Seismic Assessment of RC Exterior Beam-Column Joints and Retrofit with Haunches Using Post-Installed Anchors

Von der Fakultät Bau- und Umweltingenieurwissenschaften
der Universität Stuttgart zur Erlangung der Würde
eines Doktors der Ingenieurwissenschaft (Dr.-Ing.)
genehmigte Abhandlung

Vorgelegt von

Giovacchino Genesio

aus Florenz, Italien

Hauptberichter:	Prof. Rolf Eligehausen
Mitberichter:	Prof. Jan Hofmann
	Prof. Stefano Pampanin
	Prof. Elizabeth Vintzileou

Tag der mündlichen Prüfung: 25. Mai 2012

Institut für Werkstoffe im Bauwesen der Universität Stuttgart
2012

Mitteilungen des Institut für Werkstoffe im Bauwesen; Band 2012/1

Genesio, G. Seismic Assessment of RC Exterior Beam-Column Joints and Retrofit with Haunches Using Post-Installed Anchors

Herausgeber: Institut für Werkstoffe im Bauwesen der Universität Stuttgart
Prof. Dr.-Ing. Harald Garrecht
Prof. Dr.-Ing. Jan Hofmann

Anschrift: Institut für Werkstoffe im Bauwesen
Pfaffenwaldring 4
70569 Stuttgart
oder:
Universität Stuttgart
Institut für Werkstoffe im Bauwesen
70550 Stuttgart
Telefon: (0711) 685 63324
Telefax: (0711) 685 63349

Redaktion: Dr.-Ing. Joachim Schwarte
Dipl.-Bibl. Monika Werner

D93

ISSN 0932-5921
ISBN 978-3-9811682-4-2

“True, our knowledge does grow, but it is threatened by greater increases in confidence, which make our increase in knowledge at the same time an increase in confusion, ignorance, and conceit.”

(N. N. Taleb – The Black Swan)

This work is dedicated to the memory of
Piero Scapini, Professor, Artist, Researcher
[Verona, 15.02.1916 – 08.01.2004]

ABSTRACT

The assessment of the shear strength of two dimensional (2D) reinforced concrete (RC) exterior beam-column joints is an open issue and its solution is still a point of discussion in the scientific community although significant research effort has been devoted to this topic in recent times. The uncertainty in the evaluation of joint shear strength is exacerbated if substandard detailing is present such as lack of transverse reinforcement in the core, the use of plain round bars and inadequate anchorage of the beam bars, typical of pre 1970s construction practice. The need of a reliable evaluation of the shear behaviour of substandard joints is highlighted within the framework of a performance based seismic assessment and retrofit of RC frames.

The first part of this thesis aims to develop a simple shear strength assessment model for typical pre 1970s beam-column connections based on mechanical principles. An experimental programme consisting of six quasi-static cyclic tests was carried out. The experimental results were used for the validation of a Finite Element (FE) model, which was used to carry out an extensive parametric study. The shear assessment model proposed was additionally validated with an experimental database. The model includes the influence of several parameters such as concrete strength, column axial load, amount and detailing of beam and column reinforcement, geometric aspect ratio and effect of beam bar yielding.

In the second part, the possibility of using post-installed anchors for the seismic retrofitting of beam-column joints is investigated. Post-installed anchors are usually fast and easy to install and they represent a valuable minimally-invasive solution to transfer high loads with reasonably low costs. The retrofit of RC beam-column connections using a fully fastened diagonal haunch element is proposed as an optimisation of an existing retrofit technique. After some preliminary analytical considerations, experimental tests and numerical simulations were carried out to develop a safe and economical design model of the proposed retrofit solution. The investigations highlighted the need of displacement oriented design provisions for post-installed anchors, because tensile and shear stiffness of the anchorages are necessary in order to evaluate their loading and the effectiveness of the retrofit solution.

KURZFASSUNG

Die Beurteilung der Schubtragfähigkeit von Stahlbetonrahmenendknoten ist ein umstrittenes Thema. Trotz der umfassenden Forschungen auf diesem Gebiet in den letzten Jahrzehnten wurde bislang keine Lösung gefunden, die allgemein akzeptiert wird. Die Unsicherheit in der Abschätzung der Knotenschubtragfähigkeit ist noch deutlicher im Fall von Bewehrungsausführungen typisch in der Baupraxis vor der Einführung von modernen seismisch orientierten Normen Anfang der siebziger Jahre (z. B. Anwendung von glatten Stäben und mangelhafte Verankerungslösung der Riegelbewehrung im Knotenbereich). Für die Bemessung einer seismischen funktionsanforderungsorientierten Ertüchtigung ist eine zuverlässige Beurteilung des Schubverhaltens von Knoten in einem Stahlbetonrahmen notwendig.

Der erste Teil dieser Arbeit zielt darauf ab, eine Bemessungsmethode für die Beurteilung der Schubtragfähigkeit von Stahlbetonrahmenknoten zu entwickeln, die nicht nach modernen seismisch orientieren Normen bemessen und gebaut wurden. Diese Methode basiert auf mechanischen Prinzipien. Ein Versuchsprogramm von sechs Prüfkörpern wurde erarbeitet. Die experimentellen Ergebnisse dienten der Validierung eines Finiten Elemente (FE) Modells, mit dem eine umfangreiche Parameterstudie durchgeführt wurde. Die Beurteilungsmethode der Knotenschubtragfähigkeit wurde mit einer experimentellen Datenbank zusätzlich validiert. Das Modell berücksichtigt den Einfluss von etlichen Parametern, wie: der Betondruckfestigkeit, der Normalkraft in der Stütze, dem Bewehrungsgrad und der Bewehrungsausführung, der geometrischen Schlankheit und dem Effekt des Fließens der Längsbewehrung des Riegels.

Im zweiten Teil wird die mögliche Anwendung von nachträglichen Befestigungsmitteln für die seismische Ertüchtigung von Stahlbetonrahmenknoten untersucht. Dübel sind normalerweise schnell und einfach zu installieren und stellen eine wirtschaftliche Lösung dar, hohe Lasten zu übertragen. Die Ertüchtigung von Stahlbetonrahmenknoten mit nachträglich befestigten Stahldiagonalen wurde als Optimierung einer vorhandenen Ertüchtigungslösung vorgeschlagen. Nach anfänglichen analytischen Betrachtungen wurden hierzu experimentelle Versuche und numerische Simulationen durchgeführt, um ein sicheres und wirtschaftliches Bemessungsmodell zu entwickeln. Die Untersuchungen zeigten den Bedarf an verschiebungsorientierten Bemessungsrichtlinien für nachträgliche Befestigungsmittel auf, da sich die Schub- und Zugsteifigkeit der Befestigung entscheidend auf die Höhe der Belastung und die Wirksamkeit der Ertüchtigungsmaßnahme auswirken.

ACKNOWLEDGMENTS

There are many people that I would like thank, for their help and support during these years of research work.

First of all I would like to thank my first PhD advisor Prof. Rolf Eligehausen. I would like to express my greatest gratitude to Prof. Eligehausen for giving me the chance to work for almost six years at the Institute of Construction Materials (IWB) of the University of Stuttgart. Under his guidance I had the chance to work on this interesting project and gain experience also in activities beyond research such as teaching, code development and organisation.

My research project would have probably never started without the contribution of ideas and experience of Prof. Stefano Pampanin. I will be forever grateful to him for welcoming me into *Team Italia* and giving me the possibility to work for five months at the University of Canterbury (Christchurch, New Zealand). This experience gave a tremendous positive input to my research work. I will also never forget our long meetings via Skype at any time of day and night.

I would also like to thank Prof. Elizabeth Vintzileou for accepting to serve as co-reviewer for my PhD Thesis and for her constructive critics to my work.

I also would like to thank Prof. Hofmann, with whom I have been working during the last (almost) two years at IWB. It was great to get involved in so many new projects and ideas. Furthermore, I would like to thank him for serving as co-reviewer for my PhD Thesis.

The numerical part of my study would have not been possible without the know-how and patient support of Prof. Ožbolt. I am sincerely thankful to him for teaching me so much about the Finite Element method.

The main reason why, I will always have a great memory about my time at IWB, is because I had the chance to work in a very pleasant and cooperative working environment. Among my colleagues I would like to thank especially Jörg Appl, Stefan Fichtner, Christian Fischer, Mattew Hoehler, Carolin Kurz, Steffen Lettow, Anita Negele, Goran Periškić, Klaus Schmid, Sabrina Senftleben, Georg Welz and Anke Wildermuth for their friendship, support, helpful discussions and suggestions. The technical discussions with Philipp Grosser have been for me extremely helpful and need to be extra-aknowledged: Thank you Philipp for your time and friendship. Thanks a lot to Monika Werner for being always extremely helpful in searching and finding all the publications I requested and for reviewing the reference chapter of this work. Dr. Fuchs was always there with his experience for suggestions and to correct my documents in German: this deserves my gratitude. Great thanks go also the IWB technicians

Peter Scherf, Eugen Lindenmeier and Paul Geiger, who taught me so much about lab working.

My stay in Christchurch, working in the laboratory of the University of Canterbury, would have not been so enjoyable and fruitful if I would have not met such great colleagues and friends. For their support and friendship I especially thank Umut Akgüzel, Anna Brignola, Weng Yuen Kam, Sara Personeni, Tobias Smith and Andrea Vezzoli. For their technical support in the laboratory great thanks go to Mosese Fifita, Gavin Keats and John Maley.

My greatest gratitude goes to Akanshu Sharma. He did so much more than just helping me in carrying out the experimental campaign at the Bhabha Atomic Research Centre (BARC). He has organised and carried out tests in the time when I could not be in Mumbai and during my stay in India he made sure that I felt comfortable in the new environment and that I could get to know some aspects of the amazing Indian culture. For this and much more he and his family will always have my gratitude. Furthermore, I would like to acknowledge the support and interest in the research Project of Mr. H. S. Kushwahwa and Dr. G. R. Reddy. For the technical support during the tests at BARC my gratitude goes to Mr. S.S. Sharma, Mr. Nagre, Mr. Murali Nayar, Mr. S.N. Bodele, Mr. R.V. Nandanwar, and Mr. Girish.

For the proof reading of my thesis thanks go to my friends Charlotte Brown and Tobias Smith.

Thanks also to the Diploma/Masters candidates that I supervised, Mutlu Sönmez, Ravi Kiran Yellavajjala and Joty Shrestha and the students who supported my work Solmaz Amiri and David Camacho Alcocer.

I would like to acknowledge the firm Würth for the financial support for the research presented in this thesis. Additionally, the DAAD (Deutscher Akademischer Austauschdienst) for my stay in New Zealand and of DFG (Deutsche Forschungsgemeinschaft) for allowing me in participating at two international conferences are kindly acknowledged for awarding me with scholarships.

Finally, I would like to thank my wonderful wife Korinna for her constant support during the last few years and patience especially during my long stays abroad and my parents, my brother and my parents-in-law for believing in me.

Giovacchino Genesio
Stuttgart, June 2011

TABLE OF CONTENTS

NOTATION

Latin Uppercase Letters

A	Area or cross section
A_b	Beam cross section
A_c	Column cross section
A_d	Cross section of the diagonal steel haunches
A_j	Joint cross section
A_{sb}	Reinforcement area in the beam in the case of symmetrical reinforcement
A_{sc}	Reinforcement area in the column in the case of symmetrical reinforcement
A_{sj}	Transverse reinforcement area in the joint
C	Compression
D	Force of the compression strut / Deformed bars
E_c	Young's modulus of concrete
E_s	Young's modulus of steel
G_c	Shear modulus of concrete
G_C	Fracture energy of concrete in compression
G_F	Fracture energy of concrete in tension
H_c	Column height
H_s	Hardening modulus of steel
K	Stiffness
K_d	Stiffness of haunch steel diagonals in [kN/mm] or [N/mm]
K_f	Frictional stiffness
K_h	Haunch stiffness
K_j	Joint rotational stiffness
K_N	Tensile stiffness of an anchorage
K_V	Shear stiffness of an anchorage
K_s	Secant stiffness
I_b	Inertial moment of the beam cross section
I_c	Inertial moment of the column cross section
L_h	Length of the haunch
L_b	Beam half length
M	Moment
M_b	Beam flexural moment at column interface
$M_{b,y}$	Beam flexural yielding moment
$M_{b,u}$	Beam flexural ultimate moment
M_c	Column flexural moment at beam interface
$M_{c,y}$	Column flexural yielding moment

$M_{c,u}$ Column flexural ultimate moment
N_c Column axial load
$N_{R,c}$ Resistance to concrete cone failure of an anchor group
$N_{R,p}$ Resistance to pullout / pull-through / combined concrete cone and pullout of an anchor group
$N_{R,s}$ Resistance to steel failure in tension of an anchor
$N_{R,sp}$ Resistance to splitting failure of an anchor group
R Plain round / smooth bar
T Tension
V Shear / Volume
V_c Column shear
V_b Beam shear
V_j Joint shear
V_{jh} Horizontal shear force in the joint core
V_{jv} Vertical shear force in the joint core
$V_{R,c}$ Resistance to concrete edge failure of an anchor group
$V_{R,cp}$ Resistance to concrete pryout failure of an anchor group
$V_{R,s}$ Resistance to steel failure in shear of an anchor

Latin Lowercase Letters

c Concrete cover / Edge distance of anchor or anchor group
e Eccentricity
d_b Beam longitudinal bars diameter
d_c Column longitudinal bars diameter
d_s Diameter of bars constituting the transversal reinforcement (i.e., stirrups)
f_a Concrete compressive stress due to column axial load
f_{bd} Bond stress
f_c Concrete compressive strength measured on cylinder
f_c' Specified concrete compressive strength according to *ACI* and *NZS*
f_{cm} Mean concrete compressive strength measured on cylinder
f_{cc} Concrete compressive strength measured on cubes
f_{cd} Design concrete compressive strength measured on cylinder
f_{ct} Concrete tensile strength
f_{ctm} Average concrete tensile strength
f_{ck} Characteristic concrete compressive strength measured on cylinder according to *EN*
f_y Steel yield strength / Specified steel yield strength according to *ACI* and *NZS*
f_{yd} Design steel yield strength
f_{yk} Characteristic steel yield strength according to *EN*
f_u Steel ultimate strength
h Overall depth of a cross-section
h_b Beam section depth
h_j Joint section depth
h_c Column section depth
h_{ef} Effective embedment depth of an anchor
j_b Internal lever arm of the beam

j_c Internal lever arm of the column
k_f Frictional stiffness in [N/mm^3]
k_N Tensile stiffness of a single anchor
k_V Shear stiffness of a single anchor
l_d Anchorage length
l_{dh} Length of the straight anchorage in the joint panel
n_c Column axial load as [%] of the compressive strength of the concrete section
p_t Principle tensile stress
p_c Principle compressive stress
s Spacing of stirrups / Spacing of anchors in a group
t Thickness
v_j Shear stress in the joint core
v_{jc} Joint shear stress resisted by concrete
v_{jh} Horizontal shear stress in the joint core
v_{js} Joint shear stress resisted by transverse reinforcement
w_b Beam section width
w_c Column section width
w_j Joint section width
z_b Beam static height, i.e., ($h_b - c$)
z_c Column static height, i.e., ($h_c - c$)

Greek Uppercase Letters

Δ Difference / Displacement
Δ_y Yielding displacement
Δ_u Ultimate displacement
Σ Sum

Greek Lowercase Letters

α_j Angle between joint diagonal and horizontal axis
α Angle between diagonal haunch and beam / Variation coefficient of column axial load
β Shear transferring factor
β_{cr} Anchor axial stiffness in service load range in cracked concrete according to *ICC-ES*
β_{uncr} Anchor axial stiffness in service load range in uncracked concrete according to *ICC-ES*
δ Displacement
δ_b Beam end displacement
δ_c Column top displacement
ε Strain
ϕ Curvature
ϕ_y Yielding curvature
ϕ_u Ultimate curvature
λ_0 $\lambda_1 \cdot \lambda_2$
λ_1 Ratio between average and characteristic yielding strength of reinforcement steel according to *Paulay & Priestley (1992)*

λ_2 Ratio between yielding and ultimate strength of reinforcement steel according to *Paulay & Priestley (1992)*
γ Partial factor according to *EN*
γ_j Joint shear distortion
μ_k Coefficient of kinetic friction
μ_s Coefficient of static friction
μ_Δ Displacement ductility
μ_ϕ Curvature ductility
ν_c Poisson ratio of concrete
ν_s Poisson ratio of steel
ρ_b Beam reinforcement ratio (tensioned bars)
ρ'_b Beam reinforcement ratio (compressed bars)
ρ_c Column reinforcement ratio (tensioned bars)
ρ'_c Column reinforcement ratio (compressed bars)
ρ_j Joint volumetric reinforcement ratio
σ Stress
ψ Factor to account for various influences in the calculation of concrete failure modes of anchorages

Common Subscripts

0 Short term
b Beam
c Column / Concrete
cr Crack
d Design / Steel diagonal
h Horizontal / Hoop / Haunch
j Joint
k Characteristic
m Mean / Average
R Resistance
S Action
s Steel
u Ultimate
y Yield
v Vertical

Symbols

∞ Long term

Abbreviations

1D one-dimensional
2D two-dimensional
3D three-dimensional

B	Beam flexural failure mode
BARC	Bhabha Atomic Research Centre
BCM	Bond Capacity Method
BJ 1	Beam flexural failure after joint shear cracking
BJ 2	Joint shear cracking after beam flexural yielding
CCM	Concrete Capacity Method (also CC-Method)
CV	Coefficient of Variation
EOTA	European Organisation for Technical Approvals
ETA	European Technical Approval
FE	Finite Element
FEA	Finite Element Analysis
GLD	Gravity Load Designed
HRS	Haunch Retrofit Solution
ICC-ES	International Code Council – Evaluation Service.
IWB	Institut für Werkstoffe im Bauwesen (Institute of Construction Materials)
JS	Joint shear failure mode
LD	Load-Displacement
MASA	MAcroscopic Space Analysis
MCFT	Modified Compression Field Theory
MRF	Moment Resisting Frame
n.a.	not available
RC	Reinforced Concrete
SAT	Strut And Tie
UC	University of Canterbury

Anchorage of beam bars in the joint panel

Type 1	Deformed bars with 90°-hooks bent into the core
Type 2	Deformed bars with 90°-hooks bent away from the core
Type 3	Deformed bars with U-shaped anchorage
Type 4	Deformed bars with big 180°-hooks
Type 5	Deformed bars with straight anchorage
Type 6	Plain round bars with 180°-hooks
Type 7	Plain round bars with 90°-hooks bent into the core
Type 8	Plain round bars with 90°-hooks bent away from the core
Type 9	Plain round bars with straight anchorage

1 INTRODUCTION

1.1 Historical Background and motivation

Since ancient times, human society has had to live with earthquakes and their consequences. Some of the most developed ancient civilisations settled in seismic prone areas (e.g., Babylonians, Greeks and Romans). Earthquakes were usually considered as the effects of the poor tempers of divine beings: Gilgamesh in the Sumerian society, Poseidon in ancient Greece, Jupiter or Mars for the Romans, the mythological Dragon and Elephant in China and India, respectively. The sudden movement of a catfish which lay under Japan and Ruaumoko, the god of volcanoes and earthquakes for the Maori in New Zealand caused these devastating events (*Dragoni, 2005*).

The first recorded attempts in scientifically explaining the origin of earthquakes were the work of Greek naturalist philosophers. They usually tried to explain the origin of these phenomena with the interaction of the four basic elements (air, earth, fire and water) (*Dragoni, 2005*). In consequence of several earthquakes (e.g., Peloponnesus in 373 BC), attention to the seismic behaviour of buildings was begun, as written by Pliny in his *Naturalis Historia*, about the temple of Diana (i.e., in Greek Artemis) at Ephesus (see Figure 1-1a) (*Calvi, 2010*):

Something that should be really admired of the Greek magnificence is the temple of Diana at Ephesus, constructed in 120 year with the contribution of all Asia. It was built on marshy soil, locating charcoal and wool furs under its foundations, to reduce its sensitivity to earthquakes and to avoid locating such big mass on unstable soil. [Liber XXXVI, xiv, 95]

The fact that the first known seismic experimental investigation was carried out on (probably) the most famous building in one of the most seismic cities of world has a great symbolic significance: Hagia Sophia in Constantinople (Figure 1-1b) in the VI Century. One of the architects, Anthemius of Tralles, built a steam machine in an underground room trying to simulate the underground winds that induce earthquakes according to theories of Aristotle.

a) Graphic reconstruction of the temple of Diana at Ephesus (550 B.C.) (Source: www.wikipedia.org)

b) Hagia Sophia, Istanbul, Turkey (Photo by G. Genesio)

Figure 1-1: Seismic design of the antiques?

After the “dark parenthesis” of the middle ages, when the origin of earthquakes was found to be exclusively in the sake of God and no scientific theory was considered acceptable (102nd Heresy in *Liber de hearesibus* by Filastrio), Aristotle’s and the Hellenistic theory was the most popular in Europe, e.g., Dante Alighieri and in the Middle East Avicenna (Ibn Sina) and Averroës (Ibn Rushd) (*Dragoni, 2005*). In the following centuries, theories involving the underground action of fire (e.g., *Pirothenica* by Vannuccio Beringuccio in 1550 and *De re metallica* by Giorgio Agricola in 1556) or water (e.g., *Mundus subterraneus* by Athanasius Kircher in 1664) were developed. We have to wait until the work of Robert Hooke (*Discourse on earthquakes*) in 1668 and Niels Stensen to find a correct interpretation of the stratified structure of the earth’s surface. Research carried out in the last part of XIX Century finally linked faultlines in the earth and seismic events (M.S. De Rossi, 1879; G.K. Gilbert, 1884 and B. Koto, 1891).

In spite of great effort spent by the philosophic / scientific community through the centuries in understanding the origin of seismic phenomena, earthquakes continued to be the subject of debate among thinkers, rather than learning how to construct in a way that reduces their effects (*Calvi, 2010*). This started changing after two major earthquakes: in San Francisco (1906) and Messina (1908) (Figure 1-2a,b). The patent of seismic isolator by the Italian Viscardini is just a sign that something is moving towards modern seismic design (Figure 1-2c).

a) San Francisco (1906)
(Source: www.wikipedia.org)

b) Messina (1908)
(Source: www.wikipedia.org)

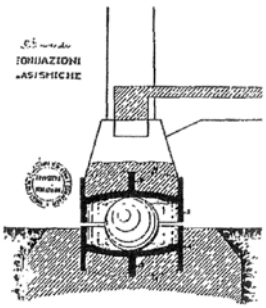

c) Patent for seismic isolator
by Viscardini in 1909

Figure 1-2: New consciousness on seismic design at the beginning of 20th century

In the 1920-30s the first seismic code provisions were developed. Generally, in the design of structures a lateral load equal to 10% of the vertical actions had to be taken into account. However, we have to wait until the 1960-70s to find a further significant improvement in the seismic design of structures, when the availability of measurements of seismographs and the development of computer based computational techniques contributed to the development of the first strength oriented design methods.

In the last four decades, the tremendous socio-economical consequences of many earthquakes provided a great impulse in the further development of seismic design. Concepts like “Capacity Design” (see chain analogy by Paulay and Priestley in Figure 1-3a), “Performance Based Design” (Figure 1-3b) (relation between seismic intensity and building response, see e.g., SEAOC Vision 2000 (*SEAOC, 1995*) and *ASCE-41-06 (2007)* and “Displacement Based Design” (design of structures in order to be able to undergo a certain displacement within a target limit state, see *Priestley at al., 2007*) were developed.

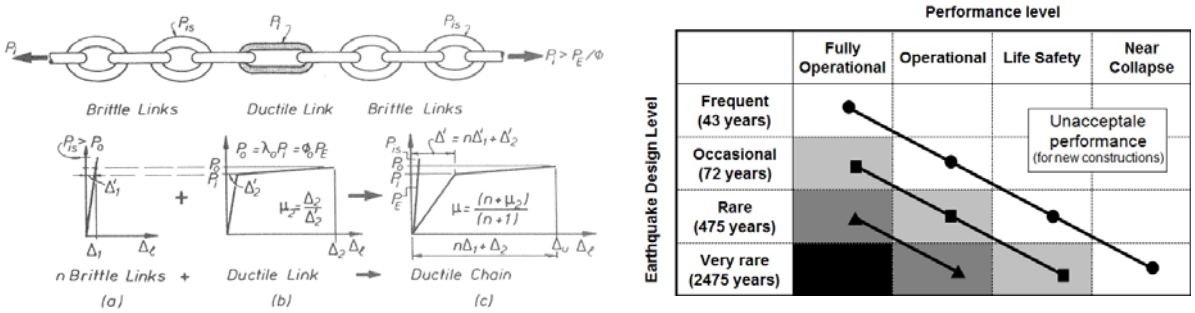

a) Basic concept of Capacity Design (*Paulay & Priestley, 1992*)

b) Performance Based Design matrix (*SEAOC, 1995*)

Figure 1-3: Development of design approaches

The above concepts need to be applied also for the assessment and retrofit of buildings, which were not built to resist seismic actions, because of the lack of knowledge from a seismological (e.g., identification and classification of seismic areas) and/or from a constructive point of view.

1.2 Context and objective of the research

Constructive deficiencies of buildings are generally not known before they are tragically highlighted by earthquakes. Several seismic events worldwide have shown the poor performance of buildings having a reinforced concrete (RC) structure built with insufficient detailing and lack of “Capacity Design” principles. Moment resisting frames (MRF) built until the end of the 1970s are generally very sensitive to lateral actions and their poor performance results often in brittle collapse during an earthquake (see Figure 1-4). This building type is globally very common, where it found widespread application in residential architecture in response to the demographical boom and urbanisation (especially in Europe) process after World War II. This is also the case for critical buildings such as schools and hospitals. In most of the cases, the causes of such undesirable behaviour of such RC structures can be identified as being due to poor detailing and deficient design of beam-column connections and in particular of exterior beam-column joints (see Figure 1-4).

a) Izmit-Kocaeli (1999) (Source: EERC, Berkeley)

b) L’Aquila (2009) (Courtesy of A. Brignola)

c) Christchurch (2011) (Courtesy of W.Y. Kam)

Figure 1-4: Joint failures in RC buildings during past earthquakes

Research of the past few decades has highlighted that the causes of low joint shear strength and consequent brittle behaviour of joints can be found in the lack of shear reinforcement in the core and deficient anchorage of the beam longitudinal bars in the joint panel (see Figure

1-5). A large variety of typologies of beam-column connections can be found in RC structures (see Figure 2-1). However, only the case of the 2-dimensional (2D) exterior joint is considered in this research project, since the evaluation of the strength of more complex joints can be carried out only after a full understanding of this basic geometrical configuration. Although a significant research effort has been spent on this topic in the last dacades, there are still major uncertainnesses in the seismic assessment of so called substandard exterior beam-column joints. Therefore, in this study the development of a shear strength model to describe the behaviour of such substandard beam-column connections is targeted.

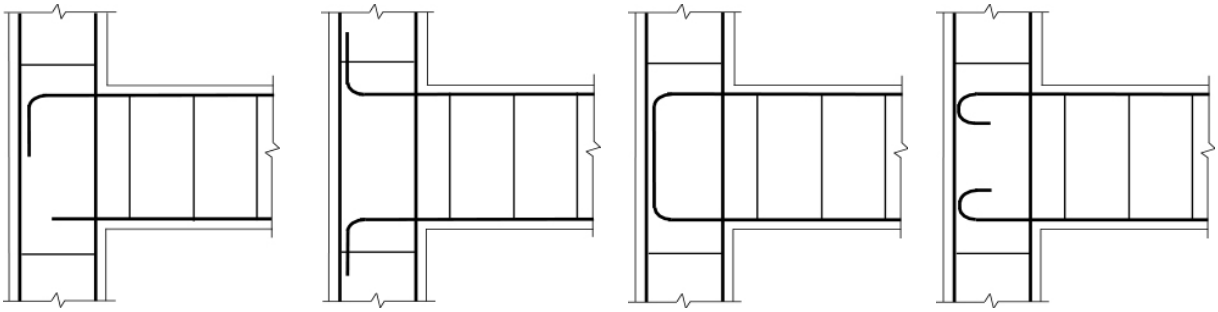

a) bent-in / straight b) Bent out c) U-Shaped d) 180°-hooks

Figure 1-5: Common detailing solutions of substandard RC exterior beam-column joint

Improvement of structural deficiencies resulting in insufficient seismic response of buildings can be achieved with the “Seismic Retrofitting”. Several techniques have been developed recently to improve the seismic performance of beam-column connections with different degrees of success. The aim of this study is to develop a low cost – minimally invasive – low tech method to retrofit beam-column joints and, hence, to improve the seismic response of MRFs. The Haunch Retrofit Solution (HRS) proposed by *Pampanin et al. (2006)* was developed to modify the internal hierarchy of strength of beam-column joints thus avoiding brittle plastic mechanisms (joint or column failure) in favour of more ductile failure modes (beam hinging). This retrofit solution constitutes the start point for this research work (Figure 1-6a).

Aiming to simplify this effective solution, the possibility of using post-installed anchor systems was investigated (Figure 1-6b). These can provide many advantages such as reduction of invasiveness, increase of durability and reduction of installation time and costs. The lower invasiveness of anchorages with post-installed anchors instead of traditional fastening methods for the connection of old and new structural elements such as clamping of steel plates with pre-tensioned threaded rods in shown in Figure 1-6a,b. The solution shown in Figure 1-6c can be easily designed since strength and stiffness are known. The strength of the connections shown in Figure 1-6d,e can be calculated using the Concrete Capacity Method (CCM) and the Bond Capacity Method (BCM) (*Eligehausen et al., 2006*), although there is still a general lack of knowledge concerning the stiffness of this kind of connection.

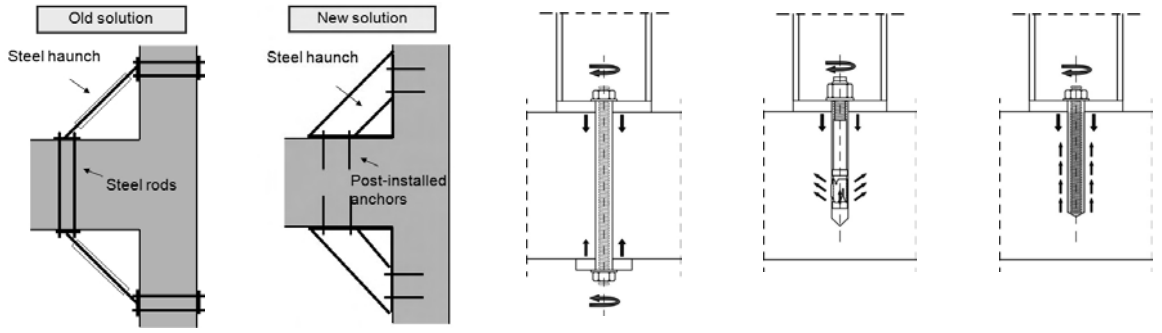

a) HRS – schema | b) New HRS - schema | c) Traditional fastening method | d) Connection with expansion anchors | e) Connection with bonded anchors

Figure 1-6: Possible connections between existing and new structural elements

1.3 Organisation of the work

After a brief overview on the state of the art inherent to the seismic assessment and retrofit of exterior RC beam-column joints and the seismic application of post-installed anchors (*Chapter 2)*, the work can be divided in two parts, dealing with the assessment and retrofit of joints, respectively.

In the first part, the seismic assessment of substandard RC exterior beam-column connections is investigated and particular focus is given to the qualitative (physical mechanism) and quantitative (determination of strength and deformation limit states) behaviour. A set of experimental tests to investigate some aspects of the behaviour of beam-column connections, which had not yet been fully understood, was carried out (*Chapter 3*). The experimental results were used to develop and validate a Finite Element (FE) model (*Chapter 4*). Based on a numerical parametric study a shear strength assessment model was proposed (*Chapter 5*). After validation using an experimental database (*Chapter 6*), the model was inserted in the framework of the "Capacity Assessment" (consistently with the principles of "Capacity Design") of beam-column joints (*Chapter 7*).

In the second part of the work, the Haunch Retrofit Solution for RC beam-column joints was analysed and its optimisation in terms of the reduction of invasiveness, simplification of installation and consequently reduction of costs was proposed. The necessary modifications of the retrofit design (*Chapter 8*) were experimentally (*Chapter 9*) and numerically (*Chapter 10*) validated. The design procedures developed on the basis of analytical, experimental and numerical investigations are contained in *Chapter 11*. Furthermore, a design format in terms of partial safety factors according to *EC8-3 (2005)* and *fib (2011)* is also proposed.

The main achievements and open questions resulting from this research work are summarised in *Chapter 12*. For reasons of completeness several appendices are attached to this work. In *Appendix A* an extensive review of joint shear strength models available in the literature is presented. The experimental database used for the validation of the assessment model and FE analyses carried out in the study (on as-built and retrofitted specimens) are listed in *Appendix B* and *C*, respectively. In *Appendix D* the assessment procedure proposed in *Chapter 7* is validated by verifying the tested specimens. In *Appendix E* the retrofit design method proposed by *Pampanin et al. (2006)* is summarised and the modified methods proposed in *Chapter 11* are applied to the investigated specimens in *Appendix F*.

2 STATE OF THE ART: ANALYSIS AND DISCUSSION

In the following sections the state of the art of the research relating to the seismic assessment and retrofit of exterior two-dimensional (2D) reinforced concrete (RC) beam-column joints as well as the seismic behaviour and application of post-installed anchors are summarised and discussed.

In the first part, after a brief introduction on the mechanics of 2D exterior beam-column joints (Section 2.1), experimental studies available in the literature are presented and the main findings are summarised and discussed (Section 2.2). The review of experimental studies is limited to monotonic and cyclic quasi-static testing of RC exterior joint designed without taking into account the provisions of modern seismic codes. The following sections discuss the use of experimental investigations as a basis for the development of numerical models (Section 2.3) and models for the evaluation of the joint shear strength (Section 2.4). Since the aim of this study is the assessment and retrofit of existing joints, it is necessary to understand the possible deficiencies that may be found in the engineering practice. Therefore, the development of some of the most relevant constructions codes in the past sixty years is briefly presented (Section 2.4.8).

Some of the strategies and techniques for the retrofit of RC moment resisting frames developed in the last decades are briefly presented in Section 2.6. In Section 2.7 post-installed anchors systems and their seismic behaviour are introduced.

Sections 2.1 to 2.4.8 provide the basis for development of a refined assessment method for the determination of the shear strength of RC exterior beam-column connections. The analysis of the historical development of construction codes (Section 2.4.8) demonstrates the need for research into the seismic assessment and retrofit of substandard joints. Sections 2.6 and 2.7 present the context for the development of the retrofit solution proposed in this research work.

2.1 Mechanics of RC exterior beam-column joints

2.1.1 General

Beam-column connections can be classified according to their geometrical configuration in corner, exterior and interior joints (see Figure 2-1) and they can be considered elastic or inelastic (*Paulay & Priestley, 1992*). From a structural point of view, a beam-column joint can be considered elastic if it is ensured that the plastic deformations of the connection occur in the beam and/or column and the joint panel remains uncracked during the entire loading history. A beam-column joint is defined as plastic if, during the loading reversals, there is some inelastic deformation in the joint panel (i.e., cracking). This latter case is typical for the

seismic behaviour of joints which were not designed according to the principles of modern advanced standards provisions (i.e., no Capacity Design, poor anchorage of beam bars in core and lack of transverse reinforcement in the joint region).

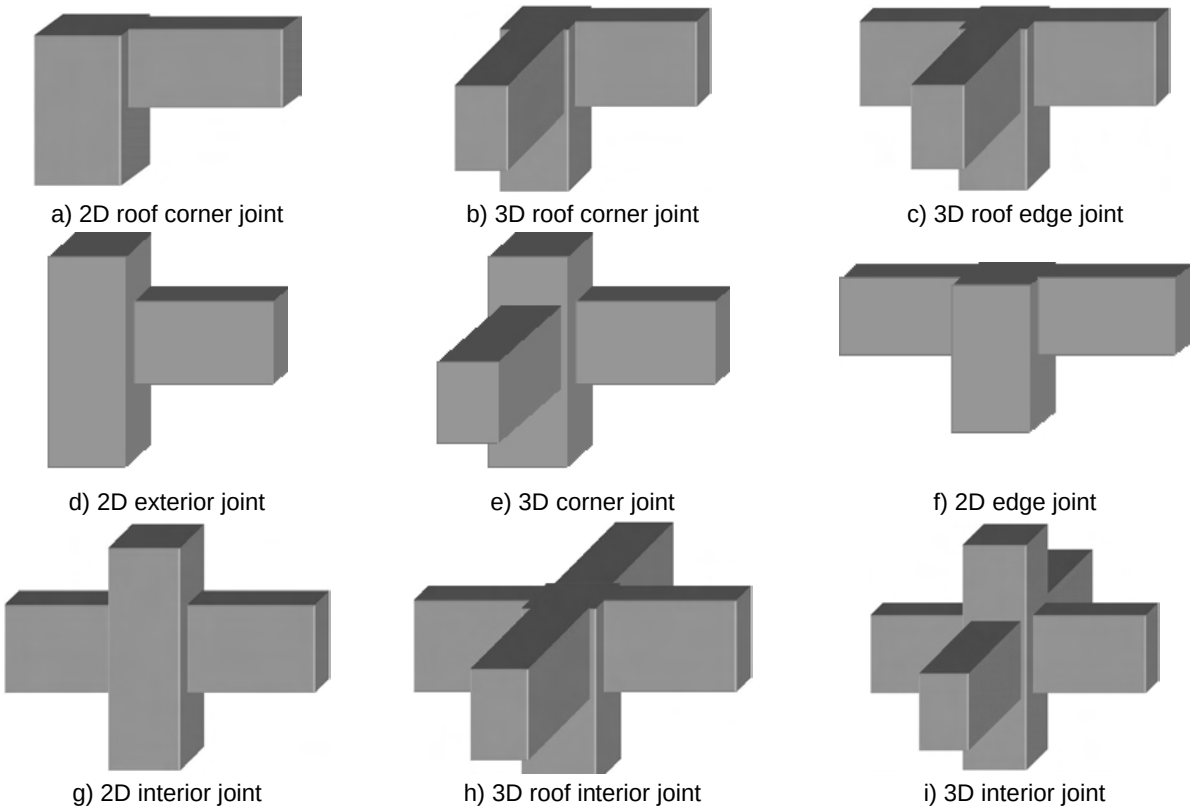

Figure 2-1: Classification of typical beam-column joints

A beam-column joint can also be defined as the region formed by the intersection of beam and column. Therefore, each of the three elements can fail under different modes as enlisted below:

- beam flexural failure;
- beam shear failure;
- column flexural failure;
- column shear failure;
- joint shear failure;
- bond failure of the reinforcement; and
- a combination of the various modes listed above.

It is well know that some of these failure modes should be avoided if the beam-column connection undergoes large plastic deformations (e.g., shear failures of beam, column or joint and bond failure of reinforcement). Due to the limited deformation capacity of such brittle plastic mechanism, a collapse of the whole frame may result.

2.1.2 Hierarchy of strength

To predict the most probable failure mode in the seismic assessment procedure of beam-column joints the concept of hierarchy of strength was introduced by *Pampanin (2006)*, as schematically shown in Figure 2-2. The performance of the beam-column connection is

expressed in a column axial load, N_c, - column flexural moment (measured at beam-column interface), M_c, domain. For a given value of N_c*, it is possible to predict the most probable failure mode in the form a sequence of events (1 to 5 in Figure 2-2). In Figure 2-2 only joint shear, beam / column flexural yielding and beam / column shear cracking are shown, but the diagram can be easily be extended to include the other failure modes mentioned above. The practical application of this seismic assessment approach of 2D exterior beam-column joints is explained in detail in Chapter 7.

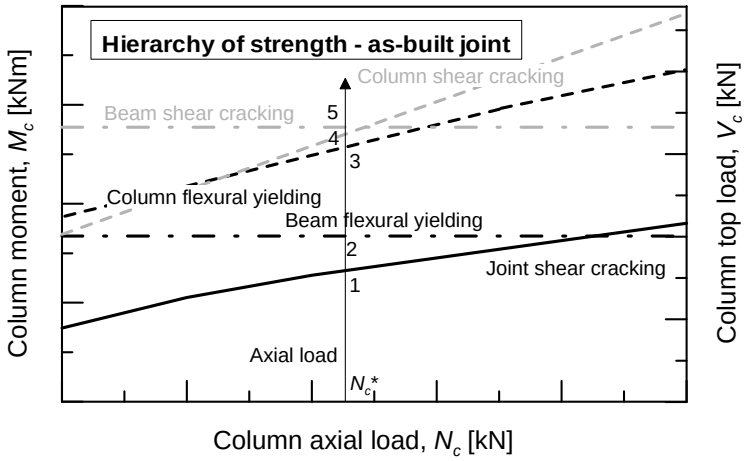

Figure 2-2: Conceptual representation of the hierarchy of strength assuming a constant column axial load, N_c*

2.1.3 Joint shear strength

As already introduced in Chapter 1, the study focus is on the shear behaviour of 2D exterior beam-column joints (Figure 2-1d). There is general agreement on the mechanics of RC beam-column joints and the stress-strain distribution which is responsible for the formation of the shear mechanism. In Figure 2-3 the forces in the beam-column connection during a seismic loading are shown (*Paulay et al., 1978*; *Paulay, 1989* and *Park, 1997*). In this study, as it is common in research practice, the geometry of the beam-column connection is given assuming the points of zero bending moment occur at the half span of the beam and half height of the column (Figure 2-3a). According to this assumption $V_a = V_c$ and $M_a = M_c$. Alternatively, the zero bending moment locations on beam and column may be evaluated by assuming a precise load distribution (gravity + seismic loads), see e.g., *Sasmal (2009)*.

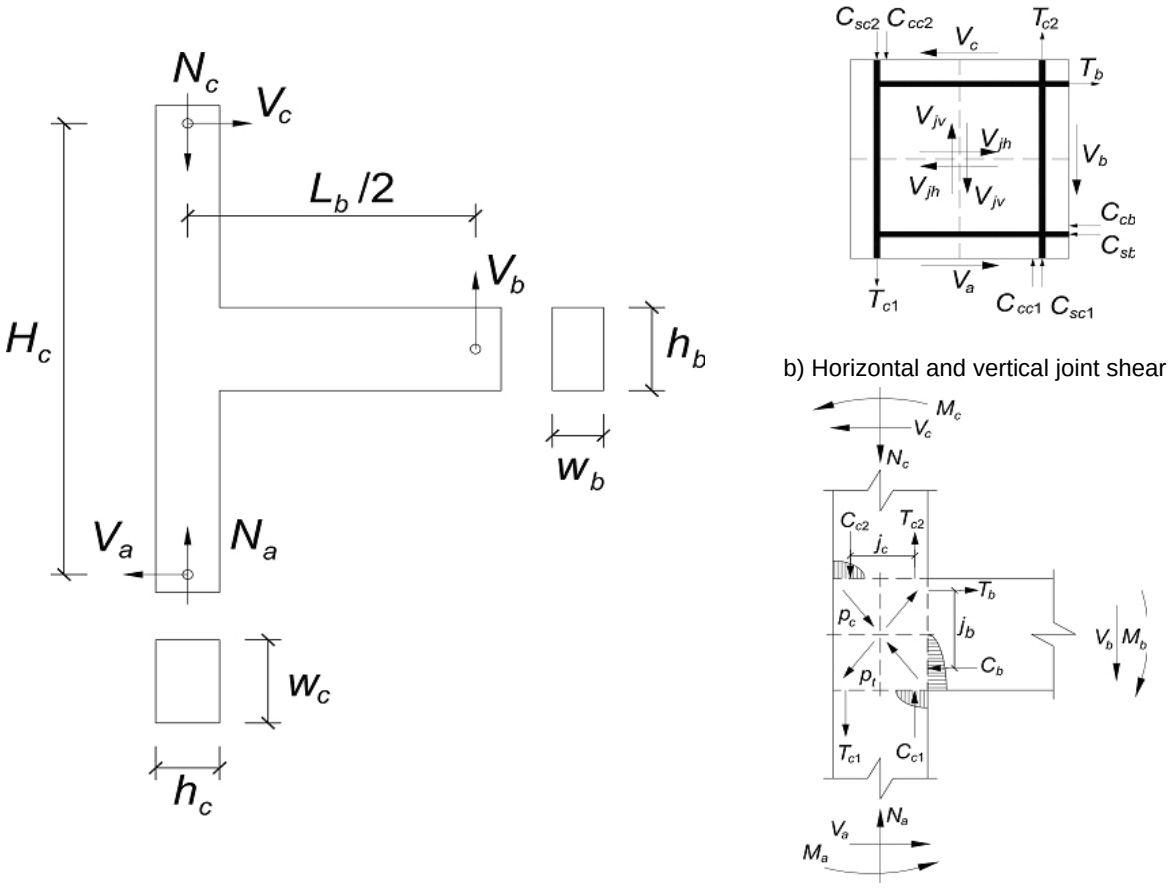

a) External actions in 2D exterior beam-column joint

b) Horizontal and vertical joint shear

c) Principle stresses in joint panel

Figure 2-3: Forces acting in exterior beam-column joint during seismic loading

For a 2D exterior beam-column connection the horizontal shear force acting across the joint region is, from first principles (Figure 2-3b):

$$V_{jh} = T_b - V_c \tag{2-1}$$

Where T_b can be calculated as:

$$T_b = M_b / j_b = V_b \left(L_b/2 - h_c/2 \right) / j_b \tag{2-2}$$

The internal lever arm of the beam, j_b, between the tensile forces and the centroid of the compressive forces can be evaluated through a moment-curvature analysis or taken as approximately 0.80 ~ 0.9($h_b - c$). In this work j_b is generally evaluated by comparing the results of moment-curvature analysis performed using the software package Response 2000 (*Response, 2001*) and the reading of strain gauges of reinforcement steel (if available in experimental tests) or values obtained in the numerical simulations.

The column top load can be calculated as:

$$V_c = V_b \cdot L_b / 2H_c \tag{2-3}$$

Substituting Equations (2-2) and (2-3) in (2-1) the following expression for V_{jh} is obtained:

$$V_{jh} = V_b \cdot \frac{L_b}{2}\left(1/j_b - h_c/2j_b - 1/H_c\right) \tag{2-4}$$

The nominal horizontal shear stress, v_{jh}, at the mid-depth of the joint core (Figure 2-3b) can be calculated as:

$$v_{jh} = \frac{V_{jh}}{w_j \cdot h_c} \tag{2-5}$$

Where the effective joint width, w_j, can be calculated using existing codes (see Section 2.5.6) or as the average of the beam and column widths. In this study b_j is calculated using the method proposed by *EC8-1 (2004)* and *NZS3101:1995* (Eq. (2-6)).

$$w_{jh} = \min\begin{cases} w_c \\ w_b \\ w_c + 0.5h_c \\ w_b + 0.5h_c \end{cases} \tag{2-6}$$

The depth of the joint can be assumed equal to the depth of the column, h_c, if the longitudinal beam bars in the core are anchored on the whole column's depth.

The nominal axial compressive stress on the column at the mid-depth of the joint core, f_a, can be calculated as:

$$f_a = \frac{N_c}{h_c \cdot w_c} \tag{2-7}$$

Most of the assessment models for the evaluation of the joint shear strength (see Section 2.4 and Appendix A) as well as most of the existing codes (see Section 2.4.8) are based on the evaluation of nominal value of v_{jh} as calculated in Equation (2-5). The contribution of the axial compressive stress on the column to the joint shear stress can be taken into account by using a variety of approaches. The method adopted in this study entails calculating the principle tension and compression stress, p_t and p_c, at mid-depth of the joint core (Figure 2-3c and point A in Figure 2-4), as found from Mohr's circle as proposed by *Hakuto et al. (2000)*:

$$p_t = -\frac{f_a}{2} + \sqrt{\left(\frac{f_a}{2}\right)^2 + v_{jh}^2} \tag{2-8a}$$

$$p_c = -\frac{f_a}{2} - \sqrt{\left(\frac{f_a}{2}\right)^2 + v_{jh}^2} \tag{2-8b}$$

Compressive stresses are taken as negative and the values of p_t and p_c of Equations (2-8a) and (2-8b) are calculated using Mohr's circle as shown in Figure 2-4. In absence of horizontal shear reinforcement in the core, the model assumes a single diagonal strut resisting all the horizontal shear forces.

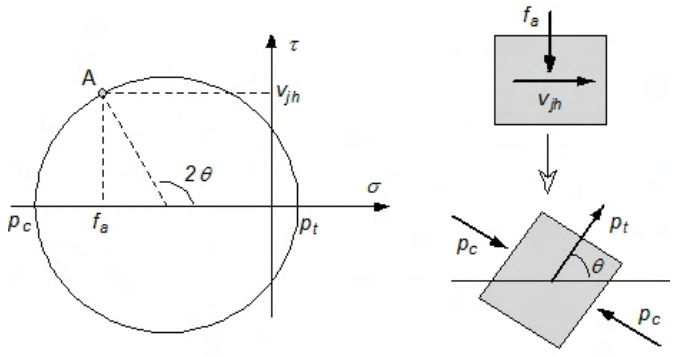

Figure 2-4: Calculation of p_t and p_c according to Mohr's circle

2.2 Experimental investigations

In the past decades many researchers carried out experimental investigations in order to understand the behaviour of RC beam-column joints. In the following sections a review of experimental investigations on monotonic (Section 2.2.1) and cyclic (Section 2.2.2) loading of beam-column joints is presented. To make the review more comprehensive, it is limited to those investigations which are closely related to this work, i.e., only 2D exterior joints (as in Figure 2-1e) without hoops in the core are considered.

2.2.1 Monotonic testing

Monotonic testing of exterior RC beam-column joints has been carried out over the past forty years. The main aim of this testing is to evaluate the joint shear strength of subassemblies built according to different code provisions and with different reinforcement detailing. These tests usually do not provide sufficient information to evaluate seismic behaviour, including joint shear deformability, ductility, energy dissipation and post peak behaviour. However, tests have shown the backbone curve of the cyclic hysterics generally follows, within acceptable limits, the monotonic load-displacement curve (*Hamil, 2000*).

Jirsa & Marques (1972) and Jirsa et al. (1977)

In these studies tests on exterior beam column connections were performed to evaluate the behaviour of standard 90° and 180° hooks conforming to *ACI 318-71* specifications (anchorage Types 1 and 4). Particular focus was given to three different types of confinement of the core: axial load, hoops in the core, longitudinal column bars and concrete cover. Tests with different aggregate types were also performed. The following conclusions were reached:

- the level of axial load does not significantly influence the behaviour of the hooked anchorages;
- the straight embedment length between the beginning of a standard hook and the critical section at the face of the column significantly influences the capacity of the anchorage;
- the configuration of the column bars does not influence the capacity of the anchorage;
- the hoops in the core have to be closely spaced relatively to the anchorage's hooks in order to be effective;
- the thickness of the concrete cover does not influence the capacity of the anchorage;

- the use of lightweight concrete does not influence the anchorage behaviour; and
- negligible performance difference was observed between 90° and 180°-hooks.

Nilsson (1973)
Research work by Nilsson was motivated by the observation that the detailing of exterior joints presented more problems than for interior joints. Seven 2/3 scaled tests, with different anchorage configurations of beam bars in the joint panel and different geometric aspect ratios, h_b/h_c, were carried out. No hoops in the joints panel were provided. All the specimens failed due to diagonal tension cracking. The joints with anchorage Type 1 exhibited much higher shear capacity than the ones with Type 2. Furthermore, it was observed that the joint shear capacity increased with decreasing ratio h_b/h_c and that the reinforcement detailing influenced the inclination of the diagonal crack.

Taylor (1974) and Taylor & Clarke (1976)
Twenty-six 3/4 scaled exterior joints were tested in these studies. The focus of the research was to investigate the influence of beam reinforcement ratio. Usually only a few hoops in the joints were provided (typically one or three). It was observed that for high beam flexural capacity the joint was not able to transfer the shear forces. Furthermore, it was recommended that the column flexural capacity should not exceed of 70% and 50% the beam flexural capacity at bottom and top joint interface, respectively. The influence of different beam reinforcement anchorage was also investigated. It was observed that for static applications anchorage Type 2 is approximately half as effective as Types 1 and 3. It was also stated that the configurations with 90°-hooks bent into and away from the joint (Types 1 and 2), are preferable than U-bars (Type 3) for seismic applications.

Hoekstra (1977)
An extensive experimental program on twenty 2/3 scaled exterior joints was carried out by Hoekstra to investigate the effect of column axial load, concrete strength, steel percentage and different configuration of hoops in the joint panel. It was observed that the concrete tensile strength has a major influence on the joint shear capacity and, to lesser extent, the column load increases the joint shear capacity. Furthermore, it was observed that for a ratio between column and beam depth of 2/3 and beam reinforcement ratio larger than 0.8%, the joint is weaker than the intersecting members. In all the tests diagonal cracking was observed in the joint core.

Scott (1992, 1994), Scott et al. (1994)
Fifteen exterior joints were tested in these studies to evaluate the effect of different joint detailing on the shear capacity. The authors observed that the British Standard *BS 8110:1985* significantly underestimates the joint shear capacity. Particular focus was given to the strain distribution in the bar anchorages, which was monitored with strain gauges (Figure 2-5). Furthermore, the following conclusions were reached:

- the column axial load increases the joint shear capacity; and
- overall, the joints with anchorage Types 1 and 3 performed much better than those with anchorage Type 2, as confirmed by the higher steel strain measured on anchoring length (Figure 2-5).

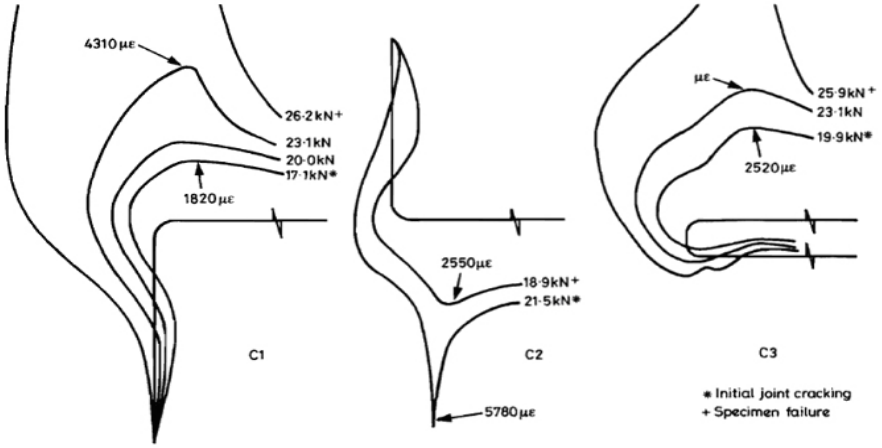

Figure 2-5: Strain distributions of anchorage Types 1, 2 and 3 (*Scott, 1992*)

Parker & Bullmann (1997)
Based on twelve monotonic tests on exterior beam-column joints, Parker and Bullmann proposed a design model to evaluate the joint shear strength. The model provided a better estimation of the shear capacity of the joint than *BS 8110:1985* and *EC2 (1992)*. The good performance of the design model could not be validated using the tests by *Scott (1992)* and *Taylor (1974)*.

Hamil (2000)
Hamil carried out forty-nine monotonic tests and twenty-six cyclic tests in order to investigate the influence of the following parameters on the shear strength:

- beam steel anchorage;
- concrete strength;
- joint ties and their positioning;
- joint aspect ratio; and
- use of high strength and steel fibre reinforced concrete.

The following main conclusions were stated by Hamil:

- beam reinforcement anchorage Type 1 is approximately 20% more effective than Type 3 at peak load, but at initial diagonal cracking the opposite behaviour was observed;
- the presence of joint ties enhances the ultimate shear capacity of the joint (Figure 2-6a), but it does not influence the strength at initial diagonal cracking (Figure 2-6b);
- the joint shear capacity decreases with increasing ratio h_b/h_c, but the capacity at first crack does not appear to be influenced by this parameter;
- the normalised shear strength of the joint in respect to $\sqrt{f_c}$ does not vary when high strength concrete is used;
- the normalised shear strength of the joint increases when fibre reinforced concrete is used; and
- low ductility of the failure mechanism, but no shear strength decrease were observed during cyclic testing compared to the monotonic tests.

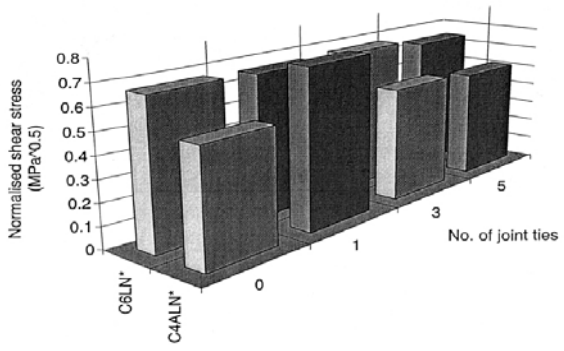

a) Effect of transverse reinforcement on initial joint shear cracking

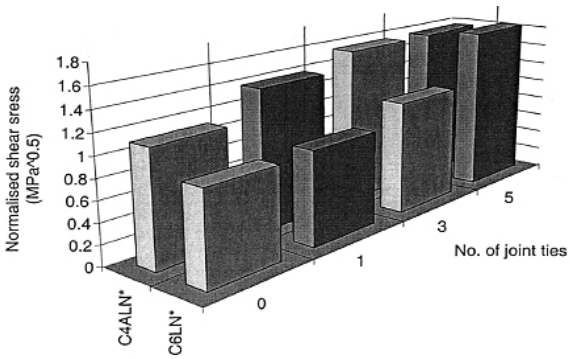

a) Effect of transverse reinforcement on joint shear ultimate strength

Figure 2-6: Investigation of the effect of joint transverse reinforcement by *Hamil (2000)*

2.2.2 Cyclic testing

The collapses and high damages observed in moment resisting frames in several earthquakes have led to a surge in research. Many of the test campaigns were aimed at the development of provisions within seismic codes. In this section, focus is given to those tests that evidenced the limits of joint shear strength.

Hanson & Connor (1967)

The first reported tests on exterior beam-column joints were carried out by *Hanson & Connor (1967)*. They outlined the necessity of incorporation of a joint shear stress limit, at which a brittle shear failure should be prevented. Their recommendations for the design of beam-column joints in monolithic reinforced concrete structures were incorporated in *ACI 318-71*, i.e., hoops should be always provided for unconfined joints (exterior and corner joints).

Morita & Fujii (1984), Kanada et al. (1985)

Tests were carried out at the University of Kyoto with the aim of investigating the following parameters:

- the effect of stirrups in the joint; and
- the influence of different beam bars anchorage types.

The following observations were made:

- the joints with bars bent out of the core (Type 2) had poorer behaviour than the specimen with 90°-hooks bent in (Type 1);
- the presence of stirrups increased the ultimate capacity of the joint; and
- specimens with anchorage shorter than the column depth exhibited a lower shear capacity. To quantify the influence of the length of such anchorages it was proposed that the effective depth of the joints should be limited to the length of the anchorage, l_{dh}, instead of the depth of the column, h_c.

Minami & Nishimura (1985), Nishimura & Minami (1985)

Tests were carried out at the University of Osaka to investigate the influence of the shape of beam bar anchorage, length of straight anchorage, axial load in the column and stirrups in the joint on joint shear capacity. It was concluded that axial load and stirrups in the joint have a positive effect on joint shear capacity. The length of the straight anchorage of the beam

bars within the joint panel was found to have also an important role, which cannot be replaced by a longer bending tail.

Hakuto et al. (2000)
Hakuto *et al.* performed tests on interior and exterior joints designed according to pre 1970s provisions. The limitation of the principle tension stress instead of the shear stress was proposed to assess the strength corresponding to the formation of the first diagonal crack in the joint panel. In this way the influence of the axial load in the column can be realistically taken into account (see Section 2.1.3).

Liu & Park (2001)
Liu tested four exterior beam-column joints with plain round bars, 90°-hooks bent in and away from the joint (anchorage Types 7 and 8) with and without column axial load. When compared with results of similar specimen reinforced by deformed bars (tests by *Hakuto et al., 2000*) less shear distortion but more opening of beam bars hooks in tension and column bar buckling were observed. Premature concrete tension cracking combined with pullout of the beam bars occurred in all the tests. Lower strength and stiffness were measured.

Clyde et al. (2000) and Pantelides et al. (2002)
Four exterior joints with non-seismic detailing according to 1960s US-American standards were tested by Clyde *et al.* under cyclic loading and two different axial load levels (10% and 20% of $A_c \cdot f_c$). The following conclusions were made:

- specimens with higher axial load level exhibited a higher joint shear strength; and
- the energy dissipation and ductility decreased with increasing axial load.

Similar results were obtained by the six tests by Pantelides *et al.* where it was confirmed that the presence of higher axial load is beneficial in terms of the joint strength, but detrimental for displacement, ductility and energy dissipation.

Calvi et al. (2001) and Pampanin et al. (2002)
After an analysis of different pre 1970s substandard exterior joints, Calvi *et al.* and Pampanin *et al.* observed that joints with plain round bars and 180° hooks as anchorage of the beam bars (anchorage Type 6) in the joint panel usually exhibit a very poor seismic performance. Two tests were carried out to show the very low joint shear capacity and poor ductility of such joints. Furthermore, the importance of considering the variation of column axial load due to the overturning moment induced by the lateral forces in the frame was highlighted in this study. Subsequently, Pampanin *et al.* introduced the concept of “concrete wedge” damage mechanism (Figure 2-7a,b).

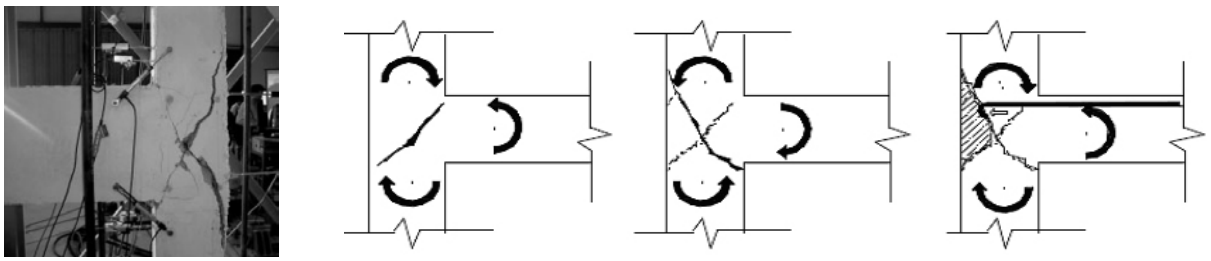

a) Exp. concrete wedge b) Schematic of “concrete wedge” damage mechanism

Figure 2-7: “Concrete wedge” damage mechanism (*Pampanin et al., 2002*)

Murty et al. (2003)

Twelve cyclic tests on exterior beam-column joints were carried out by Murty *et al.* to evaluate the influence of different beam-bars anchorage configurations (U-bars, ACI standard hooks with tail extension of $12d_b$, full seismic anchorage according to Indian Standard with tail extension of $38d_b$ (see *IS 456:1978* and *SP 34:1987*) and static anchorage with straight anchorage of the beam bottom reinforcement). The influence of transverse reinforcement details (hair clips and closed ties) was additionally investigated. It was found that the full anchorage of $38d_b$ does not improve the joint performance in comparison to the standard hook with tail of $12d_b$. The hair clips appeared to be the most effective form of transverse reinforcement.

Hertanto (2005) and Chen (2006)

Six tests on exterior beam column joints, designed for gravity loads only, were carried out by Hertanto and Chen. The effect of the following parameters was investigated:

- plain round bars with 180°-hooks (Type 6) and deformed bars with 90°-hooks bent into the core (Type 1);
- different failure modes: shear failure of joint core and beam flexural failure;
- deep and shallow beams; and
- particular focus was given to the deformation capacity of the joint panel (Figure 2-8).

The following conclusions were made:

- joints with anchorage Type 6 have poorer behaviour than those with Type 1;
- the joint shear failure mode has a lower energy dissipation capacity such that the beam flexural failure and high strength and stiffness degradation occurs after the peak load; and
- the specimens with a shallow beam generally exhibit a less brittle behaviour than those with a deep beam.

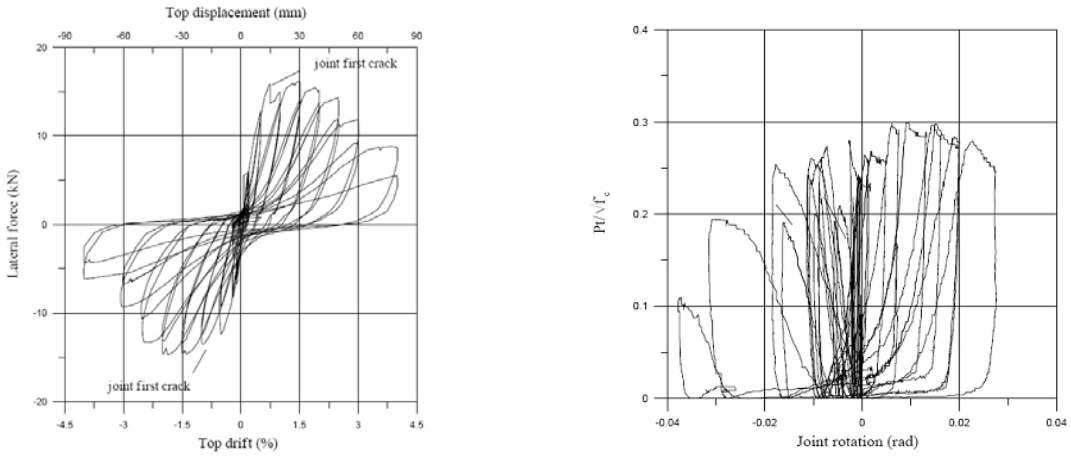

a) Hysteretic behaviour of beam-column connection b) Hysteretic behaviour of joint panel

Figure 2-8: Characterisation of joint shear behaviour (*Hertanto, 2005*)

Kuang & Wong (2006) and Wong & Kuang (2008)

Two different experimental test series on beam-column joint designed without seismic detailing (i.e., without transverse reinforcement in the core) were performed. The influence of

the beam bar anchorage (*Kuang & Wong, 2006*) and the beam-column depth ratio on the joint shear behaviour were evaluated (*Wong & Kuang, 2008*). It was shown that the form of beam anchorage significantly influenced the joint shear capacity. The need to include the effect of beam-column depth ratio in the design of the joint was also stated.

2.2.3 Summary of the experimental studies

The behaviour of exterior beam-column joints has been extensively investigated in the last forty years. The main influencing parameters on the shear strength of such connections have been determined to be:

- concrete compressive strength, f_c;
- anchorage detailing of longitudinal beam bars in the joint region;
- axial load in the column;
- geometric aspect ratio of the joint, h_b/h_c; and
- some authors also indicated an influence of reinforcement ratio in beam and column, ρ_b and ρ_c, respectively.

However, most of the authors did not fully investigate the effect of the all above parameters. This is likely to be because of the different interests associated with single national design standards and above all due to the difficulty in carrying out extensive experimental tests programmes. Furthermore, the influence of some parameters such as the axial load in the column was not always recognised.

Only a few authors have measured the joint shear deformation (e.g., *Clyde, 2000*; *Pantelides, 2002* and *Hertanto, 2005*). In most of the tests the focus was given to the ultimate shear strength of the joint. Recent studies (e.g., *Hertanto, 2005*) have shown that the limit state corresponding to the formation of the first diagonal crack in the joint significantly influences the shear deformability of the joint region.

2.3 Numerical studies

In the last decades a large number of numerical approaches for the simulation of beam-column joints have been developed. These methods may be divided into two groups with reference to the ultimate aim of the numerical analysis. The first group of models aims to simulate the joint strength and rotation within a MRF. They are aimed by the observation that the plastic behaviour of a frame cannot be properly simulated taking into account only the strength-deformation contribution of beam and column while neglecting the joint shear strength and distortion. In this type of models the behaviour of the joint is assumed to be known. Examples of this type of models are:

- rotational hinge models (Section 2.3.1);
- multi-spring models; and (Section 2.3.2); and
- fibre models (Section 2.3.3).

The models of the second group are more sophisticated. These models usually involve the Finite Element (FE) method, are often aimed at the investigation of joint load-deformation behaviour and the effect of different parameters. These types of models are very demanding in terms of computational requirements and are usually not suitable for the analysis of full

structures. They are generally meant to be used to save much more expensive experimental tests. In Section 2.3.4 a short overview on different FE models is given.

2.3.1 Rotational hinge models

Rotational hinge models typically comprise a bi- or trilinear monotonic envelope curve and an associated set of hysteretic rules which define the behaviour of the joint under cyclic load reversals. Several researchers have proposed such models based on analytical formulations derived from experimental evidences.

Otani (1974) used a bilinear idealisation of an envelope curve to compute the characteristic points of the curve. In doing this Otani assumed that bond stresses are constant along the development length of the reinforcing bars and that the reinforcing embedment length is long enough to develop sufficient steel forces. The fixed end rotation was found to be proportional to the square of the moment acting at the beam-column interface. *Takeda et al. (1970)* rule was used as the associated hysteretic rule. The pinching effect due to bond stress-slip and shear sliding was included by *Banon et al. (1981)*. Several other models have been proposed in the literature; however, they do not generally consider the joint shear behaviour, but only the beam and column moment-rotation capacity (*Fillipou et al., 1983* and *Fillipou & Issa, 1988*). *Kunnath et al. (1995a,b)* modified the beam flexural capacity to take into account the failure of the anchorages of the longitudinal bars in the beam. The joint shear deformation was modelled with a rotational spring model with deteriorating hysterics by *Alath and Kunnath (1995)*. *Pampanin et al. (2003)* proposed a moment-rotation relationship of the spring derived from plotting the principal tension stress in the core against the joint shear distortion (See Figure 2-9). As similar model, which is valid, at the moment, only for monotonic loading has been recently proposed by *Sharma et al. (2011)*.

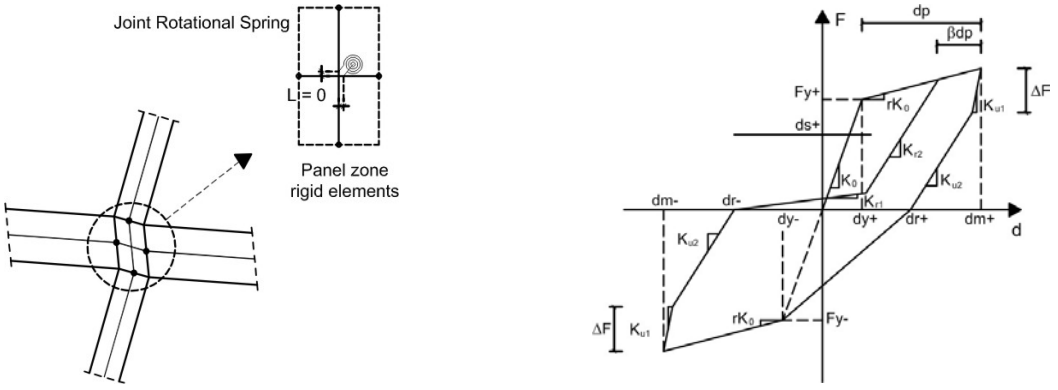

a) Joint modelling b) Hysteretic rule with pinching

Figure 2-9: Rotational hinge model proposed by *Pampanin et al. (2003)*

2.3.2 Multi-spring models

The basic idea of multi-spring models is to simulate the behaviour of beam-column connections by isolating the contribution of several factors such as bond stress-slip behaviour of longitudinal reinforcement and crushing of concrete at each beam-column interface. These types of models are usually based on mechanical principles and calibrated on experimental results.

Biddah & Ghobarah (1999) proposed the use of rotational springs to simulate the joint shear behaviour and the bond stress-slip of the longitudinal beam bars (Figure 2-10a). *Elmorsi et*

al. (2000) proposed an approach where beams and columns are described by elastic elements and are connected to the joint through the interposition of non-linear transitional elements. The effective node panel region is modelled with another element. This model allows the description of material behaviour using stress-strain relationships of steel and concrete. Concrete is defined by two different relationships which represent pre- and post-cracking behaviour. Longitudinal reinforcing steel bars are modelled with non-linear elements along the upper and lower sides of the joint panel. Furthermore, this model allows the introduction of a "bond-slip element" to represent the slipping of steel bars (Figure 2-10b). *Youssef & Ghobarah (2001)* modified the previews model (Figure 2-10a) inserting two diagonal translational springs connect the opposite corners of the panel zone to simulate joint shear deformation (Figure 2-10c). Similar models were proposed by *Lowes & Altoontash (2003)* with refinements and simplifications by *Altoontash (2004)* using the Modified Compression Field Theory (MCFT) by *Vecchio & Collins, 1986*) to define the envelope of the shear stress-strain relationship in the panel zone (see Figure 2-10d,e). Joints with no transverse reinforcement, typical in Gravity Load Designed (GLD) RC frames, were excluded from this study. It was noted that in joints with low or no transverse reinforcement shear is transferred primarily through a compression strut mechanism which is stronger and stiffer than predicted by the MCFT. The model proposed by *Shin & LaFave (2004)* is based on a similar approach to Lowes & Altoontash. The model was calibrated using joint shear stress-strain relationships from more than fifty interior joints tests available in the literature (Figure 2-10f).

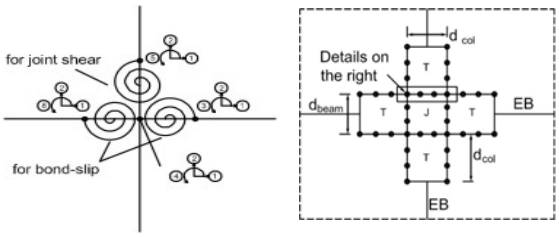

a) *Biddah & Ghobarah (1999)*

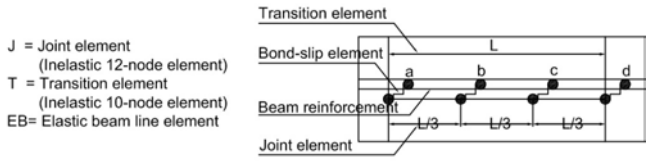

b) *Elmorsi (2000)*

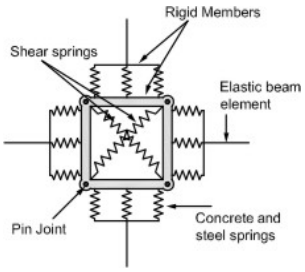

c) *Youssef & Ghobarah (2001)*

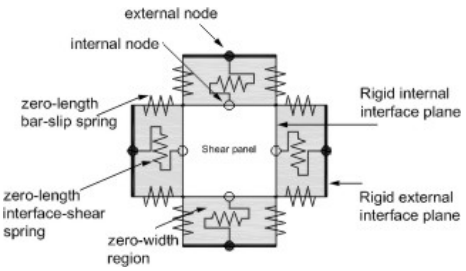

d) *Lowes & Altoontash (2003)*

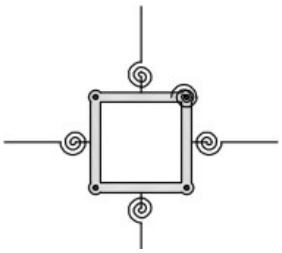

e) *Altoontash (2004)*

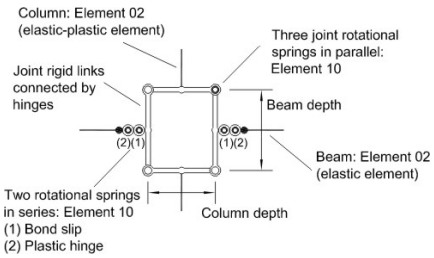

f) *Shin & LaFave (2004)*

Figure 2-10: Multi-spring models

2.3.3 Fibre models

In fibre models the element is divided into longitudinal fibres. Fibre models are commonly used to simulate the behaviour of flexural members like beams or columns. However, some researchers also apply this type of model to simulate beam column joints. Special elements are used to reproduce the bond stress-slip behaviour of the anchorages (e.g., *Braga et al., 2001b*).

2.3.4 Finite elements models

Finite Element Analysis (FEA) represents the most powerful and complete tool to simulate the behaviour of structures. Due to the large amount and complexity of analyses, usually requiring a high computational time to obtain a reliable model, this method is more suitable for the analysis of single structural elements as opposed to whole structures. The aim of FEA is to simulate experimental tests to obtain information on the stress-strain behaviour of concrete and reinforcement, which are difficult to measure experimentally.

The suitability of the microplane model in its formulation with relaxed kinematic constraint (*Ožbolt et al., 2001*) adopted by the FE code MASA (MAcroscopic Space Analysis) for the 3D non linear cyclic analysis of exterior beam-column joints was demonstrated by *Ožbolt et al. (1998)*, *Eligehausen et al. (2006b)*, *Eligehausen et al.* (*2009), Mahajan (2009)* and *Genesio et al. (2010a)*. This FE code is also used in the framework of this research and further information are provided in Chapter 4. Other researchers successfully applied FEA for the simulation of beam-column joints. 2D Monotonic analyses were carried out by *Hamil (2000)*, *Baglin & Scott (2000)* and *Hegger et al. (2004)* using the package SBETA and ATHENA. 2D cyclic analyses based on MCFT (*Vecchio & Collins, 1986*) and Distributed Stress Field Model (DSFM) (*Vecchio, 2000*) analyses were carried out by *Sagbas (2007)* using the package VecTor2. Typical representations of cracking patterns obtained from FEA for monotonic and cyclic analysis are shown in Figure 2-11 and Figure 2-12, respectively.

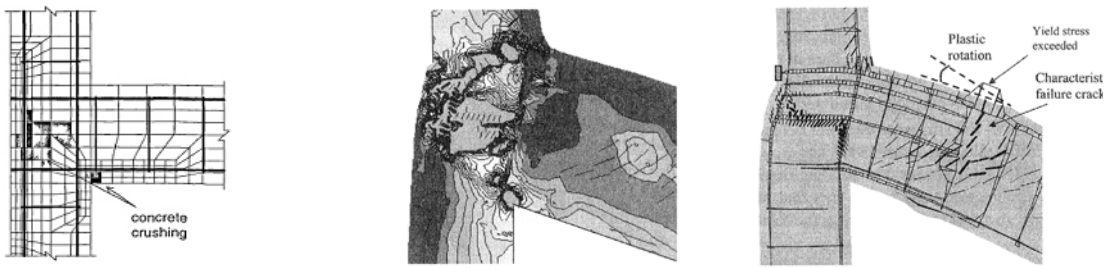

a) Joint shear failure (*Baglin & Scott, 2000*) | b) Joint shear failure (*Hegger et al., 2004*) | b) Beam flexural failure (*Hegger et al., 2004*)

Figure 2-11: Simulations of monotonic tests on exterior beam-column joints

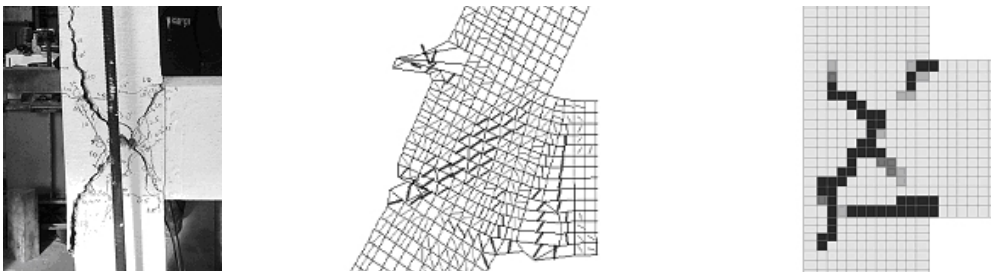

a) Test by *Hertanto (2005)* | b) FE by *Sagbas (2007)* | c) FE by *Genesio & Eligehausen (2008)*

Figure 2-12: Simulations of cyclic tests on exterior joints by *Hertanto (2005)*

2.3.5 Summary of numerical studies

In past decades the importance of modelling the shear and bond-slip behaviour of RC joints has been recognised. This aspect is particularly relevant for the analysis of fragility and prediction of damage state probabilities of GLD frames (*Celik & Ellingwood, 2008*). Rotational hinge models are well suited to this due to their simplicity. Multi-spring models offer the ability to account separately for strength and deformation contributions from joint shear cracking and bond-slip behaviour of beam and column reinforcement bars. However, the model calibration is more difficult and their implementation in the analysis of multi-storey MRF is computationally demanding. Both these types of models are primarily based on experimental and phenomenological evidence. FEA offers the possibility not only to replicate experimental results, but also to carry out parametric studies. This reduces the amount of experimental testing required and allows measurement of stress and strain in any portion of concrete and reinforcement of a specimen. However, currently it is not possible to effectively apply this method for the analysis of multi-storey frames, due to limitations of computational resources. A combination of FEA and rotational hinge modelling for the analysis of beam-column joint subassemblies and multi-storey frames, respectively, appears to be the most effective applications of numerical simulation.

2.4 Joint shear strength models

Several joint shear strength models have been proposed in past decades. In the following sections a review of existing methods is presented. A detailed description of the main models available in the literature is given in Appendix A.

2.4.1 Empirical models

Empirical models are those that are based on the extraction of the parameters affecting the joint shear capacity from test results. The parameters are generally obtained using regression analysis under the assumption that each parameter is independent from the others. The majority of empirical models are based on the analysis of experimental databases (e.g., *Sarsam & Phipps, 1985*; *Vollum & Newman, 1999*; *Bakir & Boduroğlu, 2002* and *Hegger at al., 2003*). With the development of more sophisticated FE codes, numerical parametrical studies are becoming used more often to develop empirical models (e.g., *Mahajan, 2009*).

2.4.2 Strut And Tie models

Strut And Tie (SAT) models define different limit states through the failure of either the tension tie (joint diagonal cracking) and/or the compression strut (ultimate joint shear capacity). It is commonly recognised that this type of model is suitable for describing the joint shear behaviour (see Section 2.1.3), however, the use in practice is limited due to its complexity. The dimension and direction of the struts, the magnitude of the ties and the size of the nodes are modelled as being interdependent and are correlated to the shear and axial forces acting in beam and column. Therefore, it is very time intensive to determine an appropriate geometry for the nodes and solutions can only be found using iterative processes. SAT models have been proposed by *Nilsson (1973)*, *Hoekstra (1977)*, *Ortiz (1993)*, *FEMA 273 (1997)*, *Parker & Bullman (1997)*, *Vollum (1998)* and *Hwang & Lee (1999)* and *Park & Mosalam (2009)*.

2.4.3 Average plane stress models

One possible approach to assess the shear strength of beam-column joints is to compare average stresses with critical values corresponding to diagonal cracking and shear strength. The majority of these kinds of models (e.g., *Taylor, 1974*; *Scott et al., 1994*; *Hamil, 2000* and *Wong, 2005*) consider a limitation of the nominal shear stress, v_{jh}, in the joint panel. This approach is used in several codes due to its simplicity (e.g., *ACI 318-02* and *NZS 3101:1995*). Several researchers have indicated that the principle tension stress, p_t, in the joint panel, as a damage indicator, is a function of both shear stress and axial load in the column and, therefore, it is better suitable than the shear stress only for the evaluation of the joint shear strength (e.g., *Priestley, 1997*; *Pampanin et al., 2003*; *Russo & Somma, 2006* and *Tsonos, 2007*).

2.4.4 Other models

According to the model proposed by *Shiohara (2004)*, the joint shear failure of beam-column connections is defined as the failure of quadruple flexural resistance. Failure criteria for concrete, steel, bond and anchorage are combined with the equilibrium conditions of the members framing into the joint evaluated on the diagonal sections of the joint panel.

2.4.5 Shear strength degradation

Several studies have shown that specimens that fail in shear after beam flexural yielding usually exhibit a lower shear strength than those where the beam longitudinal bars remain elastic (e.g., *Shin & LaFave, 2004*). For this reason some authors recognised the importance of defining shear strength degradation curves to account for joint shear failure occurring after the formation of a flexural plastic hinges in the beam. *Park (1997)* and *Hakuto et al. (2000)* proposed linear degradation of joint shear strength with increasing ductility of the frame beam (Figure 2-13).

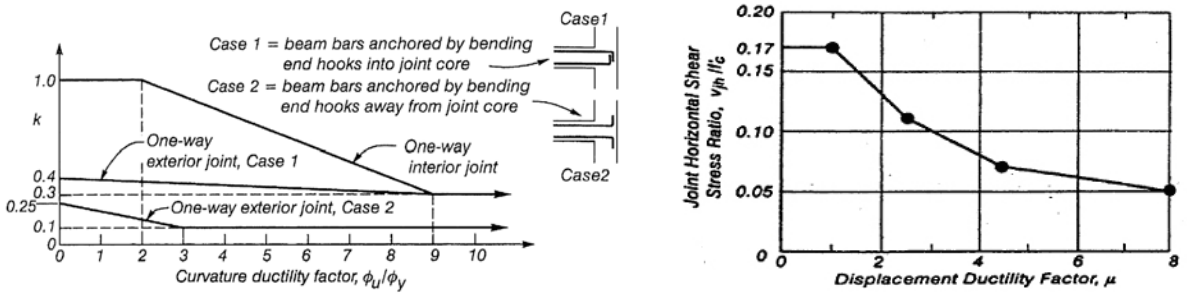

a) *Park (1997)* b) *Hakuto et al. (2000)*

Figure 2-13: Joint shear strength degradation curves

2.4.6 Effect of transversal reinforcement in the joint panel

It is commonly accepted and included in all the most advanced building codes (e.g., *ACI 318-02*; *NZS 3101:1995* and *EC8-1, 2004*) that the presence of adequate transversal reinforcement in the core may highly enhance the shear strength and rotational capacity of the joint. The main functions of transverse reinforcement are: (i) the transfer of tension forces following diagonal cracking of the joint and (ii) confinement of concrete in the joint panel. Most of the existing design models consider the influence of transversal reinforcement independent of the concrete contribution (e.g., *Sarsam & Phipps, 1985*; *Vollum & Newman, 1999*; *Bakir & Boduroğlu, 2002* and *Hegger et al., 2003*), as shown in Equation. (2-9):

$$v_j = v_{jc} + v_{js} \tag{2-9}$$

where v_{js} is usually equal to $\alpha A_{js} f_y$ and α is transverse reinforcement efficiency factor. α is usually related to the amount, location and type of reinforcement (stirrups or hairpins). Several studies were carried out to evaluate the influence of different stirrup configurations on joint shear strength, however, no general agreement has been reached yet. *Hegger et al. (2003)* and *Murty et al. (2003)* found that hairpins are generally more effective than stirrups, while *Hamil (2000)* observed the opposite, due to the potentially inadequate anchor lengths of the hairpins. Some studies showed that stirrups can be considered effective (i.e., the joint ultimate strength increased) only if located above the flexural compressive zone of the incoming beam and below the main beam reinforcement (e.g., *Vollum & Newman, 1999* and *Mahajan, 2009*). Some authors observed, on the basis of experimental evidence, that joint shear reinforcement does not influence the limit state corresponding to the first diagonal cracking of the joint panel (i.e., *Hamil, 2000* and *Shiohara, 2004*). According to *Mahajan (2009)* joint transverse reinforcement also influences the shear resisted by the concrete, since the concrete properties are modified by the confinement. More details about the effect of transverse reinforcement on the joint shear stress are given in Appendix A. However, in the present study this parameter is not taken into account, since the focus is given on joint with substandard detailing, such as no stirrups in the joint panel.

2.4.7 Summary of shear strength models

In Table 2-1 a schematic summary of the shear strength models described in detail in Appendix A is shown. Generally, two different limit states for the shear mechanism of beam-column joint can be distinguished:

- 1st diagonal cracking in the joint region
- Peak load

However, only a few authors proposed design equations for both limit states (*Nilsson, 1973*; *Hoekstra, 1977*; *Sarsam & Phipps, 1985*; *Hamil, 2000* and *Priestley, 1997)*. It is generally recognised that 1st joint diagonal cracking should be considered as a serviceability limit state (i.e., limitation of crack width). *Priestley (1997)* and *Pampanin et al. (2003)* identified this limit state as crucial for the shear distortion of the joint panel, since after this cracking the joint loses part of its stiffness and starts to deform plastically.

Most of the models assume proportionality between the joint shear capacity and the square root of the concrete compressive strength, $\sqrt{f_c}$. A few models consider the strength corresponding to the first diagonal crack to be related to the concrete tensile strength, f_{ct} (e.g., *Nilsson, 1973*; *Taylor, 1974* and *Hoekstra, 1977*). Others consider f_c, for example some SAT models assume the crushing of the compressive strut as failure condition (e.g., *Zhang & Jirsa, 1982* and *Hwang & Lee, 1999*). *Hegger et al. (2003)* and a few other authors proposed a relation between the joint shear stress and $\sqrt[3]{f_c}$ to calibrate their model on high strength concrete.

The effect of the column axial load on the joint shear strength is still not clear from the literature. Some models take it into account as positive contribution to the joint shear strength

(e.g., Sarsam & Phipps (1985); *Priestley 1997* and *Hamil, 2000*), while others ignore it (e.g., *Bakir & Boduroğlu, 2002; Vollum & Newman, 1999* and *Hegger et al., 2003*).

The influence of various parameters has been investigated in several studies in the past years. In the case of pure shear mechanism of the joint (i.e., where no yielding of the longitudinal bars in the beam and column occurs) the amount of beam and column reinforcement (ρ_b and ρ_c, respectively) is only believed to influence the joint shear strength by a few researchers.

It is commonly recognised that the joint geometric aspect ratio h_b/h_c significantly influences the joint shear strength and that joints with lower values of h_b/h_c usually exhibit a higher shear capacity.

Many experimental studies have shown that the concrete contribution to the joint shear strength is influenced by anchorage detailing of the beam bars in the core. However, only a few models take this parameter into consideration. The reason for that can be found in the aim of most of the models, which largely address beam-column connections designed according to valid standard codes. Usually the allowed anchorage detailing is prescribed by the code (see Section 2.4.8). Some models consider two different types of anchorage (Type 1 and 3), e.g., *Vollum & Newman (1999)* and *Hegger et al. (2003)*. Only the model proposed by *Priestley (1997)* and extended to joints with plain round bars by *Pampanin at. (2003)* considers the case of other anchorages types (Types 1, 2 and 6).

A few models consider other influencing parameters such as the presence of eccentricity between beam and column (*Mahajan, 2009*) and the axial load in the beam (*Hoekstra, 1977*).

In the past few years several authors carried out comparative studies of the performance of different models (*Park & Mosalam, 2009*; *Lima et al., 2010*). Generally, the accuracy of different models has a coefficient of variation, CV = 15~30%, mainly dependent on the choice of the sample for the experimental database.

Table 2-1: Qualitative comparison of shear strength models

	Model	1st crack	Peak load	γ_j	f_c	f_{ct}	f_a	ρ_b	ρ_c	h_b/h_c	Ancho -rage	Other / Note
Empirical models	Sarsam and Phipps	■	■		a)		■		■	■		
	Vollum and Newman		■		a)					■	■	
	Bakir and Boduroğlu				a)			■		■	■	
	Hegger *et al.*		■		b)				■	■	■	
	Mahajan		■		a)		■			■		Eccentricity; Confinement
SAT models	Nilsson	■				■						
	Hoekstra	■				■						Beam axial stress
	Zhang & Jirsa		■		c)		■			■		Beam yielding; trans. beam
	Ortiz		■		c)					■		
	FEMA 273				a)							
	Vollum		■		a)					■		
	Parker and Bullman				c)					■	■	
	Park and Mosalam		■		a)					■		Beam yielding
Ave. plane stress models	Hwang & Lee		■		c)					■		
	Taylor	■	■			■	■	■		■		
	Scott		■		a)					■		
	Hamil	■	■		a)		■			■		
	Wong		■		a)					■		
	Priestley – Pampanin	■	■	■	a)		■				■	
	Tsonos		■		a)		■			■		
	Russo and Somma		■		■		■					
	Shiohara		■		■					■		

[a] Proportional to $\sqrt{f_c}$; [b] Proportional to $\sqrt[3]{f_c}$; [c] Proportional to f_c

2.4.8 Joint shear deformation

Only very limited tests in the literature contain information about the joint shear distortion, γ_j. In the document *FEMA 356 (2000)* the relationship shown in Figure 2-14a is suggested for the modelling of substandard exterior beam-column joints within a non-ductile moment resisting frame. In Figure 2-14a, V is the design shear force and V_n is the shear strength of the joint. *Priestley (1997)* proposed p_t-γ_j relationships for joints without transverse reinforcement in the core and different detailing configurations with deformed bars (Types 1 and 2). *Pampanin et al. (2003)* extended this to include plain round bars anchored with180°-hooks (Type 6) in the joint region (Figure 2-14b).

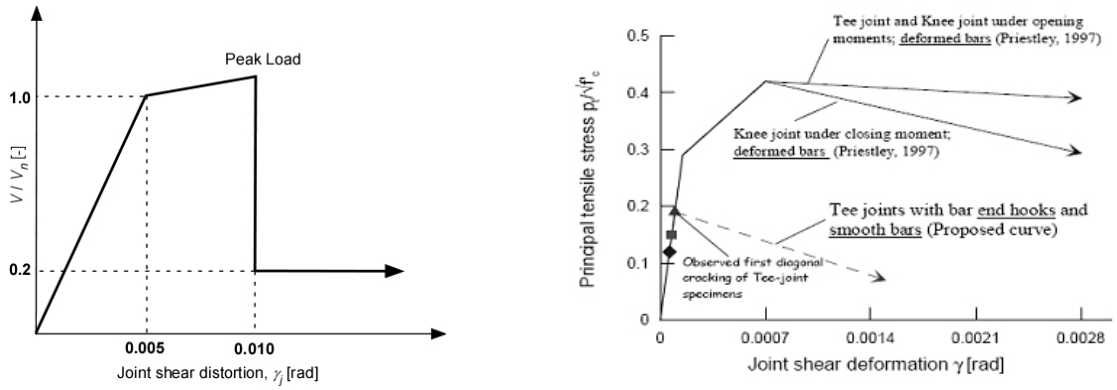

a) *FEMA 356 (2000)* b) *Priestley (1997)* and *Pampanin et al. (2003)*

Figure 2-14: Joint shear deformation relationships

2.5 Development of codes provisions

To better understand the possible deficiencies of old RC frames designed without following the prescriptions of modern seismic provision, it is necessary to review the development of constructions standards. In the following sections the development of some standards during the last fifty years is presented. Special emphasis is given to the requirements of beam bar anchorage in the joint and transverse reinforcement. The standards of USA (Section 2.5.1), Japan (Section 2.5.2) and New Zealand (Section 2.5.3) are considered, because they usually have been considered to be the most advanced. The Italian standard (Section 2.5.4) can be taken as an example for the Mediterranean context. India (Section 2.5.5) is taken as example for developing countries in Asia. All the considered countries present areas of moderate to high seismicity. Finally, the requirements of the most recent and advanced US, New Zealand and European standards are compared (Section 2.5.6).

2.5.1 USA

The importance of beam-column joint design and detailing was first highlighted in the *SEAOC (1966)* (Structural Engineers Association of California). According to ACI 318, until the beginning of the 1970s only provisions for the anchorage length of beam bars in the joint were given (*ACI 318-51* and *ACI 318-63*, see Figure 2-15a). *ACI 318-71* contained an appendix of special provision for seismic design including provisions for beam-column joint shear design based on the work of *Hanson & Connor (1967)*. However, no Capacity Design provisions were specified. In the recommendations of *ACI 318-71* and of *SEOC (1966, 1973)* anchorages of longitudinal beam bars in joint region with 90°-hooks bent away (Type 2) and with 180°-hooks (Type 4 and 6) were allowed, although the 90°-bent in hooks (Type 1) was preferred (see Figure 2-15b). *ACI 352-76* was the first document that extensively addressed the design of beam column joints. Special focus was given not only to the anchorage length of the beam bars, but also to the transverse reinforcement and the resistance of the confining members. The joint detailing provided by the *ACI 318-83* is still valid nowadays. A chronological overview of the code's requirement on anchorage length of beam longitudinal bars in the joint region is given in Table 2-2.

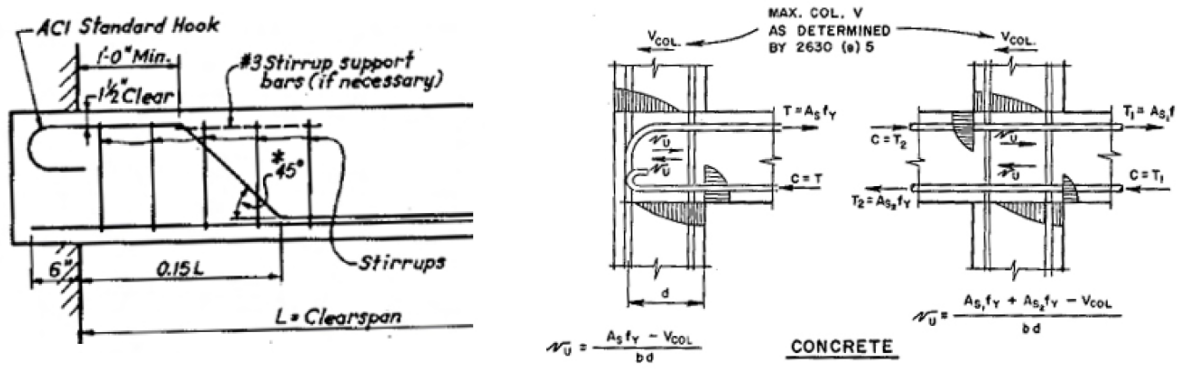

a) *ACI 318-63* b) *SEAOC (1973)*

Figure 2-15: Design and detailing of beam-column joints in USA

Table 2-2: Detailing of exterior beam-column-joints according to US American standards

ACI 318-51	
Bond stress not higher than $0.045 \cdot f_c'$ and $0.1 \cdot f_c'$ for plain round and deformed bars, respectively. The anchorage length shall be at least $12d$.	
ACI 318-63 (*ACI 318, 1963*)	
See Figure 2-15a for detailing of hooked and straight anchorages.	
ACI 318-71 (*ACI 318, 1971*)	
$l_d = \frac{0.04 \cdot A_b \cdot f_y}{\sqrt{f_c'}}$ (for reinforcement steel ≤ 60 ksi) $l_d = \frac{0.04 \cdot A_b \cdot f_y}{\sqrt{f_c'}} \cdot 1.4 \cdot \left(2 - \frac{60000}{f_y}\right)$ (for reinforcement steel > 60 ksi)	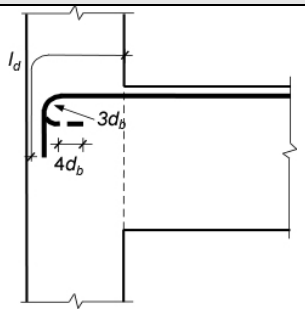
ACI 318-77 (*ACI 318, 1977*)	
$l_d = \frac{0.04 \cdot A_b \cdot f_y}{\sqrt{f_c'}}$ (for reinforcement steel ≤ 60 ksi) $l_d = \frac{0.04 \cdot A_b \cdot f_y}{\sqrt{f_c'}} \cdot 1.4 \cdot \left(2 - \frac{60000}{f_y}\right)$ (for reinforcement steel > 60 ksi) Minimum joint shear reinforcement shall be provided	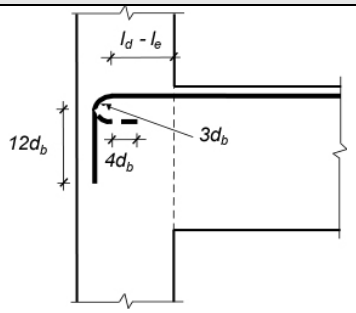
ACI 318-83 (*ACI 318, 1983*)	
$l_{dh} = \frac{1200 \cdot d_b}{\sqrt{f_c'}}$ (for reinforcement steel = 60 ksi) $l_{dh} = \frac{1200 \cdot d_b}{\sqrt{f_c'}} \cdot \frac{f_y}{60000}$ (for reinforcement steel ≠ 60 ksi) Minimum joint shear reinforcement shall be provided	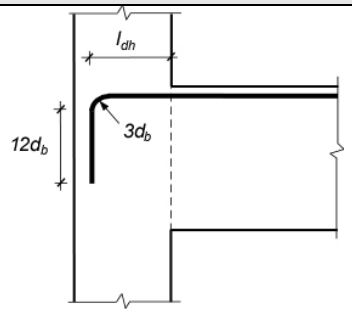

2.5.2 Japan

Until the late 1980s the Japanese Building Standard Law contained no requirements for the safety of joints under seismic forces (*Kurose, 1987*). The AIJ (Architectural Institute of Japan) Standard for RC Structures (*AIJ, 1982*) prescribed only requirements for the development length of reinforcing bars anchored in the joint. The transverse reinforcement was usually provided in the form of 10 dia. bars with a spacing of 150 mm for normal buildings, while more attention for joint design was given in high rise buildings (*Kurose, 1987*). It was common construction practice in Japan to anchor plain round bars using 180°-hooks and deformed bars by using 90°-hooks bent in or away from the joint (Figure 2-16). Generally, the contribution of transverse reinforcement was not taken into account in the design with resulting in massive cross sections of columns. Therefore, the anchorage straight length of longitudinal bars limited to the mid of the column height was not uncommon (see Figure 2-16)

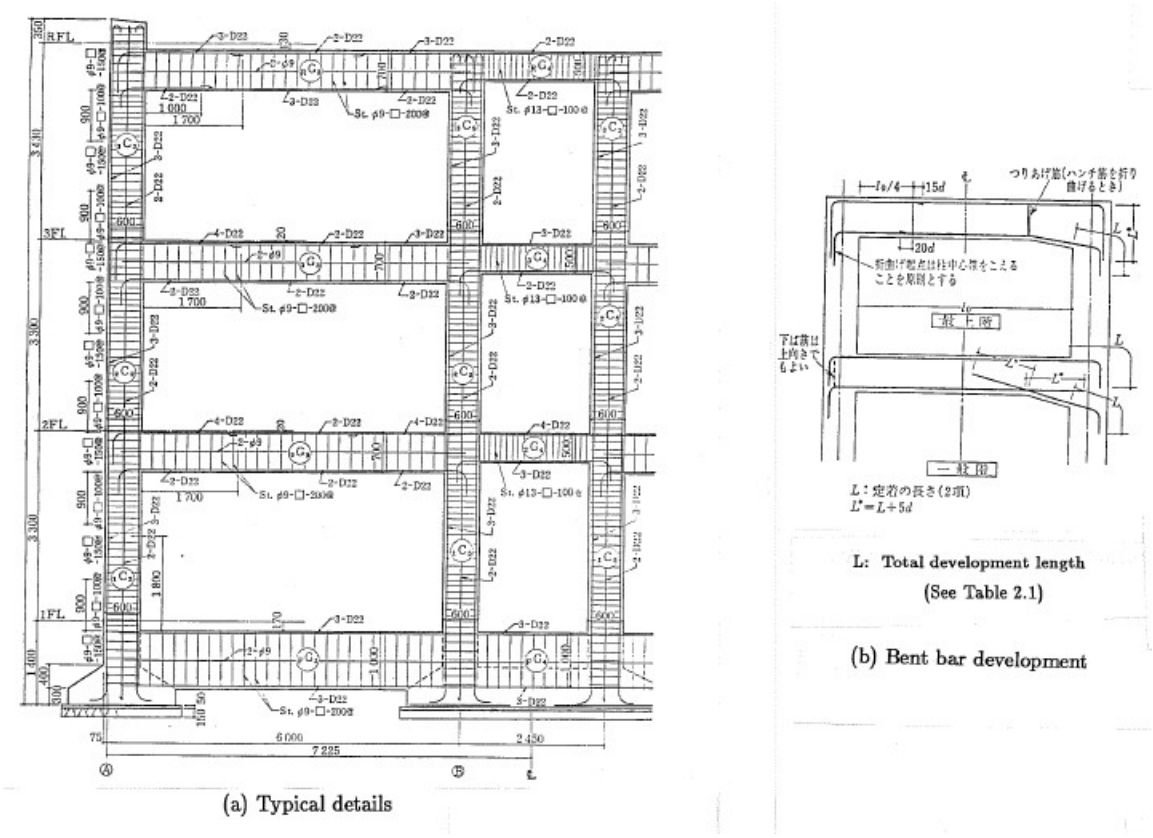

Figure 2-16: Reinforcement details in Japanese practice (*Kurose, 1987*)

2.5.3 New Zealand

In New Zealand the use of plain round bars was predominant until the end of the 1960s. The *NZS 95:1955* prescribed the anchorage of such bars with 180°-hooks in presence of tensile forces (Figure 2-17). *Hollings (1969)* concluded in his research that that beam hinging is the most preferable plastic mechanism for MRF and this conclusion was a prelude to the concept of Capacity Design. Pre-1970s engineering practice in New Zealand was similar to USA and British practice, because of language and cultural reasons. During the 1970s several innovative advancements in the detailing of reinforced concrete members were introduced such as column confinement, anti-buckling transverse reinforcement and shear reinforcement in the joint zone (*NZS3101:1972* and *NZS4203:1976*). The *NZS 3101:1982*

provisions for detailing of exterior beam-column joints are mostly still valid today (Table 2-3). More detailed historical reviews of the development of seismic design in New Zealand are available in the literature (e.g., *Megget, 2006*).

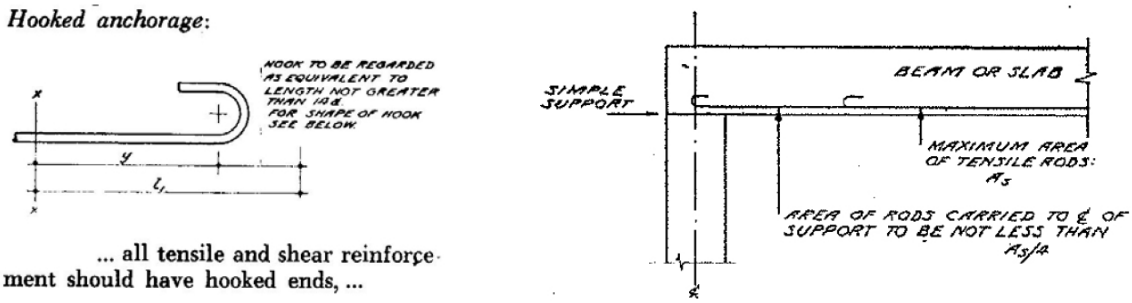

Figure 2-17: Plain round reinforcement anchorage according to *NZS (1955)*

Table 2-3: Detailing of exterior beam-column-joints according to New Zealand standards

NZS3101:1982 (*NZS, 1982*)	
Calculation of straight anchorage length: $l_{hb} = \frac{66 \cdot d_b}{\sqrt{f_c'}} \cdot \frac{f_y}{275}$ Minimum joint shear reinforcement shall be provided (see Table 2-5)	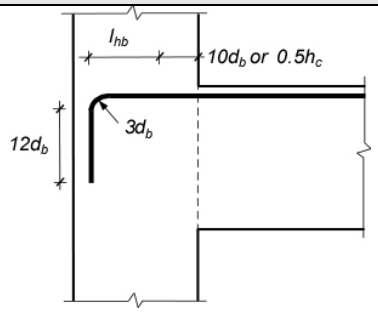

2.5.4 Italy

Until the early 1970s the design recommendations provided by the Italian national design code (*Regio Decreto, 1939*) had to be followed and, where necessary, integrated by textbooks broadly adopted in engineering practice (e.g., *Santarella, 1957*). Until that point the use of plain round bars was predominant in Italian construction practice (*Verderame et al., 2001*). No design provision was given for exterior beam-column joints. For tensioned plain round bars anchorage with 180°-hooks was required. After the publication of the *D.M. 30/05/1972* the use of deformed bars became common practice. The earthquake in Friuli in 1976 can be considered the event that induced a new consciousness about the seismic risk in Italy. The earthquake caused the death of almost 1000 people and the destruction of many towns and villages in the north east mountain region of Italy. After that event much greater attention was given to the seismic design. Provisions concerning the minimum anchorage length of bars were contained in *D.M. 14/02/1992*. The design of exterior beam-column joints was explicitly addressed for the first time in the *D.M. 16/01/1996* (See Table 2-4).

Table 2-4: Detailing of exterior beam-column-joints according to Italian standards

D.M. 14/02/1992 (*DM, 1992*)
$f_{bd} = \frac{0.32}{\gamma_c} \cdot \sqrt{f_{cc}}$ for plain round bars; $f_{bd} = 2.25 \cdot \frac{f_{ct}}{\gamma_c}$ for deformed bars 180°-Hooks is equivalent to 20 bar diameters straight anchorage. It is mandatory for anchorages with plain round bars. Hooks may be omitted in the case of deformed bars 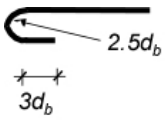
D.M. 16/01/1996 (*DM, 1996*)
$l_d = \frac{1.25 \cdot f_{yk} \cdot d_b}{4 \cdot \tau_{ad}}$ τ_{ad} = 1.5· τ_{c0} for plain round bars; τ_{ad} = 3.0· τ_{c0} for deformed bars ($\tau_{ad} = f_{bd}$ and $\tau_{c,0}$ = concrete shear strength) Transverse reinforcement in the joint panel with spacing not smaller than the spacing of the stirrups of the column 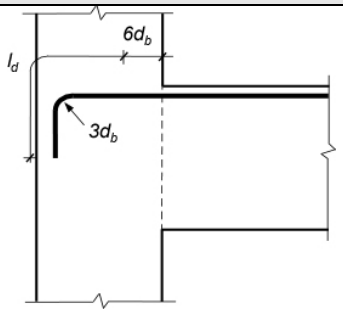

2.5.5 India

Provisions concerning the anchorage of smooth and deformed longitudinal deformed bars of reinforced concrete members are provided in the “Handbook of Concrete Reinforcement and Detailing”, *SP 34:1987* for non-seismic applications (Figure 2-18a). The handbook is an explanatory document of *IS 456:1978*. The “Explanatory Handbook on Codes for Earthquake Engineering”, *SP 22:1982* is an explanatory document of *IS 1893:1975* and *IS 4326:1976*. This handbook directly addresses the detailing of beam-column joints requiring larger anchorage length (L_d + 10*d*) and the presence of transverse reinforcement (Figure 2-18b). Similar provisions are required by the code for “Ductile Detailing of Reinforced Concrete Structures Subjected to Seismic Forces” (*IS 13920:1993*). Similar detailing requirements are contained in newer version of the Indian seismic standard (e.g., *IS 1893:2002*). Calculation and limitation of shear strength in the joint region is not required by any of the mentioned codes.

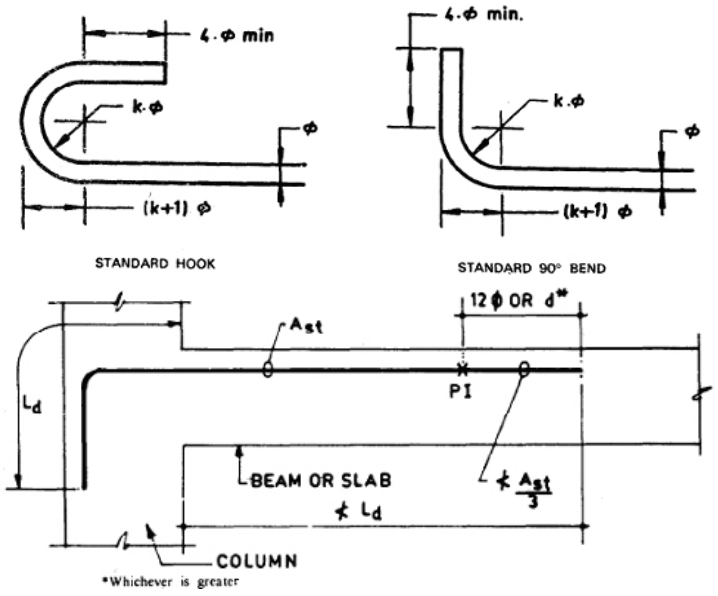

$$L_d = \frac{d_b \cdot \sigma_s}{4 \cdot \tau_{ad}}$$

with: σ_s = tension stress of reinforcement steel and
1.0 MPa < τ_{ad} < 1.0 MPa for diameter between M15 and M40.

a) Anchorage requirements according to *SP 34:1987*

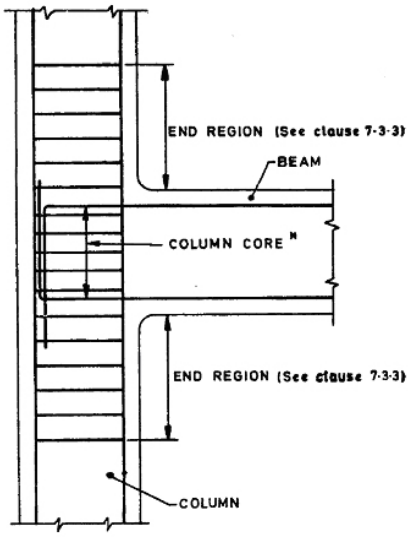

b) Joint detailing according to *SP 22:1982*

Figure 2-18: Requirements of Indian Standards

2.5.6 Current practice

Today joint detailing plays an important role in the design of MRF. A comparison of three of the most advanced building codes, *ACI 318-02*, *NZS 3101-1:1995* and the *Eurocode 8 of EN 1998-1:2004* (*EC8-1, 2004*) is given in Table 2-5. The comparison is based on the anchorage length, effective width of the joint, joint transverse reinforcement, determination of characteristic joint shear strength and Capacity Design provisions (i.e., weak beam – strong column).

Table 2-5: Comparison of modern codes provisions

Parameter	*ACI 318-02*	*NZS 3101-1 (1995)*	*EC8-1 (2004)*
Development length of anchorage	$l_{dh} = \frac{f_y \cdot d_b}{5.4 \cdot \sqrt{f_c'}}$	$l_{dh} = 0.24 \cdot \alpha_b \cdot \alpha_1 \cdot \alpha_2 \frac{f_y \cdot d_b}{\sqrt{f_c'}}$	Limitation on d_b to avoid bond failure: $\frac{d_b}{h_c} \le \frac{7.5 \cdot f_{ctm}}{\gamma_{Rd} \cdot f_{yd}} (1 + 0.8 \cdot f_a)$
Critical section from the column face	Column face	min(h_c/2; 8d_b)	5d_b
Tail extension	12d_b	12d_b	10d_b
Flexural strength of the column	$\sum_c M_{n,c} \ge 1.2 \cdot \sum_b M_{n,b}$	$\sum_c M_{n,c} \ge 1.4 \cdot \sum_b \phi_0 \cdot M_{n,b}$	$\sum_c M_{Rc} \ge 1.3 \cdot \sum_b M_{Rb}$
Effective width of the joint $w_c > w_b / w_c < w_b$	min(w_b+h_c; w_b+2x) [a)]	min(b_c;w_b+0.5h_c)	min(b_c; w_b+0.5h_c)
	w_c	min(b_b; w_c+0.5h_c)	min(b_b; w_c+0.5h_c)
Amount of joint transverse reinforcement	$A_{sh} \begin{cases} = 0.3 \cdot (s \cdot h_c'' \cdot f_c') \cdot \left(\frac{A_g}{A_{ch}} - 1 \right) \\ \ge 0.09 \frac{s \cdot h_c'' \cdot f_c'}{f_{yh}} \end{cases}$	$A_{jh} = \frac{6 \cdot \upsilon_{jh}}{f_c'} \beta \cdot \left(0.7 - \frac{C_j \cdot f_a}{f_c'} \right) \cdot \frac{f_y}{f_{yh}} \cdot A_{s1}$	$\frac{A_{jh} \cdot f_{yhd}}{w_j \cdot h_{jw}} \ge \frac{2 \frac{V_{jh}}{w_j \cdot h_{jc}}}{f_{ctd} + \frac{f_a}{f_{ck}} \cdot f_{cd}} - f_{ctd}$
Amount of vertical reinforcement	-	$A_{jv} = \alpha_v \frac{h_b}{h_c} A_{jh} \frac{f_{yh}}{f_{yv}}$ with: $\alpha_v = 0.7 / (1 + f_a)$	$A_{sv,i} = (2/3) \cdot A_{sh} \frac{h_{jc}}{h_{jw}}$ Assumption: Intermediate column bars carry approximately half of the yield load
Vertical spacing of horizontal hoops	min(h_c/4; 6d_b; S_x)	min(10 d_b; 200)	min (b_0/2; 8 d_b; 175)
Horizontal spacing of vertical reinforcement	No more than 350	min(h_c/4; 200)	150
Shear strength	Confined on 4 faces: $v_{jh} = 1.5 \cdot \sqrt{f_c'}$ Confined on 3 or 2 faces: $v_{jh} = 1.2 \cdot \sqrt{f_c'}$ Other cases: $v_{jh} = 1.0 \cdot \sqrt{f_c'}$	$v_{jh} = 0.2 \cdot f_c'$	$v_{jh} = 0.8 \cdot f_{cd} \cdot \sqrt{1 - \frac{f_a}{\eta \cdot f_c'}}$ with: $\eta = 0.6 (1 - f_{ck}^2 / 250)$

[a)] x = distance of the column edge beyond the edge of the beam in the direction of loading

2.5.7 Summary

Comparing the provisions of the most advanced building codes (Section 2.5.6) with worldwide provisions from the last decades (see Sections 2.5.1 to 2.5.5) several discrepancies may be observed. Joints designed without sufficient anchorage length or anchorage type other than Type 1 and with lack of transverse reinforcement in the core are usually addressed as pre-1970s joints. However, it can be noted that this indication is valid for USA or New Zealand, but not for other countries, where the development of building codes took more time. The greatest deficiency in the seismic response of such beam-column connections is the lack of Capacity Design in order to assure the establishment of a ductile

plastic mechanism. Secondly, for those joints the prediction of shear strength based on modern code provisions is generally over estimated. Furthermore, the calculation of the shear strength according to most of the existing code provisions does not take into account the influence of factors such as joint aspect ratio and axial load on the column. This fact emphasises the need of development of more accurate design models (see Section 2.4). Another factor in the uncertainty of the seismic resistance of structures is the constant development of seismicity maps in different countries, i.e., regions with no or only moderate seismic risk have been often re-evaluated on the basis of new results of seismological research. In Figure 2-19 the development of seismic maps of Italy is shown as an example.

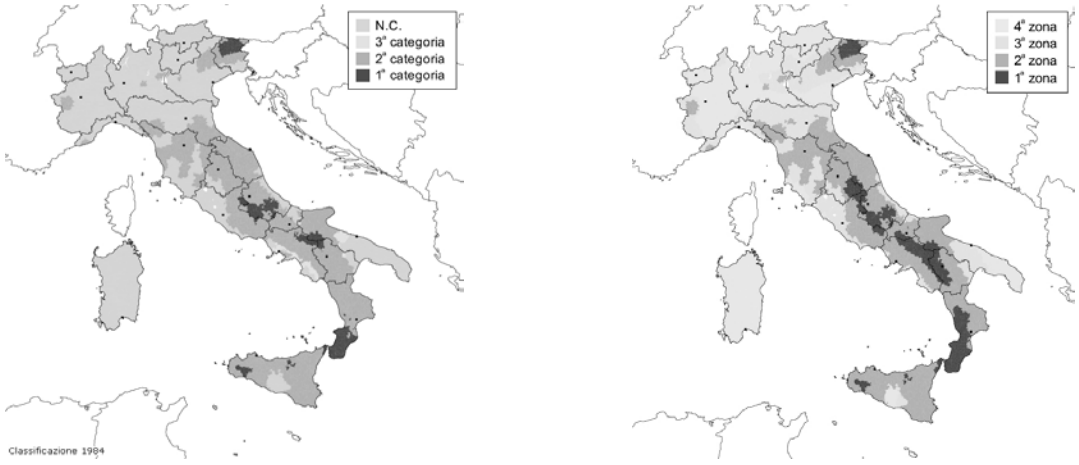

a) *DM (1984)* b) *OM 3274 (2003)*

Figure 2-19: Development of seismic maps of Italy (source: www.ingv.it)

Understanding of the development of building codes in different areas can give important, but not exhaustive information on possible deficiencies of existing structures. The analysis of the damages occurred in RC structures in the recent earthquakes in Sichuan (China) in May 2008 and L'Aquila (Italy) in April 2009 have shown that a primary role is played by the poor quality of materials and workmanship (*Decanini et al., 2010*). Few researchers have carried out statistical investigations to estimate the average mechanical properties of construction materials used and common structural typology used in certain contexts, e.g., *Verderame et al. (2001)* in Italy and *Inel et al. (2010)* in Turkey.

2.6 Seismic retrofit of RC frames

Seismic retrofit of buildings is intended to upgrade the structural performance of a building to resist certain design earthquake eccitation with no or an acceptable damage level. The level of retrofit will be related to the building's socio-economic value. Retrofit strategies may follow one of the schemes presented in *CEB (1995)* and shown in Figure 2-20 such as increase of strength (a), ductility (b) or a combination of both (c). Strategies which address an increase in strength of a building usually require a "global retrofit" in order to transfer the loads safely from the top of the structure to the foundation (see Section 2.6.1). To increase the ductility of a construction, in most cases "local retrofit" is sufficient to eliminate the sources of brittleness (Section 2.6.2). It is also important to distinguish between "retrofitting" and "repairing". "Retrofitting" is where only undamaged buildings are considered and the target is their upgrade. Seismic "repairing" addresses structures which have suffered a moderate damage during a seismic event. Reparing techinques primarily aim to re-estabilish the previous

structural performance, but they are ususally combined with retrofit strategies in order to improve the strength and/or ductility of a building. In this section no reference to repairing techniques is given, although some retrofit methods may be used also for repairing, such as FRP (Fibre Reinforced Polymers) wrapping of structural components.

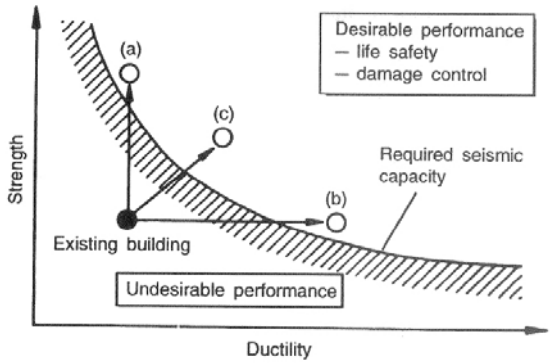

Figure 2-20: Basic concept for seismic retrofit (*CEB, 1995*)

2.6.1 Global retrofitting

Global strategies may be adopted to enhance the resistance of structures to lateral loads such as the insertion of shear walls or steel bracing (Figure 2-21a). Strategies may be used to reduce the effect of seismic action through damping systems (Figure 2-21b) or base isolation (Figure 2-21c). It is not the objective of this work to investigate in depth these kind of retrofit solutions. However, they have some common features, which clearly distinguish them from local strategies:

- in comparison to local retrofitting they are characterised by their significant aesthetical and/or functional invasiveness either only during their construction (e.g., seismic isolation) and/or during normal life of the building (e.g., stiffening techniques and damping systems); and
- due to their high costs they are usually not economically applicable to most structures such as residential and commercial buildings, therefore they are usually meant for strategic buildings such as hospitals and schools, which need to substantially maintain their functionality following a seismic event.

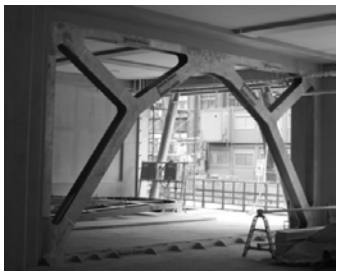

[Source: EERC, Berkeley]
a) Steel bracing

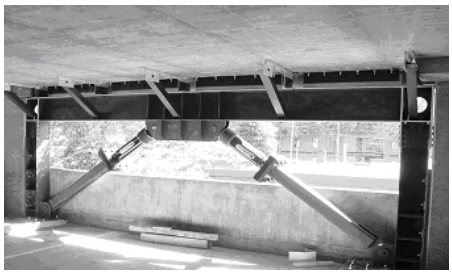

[Source: www.staaleng.com]
b) Viscous dampers

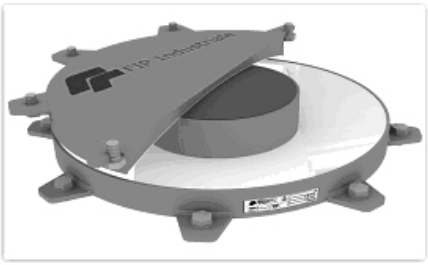

[Source: www.fip-group.it]
c) Seismic isolation

Figure 2-21: Global retrofit strategies

2.6.2 Local retrofitting

Local strategies are usually chosen to prevent brittle mechanisms of structural elements, such as shear failure of walls and columns. The main deficiencies in seismic performance of

RC frames designed for gravity loads only, are generally more related to lack of ductility rather than to inadequate lateral strength. This is usually due to poor detailing of reinforcement and lack of a Capacity Design philosophy (*Priestley, 1997*). As a consequence of the lack of Capacity Design considerations in the design process, there is no assurance that a suitable hierarchy of strength exists to avoid brittle mechanisms. Typical collapse of RC frames may be due to shear failure or occurrence of a plastic hinge in the column which may result in a limited-ductile mechanism such as “strong beam - weak column” (Figure 2-22a, *Priestley, 1997*). Furthermore, poor detailing of the reinforcement in frame joints (i.e., insufficient anchorage of longitudinal reinforcement, total lack of or inadequate shear reinforcement in the core) may lead to a premature failure of the joint. The concept of a shear hinge was introduced by *Pampanin et al. (2003)* (Figure 2-22b) after the observation of the poor load-displacement capacity of substandard exterior beam-column joint failing in shear. It is generally recognised that the formation of a plastic beam mechanism allows a frame to undergo larger horizontal displacements without collapsing (Figure 2-22c).

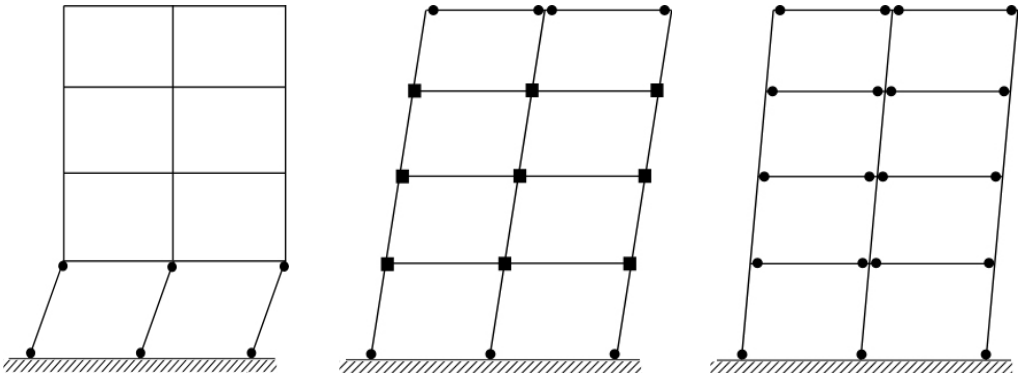

a) Column sway b) Joint sway c) Beam sway

Figure 2-22: plastic mechanisms typical of RC frames

Several strategies have been investigated in the past years to increase the column and joint shear strength. *Alcocer & Jirsa (1993)* tested the effect of repair and retrofit of four interior joints with RC jacketing (Figure 2-24a). An improvement of the confinement of the joint zone with corrugated iron was investigated by *Ghobarah et al. (1997)* (Figure 2-24b). *Tsonos (1999)* proposed a strengthening strategy consisting of enlarging the sections of the beam-column connection and increasing the anchorage length of the beam bars in the core using traditional RC (Figure 2-24c). Several other studies have been carried out in the recent past to evaluate the possibility of repairing and retrofitting damaged joints using RC jackets such as *Karayannis et al. (2008)*.

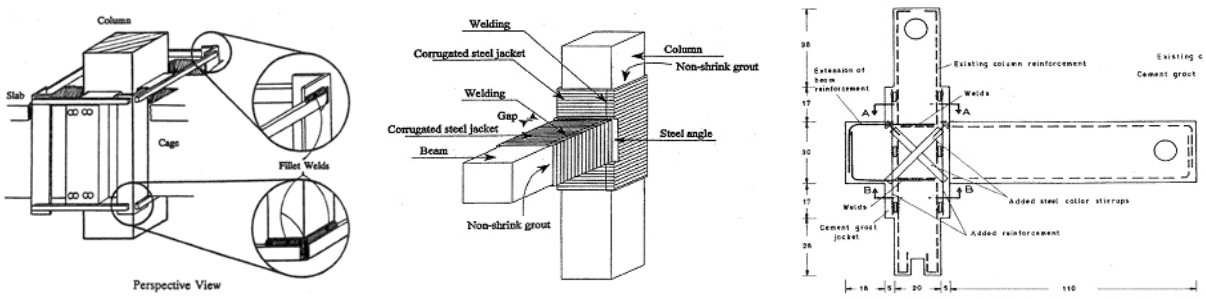

a) *Alcocer & Jirsa (1993)* b) *Ghobarah et al. (1997)* c) *Tsonos (1999)*

Figure 2-23: Retrofit strategies based on jacketing of the joint with traditional materials

More recently the use of composite materials such as carbon laminates and glass fibres has become more and more popular among the researchers and in the construction practice. These newly developed techniques present several advantages compared with traditional RC and steel jacketing. They include negligible modification of the original sections and shorter time required for the construction. On the other hand, these techniques require higher quality workmanship and higher material costs. Many studies in this field can be found in the literature (e.g., *Gergely et al., 2000*; *Ghobarah & Said, 2001*; *Antonopoulos & Triantafillou, 2003*; *Mukherjee & Joshi, 2005*; *Pampanin et al., 2007*; *Le-Trung et al., 2010*; *Sasmal, 2009* and *Akgüzel, 2011*). Some examples are shown in Figure 2-24.

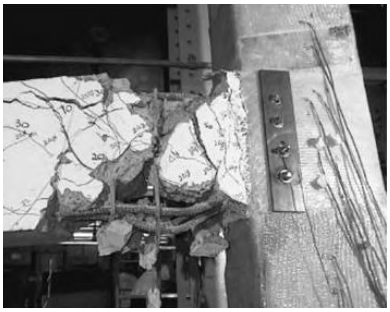

a) *Ghobarah & Said (2001)*

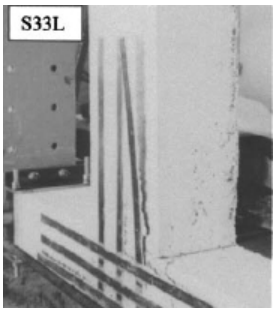

b) *Antonopoulos & Triantafillou (2003)*

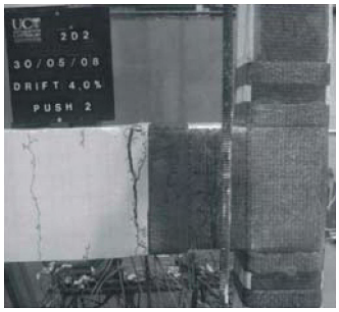

c*) Akgüzel (2011)*

Figure 2-24: Retrofit strategies involving the use of advanced polymeric materials

Other researchers adopted different strategies to prevent a brittle joint shear failure. One possibility consists of reducing the shear stress demand in the joint panel instead of increasing its strength. *Said & Nehdi (2001)* investigated the possibility of reducing the joint shear demand using steel diagonals. The test of the retrofit solution showed a considerable increase of shear capacity in the beam-column connection, which failed in shear at much higher level of lateral load and displacement (Figure 2-25a). A similar but more rigorous application of this strategy was proposed by *Pampanin et al. (2006)*. The geometry and stiffness of the steel diagonal were chosen to protect the joint panel and induce the formation of a flexural hinge in the beam (Figure 2-25b). This retrofit solution is described in detail in Chapter 6 and Appendix D, since it is considered as starting point for the retrofit solution proposed in this study. *Chaimahawan & Pimanmas (2009)* successfully investigated the possibility of protecting the joint from a brittle failure by increasing its in-plane surface (Figure 2-25c). Innovative techniques involving weakening of the beam in order to reduce the shear forces entering in the joint panel combined with a post-tensioning solution have also recently been developed by *Kam (2011)* (Figure 2-25d). *Bendirhanoglu et al. (2010)* successfully improved the joint shear strength of beam-column connections with plain round bars and 90° bent in hooks (Type 7) of approximately 30% by welding together bottom and top bars obtaining a U-shaped anchorage.

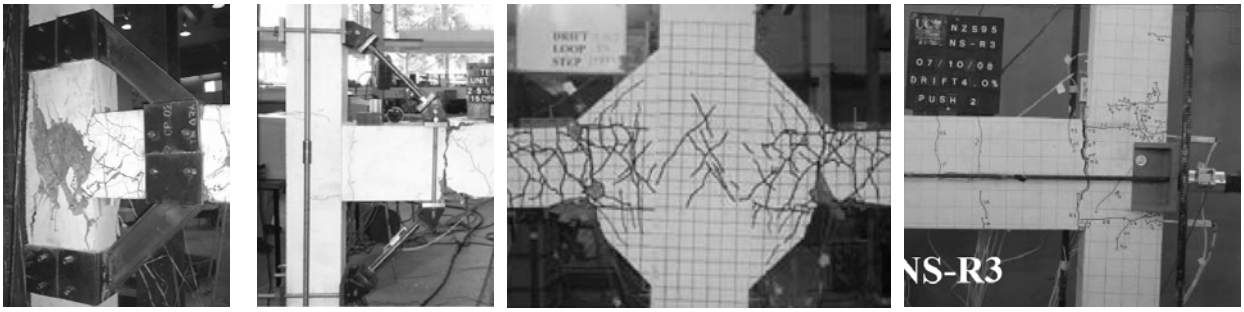

a) *Said & Nehdi (2001)* b) *Pampanin et al. (2006)* c) *Chaimahawan & Pimanmas (2009)* d) *Kam (2011)*

Figure 2-25: Alternative retrofit strategies for RC joints involving unloading of the joint panel

One of the most challenging tasks is the choice of the optimal retrofit solution as function of:

- structural deficiencies of the existing structure;
- target capacity of the retrofitted structure; and
- socio-economic value of the building.

Some authors have carried out research studies comparing different retrofit solutions, e.g., *Engindeniz et al. (2005)* and *Pampanin (2006)*. Several documents have been published in the past few years to provide guidance to the designer in the choice of the most suitable retrofit solution, e.g., *UNIDO (1983)*; *FEMA 273 (1997)*; *FEMA 356 (2000)*; *FEMA 547 (2006)* and *fib (2003)*.

2.7 Seismic behaviour of post-installed anchors

Post-installed anchors constitute a reliable and economical solution to connect both non-structural (e.g., façade, suspended ceilings, pipelines etc.) and structural elements (e.g., connection between existing and new structures) to an existing RC structure. The use of post-installed anchors is also required in many seismic retrofit and strengthening techniques (see Section 2.7.5). To address some of the aspects which have to be considered for the choice of appropriate anchor types for economic installation and adequate load-carrying capacity, a short overview on the state of the art fastening technology is given in the following sections.

2.7.1 Types of post-installed anchors

The load-transfer mechanisms of post-installed anchors into the concrete member are typically identified as friction, mechanical interlock and bond or a combination of those (see Figure 2-26).

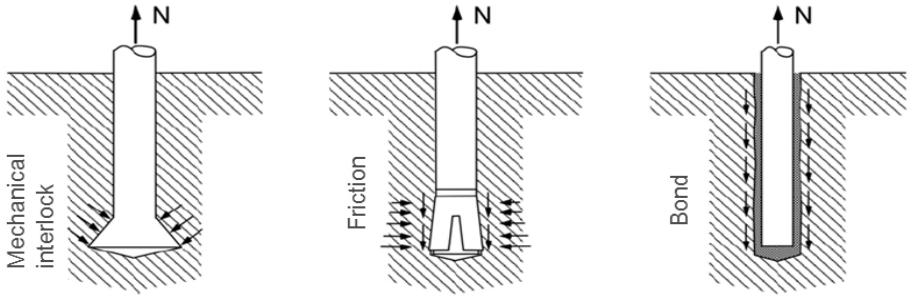

Figure 2-26: Load-transfer mechanisms of anchors

Post-installed anchors for use in concrete are usually inserted into a pre-drilled hole. They may be distinguished as mechanical expansion anchors, undercut anchors, screw anchors and bonded anchors usually used for the transfer of high loads (Figure 2-27a to j). For the transfer of smaller loads, ceilings, hangers and plastic anchors may also be suitable (Figure 2-27k,i). The anchor types presented below can be distinguished by their load-transfer mechanism (compare Figure 2-26 and Figure 2-27), by their different load-displacement behaviour (*Fuchs et al., 1995*) and their capacity to carry loads in cracked and uncracked concrete (*Eligehausen & Balogh, 1995*). Detailed descriptions of the various anchor types available on the market are provided in *Eligehausen et al. (2006a)* and in several studies available in the literature, e.g., *Küenzlen (2005)* for screw anchors and *Appl (2009)* for bonded anchors.

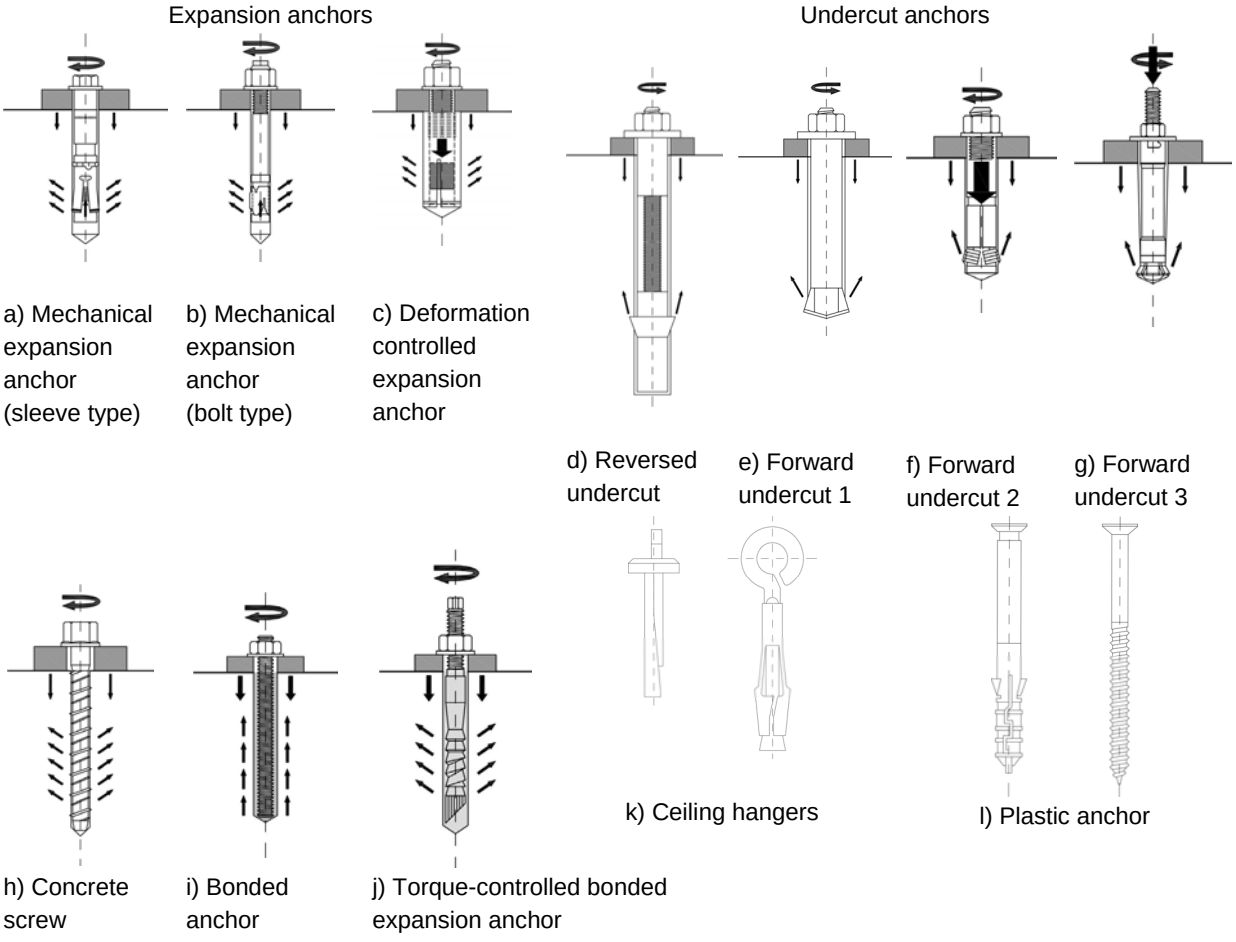

Figure 2-27: Typical post-installed anchors (*fib, 2011*)

2.7.2 Load-bearing behaviour under monotonic loading

The anchorages may be loaded in tension, shear, combined tension and shear, or by bending moment (see Figure 2-28).

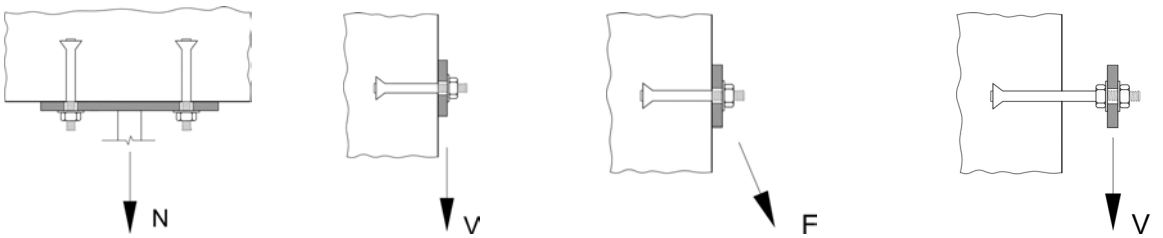

a) Tension | b) Shear | c) Combined tension and shear | d) Bending moment

Figure 2-28: Loading on anchorages and on anchors (*fib, 2011*)

For anchors loaded in tension the following failure modes can be distinguished: pullout failure (Figure 2-29a_1), pull-through failure (Figure 2-29a_2), combined pullout and concrete cone failure (Figure 2-29a_3), concrete cone failure (Figure 2-29$b_{1,2,3}$), blowout failure (Figure 2-29b_4), splitting failure (Figure 2-29$c_{1,2,3}$) and steel failure (Figure 2-29d).

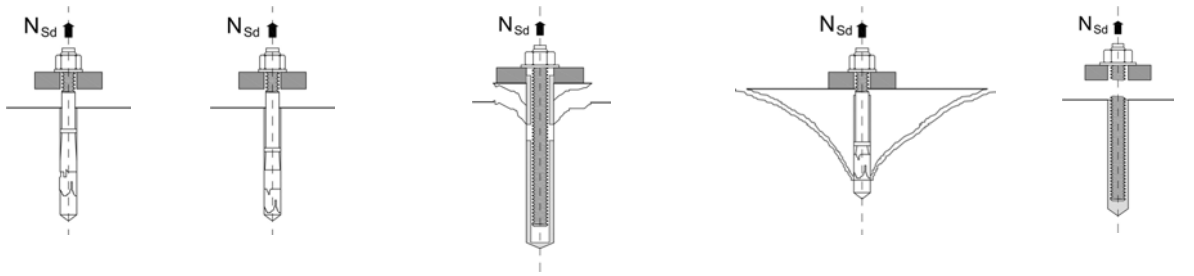

a_1) Pullout failure | a_2) Pull-through failure | a_3) Combined pullout and concrete cone failure | b_1) Concrete cone failure | d) Steel failure

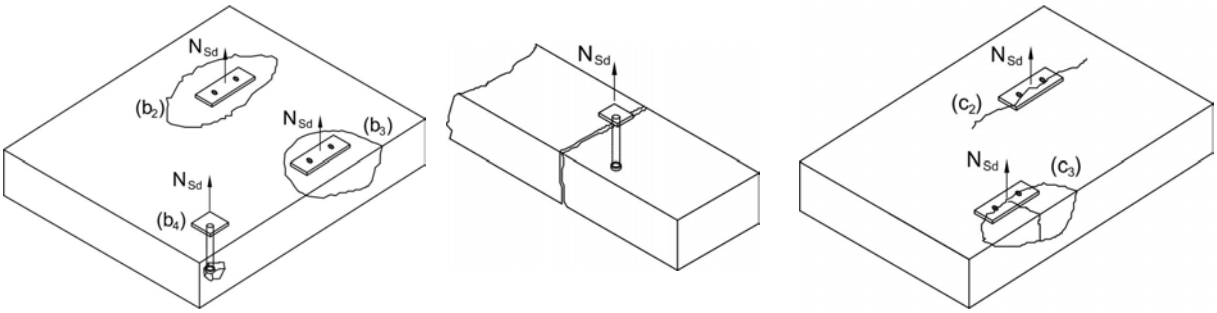

$b_{2,}$) Group breakout; b_3) Edge breakout; b_4) Blowout failure | c_1) Splitting failure | c_2) Group splitting failure; c_3) Near edge splitting failure

Figure 2-29: Failure modes associated with tension loading (*fib, 2011*)

For anchors loaded in shear the following failure modes can be distinguished: steel failure (Figure 2-30a), concrete edge failure (Figure 2-30$b_{1,2,3,4,5}$), pryout failure (Figure 2-30c) and pullout failure (Figure 2-30d).

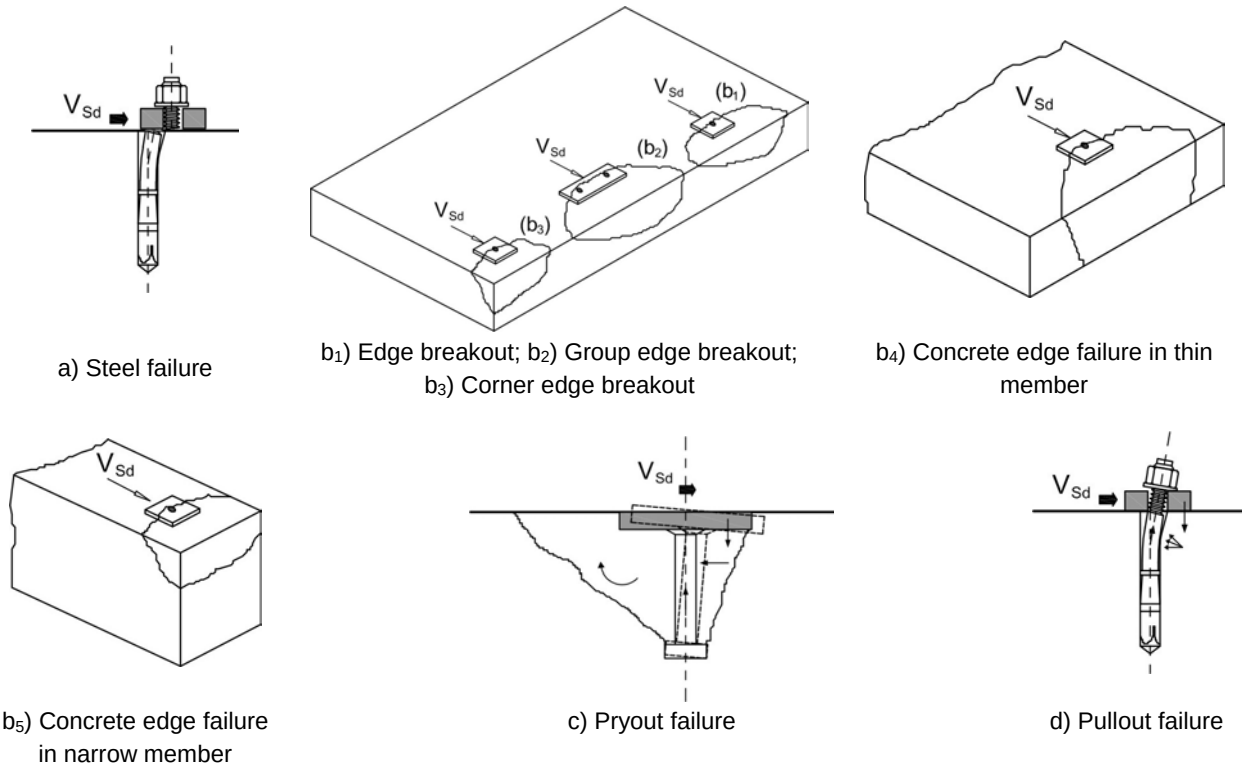

a) Steel failure

b_1) Edge breakout; b_2) Group edge breakout; b_3) Corner edge breakout

b_4) Concrete edge failure in thin member

b_5) Concrete edge failure in narrow member

c) Pryout failure

d) Pullout failure

Figure 2-30: Failure modes associated with shear loading (*fib, 2011*)

Analytical methods to calculate the ultimate loads of different anchor types (see Figure 2-27) and anchorages for the failure modes mentioned in Figure 2-29 and Figure 2-30, under monotonic loading, are available in the literature (e.g., *Eligehausen et al., 2006a* and *fib, 2011*).

2.7.3 Load-bearing behaviour under seismic conditions

During an earthquake an anchorage may be cyclically loaded by a combination of tensile and shear forces and the concrete element should generally be considered cracked. The general behaviour of anchors under such conditions is basically as briefly shown in Section 2.7.2. However, some factors have to be taken into account for the definition of prequalification procedures for the seismic suitability of anchors:

- The behaviour of anchors is influenced by the crack width and by the opening and closing of the cracks due to the cyclic loading of the concrete member. Research studies available in the literature (i.e., *Hoehler, 2006*) have suggested it is necessary to assume that there can be a significantly higher maximum crack width than for the case of static loading (e.g., $\Delta w = 0.8$ mm instead of 0.3 mm). The width of cracks negatively influences stiffness and the strength of the anchors and it may also induce a change of the failure mechanism.
- The anchors are generally subjected to cyclic loading. Experimental tests by *Hoehler (2006)* showed that the behaviour of anchors under pulsating tension follows the backbone curve defined by the monotonic loading. Investigations by *Simons (2007)* on the cyclic behaviour of post-installed reinforcing bars under alternating axial load well agrees with the bond stress-slip behaviour of reinforcing bars shown by *Eligehausen et al. (1983)*. Tests on post-installed anchors under alternating shear, carried out by *Genesio (2007b)*, showed a reduction of the shear strength due to low

cycle fatigue. The amount and amplitude of loading cycles may influence the anchors load-displacement behaviour (*Hoehler, 2006*).

- The loading rate expected during an earthquake is typically between 10 kN/s and 2000 kN/s (*Fujikake at al., 2003*). Investigations by Hoehler showed an increase of failure load for a concrete cone failure, but not a significant influence for the other failure modes (steel failure and pullout / pull-through failure). Experimental investigations on tensioned anchors in cycled cracks showed no influence of the cycles opening/closing rates on the load-displacement behaviour of the anchors (*Mahrenholtz et al., 2010*).
- A few experimental investigations have been carried out to evaluate the influence of cracked concrete with $\Delta w = 0.8$ mm (*Genesio, 2007a*) and cyclic loading and $\Delta w = 0.5$ mm (*Guillet & David, 2007* and *Guillet, 2011*) on anchors loaded in combined tension and shear. According to those tests the fulfilment of Equation (2-10) gives a conservative estimation of the anchor resistance to the combined tension and shear:

$$\left(\frac{N_{Sd}}{N_{Rd}}\right)^{k} + \left(\frac{V_{Sd}}{V_{Rd}}\right)^{k} \leq a \qquad \text{with } k = 1.0 \text{ and } a = 1.0 \tag{2-10}$$

  Investigations by *Dieterle et al. (1990)* on various anchor types loaded monotonically in with $\Delta w = 0.4$ mm indicated that $a = 1.2$ may be used.

Experimental tests on single anchors located in cracked concrete carried out by *Dieterle et al. (1990)* (bonded anchors) and *Genesio (2007a)* (expansion and undercut anchors) highlighted that for small angles against the anchor axis the shear load component has a favourable effect on the tensile resistance and therewith the anchors are generally less sensitive to concrete cracking. For bonded anchors it appears that this effect counterbalances the negative influence of the cracked concrete inducing a strength increase in comparison to pure tension of 30% or more. (see Figure 2-31a). For mechanical anchors the same strength increase is limited to approximately 10% (see Figure 2-31b). The different behaviour can be explained with the different load carrying mechanism (see Figure 2-26) of different anchor types. In the case of bonded anchors the load is resisted on the entire embedded length of the steel element, while for the expansion and undercut anchors the load is resisted along a short length at the end of the anchor, where the load is transferred into che concrete by friction and/or mechanical interlocking.

Tests by *Guillet & David, 2007* and *Guillet, 2011* highlighted the descrese of shear capacity of single anchors loaded by alternating shear up to failure and different levels of axial load (see Figure 2-32).

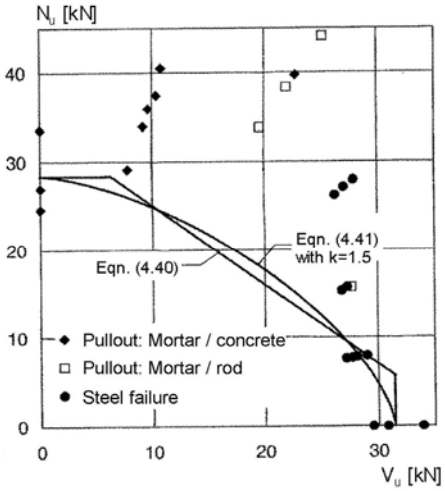

a) Tests on bonded anchors (M12, h_{ef} = 110 mm, f_c ~ 23 MPa and Δw = 0.4 mm) (*Dieterle et al., 1990*)

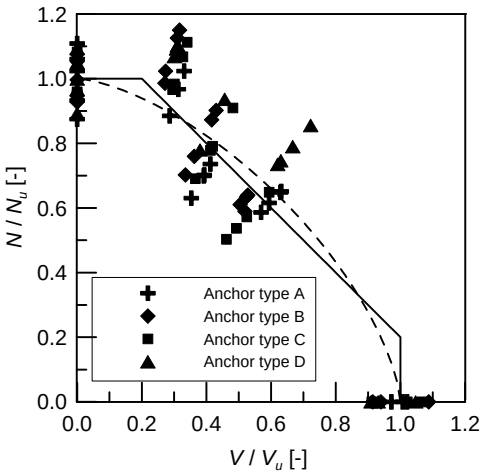

b) Tests on undercut anchors and expansion anchors (d_{nom} = 16-20, h_{ef} = 80-100 mm, f_c ~ 30 MPa and Δw = 0.8 mm) (*Genesio, 2007a*)

Figure 2-31: Behaviour of post-installed anchors located in cracked concrete and loaded in combined tension and shear

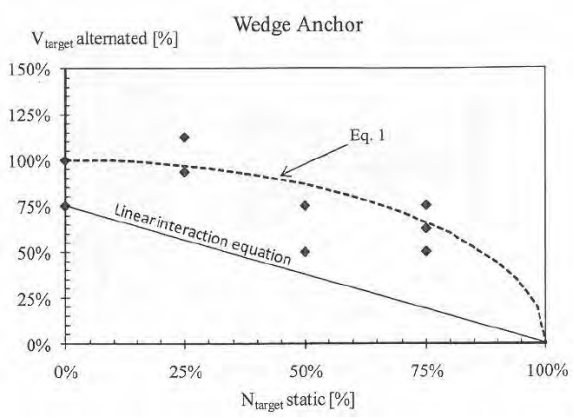

a) Expansion anchor (sleeve) type A

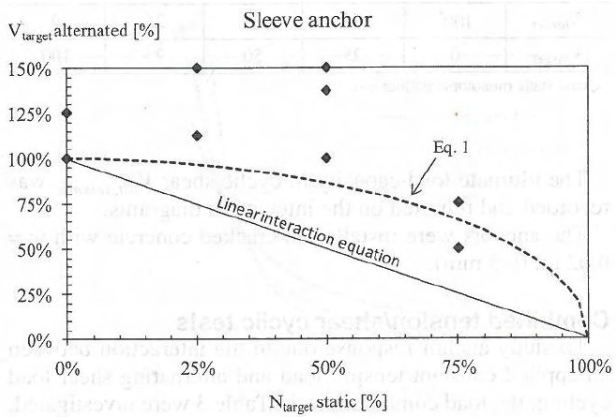

b) Expansion anchor (sleeve) type B

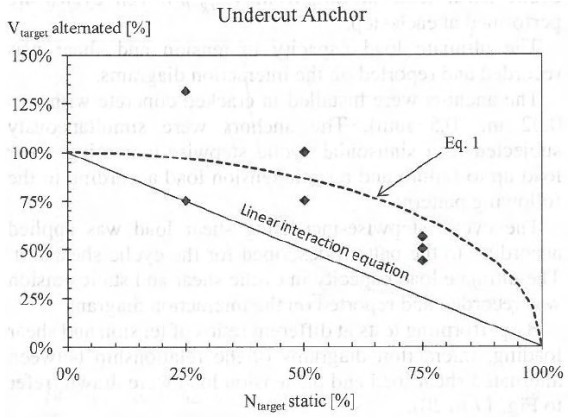

c) Undercut anchor

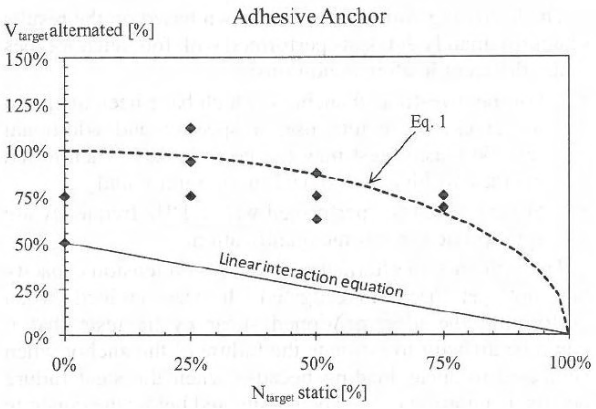

d) Bonded anchor

Figure 2-32: Effect of the combined shear and tension under alternate shear loading and constant axial loading (*Guillet, 2011*)

2.7.4 Normative standards for anchors under seismic actions

An overview of the most relevant standards in Europe and North America can be found in *Hoehler (2006)*, *Silva & Hoehler (2007)* and *Nuti & Santini (2008)*.

It is not the objective of this study to analyse the requirement of existing standards for prequalification as well as for design of anchors under seismic application. However, it is worthwhile mentioning that the requirements of existing codes are strictly force oriented. Anchors are considered as qualified for seismic application if they do not fail during the load (or crack) cycles and if the average required anchor capacity measured after the cycling is at least α-times (or β-times) the average capacity without cyclic loading (or crack opening/closing) measured in reference tests ($N_{u,m}$, $V_{u,m}$) (Equation (2-11). In general the factors α and β are taken to be < 1.0. At the moment only few information about the load-displacement behaviour of anchors are provided by existing prequalification procedures.

$$\begin{aligned} N_u &\le \alpha \cdot N_{u,m} \\ V_u &\le \beta \cdot V_{u,m} \\ \alpha, \beta &< 1.0 \end{aligned} \qquad (2\text{-}11)$$

Post-installed anchors qualified to be used under seismic conditions may be designed according to the relevant code of practice (e.g., *CEN, 2009*; *ACI 318-08 Appendix D* and *fib, 2011*). Some design codes (e.g., *fib, 2011*) require consideration of seismic actions including a form of Capacity Design. A ductile plastic deformation must be guaranteed by the anchors, the fixture or the attached element. Alternatively, an incremental factor (usually equal to 2.5) has to be considered on the actions side. Recent studies on anchor load-displacement behaviours have shown that only limited ductility and energy dissipation can be provided by the anchors, therefore, ductility requirements should be generally satisfied by the attached elements (*Hoehler, 2006* for tension and *Genesio, 2007b* for shear).

2.7.5 Application of post-installed anchors for seismic retrofit techniques

In many of the seismic retrofit techniques developed and put into practice in the last decades fastening systems find an application (e.g., *Akiyama et al., 2007* and *Hattori & Yamamoto, 2007*). A state of the art report of retrofitting techniques with emphasis on the use of fastening systems was published in 1995 (*CEB, 1995*). A few examples are shown in Figure 2-33. However, there is a general lack of guidelines for the design of anchorages with post-installed anchors for retrofit techniques.

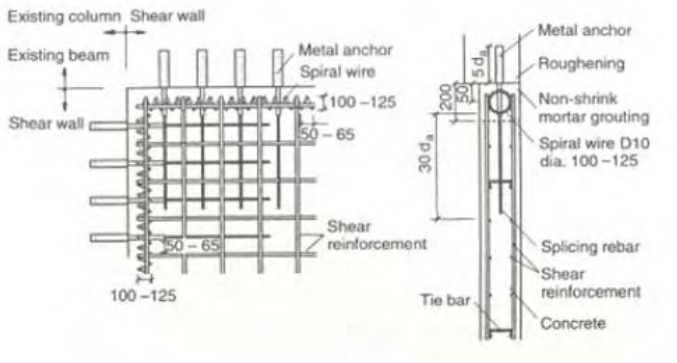

a) Infilled RC shear wall (*Sawabe & Okuzawa, 1984*)

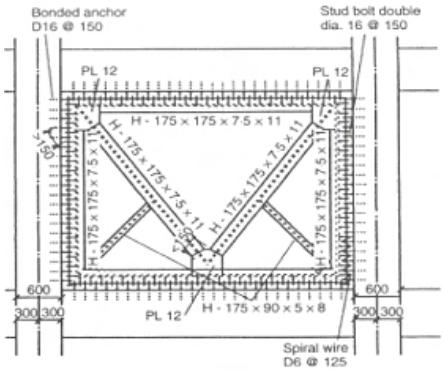

b) Framed steel bracing (*JBPA, 1990*)

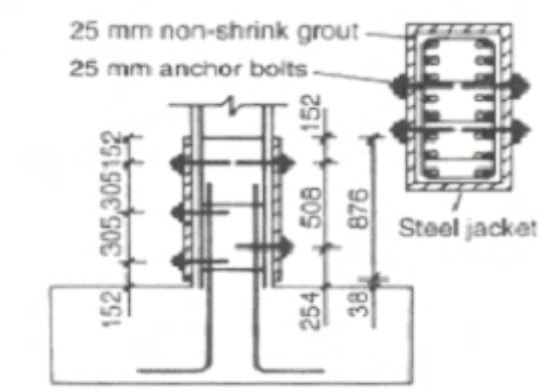

c) Steel jacketing of column with inadequate lap splices (*Aboutaha et al., 1994)*

d) Mechanically anchored FRP laminates (*Lopez & Nanni, 2006*)

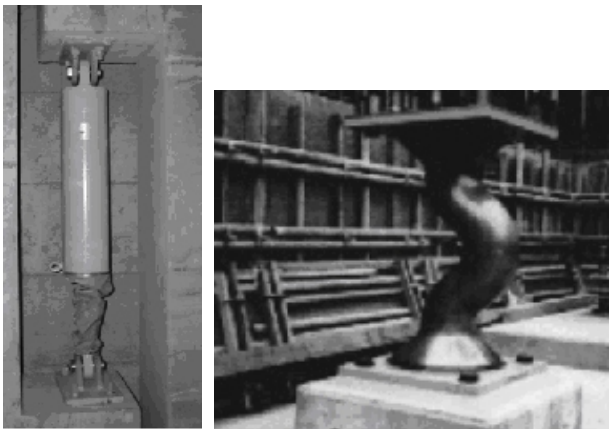

e) Anchorage of dampers
[Source: www.jssi.or.jp]

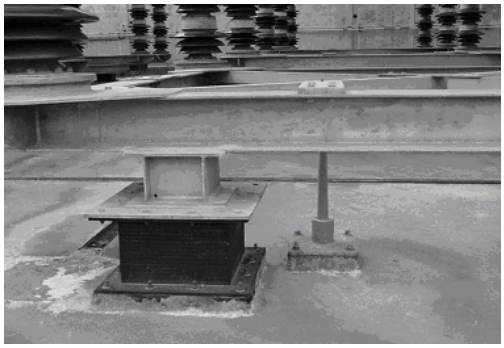

f) Anchorage of seismic isolators
[Source: www.seismicisolation.com]

Figure 2-33: Applications of post-installed anchors for seismic retrofitting

3 EXPERIMENTAL INVESTIGATIONS ON AS-BUILT JOINTS

In this chapter the experimental tests on as-built beam-column joints carried out in this study are presented. After the motivation of the experimental work (Section 3.1), the test programme (Section 3.2), the description of the testing procedures (Section 3.3) and the tests results (Section 3.4) are presented. In Section 3.5 the results of the tests are evaluated using different joint shear strength models available in the literature (Section 3.5.1) and special focus is given to the assessment method proposed by *Priestley (1997)* and *Pampanin et al. (2003)* (Section 3.5.1). The findings of the tests are finally summarised in Section 3.6. The complete tests reports are available in *Genesio & Akgüzel, (2009)* and *Genesio & Sharma (2010a)*.

3.1 Motivation

As presented in Chapter 2 a lot of research has been carried out in past decades to understand the shear behaviour of beam-column connections. Many experimental results are available and several assessment models have been proposed. To date, however, no general agreement on the shear behaviour of beam-column connections has been reached in the scientific community.

In this study new tests have been carried out. The primary objectives of these tests were:

- to determine the relative performance of exterior beam-column connections without transverse reinforcement in the core and with different beam longitudinal bar anchorage;
- to quantify the behaviour of such joints in terms of two strength limit states: initial diagonal cracking of the core and peak load;
- to define limit states of the joint shear distortion; and
- to provide a reliable benchmark for the validation of a numerical model (see Chapter 4).

3.2 Test programme

The test programme summarised in Table 3-1 can be divided into two parts. The first test (2D pre 1970s) was carried out as part of a research collaboration between the University of Stuttgart and the University of Canterbury (UC) on a 2/3 scaled specimen. The aim of the project was the development of assessment and retrofit methods for exterior RC beam-column joints that fail with a brittle plastic mechanism – that is by formation of a shear hinge in the core. The test presented in this section is the benchmark for the experimental investigation of the feasibility of the retrofit solution presented in Chapter 9 as well as for the retrofit solutions investigated by *Kam (2011)* and *Akgüzel (2011)*. The specimen “2D pre

1970s" is characterised by the use of plain round bars terminating with 180°-hooks in the joint region.

Five more tests on full scaled as-built beam-column joints (JT1-1 to JT5-1) were carried out in the laboratory of Bhabha Atomic Research Centre (BARC) (*Genesio & Sharma, 2010a*). As shown in Table 3-1 the test specimens had similar properties except for the anchorage of beam longitudinal bars in the joint region. For all specimens, with the exception of JT2-1, deformed bars were used. The specimens JT1-1, JT2-1, JT3-1 and JT4-1 were designed to fail in shear in the joint region before the yielding of beam or column reinforcement. The test JT5-1 was not included in the initial test programme but it was added at a later stage in order to validate the results of numerical simulations investigating the effect of the interaction between joint shear cracking and beam bar yielding (preliminary analysis by *Genesio et al., 2010a* and further investigations by *Mahajan et al., 2010*). Specimen JT5-1 was designed for a failure mode of beam flexural yielding after initial diagonal cracking in the joints. The tests carried out at BARC, and more specifically the specimen JT1-1, represent the benchmark for the investigation of the retrofit technique presented in Chapter 8 performed in addition to the feasibility study carried out at UC. The length and bend of the beam bars in the joint region for all the specimens were designed to meet the minimal provisions of *ACI 318-71*.

Table 3-1: Test programme on as-built specimens

Specimen	f_c [MPa]	f_{ct} [a)] [MPa]	f_y [MPa]	Col. rein.	Beam rein. [b)]	Anchorage [c)]	Failure [d)]
2D pre 1970s	17.7	1.9	430	3+3 R10	4+4 R10	180°-hooks	JS
JT1-1	25.4	n.a.	560	3+3 D20	2 D20 + 1D16	90°-bent in	JS
JT2-1	24.4	3.5	310	3+3 D20	2 R20 + 1R16	180°-hooks	JS
JT3-1	27.5	n.a.	560	3+3 D20	2 D20 + 1D16	90°-bent in / 150 mm straight	JS
JT4-1	28.2	3.0	560	3+3 D20	2 D20 + 1D16	90°-bent in / 90°-bent out	JS
JT5-1	24.6	3.4	540	3+3 D20	4 D12	90°-bent in	BJ

[a)] f_{ct} by splitting test; [b)] D = deformed bars; R = plain round bars (symmetrical reinforcement for top and bottom layer); [c)] Anchorage of top / bottom bars; [d)] JS = Joint shear failure before yielding of the beam bars, BJ = Yielding of the beam bars after joint diagonal cracking

3.3 Test Setup and procedure

The test setups and the geometry of the specimens used in the experimental investigations at UC and BARC are shown in Figure 3-1 and Figure 3-2, respectively. For the test at UC the bottom of the column was hinged and the top was free to move horizontally and vertically. Axial load was applied on the top of the column and the joint was cyclically loaded in the horizontal direction. The specimens tested at BARC were cyclically loaded in vertical direction at the beam end and the column was hinged at the top and bottom. No axial load was applied. The different static systems used are equivalent in terms of specimen loading, however, the deformation shapes are different. Discussion on different test setups is availabe in Section 5.1.7.

In the test carried out at UC the displacement in horizontal direction was measured at the top of the column (point of application of lateral loading) and at the end of the beam. In the tests at BARC the vertical displacement of the end of the beam (point of application of the cyclic

loading) was recorded. Furthermore, in both testing campaigns the strain in selected locations of the reinforcement bars of the beam and column was measured. The objective of the measurement with the strain gauges was to verify that the designed sequence of events occurred in the tests, i.e., joint shear failure before yielding of beam and/or column bars (except in the test JT5-1, see Section 3.4.6). The slip of the logitudinal beam bars out of the joint panel was measured only in the first test "2D pre 1970s". Linear potentiometers were used to quantify the contribution of beam, column and joint to the global deformation of the specimen.

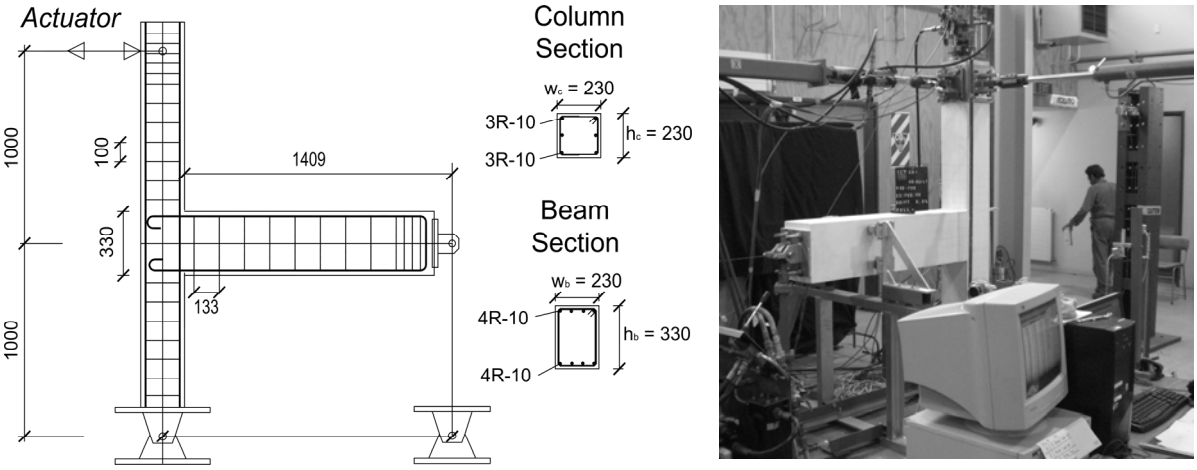

a) Test specimen 2D pre 1970s b) Test setup at UC

Figure 3-1: Test setup and geometry of the specimen for the test at UC

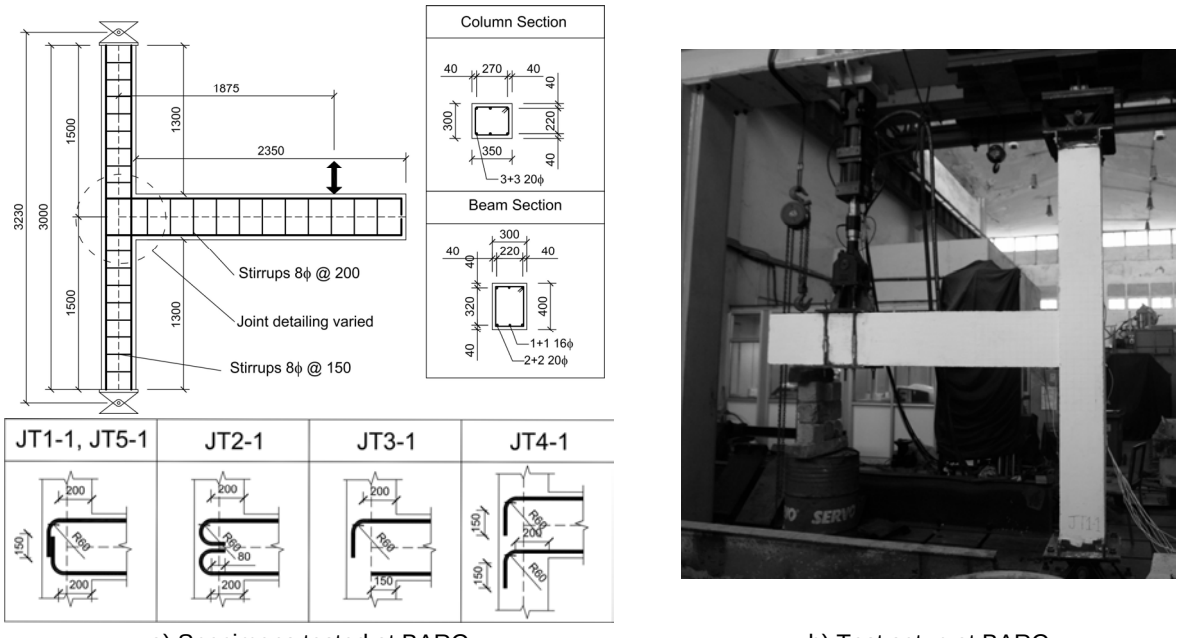

a) Specimens tested at BARC b) Test setup at BARC

Figure 3-2: Test setup and geometry of the specimens for the tests at BARC

The cyclic loading patterns used for the different test setups are shown in Figure 3-3. In both cases the loading consisted of cycles at increasing drift level with 2 cycles at each stage. The loading rate was chosen to reproduce quasi-static loading conditions. The requirements of *ACI 374-05* for cyclic assessment of moment resisting frames were not fullfilled, since 3 cycles at each drift level would have been required. However, the loading protocol is

considered adequate for the testing of substandard beam-column connections. The top drift for testing is defined: with horizontal loading of the top of the column (UC) according to Equation (3-1a); or vertical loading of the end of the beam (BARC) according to Equation (3-1b):

$$Top\,drift_c = \frac{\delta_c}{H_c} \cdot 100 \ [\%] \tag{3-1a}$$

$$Top\,drift_b = \frac{2\delta_b}{L_b} \cdot 100 \ [\%] \tag{3-1b}$$

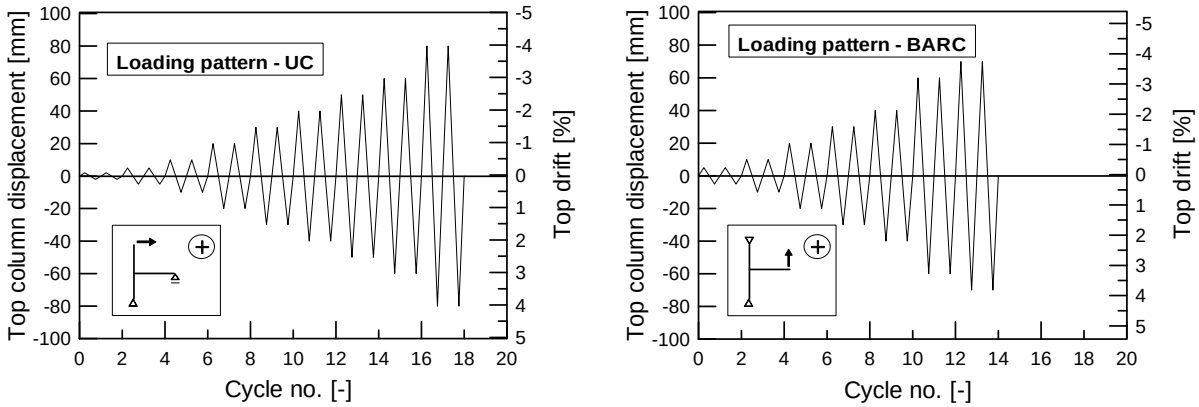

a) Cyclic loading UC c) Cyclic loading BARC

Figure 3-3: Testing procedures at UC and BARC

In the test carried out at UC the axial load in the column, N_c, was varied to account for the overturning moment induced by the lateral loading of a prototype frame (*Akgüzel, 2011*) according to Equation (3-2) and Figure 3-4.

$$N_c = N_{c,0} - \alpha \cdot V_c \tag{3-2}$$

with:

$N_{c,0}$ = static axial load
V_c = later shear force
α = axial load variation factor according to Figure 3-4

The schematic used for the calculation of the variation of axial load is shown in Figure 3-4a. The variation of axial load, ΔN, at the exterior columns of the frame can be approximated by assuming an equivalent lateral loading, F, acting at an height of 2/3 of the total building height, H, inducing an overturning moment that is resisted by ΔN times the total bay length, L (Eq. (3-3a)). The factor α, introduced in Equation (3-3b), can be calculated for a given plastic mechanism of the frame. Considering the flexural yielding moment of the column, $M_{c,y}$, the corresponding beam moment, $M_{b,eq}$ and the related shear forces, $V_{c,i}$, with i equal to the number of columns of the frame the factor α can be calculated using Equation (3-3d). The axial load variation adopted in the test is shown in Figure 3-4b. The factor α = 4.63 as well as $N_{c,0}$ = 110 kN used in this test is based on the design of the retrofit solution using GFRP proposed by *Akgüzel (2011)*.

$$2/3 \cdot F \cdot H = \Delta N \cdot L \tag{3-3a}$$

$$\Delta N = \alpha \cdot V_c \tag{3-4b}$$

$$F = \sum_i V_{c,i} \tag{3-5c}$$

$$\alpha = \frac{2}{3}\frac{H}{L}\sum_i V_{c,i}/V_{c,1} \quad \text{(for the exterior beam-column joint of the 1st floor)} \tag{3-2d}$$

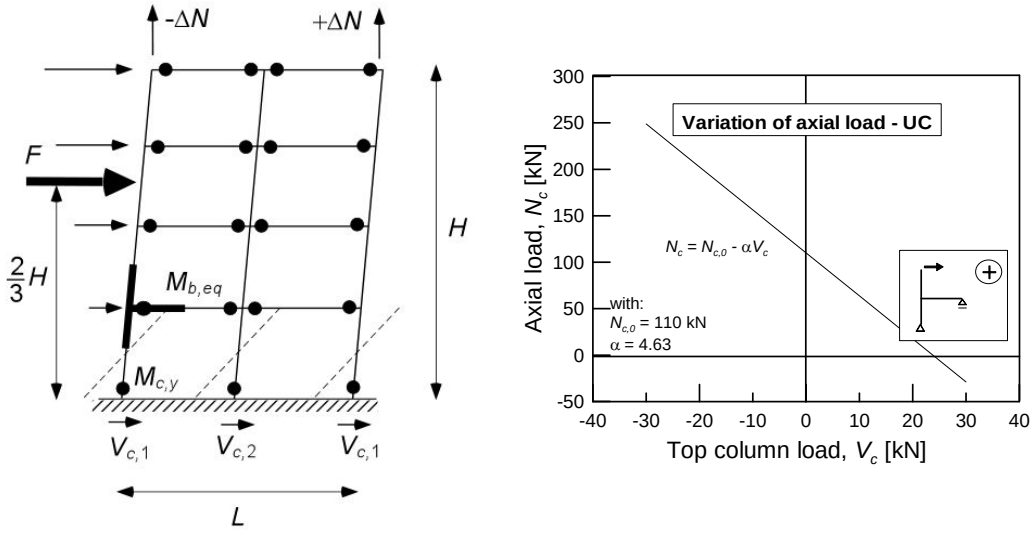

a) Schematic of the variation of axial load during lateral loading

b) Variation of axial load (*Akgüzel, 2011*)

Figure 3-4: Variation of axial load

3.4 Results of the tests

In Table 3-2 the main results of the tests on the joints are shown. The limit states corresponding to 1st joint shear cracking and peak load are distinguished. The shear strength of the joints is expressed in terms of beam / column shear load and the ratio of principle tensile stress, p_t, to $\sqrt{f_c}$ as explained in Section 2.1.3. The deformability of the specimen is given by the drift (see Eqs. (3-1a) and (3-1b)) and the joint shear distortion, γ_j, at each limit state. γ_j is calculated based on the measurements of the linear potentiometers (Figure 3-5) and using Equation (3-6). In the following sections the experimental observations are described in detail.

$$\gamma_j = \gamma_1 + \gamma_2 = \frac{\delta_j - \delta_j'}{2 \cdot l_j}\left(\tan\alpha_j + \frac{1}{\tan\alpha_j}\right) \tag{3-6}$$

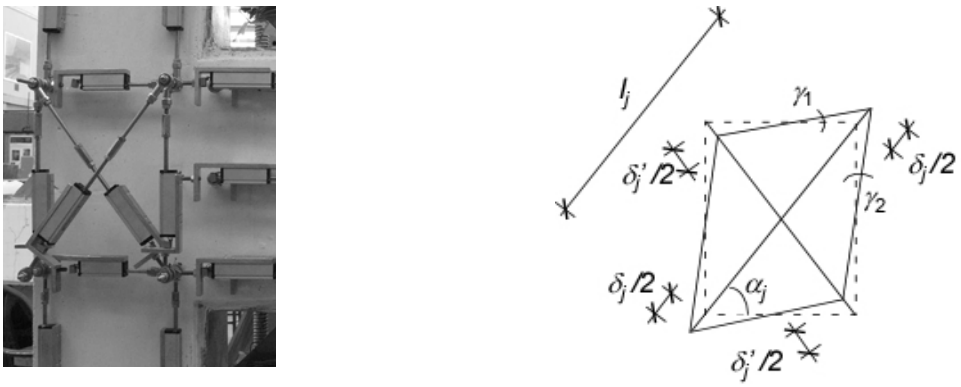

a) Measurement of joint shear distortion

b) Schematic for the calculation of joint shear distortion

Figure 3-5: Measurement and calculation of joint shear distortion

Table 3-2: Main results of the experimental tests

Specimen	1st Joint shear cracking				Peak load			
	Drift [%] a)	Load [kN] a)	$p_t l \sqrt{f_c}$ [-] a)	γ_j [rad] a)	Drift [%] a)	Load [kN] a) b)	$p_t l \sqrt{f_c}$ [-] a)	γ_j [rad] a)
2D pre 1970s	0.89 / 0.97	14.4 / 18.9	0.28 / 0.22	0.002 / 0.000	2.00 / 0.97	14.9 / 18.9	0.30 / 0.22	0.009 / 0.000
JT1-1	2.33 / 1.11	67.6 / 39.3	0.61 / 0.35	0.002 / 0.001	3.20 / 2.13	76.9 / 61.5	0.71 / 0.55	0.005 / 0.004
JT2-1	0.90 / 0.84	28.8 / 26.6	0.26 / 0.26	0.002 / 0.001	3.20 / 2.13	41.5 / 39.1	0.38 / 0.36	0.008 / 0.009
JT3-1	0.92 / 1.13	25.5 / 40.9	0.22 / 0.35	0.001 / 0.001	3.05 / 2.28	38.0 / 53.5	0.33 / 0.46	0.004 / 0.004
JT4-1	0.68 / 1.45	26.1 / 46.6	0.22 / 0.40	0.001 / 0.003	3.20 / 2.13	40.5 / 57.8	0.34 / 0.48	0.014 / 0.007
JT5-1	1.60 / 1.19	50.2 / 35.7	0.46 / 0.32	0.001 / 0.001	2.13 / 2.13	51.0 / 39.5	0.46 / 0.36	0.003 / 0.009

a) Positive / Negative loading direction; b) Load is V_c for "2D pre1970s" and V_b for the other test specimens

3.4.1 Test 2D pre 1970s

The behaviour of the beam-column connection was characterised by the formation of several flexural cracks in the beam and the column up to a maximum drift of 0.5% (Figure 3-6c$_1$). In the first 1.0% cycle a shear diagonal crack appeared in the joint region at 0.89% and 0.97% drift in the positive and negative direction, respectively (Figure 3-6a,c$_{2,3}$). In the negative loading direction the width of the first shear crack was much smaller than in the positive direction due to the higher level of axial load (194.6 kN vs. 46.34 kN). After initial joint shear cracking, the overall deformation of the specimen increasingly concentrated in the joint region. No new cracks occurred in the beam or column and the width of the existing flexural cracks gradually decreased. As shown in Figure 3-6a, the ultimate capacity of the joint was almost constant up to the 1st cycle at 2.5% drift. During the 2nd cycle a 3.0% drift in the negative direction (increasing axial load) the longitudinal column reinforcement bars buckled inducing a drastic loss of resistance of the joint and a "concrete wedge" formed (Figure 3-6c$_4$). The joint shear distortion, in both loading directions, was almost negligible up to the first diagonal cracking, but later it increased significantly (Figure 3-6b). The overall hysteretic behaviour of the joint was characterised by high pinching and low energy dissipation. It is worth noting that in the negative loading direction (increment of axial load) the general behaviour was very brittle, with strength reduction starting from the 1st shear cracking (Figure 3-6a,b). In the positive loading direction (decrement of axial load) a slight increment of strength after the 1st shear cracking up to 2.5% drift was observed (Figure 3-6a,b). The ratio $p_t/\sqrt{f_c}$ was smaller in the negative loading direction (Figure 3-6b). The strain gauge readings indicated the yielding of the top beam bars at approximately the peak load in the negative loading direction. The strains in column longitudinal bars remained below the yielding level up to the bukling during the 3% drift cycle. The slip of the beam bars out of the joint panel was negligible.

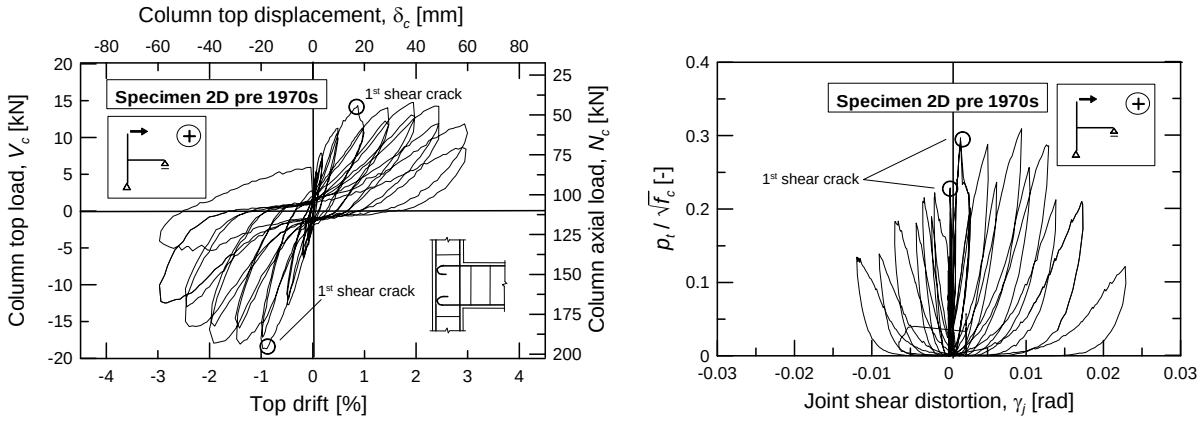

a) Hysteretic behaviour b) Joint shear deformation

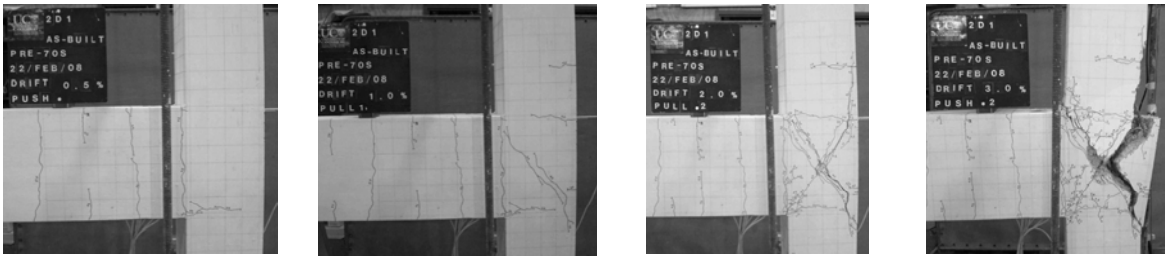

c$_1$) +0.5% c$_2$) +1.0% c$_3$) +2.0% c$_4$) -3.0%

c) Cracking patterns at increasing top drift levels

Figure 3-6: Test 2D pre 1970s

3.4.2 Test JT1-1

Up to 0.5% drift, flexural cracks occurred mainly in the beam and at the interface between column and joint region. The first cracks in the joint region occurred in the 1st 20 mm cycle and they were due to splitting caused by the high bond stresses induced by the deformed bars (Figure 3-7c$_1$). At the beginning of the 30 mm cycle diagonal cracking of the joint panel occurred in the negative direction (Figure 3-7c$_2$). A symmetric behaviour was expected because of the lack of column axial load and the symmetric detailing of the joint. However, in the positive loading direction the 1st joint shear cracking occurred at a much higher deformation (> 2.0% vs. 1.0% top drift) and higher load (67.6 kN vs. 39.3 kN) than that observed in the negative loading direction (Figure 3-7a). In both loading directions the peak load was reached at a drift of approximately 3.0% followed by brittle behaviour (Figure 3-7a). However, in the positive direction the peak load was significantly higher than in the negative direction (79.9 kN vs. 61.5 kN). Also in this test the joint shear distortion became significant only after the first shear cracking (Figure 3-7b). Further cracks in the joint region were observed along the column longitudinal bars (Figure 3-7c$_3$). At the end of the test the damage was mainly observed in the joint panel (Figure 3-7c$_4$). The extension of the joint shear cracks in the column in the form of vertical cracks (Figure 3-7c$_{3,4}$) let assume that the presence of axial load would have a deleterious effect on the deformation of the specimen as consequence of the *P-Δ* effect. According to the strain gauge readings, no yielding of beam and/or column bars occurred during the entire loading pattern.

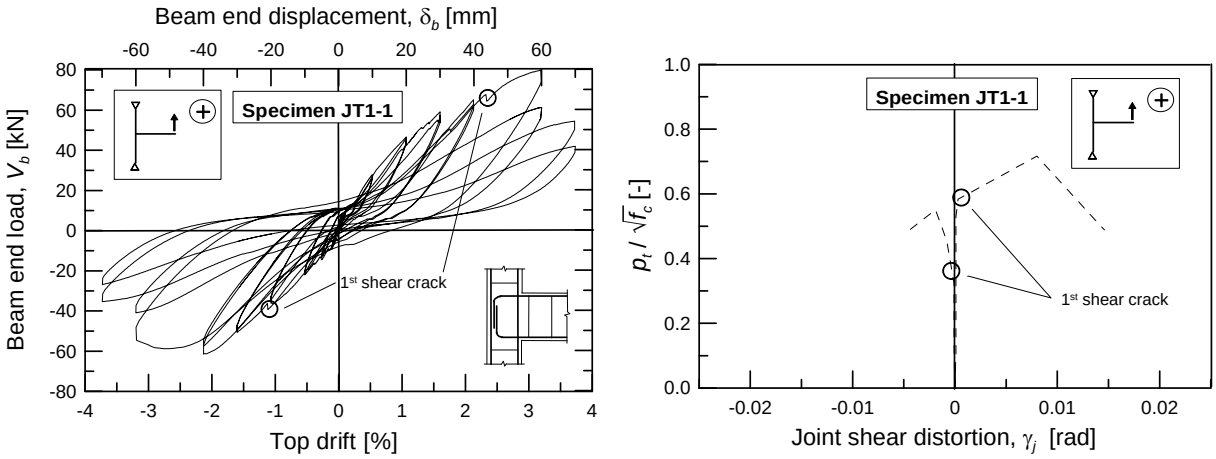

a) Hysteretic behaviour

b) Envelope of shear deformation

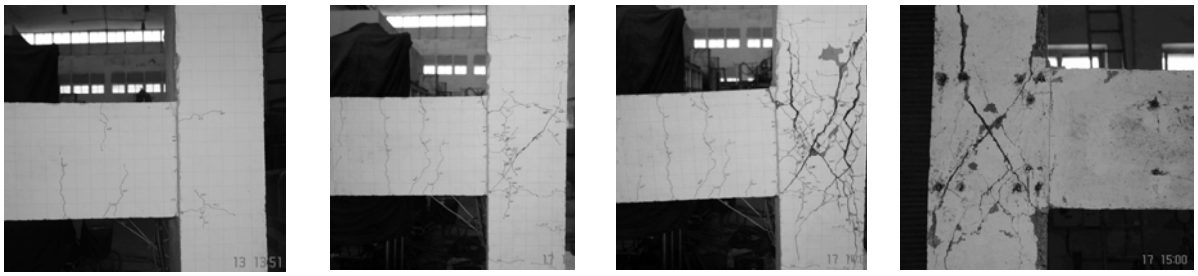

c$_1$) -20 mm c$_2$) -30 mm c$_3$) -70 mm c$_4$) End of the test – back side

c) Cracking patterns at increasing beam end displacement levels

Figure 3-7: Test JT1-1

3.4.3 Test JT2-1

In this test similar joint detailing to the test presented in Section 3.4.1 was investigated - including the use of plain round bars with 180°-hooks. However, the hooks were much bigger than in the specimen "2D pre 1970s" (compare Figure 3-1 and Figure 3-2), because of the use of beam bars with larger diameter (16 and 20 mm vs. 10 mm). In this test only flexural cracks in beam and column were observed up to a drift of approx. 1.0% (Figure 3-8c_1) . As expected no bond cracks were observed during the test, because the smooth bars were not able to develop sufficient stresses. Diagonal cracking of the joint was observed at 0.90% and 0.84% top drift in positive and negative loading directions, respectively, at similar load levels (28.8 kN and 28.6 kN) (Figure 3-8a,$c_{2,3}$). A symmetric load-deformation behaviour was observed for both hysteretic loops and joint shear deformation (Figure 3-8a,b). At a drift of approximately 2.0% the yielding of the 16 mm diameter bars was measured at the beam-column interface. The strength of the specimen increased up to a drift of approximately 3.0%. The strength significantly decreased from the 2ndcycle at ±60 mm. The final cracking pattern was characterised by two major diagonal cracks in the joint region extending in form of vertical large cracks in the column at distance from the outer face corresponding to concrete cover of the loagitudinal bars and by a few minor flexural cracks in beam and column (Figure 3-8c_4). No yielding of beam and/or column bars was observed.

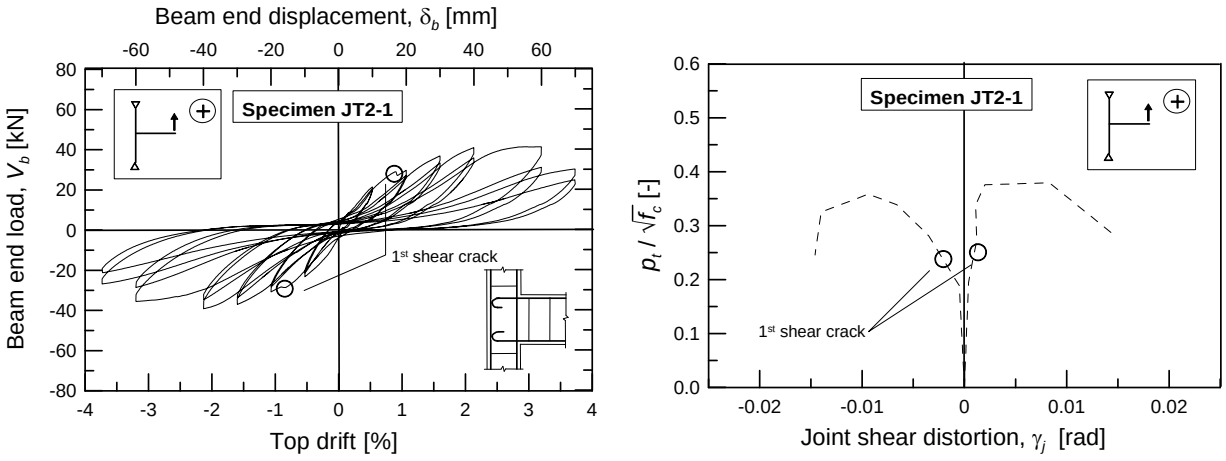

a) Hysteretic behaviour

b) Envelope of joint shear deformation

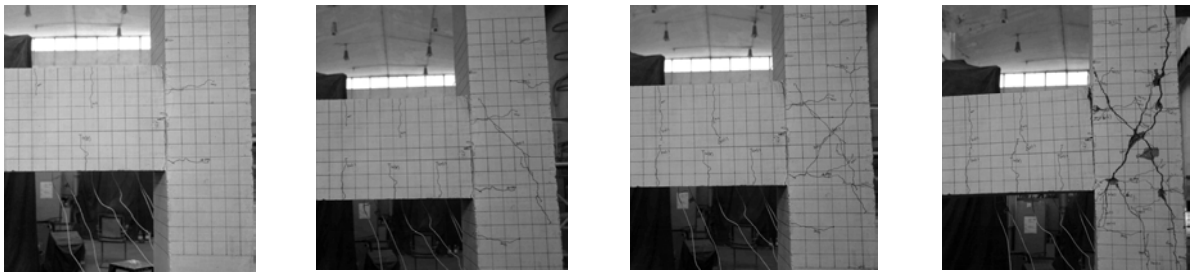

c_1) -10 mm c_2) + 20 mm c_3) -20 mm c_4) -70 mm

c) Cracking patterns at increasing beam end displacement levels

Figure 3-8: Test JT2-1

3.4.4 Test JT3-1

In the test JT3-1 the performance of typical static beam anchorage, using deformed bars in the joint core with 90°-hooks and 150 mm straight anchorage (6 inches according to *ACI 318-71*) for top and bottom layers, respectively, was investigated. In positive loading direction the first diagonal crack occurred at 0.92% drift and 25.5 kN (Figure 3-9a). The crack started at the end of the straight anchorage approximately at the mid-depth of the column (Figure 3-9c$_2$). In the negative direction the behaviour observed was approximately the same as in the test JT1-1 (negative loading direction), with diagonal cracking of the joint occurring at 1.13% drift and 40.9 kN (Figure 3-9c$_3$). In both loading directions the load increased up to approximately 3.0% drift (Figure 3-9a). However, in positive loading direction the behaviour of the joint moved from shear cracking to pullout of the beam bars with straight anchorage due to the bond degradation induced by the cyclic loading. This behaviour can be seen in the decrease of the joint shear distortion in the last part of the backbone curve (Figure 3-9b). It is also evidenced by the formation of parabolic cracks at failure starting from the mid depth of the joint and going to the bottom and top of the beam (Figure 3-9c$_4$). Vertical cracks in the column appeared in the last part of the test (Figure 3-9c$_4$). Also in this test no yielding of the beam and/or column bars was measured.

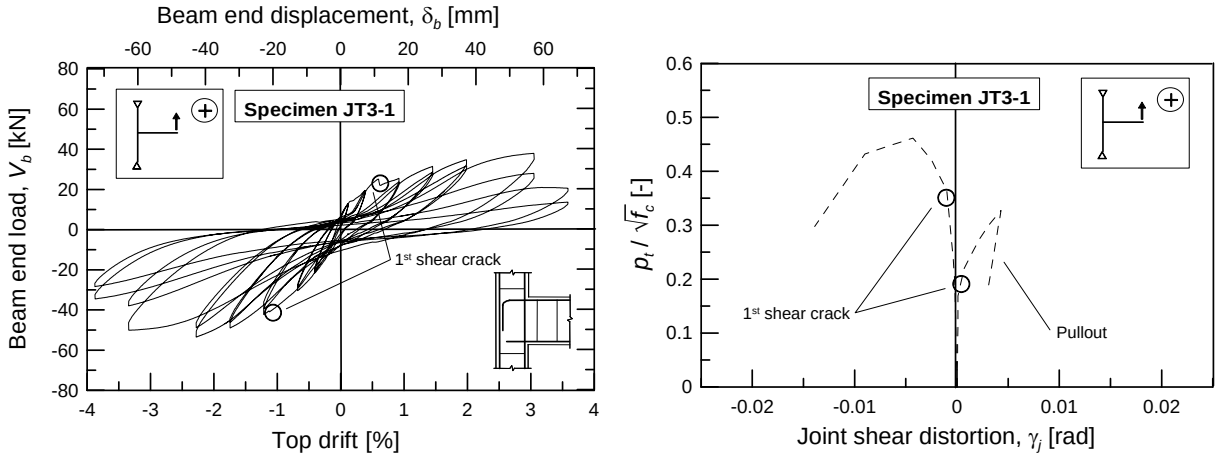

a) Hysteretic behaviour b) Envelope of joint shear deformation

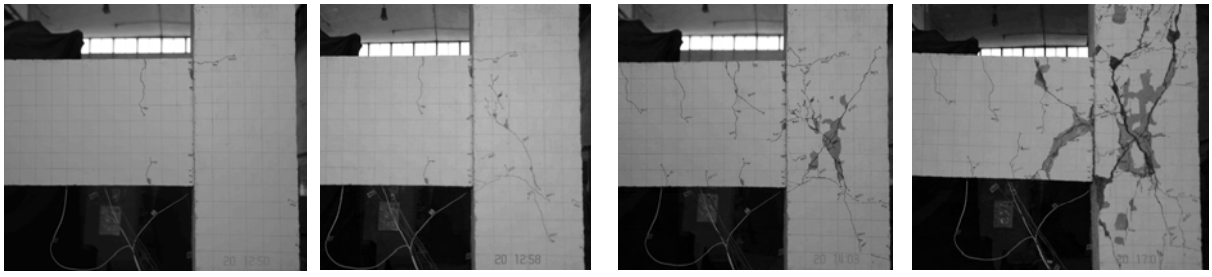

c$_1$) -10 mm c$_2$) +20 mm c$_3$) -30 mm c$_4$) +70 mm

c) Cracking patterns at increasing beam end displacement levels

Figure 3-9: Test JT3-1

3.4.5 Test JT4-1

The test JT4-1 focused the different behaviour of beam bars anchored with 90°-hooks bent in or away from the core (Types 1 and 2, respectively). In the positive loading direction (anchorage Type 2) premature diagonal cracking occurred at 0.68% drift and 26.1 kN beam end load (Figure 3-10a,c_2). In the negative direction, with the better anchorage (Type 1), the diagonal joint cracking occurred at 1.45% drift and 46.6 kN load (Figure 3-10a,c_3). It is worth noting that the inclination of the diagonal crack of the Type 2 anchorage is much flatter than for the Type 1 anchorage (Figure 3-10$c_{3,4}$). This confirms the observation of other tests available in the literature such as by *Hakuto et al. (2000)* and *Kuang & Wong (2006)*. The ultimate shear strength of the joint was reached in both loading directions at approximately 3.0% drift. The joint shear distortion was qualitatively similar to the tests JT1-1, JT2-1 and JT3.1 (Figure 3-10b). The development of the cracking pattern shown in (Figure 3-10$c_{1\text{-}4}$) follows the sequence of the previews tests starting with flexural cracking of beam and column, bond cracking in the joint and finally diagonal cracking. At the end of the test two major cracks were observed in the joint panel and extending in the column (Figure 3-10c_4). The readings of the strain gauges indicated that, as per the intended design, the beam-column connection reached its ultimate strength in both loading directions before the yielding of beam and/or column could occur.

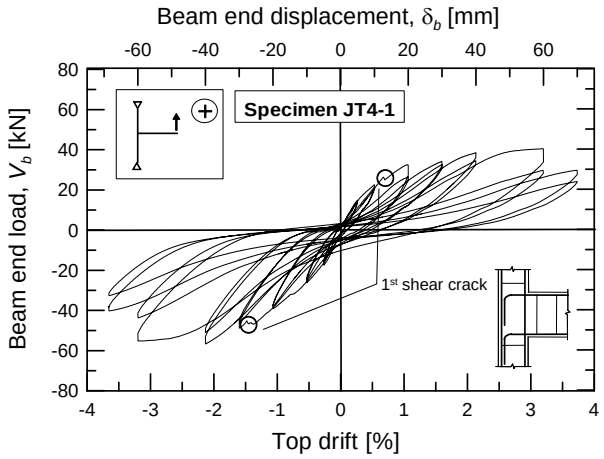

a) Hysteretic behaviour

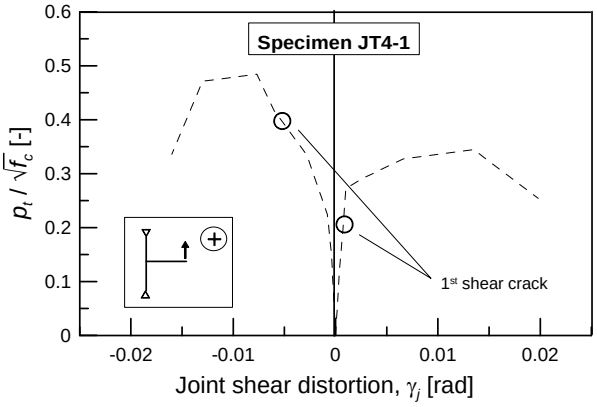

b) Envelope of joint shear deformation

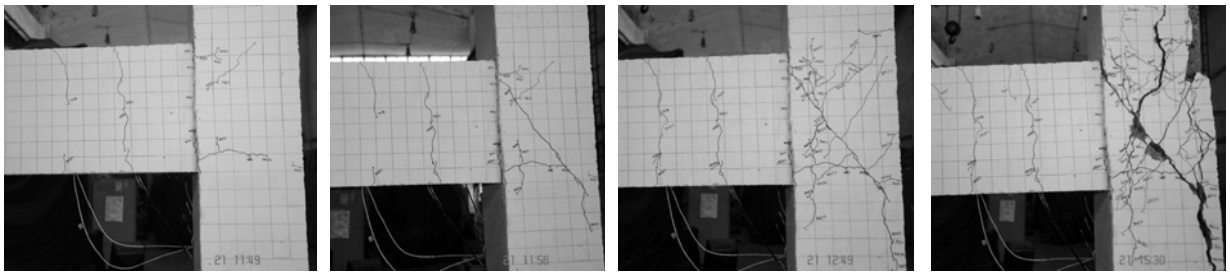

c_1) -10 mm c_2) +20 mm c_3) -30 mm c_4) -70 mm

c) Cracking patterns at increasing beam end displacement levels

Figure 3-10: Test JT4-1

3.4.6 Test JT5-1

This specimen had the same detailing as JT1-1, but the beam reinforcement ratio was reduced to induce the yielding of the longitudinal beam bars after the formation of the first diagonal cracking in the joint region. The joint behaviour was characterised by the formation of flexural and bond cracks up to a drift of 1.0% (Figure 3-11c$_1$). The first diagonal crack in the positive loading direction occurred at a later stage than expected: at 1.60% drift and 50.2 kN load (Figure 3-11a,b,c$_2$) and at approximately the yielding point of the beam bars (compare with other tests with anchorage Type 1). As expected, the joint strength did not increase further because it was limited by the beam flexural capacity. No higher ductility was obtained with the modification of the failure mode. In negative direction the first diagonal crack occurred at 1.19% drift and 35.7 kN load (Figure 3-11a,b,c$_3$). In this loading direction the yielding of the beam was not achieved and the peak load was reached at 2.13% drift with negligible strength increase from that observed at 1st diagonal cracking. At the end of the test the damage was concentrated in the joint region with two major diagonal cracks and spalling of concrete in the middle of the core (Figure 3-11c$_3$).

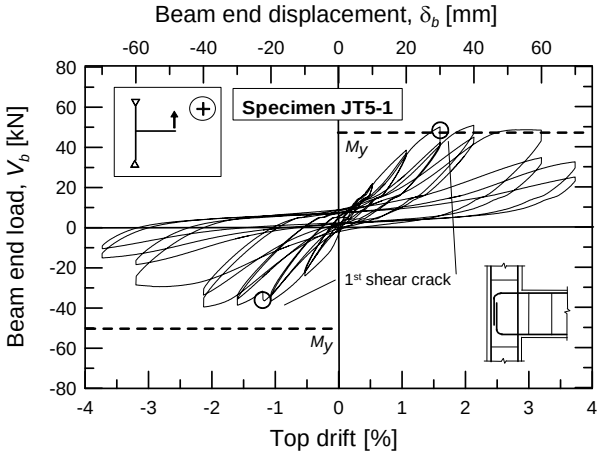

a) Hysteretic behaviour

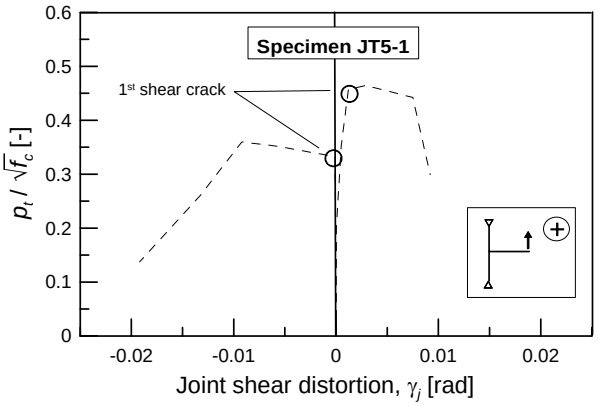

b) Envelope of joint shear deformation

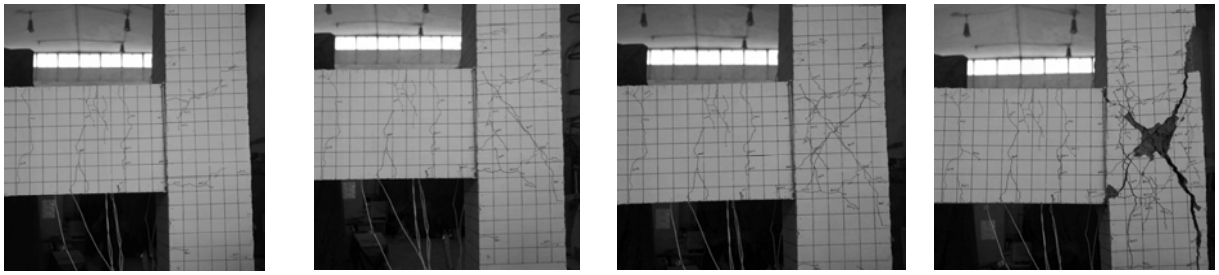

c$_1$) -20 mm c$_2$) +30 mm c$_3$) -30 mm c$_4$) +70 mm

c) Cracking patterns at increasing beam end displacement levels

Figure 3-11: Results of the test JT5-1

3.5 Evaluation of the results using analytical models

3.5.1 Evaluation of joint shear strength models available in the literature

As qualitatively discussed in Chapter 2, most of the existing joint shear strength may not be adequate for the assessment of substandard beam-column connections such as the specimens tested in this study. In Table 3-3 the estimation the joint shear stress, v_{jh}, at initial shear cracking according to several models is shown. The models by *Taylor (1974)* and *Sarsam & Phipps (1985)* significantly overestimate the strength corresponding to this limit

state for anchorages of the beam bars different than Type 1 (Exp/Calc < 0.6) with the exception of the specimen "2D pre 1970s", while for Type 1 the calculations diverge from the experimental measurement within an acceptable percentage of ±25%. The estimation using *Nilsson (1973)*, *Hoekstra (1985)* and *Hamil (2000)* are slightly better, however, the ratio Exp/Calc is generally smaller than 1.0, i.e., the predictions are unconservative.

Table 3-3: Evaluation of shear strength models (1st joint shear cracking)

Test	1st Joint shear cracking – Ratio Exp / Calc									
	Nilsson (1973)		*Taylor (1974)*		*Hoekstra (1977)*		*Sarsam & Phipps (1985)*		*Hamil (2000)*	
	Pos	Neg	Pos	Neg	Pos	Neg	Pos	Neg	Pos	Neg
2D pre 1970s	0.90	1.14	1.06	0.94	1.85	2.39	0.75	0.84	0.76	0.92
JT1-1	1.38	1.06	1.53	0.89	2.10	1.22	1.26	0.73	1.90	1.10
JT2-1	0.83	0.79	0.55	0.56	0.76	0.77	0.54	0.54	0.80	0.81
JT3-1	0.65	0.92	0.58	0.93	0.79	1.27	0.47	0.75	0.72	1.15
JT4-1	0.77	0.97	0.59	1.05	0.81	1.44	0.48	0.85	0.73	0.73
JT5-1	0.73	0.53	0.96	0.70	1.31	0.96	0.90	0.66	1.35	1.35

The performance of eight different joint shear strength models developed during the past twenty-five years for the estimation of the ultimate limit state in terms of v_{jh} highlights the inadequateness of most of all of them for the assessment of substandard joints (see Table 3-4). Only the empirical model by *Baikir & Boduroğlu (2002)* appears to agree acceptably well with the experimental predictions, however, this model does not consider joint with anchorages Type 2, 5 and 6 and it ignores the influence of column axial load. For all the other models, the experimental results correspond to 30% to 60% of the calculated v_{jh}, which is an unacceptable difference.

Table 3-4: Evaluation of shear strength models (Peak load)

Test	Peak load – Ratio Exp / Calc															
	Sarsam & Phipps (1985)		*Scott et al. (1994)*		*Vollum & Newmann (1999)*		*Hamil (2000)*		*Baikir & Boduroğlu (2002)*		*Hegger et al. (2003)*		*Mahajan (2009)*		*Park & Mosalam (2009)*	
	pos	neg	pos	neg	pos	neg	pos	neg	pos	neg	pos	neg	pos	neg	pos	neg
2D pre 1970s	0.34	0.40	0.37	0.47	a)	a)	a)	a)	a)	a)	a)	a)	0.72	0.62	0.74	0.94
JT1-1	0.63	0.48	0.68	0.52	0.82	0.63	0.71	0.55	1.36	1.04	0.77	0.59	1.14	0.87	0.89	0.68
JT2-1	0.33	0.31	0.36	0.34	a)	a)	a)	a)	a)	a)	a)	a)	0.61	0.58	0.46	0.44
JT3-1	0.29	0.41	0.31	0.44	a)	0.53	a)	0.46	a)	0.87	a)	0.50	0.50	0.71	0.42	0.60
JT4-1	0.34	0.43	0.36	0.46	a)	0.55	a)	0.48	a)	0.91	a)	0.52	0.58	0.73	0.50	0.63
JT5-1	b)	b)	b)	b)	b)	b)	b)	b)	b)	b)	b)	b)	b)	b)	1.06	0.77

[a)] This anchorage detailing not considered by this model; [b)] Prediction of BJ mode not possible with this model
Note: models which do not address any specific anchorage detailing were used to estimate the shear strength of all anchorage types.

The reason of the significant discrepancy between experimental and analytical results may be found in the followings:

- lack of consideration of beam bars anchorage types different than Type 1;
- the effect of the column axial load is often not adequately taken into account; and

- the calibration of most models was carried out on experimental databases including specimen with and without shear reinforcement in the core. This may lead to an overestimation of the concrete contribution on the joint shear strength and lack of consideration of the effect of the initial diagonal cracking.

3.5.2 Evaluation of the Priestley-Pampanin model

Priestley proposed a semi-empirical phenomenological method based on experimental evidences to estimate the failure of unreinforced (i.e., without transverse reinforcement in the core) exterior beam-column joints defining limits of, k, the ratio $p_t/\sqrt{f_c}$ (Eq. (3-7)) (*Priestley, 1997*). The extension of the model to joints with plain round bars and 180°-hooks (anchorage Type 6) was proposed by *Pampanin et al. (2003)*.

$$k = \sqrt{f_c}/p_t \tag{3-7}$$

with:
k = 0.42 for beam deformed bars bent into the joint (Type 1)
k = 0.29 for beam deformed bars bent away from the joint (Type 2) and 1st diagonal cracking for anchorage Type 1
k = 0.20 for beam plain round bars with 180°-hooks (Type 6) (*Pampanin et al., 2003*)

In Table 3-5 the prediction of the strength of the tested specimen with the model Priestley-Pampanin is compared with the experimental results. The model could conservatively predict the results with an error between 10% and 30% for anchorages Types 1 and 2 and almost 100% for the anchorage Type 6. The model presents the advantages of being simple and based on principle of mechanics using p_t instead of v_{jh} as damage indicator, taking in this way the effect of axial load realistic into consideration as shown in *Eligehausen et al. (2009)*. At the same time the most relevant parameters for the assessment of unreinforced joints (i.e., f_c and the anchorage and type of beam bars) are realistically taken into account, e.g., has shown by tests by *Hertanto (2005)*. In the following chapters investigations will be carried on in order to evaluate the possibility of refinement of this model eventually including the influence of other parameter such as geometric aspect ratio of the joint, h_b/h_c and reinforcement amount in beam and column, ρ_b and ρ_c.

Table 3-5: Evaluation of the assessment Priestley-Pampanin model

Specimen	1st Joint shear cracking [a]						Peak load					
	$(p_t/\sqrt{f_c})_{Exp}$ [-]		$(p_t/\sqrt{f_c})_{Calc}$ [-]		Exp / Calc [-]		$(p_t/\sqrt{f_c})_{Exp}$ [-]		$(p_t/\sqrt{f_c})_{Calc}$ [-]		Exp / Calc [-]	
	pos	neg	pos	neg	pos	neg	pos	neg	pos	neg	pos	neg
2D pre 1970s	0.28	0.22	0.20	0.20	1.40	1.10	0.30	0.22	0.20	0.20	1.50	1.10
JT1-1	0.61	0.35	0.29	0.29	2.10	1.21	0.71	0.55	0.42	0.42	1.69	1.31
JT2-1	0.26	0.24	0.20	0.20	1.30	1.20	0.38	0.36	0.20	0.20	1.90	1.80
JT3-1	0.22	0.35	-	0.29	-	1.21	0.33	0.46	-	0.42	-	1.10
JT4-1	0.22	0.40	0.29	0.29	0.76	1.38	0.34	0.48	0.29	0.42	1.17	1.14
JT5-1	0.46	0.32	0.29	0.29	1.59	1.10	0.46	0.36	-	-	-	-

[a] Diagonal cracking in the joint panel

The model also includes indication on the joint shear deformability (*Pampanin et al., 2003*):

- Undamaged (uncracked): $\gamma_j < 0.0002$

- Limited damage (initial cracking): $0.0002 \leq \gamma_j < 0.005$
- Extensive damage: $0.005 \leq \gamma_j < 0.01$
- Critical damage (reparability issues arise): $0.01 \leq \gamma_j < 0.015$
- Incipient collapse: $\gamma_j \geq 0.015$

The above deformation limit states are similar to the values observed in the experimental tests carried out in this study (see Table 3-2).

3.6 Summary and discussion

The main findings of the experimental tests carried out in this research are summarised below:

- The test "2D pre 1970s" confirmed poor behaviour of joints with plain round bars and anchorage Type 6 (180°-hooks).
- The joint shear strength of substandard joints is much less than the one considered as the lower limit by the most advanced seismic codes (compare Figure 3-12a and Section 2.5.6).
- The tests JT1-1, JT2-1, JT3-1 and JT4-1 showed poor performance of non-Type 1 anchorages (i.e., different than 90°-bent in hooks) confirming that the anchorage of longitudinal reinforcement beam bars in the joint region has a major influence on the joint shear capacity (Figure 3-12a). However, in none of the investigated cases, significant pullout the beam bars out of the joint panel up to the ultimate load was observed.
- The specimen JT1-1 behaved in very different ways in the two loading directions, although the detailing was perfectly symmetric. In particular the shear strength recorded in the positive loading direction was surprisingly high in comparison to the other tests (JT3-1 and JT4-1, negative loading direction) and to similar tests available in the literature. For this reason those values are not considered in the further analyses.
- JT2-1 behaved similarly to "2D pre 1970s" up to the 1st joint diagonal cracking. In contrast to "2D pre 1970s" a significant strength increment could be achieved after this event. This difference may be justified by:
    - lack of axial load in the column in the test JT2-1,
    - significantly bigger ending hooks of the beam bars, because of the larger bars diameter (20 mm by JT2-1 vs. 10 mm by "2D pre 1970s"), and
    - different test setup (see Section 5.1.7 for more details)
- The performance of the straight anchorage of the beam bars in the core (test JT3-1) was surprisingly good. No complete pullout occurred and the joint failed in shear with strength comparable to the Types 2 and 6 anchorages.
- In the test JT4-1 the different shear strength and cracking patterns in the joint region due to anchorage of the beam bars Types 1 and 2 were observed confirming observations available in the literature (e.g., *Hakuto et al., 2000* and *Kuang & Wong, 2006*).
- The joint shear distortion, γ_j, appears to be only slightly influenced by the anchorage of the beam bars in the core as shown in Figure 3-12b.

- The initial joint diagonal cracking and the peak load occurred at a range of γ_j between 0.001 and 0.002 rad and 0.05 and 0.015 rad, respectively.

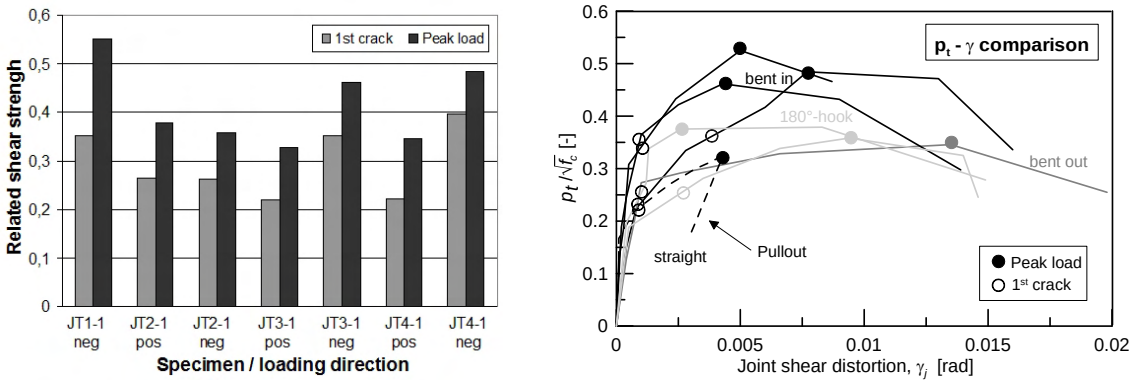

Note: JT1-1-pos is not considered in this comparison
(Smallest related shear strength according to *ACI 318-95* equal to 1.0 assuming no column axial load)

a) Comparison of joints shear strength b) Comparison of joints shear distortion

Figure 3-12: Comparison of tests results of JT1-1, JT2-1, JT3-1 and JT4-1

- The limit state defined as initial diagonal cracking of the joint panel is a crucial event and significantly influences the hysteretic behaviour of subassemblies without transverse reinforcement in the core. After initial cracking the damage and deformation of the specimens start concentrating in the joint region. The joint contribution to the overall deformation of the specimens at increasing drift levels is shown in Figure 3-13. Despite a high scattering of results, on average the joint shear distortion represents approximately 10%, 25% and 40% of the overall deformation at 1.0%, 2.0% and 3.5% top drift level, respectively.

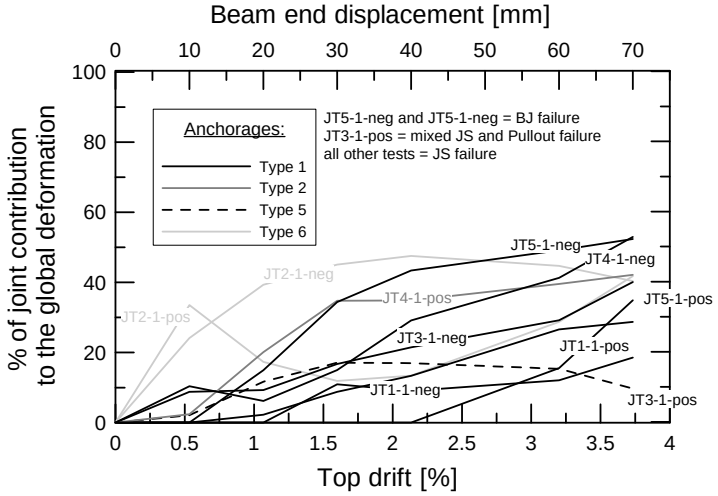

Figure 3-13: Joint contribution to the global deformation

- The test JT5-1 showed that after the formation of the 1st joint diagonal crack, beam flexural hinging does not lead to a ductile plastic mechanism.
- The results of the experimental test highlighted the inadequateness of most of existing joint shear strength model in the assessment of substandard beam-column connections (see Section 3.5.1).

- The validity of the assessment model by Priestley-Pampanin has been confirmed, but a refinement of the model itself to take into account for the influence of other parameters, such as the ratio h_b/h_c is necessary (see Section 3.5).

4 FINITE ELEMENT PROGRAM, MODELLING AND VALIDATION OF THE MODEL

The theoretical background of the non-linear Finite Element (FE) code used for the simulation of the load-displacement behaviour of beam column joints under monotonic and cyclic loading failing in shear is described in Section 4.1. After the presentation of the modelling technique adopted (Section 4.2), the numerical model validation by simulating experimental tests of beam-column connections available in the literature is presented. Joints with various reinforcement detailings exhibiting ductile as well as brittle plastic mechanisms were considered for the validation of the FE model (Section 4.3). As preliminary work for the FE parametric study described in Chapter 5, the experimental tests on as-built joints carried out in this study (Chapter 3) were simulated and the results are compared (Sections 4.3.6 to 4.3.11).

4.1 Non-linear Finite Element code MASA

The FE code MASA (Macroscopic Space Analysis) has been developed at the Institute of Construction Material (IWB) of the University of Stuttgart (*Ožbolt, 1998*). The program can be used for the simulation of three-dimensional (3D) structural elements. Different material models, such as microplane, plasticity and damage type of models are incorporated in the program. The microplane material model is used for the simulation of quasi brittle materials like concrete (*Ožbolt et al., 2001*) (Section 4.1.1). The program has been mainly validated for the simulation of RC members (*Ožbolt et al., 1999*). Damage and fracture phenomena (cracks) are treated in a smeared way (smeared crack approach) (Section 4.1.2).

In the numerical analysis of materials, which exhibit fracture and damage phenomena, such as concrete, a localisation limiter is necessary. A localisation limiter is used to prevent localisation of damage and to limit the dependence of analysis results from the mesh size. In MASA two approaches are used for this: crack band approach and local approach of integral type (Section 4.1.2).

The component to be analysed may be discretised using eight node (hexahedral) or four node (tetrahedral) solid elements (Sections 4.1.1 and 4.2.1). The steel reinforcement can be modelled with 3D elasto-plastic elements (Von Mises model) or one-dimensional (1D) truss element (Section 4.1.3). The bond-slip stress-strain relationship between reinforcement and surrounding concrete can be simulated in a smeared way (a layer of elements with appropriate mechanical properties) or in a discrete way, using the discrete bond model incorporated in the program and briefly presented in Section 4.1.4.

The analysis is incremental and, therefore, the total applied load or displacement has to be divided into a number of increments. Besides static analysis under monotonic loading, cyclic and dynamic analysis can be performed as well. The program can also be used to analyse creep, shrinkage, corrosion and high temperature effects in concrete.

Regarding the global solution strategy, two options are commonly used:

- Constant Stiffness Method (CSM): The stiffness matrix is calculated only at the beginning of each load/displacement step (generally this method has been employed in this study);
- Secant Stiffness Method (SSM): The stiffness matrix is calculated at the beginning of each load step and every 25 iterations (more precise, but more time consuming than CSM).

Further analysis parameters, which may influence the results of the simulation and had to be chosen carefully, are: amplitude of load-displacement steps and convergence criteria (see Section 4.3.1).

The preparation of input data and the display of analysis results were carried out with the commercial pre- and post- processing package FEMAP. In this program the geometry, the mesh (nodes and elements), boundary conditions, loads and material IDs of the model are defined. The material properties, loading history and all the parameters of the numerical analysis are defined through the user interface of MASA. At the end of the analysis the results may be exported to FEMAP for the post-processing and graphic visualisation.

4.1.1 Constitutive law for concrete – Microplane material model

The microplane model is a macroscopic 3D material model. It is particularly suitable for the modelling of damage and fracture phenomena under general state of stress of quasi brittle materials like concrete. *Taylor (1938)* described the idea of defining the inelastic behaviour of various orientations independently within the material. This inelastic effect on all the planes was then superimposed to obtain the plastic strain on the metallic crystals. The generalisation of Taylor's concept was applied to concrete by *Bažant (1984)*. In the microplane model the material is characterised by a relation between stress and strain components on planes of various orientations. The planes represent the damage or weak planes in the macrostructure, such as contact layers between aggregate and cement paste in concrete (Figure 4-1a). *Ožbolt & Bažant (1992)* proposed the microplane model for nonlinear tri-axial behaviour of concrete under cyclic loading and loading rate effect. The model predicted failure and the correct hysteretic loop area with steep initial unloading slope and pinched form of hysteretic loop in shear.

The microplane model incorporated in the FE program, MASA, was proposed by *Ožbolt et al. (2001)*. It is based on the "relaxed kinematic constraint" and it is a modification of the model proposed by *Bažant & Prat (1988)*. It is assumed that the strain components at each microplane are the projections of the macroscopic strain tensor. If the stress-strain relationships of each component of the microplane are known, they can be used for the calculation of the macroscopic stiffness and stress tensor by integrating all the contributions. The stress-strain boundaries under compression are defined on the microplanes separately

for volumetric and deviatoric components (Figure 4-1b). A detailed description of the model can be found in *Ožbolt et al. (2001)*.

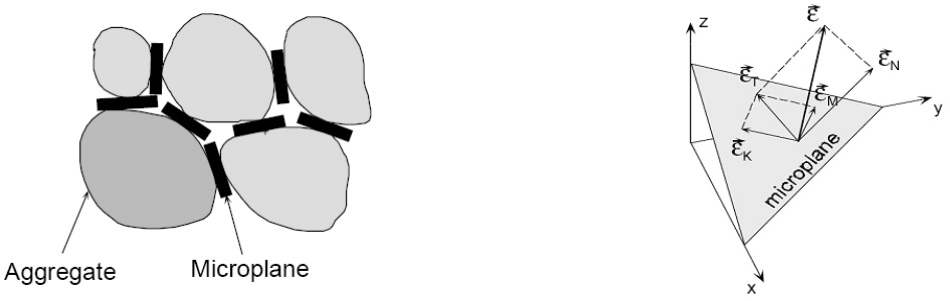

a) Schematic representation of microplanes b) Microplane and strain components

Figure 4-1: Basic concept of microplane material model (*Ožbolt et. al, 2001*)

4.1.2 Crack width localisation limiter

In the classical continuum approach for quasi-brittle materials the softening process due to cracking is very sensitive to the mesh size. In Figure 4-2 this behaviour is schematically shown for two simple FE models (A and B) with the same geometry, but different mesh size.

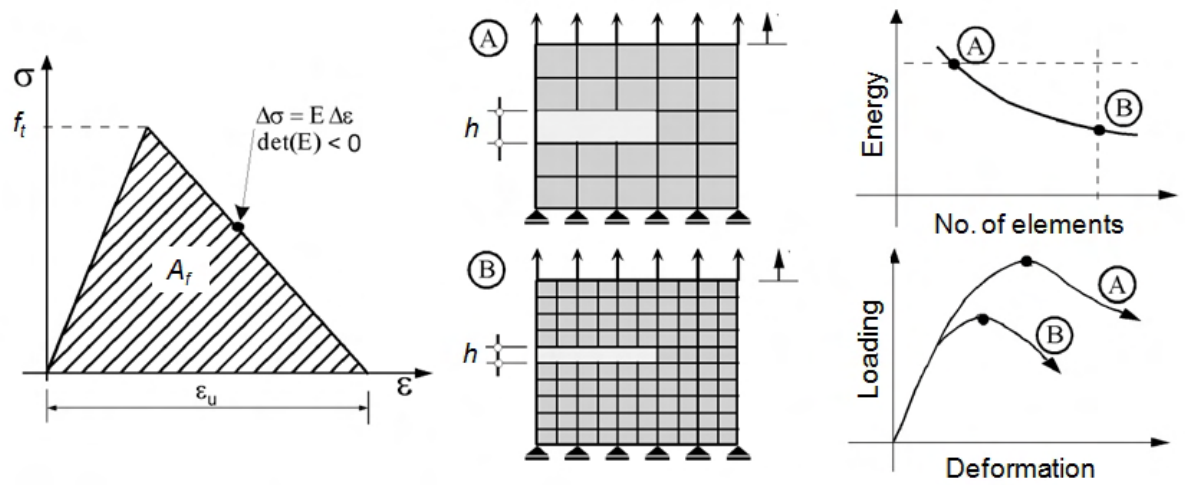

Figure 4-2: Influence of the element size in the continuum analysis (*Bažant & Cedolin, 1979)*

According to *Bažant & Cedolin (1979)* in the case of the more coarse mesh (model A in Figure 4-2) the damaged volume and the resulting dissipated energy is bigger than in the case of a fine mesh (model B in Figure 4-2). Theoretically, if the size of the element is almost zero then the dissipated energy is zero, which is physically impossible. In order to avoid a localisation of the damage and a high sensibility of the analysis to the mesh size a localisation limiter was introduced. Two possible approaches can be used to avoid this problem: “crack band method” (Section 4.1.2.1) and the “nonlocal integral approach” (Section 4.1.2.1).

However, there are still a number of problems, which make the use of these approaches difficult in practical applications for concrete and reinforced concrete structures. The results are generally realistic only for relatively fine meshes in the damaged zone. Consequently, the computational costs are often too high and the approach cannot be used for large

components. An example of different results due to the use of a too coarse model mesh is shown in *Eligehausen et al. (2006b)*.

4.1.2.1 Crack band method

The basic assumption of the crack method is that the damage (crack) is localised in a row of finite elements (*Bažant & Oh, 1983*). In order to keep the energy dissipation, due to the crack opening, constant and independent from the mesh size, the fracture energy has to be kept constant. The softening law has to be modified according to Equation (4-1).

$$G_F = A_f \cdot h = const. \tag{4-1}$$

with:

A_f = Surface under the local stress-strain-curve under tension

h = Size of the element or assumed width of the crack band

The representative size of the element, h, is calculated as $\sqrt{A}$, $\sqrt[3]{V}$, and $1/5\sqrt[3]{V}$ for 2D and 3D hexa and tretra elements, respectively. For this reason in order to minimise the influence of the mesh on the results of the analysis, it is generally suggested regularity for the geometry of the elements (i.e., sides with approximately the same length and no excessive variation of the mesh size between two adjacent rows of elements).

The same approach is used for the softening under compression loading assuming that the fracture energy for compression loading, G_C is equal to $100 \cdot G_F$. In this way the constitutive law is adapted for both one-axial tension and compression.

4.1.2.2 Nonlocal integral approach

The nonlocal integral continuum approach offers the possibility of avoiding spurious mesh dependency in the smeared fracture analysis of quasi-brittle materials. An effective form of the approach is where all variables that control the softening are nonlocal and all others are local (*Pijaudier-Cabot & Bažant, 1987* and *Bažant & Ožbolt, 1990*). The key parameter in this approach is the "characteristic length", l_{ch}. l_{ch} controls the size of the representative volume in which the local quantities are averaged. In the first phase of the development of this approach the characteristic length was assumed to be a material constant. In the case of concrete it was related to the maximum size of the aggregate, d_a, ($l_{ch} = 3d_a$). Recent evidence indicates that l_{ch} also depends on the stress-strain field in the neighbouring area of the cracking zone (*Bažant, 1991*). Therefore, a new nonlocal approach was developed (*Ožbolt & Bažant, 1996*).

This method is more general than the "crack band method" which was used for the analyses in carried out in this study. However, the results are realistic only for very fine meshes. Consequently the computational costs of the "Nonlocal integral approach" are often too high".

4.1.3 Modelling of reinforcement steel

In this work the reinforcement steel was modelled using 1D truss elements. Alternatively, the reinforcement can be modelled using 3D solid elements, but this option was discarded for simplicity of the modelling. The 1D truss elements are able to transfer tension and compression forces, but no bending moment. In such locations of the reinforcement where bending stiffness is required (i.e., anchorage hooks of the beam reinforcement in the joint

region), a flexural rigid connection between the truss elements was defined. The constitutive law used consists of an elastic branch up to the yielding strength, f_y, and a linear behaviour from f_y up to the ultimate strength, f_u. The slope of the two branches gives the elastic modulus, E_s, and hardening modulus, H_s, of reinforcement steel, respectively. After reaching f_u, the steel strain increases at constant stress, i.e., no tensional rupture of the reinforcement steel can be simulated. However, tensional rupture was not required in the present study. The loading-unloading response of the model under monotonic and cyclic loading is shown in Figure 4-3.

A more realistic phenomenological model for steel, which includes: yield plateau, nonlinear strain hardening and degradation of the yield limit as a function of the plastic strain hardening degradation and strain history (Bauschinger effect), was proposed by *Hoehler & Stanton (2006).* This model is also incorporated in MASA. Preliminary FE simulations showed that the use of the constitutive law for reinforcement steel shown in Figure 4-3b instead of the one of Figure 4-3a does not significantly influence the results. This is because the steel usually remains in the elastic range. Furthermore, the calibration of the empirical coefficients of the model by Hoehler and Stanton requires information about the hysteretic behaviour of reinforcement steel which is usually not known.

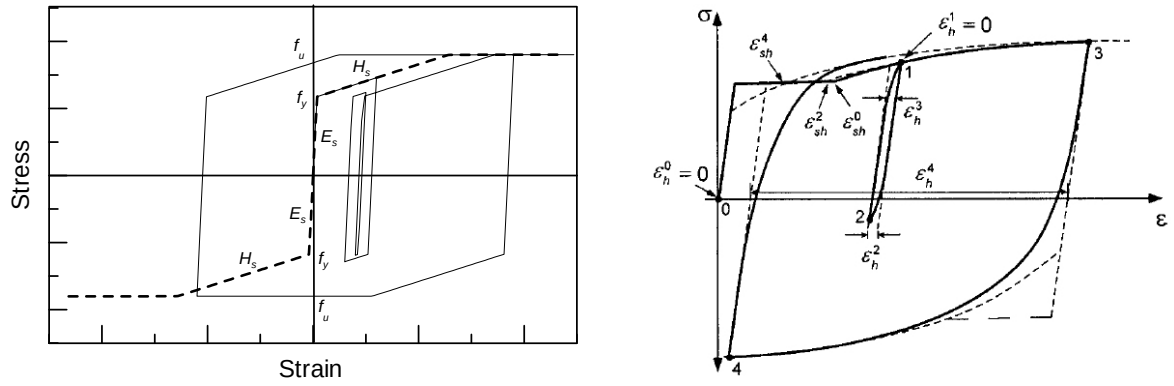

a) three-linear constitutive law b) Hoehler & Stanton model

Figure 4-3: 1D constitutive law for reinforcement steel

4.1.4 Discrete bond model

Two possible strategies can be followed to simulate the bond stress-slip behaviour between reinforcement steel and the surrounding concrete. The bond can be simulated in a smeared way by defining a layer with calibrated material properties. This is the most common method used in Finite Element Analysis (e.g., *Hoehler & Ožbolt, 2001* and *Sagbas, 2007*). In this study a discrete approach was adopted. The bond stress-slip relationship was modelled as shown in Figure 4-4. The discrete bond model defines the bond strength and stiffness as function of the relative slip between the concrete and the reinforcing bar. Two zero thickness spring elements connect the bar element with the surrounding concrete solid elements. The bond elements allow relative displacement between concrete and reinforcement steel only along the axis of the bar element (i.e., in the direction of the slip). The connection of the elements perpendicular to the bar axis is considered perfect (i.e., no slip).

The bond stress-strain relationship for deformed bars under monotonic and cyclic loading is based on the work of *Eligehausen et al. (1983)*. In Figure 4-5a the monotonic bond, τ, and slip, s, relationship of deformed bars is schematically shown. The bond stress is divided into

mechanical (τ_m) and frictional (τ_f) components. Bond degradation is assumed to occur after a critical slip due to the mechanical damage of the concrete-steel interface produced by the ribs of the reinforcement bars. For larger displacement the bond strength is limited to the frictional force. The tangential and radial stresses are generated on the concrete solid elements when the ribbed bar is pulled out from concrete. Experiments showed that under cyclic loading, the bond strength significantly decreases with an increase in the number of cycles (*Eligehausen et al., 1983*). This effect is accounted for in the program by using a factor based on the shear energy dissipation and the area under the monotonic bond-slip curve (*Ožbolt et al., 2002*). The bond stress-slip hysteretic behaviour for deformed bars is qualitatively shown in (Figure 4-5b and Figure 4-6b).

The bond-slip response in MASA is described by 9 parameters (see Figure 4-5a) to account for different geometries (i.e., related rib area). The model takes into account the stress-strain conditions of the reinforcement steel (i.e., decrease of bond strength due to steel yielding) and of the surrounding concrete (i.e., increase of bond strength due to compression of the concrete). For further information, refer to the discrete bond model by *Ožbolt et al. (2002)* and *Lettow, (2006)*. In this study the bond-slip parameters for deformed bars proposed by *Lettow (2006)* were used.

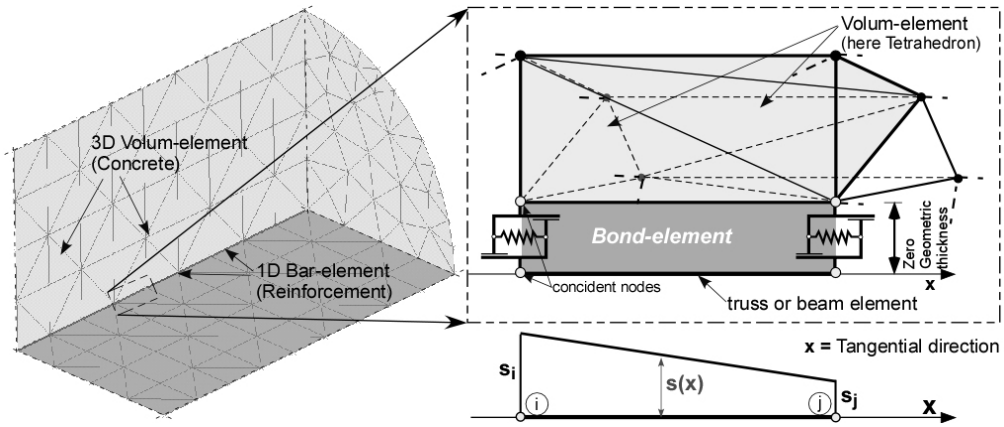

Figure 4-4: Implementation of the discrete bond model in MASA (*Lettow, 2006*)

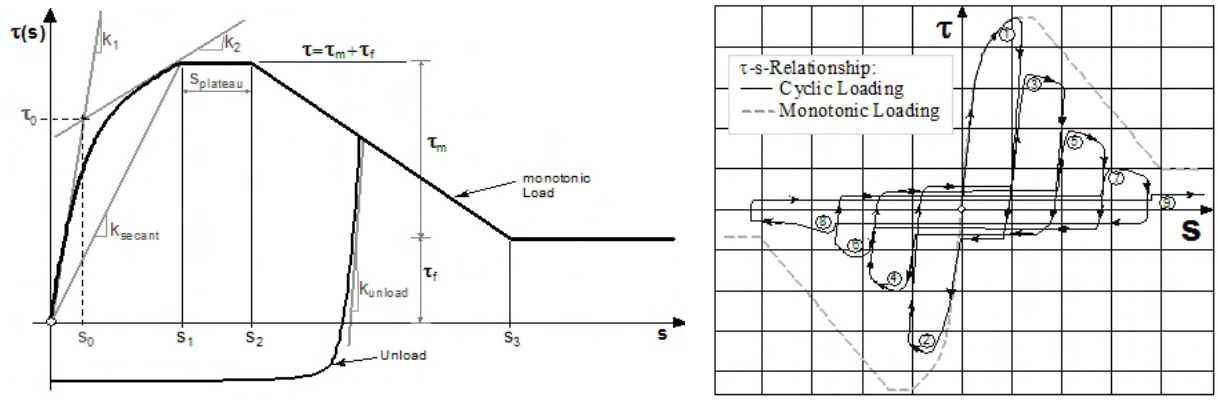

a) Monotonic (*Lettow, 2006*) c) Cyclic (*Eligehausen et al., 1983*)

Figure 4-5: Bond stress-slip relationship for deformed bars

The discrete bond model was also employed for the simulation of bond stress-slip behaviour of plain round bars. Only a few tests on the bond stress-slip behaviour of plain round bars are available in the literature. In this study the beam tests according to *Rilem (1982)* by

Fabbrocino et al. (2002) are considered for the calibration of the discrete bond model of smooth bars (Figure 4-6a).

The shape of the bond stress-slip curves obtained by *Fabbrocino et al. (2002)* can be fairly reproduced using the parameters of the discrete bond model in MASA (compare Figure 4-5a and Figure 4-6a). However, the physical rationale of the decomposition of the bond stress (τ_m + τ_f) is different. In the case of plain round bars no mechanical interlock of ribs can be activated. In the tests by *Fabbrocino et al. (2002)* an initial stiff branch can be observed before the activation of the frictional stress (Figure 4-6a). This can be interpreted as the initial adhesion. The initial adhesion is characterised by a very high stiffness, approximately 5-times the initial stiffness assumed for deformed bars. For the frictional resistance a much lower value should be assumed, i.e., approximately 1/5 to 1/10 of the strength adopted for deformed bars. Figure 4-6b shows a comparison between the bond stress-slip relationships of 12 mm dia. deformed and plain round bars embedded in concrete with f_c = 20 MPa. It is worth noting that it can be assumed that the bond stress-slip behaviour is not related to the concrete strength. This is contrary to the case of deformed bars, since no damage of concrete may occur by pulling out the reinforcing bars.

The cyclic behaviour of plain round bars is assumed to be qualitatively similar to the one assumed for deformed bars. *Braga et al. (2001b)* proposed that the hysteretic bond stress-slip curve should have the monotonic relationship as backbone curve without exhibiting strength degradation as in Figure 4-5b, since no damage of the concrete-steel interface occurs.

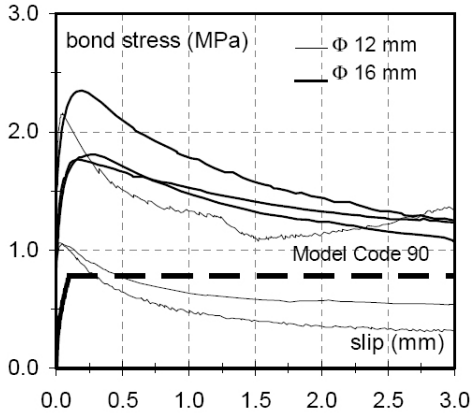

a) Results of the tests by *Fabbrocino et al. (2002)*

Parameter		Deformed bar	Plain round bar
τ_m	[MPa]	6.4	0.5
τ_f	[MPa]	4.3	0.5
k_1	[N/mm^3]	28.6	100
k_{sec}	[N/mm^3]	13.0	80
k_2	[N/mm^3]	1.0	10
k_{unload}	[N/mm^3]	28.6	100
s_1	[mm]	0.82	0.01
s_2	[mm]	1.6	0.1
s_3	[mm]	8.5	1.0

b) Bond parameters for 12 mm bars (f_c = 20.0 MPa)

Figure 4-6: Bond stress-strain relationship for plain round bars

4.2 Finite element analyses

The FE Code MASA was employed for the simulation of exterior RC beam-column connections. Preliminary numerical investigations were carried out to assess the suitability of the modelling principles (Section 4.2.1) to realistically reproduce the mechanical behaviour of the RC beam-column joints (Sections 4.3.1 to 4.3.5). Second, the model was verified on some of the experimental tests described in Chapter 3 (Sections 4.3.6 to 4.3.10). The verified models ware used to carry out a parametric study to evaluate the influence of several parameters on the load carrying capacity and deformability of beam-column joints failing in shear (Chapter 5).

4.2.1 Modelling and discretisation

The concrete was discretised by eight nodes 3D hexahedral elements. Since the increase in the number of nodes increases the computational time and cost (i.e., the equilibrium conditions must be satisfied for a larger amount of nodes), a relatively fine mesh was adopted in the joint region using approximately cubic elements with 20 mm side length (Figure 4-7). A coarser mesh with elements with side lengths up to 100 mm and geometric aspect ratios up to 2.5 (i.e., length / height of the element) was adopted in those portions of beam and column where the concrete was supposed to remain elastic during the entire loading history (Figure 4-7).

The reinforcement and the bond stress-slip relationship between steel and concrete were modelled according to the principles explained in Sections 4.1.3 and 4.1.4, respectively.

A rigid connection was adopted between transverse reinforcement (i.e., stirrups) and concrete elements, i.e., the influence of the relative displacement between stirrups and concrete was considered negligible. The stirrups were modelled as “perfectly closed”, since no stirrups opening was aimed to be simulated.

Load and boundary conditions schematically shown in Figure 4-7, were applied as nodal loads and constraints in the FE model. To prevent local failure of the concrete elements due to the concentration of high stress in the vicinity of the supports and at the point of application of axial and lateral load, the concrete behaviour was assumed as linear elastic (darker elements in Figure 4-7). In the analyses the vertical symmetry plane of the specimen was utilised, i.e., only one-half of the specimen was modelled. On the plane of symmetry the nodes displacement was constrained in the y-direction.

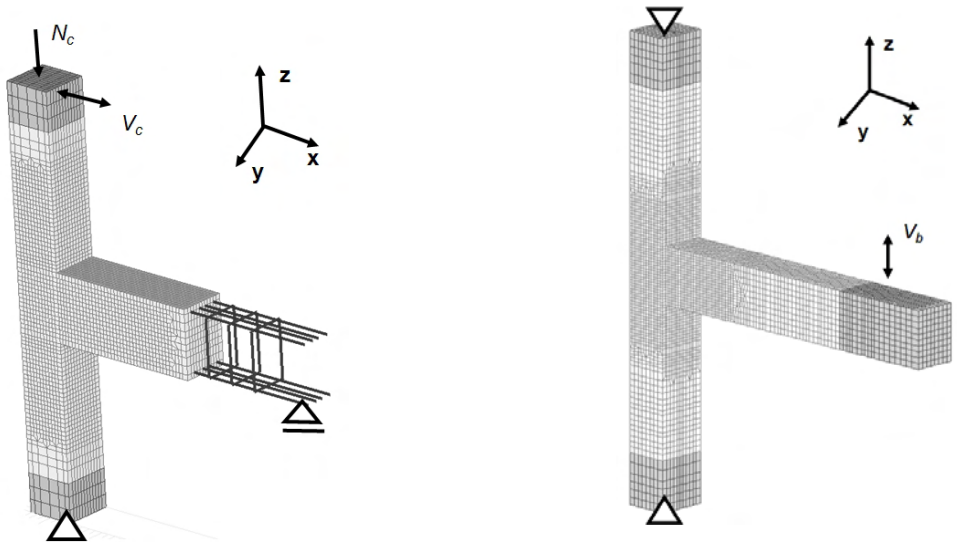

a) Model of the UC specimen b) Model of the BARC specimen

Figure 4-7: Modelling of UC and BARC specimen (utilisation of symmetry plane not shown)

The modelling of the anchorage of the beam longitudinal reinforcement was very important, since the model needed to realistically take into account its effect on the joint shear strength that was evidenced in the experimental investigations (see Chapter 3). The round bending of

reinforcement bars was simplified with diagonal elements. Two different approaches were employed and their efficiency was validated:

- imposition of bending stiffness of the diagonal reinforcement truss elements representing the bending of the bars (Figure 4-8a) (method used for the simulation of the UC specimens); and
- definition of the concrete elements surrounding the bending of the reinforcement as linear elastic (Figure 4-8b) (method used for the simulation of the BARC specimens).

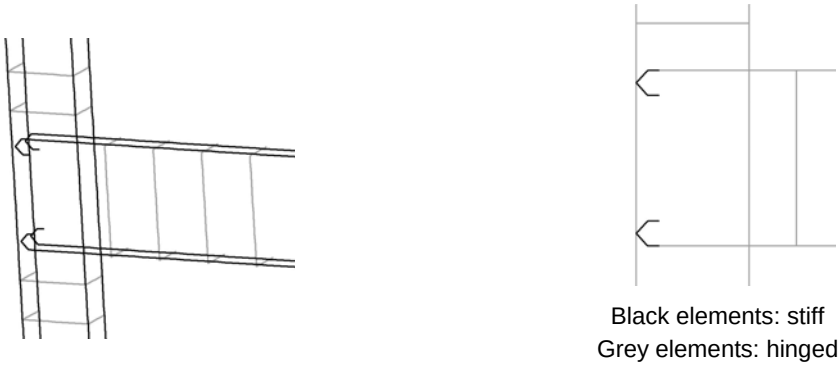

a) Modelling of Reinforcement and of bending of anchorages (Specimen UC, half specimen shown only)

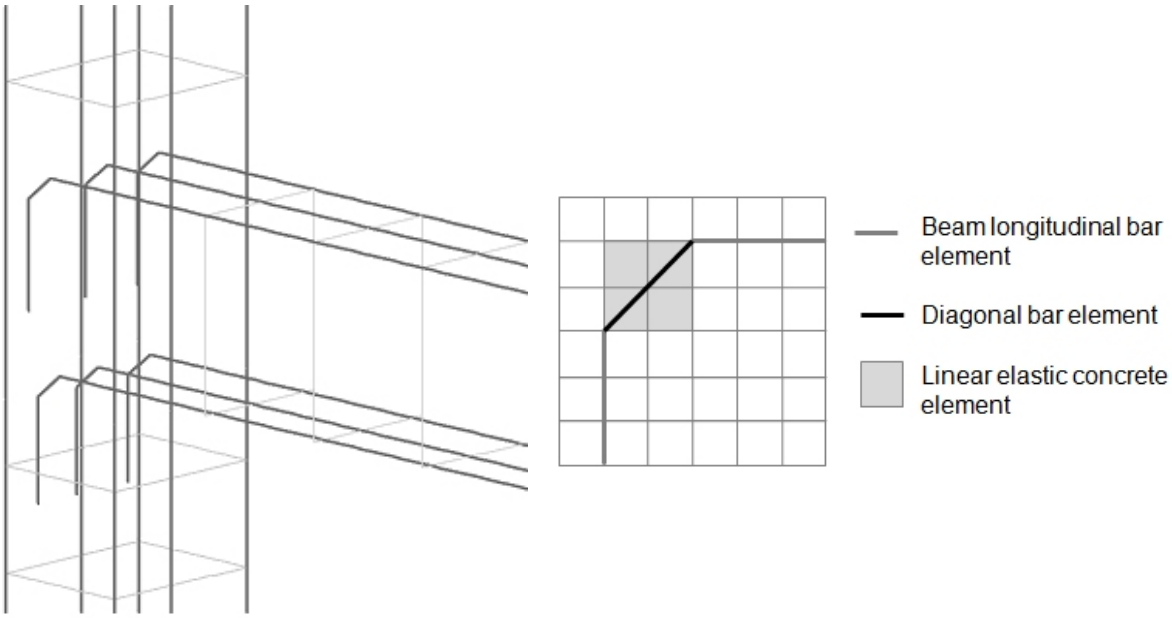

b) Modelling of Reinforcement and of bending of anchorages (Specimens BARC)

Figure 4-8: Details of the modelling of the reinforcement bending

4.3 Verification of the finite element model

In the following sections the adopted FE model is verified. The possible sources of errors and uncertainties in the numerical simulation results are evaluated (Section 4.3.1). The mechanic that governs the shear behaviour of the joint is shown by plotting the principle stresses and strain fields in the joint panel (Section 4.3.2). The reliability of the model to reproduce joint shear behaviour under different conditions of loading and reinforcement detailing is necessary for the parametric study presented in Chapter 5. In Section 4.3.3 the relevance of the modelling of the bond-stress slip relationship between reinforcing steel and concrete is

discussed. The ability of the model to distinguish different failure modes was also assessed by investigating the interaction with the beam flexural failure (Section 4.3.4). The results of tests available in the literature including joints with various reinforcement detailings and failure modes were reproduced (Section 4.3.5).

4.3.1 Sources and evaluation of errors

To evaluate the quality and reliability of the numerical simulation it is necessary to identify the possible sources of errors. They may be grouped in three categories: (i) modelling, (ii) materials and (iii) numerical calculation.

4.3.1.1 Modelling

The major sources of errors in the modelling are related to the high concentration of stresses at the interface of different materials such as between steel and concrete at the anchorages of the beam bars in the joint core. As already mentioned in Section 4.1.2, the analysis results are approximately mesh independent only if the element dimension is small enough in the zones where the damage (cracking) occurs. Furthermore, experience has shown that mesh regularity, such as gradual variation of element size, and a small ratio between the sides of the 3D elements, reduces the error. Errors can also arise if the application of constraints and loads does not closely correspond to the conditions of the tests. Commonly, the first ascending branch of the load-displacement curve of the numerical simulation results is stiffer than in the one of the experimental tests. The main reason for this difference is the idealisation of the boundary conditions of the specimen in the numerical modelling.

4.3.1.2 Materials

The material properties used in the numerical simulations are the same as measured in the tests. However, some material properties required for the input of the FE analysis are not usually measured in experimental practice. These are:

- Young's modulus of concrete, E_c;
- concrete tensile strength, f_{ct} (which may vary significantly also within a concrete member);
- concrete fracture energy, G_F; and
- bond properties (especially in the case of plain round bars where there is a lack of available experimental investigations on the bond stress-slip relationship).

Preliminary monotonic analyses using the model of the "2D pre 1970s" specimen (Section 4.3.6) were carried out to evaluate the influence of the above parameters. Young's modulus of concrete, E_c, has a minor influence since the notable non-linearity of concrete behaviour is mainly due to the cracking (Figure 4-10a). The scattering of the concrete tensile strength influences the joint behaviour more significantly. As shown in Figure 4-10b, f_{ct} has an influence on the shear strength and on the post-peak behaviour of the specimen. In this study, when no direct measurements were available, the value of f_{ct} was assumed to be dependent on f_c according to the Heilmann's formula adopted in the CEB-FIB Model Code 1990 (*CEB, 1993*) (Eq. (4-2)).

$$f_{ct} = 0.3 f_c^{2/3} \tag{4-2}$$

The fracture energy of the concrete, G_F plays a major role in the adopted damage model and specifically in the "Crack Band Method" used as localisation limiter (see Section 4.1.2.1). For the calculation of G_F the formula proposed by the CEB-FIB Model Code 1990 (*CEB, 1993*) can be used (Eq. (4-3)).

$$G_F = G_{F0}\left(f_c / f_c^0\right) \tag{4-3}$$

with:

f_c^0 = 10 Mpa

G_{F0} = 0.025, 0.030, 0.058 for maximum aggregate diameters $d_{a,max}$ = 8, 16, 32 mm, respectively

Equation (4-3) does not take into account the influence of several other parameters, which significantly affect the fracture energy of concrete such as the mechanical properties and shape of the aggregates. The high variability of experimental measurements of fracture energy of concrete is shown in Figure 4-9. Furthermore, tests by *Remmel (1994)* evidenced that Equation (4-3) may underestimate the value of G_F for low and normal strength concrete (see Figure 4-9b) and proposed another formula valid for $d_{a,max}$ = 16 mm (Eq. (4-4)).

$$G_F = 0.065 \cdot \ln\left(1 + f_c / f_c^0\right) \approx 0.0307 \cdot f_{ct} \tag{4-4}$$

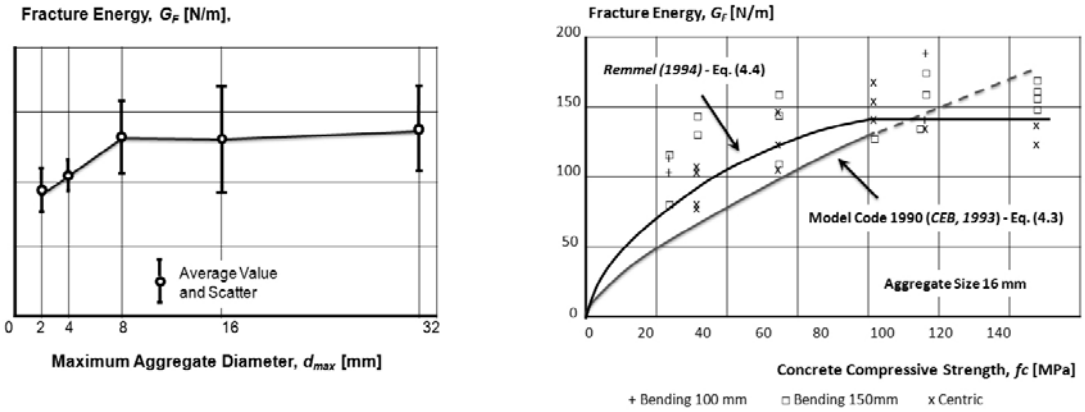

a) Influence of aggregate size (*Wolinski et al., 1987*) b) Influence of f_c (*Remmel, 1994*)

Figure 4-9: Variability of fracture energy of concrete

Figure 4-10c shows that the variation of the fracture energy has a not negligible influence on shear strength and on the post peak behaviour of the specimen.

The calibration of the bond model is based on extensive data on deformed bars (*Eligehausen et al., 1983* and *Lettow, 2006*) and limited experimental investigations for plain round bars (*Fabbrocino et al., 2002*). In Figure 4-10d,e the main bond parameters (i.e., stiffness and strength) have been varied to investigate the sensitivity of the specimen response. While the bond stiffness does not appear to have a significant influence on the joint response (Figure 4-10d), with increasing bond strength the joint shear capacity also increases (Figure 4-10e). Due to the difficulty of verifying these results for the bond calibration the parameters established by *Fabbrocino et al. (2002)* were used.

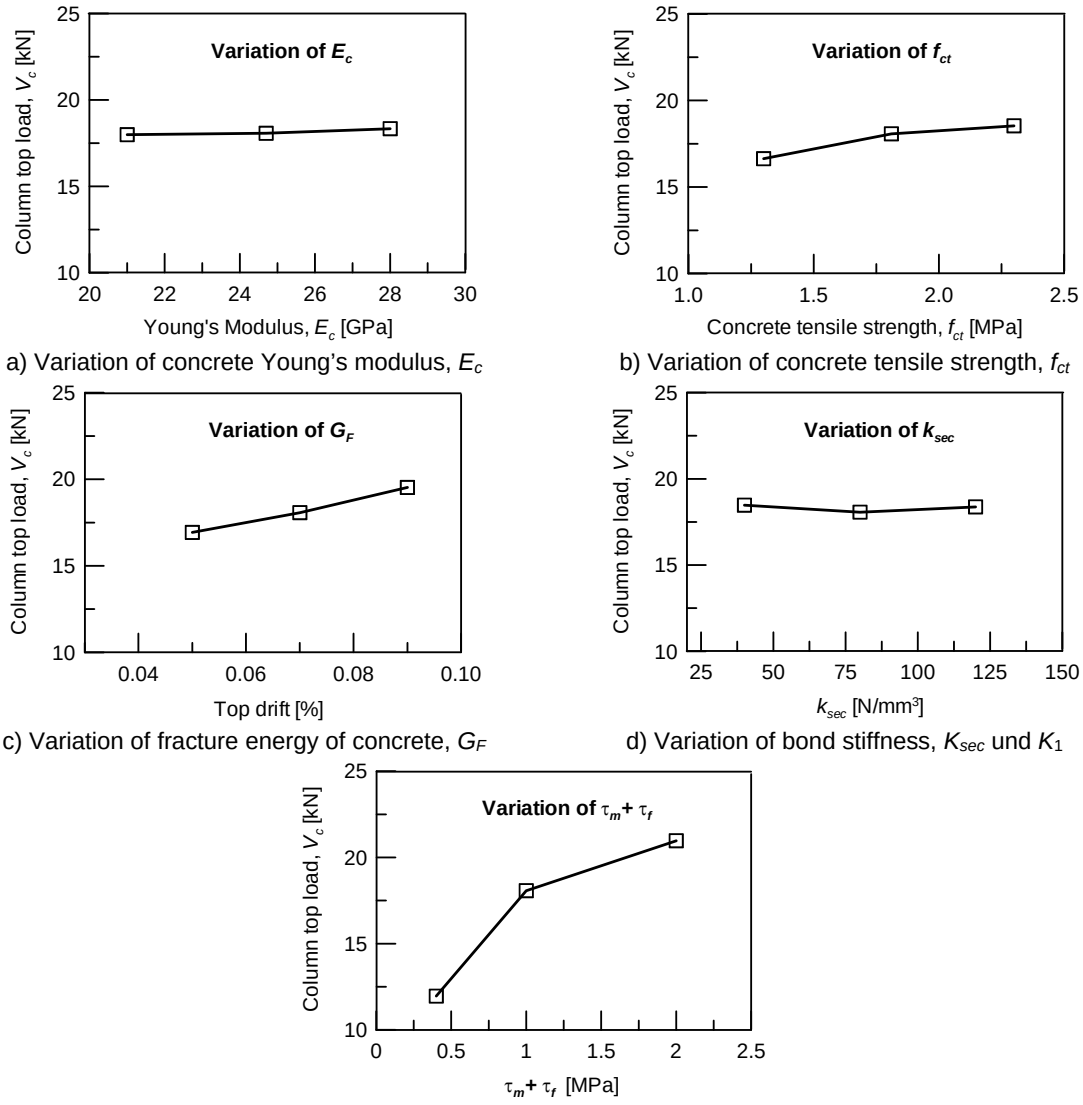

a) Variation of concrete Young's modulus, E_c

b) Variation of concrete tensile strength, f_{ct}

c) Variation of fracture energy of concrete, G_F

d) Variation of bond stiffness, K_{sec} und K_1

e) Variation of bond strength

Figure 4-10: Sensitivity analyses on the "2D pre 1970s" model

4.3.1.3 Numerical calculation

The RC specimen was loaded by incremental displacement steps. At each loading step the force equilibrium in each node of the model had to be established. The accuracy of the results is highly dependent on the length of the displacement steps. The calculation method for the stiffness matrix, the number of iterations to reach the equilibrium and the limit of the iteration criteria also influence the results. The convergence criterion has to be met for each node and element of the model according to Equation (4-5).

$$tol = \sqrt{\sum_{i=1}^{n} R_{residual,i}^2 \Big/ \sum_{j=1}^{m} R_{load,j}^2} \tag{4-5}$$

with:

$R_{residual,I}$ = Reaction force in the element i

$R_{load,j}$ = Load in the node j

4.3.2 Simulation of the mechanics of shear failure of exterior joints

The basic mechanics of exterior RC beam-column joints have been presented in Section 2.2. Generally, it is not possible to obtain from experimental tests a clear image of the stress-strain distribution in the joint panel, mainly due to the difficulty of measuring stress and strain field of a concrete region. Stresses and strains can be indirectly evaluated from stress strain distribution in the reinforcement and global deformations, which are easier to measure. The FE analysis offers the opportunity to visualise the development of the stress-strain distribution in the joint region that leads to diagonal cracking and shear failure of the joint.

In Figure 4-11 typical tensile (σ_{11}) and compressive (σ_{33}) stress fields are shown at three loading stages for a specimen with beam bars anchored with 90°-bent in hooks in the joint region: (i) flexural cracking in the beam and joint region uncracked, (ii) initial shear cracking of the core, (iii) peak load. Furthermore, the principle tensile strains (ε_{11}), which represent the corresponding cracking pattern, are also shown. The contour levels adopted in Figure 4-11 go from clear grey to black with increasing stress, where $\sigma_{11,max} = f_{ct}$ and $\sigma_{33,max} = f_c$. The strain level, ε_{11}, corresponding to the formation of a macrocrack (i.e., visible crack of approximately width, w = 0.2 mm) is 1.0% and at that level and above the element's contour is black.

As long as the joint region is uncracked (Figure 4-11g), the tensile stresses are transferred through the entire panel (Figure 4-11a). After reaching the concrete tensile strength the 1st diagonal crack starts (Figure 4-11b,h). After this event the tensile stresses need to find an alternative path to enable the beam-column connection to further transfer the shear through the core. In the absence of transverse reinforcement, the only possibility is the utilisation of the pullout strength of the longitudinal beam bars (Figure 4-11c,f). Therefore, the anchorage detailing of the beam bars in the core influences the joint shear strength significantly as observed in the tests shown in Chapter 3. The strut responsible for the transfer of the compression stress is shown in Figure 4-11d. At the formation of the first diagonal crack the strut is weakened and split into two thinner struts (Figure 4-11e,f). The numerical analysis shows that at the peak load one of the struts starts crushing (Figure 4-11f).

The axial load in the column also plays a central role. With increasing axial load the tensile tie is unloaded, but the strength demand in the compressive strut increases. The evaluation of these opposed effects is discussed in the parametric study presented in Chapter 5.

The limit states of the 1st shear cracking and peak load correspond to the failure of the tensile tie and compressive strut, respectively. Theoretically, it is also possible that the first event is the failure of the compressive strut with consequent crushing of the concrete, but it is highly improbable for exterior joints, because of the low axial load.

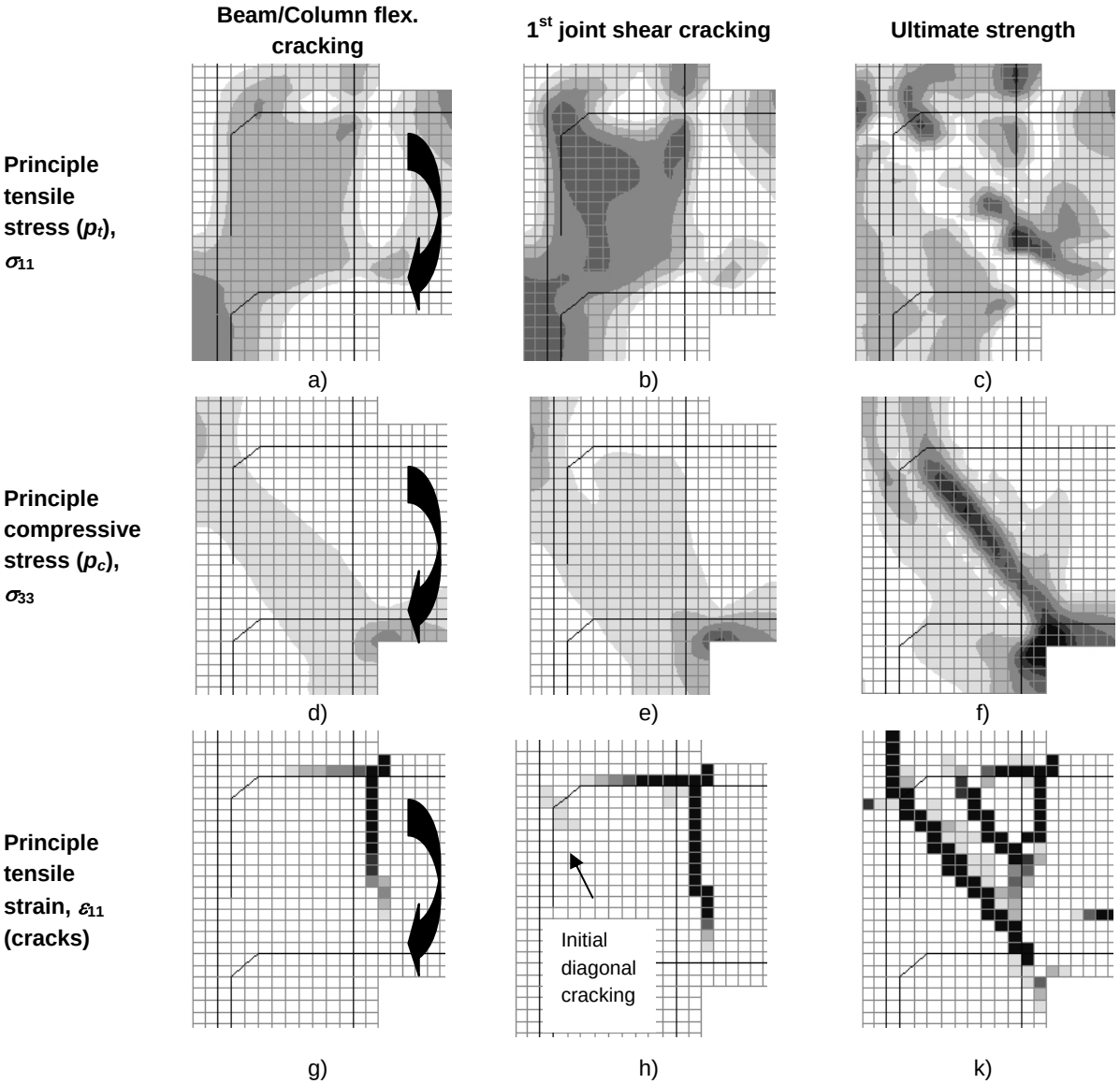

Figure 4-11: Stress and strain fields in the joint core from FE analysis (anchorage Type 1)

In the case of cyclic loading, the diagonal cracking of the joint panel in one loading direction does not theoretically have any influence on the development of stress-strain fields in the opposite direction, because the existing crack is parallel to the direction of p_t. Therefore, for joints with symmetrical reinforcement detailing and boundary conditions the same shear strength in both loading directions may be expected. The difference between the theoretical behaviour presented here and the collection of experimental observations in the literature, is discussed in Chapter 6.

For comparison, the distribution of σ_{33} and ε_{11} is also shown for joints with deformed bars with 90°-hooks bent away (Type 2) in Figure 4-12. Similar to what was observed in the experimental tests, the anchorage Type 2 induced a different inclination of the strut (compare Figure 4-12a with Figure 4-11f) and of the crack (compare Figure 4-12b with Figure 4-11k). As already discussed in Chapter 3, the form, inclination and thickness of the struts depend

on the geometric aspect ratio of the joint panel and the detailing of the anchorage of the beam bars.

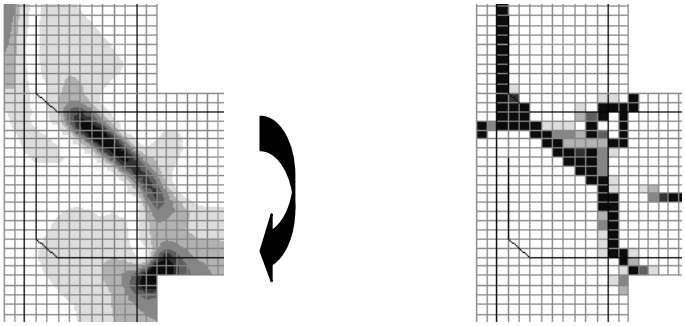

a) Principle compressive stress (p_c), σ_{33} b) Principle tensile strain, ε_{11} (cracks)

Figure 4-12: Stress and strain field in the joint core from FE analysis (anchorage Type 2)

In Figure 4-13 a schematic summary of the observations from the numerical simulation is shown. A typical load-displacement curve (or the backbone curve of the hysteretic loops) for exterior joints without transverse reinforcement is idealised in Figure 4-13a. The initial stiffness decreases with increasing flexural cracking in the beam and column. The 1st diagonal crack in the joint is generally followed by a loss of resistance, but after maximum 1-2 mm of displacement the strength increases again up to the peak load. The post-peak branch is generally very steep denoting the brittleness of the failure mode. Up to the formation of the 1st joint shear crack the SAT scheme shown in Figure 4-13b is valid. After this event the concrete strut is dived in 2 or more thinner struts. The peak load corresponds to the crushing of the weakened concrete strut (darker strut in Figure 4-13c) or with the pullout of the beam longitudinal reinforcement from the joint core, if the anchorage is insufficient to transfer the tension forces to reach another failure mechanism. The Strut-And-Tie (SAT) mechanism observed in the FE analysis is presented in Figure 4-13b,c.

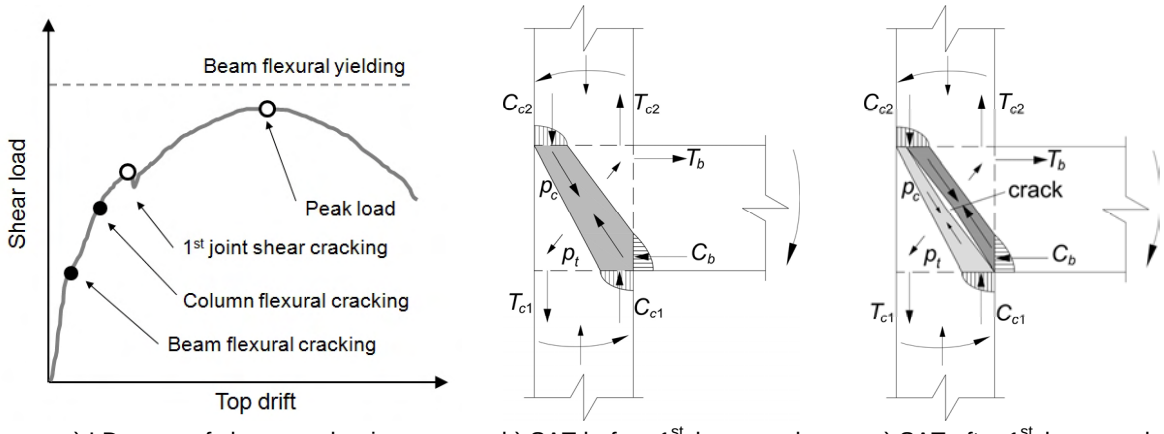

a) LD curve of shear mechanism b) SAT before 1st shear crack c) SAT after 1st shear crack

Figure 4-13: Schematic representation of shear behaviour of exterior RC joints

It would be reasonable to consider p_t as an index for the joint cracking and p_c for the ultimate strength. The evaluation of p_c is difficult because of the uncertainties in the determination of the form and inclination of the strut after cracking of the core (compare Figure 4-11f and Figure 4-12a). Therefore, this approach is disregarded in this study.

4.3.3 Relevance of simulation of bond between reinforcing steel and concrete

Preliminary numerical analyses evidenced the importance of the modelling of the bond between reinforcing steel and concrete for a realistic simulation of exterior beam column joints. The following aspects have been observed:

- in the case of plain round bars, neglecting of the influence of bond effect (perfect connection between steel and concrete) generally induces a significant overestimation of the joint shear capacity and in the worst case the prediction of a more ductile failure mode (*Eligehausen et al., 2009*). Figure 4-14 shows the analysis results with and without modelling of bond in the case of joint with plain round bars (see test 2DP2 in Section 4.3.5 for experimental results);
- for the cyclic simulation of beam-column joints with plain round bars, the approaches of *Eligehausen (1983)* and *Braga et al. (2001b)* led to similar results (*Eligehausen et al., 2006b*);
- in the case of deformed bars, the assumption of a perfect connection between steel and concrete leads to a slight overestimation of the ultimate strength if compared to the use of the discrete-bond model (*Sharma et al., 2009*); and
- the use of the discrete bond model generally leads (for both deformed and plain round bars) to a more realistic cracking pattern and post-peak behaviour especially under cyclic loading (*Lettow, 2006*; *Eligehausen et al., 2009* and *Sharma et al., 2009*).

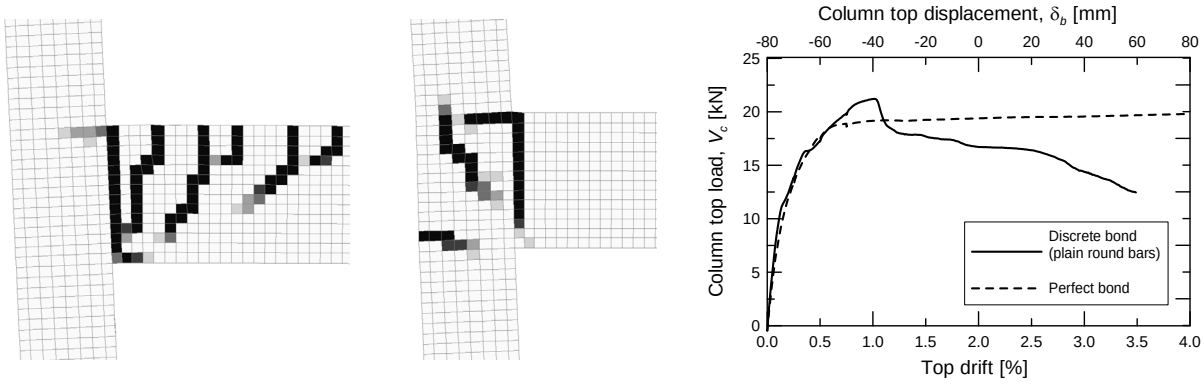

a) Cracking pattern with perfect bond

b) Cracking pattern with discrete bond model

c) Comparison of load-displacement curves

Figure 4-14: Investigation of influence of bond modelling for joint with plain round bars

4.3.4 Interaction of failure modes

In the context of the seismic assessment of a moment resisting frame, and more specifically of an exterior beam-column joint, the evaluation of the strength and deformability should be accompanied by the estimation of the ductility of the expected plastic mechanism. It is not the objective of this work to provide values of expected ductility, but to predict with reasonable confidence the failure mode which will most probably occur. In this context, the concept of hierarchy of strength based on the capacity design of RC structures, as introduced by *Paulay & Priestley (1992)* and formalised for the assessment beam-column joints by *Pampanin (2006),* shown in Section 2.1.3, is adopted. The first step for the design of the retrofit solution is to establish, if the as-built joint would exhibit a ductile (i.e., beam flexural hinging) or brittle (i.e., joint, beam and column shear failure, and column flexural

hinging) plastic mechanism. Experimental results available in the literature, as well as the test JT5-1 (Section 3.4.6), have shown that the flexural yielding of the beam does not usually lead to the formation of a ductile plastic mechanism if it is accompanied by joint shear cracking. Some authors proposed a formulation of joint shear degradation as a function of beam ductility (*Park, 1997* and *Hakuto et al., 2000*).

Figure 4-15 shows the variation of the beam flexural capacity of the FE model for specimen JT1-1. Four cases can be distinguished:

(1) joint shear failure without yielding of the beam bars (JS);
(2) beam flexural yielding after 1st shear cracking of the joint and successive brittle behaviour (BJ1);
(3) beam flexural yielding followed by joint shear cracking and successive loss of strength (BJ2); and
(4) beam flexural failure (B).

The load-displacement curves in Figure 4-15a confirm that the beam flexural yielding does not guarantee a ductile behaviour of the beam-column connection if the joint becomes inelastic before the top drift target is reached. The influence of the joint shear deformation, γ_j, is confirmed in Figure 4-15b. There it is shown that specimens with lower joint deformation exhibit a more ductile behaviour (compare Figure 4-15a and Figure 4-15b).

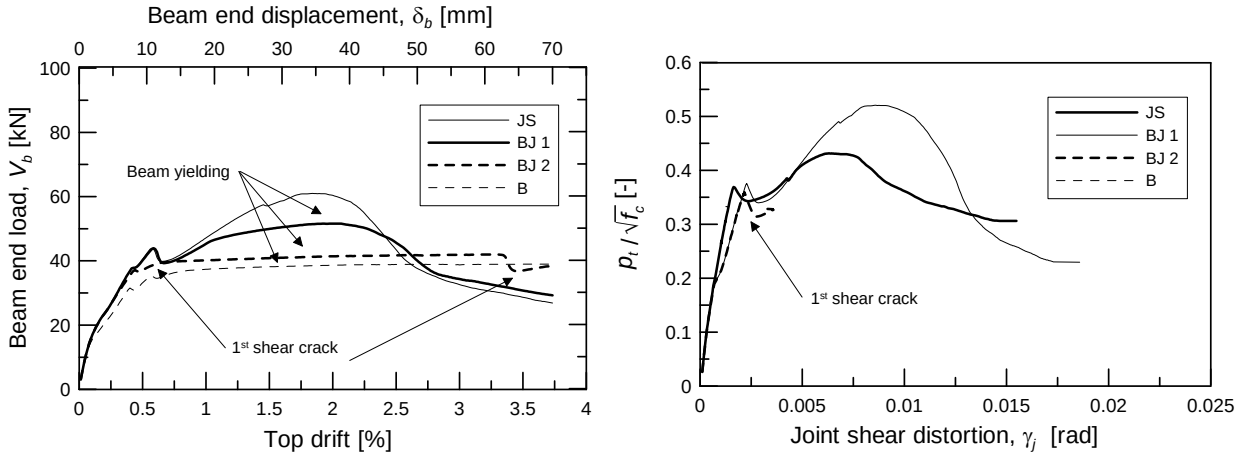

Figure 4-15: Interaction between beam flexural yielding and joint shear failure – FE simulations

The numerical and experimental investigations carried out in this study suggest that two cases may be distinguished:

- flexural yielding of the beam before joint shear cracking → ductile behaviour; and
- flexural yielding of the beam after joint shear cracking → brittle behaviour.

The numerical simulations indicate that the yielding of the beam bars at the beam-column interface negatively influence the joint shear strength. This is mainly because of strain penetration and the consequent increase of the tensile force transmitted directly by the hooked anchorage rather than being transferred by the concrete-reinforcement bond stress. In Figure 4-16 the tensile stresses in the longitudinal beam bars of two specimens with different curvature ductility, μ_ϕ, (2.0 vs. 7.7) are shown. The specimen with lower μ_ϕ exhibited

a strain penetration length, L_{sp}, of approximately 80 mm (Figure 4-16a). The specimen with $\mu_\phi = 7.7$ exhibited $L_{sp} \sim 220$ mm (Figure 4-16b). The specimen with lower μ_ϕ exhibited a higher ratio $p_t/\sqrt{f_c}$ (0.443 vs. 0.381).

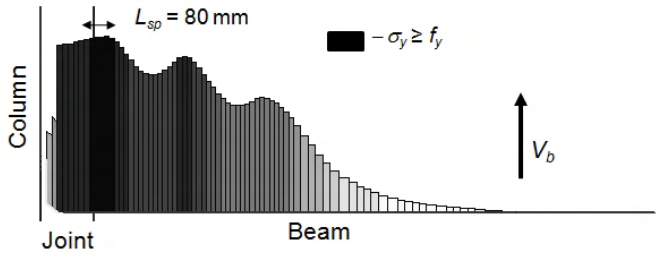

a) Specimen with $\mu_\phi = 2.0$ and $p_t/\sqrt{f_c} = 0.443$

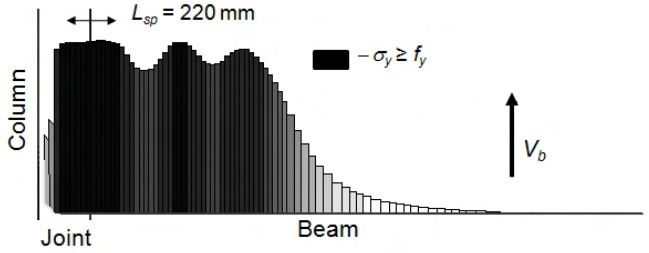

b) Specimen with $\mu_\phi = 7.7$ and $p_t/\sqrt{f_c} = 0.381$

Figure 4-16: Effect of strain penetration and ductility on joint shear strength

The negative effect of strain penetration due to the formation of plastic hinge in the beam on the effective anchorage length of the beam bars in the joint is taken into account by some code provisions, e.g., *NZS 3101:1995* and *EC8-1 (2004)*. According to both these codes the anchorage length has to be measured at a certain distance from the column face, which is a multiple of the bars diameter (see Table 2-5).

4.3.5 Preliminary analyses

The suitability of FE code MASA and of the proposed modelling approach for the simulation of monotonic and cyclic behaviour of beam-column joints failing in shear was verified by several studies (e.g., *Eligehausen et al., 2006b* and *Eligehausen et al., 2009*). In the framework of this study the suitability of the model to simulate different failure modes and the influence of different detailing solutions, such as deformed or plain round bars and different anchorage types (Types 1 and 6), was investigated. The need of these preliminary investigations is clearly given in the frame of the parametric study (Chapter 5) in order to relate the obtained results to the corresponding failure mode. The experimental tests by *Hertanto (2005)* were considered as benchmark. In Table 4-1 the main material properties of the test specimens (also used for the numerical simulations) are listed.

Table 4-1: Material properties of the specimens tested by *Hertanto (2005)*

Test	h_b/h_c [-]	f_c [MPa]	ρ_b / ρ'_b [-]	ρ_c [-]	N_c [-]	Rein. type	Anchorage type	f_y [MPa]	Failure mode
TDD1	1.43	23.3	0.26/0.51	0.50	Var.	Deformed	90° bent in	324	B
TDD2	1.43	24.7	0.51/0.77	0.50	Var.	Deformed	90° bent in	354	JS
TDP2	1.43	25.0	0.51/0.51	0.50	Var.	Plain round	180° hook	333	JS

In Figure 4-17 the results of the analysis of the specimen TDD1 (deformed bars and anchorage Type 1) are shown. The hysteretic behaviour (Figure 4-17a) as well as the

cracking pattern (Figure 4-17b) were realistically reproduced. The observed failure mechanism consisted in the formation of a plastic hinge in the beam in both loading directions.

Figure 4-18 shows the results of the simulation of specimen TDD2. The beam reinforcement consisted also of deformed bars bent into the joint with anchorage Type 1. However, the reinforcement ratio, ρ_b, was about twice as high as in TDD1. The observed plastic mechanism was joint shear failure with strength degradation after the peak load, high pinching of the hysteretic behaviour and consequently with lower energy dissipation compared to TDD1. The behaviour of the specimen TDD2 in the negative direction was expected to be similar to TDD1 in the positive direction because of the same amount and strength of beam longitudinal reinforcement (see Table 4-1). However, the yielding of beam bottom bars observed in the FE analysis induced a more ductile behaviour than in the experimental test, where the specimen failed before reaching the beam flexural yielding strength.

The test specimen TDP2 contained plain round beam bars anchored by 180°-hooks in the joint (Type 6). As shown in Figure 4-19, the specimen failed by joint shear cracking, which induced a brittle behaviour of the specimen with significant strength reduction after peak load and low energy dissipation. In the tests TDD2 and TDP2 the positive effect of the axial load on the joint shear strength was correctly simulated. It was observed that in both cases the peak load was higher in positive than in the negative loading direction, because of the favourable influence of the increase in axial load.

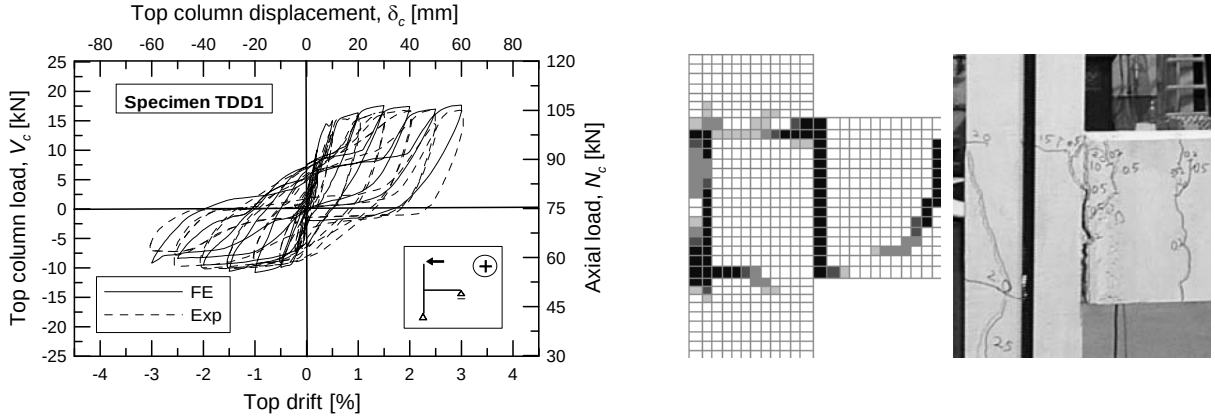

a) Hysteretic behaviour b) Cracking pattern

Figure 4-17: Validation of the FE model for specimen TDD1

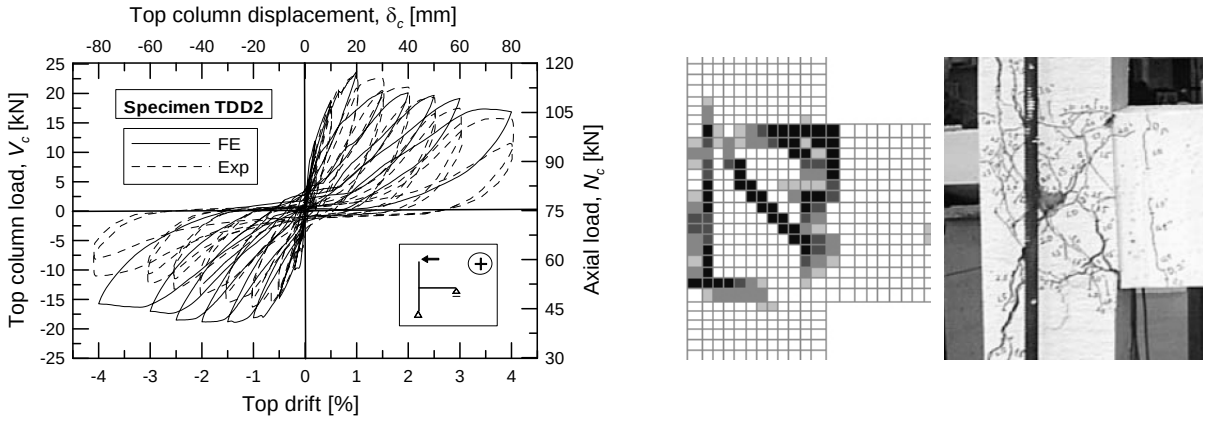

a) Hysteretic behaviour b) Cracking pattern

Figure 4-18: Validation of the FE model for specimen TDD2

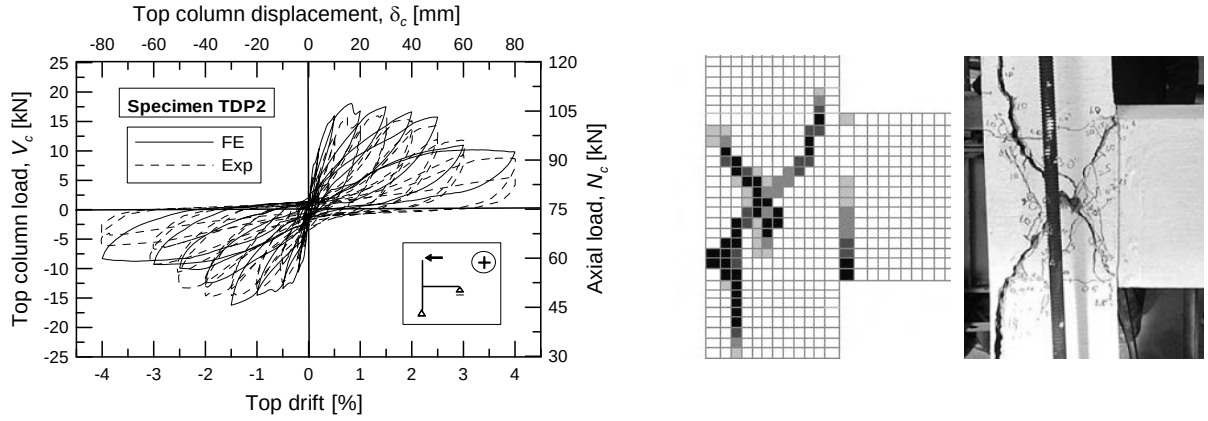

a) Hysteretic behaviour b) Cracking pattern

Figure 4-19: Validation of the FE model for specimen TDP2

The comparison between experimental tests and FE simulations is summarised in Table 4-2. All results confirm the capability of the numerical model to satisfactorily reproduce the global hysteretic behaviour of the analysed joints within acceptable errors. The initial stiffness of the specimen was generally overestimated by more than 50%, because of the difficulty in reproducing the effective boundary conditions of the tests (i.e., small slippage of external constraints). However, the shear strength of the joints, at both limit states, was generally predicted with less than 20% confidence for all analysed specimens.

Table 4-2: Comparison between experimental and FE results of tests by *Hertanto (2005)*

	EXP			FE			FE / EXP		
Test	**Initial stiffness [kN/m] a)**	**Load at 1st crack [kN] a)**	**Peak load [kN] a)**	**Initial stiffness [kN/m] a)**	**Load at 1st crack [kN] a)**	**Peak load [kN] a)**	**Initial stiffness [-] a)**	**Load at 1st crack [-] a)**	**Peak load [-] a)**
TDD1	3300 / 2200	n. a.	16.8 / -10.2	3100 / 3050	n. a.	17.7 / -10.8	0.94 / 1.39	n. a.	1.05 / 1.06
TDD2	3200 / 2450	21.1 / -15.8	23.1 / -16.3	4650 / 4450	20.6 / -17.8	23.7 / -18.9	1.45 / 1.82	0.98 / 1.13	1.03 / 1.16
TDP2	1500 / 1500	15.8 / -12.4	16.2 / -14.7	2600 / 2600	18.5 / -13.9	18.1 / -16.2	1.73 / 1.73	1.12 / 1.10	1.17 / 1.10

a) Positive / Negative loading direction

4.3.6 Test 2D pre 1970s

The test specimen “2D pre 1970s” was used for most of the preliminary analyses, and the parametric study for the joint with plain round bars and anchorage of the beam bars in the core with 180°-hooks (Type 6). The hysteretic behaviour of the numerical model was reproduced with reasonable confidence (Figure 4-20a). The joint diagonal cracking occurred at almost the same drift level in the experiment and the numerical simulation. The collapse of the specimen occurred in the 3.0% drift cycle in the negative direction, due to the buckling of the column bars (Figure 3-6c). The different behaviour of the specimen in the positive and negative loading direction, due to the variation of axial load (Section 3.3), could also be realistically simulated. The joint shear distortion observed in the experimental test can be compared with the one of the numerical monotonic simulation (Figure 4-20b). In the FE analysis the joint shear distortion is measured by the nodal displacements. The smeared crack approach induces large nodal displacements in the damaged zones, therefore, realistic nodal displacements cannot be assured in those regions. For this reason the measurement of the joint shear distortion during cyclic analysis is generally not reliable (see Figure 4-21). In Figure 4-20c,d the contributions to the global deformation of the beam, column and joints measured in the experimental tests and in the monotonic analysis are shown. The similarity between the experiments and the FE analysis can be seen by the comparison of the cracking patterns at different drift levels (Figure 4-21).

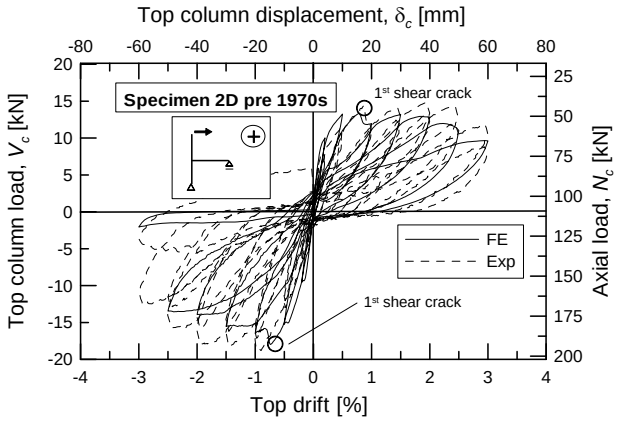

a) Hysteretic behaviour

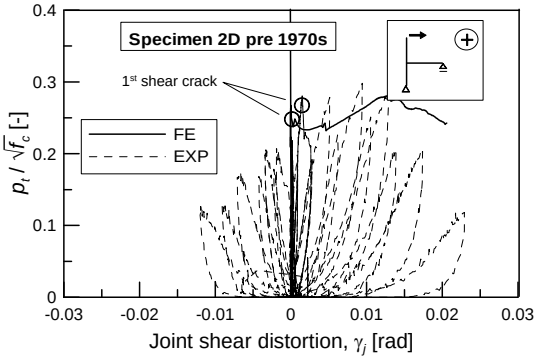

b) Joint shear distortion

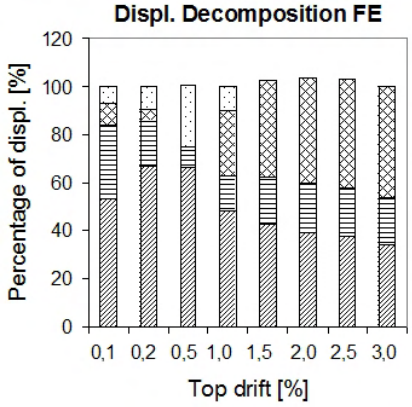

c) Decomposition of displacement - FE

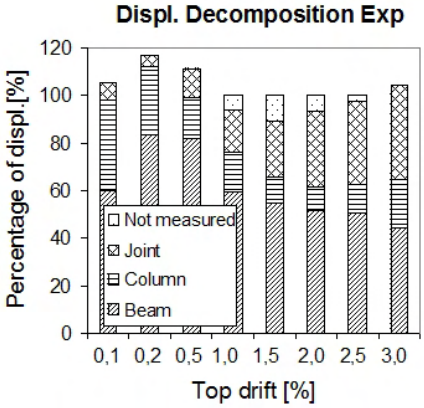

d) Decomposition of displacement - Experimental

Figure 4-20: Validation of the FE model of the specimen “2D pre 1970s”

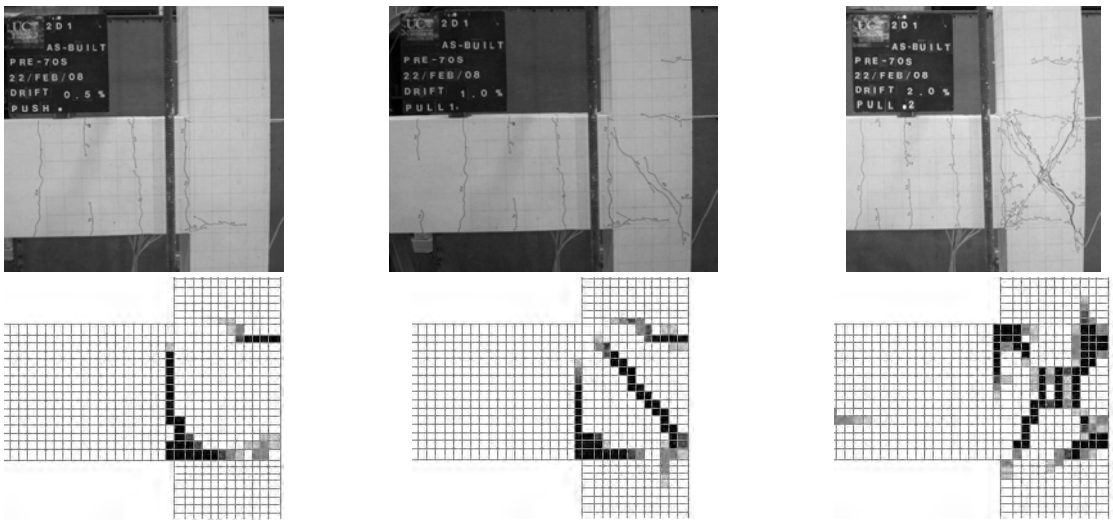

a) Top drift 0.5 % b) Top drift 1.0% c) Top drift 2.0%

Figure 4-21: Comparison of the cracking patterns of the specimen "2D pre 1970s" observed in the exp. test and in the FE simulation

4.3.7 Test JT1-1

As already mentioned in Section 3.4.2, the hysteretic behaviour of the specimen JT1-1 observed in the experiment was not symmetric as expected. The numerical simulation predicted symmetric behaviour similar to the experimental observations in the negative loading direction. The main differences are the overestimation of the initial stiffness and of the strength degradation by the FE analysis, compared to the experimental tests (Figure 4-22a). The joint shear distortion predicted by the numerical simulation slightly exceeds the experimental measurement (Figure 4-22b) and the cracking pattern agrees fairly well with the experimental observations (Figure 4-23a,b,c).

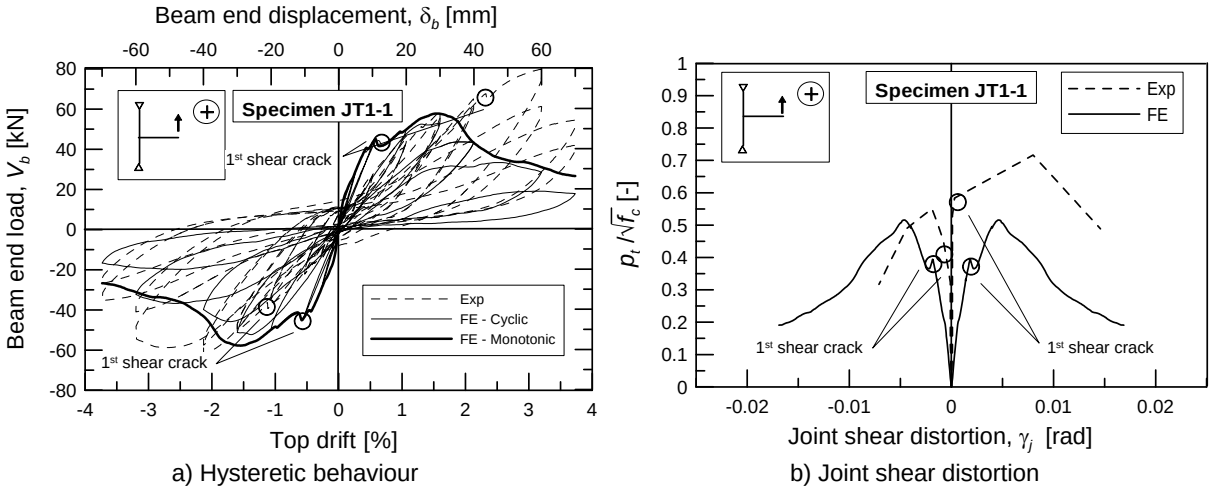

a) Hysteretic behaviour b) Joint shear distortion

Figure 4-22: Validation of the FE model of the specimen JT1-1

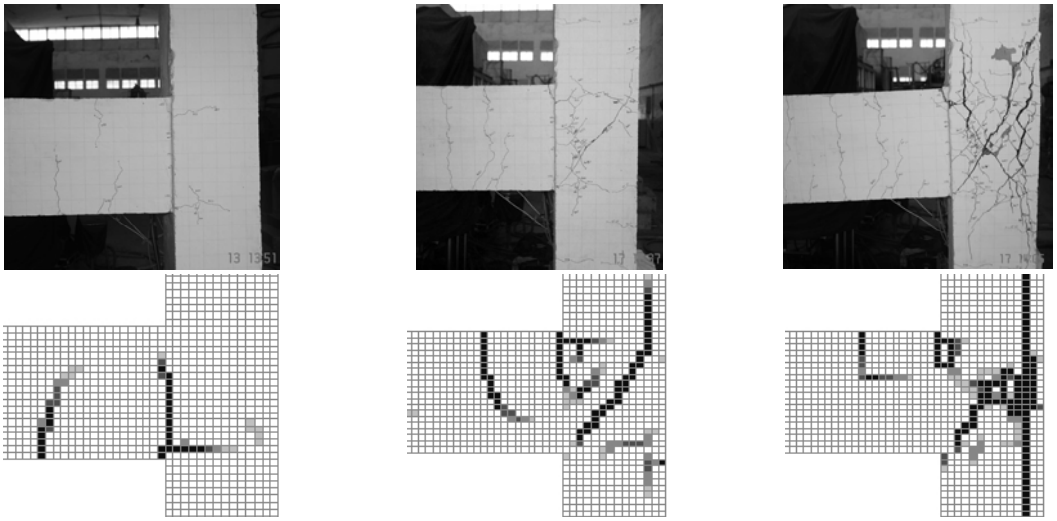

a) Beam end displ. +20 mm b) Beam end displ. -30 mm c) Beam end displ. -70 mm

Figure 4-23: Comparison of the cracking patterns of the specimen JT1-1 observed in the exp. test and in the FE simulation

4.3.8 Test JT2-1

Even though the specimen JT2-1 has the same detailing as "2D pre 1970s", JT2-1 was also used a benchmark for the FE parametric study. JT2-1 is a better comparison to the specimens with different detailing (JT1-1, JT3-1 and JT4-1) because it had the same geometry and reinforcement characteristics and it was tested with the same test setup. The two limit states considered could also be observed in the experimental tests and in the numerical analysis since there was no axial load in the column. The FE analysis closely simulated the behaviour of this specimen. Also in this case the numerical analysis predicted a stiffer initial behaviour than observed in the test (Figure 4-24a). The initial shear crack was reached in the FE analysis at 32.8 kN, which slightly overestimated the values obtained in the test (28.8 kN and 26.6 kN), with a $\gamma_j = 0.0015$ rad (0.002 rad and 0.001 rad was measured in the test) (see Figure 4-24a,b). The numerical analysis simulated the load increase up to 39.4 kN and 43.2 kN, similarly to the experimental results (41.5 kN and 39.2 kN). The cracking pattern obtained in the analysis reproduced the experimental observation at different loading stages. This confirmed the capability of the model to follow the sequence of events of the tests (Figure 4-25a,b,c).

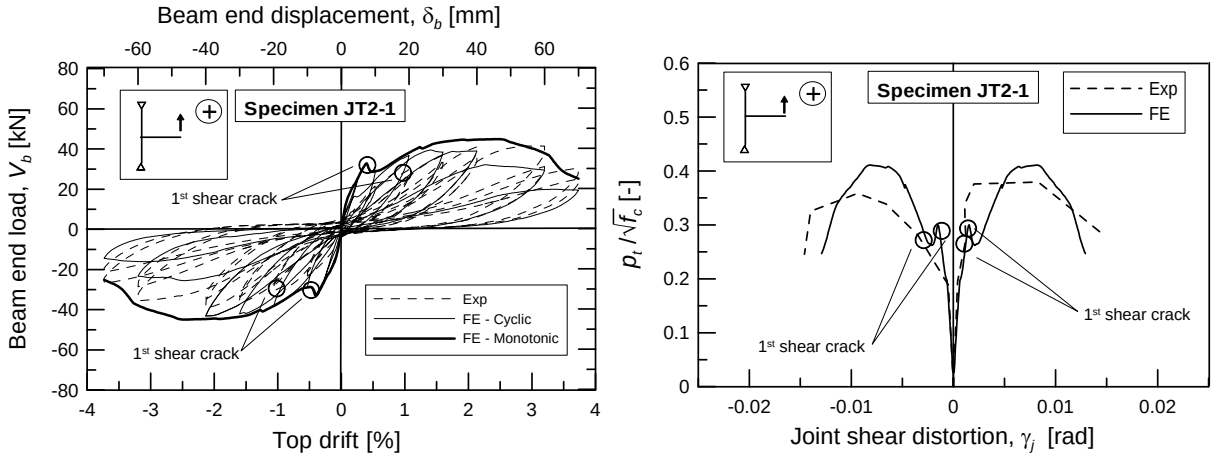

a) Hysteretic behaviour b) Joint shear distortion

Figure 4-24: Validation of the FE model of the specimen JT2-1

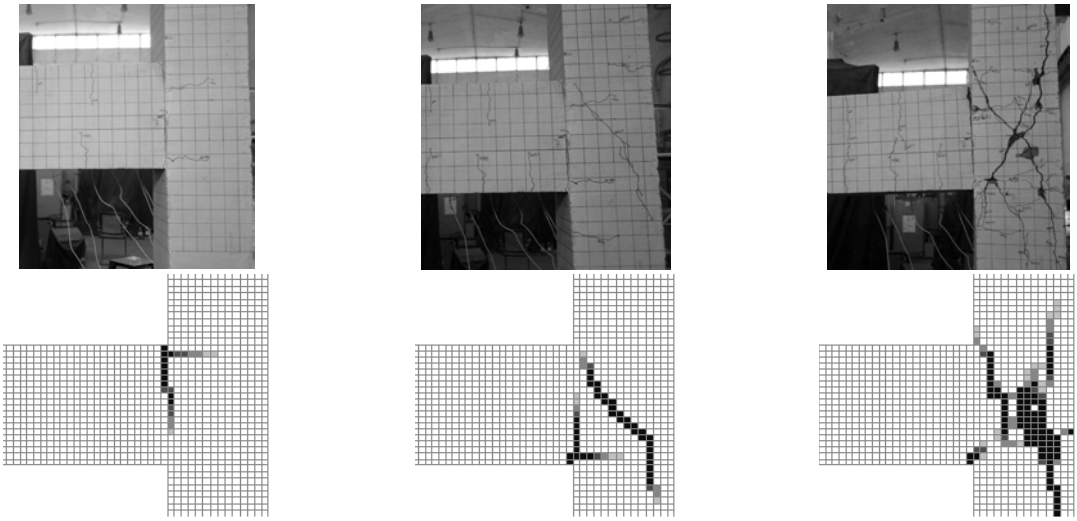

a) Beam end displ. -10 mm b) Beam end displ. +20 mm c) Beam end displ. -70 mm

Figure 4-25: Comparison of the cracking patterns of the specimen JT2-1 observed in the exp. test and in the FE simulation

4.3.9 Test JT4-1

The test JT4-1 was used as a benchmark for the parametric study on joints with deformed bars anchored with 90°bent out and bent in hooks (Types 2 and 1, respectively) in positive and negative loading directions, respectively. The unsymmetrical behaviour of the specimen due to the different anchorage solutions of beam top and bottom bars was closely simulated by the FE analysis (Figure 4-26a). From the comparison of the hysteric loops shown in Figure 4-26a, a significantly higher initial stiffness can be seen in the numerical model. This was also reflected by the drift level at which the first diagonal crack occurred in both loading directions. The difference in stiffness between numerical and experimental results did not affect the joint shear distortion, which is well correlated as shown in Figure 4-26b. The effect of the Type 2 anchorage was observed also in the simulation of the cracking pattern (Figure 4-27). The diagonal crack through the joint region was generally flatter in the case of anchorage with 90°-hooks bent away from the core than in other cases. This behaviour was observed in the experimental and numerical tests carried out in this study (compare Figure 4-21 and Figure 4-27) as well as in tests by other authors available in the literature (see Figure 5-21).

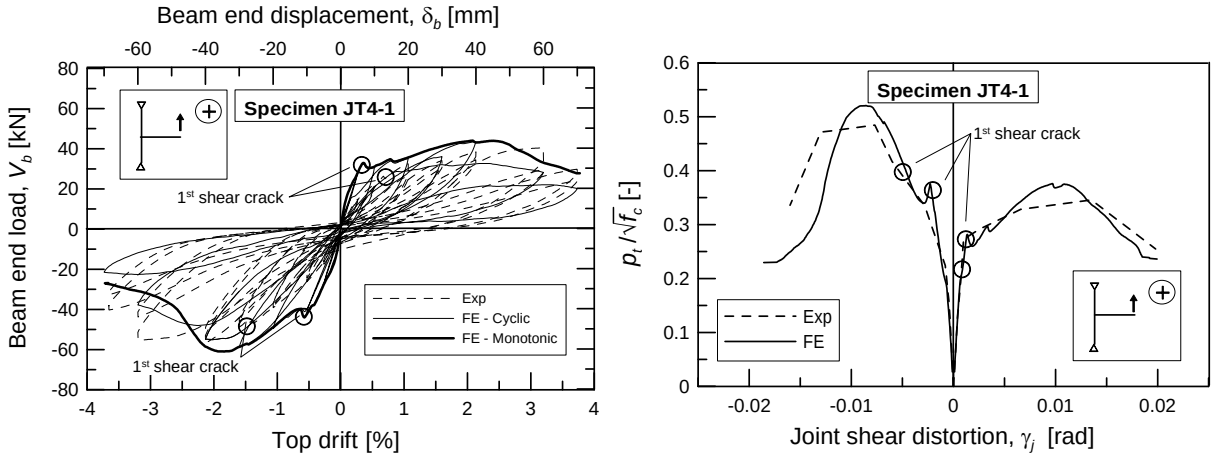

a) Hysteretic behaviour b) Joint shear distortion

Figure 4-26: Validation of the FE model of the specimen JT4-1

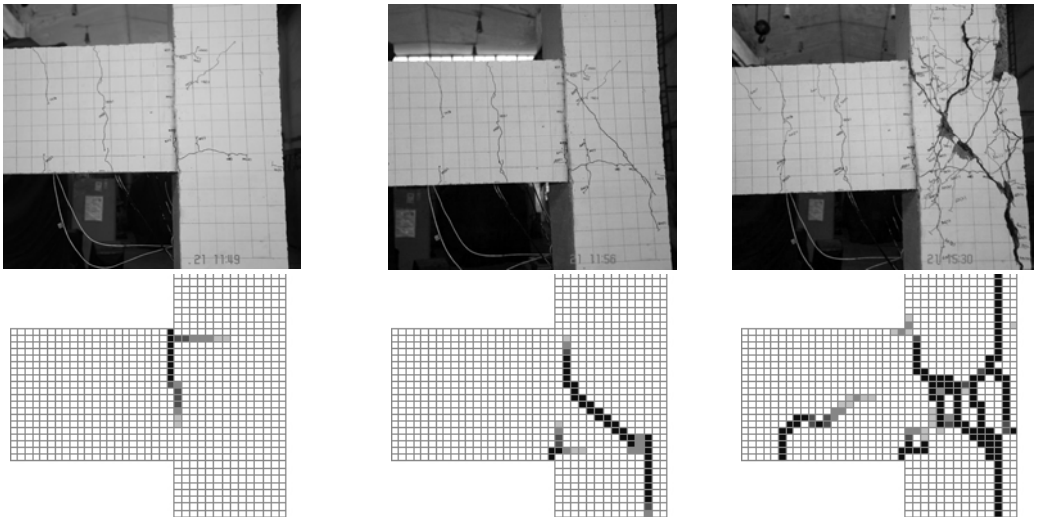

a) Beam end displ. -10 mm b) Beam end displ. + 20 mm c) Beam end displ. -70 mm

Figure 4-27: Comparison of the cracking patterns of the specimen JT4-1 observed in the exp. test and in the FE simulation

4.3.10 Test JT5-1

The importance of a realistic simulation of the test JT5-1 is related to the investigations of the interaction of different failure modes (joint shear failure and beam flexural yielding) and/or the joint shear degradation with increasing specimen's ductility (Section 4.3.4). As shown in Figure 4-28a, the global behaviour of the specimen was realistically simulated. However, as already observed in Section 3.4.6, in the positive loading direction the first shear crack occurred at a higher load level than expected. The behaviour in negative direction was negatively influenced by the damage occurred in the previous half-cycle. Both factors induced a poorer strength response and higher joint deformation (Figure 4-28b). The numerical simulation could not reproduce this joint behaviour and the predicted hysteretic loops were approximately symmetric in positive and negative loading directions. The FE analysis confirmed that the cracking pattern observed does not substantially differ from the joint shear failure without yielding of the beam longitudinal bars and agreed well with the experimental observations (Figure 4-29).

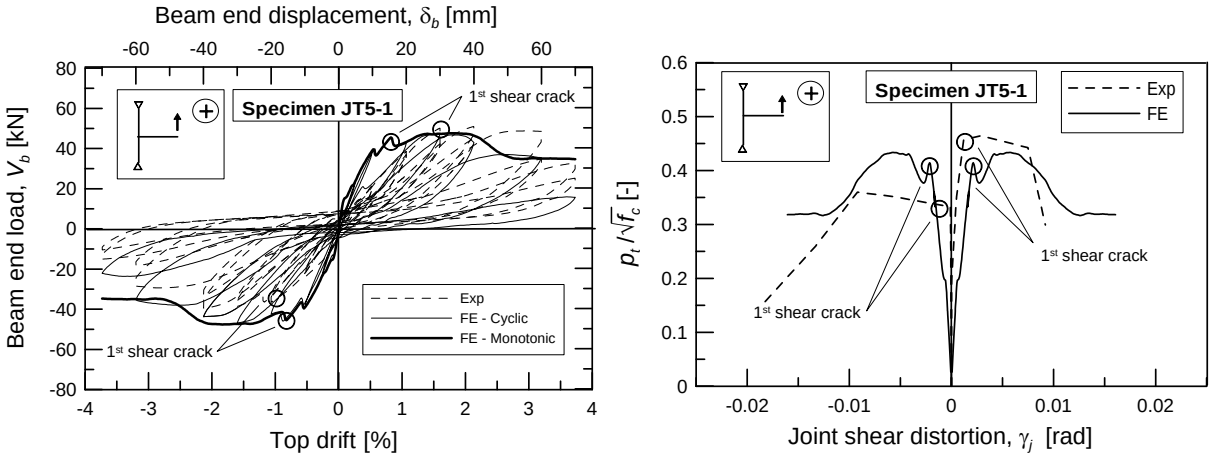

a) Hysteretic behaviour b) Joint shear distortion

Figure 4-28: Validation of the FE model of the specimen JT5-1

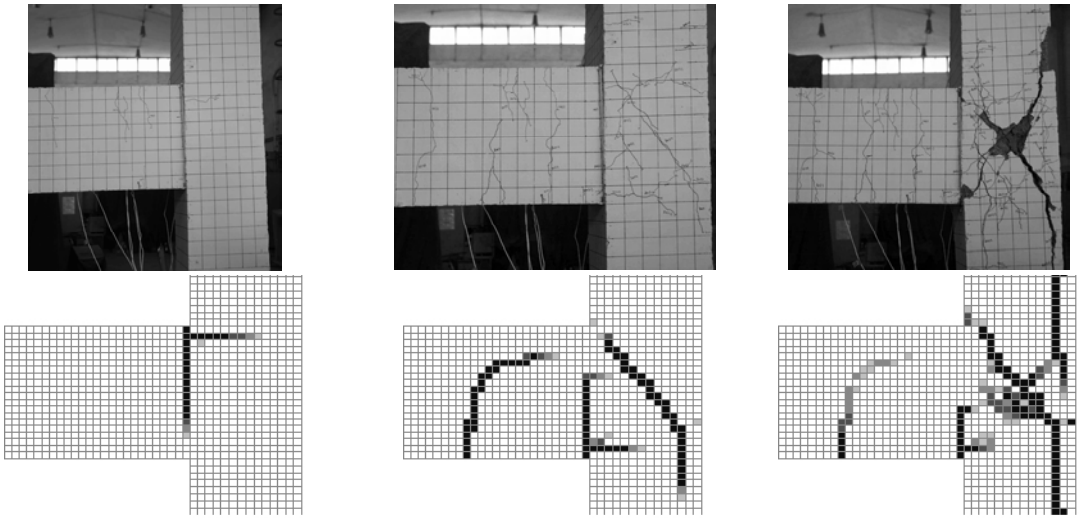

a) Beam end displ. -10 mm b) Beam end displ. +30 mm c) Beam end displ. +70 mm

Figure 4-29: Comparison of the cracking patterns of the specimen JT5-1 observed in the exp. test and in the FE simulation

4.3.11 Summary of the validation of the numerical model

In Table 4-3 and Table 4-4 a summary of the comparison of experimental and numerical results, in terms of strength and joint shear distortion, is shown. The general behaviour of the tested specimens was realistically reproduced by the FE simulations, as shown in the previous sections (see Figure 4-20 to Figure 4-29). The quantitative comparison presented in Table 4-3 shows that the most significant discrepancies between the numerical and experimental results was the general overestimation of the initial stiffness for the specimens tested at BARC (JT1-1, JT4-1 and JT5-1). The agreement of the other results, within an error confidence interval of less than ±20%, can be considered satisfactory. The size of the error takes into account the normal scattering of the behaviour of RC structures and that the experimental results refer to single tests and not the average of multiple test series. The agreement of the joint shear deformations measured in the tests and in the FE analyses shown in Table 4-4 was also considered acceptable.

Table 4-3: Strength comparison between experimental and numerical results

	EXP			FE			FE / EXP		
Test	**Initial stiffness [kN/m] [a)]**	**Load at 1st crack [kN] [a) b)]**	**Peak load [kN] [a) b)]**	**Initial stiffness [kN/m] [a)]**	**Load at 1st crack [kN] [a) b)]**	**Peak load [kN] [a) b)]**	**Initial stiffness [-] [a)]**	**Load at 1st crack [-] [a)]**	**Peak load [-] [a)]**
2D pre 1970s	2900 / 2000	14.3 / 18.8	14.3 / 18.8	2600 / 1500	13.3 / 18.0	13.3 / 18.0	0.90 / 0.75	0.93 / 0.96	0.93 / 0.96
JT1-1	2700 / 2900	67.6 / 39.3	76.9 / 61.5	5800 / 5800	44.7 / 44.4	59.9 / 52.3	2.15 / 2.00	0.66 / 1.13	0.78 / 0.85
JT2-1	2400 / 3100	28.8 / 26.6	41.5 / 39.1	5200 / 5200	32.8 / 32.8	39.4 / 43.2	2.17 / 1.68	1.14 / 1.23	0.95 / 1.10
JT4-1	3000 / 3500	26.1 / 46.6	40.5 / 57.8	5600 / 5500	32.6 / 41.2	43.5 / 58.7	1.87 / 1.58	1.25 / 0.88	1.07 / 1.03
JT5-1	2400 / 3200	50.2 / 35.7	51.0 / 39.5	4800 / 4700	39.9 / 37.8	47.4 / 46.9	2.00 / 1.47	0.93 / 1.06	0.93 / 1.19

[a)] Positive / Negative loading direction; [b)] Load is V_c for "2D pre1970s" and V_b for the other test specimens

Table 4-4: Deformation comparison between experimental and numerical results

	EXP		FE		FE / EXP	
Test	**η at 1st crack [rad] a)**	**η at Peak load [rad] a)**	**η at 1st crack [rad] a)**	**η at Peak load [rad] a)**	**η at 1st crack [-] a)**	**η at Peak load [-] a)**
2D pre 1970s	0.0015 / 0.0002	0.0094 / 0.0002	0.000 / 0.000	0.0081 / 0.0001	N. A.	0.86 / 0.50
JT1-1	0.002 / 0.001	0.005 / 0.004	0.0018	0.0047	0.90 / 1.80	0.94 / 1.18
JT2-1	0.002 / 0.001	0.008 / 0.009	0.0015	0.0065	0.75 / 1.50	0.81 / 0.72
JT4-1	0.001 / 0.003	0.014 / 0.008	0.0014 / 0.0023	0.0098 / 0.0088	1.40 / 0.77	0.70 / 1.10
JT5-1	0.001 / 0.001	0.003 / 0.009	0.0021	0.0045	2.10 / 2.10	1.50 / 0.5

a) Positive / Negative loading direction

5 NUMERICAL PARAMETRIC STUDY AND DEVELOPMENT OF THE ANALYTICAL MODEL OF JOINT SHEAR STRENGTH

The preliminary investigations described in Chapter 4 demonstrated the suitability of the Finite Element (FE) model to realistically reproduce the mechanics of exterior 2D RC beam-column connections and to quantify the joint shear strength with acceptable error limits. The validity and the limits of the assessment model proposed by Priestley-Pampanin (*Priestley, 1997* and *Pampanin et al., 2003*) have also been shown (Section 3.5). In this chapter the results of a FE parametric study (Section 5.1) are presented and the refinement of the above assessment model is proposed (Section 5.2).

5.1 Parametric study

The parameters to be varied were chosen after the analysis of experimental data available in the literature (see Chapter 2). The following parameters were varied:

- concrete compressive strength, f_c;
- column axial load expressed in percentage of the compressive strength of the column concrete section, n_c (see Eq. (5-1));
- beam reinforcement ratio, ρ_b;
- column reinforcement ratio, ρ_c; and
- joint geometric aspect ratio, h_b/h_c.

The range of variation of different parameters was chosen to represent realistic conditions for pre 1970s beam-column connections (i.e., no high strength concrete with $f_c > 50$ MPa and reinforcement ratio in beam and column, ρ_c and ρ_c, not greater than 2.0%). Furthermore, the analyses with such combinations of parameters that led to the formation of a plastic mechanism in the specimen other than joint shear failure without yielding of beam and/or column bars were not taken into consideration. The range of parameters is shown in Table 5-1.

Table 5-1: Matrix of the parametric study

Anchorage	f_c [MPa]	Axial load, n_c [%]	ρ_b [%]	ρ_c [%]	h_b/h_c [-]
Type 1	20 - 50	0 – 41	0.56 – 1.82	0.37 – 2.16	1.17 – 2.0
Type 2	20 – 50	0 – 41	0.56 – 1.82	0.37 – 2.16	1.17 – 2.0
Type 6	12 – 43 [a)]	0 – 18 [a)]	0.45 – 1.78 [a)]	0.50 – 2.00 [a)]	1.26 – 1.98 [a)]
	20 – 50 [b)]	0 – 47 [b)]	0.56 – 1.82 [b)]	0.37 – 2.16 [b)]	1.17 – 2.0 [b)]

[a)] Benchmark specimen "2D pre 1970s"; [b)] Benchmark specimen JT2-1

The structure of the matrix (Table 5-1) implies that the parameters (f_c, P_c, ρ_b, ρ_c and h_b/h_c) are not correlated with each other. However, it is assumed that the influence of those parameters may be different for different anchorage detailing of the beam bars in the joint core. The basic models for the parametric study are: the models validated on the test JT4-1 (Section 4.3.9) for anchorages Types 1 and 2; and the models of the test specimens "2D pre 1970s" and JT2-1 (Sections 4.3.6 and 4.3.8) for anchorage Type 6. A comparison of the parametric study carried out with the specimens "2D pre 1970s" and JT2-1 for anchorage Type 6 should provide information regarding the following aspects:

- specimens loaded in different test setups;
- effect of axial load in the column;
- evaluation of effect of scaling of the specimen (2/3 vs. full scale); and
- effect of different reinforcement detailing between JT2-1 and JT4-1.

The material properties used for the analysis of the basic models were taken from experimental data and, if not available (e.g., bond stress-slip relationship), from relevant literature. An overview is given in Table 5-2 and Table 5-3.

Table 5-2: Material properties of the basic models "2D pre 1970s" and JT2-1

Model "2D pre 1970s"					Model JT2-1				
Concrete	f_c =	17.7 [a)] MPa	E_c =	24.7 GPa	Concrete	f_c =	24.4 [a)] MPa	E_c =	25.0 GPa
	f_{ct} =	1.8 [a)] MPa	G_F =	0.07 N/mm		f_{ct} =	2.3 [a)] MPa	G_F =	0.07 N/mm
	υ_c =	0.18				υ_c =	0.18		
Steel R10 [b)]	f_y =	430 [a)] MPa	E_s =	200 [a)] GPa	Steel D16 [b)]	f_y =	312 [a)] MPa	E_s =	200 GPa
	f_u =	527 [a)] MPa	H_s =	10 [a)] GPa		f_u =	478 [a)] MPa	H_s =	10 GPa
	υ_s =	0.33				υ_s =	0.33		
Steel R6	f_y =	397 [a)] MPa	E_s =	196 [a)] GPa	Steel D20 [b)]	f_y =	308 [a)] MPa	E_s =	200 GPa
	f_u =	452 MPa	H_s =	10 [a)] GPa		f_u =	482 [a)] MPa	H_s =	10 GPa
	υ_s =	0.33				υ_s =	0.33		
Note: N_c = 110 kN (P_c = 12%)					Steel D8	f_y =	301 [a)] MPa	E_s =	200 GPa
						f_u =	458 [a)] MPa	H_s =	10 GPa
						υ_s =	0.33		
					Note: N_c = 0 kN				

[a)] Measured value; [b)] Bond parameters in Appendix C

Table 5-3: Material properties of the basic model JT4-1

Model JT4-1				
Concrete	f_c =	28.2 [a)]	E_c =	28.5 GPa
	f_{ct} =	3.0 [a)]	G_F =	0.075
	υ_c =	0.18		
Steel D16 [b)]	f_y =	552 [a)] MPa	E_s =	200 GPa
	f_u =	672 [a)] MPa	H_s =	10 GPa
	υ_s =	0.33		
Steel D20 [b)]	f_y =	558 [a)] MPa	E_s =	200 GPa
	f_u =	688 [a)] MPa	H_s =	10 GPa
	υ_s =	0.33		
Steel D8	f_y =	548 [a)] MPa	E_s =	200 GPa
	f_u =	652 [a)] MPa	H_s =	10 GPa
	υ_s =	0.33		

Note: N_c = 0 kN; [a)] Measured value; [b)] Bond parameters in Appendix C

In the parametric study monotonic analyses were carried out as it was assumed that they represent the backbone curve of the hysteretic loops. Note, however, that this assumption is valid only for displacement levels before the collapse of the specimen. That is where no buckling of the bars occurs, the slippage of reinforcement is limited and there is no significant spalling of concrete cover.

In the following sections the main results are analysed and discussed. Particular emphasis is given to:

- determination of strength limit states (1st diagonal crack and peak load) in terms of ratio between principle tensile strength, p_t, and $\sqrt{f_c}$, and
- deformation of the specimen in terms of top drift and of joint shear distortion, γ_j.

5.1.1 Influence of concrete strength

The variation of the concrete compressive strength implies variation of other concrete properties such as: tensile strength, f_{ct}, Young's modulus, E_c, and fracture energy, G_F. These properties are conventionally calculated as a function of the concrete compressive strength, f_c as explained in Section 4.3.1.2 and shown in Appendix C. However, it is well known that they may vary significantly in relation to other parameters such as type, form and dimension of the aggregate. A variation of 12 MPa ≤ f_c ≤ 50 MPa was chosen to cover the most probable range of concrete strength found in existing pre 1970s structures.

The variation of concrete strength implies also a variation of the bond stress-slip characteristic of deformed bars (see *Lettow, 2006* and Appendix C). For plain round bars it was assumed that the variation of the concrete strength has a negligible influence on the bond-stress strain relationship, since no mechanical damage takes place at the steel-concrete interface.

In Figure 5-1 to Figure 5-3 the effect of the variation of concrete strength, f_c, on joints with different beam longitudinal bar anchorage detailing is shown. In Figure 5-1a, Figure 5-2a and Figure 5-3a,c the load-displacement curves are shown. Generally, an increase of the concrete strength induced an increase of the joint shear strength at both considered limit states. The corresponding top drift also increased, but less significantly. The conversion of the load into $p_t/\sqrt{f_c}$ confirms the validity of the approach proposed by *Priestley (1997)* and *Pampanin et al. (2003)* (Figure 5-1b, Figure 5-2b and Figure 5-3b,d). In the investigated range of concrete strength $p_t/\sqrt{f_c}$ was approximately constant with varying f_c for the considered limit states and anchorage configurations. The joint shear distortion shown in the same figures does not seem to be influenced by the variation of f_c. Comparing Figure 5-3a,b with Figure 5-3c,d it can be seen that, for the specimens with constant axial load (2D pre 1970s), the initial joint shear cracking also corresponds to the peak load. In the case of JT2-1 (no column axial load) two limit states similar to the results in Figure 5-1 and Figure 5-2 can be observed.

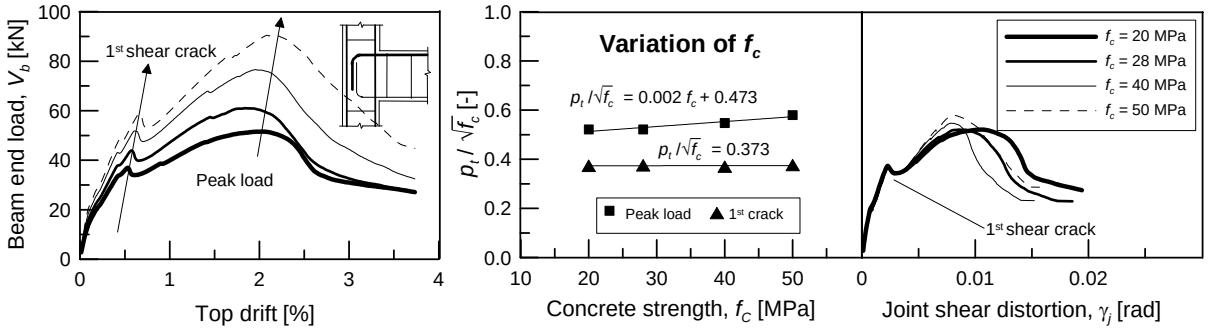

a) LD curves b) Influence of f_c on strength and deformability

Figure 5-1: Influence of concrete strength, f_c, for anchorage Type 1

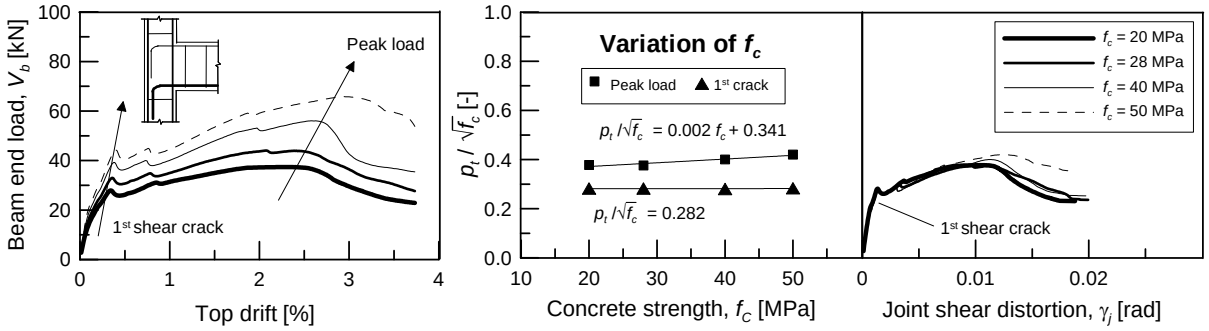

a) LD curves b) Influence of f_c on strength and deformability

Figure 5-2: Influence of concrete strength, f_c, for anchorage Type 2

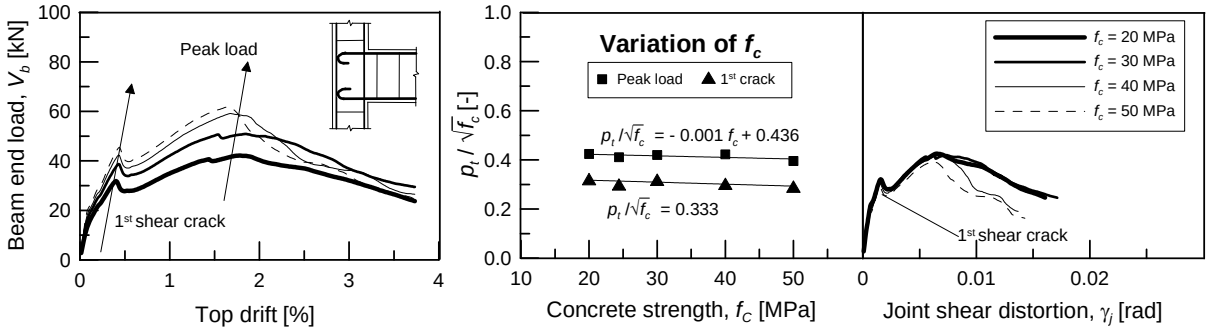

a) LD curves (JT2-1) b) Influence of f_c on strength and deformability (JT2-1)

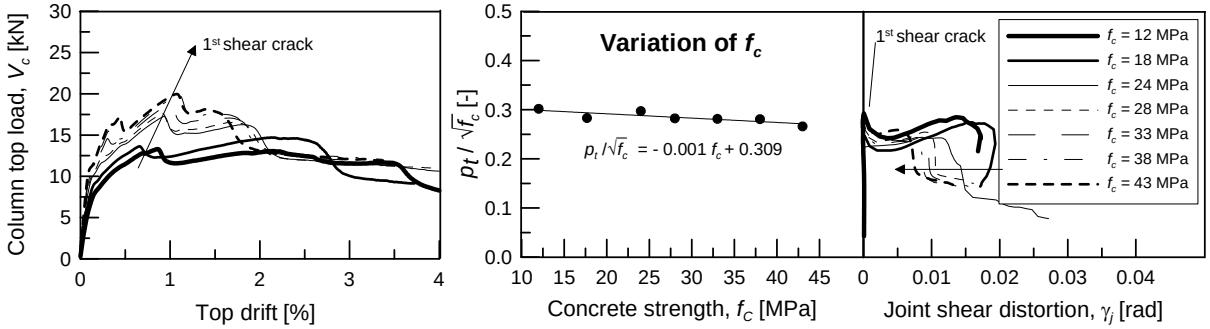

c) LD curves (2D pre 1970s) d) Influence of f_c on strength and deformability (2D pre 1970s)

Figure 5-3: Influence of concrete strength, f_c, for anchorage Type 6

5.1.2 Influence of axial load in the column

The influence of axial load in the column, n_c, on the joint shear strength is still a controversial topic in the scientific community. In engineering practice, the axial load level acting at different storey levels of a moment resisting frame can only be determined statistically. Additionally, the axial load varies during lateral loading of the RC frame in order to

counterbalance the resulting overturning moment (see Figure 3-4). The axial load level, n_c, is defined by Equation (5-1)

$$n_c = \frac{N_c}{h_c \cdot w_c \cdot f_c} \cdot 100 \ [\%] \qquad (5\text{-}1)$$

with N_c being the axial load in the column expressed in [N]

The estimation of the axial load on the column of an exterior joint can be done only on a probabilistic basis, i.e., most codes suggest taking into account a decreasing percentage of live loads with increasing numbers of storeys. It is not the objective of this study to investigate this. However, considering the partial safety factors on loads and materials (reduction factor between 3 and 5), as well as the fact that the design of the exterior column in moment resisting frames is more influenced by the bending moment than by the axial load, it is reasonable to assume that the axial load under static conditions will probably not be higher than 15% to 20% of the ultimate compressive strength of the column. The variation of axial load due to the lateral loading can realistically be equal to 10%~15%. On the basis of these considerations, the variation of the column axial load was taken to be between 0% and 40% of the column compressive strength.

In the approach used in this study the positive effect of axial load in the column on the joint shear strength is taken into account by considering the principle tensile stress, p_t, instead of the joint shear stress, v_{jh}, as limit state indicator (see Section 2.1.2).

The favourable effect of the axial load on the joint shear strength is shown to be qualitatively independent of the joint detailing in the load-displacement curves (Figure 5-4a, Figure 5-5a and Figure 5-6a). As shown in Figure 5-4b, Figure 5-5b and Figure 5-6b, the ratio between the considered limit states (Peak load / 1st shear crack) decreases with increasing n_c. For high values of n_c, the ultimate capacity of the joint corresponds to strength at 1st joint shear cracking. The observation confirms the validity of the SAT model presented in Section 4.3.2, since the axial load influences the strength limit states in different ways.

1st joint shear cracking: the increase of axial load induces an increase in load corresponding to the initial diagonal cracking. This effect can be accounted for by the formulation of joint shear strength in terms of $p_t/\sqrt{f_c}$. This is valid for the three detailing solutions analysed in this study (Figure 5-4b, Figure 5-5b and Figure 5-6b). The physical rationale of this behaviour is the reduction of tensile stress in the tie due to the axial load. The expression of p_t according to Mohr's circle theory (Section 2.1.3) theoretically supports the increase of v_{jh} in the joint with increasing column compressive stress, f_a. Since p_t remains constant for variable f_a, it can be used as indicator of the initial joint cracking.

Peak load: The axial load increases the compression demand in the strut. However, the width of the strut is simultaneously increased by the enlargement of the compression zone in the column, above and below the joint panel. This behaviour induces an increase in ultimate shear capacity of the joint (Figure 5-4a, Figure 5-5a and Figure 5-6a) and variable p_t. For low axial load levels the peak load corresponds to the failure of the compressive strut. The strength increase, conversely to the failure of the tensile tie (1st diagonal crack), decreases with increasing axial load. For high axial load levels the peak load coincides with the 1st

shear crack in the joint, i.e., after joint cracking the weakened strut (see Figure 4-13c) of the joint is not able to transfer enough compressive stress without transferring tensile stresses through the core. The axial load limit between the compression failure of the joint and the failure load corresponding to the 1st diagonal cracking depends on the anchorage detailing. The more efficient the anchorage of the beam bars in core is, the higher the possible strength increase after the joint diagonal cracking is and the higher the axial load level after which the 1st shear crack is. This coincides with the peak resistance of the specimen.

On the basis of the numerical simulations (Figure 5-4b, Figure 5-5b and Figure 5-6b), for no axial load (n_c = 0%) the ratio between the limit states was approximately 1.3 for the anchorage Types 1, 2 and 6. The limit of n_c, after which there distinction between the two limit states could be observed, was 20% for the anchorage Type 1 and 10% for Types 2 and 6.

With increasing n_c the drift levels corresponding to the analysed limit states also increased, as did the brittleness of the specimen, i.e., the negative inclination of the descending branch of the curve, also increased (Figure 5-4a, Figure 5-5a and Figure 5-6a). The joint shear distortion corresponding to the 1st joint diagonal cracking increased with increasing value of n_c (Figure 5-4b, Figure 5-5b and Figure 5-6b).

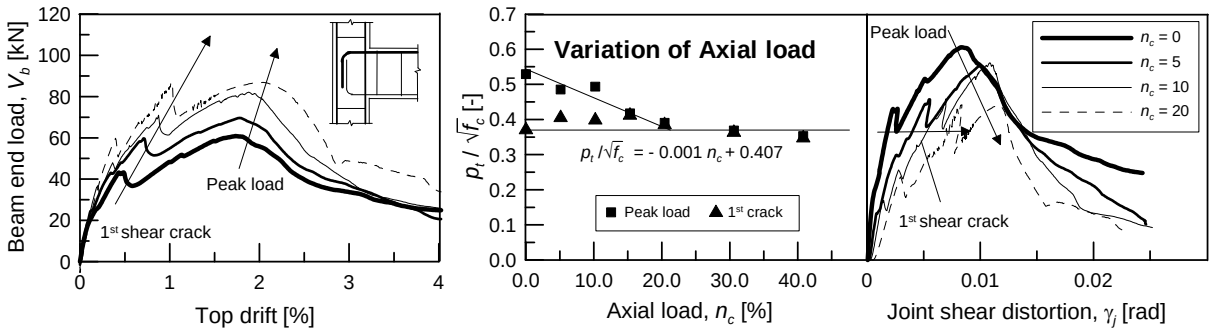

a) LD curves b) Influence of axial load on strength and deformability

Figure 5-4: Influence of axial load in the column, n_c, for anchorage Type 1

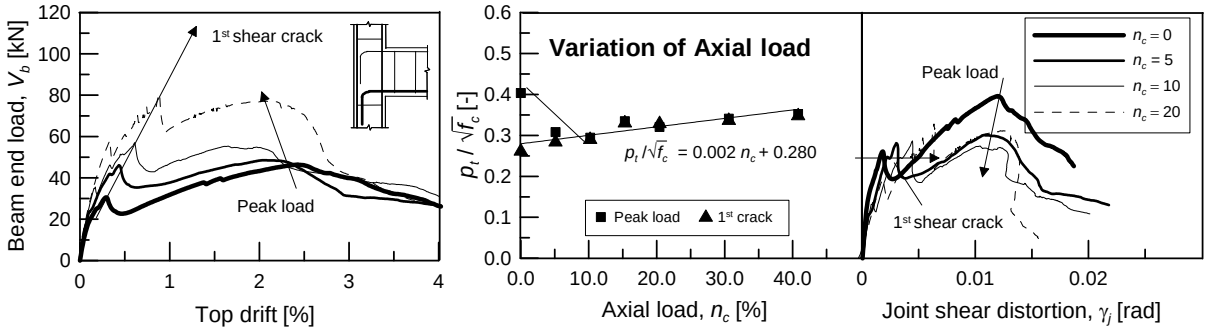

a) LD curves b) Influence of axial load on strength and deformability

Figure 5-5: Influence of axial load in the column, n_c, for anchorage Type 2

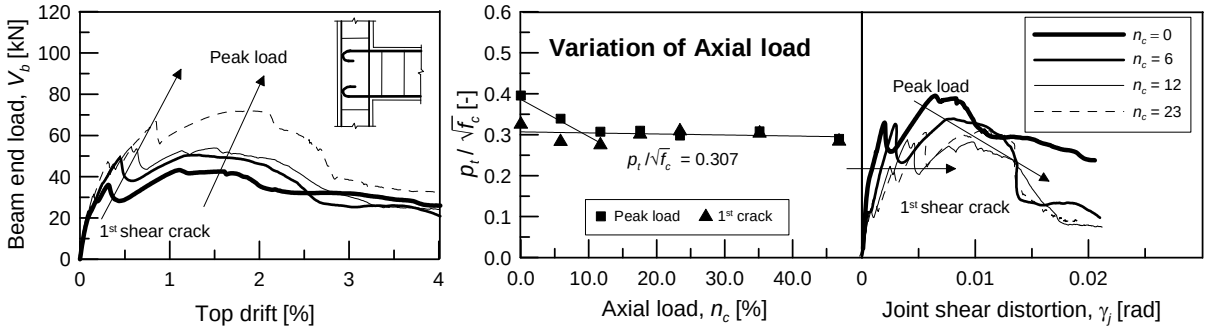

a) LD curves (JT2-1) b) Influence of axial load on strength and deformability (JT2-1)

Figure 5-6: Influence of axial load in the column, n_c, for anchorage Type 6

5.1.3 Influence of beam reinforcement ratio

The amount and distribution of the longitudinal reinforcement framing into the joint region influences the stress-strain field in the joint region. The lateral area of the reinforcement is directly proportional to the force transmitted via the bond of the reinforcement with the concrete. In the case of the beam longitudinal bars, the tension force induced by the bending moment at the beam-column interface is transferred to the joint region via the bond and the mechanical anchorage at the end of the bars. Assuming that the shear failure of the joint corresponds to the failure of the strut starting at the anchorage of the beam reinforcement (see Section 4.3.2), it can be argued that increasing the portion of tensile forces transferred by bond (i.e., an increase of beam reinforcement ratio, ρ_b), the concrete strut will fail at a higher load. Furthermore, with increasing ρ_b the bending of the reinforcement would become more efficient in supporting the concrete strut. In Figure 5-7 the forces transferred by the beam reinforcement into the joint region are shown.

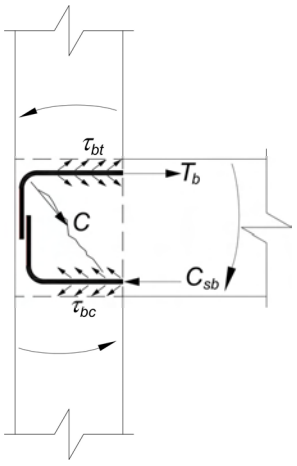

Figure 5-7: Forces transferred by the beam into the joint region

In the numerical models with deformed bars, the diameter of the 3 bottom and top bars of the benchmark test JT4-1 were varied between D12 and D25 (3 and 4 bars D25). In the numerical simulations the cross sectional area of the reinforcement was changed accordingly and the bond properties were modified as proposed by *Lettow (2006)* and shown in Appendix C.

The load-displacement curves shown in Figure 5-8a and Figure 5-9a denote, as expected, an increase in the initial stiffness of the specimen with increasing ρ_b. The increase of the load

corresponding to the first joint diagonal cracking was in both cases very low and, therefore, it was neglected. The increase of the ultimate joint shear capacity with increasing ρ_b was more significant, especially in the case of beam bars with anchorage Type 1, as opposed to Type 2 (compare Figure 5-8b and Figure 5-9b). The joint shear distortion was not significantly influenced by the variation of ρ_b (see Figure 5-8b and Figure 5-9b).

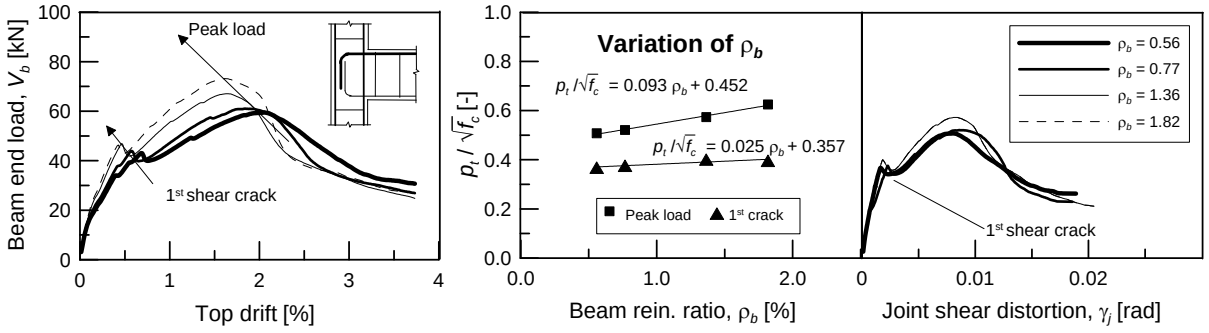

a) LD curves b) Influence of ρ_b on strength and deformability

Figure 5-8: Influence of beam reinforcement ratio, ρ_b, for anchorage Type 1

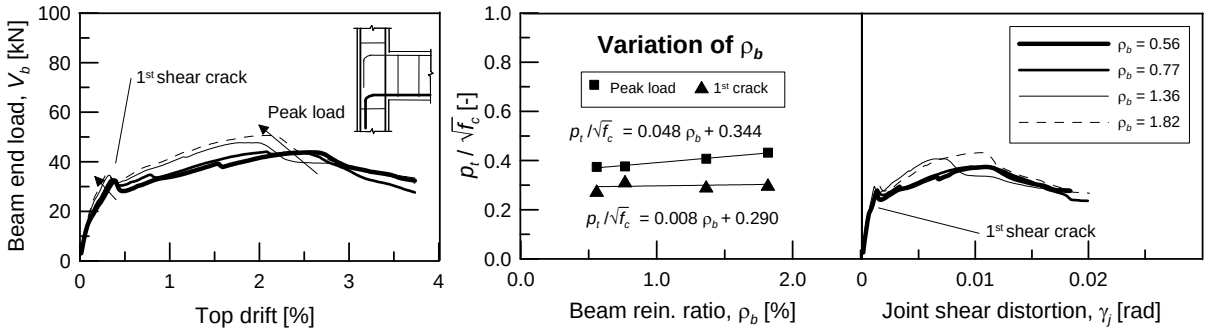

a) LD curves (2D pre 1970s) b) Influence of ρ_b on strength and deformability

Figure 5-9: Influence of beam reinforcement ratio, ρ_b, for anchorage Type 2

For plain round bars (specimen JT2-1), 3 top and bottom bars similar to specimen JT4-1 were considered (ranging from R16 to R25). In addition, a configuration with 4 top and bottom longitudinal beam bars, as in the test "2D pre 1970s", was also considered. A range of bar sizes between R10 and R20 were used. Since it is not known if bar diameters bigger than 20 mm were available in the pre 1970s construction industry, the analysis with R25 only has a theoretical relevance. The tests of *Fabbrocino et al. (2002)* provide indications about the bond properties of plain round bars R12 and R16. The bond stress-slip relationships for the other investigated diameters (R10 and R14 to R25) were obtained by linear interpolation (see Appendix C).

The variation of ρ_b has, in the case of plain round bars, a similar influence on the shear strength and deformability of the joint as for deformed bars (Figure 5-10a,b). However, the contribution of bond forces is smaller than for deformed bars. Less significant influence of bond forces was observed for the specimen "2D pre 1970s", where the initiation diagonal cracking in the joint region corresponded to the ultimate strength (Figure 5-10c,d).

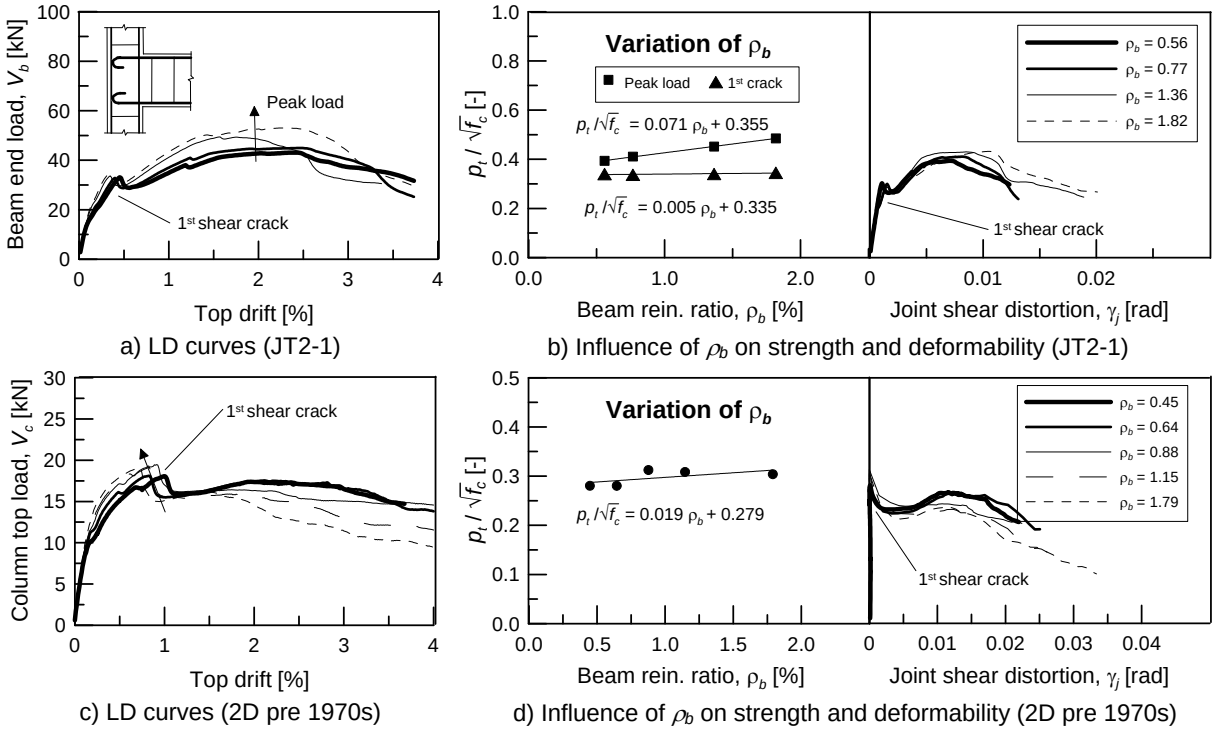

a) LD curves (JT2-1)

b) Influence of ρ_b on strength and deformability (JT2-1)

c) LD curves (2D pre 1970s)

d) Influence of ρ_b on strength and deformability (2D pre 1970s)

Figure 5-10: Influence of beam reinforcement ratio, ρ_b, for anchorage Type 6

It was considered necessary to evaluate the combined effect of varying ρ_b and n_c, since in the simulations presented in the above diagrams no axial load of the column was applied (n_c = 0%) and both parameters (ρ_b and n_c) influence the strength of the concrete strut. The results plotted in Figure 5-11 indicate that the effect of ρ_b on the joint ultimate shear strength decrease with increasing axial load level. For joints with anchorage Types 1 and 6 the increase of shear strength with increasing ρ_b from 0.77% to 1.82% at n_c = 0 is about 25% (compare Figure 5-11a,c with Figure 5-8b and Figure 5-10b,d). For anchorage Type 2 the strength increase in the same conditions is only 10% (compare Figure 5-11b and Figure 5-9b). This behaviour is reasonable, because the anchorage Type 2 does not support the concrete strut effectively being bent out of the joint panel. In all cases the influence of ρ_b decreased with increasing n_c. For axial load levels, where the ultimate strength of the joints corresponded to the strength at initial diagonal cracking, the variation ρ_b did not induce joint strength variation, because it did not influence that limit state as discussed above.

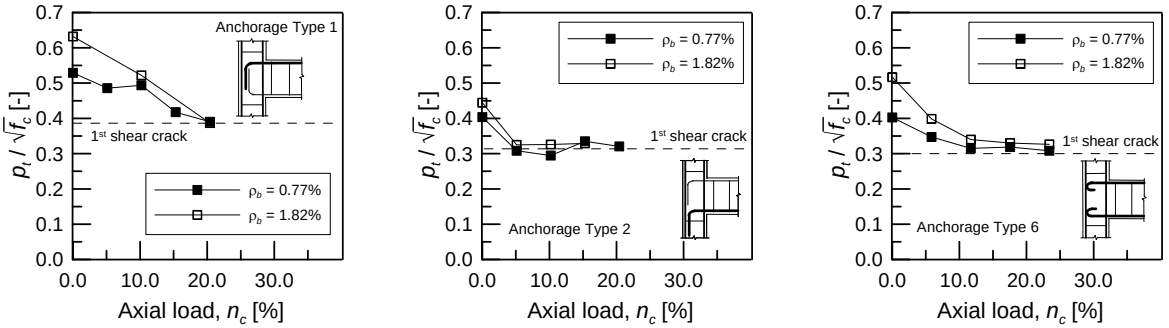

a) Anchorage Type 1

b) Anchorage Type 2

c) Anchorage Type 6

Figure 5-11: Influence of ρ_b at different axial load levels

5.1.4 Influence of column reinforcement ratio

The variation of the column reinforcement ratio, ρ_c, similar to the case of ρ_b, influences the stress-strain field in the joint region by varying the amount bond stresses transferred by the reinforcement to the concrete. In the specimens considered, the longitudinal column bars were not interrupted in the joint region (i.e., no lap splices were considered). In Figure 5-12 the bond forces transferred by the column reinforcement into the joint region are shown. It is possible that these forces contribute to limit the 1st diagonal crack in the core more effectively than in the case of the beam bars because of the continuity of the reinforcement through the entire height of the joint and the bond forces keeping the joint intact and because in the considered subassemblies typologies $h_b \geq h_c$. Furthermore, the bond forces shown in Figure 5-12 may effectively reduce the tensile stress field in the joint panel.

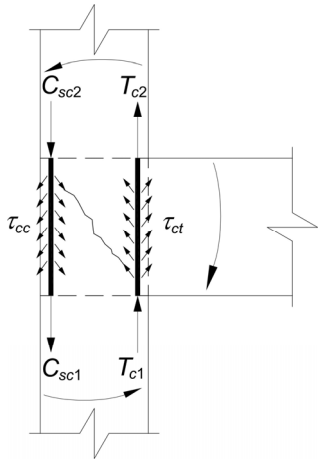

Figure 5-12: Forces transferred by the column into the joint region

In the numerical models with deformed and plain round bars, the column reinforcement bars were kept constant in number (3+3 as for the benchmark specimens) and their diameter was varied between D12 and D25 (including 4+4 D25). The parameters of the discrete bond model were also in this case accordingly varied (see Appendix C).

The numerical analyses showed a negligible difference in the ultimate capacity of the specimen for variable ρ_c and a slight increase of the load corresponding to the 1st joint shear cracking with increasing ρ_c (see Figure 5-13 to Figure 5-15). The joint shear distortion was not influenced by the variation of ρ_c in a significative manner (see Figure 5-13b, Figure 5-14b and Figure 5-15b), while at peak load no significant variation was observed. On the basis of these analyses and because of the lack of different indications in the relevant literature (see Table 2-1 and Appendix A), it was decided to neglect the influence of ρ_c on the assessment of the joint shear strength.

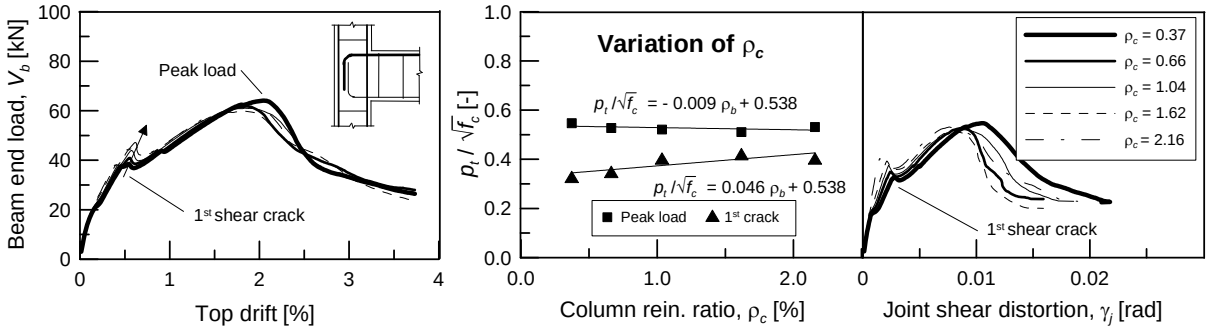

a) LD curves b) Influence of ρ_c on strength and deformability

Figure 5-13: Influence of column reinforcement ratio, ρ_c, for anchorage Type 1

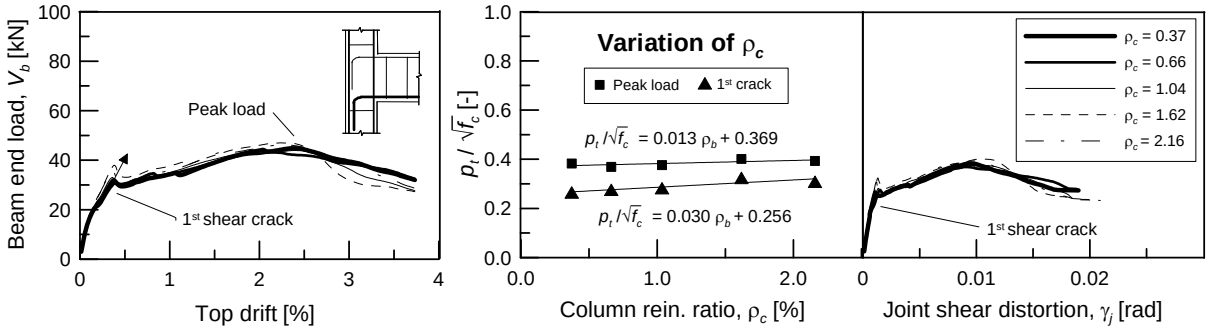

a) LD curves b) Influence of ρ_c on strength and deformability

Figure 5-14: Influence of column reinforcement ratio, ρ_c, for anchorage Type 2

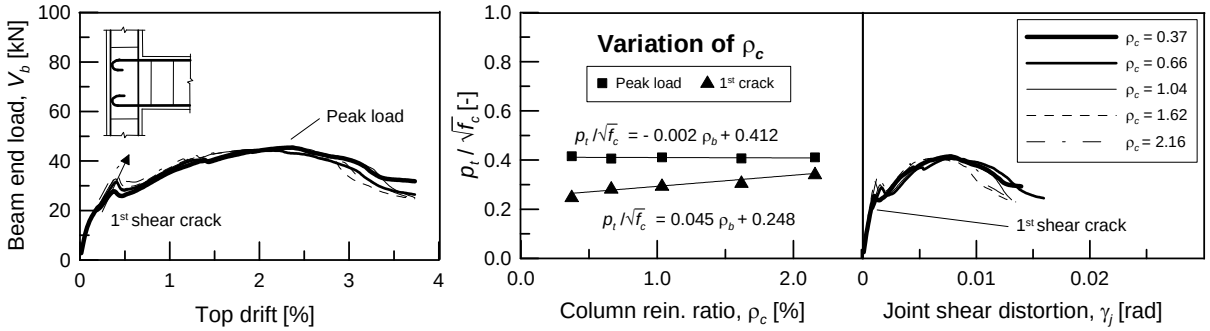

a) LD curves (JT2-1) b) Influence of ρ_c on strength and deformability (JT2-1)

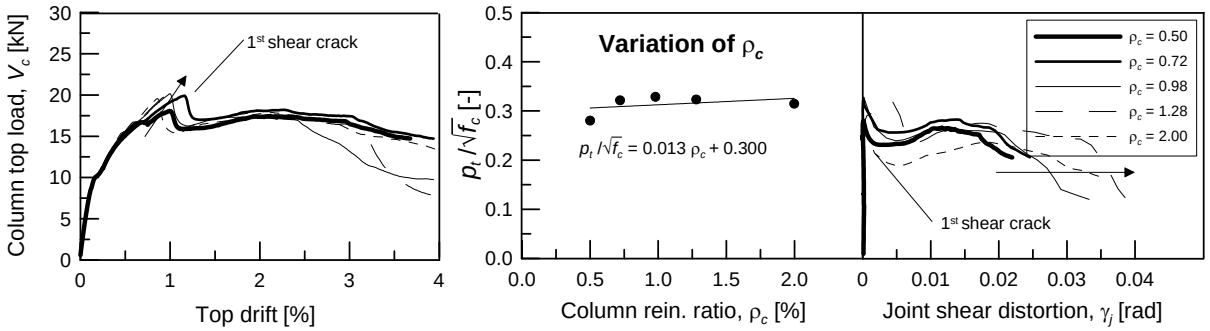

c) LD curves (2D pre 1970s) d) Influence of ρ_c on strength and deformability (2D pre 1970s)

Figure 5-15: Influence of column reinforcement ratio, ρ_c, for anchorage Type 6

5.1.5 Influence of aspect ratio

Most of the models proposed in the literature to estimate the joint shear capacity indicate that with increasing joint geometric aspect ratio, h_b/h_c, the joint shear capacity increases. The rationale for this behaviour can be easily explained by the SAT model used to visualise the internal forces acting in the joint region (see Figure 5-16); i.e., with decreasing ratio h_b/h_c the

strength demand in the concrete strut, *C*, needed to counterbalance the tension force, *T*, decreases. According to the comparison shown in Figure 5-16a,b between two joints with h_b/h_c = 1.00 and 2.00 respectively, the ratio of the joint shear strength of those joints should be 1 to 0.64. However, it is reasonable to think that the theoretical calculation shown in Figure 5-16c is, in reality, influenced by factors such as the detailing of the anchorage of the beam bars, including concrete cover, radius of curvature of the bars and above all the form of the anchorage.

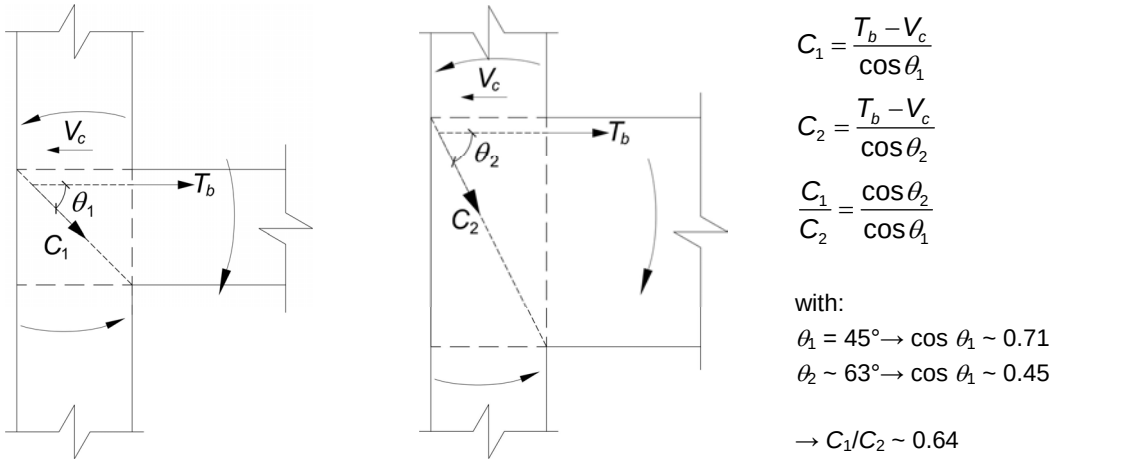

a) h_b/h_c = 1.00 b) h_b/h_c = 2.00 c) Theoretical ratio C_1/C_2

Figure 5-16: Compression demand in the strut for equal T_b - V_c and different h_b/h_c

The analysis of the ratio h_b/h_c was carried out by varying the height of the beam, h_b and keeping the height of the column, h_c, constant (note: it was verified that the variation of h_c instead of h_b carries to the same results). ρ_b was varied to keep the bond forces approximately constant in the different analyses. For joints with anchorage Type 1 the increase of h_b/h_c induced a stiffening of the initial branch of the load-displacement curve and an increase of the joint shear strength at both limit states (Figure 5-17a). The expression of the results in terms of nominal principle tensile stress in the core showed that with increasing h_b/h_c, p_t decreased for both 1st shear crack and peak load (Figure 5-17b). The ratio of the strength between the simulations with h_b/h_c = 1.17 and 2.00 was equal to 0.69 and 0.78 for 1st shear crack and peak load, respectively. 0.69 would have been the ratio according to the simplified theoretical model shown in Figure 5-16. The joint shear distortion increased with increasing ratio h_b/h_c (Figure 5-17b). Figure 5-18 shows that with increasing ratio h_b/h_c the diagonal shear crack in the core becomes steeper.

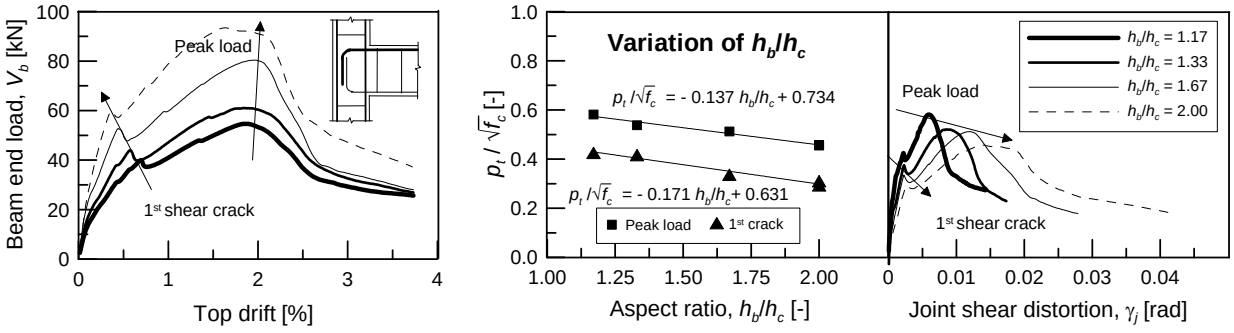

a) LD curves b) Influence of ratio h_b/h_c on strength and deformability

Figure 5-17: Influence of aspect ratio, h_b/h_c, for anchorage Type 1

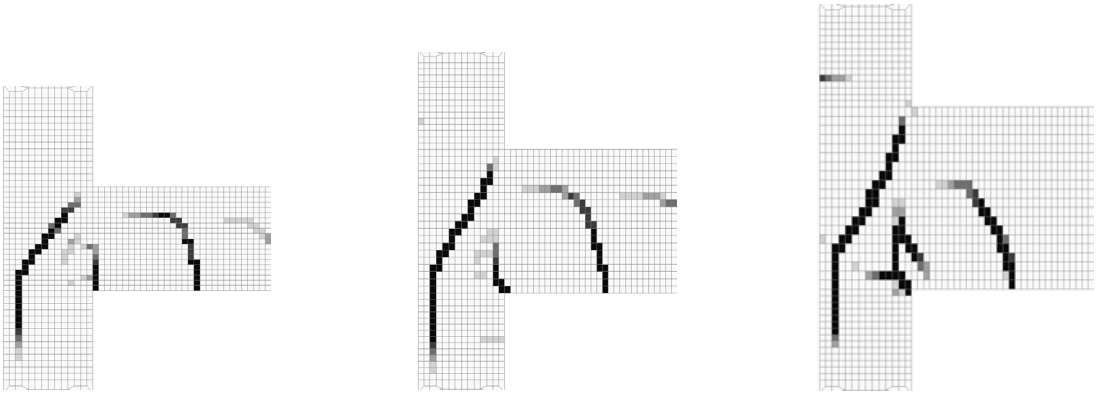

a) h_b/h_c = 1.17 b) h_b/h_c = 1.5 b) h_b/h_c = 2.0

Figure 5-18: Inclination of diagonal shear crack with increasing ratio h_b/h_c (anchorage Type 1)

For beam bars anchored with 90°-hooks bent away from the core (Type 2), the variation of the load-displacement curve with increasing ratio h_b/h_c was qualitatively similar to results of anchorage Type 1 (compare Figure 5-17a with Figure 5-19a). However, the analysis of the results in terms of $p_t/\sqrt{f_c}$ showed that no substantial variation was observed in the investigated range of $1.17 \leq h_b/h_c \leq 2.00$ for both limit states (Figure 5-19a). Also, in this case the joint shear distortion increased with increasing geometric aspect ratio of the joint panel (Figure 5-19b). The reason for this behaviour can be found in the typical cracking pattern observed in the Type 2 joint failing in shear. Comparing Figure 5-20 with Figure 5-18 it can be seen that in the case of anchorage Type 2 the inclination of the diagonal crack does vary significantly with increasing ratio h_b/h_c. In Figure 5-21 the cracking pattern observed in the test JT4-1 (Type 2 anchorage of the bottom bar in Figure 5-21a) is compared to other tests available in the literature. In all cases the diagonal cracks did not follow the geometric diagonal of the joint, but they were much flatter. Increasing the joint ratio h_b/h_c did not really affect the diagonal strut and the nominal principle tensile stresses distribution in the joint was also constant.

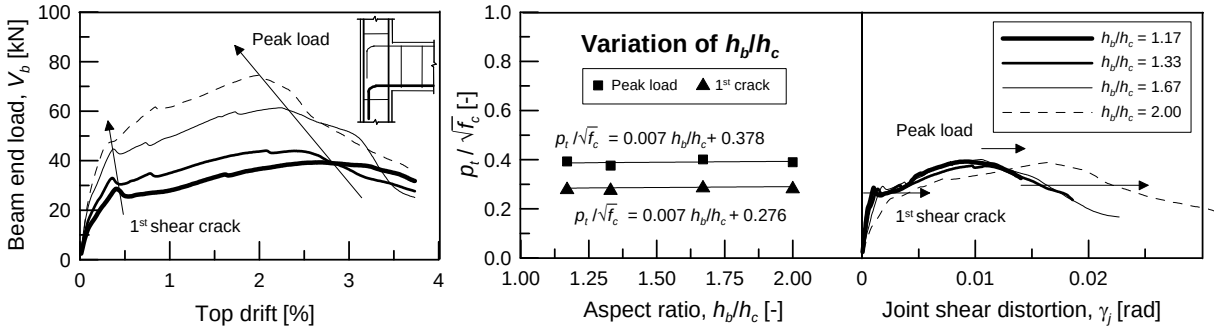

a) LD curves b) Influence of ratio h_b/h_c on strength and deformability

Figure 5-19: Influence of aspect ratio, h_b/h_c, for anchorage Type 2

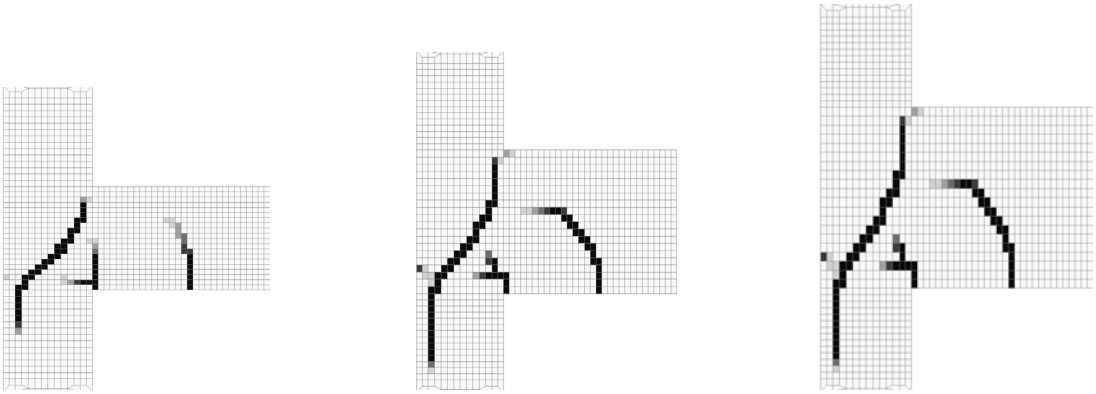

a) h_b/h_c = 1.17 b) h_b/h_c = 1.5 b) h_b/h_c = 2.0

Figure 5-20: Inclination of diagonal shear crack with increasing ratio h_b/h_c (anchorage Type 2)

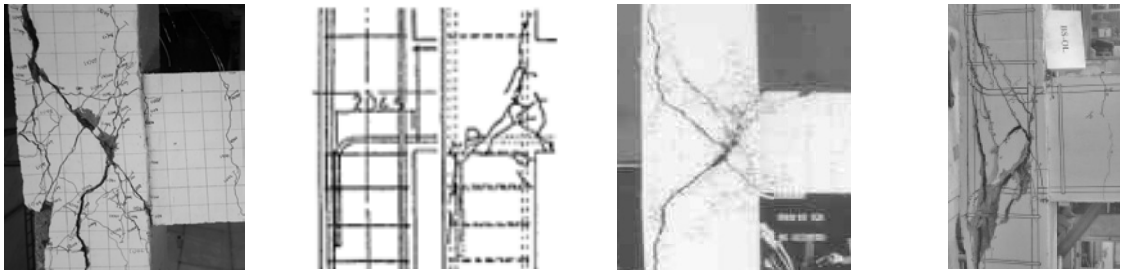

a) *Genesio & Sharma (2010a)* b) *Minami & Nishimura (1985)* c) *Hakuto et al. (2000)* d) *Kuang & Wong (2006)*

Figure 5-21: Typical cracking pattern for joints with anchorage Type 2

For the joint with plain round bars and anchorage with 180°-hooks (Type 6) the qualitative influence of the variation of the aspect ratio, h_b/h_c, was similar to anchorage Type 1 (compare Figure 5-22a with Figure 5-17a). Considering the specimen JT2-1 (Figure 5-22a,b), the ratio of the strength between the simulations with h_b/h_c = 1.17 and 2.00 was equal to 0.53, while 0.69 is the ratio according to the simplified theoretical model shown in Figure 5-16. Considering the specimen "2D pre 1970s" (Figure 5-22c,d) similar ratios were obtained: 0.543 (FE) vs. 0.716 (theoretical). The joint shear distortion did not appear to be affected by the variation of h_b/h_c (see Figure 5-22b).

The assumption of a linear influence of the ratio h_b/h_c on the joint shear strength appears to be reasonable, since the variation of $\cos\theta$ for $45° \leq \theta \leq 60°$ (see Figure 5-16) can be taken as linear with good approximation.

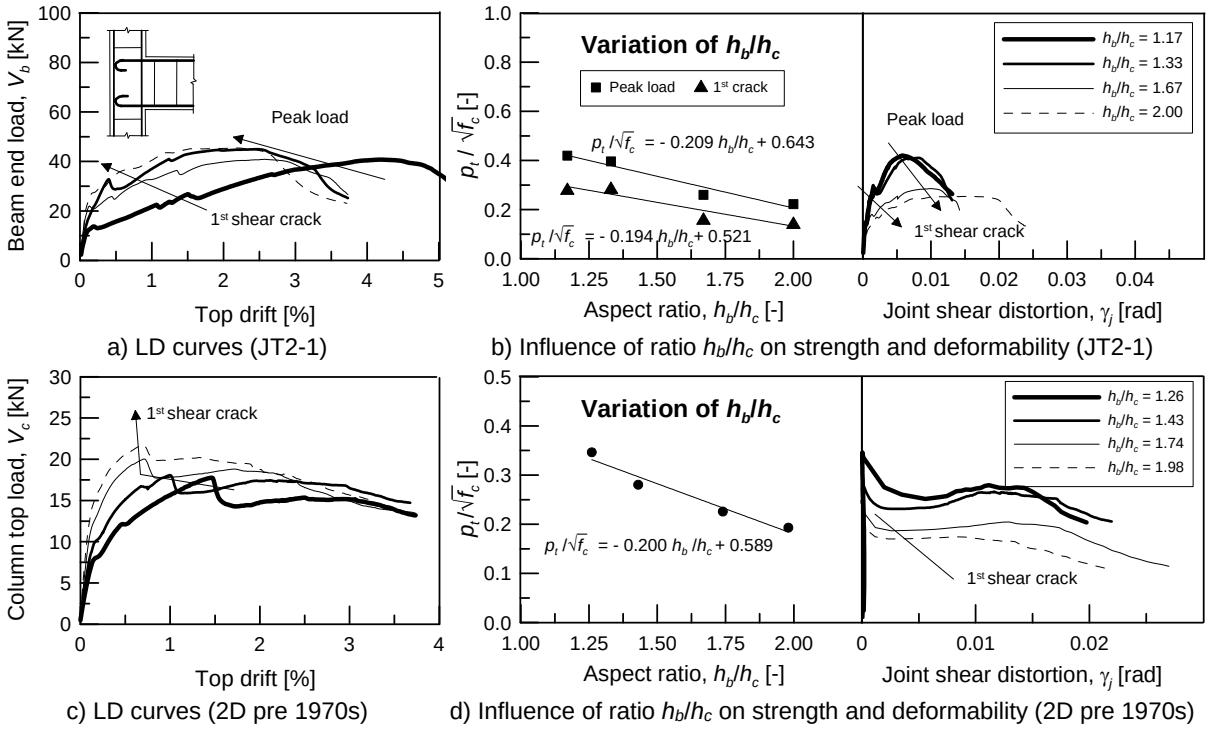

Figure 5-22: Influence of aspect ratio, h_b/h_c, for anchorage Type 6

5.1.6 Findings of the FE parametric study

From the numerical parametric study presented and discussed in the previews sections the following main conclusions can be drawn:

- the increase of joint shear strength with increasing concrete strength is linearly proportional to $\sqrt{f_c}$;
- the increase of shear strength due to the increase of axial load in the column corresponding to the 1st diagonal cracking in the core can be taken into account by considering the principle tensile stress, p_t, instead of the horizontal shear stress, v_{jh}, as proposed by *Priestley (1997)*;
- the increase of shear strength due to the increase of axial load in the column corresponding to the ultimate joint shear strength cannot simply be taken into account by limiting the principle tensile stresses. The ratio between peak load and load at 1st joint diagonal cracking decreases with increasing axial load until the limit of the axial load, after which the peak load corresponds to the 1st joint diagonal cracking. This limit depends on the anchorage type of the beam bars in the core;
- beam and column reinforcement ratios slightly influence the joint strength corresponding to the peak load and initial diagonal cracking, respectively;
- the joint geometric aspect ratio, h_b/h_c, significantly influences the shear strength of the joint, except if beam bars are bent away from the core; and
- the deformability of the specimen evaluated in terms of top drift at the considered limit states increases with increasing f_c and n_c, while the specimen becomes stiffer with increasing ρ_b, ρ_c and h_b/h_c.

The effect of the investigated parameters on the joint shear distortion is discussed in Section 5.2.4.

5.1.7 Influence of test setup

Two different setups for the testing of beam-column joints were used in this study. As shown in Section 3.3, in the test at UC the bottom of the column was hinged and the top was free to move horizontally. The joint was loaded in the horizontal direction on the top of the column and axial load was applied. The specimens tested at BARC were loaded vertically at the beam end and the column was hinged at the top and bottom ends. The static systems used are equivalent for the loading of the specimen, however, the deformation shapes are different. The results are generally considered equivalent.

FE simulations were carried out to verify this assumption. For each of the joint configurations investigated in this study (anchorage Types 1, 2 and 6) three analyses with different boundary conditions were performed. Two analyses correspond to the idealisation of the setups used for the tests carried out at UC and BARC. One analysis was performed assumining that the top and bottom of the column are fixed instead of hinged and the end of the beam is loaded vertically. This configuration should simulate the maximum difference between ideal and real boundary conditions, i.e., full restraint of the flexural moment at both column ends.

In Figure 5-23 the comparison of the monotonic behaviour of beam bar anchorage in the joint region of Type 1 and different boundary condition is shown as an example. The simulations are distiguished by the condition of the top of the column as “free” (as test setup UC), “hinged” (as setup of BARC) and “fixed” (theoretical setup with moment restrain at top and bottom of the column). In Table 5.4, the ratios of the strength values obtained for joints with different reinforcement detailings and boundary conditions are summarised. The calculated factors, α_{setup}, may be used to convert results from one test setup to another.

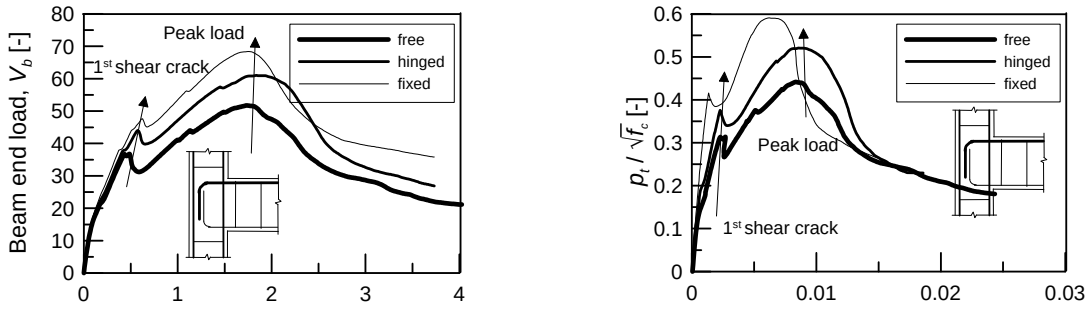

a) Load-displacement behaviour b) Joint shear distortion

Figure 5-23: Influence of test setup for joint with anchorage Type 1

Table 5.4: Ratios of joint shear strength measured for different boundary conditions (α_{setup})

Boundary conditions	Free	Hinged	Fixed
Free	1 [a)]	0.85 [a), b)]	0.75 [a)]
Hinged	1.18* [a)]	1 [a)]	0.90 [a)]
Fixed	1.33 [a)]	1.11 [a)]	1 [a)]

[a)] Values average on FE simulations with joint with anchorage Types 1, 2 and 6 for 1st shear cracking and peak load limit states (maximum CV = 7.4%); [b)] Example: ratio free / hinged

The different joint shear strength measured varying the boundary conditions can be explained by observing the different internal action and deformed shapes that result from the same external loading (V_b or V_c) shown in Figure 5-25. Differences may be observed in the distributions of the bending moment ("hinged" and "free" vs. "fixed") and axial force ("hinged" and "fixed" vs. "free"). However, the greatest difference is in the deformed shapes. It appears that if the joint deformation is less restrained (case "free"), the shear strength is smaller than for a higher degree of restraint (cases "hinged" and "fixed"). It is worth mentioning that the boundary condition with the joint loaded laterally on the top of the column is the closest to the reality of a moment resisting frame for loading pattern and deformation shape. In Figure 5-24 the distribution of principle compressive stresses, σ_{33}, in the joint panel and in the column for the three considered boundary conditions are compared at the load step corresponding to the ultimate strength. Consistently to the strength prediction of the numerical simulations, the compression field in the case of joint "fixed" is larger than for the cases "hinged" and "free". Furthermore, in the case "free" after the joint shear cracking only one strut is clearly visible, while in the other investigated configurations two asymmetric struts can be distinguished (compare Figure 5-24a and Figure 5-24b,c).

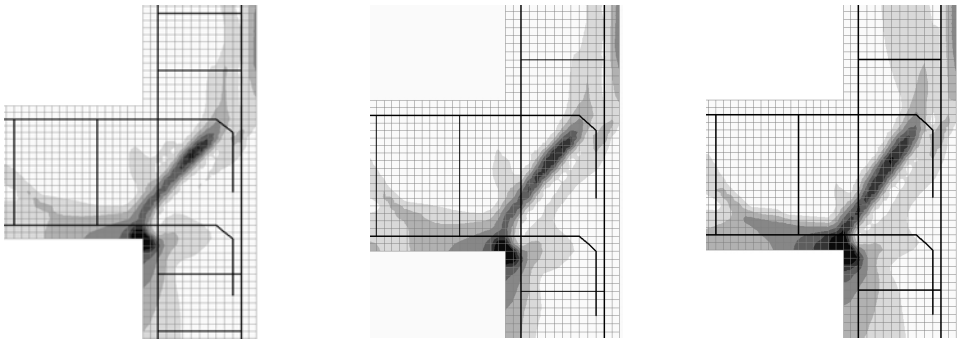

a) Joint "free" b) Joint "hinged" c) Joint "fixed"

(Darker elements → higher σ_{33}, Black elements → $\sigma_{33} = f_c$)

Figure 5-24: Distribution of principle compressive stresses, σ_{33}, at ultimate strength

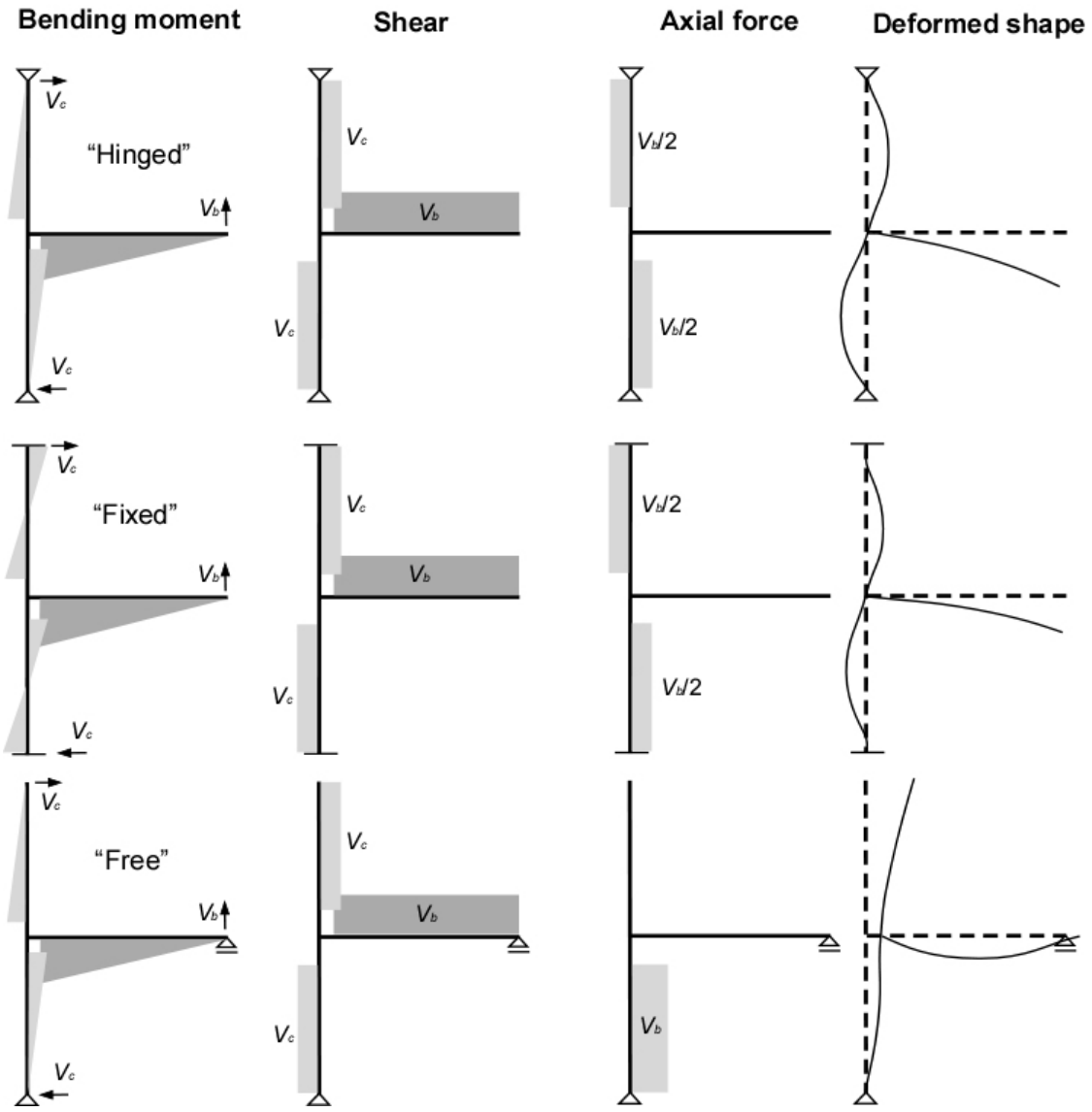

Figure 5-25: External actions, internal forces and deformed shapes of beam-column joint with different boundary conditions

5.2 Analytical model for joint shear strength and deformation based on results of the FE investigations

5.2.1 Strength limit states

On the basis of the numerical parametric study a refinement of the assessment model of Priestley-Pampanin (*Priestley, 1997* and *Pampanin, 2003*) is proposed (see Section 3.5.2).

According to the numerical investigations, it is believed that the influence of the ratio h_b/h_c should be taken into account. Additionally, the positive affect of column axial load on the peak load for no or low axial load levels should be taken into account. This influence cannot be realistically described by p_t, since the failure is determined by the crushing of the cracked compressive strut (see Section 4.3.2). Therefore, it is taken into account by adding an empirical component to Equation (5-3a)).

Equation (5-2) describes the assessment of the initial diagonal cracking of the joint region.

$$\frac{p_t}{\sqrt{f_c}} = k_0 + k_1\left(2 - \frac{h_b}{h_c}\right) \tag{5-2}$$

where k_0 and k_1 are non-dimensional empirical coefficients depending from the joint detailing

The ultimate limit state is defined by Equations (5-3a,b).

$$\frac{p_t}{\sqrt{f_c}} = k_0 + k_1\left(2 - \frac{h_b}{h_c}\right) + \frac{\left(n_{c,0} - n_c\right)}{100}\cdot k_2 \cdot \rho_b \qquad \text{for } n_c \le n_{c,0} \tag{5-3a}$$

$$\frac{p_t}{\sqrt{f_c}} = k_0 + k_1\left(2 - \frac{h_b}{h_c}\right) \qquad \text{for } n_c > n_{c,0} \tag{5-3b}$$

where $n_{c,0}$ is the upper limit value of axial load after which the peak load is coincident with the 1st joint shear cracking. The influence of ρ_c is considered negligible and, therefore, this parameter is not included in the above equations. k_2 is also an empirical coefficient.

The values of k_0, k_1, k_2 and $n_{c,0}$ for the considered joint configurations are given in Table 5-5 and their statistical evaluation is shown.

Table 5-5: Empirical coefficients of the FE assessment model and statistical evaluation

Anchorage	k_0 [-]	k_1 [-]	k_2 [-]	$n_{c,0}$ [%]	No. of FE analyses	$\frac{\left(p_t/\sqrt{f_c}\right)_{FE}}{\left(p_t/\sqrt{f_c}\right)_{Calc}}$		CV [%]	
						1st crack	Peak load	1st crack	Peak load
Type 1	0.15	0.3	1.2	20	20	1.15	1.02	18.2	11.7
Type 2	0.20	0.0	0.9	10	20	1.48	1.47	7.6	9.7
Type 6 [a)]	0.10	0.3	1.2	10	21+24 [b)]	1.05	1.08	13.4	12.6

[a)] α_{setup} according to Table 5.4 was used to convert the results obtained with the UC setup into BARC setup;
[b)] 21 and 24 analyses based on JT2-1 and "2D pre 1970s", respectively

5.2.2 Discussion of the empirical coefficients

The empirical coefficients proposed in Table 5-5 were calibrated on the FE simulations as well as on specific experimental studies available in the literature, i.e., test series where only one parameter was varied.

The k_0 value for anchorage Type 2 was taken to be lower than the value of the numerical simulations (0.2 instead of 0.3) because the comparison of the FE model with the experimental results had evidenced an overestimation of the limit state corresponding to the initial joint shear cracking by the numerical analysis (see Table 4-3).

The coefficient k_1 for anchorage Type 1 and 6 was increased from 0.2 (best fitting from FE simulations) to 0.3 to better describe experimental evidence available in the literature. In Figure 5-26a the influence of the ratio h_b/h_c from two different experimental studies is shown. Values between 0.1 and 0.4 appear to be plausible. In *Vollum & Newmann (1999)* the influence of h_b/h_c is accounted for by a factor of 0.55. A factor of 0.3 was assumed by *Hegger et al. (2003)* on the basis of the analysis of a large experimental database of exterior beam column joints with and without shear reinforcement in the core. FE investigations carried out using different basic models than the one adopted for the study shown in Section 5.1.5 and varying the ratio h_b/h_c are shown in Figure 5-26b. The model 2D-Types 1 and 2 are based on

"2D pre 1970s", while the model TDD2 is the same presented in Section 4.3.5. The slight variation of the influence of the ratio h_b/h_c on the related shear strength, $p_t/\sqrt{f_c}$, is due to the different mesh sizes adopted in the models and consequent slightly different diagonal crack propagation in the joint panel. Similarly, the different trend lines obtained in the experiments (Figure 5-26a) may be due to different cracking patterns and consequent different parameters of the compressive strut (i.e., inclination and width).

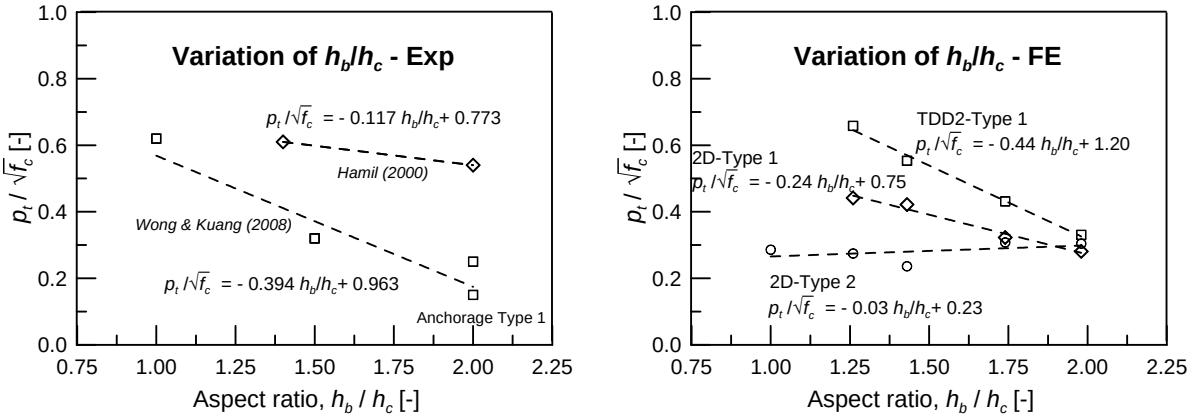

a) Experimental studies

a) FE analyses with different models

Figure 5-26: variation of h_b/h_c (anchorags: Type 1: 90° bent in hooks; Type 2: 90° bent out hooks)

The choice of values of normalised axial loads, $n_{c,0}$, was validated with a few experimental studies, where the axial load was varied and the other parameters were kept constant. In Figure 5-27a the tests results with anchorage Type 1 are analysed in terms of $p_t/\sqrt{f_c}$. A decrease of the ratio $p_t/\sqrt{f_c}$ with increasing n_c is confirmed. For the tests by *Parker & Bullmann (1997)* the value of $n_{c,0}$ could be assumed to be equal to 10% assuming $(p_t/\sqrt{f_c})_{crack}$ = 0.25 (calculated with Equation (5-2), and h_b/h_c = 1.67). Tests by *Clyde (2000)* suggest a limit of $n_{c,0}$ = 30%. In Figure 5-27b similar investigations with anchorage Type 4 (see Figure 6-6) are shown (*Pantelides et al., 2002*). In this case the limit of $n_{c,0}$ appears to be between 25% and 30%. This uncertainness may be also related to the high variability of the cracking pattern (as for the evaluation of the ratio h_b/h_c) that can be observed in the joint panel during experiments. In fact, different inclinations and widths of the compressive strut induce different responses of the beam-column connection to the column axial load.

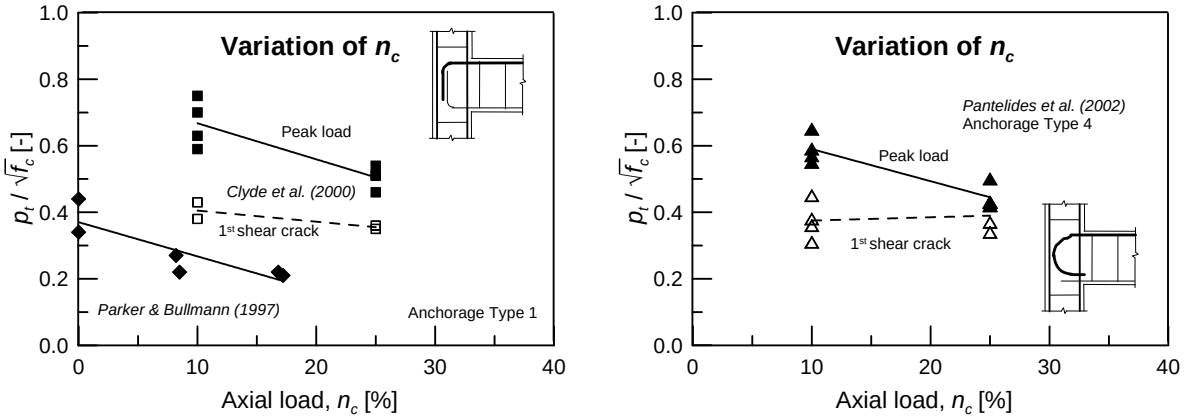

a) Tests with anchorage Type 1

a) Tests with anchorage Type 4

Figure 5-27: Experimental variation of n_c

5.2.3 Effect of yielding of the beam bars

As shown in Section 4.3.4 the yielding of the longitudinal beam bars negatively affect the joint shear strength. Numerical simulations confirmed the suitability of the approach of *Park (1997)*, who proposed the shear strength degradation was related to the curvature ductility factor, μ_ϕ.

Figure 5-28 shows the comparison of Park's proposed shear strength degradation for 2D exterior joints with anchorage Type 1 and no transversal reinforcement in the core and the FE simulations carried out in this study. 24 simulations of joints failing in shear after yielding of the beam bars (i.e., failure modes BJ1 and BJ2) are considered. The trend line of the numerical simulation is approximately parallel to Park's model. The offset is due to the different ratio of h_b/h_c and/or of axial load of the tests considered by Park. Park's model led to a shear strength limit of $p_t/\sqrt{f_c} \sim 0.4$ for pure shear failure, while the benchmark model of the FE analyses (JT1-1) failed in shear in the joint at $p_t/\sqrt{f_c} \sim 0.5$. In both cases, the minimum value of the joint shear strength corresponds approximately to the 1st shear cracking limit state.

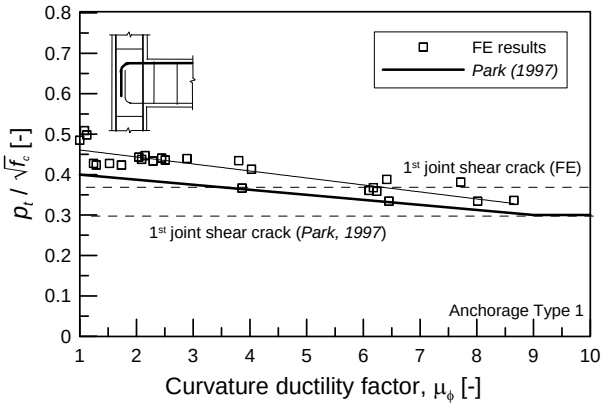

Figure 5-28: Comparison between FE simulations and joint shear degradation curve proposed by *Park, 1997* (anchorage Type 1)

Further FE simulations were carried out to evaluate the influence of the beam flexural hinging on the joint shear strength for anchorage Type 2 and 3. The proposal of the joint shear degradation by *Park (1997)* for joints with beam bars bent away from the core (Type 2) is much more conservative than the results obtained in the numerical simulations (see Figure 5-29a). The FE simulations indicate shear strength degradation up to $\mu_\phi \sim 6$. For higher beam curvature ductility factors the joint shear strength corresponds approximately to the initial joint shear cracking limit state. Park proposed a limit of $\mu_\phi \sim 3$ and a constant $p_t/\sqrt{f_c} \sim 0.1$. For joints with plain round bars and 180°-hooks (anchorage Type 6) no experimental studies on the joint shear degradation are available. As shown in Figure 5-29b, the FE analyses indicate that beam flexural ductility has a small influence on the joint shear strength for the case of plain round bars and anchorage Type 6. A shear strength reduction, up to the initial joint cracking limit state, occurs at $\mu_\phi \sim 25$. This result appears to be reasonable, since the strain penetration does not have a significant effect in reducing on the bond capacity of plain round bars.

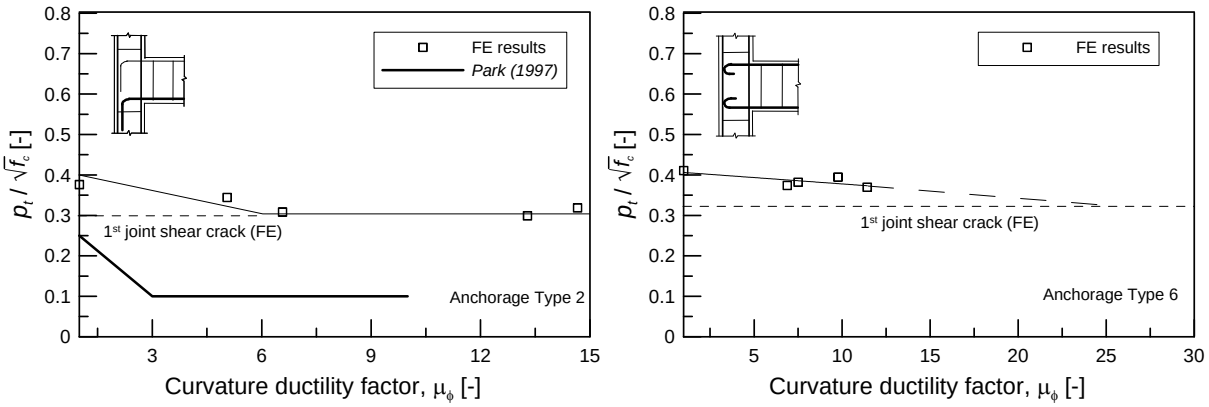

a) Anchorage Type 2, FE vs. *Park (1997)* b) Anchorage Type 6 , FE

Figure 5-29: Comparison between FE simulations and joint shear degradation curves

Generally, the lower bound of the joint shear strength can be described with the Equation (5-2), while the Equation (5-3a) can be modified as follows to take into account the flexural yielding of the beam.

$$\frac{p_t}{\sqrt{f_c}} = k_0 + k_1\left(2 - \frac{h_b}{h_c}\right) + \left[\frac{\left(n_{c,0} - n_c\right)}{100} \cdot k_2 \cdot \rho_b\right] \cdot \alpha_y \quad \text{for } n_c \le n_{c,0} \tag{5-4a}$$

with:

$$\alpha_y = 1 - \mu_\phi / 6 \tag{5-4b}$$

for $\mu_\phi > 6$ the ultimate strength of the joint corresponds to the initial diagonal cracking. For simplicity, this limit is assumed to be valid for all anchorage types of beam bars in the core.

5.2.4 Deformation limit states

The joint shear deformability, γ_j has also been investigated in the parametric study and it has been evaluated at the considered limit states ($\gamma_{j,crack}$ and $\gamma_{j,peak}$). The main observations can be summarised as follows:

- the joint detailing (form of the anchorages hooks and plain round vs. deformed bars) does not significantly influence the joint shear distortion;
- the variations of f_c, ρ_b and ρ_c do not influence the joint deformability;
- increasing the axial load level, n_c, from 0% up to 40%, γ_j corresponds to a 1st diagonal cracking increase from 0.001 rad up to approximately 0.007 rad, while γ_j corresponding to the peak load is not significantly influenced; and
- with increasing ratio h_b/h_c, γ_j corresponding to both limit states increases. For $h_b/h_c = 1.0$ γ_j appears to be negligible, while for h_b/h_c up to 2.0 $\gamma_{j,crack}$ and $\gamma_{j,peak}$ increase to 0.001 rad and 0.015 rad, respectively.

On the basis of the FE analyses a tri-linear general p_t - γ_j curve is proposed (black curve in Figure 5-30). The first branch corresponds to the joint elastic shear deformation and it is limited by the 1st joint shear cracking. The second branch is less stiff and its inclination depends on the axial load level on the column, n_c. With increasing ratio h_b/h_c the shear stiffness of the joint panel decreases. However, a quantification of the influence of n_c and h_b/h_c is not proposed, because in reality the scatter of the p_t-γ_j curves is extremely large (see

Section 6.6). The values derived in this FE parametric study (see above at the beginning of this section) can be assumed as a first approximation. After the peak load no plateau is generally observed and a linear descending branch can be introduced. For comparison curves for increasing n_c and h_b/h_c are schematically sketched.

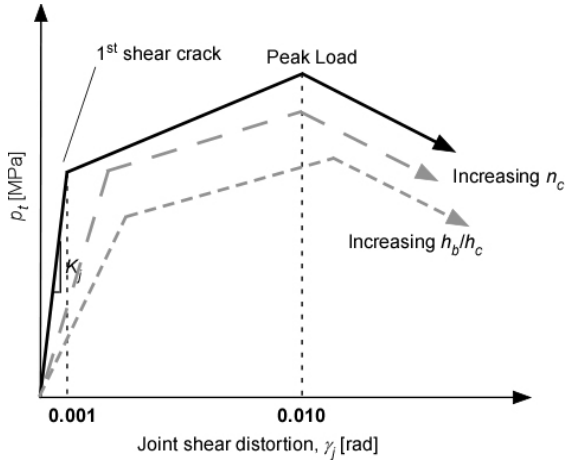

Figure 5-30: Schematic of joint shear distortion

5.3 Summary of FE parametric study and development of the analytical model

A parametric study on 2D RC exterior beam column joints has been carried out. Three different anchorage dailings of the loagitudinal beam bars in the joint panel have been taken into consideration:

- deformed bars with 90° bent into the core (Type 1),
- deformed bars with 90° bent away from the core (Type 2) and
- plain round bars with 180° hooks (Type 6).

The following parameters have been varied:

- Concrete compressive strength, f_c
- Column axial load, n_c
- Beam reinforcement ratio, ρ_b
- Column reinforcement ratio, ρ_c
- Joint geometric aspect ratio, h_b/h_c

An analytical model for the evaluation of the joint shear strength has been developed. Two limit states are distinguished: 1st diagonal joint cracking and peak load. The model constitutes a refinement of the Priestley-Pampanin model (*Priestley, 1997* and *Pampanin et al., 2003*). It is based on principles of mechanics (i.e., Mohr circle's theory) and empirical factors to take into account the influence of different parameters. The model takes into account the detrimental effect of the beam bars yielding on the joint shear strength.

Furthermore, indications on the joint shear deformability are provided.

6 COMPARISON BETWEEN TEST RESULTS AND PROPOSED ANALYTICAL JOINT SHEAR STRENGTH MODEL

In Chapter 5 the assessment method for the evaluation of the shear strength 2D exterior beam-column joints without shear reinforcement in the core was developed and proposed on the basis of a numerical parametric study. In this chapter the same model is validated by comparing it with an experimental database including tests on beam-column connections carried out worldwide in the past forty years (see literature review in Section 2.2). In Section 6.1 the experimental database is discussed and the principles used for its analysis are presented. In Section 6.2 the capability of the assessment model to capture the influence of the considered parameters is shown. In Section 6.3 the influence of other types of anchorages on the shear strength of beam-column joints tested in the literature are evaluated using the proposed assessment model. In Section 6.4 the model is statistically evaluated and characteristic strength values for substandard joints are proposed.

The influence of the beam flexural ductility on the joint shear strength investigated in Section 5.2.3 could not be further evaluated due the lack of experimental data available in the literature (Section 6.5). In Section 6.6 the proposed deformability limit states, in terms of joint shear distortion, are compared with values from the literature.

6.1 Experimental database of exterior beam-column joints

6.1.1 General description

The considered experimental database includes tests on exterior 2D beam-column joints failing in shear in the joint (Table 6.1). Additionally, tests of beam-column connections failing in shear after flexural yielding of the beam are considered if the joint shear cracking occurred before the yielding of the beam longitudinal bars. These tests were evaluated for the initial shear cracking limit state. In general only tests on joints without any transverse reinforcement in the core are considered. For the large majority of the tests, only the ultimate shear strength of the specimen was reported. The minority of the tests recorded the 1st diagonal crack in the core and in much fewer cases the joint shear distortion was measured. Only results of tests, where sufficient documentation was available (i.e., material characteristics, geometry, test setup and description of the behaviour) were taken into consideration. According to experimental results available in the literature (e.g., *Hamil, 2000*) the presence of transverse reinforcement does not have any influence of the initial diagonal cracking of the core. For this reason additional results of tests on specimens with transversal reinforcement can be considered for the evaluation of 1st joint shear cracking. Therefore, these kinds of tests have been included in the data base, but only for the evaluation of limit state corresponding to the initial cracking of the joint core.

Table 6.1: Summary of the experimental database

Anchorage	n [a)]	f_c [MPa]		n_c [%]		ρ_b [%]		ρ_c [%]		h_b/h_c [-]	
		min	Max	min	Max	min	Max	min	Max	min	Max
Type 1	32 / 64	19.3	46.2	0.0	38.3	0.51	2.30	0.28	2.33	0.89	2.00
Type 2	7 / 20	24.6	45.6	0.0	30.0	0.65	1.35	0.45	2.23	1.00	2.00
Type 3	12 / 16	19.3	47.4	4.7	47.4	0.55	2.03	1.13	3.48	1.40	2.00
Type 4	8 / 8	31.0	31.7	10.0	25.0	1.71	1.71	1.36	1.36	1.00	1.00
Type 5	6 / 6	25.5	34.0	0.0	25.0	0.77	1.71	0.90	1.36	1.00	1.60
Type 6	11 / 13	17.4	25.0	0.0	20.8	0.35	0.77	0.43	1.04	1.33	1.65
Total	**76 / 127**										

[a)] *X*/*Y*: *X* tests out of *Y* with information about 1st diagonal crack in the joint

For the evaluation of the experimental database the following criteria were used:

- Results from monotonic and cyclic tests are generally comparable, as shown by *Hamil (2000)*;
- the anchorage detailing of the beam top/bottom bars in the core is not influenced by the detailing of the bottom/top layer of reinforcement as shown by tests by *Pantelides et al. (2002)*, *Murty et al. (2003)* and the tests presented in Chapter 3;
- the length of the tail extension of beam bar anchorage in the core does not significantly influence the joint shear strength as long as it is sufficient to avoid a pullout failure. This assumption is justified by the observations of *Scott (1996*) and; and *Murty et al. (2003).*
- only specimens with straight anchorage of beam bars through the entire depth of the column and bending just before the concrete cover are considered. Tests by *Morita & Fuji (1984)* and *Nishimura & Minami (1988)* showed the decreased effectiveness of beam bar anchorage with bending starting mid-depth of the column. These cases are discussed in Section 6.3.
- For cyclic tests, the strength and deformation at the considered limit states in both loading directions are not assumed to be correlated. No specific studies are known in the literature to suggest otherwise. However, it is commonly accepted that for cyclic loading of beam-column joints, the lowest resistance (for closing or opening joint) is considered to be the ultimate limit state. This approach does not allow the results from monotonic and cyclic tests to be realistically compared. The analysis of the database, taking into consideration only cyclic tests on perfectly symmetrical specimens, shows that the average of ratios between resistances (smaller resistance in loading direction 1 or higher resistance in loading direction 2) is 0.90 and 0.92 for 1st cracking and ultimate strength respectively. The Coefficients of Variations, CV, are equal to 8.4% and 8.3%, respectively. The ratio between the resistances in both loading directions is close to 1.0 with reasonably small CV. These values are well below the typical scattering of the results for these kinds of tests (15-20%) and confirm that both values can be compared to the joint shear strength calculated by the model presented in Chapter 5.

It is worth mentioning that in some cases the definition of the 1st diagonal cracking of the joint panel by different authors could not be verified (i.e., no photos or definition of the cracking pattern are available). In these cases the results were not taken into consideration (e.g., tests

by *Scott, 1996*). The cracking pattern in the core shown in Figure 6-1a is not considered to be initial joint shear cracking, because the Strut-And-Tie mechanism explained in Section 4.3.2 is not influenced by these cracks. The joint panel shown in Figure 6-1b is considered cracked.

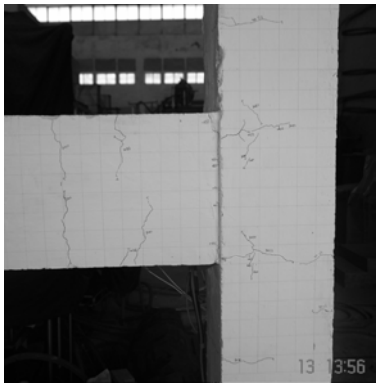

a) Joint panel uncracked

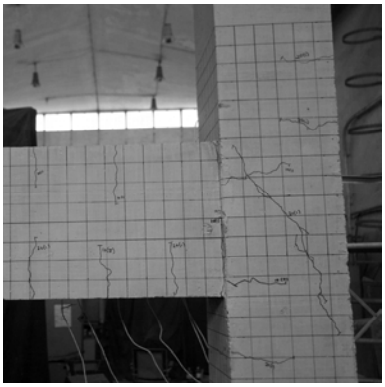

a) Joint panel cracked

Figure 6-1: Definition of 1st diagonal shear crack

The test specimens of the database are different in dimension and scale, typically between half and full scale. Tests by *Abrams (1987)* on interior and exterior joints showed that specimens scaled from 1/4 to 3/4 provided comparable force-deflection relations. The dimensions range of the tests constituting the database is shown in Table 6.2. All relevant information of the tests included in the database are summarised in Appendix B.

Table 6.2: Summary of the dimensions of the tests specimens

H_c		$L_b/2$		h_b		w_b		h_c		w_c	
min	**Max**	**min**	**Max**	**min**	**Max**	**min**	**Max**	**min**	**Max**	**min**	**Max**
1500	3900	570	2130	200	625	110	406	150	460	150	500

All measures in [mm]

6.1.2 Influence of test setup

Different test setups can be found in the literature and they may influence the load-deformation behaviour of the beam-column connection. No comparative experimental studies are available and, therefore, the α_{setup} obtained in the numerical study (see Section 5.1.7) were used. Typical setups are shown in Figure 6-2.

The large majority of the experimental tests of the databse considered in this study are constrained according to the scheme “hinged” (top and bottom column hinge and vertical loading of at the beam end) and only a few are horizontally loaded at the top of the column (scheme “free”). Therefore, all the results obtained with test setups of type “free” are accordingly converted into type “hinged” by multiplying them with the approriate α_{setup} (see Table 5.4).

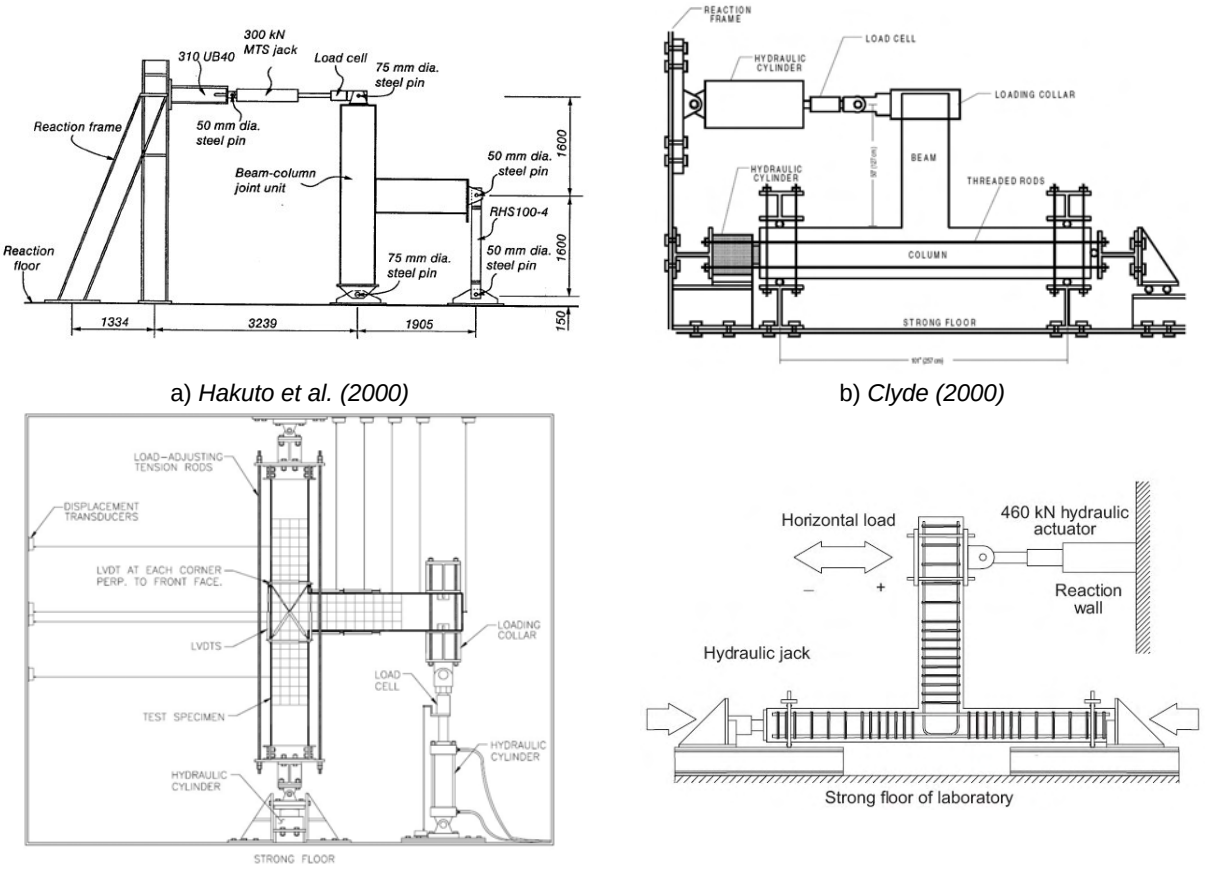

a) *Hakuto et al. (2000)* b) *Clyde (2000)*

c) *Pantelides et al. (2002)* d) *Kuang & Wong (2006)*

Figure 6-2: Typical test setups

6.2 Evaluation of the investigated parameters

In the following sections the assessment model based on the numerical parametric study (Chapter 5) is validated using the experimental database. For this comparison, only the tests summarised in Table 6.1 and with joint detailing corresponding to Types 1, 2 and 6 are considered.

In Figure 6-3 to Figure 6-7 the assessment model presented in Chapter 5 is verified using the experimental database. Each considered parameter (f_c, n_c, ρ_b, ρ_c and h_b/h_c) for each different anchorage detailing is evaluated and the best fitting linear trends are shown. The linear trends can be considered reliable for tests with anchorage Type 1 (32 and 61 specimens for 1st shear cracking and ultimate strength, respectively), but less for Type 2 (7 and 16 specimens for 1st shear cracking and ultimate strength, respectively) and Type 6 (11 and 13 specimens for 1st shear cracking and ultimate strength, respectively), because of the small amount of tests available for the comparison. However, the influence of the considered parameters can be captured with acceptable confidence for both limit states with few exceptions.

The influence of f_c is realistically captured for all anchorage types. The model appears to be less conservative in the prediction of the ultimate strength for $f_c \geq 40$ MPa (see Figure 6-3b). The six tests which determined this trend were carried out by *Parker & Bullmann (1997)* and they exhibit a ratio $(p_t/\sqrt{f_c})_{Exp}$ / $(p_t/\sqrt{f_c})_{Calc}$ between 0.65 and 0.95. The reliability of those tests, however, was criticised also in *Hegger & Roeser (2002)* and *Vollum and Newmann (1999)*.

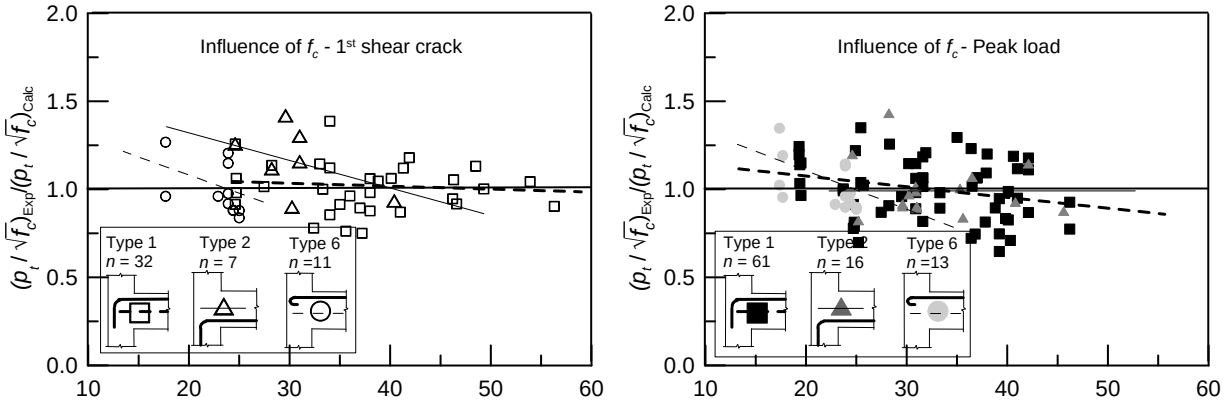

a) 1st joint shear crack b) Joint ultimate strength

Figure 6-3: Comparison between FE and Exp results (influence of f_c)

The effect of variation of the normalised axial load, n_c, is captured by the model with acceptable confidence for all anchorage types for both limit states (see Figure 6-4). However, it should be noted that the model is conservative for high values of axial load and anchorage Type 1 ($n_c \geq 25\%$). This aspect was already discussed in Section 5.2.2 (see Figure 5-27).

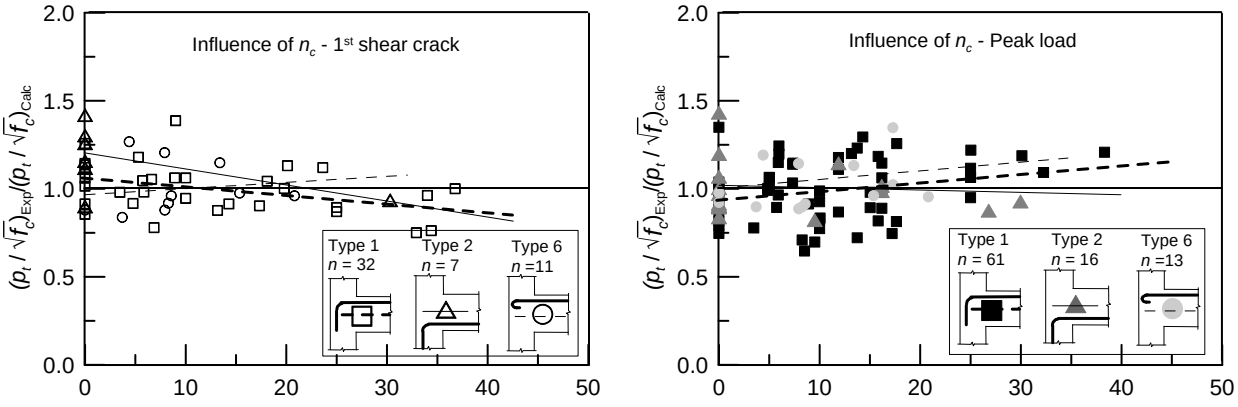

a) 1st joint shear crack b) Joint ultimate strength

Figure 6-4: Comparison between FE and Exp results (variation of n_c)

The effect of variation of beam (ρ_b) and column (ρ_c) reinforcement ratios is captured by the model with acceptable confidence for all anchorage types for both limit states (see Figure 6-5 and Figure 6-6). Some minor uncertainness related to the small amount of tests are present in the evaluation of joints with anchorage Types 2 and 6 for the initial shear cracking limit state (Figure 6-5a and Figure 6-6a). The assessment of initial cracking for the anchorage Type 2 appears to be slightly conservative.

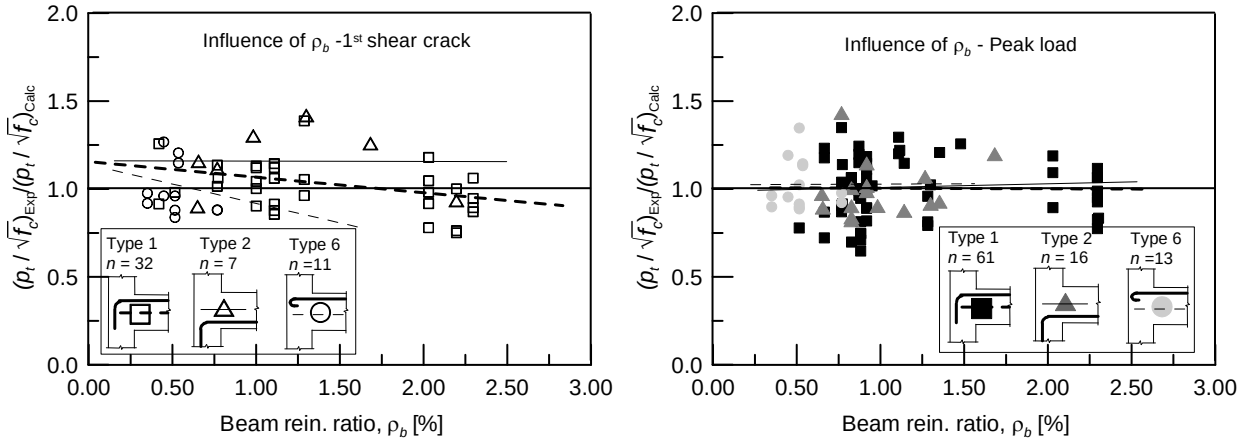

a) 1st joint shear crack b) Joint ultimate strength

Figure 6-5: Comparison between FE and Exp results (variation of ρ_b)

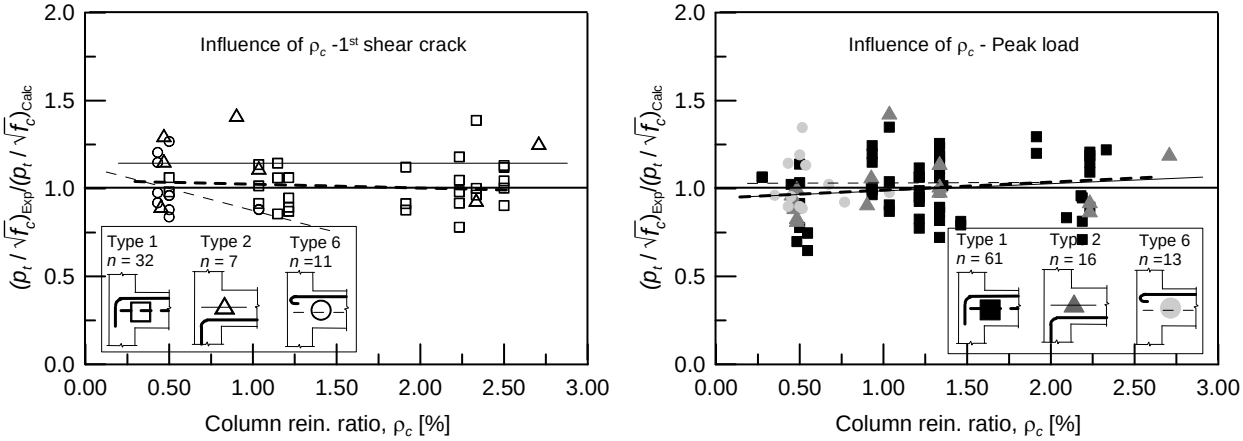

a) 1st joint shear crack b) Joint ultimate strength

Figure 6-6: Comparison between FE and Exp results (variation of ρ_c)

The trends lines for the evaluation of the ratio h_b/h_c diverge significantly from the ideal one for the anchorage Types 2 and 6, but this is mainly due to the low amount of specimens available for the evaluation of the model as shown in Figure 6-7 and Figure 6-8. The trendline for 1st shear cracking of anchorage Type 2 (Figure 6-7a) indicates an increase of $p_t/\sqrt{f_c}$ with increasing ratio h_b/h_c, which is physically not reasonable. However, it should be noted that the few available test results cover a small range of $1.00 \le h_b/h_c \le 1.40$. The trendline for anchorage Type 6 is also based for both limit states on a very small range $1.43 \le h_b/h_c \le 1.65$ (Figure 6-7a,b). The same figures indicate a good agreement of the assessment model with the available experimental results for the anchorage Type 1 at both limit states.

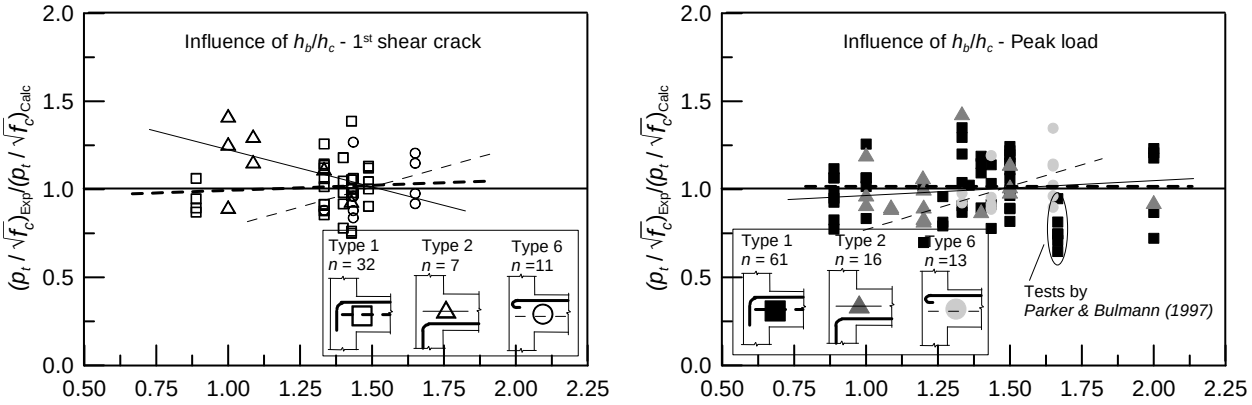

a) 1st joint shear crack b) Joint ultimate strength

Figure 6-7: Comparison between FE and Exp results (influence of h_b/h_c)

The assessment model proposed in Chapter 4 can be considered valid in the range of parameters described in Table 6.2 and Table 5.4 for the anchorage Type 1, 2 and 6.

6.3 Influence of different detailing of beam bar anchorage in the joint

The assessment model of the joint shear strength was developed considering the three of the most common beam bar anchorage detailing in the core in pre 1970s practice (Types 1, 2 and 6). In the literature other detailing types can be found.

6.3.1 U-Shaped anchorage with deformed bars (Type 3)

Several authors investigated the effect of U-shaped beam bar anchorage in the core (e.g., *Taylor, 1974*; *Hoekstra, 1977*; *Scott, 1996*, *Hamil, 2000* and *Kuang & Wong, 2006*). According to the available data both strength limit states can be estimated by the proposed assessment model with good approximation by assuming the same parameters (k_0, k_1, k_2 and $n_{c,0}$) and 90°-hooks bent into the joint (anchorage Type 1). It should be noted that some authors observed a strength decrease of 10~15% for joints with anchorage Type 3 in comparison to Type 1 (*Vollum & Newmann, 1999* and *Hegger, 2002*).

6.3.2 180°-big hooks with deformed bars (Type 4)

Pantelides at al. (2002) tested exterior joints with beam bar anchorage comprising 180°-hooks with large diameters (Figure 6-8a). The results of those tests suggest that for this detailing (anchorage Type 4) the joint ultimate shear strength is approximately the same as for anchorage Type 1. The strength corresponding to the initial joint shear cracking is slightly lower than for anchorage Type 1. This may be due to the large curvature radius of the hooks and use of beam bars with large diameter, d_b = 28.5 mm and consequently short length of straight anchorage, l_{dh}, in respect to the column depth, h_c (l_{dh} = 114 mm with h_c = 406 mm, Figure 6-8a). A large curvature radius of hook and short straight anchorage may be unfavourable, because the effective joint depth, where the tensile stress field in the concrete develops, is reduced. The same does not influence the compressive strut. Furthermore, observing the cracking patterns shown in Figure 6-8b,c, it can be seen that most of the diagonal cracks are steeper than the geometric diagonal of the joint. This is an indication that the cracks start at the beginning of the bending of the beam bars reducing the effective depth

of the joint core. For anchorage Type 4, the same formulation of the assessment equation as in the case of anchorage Type 1 is proposed, but the coefficient k_0 is conservatively taken as 0.10 instead of 0.15.

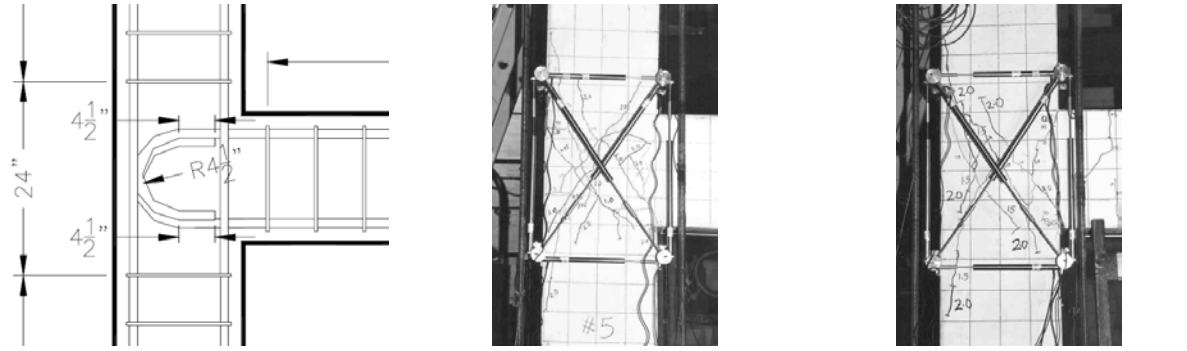

a) Reinforcement detailing b) Cracking pattern specimen #5 b) Cracking pattern specimen #6

Figure 6-8: Reinforcement and cracking patterns of tests by *Pantelides et al. (2002)*

6.3.3 Straight anchorage with deformed bars (Type 5)

A few studies on the behaviour of straight anchorage (Type 5) are also available. According to *Morita & Fuji (1984)*, in the case of anchorage of the beam bars that do not utilise the whole column depth, h_c, l_{dh} should be substituted for h_c in the calculations of the joint shear stress, v_{jh} (compare Figure 6-9a,b). This approach was validated by the tests of *Nishimura & Minami (1988)*. This situation typically occurs in the case of static detailing of the bottom beam bars (e.g., l_{dh} = 150 mm according to *ACI 318-71* in the case of straight anchorage of beam reinforcing bars). In the test with straight anchorage carried out in this study, JT3-1 (see Section 3.4.4), it was also observed that the portion of the joint panel between the end of the beam bars and the back side of the column remained undamaged during the entire test. This observation suggests that no significant stresses were acting in that region.

In Table 6.3 the results available are analysed according to the above concept. The straight anchorage, l_{dh}, induces a much lower joint strength than the case of hooked ends, if the anchorage is shorter than the column depth, h_c (tests by *Pantelides et al., 2002*, T1 and T2 and JT3-1 in Figure 6-9a). If l_{dh} is approximately as long as h_c the straight anchorage appears as affective as the hooked end, as shown by the analysis of the tests by *Pantelides et al. (2002)*, T3 and T4. If the ratio $p_t/\sqrt{f_c}$ is recalculated replacing h_c with $l_{dh} + c$ (c = concrete cover), the results with anchorage Type 5 are very similar to anchorage Types 1 and 4. The concrete cover, c, is taken in the account in the calculation shown in Figure 6-9d to be consistent with the calculation in Figure 6-9c, where $h_c = l_{dh}$ + c is used instead of l_{dh}. The test T14 described in *Nilsson (1974)* is also included in the comparison, although its behaviour is captured with less accuracy by the proposed model. The reason can be found observing the cracking pattern in Figure 6-9b, which shows that one diagonal shear cracks starts in the middle of the anchorage reducing the efficiency of the same.

The results shown suggest that the related shear strength, $p_t/\sqrt{f_c}$, of the joint with straight anchorage approximately corresponds to anchorage Type 1 (or 4) if the h_c is replaced by $l_{dh} + c$ in the calculation of the joint horizontal shear stress, v_{jh} (as shown in Figure 6-9c,d) and the geometric aspect ratio of the joint is taken as $h_b/(l_{dh} + c)$. The compression stress due to the column axial load, f_a, should still be evaluated considering the entire column cross section.

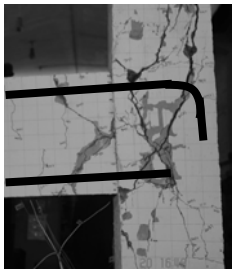

a) Test JT3-1 (see Chapter 3)

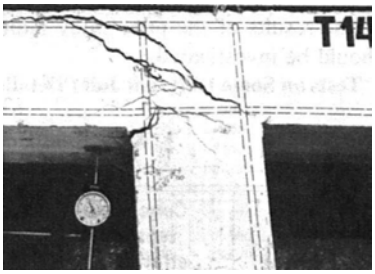

b) Test T14 *Nilsson (1973)*

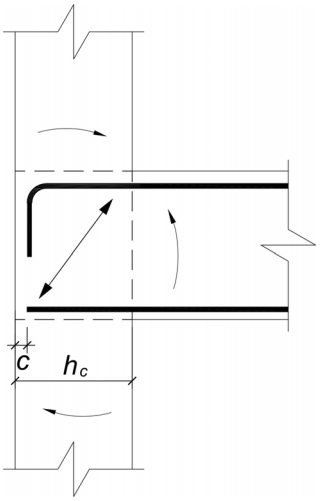

$$v_{jh} = V_{jh} \Big/ \left(w_j \cdot h_c \right)$$

c)

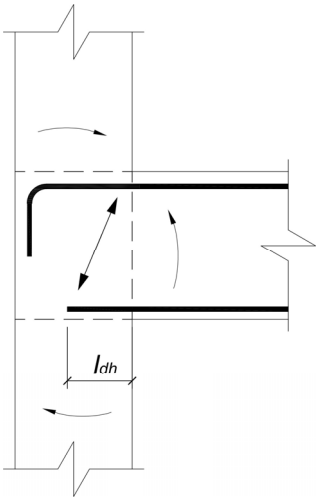

$$v_{jh} = V_{jh} \Big/ \left[w_j \cdot \left(l_{dh} + c \right) \right]$$

d)

Figure 6-9: Typical cracking pattern associated to straight anchorage and calculation of v_{jh} for different anchorage lengths

Table 6.3: Analysis of tests on joints with straight anchorage

1st Author / Test	l_{dh} / h_c [mm]	$p_t l \sqrt{f_c}$ measured straight bars with h_c c)		$p_t l \sqrt{f_c}$ calculated straight bars with $l_{dh} + c$ c)		$p_t l \sqrt{f_c}$ measured hooked ends c)	
		1st crack	ultimate	1st crack	ultimate	1st crack	ultimate
Pantelides / T1 a)	150 / 406	0.20	0.22	0.59	0.64	0.45	0.59
Pantelides / T2 a)	150 / 406	0.18	0.22	0.63	0.63	0.42	0.42
Pantelides / T3 a)	350 / 406	0.41	0.58	0.43	0.61	0.38	0.57
Pantelides / T4 a)	350 / 406	0.40	0.46	0.43	0.49	0.43	0.50
Genesio / JT3-1 b)	150 / 300	0.22	0.33	0.35	0.52	0.36	0.46
Nilsson T14	174 / 200	0.31	0.40	0.31	0.40	0.45 d)	0.61 e)

a) Reference anchorage Type 4; b) Reference anchorage Type 1; c) 1st shear crack / peak load; d) Value calculated using Equation (5-2); e) Value calculated using Equation (5-3a)

In the same way, the tests by *Nishimura & Minami (1988)* on joints with anchorage Types 1 and 2 and ending at mid depth of the column can be evaluated and included in the statistical analysis of the model.

6.3.4 90°-hooks bent in / bent out with plain round bars (Types 7 and 8)

The anchorage of tensioned plain round bars with anchorage different than 180°-hooks (Type 6) was not allowed by any of the code provisions considered in this study (see Section 2.4.8). However, anchorage solutions 90°-hooks bent in (Type 7) and bent out (Type 8) can be found in the literature. Tests with this type of joint detailing were carried out by *Liu & Park (2001)* and they highlighted a lower strength in comparison to similar tests with deformed bars and the joint shear strength could not be reached, because of opening and consequent pullout of the 90°-hooks. Because of the lack, of further available data the shear strength of joints with anchorage Type 7 and 8 can be conservatively limited to the pullout strength of the beam bars.

6.3.5 Straight anchorage with plain round bars (Type 9)

No tests with beam plain round bars and straight anchorage in the joint core are known to be available. However, it may be reasonably assumed that in that case a pullout of the bars would occur before the joint shear strength is reached. For example, considering the test specimen "2D pre 1970" (see Section 3.4.1), the joint shear force V_{jh} at peak load was equal to 86 kN and 109 kN in positive and negative loading direction, respectively. Assuming, the same beam-column joint, but with beam bars with straight anchorages in the core though the entire beam height, h_c, instead of 180°-hooks, the maximum pullout resistance of the beam bars would be approximately 26 kN (assuming the maximum bond-stress $\tau_f + \tau_m$ = 1.0 MPa according to Figure 4-6).

6.4 Statistical evaluation of the proposed assessment model

The model was statistically evaluated and the 5%-fractile was estimated on the basis of number of results, n, and the coefficient of variation, CV. The coefficient of confidence was assumed equal to 0.75 (*Fischer, 1995*). As suggested by *Fischer (1995)* a normal distribution and logarithmic distributions of the results were assumed when CV ≤ 20% and CV > 20%, respectively.

In Table 6-4 the parameters, k_0, k_1, k_2 and $n_{c,0}$ for the different anchorages of beam bars in the core, that can be commonly found in pre 1970s construction practice, are summarised. The statistical evaluation in terms of average values and coefficients of variations is also shown. On the basis of the work of *Fischer (1995),* the coefficients $\alpha_{5\%}$ have been calculated for each reinforcement detailing and for the entire model. Multiplying the values of joint shear strength calculated with Equations (5-2), (5-3a,b) and (5-4a) by $\alpha_{5\%}$ (See Eqs. (6-1) to (6-2b)), it is possible to determine the characteristic shear strength of the joint. The value $\alpha_{5\%}$ ~ 0.7 calculated for the global model is very close to the typical value of 0.75 generally used for RC structures. The latter is derived assuming a normal distribution with CV = 15% and "large" amount of specimens (generally n > 100)

1st joint shear cracking:

$$\frac{p_t}{\sqrt{f_c}} = \left[k_0 + k_1 \left(2 - \frac{h_b}{h_c} \right) \right] \cdot \alpha_{5\%} \qquad (6\text{-}1)$$

Ultimate limit state:

$$\frac{p_t}{\sqrt{f_c}} = \left\{ k_0 + k_1 \left(2 - \frac{h_b}{h_c} \right) + \left[\frac{\left(n_{c,0} - n_c \right)}{100} \cdot k_2 \cdot \rho_b \right] \cdot \alpha_y \right\} \cdot \alpha_{5\%} \qquad \text{for } n_c \le n_{c,0} \qquad (6\text{-}2a)$$

$$\frac{p_t}{\sqrt{f_c}} = \left[k_0 + k_1 \left(2 - \frac{h_b}{h_c} \right) \right] \cdot \alpha_{5\%} \qquad \text{for } n_c > n_{c,0} \qquad (6\text{-}2a)$$

Table 6-4: Empirical coefficients of the assessment model and statistical evaluation

Anchorage Type	k_0 [-]	k_1 [-]	k_2 [-]	$n_{c,0}$ [%]	No. of exp. tests [a)]	$\frac{\left(p_t/\sqrt{f_c}\right)_{Exp}}{\left(p_t/\sqrt{f_c}\right)_{Calc}}$ [a)]	CV [a)] [%]	$\alpha_{5\%}$ [a)] [-]
1	0.15	0.30	1.2	20	32 / 64	1.00 / 0.99	14.1 / 17.1	0.73 / 0.68
2	0.20	0.00	0.9	10	7 / 20	1.16 / 1.00	15.5 / 15.4	0.75 / 0.70
3	0.15	0.30	1.2	20	12 / 16	1.04 / 1.02	26.7 / 24.0	0.48 / 0.41
4	0.15	0.30	1.2	20	8 / 8	0.96 / 1.05	12.3 / 10.5	0.69 / 0.80
5	0.15	0.30	1.2	20	6 / 6	1.03 / 1.00	27.3 / 23.9	0.45 / 0.44
6	0.10	0.30	1.2	10	11 / 13	1.00 / 1.02	21.8 / 16.3	0.54 / 0.66
Global	-	-	-	-	76 / 127	1.02 / 1.01	18.2 / 17.6	0.68 / 0.71

a) 1st joint shear cracking / peak load

In Figure 6-10 the statistical distributions of the ratio $(p_t/\sqrt{f_c})_{Exp}/(p_t/\sqrt{f_c})_{Calc}$ for both limit states are shown.

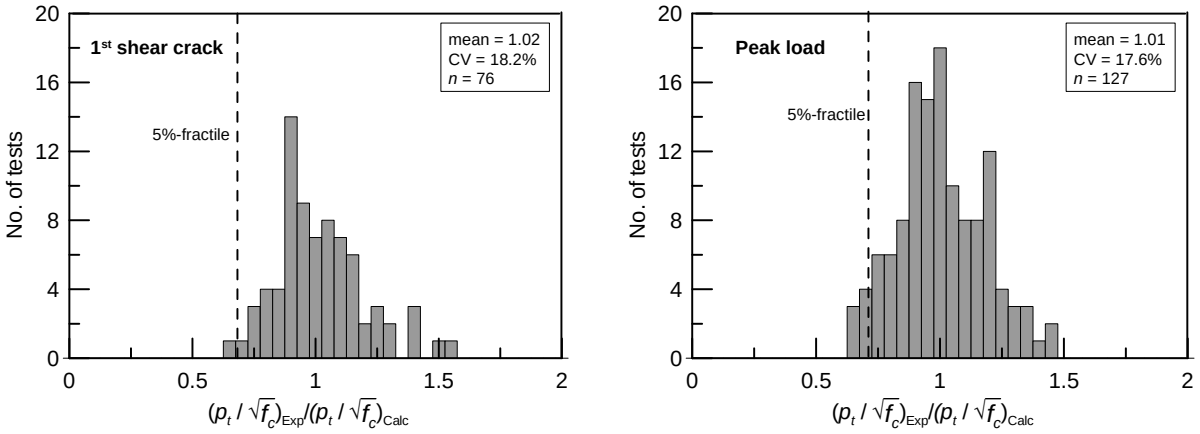

a) 1st joint shear crack b) Joint ultimate strength

Figure 6-10: Statistic evaluation of the assessment model

In Figure 6-11 to Figure 6-16 the ratio $p_t/\sqrt{f_c}$ calculated from the experimental tests and using the proposed assessment model, is compared for each anchorage type and strength limit states. Both limit states are predicted realistically but slightly conservatively for most of the investigated joint detailing types (mean ≥ 1.0) and strength limit states. Most of the tests for which the model overestimates the 1st shear crack strength are characterised by use of beam longitudinal bars with large diameter, d_b = 28.5 mm and consequently hooks with very large curvature radius, as shown in Figure 6-14a (tests by *Pantelides et al., 2002*). This is assumed to be the reason for the lower strength, as already discussed above. However, the use of reinforcing bars with such large diameters was not common in pre 1970s construction practice. For most of the anchorage Types and limit states a satisfactory CV ~ 15% was obtained by comparing the proposed model with the experimental database (Types 1, 2, 4 and 6). The controversy in the interpretation of the performance of joints with anchorages Type 3, which is found in the literature (see Section 6.3.1), is reflected by the high Coefficient of Variation, CV > 20% displayed by evaluation of the assessment model shown in Figure 6-13a,b. CV > 20% was obtained also for the anchorage Type 5, but this poor performance of the model should be attributed to the small amount of available tests.

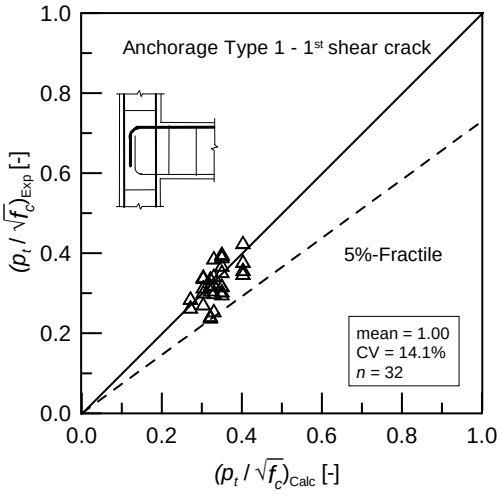

a) 1st joint shear crack

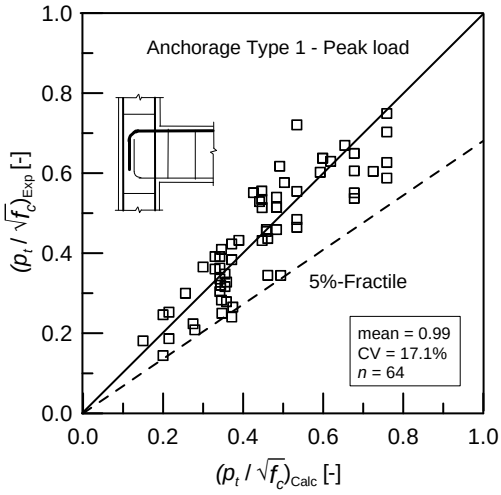

b) Joint ultimate strength

Figure 6-11: Evaluation of the assessment model (Anchorage Type 1)

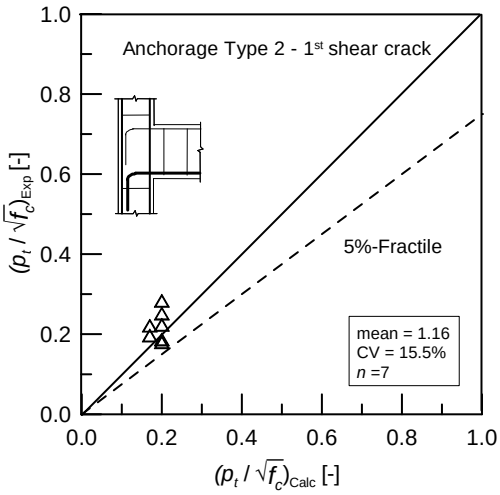

a) 1st joint shear crack

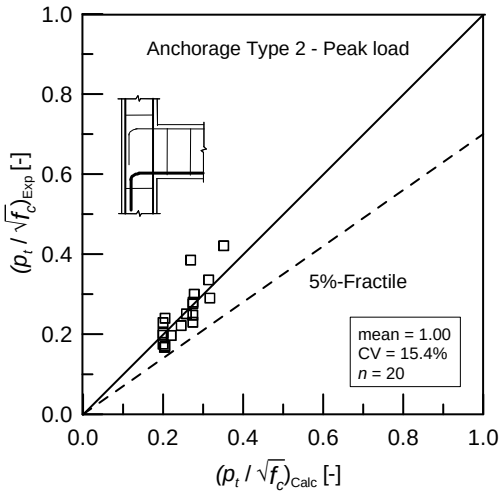

b) Joint ultimate strength

Figure 6-12: Evaluation of the assessment model (Anchorage Type 2)

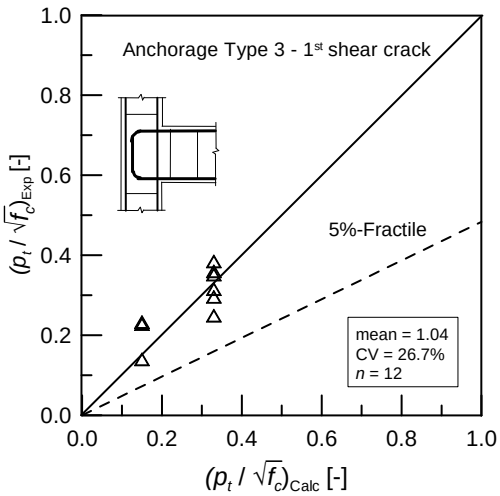

a) 1st joint shear crack

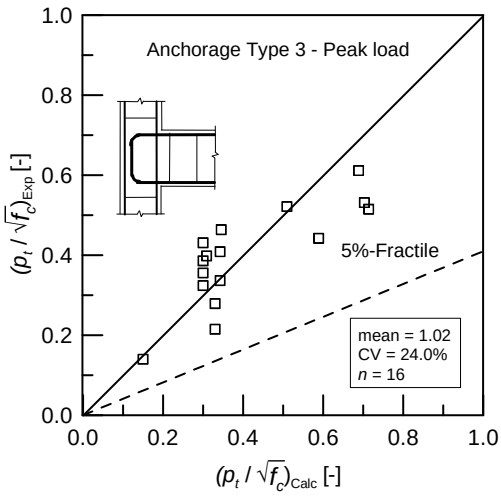

b) Joint ultimate strength

Figure 6-13: Evaluation of the assessment model (Anchorage Type 3)

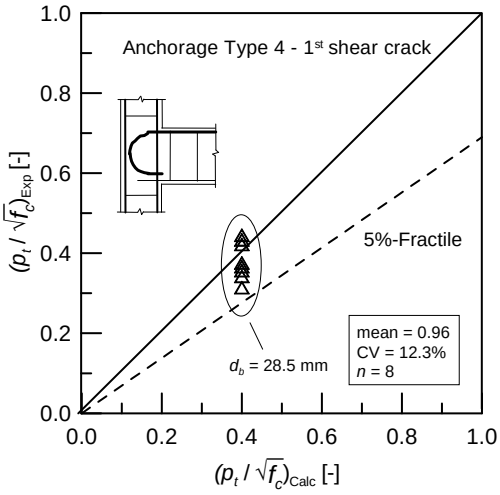

a) 1st joint shear crack

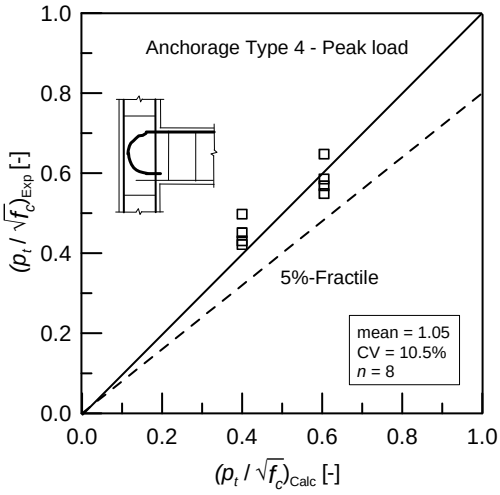

b) Joint ultimate strength

Figure 6-14: Evaluation of the assessment model (Anchorage Type 4)

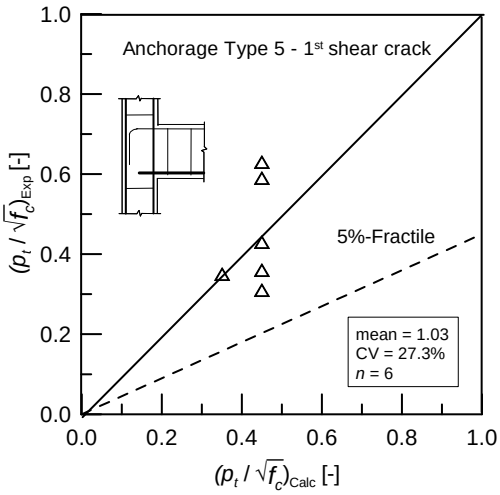

a) 1st joint shear crack

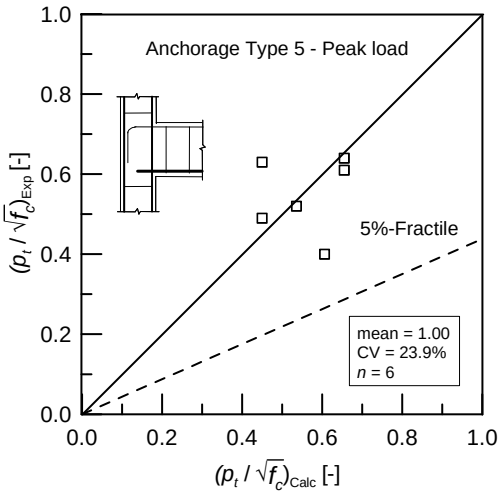

b) Joint ultimate strength

Figure 6-15: Evaluation of the assessment model (Anchorage Type 5)

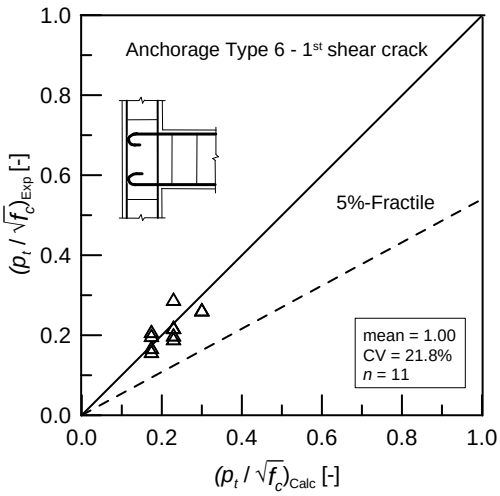

a) 1st joint shear crack

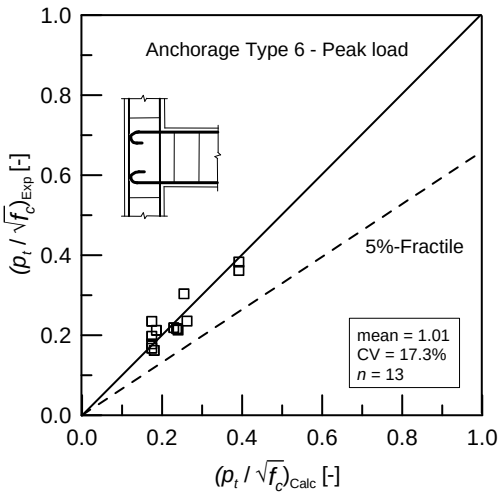

b) Joint ultimate strength

Figure 6-16: Evaluation of the assessment model (Anchorage Type 6)

6.5 Effect of yielding of beam bars

The validity of the Equation (5-4a,b) could not be verified by the experimental database due to a lack of information on the curvature ductility, μ_ϕ, for the tests where joint shear failure was observed after beam flexural yielding. However, in the majority of the tests known (e.g., *Sarsam & Phipps, 1985*, *Tsonos, 1999* and *Hegger & Roeser, 2002*), the beam yielding followed the initial diagonal cracking of the core and induced a brittle behaviour of the specimen. Only one test is known where the beam yielding occurred before the joint cracking (test TDP1 by *Hertanto, 2005*). In that case, the behaviour of the specimen was ductile as long as the joint was elastic and the diagonal cracking induced a sudden loss of strength. This occurred at a drift level of almost 3%. The possibility of evaluating the displacement instead of curvature ductility ($\mu_\Delta$instead of μ_ϕ) would allow the simpler analysis of experimental results in the literature. This possibility was discounted because μ_Δ is also influenced by other factors such as the flexural stiffness of beam and column.

6.6 Joint deformation capacity

On the basis of the experimental tests and FE parametric study carried out in this study, the joint shear distortion can be idealised according to a tri-linear p_t-γ_j relationship. At the limit states considered in this study, 1st joint diagonal cracking and peak load, γ_j, can be assumed to be equal to 0.001 rad and 0.01 rad, respectively (see Figure 5-30). γ_j is calculated according to Equation (3-6). The joint deformability increases with increasing ratio h_b/h_c and axial load, n_c, while all the other investigated parameters appear to have negligible influence.

In Figure 6-17a,b the analysis of the results available in the literature for both limit states is shown. The small number and highly scattered experimental results available do not allow a statistical evaluation of the joint shear deformability to be carried out. However, $\gamma_{j,crack}$ = 0.001 rad seems to be a realistic limit for the initial joint diagonal cracking, while $\gamma_{j,peak}$ = 0.007 rad is the approximate average value for the ultimate limit state. Similar values have been proposed by other authors such as *Shin & LaFave (2004)* and *Kam (2011)*. Test by *Hegger et al. (2002)* indicates $\gamma_{j,peak}$ = 0.006 rad.

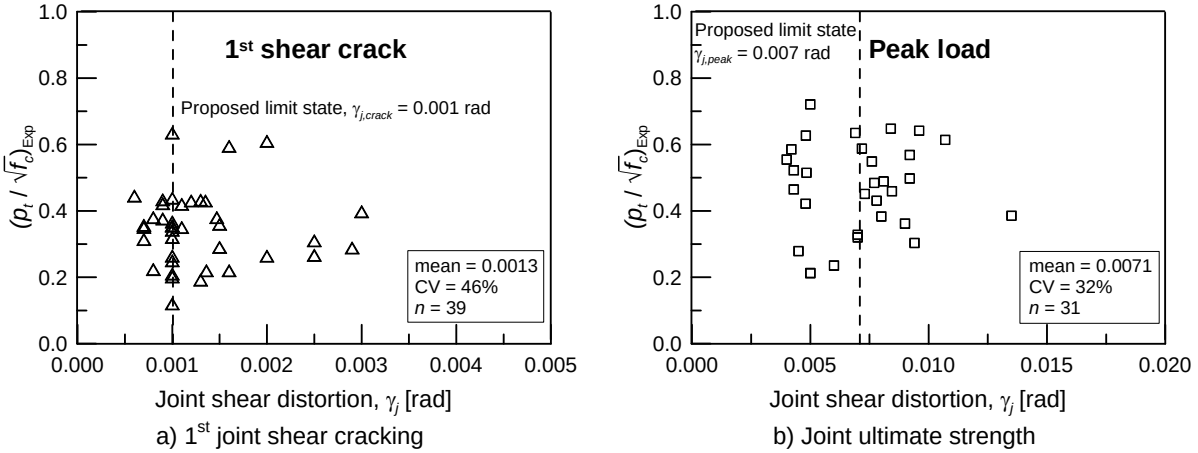

Figure 6-17: Joint shear distortion from tests of the database (see Appendix D)

In the case of BJ failure mode of the beam-column connections, the results of the test JT1-5 (see Section 3.4.6) and the numerical simulations by *Mahajan et al. (2010)* suggest a value of $\gamma_{j,peak}$ not larger than 0.005 rad.

6.7 Summary of the experimental validation of the proposed model

In this chapter the analytical model for the assessment of the joint shear strength of 2D RC exterior beam-column joints developed in Chapter 5 has been validated with a database of experimental tests. Furthermore, the following anchorage detailing types of the beam bars in the joint panel have been additionally included:

- Deformed bars with U-shaped anchorages (Type 3)
- Deformed bars with 180° big hooks (Typ 4)
- Deformed bars straight anchored (Type 5)

The experimental validation allowed the evaluation of the accuracy of the model and the derivation of characteristic joint shear resistance to be used in the design/assessment.

7 SEISMIC ASSESSMENT OF SUBSTANDARD EXTERIOR RC BEAM-COLUMN JOINTS

In this chapter the shear strength model for pre 1970s 2D exterior beam-column connections failing in shear (proposed in Chapter 5 and validated by comparing it with a database of experimental tests available in the literature in Chapter 6) is incorporated in a seismic assessment procedure. The procedure aims to establish a hierarchy strength in the framework of the Capacity Design (in this context "Capacity Assessment") as proposed by *Paulay & Priestley (1992)*. The plastic mechanism of the structures can be determined by identifying the weakest link within the system according to the chain analogy adopted in *Paulay & Priestley (1992)* (Figure 1-3a). If the weakest link of the chain corresponds to a ductile failure mode, the global behaviour of the structure will be ductile. Conversely the failure of a brittle link would lead to brittle failure and thus the sudden collapse of the entire structure.

The failure mode of beam-column connections within a moment resisting frame determines the global behaviour of the building (see Figure 2-22). In this study the most probable plastic mechanism of the beam-column joint is determined following the procedure proposed by *Pampanin (2006)* which compares the strength of the beam, column and joint.

The application of the proposed assessment procedure is shown for the investigated as-built specimens in Appendix D. It should be noted that in this chapter only mean resistances are considered, indications on a possible safety concept to be adopted are contained in Chapter 11.

7.1 Hierarchy of Strength

The strength and deformation capacity of a beam-column connection depends on its internal hierarchy of strength (see Section 2.1.2) which is typically evaluated in the framework of Capacity Design of RC structures (*Paulay & Priestley, 1992*). The concept of hierarchy of strength can be applied to different limit states. In this study the primary concern is related to the life-safety and collapse prevention limit states. For seismic assessment of RC moment resisting frames this means the establishment of a ductile plastic mechanism that allows the frame to undergo the target displacement or global interstorey drift without collapsing. The estimation of the target displacement of a RC frame required to withstand a certain seismic action (e.g., according to a time history analysis) is not object of this study.

As briefly mentioned in Section 2.1.2, the hierarchy of strength of a beam column connection and the most probable sequence of events can be graphically represented by plotting the column moment, M_c (alternatively the beam flexural moment, M_b or the shear forces V_c or V_b can be used) against the column axial load, N_c (see Figure 2-2).

The equivalent column/beam moments and shear are simply related according to the following equations:

$$M_c = M_b \frac{2L_b}{H_c} \frac{(H_c - h_b)}{(L_b - h_c)} \tag{7-1}$$

$$V_c = V_b \frac{L_b}{2H_c} \tag{7-2}$$

with L_b, H_c, h_b and h_c defined in Figure 2-3a

Each considered limit state (i.e., beam flexural failure, column flexural failure, joint shear failure, etc.) can be expressed for a given N_c. The column axial load, N_c, varies during lateral loading, as briefly explained in Section 3.3. Therefore, the diagram of the hierarchy of strength has to be modified as shown in Figure 7-1 (compare Figure 7-1 with Figure 2-2), where $N_{c,0}$ is the assumed static axial load. The choice of $N_{c,0}$ is very important for the evaluation of the hierarchy of strength and, as shown in Figure 7-1, its overestimation may lead to an unconservative prediction of brittle plastic mechanisms such as column flexural strength and joint shear strength. $N_c = N_{c,0} \pm \alpha V_c$ and α depends primarily on the geometry of the RC frame and increases with increasing slenderness (*Akgüzel, 2011*; *Kam, 2011*). It can be shown using the equations contained in Section 3.3 that typical values for α may vary between approximately 2 and 6 for exterior joints of frames with 1 to 3 bays with 5 m length and 3 to 7 floors with 3 m height. The sequence of failure modes is determined by comparing the strength (shear and flexure) of the structural elements (beam, column and joint).

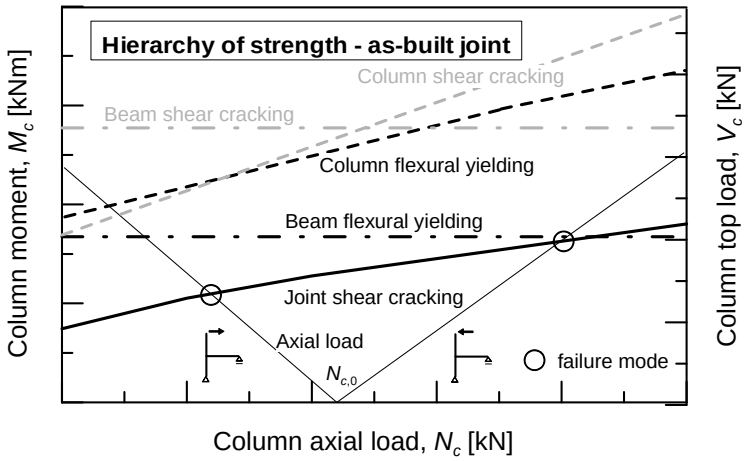

Figure 7-1: Conceptual representation of the hierarchy of strength considering the effect of varying column axial load

Upon establishing the strength and plastic mechanism of the beam-column connection, the deformation capacity, θ, and the related available ductility should be assessed. It has already been shown in this study, how the deformation of the beam-column connection may negatively influence the joint shear strength (see Section 5.2.3). The strength of single

structural elements (joint, beam and column), expressed in terms of M_c in Figure 7-1, and their deformation capacities are discussed in the following sections.

7.1.1 Joint shear strength

The average and characteristic joint shear strength can be evaluated according to the model presented in Chapter 6. It is suggested to consider the joint 1st diagonal cracking as the limit state for the following reasons:

- The experimental tests presented in Chapter 3 have shown that the 1st diagonal cracking initiates the brittle plastic mechanism with a concentration of deformation in the connection of the joint panel.
- In Chapter 4 the influence of the diagonal cracking on the mechanics of the joint have been shown by analysing the numerical simulations.
- The FE analyses have shown that the joint strength corresponding to the 1st diagonal cracking can be exceeded for low column axial load levels up to a critical value of n_c, after which the initial diagonal cracking corresponds to the ultimate strength of the connection. The magnitude of this strength increase depends on the joint detailing and loading history. The amplitude of the axial load can be determined only using a probabilistic approach and varies during seismic lateral loading (see Section 7.1).
- The joint shear strength decreases as a function of adjacent plastic hinge curvature. The formulation of the joint shear degradation proposed by *Park (1997)* was confirmed by numerical simulations carried out in this study for the case of joints with anchorage of the beam bars in the core Type 1 (see Section 5.2.3). Similar behaviour has been observed in the FE analyses on joints with anchorage Types 2 and 6. The numerical results shown in Figure 5-28 and Figure 5-29 indicate that the yielding of the beam bars has a negligible influence on the limit state corresponding to initial diagonal cracking.
- Last, the cracking of joints region is generally undesirable, because of the difficulty of access for repair.

The strength assessment of the joint can be carried out using the Equations (7-3) to (7-7):

$$V_{jh} = T_s - V_c = \frac{M_b}{j_b} - \frac{2M_c}{(H_c - h_b)} \tag{7-3}$$

$$v_{jh} = \frac{V_{jh}}{w_j \cdot h_c} \tag{7-4}$$

$$f_a = \frac{N_c}{w_c \cdot h_c} \tag{7-5}$$

$$p_{tm} = -\frac{f_a}{2} + \sqrt{\left(\frac{f_a}{2}\right)^2 + \left(v_{jh}\right)^2} \le k\sqrt{f_{cm}} \tag{7-6}$$

$$k = \left[k_0 + k_1\left(2 - h_b/h_c\right)\right] \cdot \alpha_{setup} \tag{7-7}$$

with:

k_0 and k_1 according to Table 6-4

α_{setup} = 0.85. As explained in Section 5.1.7, the most realistic test setup corresponds to the lateral loading at the top of the column, but the model was developed on tests

where the beam end was vertically loaded. For this reason the coefficient α_{setup} = 0.85 has to be applied.

The joint shear deformability can be assumed according to the empirical indications presented in Section 6.6.

In this study only the load-deformation behaviour of the 2D beam-column joint has been considered. In a RC moment resisting frame the seismic performance of the exterior joint can be influenced by several connected structural elements such as floor slab, transverse beam and, in the case of corner joints, bi-axial loading. In the following sections a short discussion on several factors that may influence the joint shear resistance is presented.

7.1.1.1 3D corner joints

Experimental tests on joints with plain round bars and 180°-hooks (anchorage Type 6) and no shear reinforcement in the joint were carried out by *Hertanto (2005)* and *Akgüzel (2011)*. In both studies one 2D joint loaded cyclically in one direction and one 3D exterior joint under bi-directional cyclic loading were tested. The corner joints exhibited a lower shear strength and more brittle behaviour. Further research is needed to modify the joint shear strength model proposed in Chapter 6 to apply it to 3D corner joints.

7.1.1.2 Effect of slab and transverse beam

The effect of a RC slab and traverse beam on the joint shear strength on 2D exterior joints was investigated by *Kam et al. (2010)*. The presence of the slab significantly increased the beam yielding moment in the negative direction (see Section 7.1.2), while the transverse beam provided an effective confinement of the joint panel avoiding brittle shear failure. In the same context *Kam et al. (2010)* investigated the effect of a RC slab in a 3D corner joint. It was observed that in that case the slab does not influence the behaviour of the joint.

7.1.1.3 Effect of eccentricity

The detrimental effect of eccentricity between beam and column longitudinal axis on the joint shear strength may be taken into account by modifying the effective width of the joint as proposed by *Mahajan (2009),* valid for the case that $w_b < w_c$. Based on the observation that the shear stress distribution for concentric and eccentric joints is different (Figure 7-2a,b), Mahajan proposed and validated the Equations (7-8a,b) for the calculation of w_j.

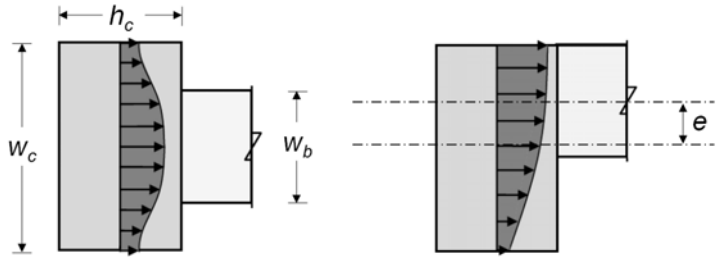

a) Concentric joint b) Eccentric joint

Figure 7-2: Distribution of shear stress across the joint width (*Mahajan, 2009*)

$$w_j = \eta \cdot w_b \tag{7-8a}$$

$$\eta = 1 + \left[1.0\left(1 - w_b/w_c\right)\right] - \left[0.75\frac{e/w_b}{h_b/h_c}\right] \quad (7\text{-}8b)$$

7.1.1.4 Pullout of the anchorage of beam bars

Pullout of the beam longitudinal bars from the joint core may occur in the case of straight anchorage or more rarely 90°-bending with substandard tail length. The bond stress, τ_b, for a reinforcement bar with diameter, d_b, cross section area, A_s, and average tensile steel stress, f_s, along an anchorage length, l_d, can be calculated using Equation (7-9).

$$\tau_{bm} = \frac{f_{sm} \cdot A_s}{\pi \cdot d_b \cdot l_d} \quad (7\text{-}9)$$

Limit values for τ_b are provided by relevant building codes for plain round and deformed bars (e.g., *CEB, 1990*). Bending tails of different form and length can be taken into account as an equivalent straight length, l_d, according to the relevant code.

The tests with deformed bars and straight anchorage with a developing length that satisfies the minimum requirements of *ACI 318-71* ($l_d \geq 150$ mm), considered in Section 6.2, have shown that this provision is usually enough to avoid the pullout of the bars. Generally, pullout would occur at a higher load than the joint shear failure even in the case of cyclic loading. Particular care in the assessment of the pullout resistance under cyclic loading of reinforcement bars should be used in the case of $l_d < 150$ mm (for deformed bars) and if plain round bars are used.

7.1.2 Beam and column flexural strength

The flexural strength of RC elements can be evaluated using moment-curvature analysis (*Paulay & Priestley, 1992*) or other analytical methods. In the case of a symmetric reinforced beam, the flexural strength depends basically on the strength of the tensioned reinforcement. The yielding moment, $M_{b,y}$, can be written as:

$$M_{bm,y} = A_s \cdot f_{ym} \cdot j_b \quad (7\text{-}10)$$

with:

A_s = area of tensioned reinforcement
f_{ym} = mean steel yielding strength
j_b = internal lever arm of the beam

The presence of a floor slab may significantly increase the negative moment capacity of the beam. The increase may be taken into account by considering the effective flange width of the slab, b_{eff}. The calculation of b_{eff} can be carried out according to the provision of different building codes (e.g., *EC8-1, 2004*; *NZ3101:1995* or *FEMA 356, 2000*). $b_{eff} = 2.2h_b$ was proposed by *Kam et al. (2010)* on the basis of experimental tests on beam-column joints with plain round bars.

The column flexural capacity is significantly influenced by the axial load acting on the column. Therefore, a moment-axial force (M_c-N_c) interaction diagram should be generated.

The curvature capacities of flexural elements, ϕ_y and ϕ_u, can be evaluated carrying out a moment-curvature analysis of the cross section and those values can be used for the calculation of the rotation capacities, θ_y and θ_u, and displacement capacities, Δ_y and Δ_u. For example, the empirical equations according to *Paulay & Priestley (1992)* (Eqs. (7-11) and (7-12)) taking into account the strain penetration length, L_{sp} (Eq. (7-13)) and the plastic hinge length, L_{ph}, (Eq. (7-14)) can be used.

$$\theta_y = 2\Delta_y / L_x = 2\left(\phi_y \left(H + L_{sp}\right)^2 / 3\right) / L_x \tag{7-11}$$

$$\theta_u = 2\Delta_u / L_x = 2\left(\Delta_y + \left(\phi_u - \phi_y\right) L_{ph}\right) / L_x \tag{7-12}$$

$$L_{sp} = 0.022 \cdot f_y \cdot d_b \tag{7-13}$$

$$L_{ph} = 0.2\left(f_u / f_y - 1\right) H + L_{sp} \le 2L_{sp} \text{ and } 2\left(f_u / f_y - 1\right) \le 0.08 \tag{7-14}$$

with:

L_x = beam span

H = length from the contra-flexural point to the centroid of the plastic hinge

Equations (7-11) to (7-14) are derived from empirical observations in tests with deformed bars and their accuracy for plain round bars has not been verified yet.

7.1.3 Beam and Column shear strength

The shear strength of a member section can be assessed using the strut and tie model according to which the compression is resisted by concrete and the tension by concrete and after reaching its tensile strength, f_{ct}, by the shear reinforcement.

Because of the difficulty in repairing the shear cracks in flexural elements (*Filialtrault & Lebrun, 1996*) and the typically low amount of transversal reinforcement in pre 1970s structures, the shear strength of beam and column may be conservatively assessed based only on the concrete tensile contribution, V_{ct}. The following Equation according to *EC-2 (2003)* may be used.

$$V_{ctm} = \left[0.1 \cdot \eta_1 \cdot \kappa \cdot \left(100 \cdot \rho_b \cdot f_{cm}\right)^{1/3} - 0.12 \cdot f_a\right] \cdot w_b \cdot \left(h_b - c\right) \tag{7-15}$$

with:

η_1 = 1.0 for normal concrete

κ = $1 + \sqrt{200 / \left(h_b - c\right)}$

Alternatively, if shear cracking is acceptable (i.e., minimum stirrups spacing is provided), the shear resistance of a RC member is given by Equation (7-16).

$$V_{Rm} = \min\left\{V_{Rm,\max}; V_{Rm,sy}\right\} \tag{7-16}$$

with:

$V_{Rm,max}$ = verification of the compressive strut (i.e., concrete) according to *EC-2 (2003)*

$V_{Rm,sy}$ = verification of the tensile tie (i.e., yielding of stirrups) according to *EC-2 (2003)*

It is generally recognised that the shear strength degradation is a function of the structural and curvature ductility. Several authors proposed empirical formulations to account for the shear strength degradation of columns failing in shear by introducing a shear strength degradation factor related to the displacement (*Sezen & Moehle, 2004*) or curvature (*Priestley et al., 1994*) ductility of the RC member.

The shear deformation of flexural elements with and without axial load, P, for shear failure, θ_s, can be determined using the following empirical formula proposed by *Elwood & Moehle (2005)*.

$$\theta_s = \Delta_s / L = 0.03 + 4\rho_s - 0.05 \cdot v_{jh} / \sqrt{f_c} - 0.025 \cdot N_c / A_c \cdot f_c \qquad (7\text{-}17)$$

with:

ρ_s = shear reinforcement ratio

v_{jh} = maximum nominal shear stress.

In regions of plastic hinges the shear strength of RC members is reduced. If no compressive axial load is applied on the RC member (e.g., beams), the shear strength is limited to the shear resistance of the reinforcing steel. In compressed members such as columns the positive affect of the axial load may be taken into account (*Paulay & Priestley, 1992*).

7.2 Summary of the assessment of substandard beam-column joints

In this Chapter a possible approach for the seismic assessment of substandard beam column joint has been presented. The main principles can be summarised as follows:

- The strength of single elements constituiting the beam-column connection can be graphically compared using the scheme of the “hierarchy of strength”.
- The evaluation of the joint shear strength for 2D exterior beam-column joint can be carried out according to the model developed in this study (see Chapters 5 and 6).
- Some consideration to take into account different geometrical configurations of exterior beam-column connections are provided in this chapter, e.g., effect of transverse beam crossing in the joint core, presence of RC slab, 3D exterior joints with bi-directional loading and eccentricity between beam and column axis.
- The evaluation of strength and deformability of beam and column under shear and flexural loading can be carried out according to the relevant standard. Some indications are provided in this chapter.

8 RETROFIT WITH HAUNCHES USING POST-INSTALLED ANCHORS: CONCEPT AND ANALYTICAL MODEL

In this chapter a possible seismic retrofit solution for beam-column joints is discussed. The "Haunch Retrofit Solution" (HRS) developed at the University of Canterbury (UC) is considered (Section 8.1) and an optimisation by using post-installed anchors is proposed Section 8.2 the analytical assessment of the new retrofit technique is discussed on the basis of analytical and theoretical considerations. Particular attention is devoted to the design of the anchorage with post-installed anchors in terms of stiffness (Section 8.2.2) and strength (Sections 8.2.3 to 8.2.5).

8.1 Haunch Retrofit Solution

The "Haunch Retrofit Solution" (HRS) represents an extension of a retrofit solution proposed for steel moment resisting frames, following a high amount of weld fractures observed after the 1994 Northridge earthquake (*Yu et al., 2000*), in order to relocate the plastic hinge away from the welded connection between beam and column (Figure 8-1).

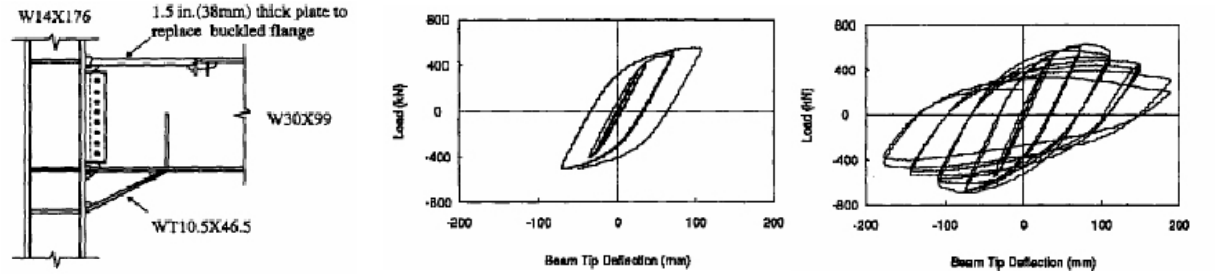

a) HRS with single haunch b) behaviour – as-built c) behaviour – after retrofit

Figure 8-1: HRS for steel beam-column joints (*Yu et al., 2000*)

The HRS of *Yu et al. (2000)* was modified for application to RC beam-column connections according to Figure 8-2a. The use of two diagonal haunches was proposed. This solution was developed in order to modify the internal hierarchy of strength of a beam-column connection and to induce the formation of a ductile flexural hinge in the beam at the end of the anchoring plates of the diagonal haunches (Figure 8-2c) rather than a brittle shear failure of the joint panel (Figure 8-2b). Tests by *Chen (2006)* confirmed the effectiveness of this seismic retrofit strategy as can be seen through the comparison of the cracking patterns (Figure 8-2b,c) and the hysteretic behaviour (Figure 8-2d,e) of the as built and retrofitted specimens. *Chen (2006)* investigated three different constructive solutions for this retrofit technique. In all tests the beam-column joints had the same geometry and reinforcing detailing as well as similar material properties. The following constructive solutions were tested with different degrees of success:

(1) Rotational hinge as connection between anchorage steel plates and diagonal haunches, which were designed to remain elastic during the entire test (see Figure 8-2a): the stiffness of the haunches was too low due to constructive tolerances and some damage in the joint core could not be avoided;

(2) Rotational hinge as connection between anchorage steel plates and diagonal haunches, which were design to yield during the tests: the yielding of the diagonal haunch could not dissipate a significant amount of energie, due to the limited elastic deformability of the beam-column connection; and

(3) Stiff connection between anchorage steel plates and diagonal haunches, which were designed to remain elastic during the entire test (see Figure 8-2c): this solution gave the best results and it was chosen for the further development in this study.

More detailed information about the application of the HRS to RC beam-column joints can be found in *Pampanin & Christopoulos (2003)*, *Chen (2006)* and *Pampanin et al. (2006)*.

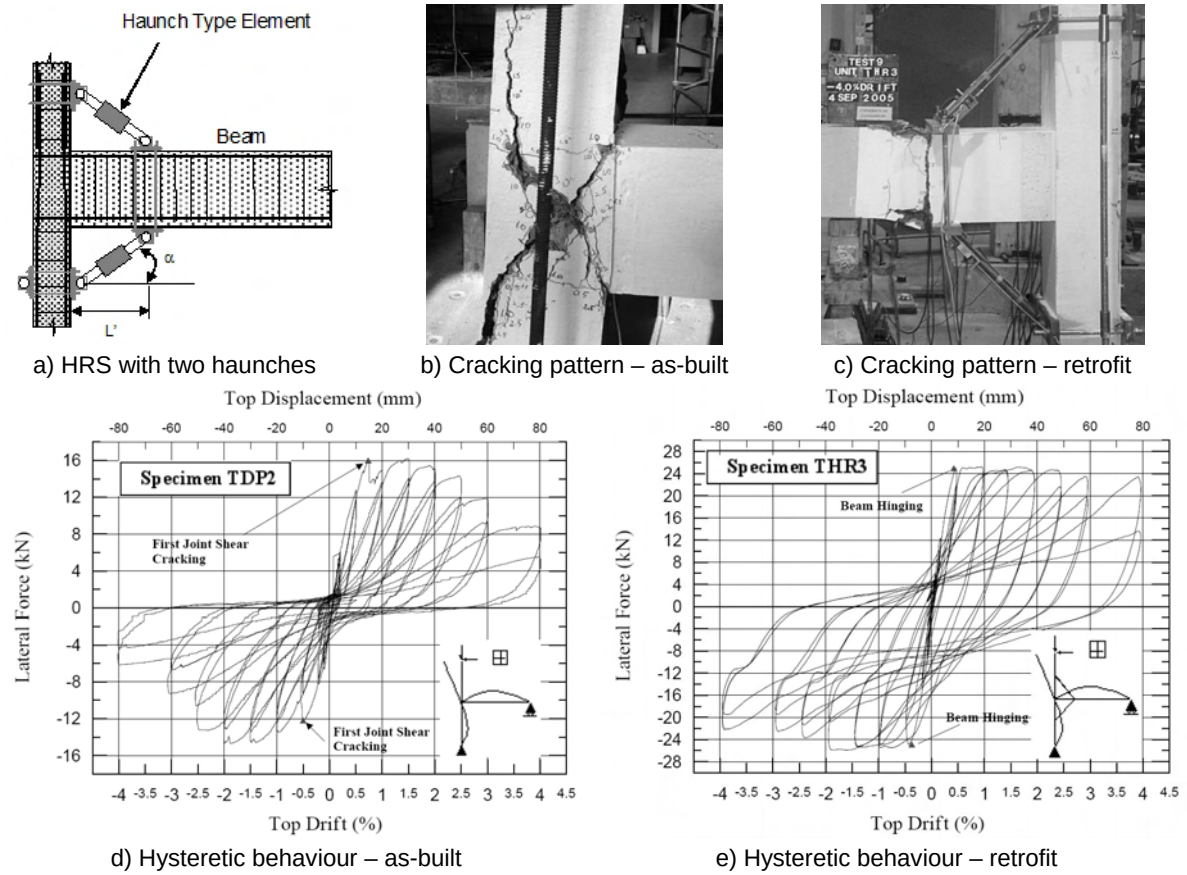

a) HRS with two haunches b) Cracking pattern – as-built c) Cracking pattern – retrofit

d) Hysteretic behaviour – as-built e) Hysteretic behaviour – retrofit

Figure 8-2: HRS for RC beam-column joints (*Chen, 2006*)

8.1.1 Assessment of the retrofitted beam-column joint

The basic idea of the HRS is the reduction of the flexural moment at the interface between the beam/column with the joint region with the aim of reducing the shear stress in the core and preventing the joint shear failure (Figure 8-3). The retrofit can improve the strength and the ductility of the beam-column connection with a maximum degree of effectiveness, if the formation of the plastic hinge in the beam in the section at the end of the diagonal haunches occurs, while the joint remains elastic as in Figure 8-2c,e.

In Figure 8-3 the internal actions (bending moment and shear force) in the beam-column after the retrofit are shown. It should be noted that this retrofit solution induces significant larger shear forces in beam and column than the as-built configuration of the joint (see Figure 8-3). Therefore, its implementation should be limited to those cases where this failure mode can be avoided by sufficient longitudinal and shear reinforcement (beam and column) and/or axial load (column). A combination with other retrofit techniques to overcome this issue (i.e., jacketing of beam and/or column) can be considered.

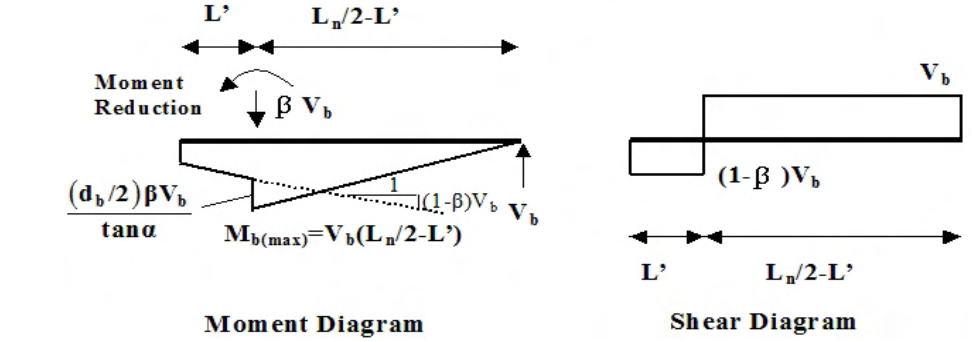

a) Beam

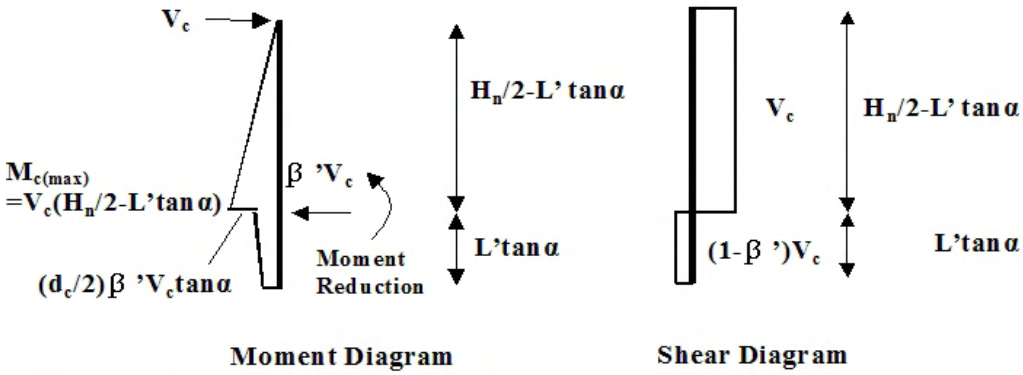

b) Column

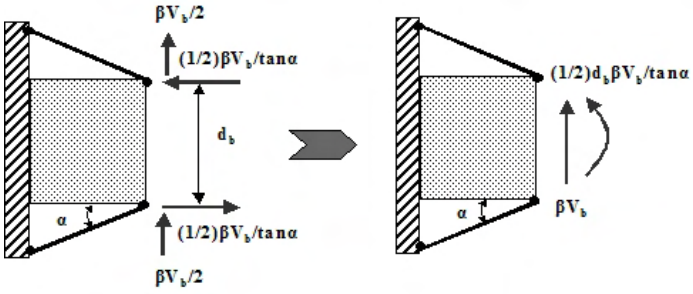

c) Eccentric force due to haunch strut action on beam

Figure 8-3: Moment and shear diagram in beam and column of the retrofitted beam-column connection (*Chen, 2006*)

The flexural moments in the beam (M_{bc}) and the column (M_{cb}) at the interface with the joint region can be written according to Equations (8-1) and (8-2), respectively:

$$M_{bc} = M_{b(\max)} + (1-\beta)V_b L' - \frac{h_b \cdot \beta \cdot V_b}{2 \cdot \tan\alpha} \tag{8-1}$$

$$M_{cb} = M_{c(\max)} + (1-\beta') \cdot V_c \cdot L' \cdot \tan\alpha - \frac{h_c \cdot \beta' \cdot V_c \cdot \tan\alpha}{2} \tag{8-2}$$

The factors β and β' are defined below after Eq. (8-6b). The shear forces acting in beam (V_{bc}) and column (V_{cb}) at the interface with the joint panel are:

$$V_{bc} = (1-\beta)\cdot V_b \tag{8-3}$$

$$V_{cb} = (1-\beta')\cdot V_c \tag{8-4}$$

The horizontal shear forces acting in the joint, V_{jh}, is written in Equation (8-5):

$$V_{jh} = \frac{M_{bc}}{j_b} - (1-\beta')\cdot V_c \tag{8-5}$$

If the joint shear strength is assessed according to the approach presented in Section 7.1.1, V_{jh} can be written as:

$$V_{jh} = A_j\sqrt{p_t^2 - \frac{p_t N_c}{A_c}} \tag{8-6a}$$

with:

$$\frac{p_t}{\sqrt{f_c}} = k_0 + k_1\left(2-\frac{h_b}{h_c}\right) \text{ and } k_0 \textit{ and } k_1 \text{ according to Table 6-4} \tag{8-6b}$$

The β-factor (and β') contained in the Equations (8-1) to (8-5) expresses the effectiveness of the retrofit solution by determining the redistribution of the shear between beam, column and haunches in the points of connection. A β_{min} which is necessary to protect the joint panel can be analytically determined. The calculation of β and β' were derived by *Chen (2006)* on the basis of the beam and column flexural deformability as explained in Appendix E (Eqs. (8-7) and (8-8)).

$$\beta = \frac{b}{a}\left(\frac{6Lh_b + 3ah_b + 6bL + 4ab + \frac{2I_b b^3}{I_c a H_c} + \frac{3I_b H L_b b^3}{2I_c a^2 H_c} + \frac{3I_b h_c H L_b b^2}{I_c a^2 H_c}}{3h_b + 6bh_b + 4b^2 + \frac{12E_c I_b}{2K_d a\cos^2\alpha} + \frac{6I_b b^2}{a^2 A_c} + \frac{2I_b h_c b^2}{I_c a} + \frac{3I_b h_c b^2}{I_c a^2} + \frac{3I_b h_c^2 b^3}{2I_c a^3}}\right) \tag{8-7}$$

$$\beta' = \beta\left(\frac{H_c}{L_b\cdot\tan\alpha}\right) \tag{8-8}$$

with:

K_d in [N/mm]

a, b = projected length of the haunches on beam and column, respectively

L = L_b - h_c - 2a (h_c = height of the cross section of the column)

H = H_c – h_b – 2b (h_b = height of the cross section of the beam)

I_b, I_c = effective inertial moment of beam and column, respectively

Due to the cyclic loading to which the beam-column connection is subjected, flexural cracks occur along beam and column. The cracks negatively influence the flexural stiffness of the section, i.e., the inertial moments, I_b and I_c. According to *Paulay & Priestley (1992)* the effective

inertial moment of a RC cracked section can be estimated as a first approximation through multiplying the theoretical value ($I_{b,0}$ and $I_{c,0}$), by a coefficient $\theta < 1.0$ (see Equations (8-9a,b)).

$$I_b = \theta_b \cdot I_{b,0} = \theta_b \frac{w_b \cdot h_b^3}{12} \text{ with } \theta_b = 0.3 \div 0.5 \quad (8\text{-}9a)$$

$$I_c = \theta_c \cdot I_{c,0} = \theta_c \frac{w_c \cdot h_c^3}{12} \text{ with } \theta_c = 0.4 \div 0.9 \quad (8\text{-}9b)$$

A more precise estimation of I_b and I_c can be provided by analytical methods, i.e., moment-curvature analysis.

For a given beam-column joint the efficiency of the retrofit solution in reducing the shear stress in the core increases with increasing values of K_d, a and b. Parallely, the shear demand in beam and column also increase and, therefore, an upper limit for the above values can be analytically determined (see Appendix E).

An iterative procedure for the design of the retrofit solution was proposed by *Pampanin et al. (2006)* and the single steps can be found in Appendix E. If properly designed, the retrofit solution is able to modify the internal hierarchy of strength of the beam-column connection (Figure 8-4). In the schematic example shown in Figure 8-4, for an assumed column axial load, N_c*, the as-built joint is expected to fail due to joint shear cracking. The retrofit solution should prevent joint and column failure. If the beam flexural strength is the smallest resistance, a ductile plastic mechanism in the beam-column joint can be achieved. It should be noted that for the graphic representation of the hierarchy of strength a V-N (beam end or column top shear - column axial load) domain is more appropriate than an M-N (Beam or column moment – column axial load) domain, because the moment diagram varies from the as-built to the retrofitted configuration at the joint panel interfaces. Conversely, beam end and column top shear are well comparable in the as-built and retrofitted specimens.

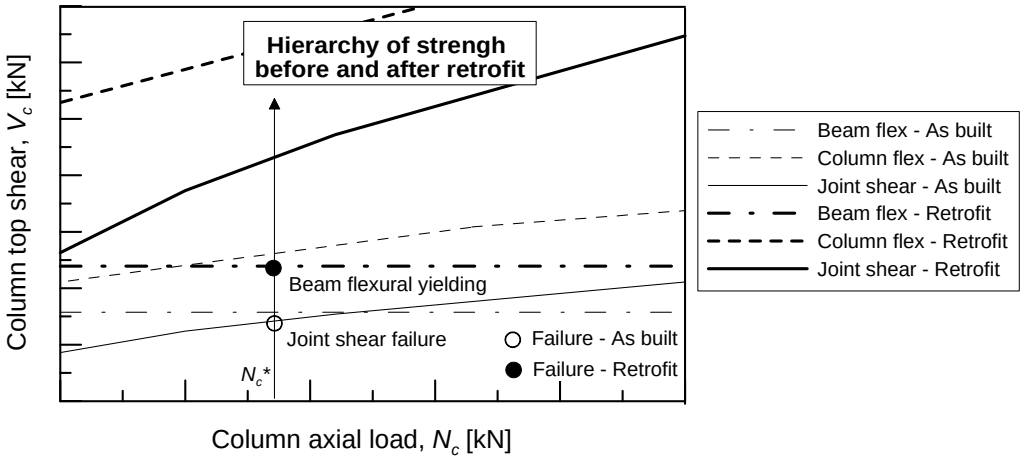

Figure 8-4: Hierarchy of strength before and after retrofit

8.2 Implementation of post-installed anchors

In order to simplify the practical application of the HRS the substitution of the external threaded rods to fix the diagonal haunch to beam and column (Figure 8-5a,b) with post-installed anchors (Figure 8-5c,d) is proposed. This new solution allows the drilling through

the floor to connect the threaded rods to the beam as well the need of external access to the building to fix them to the column to be avoided. The invasiveness of the retrofit technique can be in this way significantly reduced. Furthermore, the durability of the steel elements is improved, because it is exposed to an interior less aggressive environment (anchorage in the column). The modification of the design of the HRS for RC exterior beam-column joints proposed to take into account the load-displacement behaviour of post-installed anchors is discussed in section 8.2.

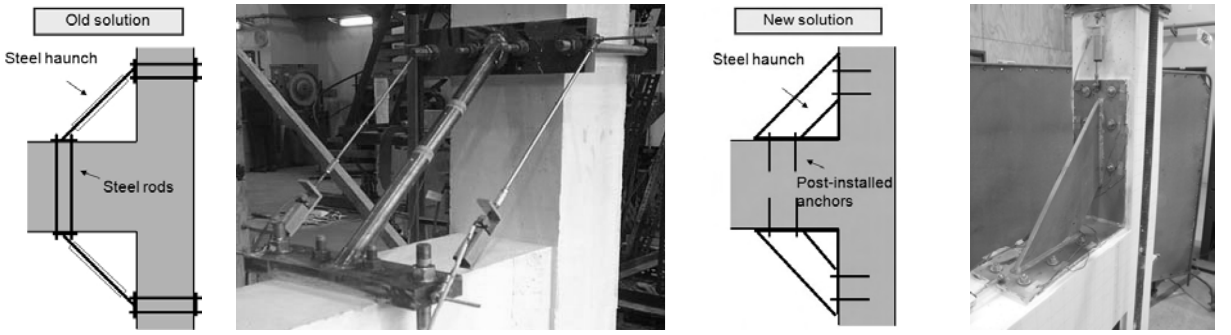

a) HRS – schema b) HRS realisation c) New HRS - schema d) New HRS realisation

Figure 8-5: Development of the "Haunch Retrofit Solution" (HRS)

8.2.1 Calculation of β-factor

As explained in Section 8.1 and Appendix E the effectiveness of the retrofit solution mainly depends on the stiffness of the steel diagonals, K_d. K_d is determined by the length L_h the cross section, A_d of the steel diagonals and the Young's modulus of steel, E_s. The shear and tensile stiffness of the connection of the anchor plates to beam and column can be considered infinite, if the external steel rods (Figure 8-5a) are adequately pretensioned. The cross section of the external steel rods is usually chosen such that it significantly exceeds strength and stiffness of the diagonal haunches. However, it should be noted that no quantification of the required pretensioning and axial stiffness of the threaded rods has been proposed yet. Furthermore, although consideration of the shear stiffness of the haunch connection with beam and column are not contained in *Chen (2006)* and *Pampanin et al. (2006)*, post-installed bonded anchors were used to increase the shear stiffness of the connection as shown in Figure 8-5b. For the haunches shown in Figure 8-5a,b K_d can be easily calculated according to Equation (8-10).

$$K_d = \frac{E_s \cdot A_d}{L_h} \tag{8-10}$$

For the HRS shown in Figure 8-5c,d the stiffness of the connection of the anchor plates with the beam and the column has to be carefully evaluated, because post-installed anchors usually exhibits slippage when loaded in tension and shear. The anchors displacement may increase significantly especially under cyclic loading in cracked concrete, which is a condition that may realistically occur in this application. The first consequence of this observation is that the stiffness of the steel diagonal is different in tension and compression. Therefore, Equation (8-7) should be modified as follows.

$$\beta = \frac{b}{a}\left(\frac{6Lh_b + 3ah_b + 6bL + 4ab + \frac{2I_b b^3}{I_c a H_c} + \frac{3I_b H L_b b^3}{2I_c a^2 H_c} + \frac{3I_b h_c H L_b b^2}{I_c a^2 H_c}}{3h_b + 6bh_b + 4b^2 + \underline{\underline{\frac{12E_c I_b}{(K_{h,c} + K_{h,t})a\cos^2\alpha}}} + \frac{6I_b b^2}{a^2 A_c} + \frac{2I_b h_c b^2}{I_c a} + \frac{3I_b h_c b^2}{I_c a^2} + \frac{3I_b h_c^2 b^3}{2I_c a^3}} \right) \quad (8\text{-}11)$$

with:
$K_{h,t}$, $K_{h,c}$ = tensile and compressive stiffness of one haunch, respectively

The projected haunch length on the beam and the column (a and b) corresponds to the distance of the centre of the anchor plate from the internal column face in the calculation of β, however, for the calculation of the effect of the retrofit, i.e., the point of application of the tensile and compressive forces in the haunches (see Figure 8-3), the centroid of anchorage should be considered. These lengths are considered to be approximately equal in the original HRS (Figure 8-5a), but this approximation is not acceptable in the new solution shown in Figure 8-5b. The position of the centroid of the anchorages of the compressed and tensioned haunches has to be carefully evaluated and it is discussed later on the base of experimental (Chapter 9) and numerical (Chapter 910) investigations.

As explained in the following sections in general $K_{h,c}$ is larger than $K_{h,t}$. For this reason the moment reduction in the beam generated by the eccentric force due to the strut action of haunch (see Figure 8-3) has to be modified and Equation (8-12) should be applied.

$$\text{Beam moment reduction} = \frac{h_b \cdot \beta \cdot V_b}{2 \cdot \tan\alpha} \frac{K_{h,t}}{K_{h,t} + K_{h,c}} \quad (8\text{-}12)$$

Similarly, the expression of the moment reduction in the column can be calculated. However, this parameter has a minor influence in the new retrofit schema (Figure 8-5c), because the force of haunches are transferred on beam and column not in a single cross section (see Figure 8-5a), but on the entire length, *L'*. Therefore, the moment reduction shown in Equation (8-12) may be conservatively neglected.

8.2.2 Evaluation of tensile and compressive stiffness of the haunches

For the evaluation of the tensile and compressive stiffness of the haunch three possible approaches may be used:

(1) the concrete members under the haunches are considered rigid (Figure 8-6);
(2) the concrete members under the haunches are considered deformable and the steel plates are taken as rigid (Figure 8-7), and
(3) a behaviour in-between (1) and (2).

In Figure 8-6 and Figure 8-7 two limit cases (1) and (2) are shown and the choice of one of the two approaches affect the distribution of forces and consequently the stiffness of the anchorages of the haunches loaded in tension and in compression. The experimental tests and numerical simulations carried out in this study (see Chapters 9 and 10) have shown that the real behaviour of the retrofitted specimen is in-between these two approaches. The concrete members cannot be considered rigid (as assumed in Figure 8-6), since in most of

the tests cracking underneath the haunches was observed. However, the deformation of the beam and column shown in Figure 8-7 is also exaggerated, since for example, in the tests no inversion of the axial loading of anchors was generally observed (compare Figure 8-6 and Figure 8-7a).

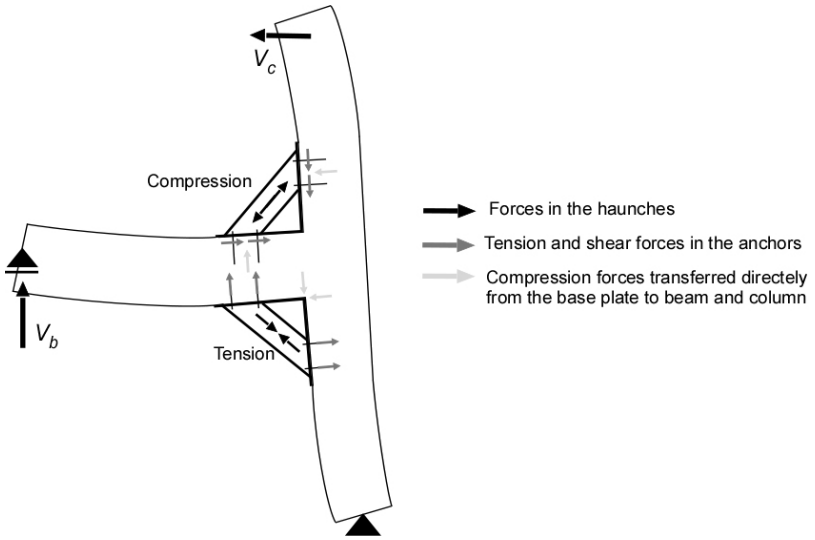

Figure 8-6: Loading of the haunches assuming perfect rigidity of the concrete members under the haunches

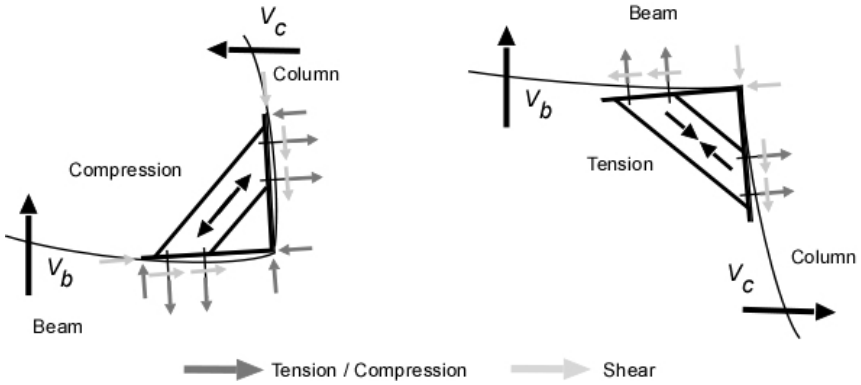

a) Compressed haunch b) Tensioned haunch

Figure 8-7: Effect of flexural deformation of beam and column on the forces distribution on the anchorage

Assuming rigid concrete members under the haunches, $K_{h,t}$ can be calculated according to Equations (8-13a,b).

$$K_{h,t} = 1 \Big/ \left(\frac{2 \cdot \sin\alpha}{K_N} + \frac{1}{K_d} \right) \tag{8-13a}$$

$$K_{h,c} = 1 \Big/ \left(\frac{2 \cdot \cos\alpha}{K_V + K_f} + \frac{1}{K_d} \right) \tag{8-13b}$$

with:

K_N = the tensile stiffness of the anchorage evaluated as: $K_N = nk_N$ (number of anchors in the group x tensile stiffness of the single anchor)

K_V = the tensile and shear stiffness of the anchorage evaluated as explained below

K_V = nk_V (number of anchors in the group x shear stiffness of the single anchor)

K_f = frictional stiffness
K_d = see (8-10)

The member "$K_v + K_f$" in Equation (8-13b) can be written as follows:

$$K_V + K_f = A_p k_f \mu_f \tan\alpha + n k_V \left(1 - \mu_f \tan\alpha\right) \tag{8-14}$$

with:
A_p = Surface area of the anchor plate in contact with the concrete face of beam/column
μ_f = frictional coefficient (see Section 8.2.2.5)
$1 - \mu_f \tan\alpha \geq 0$. If $1 - \mu_f \tan\alpha < 0 \rightarrow K_V = 0$, because the anchors are not loaded in shear

In the above calculations of $K_{h,t}$ and $K_{h,c}$ (Eq. (8-13a,b)), it is assumed that the shear forces transmitted by the haunch under tension are directly transferred to the beam and column without loading of the anchors and that the compression forces from the haunches do not compress the anchors (see Figure 8-6).

If the deformability of beam and column is taken into account and the steel plates are assumed as rigid, a force distribution as shown in Figure 8-7 should be considered. In this case, for the evaluation of $K_{h,t}$ the Equation (8-13a) should be replaced by Equation (8-15).

$$K_{h,t} = 1 \Bigg/ \left(\frac{2}{\sqrt{\left(n k_N \cdot \sin\alpha\right)^2 + \left(n k_V \cdot \cos\alpha\right)^2}} + \frac{1}{K_d} \right) \tag{8-15}$$

For the determination of $K_{h,c}$ the contribution of friction should be reduced, but at the contact surface between beam/column and the end of the steel plates compression forces occur (see Figure 8-7a). With increasing deformation of the concrete members the friction will decrease and compression forces will increase. For simplicity and because of the lack of specific investigations the Equation (8-13b) is still considered valid.

The evaluation of $K_{h,t}$ and $K_{h,c}$ is further discussed on the basis of the experimental validation and numerical analysis of the HRS with post-installed anchors presented in Chapters 9 and 10, respectively.

A great uncertainty in the design of the HRS using post-installed anchors is also the assumption of the shear and tensile stiffness of the anchors. The design of post-installed anchors according the most advanced design provisions (e.g., *ACI 318, Appendix D, 2008*, *CEN, 2009* and *fib, 2011*) are basically force oriented. The load-displacement characteristics of anchors are strongly product dependent and generally associated with large scatter (*Silva, 2007*). In Sections 8.2.2.1 to 8.2.2.4 the evaluation of shear and tensile stiffness of anchors is discussed. Section 8.2.2.5 contained considerations about the friction which acts parallely to the shear according to Equation (8-13b).

8.2.2.1 Evaluation of anchors tensile stiffness

It is well know that the anchor tensile stiffness increases with increasing diameter and secondarily with the increase of the strength of the base material, f_c. The cracking of the concrete has a detrimental effect on the stiffness (see Figure 8-8 and Table 8-1). The tensile

stiffness depends mainly on the load-transfer mechanism (see Figure 2-26). If all other relevant parameters are kept constant, bonded anchors (bond mechanism) are usually stiffer than concrete screws and undercut anchors (mechanical interlock), which are stiffer than expansion anchors (friction). The significant non-linearity of the anchors load-displacement behaviour exacerbates the already problematic issue of the determination of anchors stiffness (Figure 8-8a,b). It should be also noted that the embedment depth, h_{ef}, significantly influences the anchor's stiffness, especially in the case of bonded anchors and screw anchors, since the tensile strength of the anchor is proportional to h_{ef} (except for steel failure modes). A quantification of the influence of the above parameters is not available at present, therefore, an analytical calculation of the stiffness is not possible.

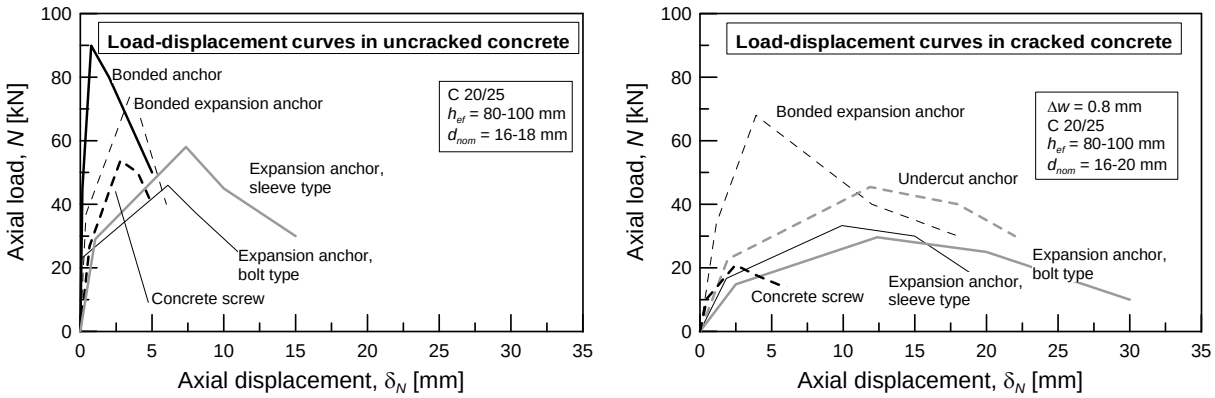

a) Comparison of different anchor types in uncracked concrete

b) Comparison of different anchor types in cracked concrete

Figure 8-8: Typical load-displacement curves of single anchors under tension loading

In Table 8-1 the axial stiffness of different anchor types and dimensions tested in uncracked and cracked concrete is shown for comparison. The secant stiffness values, $k_{s,N}$ calculated using Equation (8-16) are presented. It is assumed that the failure mode does not influence the $k_{s,N}$ up to $0.5N_u$ (with N_u = ultimate anchor tensile strength).

$$k_{s,N} = \frac{N_u}{2} \Big/ s_{N_u/2} \tag{8-16}$$

The values contained in Table 8-1 are taken from the analysis of prequalification tests carried out in the laboratory of the Institute of Construction Material of the University of Stuttgart recently according to *EOTA (1997)*, *ICC-ES (2010)* and *ICC-ES (2009)* or earlier versions of these documents. For bonded anchors the Coefficient of Variation, CV, is approximately 10~15%, while for other anchor types it is usually larger up to 20~30%.

Table 8-1: Typical values of tensile stiffness in [kN/mm] of different types of single anchors

	$d_{nom,1}$		$d_{nom,2}$		$d_{nom,3}$	
Anchor type (diameter)	**uncr**	**cr**	**uncr**	**cr**	**uncr**	**cr**
Bonded anchors (3/8", 5/8", 3/4" in.)	110 – 135	35 – 75 [a)]	170 – 180	80 – 105 [a)]	520 – 620	n.a.
Bonded expansion anchors (8, 12, 16 mm)	35 – 60	15 – 30	55 – 80	20 – 40	30 - 50	65 - 100
Concrete screws (12, 16 mm)	55 – 80	10 – 30	30 – 50	n.a.	-	-
Expansion anchors (sleeve type) (12, 18 mm)	25 – 45	10 – 20	20 – 35	25 – 50	-	-
Expansion anchors (bolt type) (8, 12, 16 mm)	35 – 75	n.a.	50 – 110	n.a.	100 – 160	n.a.

[a)] Δw = 0.5 mm; Note: all values in [N/mm]

A few researchers collected and analysed values of tensile stiffness of different anchors types and dimensions (*Mahrenholtz, 2011* and *Fichtner, 2011)*. They observed a very high scattering of the stiffness values with CV up to 50%.

8.2.2.2 Evaluation of anchors shear stiffness

In Table 8-2 a statistical analysis on the shear stiffness of anchors (different types, dimensions and failure mechanisms) carried out by *Mahrenholtz (2011)* and *Grosser (2012)* is summarised. A CV between 20 and 40% was generally observed. *Grosser (2012)* investigated the stiffness of bonded anchors of different dimensions loaded parallel and perpendicular to the edge. The analysis by *Mahrenholtz (2011)* and *Grosser (2012)* indicate similar shear stiffness values. The analysis contained in *Grosser (2012)* focuses the following aspects:

- The anchor stiffness is not influenced by the shear loading direction (i.e., parallel or perpendicular to the edge), by the embedment depth, h_{ef}, or by the edge distance, c_1.
- The anchor stiffness increases with increasing diameter, d_{nom}.

Analogous to the axial stiffness the shear secant stiffness, $k_{s,V}$ is calculated according to Equation (8-17) with V_u being the ultimate shear strength of a single anchor.

$$k_{s,V} = \frac{V_u}{2} \Big/ s_{V_u/2} \tag{8-17}$$

Table 8-2: Average shear stiffness of single anchors

	d_{nom} = 8 mm	d_{nom} = 12 mm	d_{nom} = 16 mm	d_{nom} = 20/24 mm
Anchor stiffness [a)] (*Mahrenholtz, 2008*)	3-10	5-20	10-30	15-40 [b)]
Anchor stiffness (*Grosser, 2012*)	5-10	n.a.	20-30	25-50 [c)]

[a)] Screw anchors, bonded anchors and expansion anchors (bolt and sleeve types) and different failure modes; [b)] d_{nom} = 20 mm; [c)] d_{nom} = 24 mm; Note: all tests in uncracked concrete and values in [kN/mm]

8.2.2.3 Cyclic behaviour of anchors

Results of cyclic testing of anchors available in the literature (e.g., *Hoehler, 2006*) indicate that mechanical anchors characterised by low stiffness and strong non-linear behaviour (see Figure 8-9a) can exhibit significant stiffness increase in the subsequent cycles ($k_{N,i} \geq k_{N,0}$). The stiffness $k_{N,i}$, is relevant for the effectiveness of the retrofit solution (i.e., calculation of β-factor) at the cycle *i*. However, the displacement, δ_0, (see Figure 8-9b) should be taken into account in the evaluation of the deformation of the joint region. If the joint shear distortion exceeds the elastic limit, can be verified assuming $k_{N,sec,i}$ in the calculations.

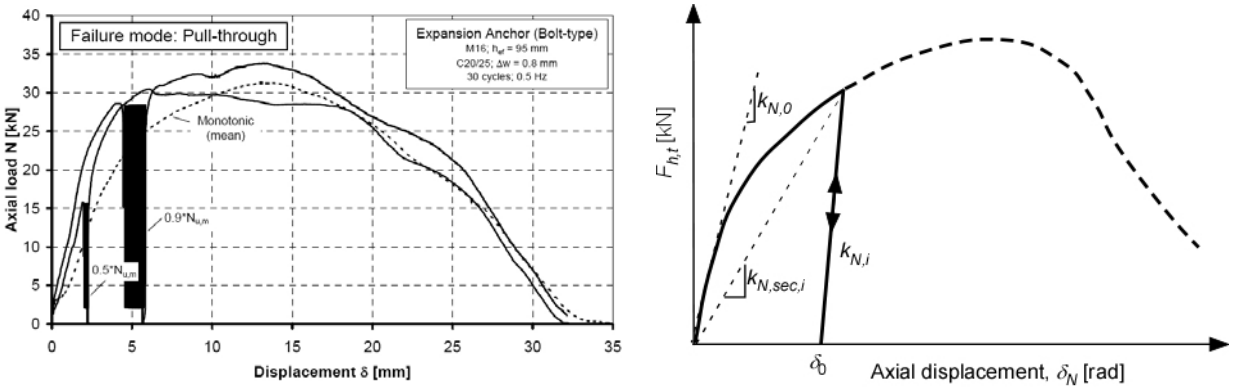

a) Experimental test (*Hoehler, 2006*) b) Anchor stiffness schematisation

Figure 8-9: Load-displacement behaviour of single anchor under tensile cyclic loading

The behaviour of anchors under shear load is significantly influenced by the presence of an hole clearance, which should be avoided, because of its deleterious effect on the anchor stiffness. In Figure 8-10 a comparison of shear cyclic behaviour on single anchors with and without hole clearance is shown.

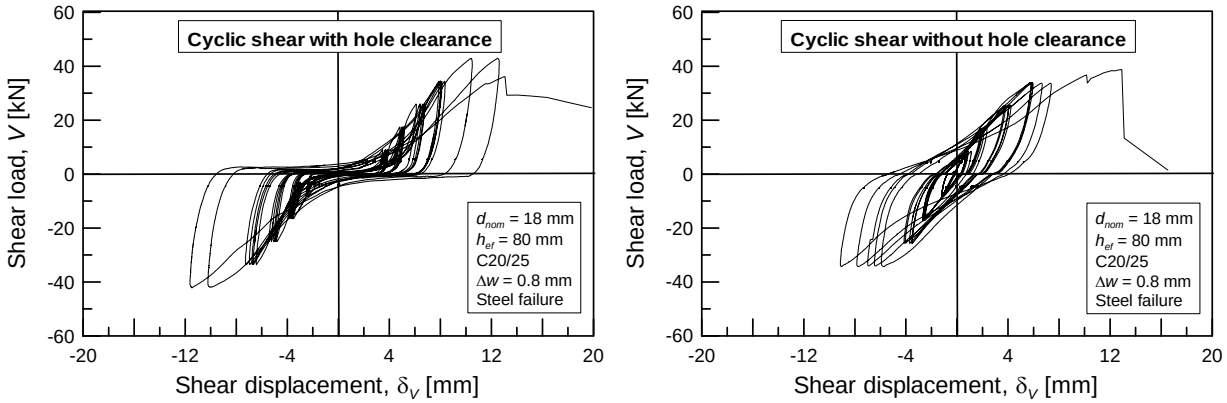

a) Test with hole clearance c) Test without hole clearance

Figure 8-10: Shear cyclic behaviour of single anchors (*Genesio, 2007b*)

8.2.2.4 Stiffness of anchors according to existing technical approvals

Technical Approvals of anchors (e.g., according to AC 193 *(ICC-ES, 2010)*, ACI 355.2-07 *(ACI 355.2, 2007)* in USA and ETAG 001 (*EOTA, 1997*) in Europe usually provide values for the estimation of the anchors deformability at the serviceability limit state ($k_{s,N}$ evaluated at approximately $N_u/3$). It is worth mentioning that the acceptance criteria of bonded anchors according to AC 308 (*ICC-ES, 2009*) do not include any information related to stiffness of the

anchor. Evaluation reports according to AC 193 (*ICC-ES, 2010*) provide only axial stiffness values of mechanical anchors.

ETAs (European Technical Approvals) for anchors according to ETAG 001 (*EOTA, 1997*) provide displacements under short term tension and shear loading (δ_{N0} and δ_{V0}) evaluated from the tests on single anchors without edge or spacing effects in concrete C20/25. The value derived should approximately correspond to the 95%-fractile for a confidence level of 90%. Furthermore, indications of the long term displacements ($\delta_{N\infty}$ and $\delta_{V\infty}$) are also provided. For anchors suitable for applications in cracked concrete, $\delta_{N\infty}$ is calculated by dividing the residual displacement resulting from the crack movement tests, δ_{M1}, by a factor equal to 1.5. The same approach is used to calculate $\delta_{V\infty}$ from a given δ_{V0}. Values of the anchor displacements are provided for cracked and uncracked concrete and different anchor diameters.

Evaluation reports according to ICC-ES (International Code Council-Evaluation Service) for anchors according to AC 193 (*ICC-ES, 2010*) indicate the minimum axial stiffness values in the service load range in uncracked and cracked concrete (β_{uncr} and β_{cr}) for different anchor diameters.

8.2.2.5 Evaluation of friction

The anchor shear stiffness, k_V, is generally much lower than the tensile stiffness, k_N, (approximately 1/3), but it acts parallel to the frictional stiffness, K_f. It is well known that the friction may significantly influence the shear load-displacement behaviour of anchorages. Typically, anchors under shear load are tested in such a way that the frictional component can be considered negligible. A teflon sheet is usually placed between the concrete surface and the steel attachment for this aim. In Figure 8-11 tests on anchors loaded in shear with and without a teflon sheet between the concrete surface and the steel fixture carried out by *Grosser (2012)* are shown. An increase of the stiffness of approximately a factor 2 was observed in the tests without teflon. The comparison of stiffness values of tests with (*Grosser, 2012*) and without teflon (*Anderson & Meinheit, 2006*) supports this thesis. In this application an even higher influence of friction may be assumed, because of the presence of levelling mortar between the steel plate and the concrete surface. However, due to the lack of specific investigations, the positive effect of friction is accounted for by a multiplication factor of 2 which could be considered realistic. Further considerations on the shear stiffness of anchors based on the analysis of available research work are presented in Section 8.2.2.2.

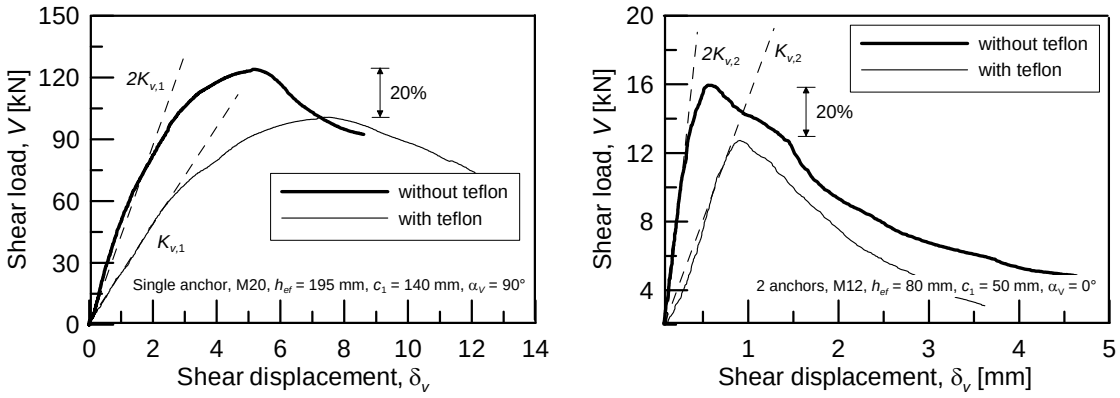

a) Single anchor loaded parallel to the edge b) Anchor group loaded towards the edge

Figure 8-11: Effect of friction shear load-displacement behaviour of anchorages (*Grosser, 2012*)

To follow the approach suggested by Equation (8-13b), the shear stiffness contribution of anchors and frictional behaviour of the anchorage plates can be consider separately. The first is given with good approximation by anchor testing using a teflon sheet between the steel fixture and the concrete surface. The second can be determined following different mechanical approaches discussed below.

For this study static and kinetic friction can be relevant. Static friction acts tangentially in the contact interface between two solid objects that are not moving relative to each other. If this force is overcome by an applied force, an object can move. When tangential relative movement for the two objects starts, the kinetic friction occurs. The relative load-displacement behaviour due to friction between two materials can be schematically represented as shown in Figure 8-12.

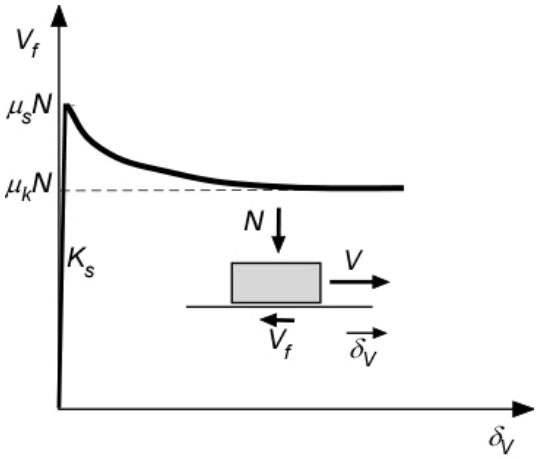

Figure 8-12: Schematic representation of friction

Tests by *Rabbat & Russel (1985)* indicated that the coefficient of static friction, μ_s, can be as high as 0.6~0.7 for concrete/steel and grout/steel interfaces. The coefficient of kinetic friction, μ_k, is typically assumed to be equal to between 0.4 and 0.6 for concrete/steel interfaces. In *EC3 (2002)* $\mu_k = 0.2$ is conservatively recommended.

Higher uncertainness concerns the estimation of the shear stiffness, K_f, related to the friction, since it is usually not measured. The classical physical approach assumes $K_f \rightarrow \infty$. However,

this approach is valid only if the friction is measured in ideal condition assuming a “perfectly stiff system”. In general, deformation due to the elasticity of materials and slip due to voids in the contact interface reduce the value of K_f. In this application the cyclic loading of the subassemblies contributes further to reduce the stiffness of the system.

Alternatively, K_f can be evaluated in analogy to the concrete-to-concrete interface friction problem. Experimental tests were carried out by *Tassios & Vintzileou (1987)* to understand the frictional behavior of smooth and rough surfaces. Some findings of the tests of Tassios and Vintzileou can be taken as a useful indication also for the frictional behaviour of the haunches on the beam and column surfaces:

- the friction coefficient is a function of the compression stress applied in the interface (σ_c in Figure 8-13a);
- the frictional stress, τ_{fr} varies between 0.2 and 0.8 Mpa (with 0.5 Mpa ≤ σ_c ≤ 2.0 Mpa for smooth surfaces, which corresponds to the case when between haunch plates and beam/column surfaces no leveling mortar is used (Figure 8-13a);
- the frictional stress, τ_f varies between 2.0 and 6.0 Mpa (with 0.5 Mpa ≤ σ_c ≤ 2.0 Mpa) for rough surfaces. The latter corresponds to the case when between haunch plates and beam/column surfaces leveling mortar is used (Figure 8-13b); and
- in the case of cyclic loading the friction-slip relationship for a smooth surface was not significantly influenced (Figure 8-13c); while in the case of rough surfaces a significant strength decrease was observed (Figure 8-13d).

Considering displacement between 0.1 and 2.0 mm of the haunch plates and a rough interface, σ_c in the same range shown in Figure 8-13b (these assumption are justified by the experimental investigations described in Chapter 9), values for the frictional stiffness, k_f, between 2.5 and 10 kN/mm^3 can be realistically assumed. To distinguish between the theoretical definitions of static and kinetic friction and the friction problem, which arise in this study, the indices *f* instead of *s* and *k* is used. The frictional coefficient, μ_f, is conservatively assumed (i.e., to avoid an overloading of the anchorage in shear (see Eq. (8-23)) equal to 0.4.

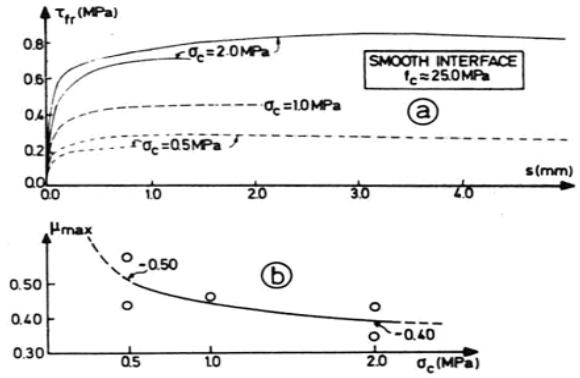

a) Smooth interfaces – Monotonic loading

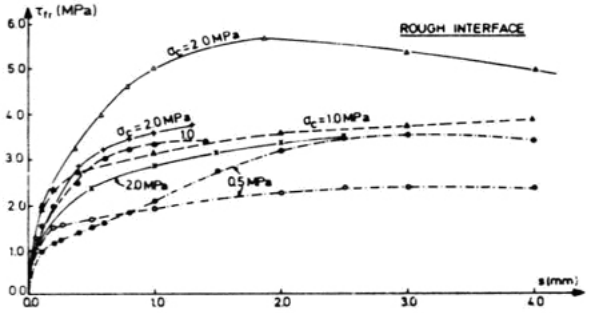

b) Rough interfaces - Monotonic loading

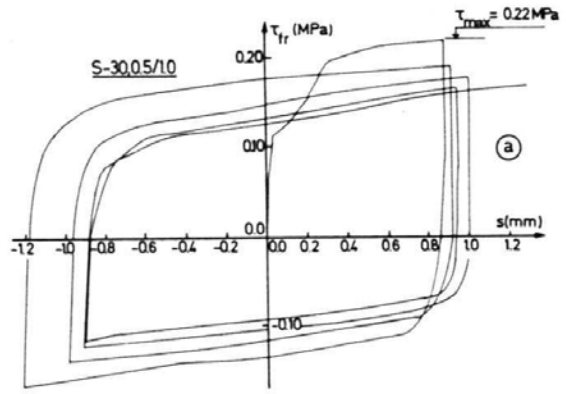

c) Smooth interfaces – Cyclic loading

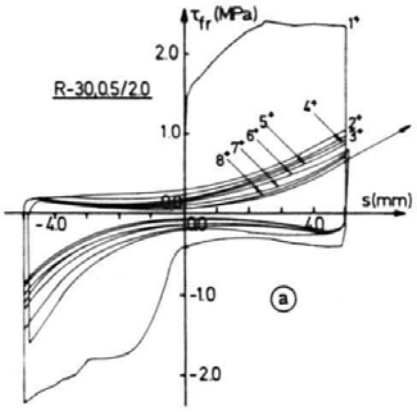

d) Rough interfaces - Cyclic loading

Figure 8-13: Friction-slip relationships in tests of *Tassios & Vintzileou (1987)*

8.2.3 Resistance of the anchorage

For the design of the anchorage, the Equation (8-18) should generally be satisfied. The partial safety factors for the action, S_d, and the resistance, R_d, should be taken according to the relevant seismic design / retrofit code and they are not considered in this chapter.

$$S_d \leq R_d \tag{8-18}$$

The forces acting on the anchorage, S_d, are discussed in Section 8.2.4.

The determination of the strength of the anchorage, R_d, is based on the CC-Method (*Fuchs et al., 1995*). The methods used for this specific anchorage for the calculation of tensile and shear strength are explained in Sections 8.2.5.1 and 8.2.5.2, respectively. As an example, the determination of the tensile and shear resistance is shown for the anchorages adopted in the experimental investigations (see Chapter 9).

8.2.4 Determination of actions and load distribution on anchors

For a given β-factor it is possible to calculate the tension and compression loading in the diagonal haunches. The axial force to be transmitted by the haunches, F_h, can be calculated according to Equation (8-19).

$$F_h = \frac{\beta \cdot V_{b,u}}{\cos\alpha} \tag{8-19}$$

with $V_{b,u}$ being the shear force in the beam corresponding to the flexural ultimate limit state of the beam at the end of haunch.

Due to the different stiffness values assumed in tension and in compression ($K_{d,t}$ and $K_{d,c}$), the haunches are loaded in tension and compression according to the Equations (8-20) and (8-21), respectively.

$$F_{h,c} = F_h \frac{K_{h,c}}{K_{h,c} + K_{h,t}} \tag{8-20}$$

$$F_{h,t} = F_h \frac{K_{h,t}}{K_{h,c} + K_{h,t}} \tag{8-21}$$

As shown in Figure 8-6 the anchorage is loaded in shear when compressed and in tension when the haunch is tensioned. The tension and shear actions on the anchorage of the tensioned haunch can be calculated according to the Equations (8-22a) and (8-22b). Note that the Equation (8-22b) applies only if the beam and column are assumed to be flexible (see Figure 8-7).

$$F_{h,N,t} = F_{h,t} \cdot \sin\alpha = \beta \cdot V_{b,u} \cdot \tan\alpha \frac{K_{h,t}}{K_{h,c} + K_{h,t}} \quad \text{(Tension force)} \tag{8-22a}$$

$$F_{h,V,t} = F_{h,t} \cdot \cos\alpha = \beta \cdot V_{b,u} \frac{K_{h,t}}{K_{h,c} + K_{h,t}} \quad \text{(Shear force)} \tag{8-22b}$$

For the compressed anchorage the shear force to be resisted can be calculated according to the Equation (8-23).

$$F_{h,V,c} = F_{h,c} \cdot \left(\cos\alpha - \mu_f \cdot \sin\alpha\right) = \beta \cdot V_{b,u} \frac{K_{h,c}}{K_{h,c} + K_{h,t}} \cos^2\alpha \left(1 - \mu_f \cdot \tan\alpha\right) \tag{8-23}$$

and if: $\left(1 - \mu_f \cdot \tan\alpha\right) \le 0 \Rightarrow F_{h,V,c} = 0$, i.e., the entire shear force is resisted by friction and the anchors are unloaded

The shear and tensile loading of the anchorage are linearly proportional to the β-factor and the ratio between $K_{h,t}$ and $K_{h,c}$. With increasing anchor stiffness the actions of the anchorage increase. For a given haunch geometry (L_h, α and K_d) the β-factor and consequently the design load of the anchorage depends on the assumed stiffness. Therefore, for the determination of actions on the anchorage, the upper bound of stiffness of the anchors chosen for the retrofit should be taken into account ($k_{N,max}$ and $k_{V,max}$). According to Equation (8-11), this approach leads to an upper bound also for the β-factor (β_{max}).

For the anchorage of the steel diagonals to the RC members, an anchor group as shown in Figure 8-14 was chosen. The dashed line in Figure 8-14a,b represents schematically the failure pattern assumed for concrete cone failure in tension and concrete edge failure for

shear parallel to the edge, respectively. The tension and shear resistances of the anchorage can be calculated according to the existing methods (e.g., *fib, 2011*). Due to the uncertainty in determining the exact position of the plastic hinge in the beam, the anchorage configuration shown in Figure 8-15 can be conservatively assumed. This shows the plastic hinge occurring in the beam cross section where the outer anchor row is situated and it represents the most unfavourable situation.

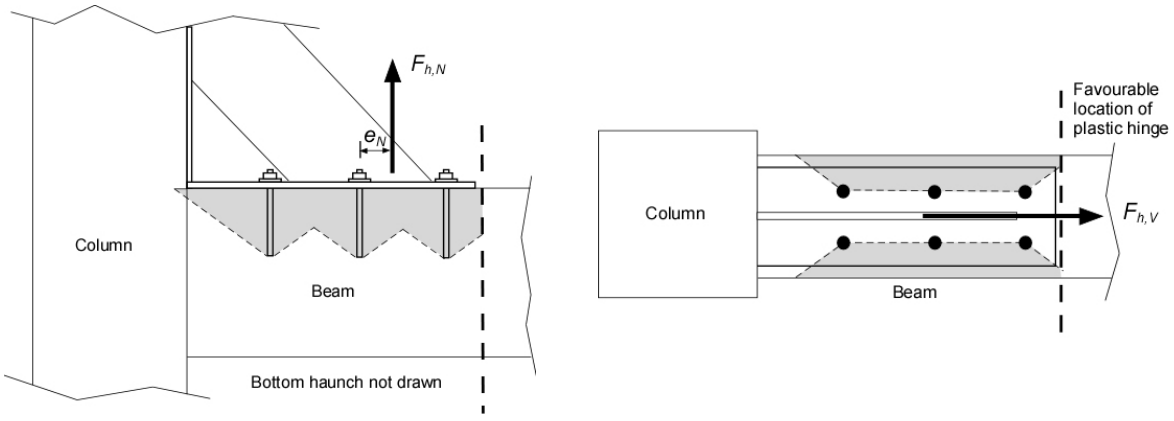

a) Side view (schema of tension loading) b) Top view (schema of shear loading)

Figure 8-14: Scheme of the loading of the anchorage (favourable location of plastic hinge)

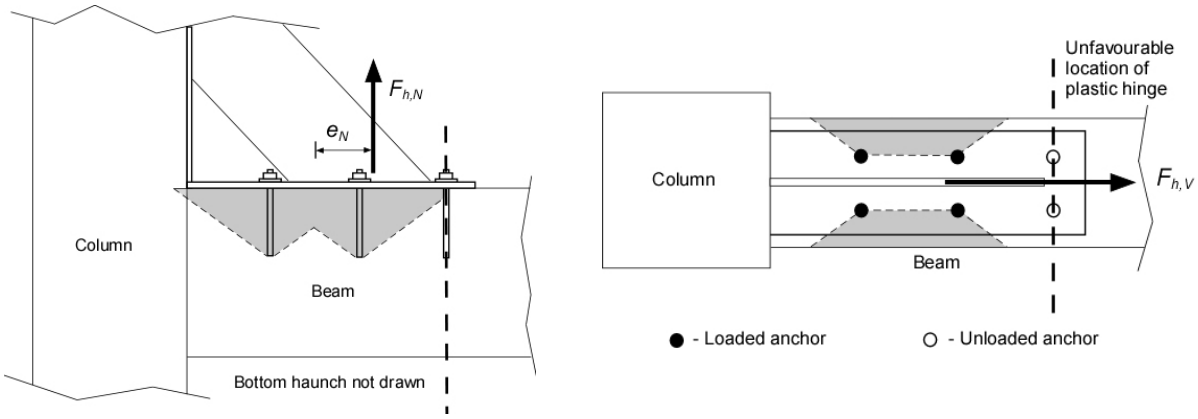

a) Side view (schema of tension loading) b) Top view (schema of shear loading)

Figure 8-15: Scheme of the loading of the anchorage (unfavourable location of plastic hinge)

The schemes shown in Figure 8-14 and the above consideration are valid also for the column. However, no plastic hinge is expected to occur in the column and flexural cracking is generally expected to be less significant in comparison with the beam (see Figure 8-3), because of the lower bending moment acting in the column and to the positive effect of the axial loading. Therefore, the resistance of the anchorage on the column is generally higher than that of the beam.

8.2.5 Determination of the mean resistance of the anchorage

While determining the resistance of the anchorage, particular care should be used for the consideration of the following aspects:

- The anchorage has to carry loads in cracked concrete, although, it is improbable that all anchors will be located in cracks;

- the most external row of anchors in the beam is located close to a plastic hinge, this has to be considered in the calculation of the projected areas for the concrete cone strength of the group (compare Figure 8-14 and Figure 8-15);
- in the design of anchorages (e.g., according to *fib, 2011*) the structural RC element, where the load is transmitted, is usually within the serviceability limit state. This is not true in this application;
- the eccentricity of the tension load has to be considered (Figure 8-14 and Figure 8-15);
- the cyclic loading pattern can negatively affect the load-carrying capacity as well as the stiffness of the anchorage; and
- Combined tension and shear loading on the anchorage may need to be considered (see Figure 8-7b).

The general rules for the calculation of the resistance of the anchorage to tension (Section 8.2.5.1), shear (Section 8.2.5.2) and combined tension and shear (Section 8.2.5.3) explained below follow the fib Design Guide “Anchorage to Concrete” (*fib, 2011*).

8.2.5.1 Calculation of tensile mean resistance of the anchorage

The mean tensile resistance, N_{Rm} of the anchorage can be calculated assuming the anchorage shown in Figure 8-14a (or Figure 8-15a). N_{Rm} is the smallest of the following resistances:

- Steel resistance, $N_{Rm,s,group}$,
- Pullout resistance, $N_{Rm,p}$,
- Concrete cone resistance, $N_{Rm,c}$,
- Combined concrete cone and pullout resistance, $N_{Rm,p}$ (only for bonded anchors); and
- Splitting resistance, $N_{Rm,sp}$.

The tensile steel resistance of a single anchor, $N_{Rm,s}$, shall be multiplied by the number of anchors of the group, n, to obtain the steel resistance of the group, $N_{Rm,s,group}$.

$$N_{Rm,s,group} = n \cdot N_{Rm,s} \tag{8-24}$$

The tensile pullout resistance of a single anchor, $N_{Rm,p}$, shall be multiplied by the number of anchors of the group, n, to obtain the steel resistance of the group, $N_{Rm,p,group}$.

$$N_{Rm,p,group} = n \cdot N_{Rm,p} \tag{8-25}$$

The concrete cone resistance, $N_{Rm,c}$, is calculated according to the *fib (2011)* provisions using the Equation (8-26).

$$N_{Rm,c} = N^0_{Rm,c} \cdot \psi_{A,N} \cdot \psi_{s,N} \cdot \psi_{ec,N} \cdot \psi_{re,N} \tag{8-26}$$

with:

$$N^0_{R,c} = k_N \cdot \sqrt{f_{cm}} \cdot h_{ef}^{1.5} \tag{8-26a}$$

where:

k_N = 10.3 or 14.7 for post-installed anchors in cracked or uncracked concrete, respectively. These empirical coefficients are strongly dependent from the product (i.e., manufacturer) and the anchor type and they may be increased up to 11.9 and 16.9, respectively (values valid for headed anchors), if suitable prequalification tests have been carried out. For instance, torque-controlled bonded expansion anchors (see Figure 2-27j) behave similarly to headed anchors according to investigations by *Pregartner & Asmus (2007)*. In this application the concrete should be considered cracked. Tests by *Mayer & Eligehausen (1984)* on groups of four anchors in cracked concrete indicated that the strength decrease with an increasing number of anchors located in cracks between 15% and 30% can be conservatively assumed. Similar tests on larger anchor groups are not known to be available in literature.

h_{ef} = effective embedment depth to be taken from the relevant technical approval

$\psi_{A,N}$ = factor to take into account the geometric effects of spacing and edge distance

$$\psi_{A,N} = A_{c,N} \big/ A^0_{c,N} \tag{8-26b}$$

In this study $A_{c,N}$ and $A^0_{c,N}$ are calculated according to Figure 8-16a,b. The section where the plastic hinge is expected to occur is conservatively considered equivalent to a free edge.

$s_{cr,N}$ and $c_{cr,N}$ (see Figure 8-16b) are equal to $3h_{ef}$ and $1.5h_{ef}$ respectively for most of anchor types.

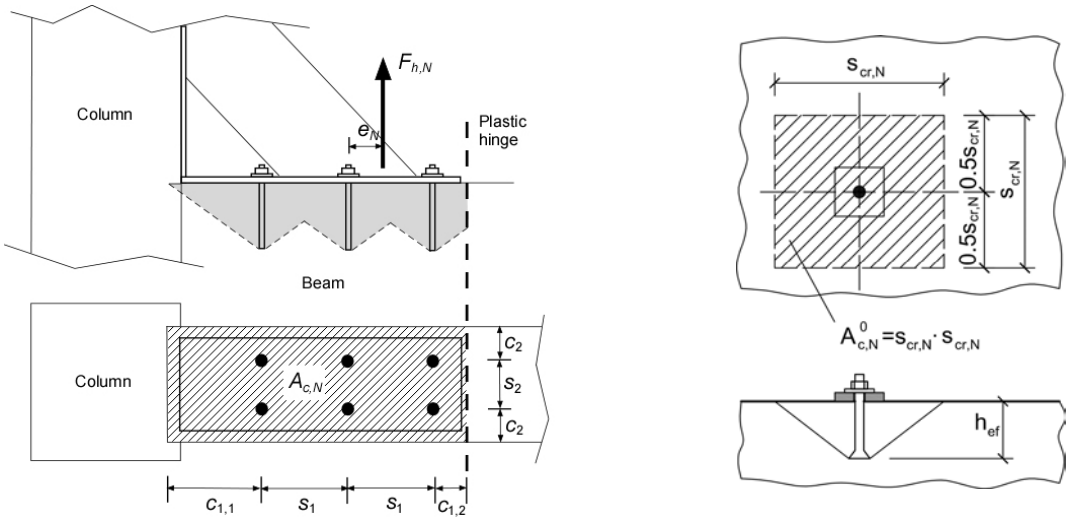

a) Anchorage considered to calculate $N_{Rm,c}$ b) Definition of $A^0_{c,N}$ (*fib, 2011*)

Figure 8-16: Anchor group considered for the determination of $N_{R,c}$

$\psi_{s,N}$ = factor accounting for the influence of the edges of the concrete member on the distribution of stresses in concrete

$$\psi_{s,N} = 0.7 + 0.3c \big/ c_{cr,N} \tag{8-26c}$$

with:

c = min($c_{1,1}$, $c_{1,2}$, c_2) according to Figure 8-16a

$\psi_{ec,N}$ = factor accounting for axial load acting with an eccentricity, e_N, in respect to the centre of gravity of the anchorage

$$\psi_{ec,N} = \frac{1}{1 + 2e_N \big/ s_{cr,N}} \tag{8-26d}$$

The length of the eccentricity, e_N, cannot be simply analytically determined as it depends on several factors such as the location of the plastic hinge in the beam and the load-

displacement behaviour of the single rows of anchors (rows arranged perpendicular to the longitudinal direction of the beam). In Figure 8-17 three cases are shown assuming flexible behaviour of the steel plates of the haunches, since perfect rigid plates would allow a perfect redistribution of the force with no eccentricity. If all three rows of anchors exhibit similar strength and stiffness, it may be assumed that the external row of anchors would take up more load than the others. The largest possible eccentricity, e_N, occurs in the case of a triangular stress-strain distribution in the diagonal haunch (Figure 8-17a). However, the trapezoidal stress-strain distribution as shown in Figure 8-17b is more realistic. It may be expected that during the loading of the beam-column connection the first flexural cracks under the haunch occur close to the section where the plastic hinge occurs. This crack may reduce the load-displacement capacity of the external rows of anchors reducing in this way the eccentricity, but at the same time also the position of the centre of gravity of the anchorage changes (Figure 8-17b). In the case of a complete loss of load carrying capacity of a row of anchors (e.g., because of the formation of the plastic hinge) a response as shown in Figure 8-17c can be expected. To obtain a conservative design of the anchorage the situation shown in Figure 8-17a may be assumed. The evaluation of e_N is further discussed in Chapter 9 on the basis of experimental measurements.

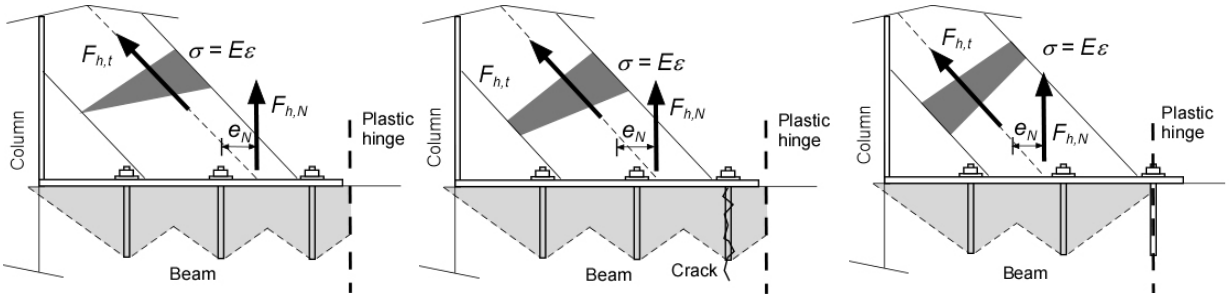

a) Favourable location of plastic hinge

b) Effect of cracked on concrete

c) Unfavourable location of plastic hinge

Figure 8-17: Evaluation of eccentricity of axial loading of the anchorage, e_N

$\psi_{re,N}$ = factor taking into account the negative effect of closely spaced reinforcement (s < 100 mm for d_s < 10 mm and s < 150 mm for d_s ≥ 10 mm) in the concrete member on the strength of anchors with an embedment depth, h_{ef} < 100 mm. $\psi_{re,N}$ may be taken equal to 1.0 in this application because the h_{ef} is generally larger than 100 mm.

If bonded anchors are used, the resistance for combined pullout and concrete cone failure according to *Appl (2009)* should be also evaluated using Equation (8-27).

$$N_{R,Np} = N^0_{R,Np} \cdot \psi_{A,Np} \cdot \psi_{s,Np} \cdot \psi_{g,Np} \cdot \psi_{ec,Np} \cdot \psi_{re,Np} \tag{8-27}$$

with:

$$N^0_{R,p} = \tau_R \cdot \pi \cdot d \cdot h_{ef} \tag{8-27a}$$

where:

τ_R = bond strength evaluated in cracked and uncracked concrete ($\tau_{R,cr}$ and $\tau_{R,uncr}$)

$\psi_{A,Np}$ = evaluated as for $N_{Rm,c}$, but $s_{cr,Np}$ and $c_{cr,Np}$ are defined by Equation (8-27b,c):

$$s_{cr,Np} = 20d\sqrt{\frac{\tau_{R,uncr}}{10}} \le 3h_{ef} \tag{8-27b}$$

$$c_{cr,Np} = 0.5s_{cr,Np} \tag{8-27c}$$

$\psi_{g,Np}$ takes into account the effect of the failure surface of the anchor group and it is defined by Equations (8-27d,e,f):

$$\psi_{g,Np} = \psi^0_{g,Np} - \sqrt{\frac{s}{s_{cr,Np}}} \cdot \left(\psi^0_{g,Np} - 1\right) \ge 1.0 \tag{8-27d}$$

$$\psi^0_{g,Np} = \sqrt{n} - \left(\sqrt{n} - 1\right)\left(\frac{\tau_R}{\max \tau_R}\right) \text{ (to be evaluated with } \tau_{R,cr} \text{ and } \tau_{R,uncr}) \tag{8-27e}$$

$$\max \tau_{R,cr} = \frac{10.3}{\pi \cdot d}\sqrt{h_{ef} \cdot f_c} \text{ and } \max \tau_{R,uncr} = \frac{14.7}{\pi \cdot d}\sqrt{h_{ef} \cdot f_c} \tag{8-27f}$$

The factors $\psi_{s,Np}$, $\psi_{ec,Np}$ and $\psi_{re,Np}$ can be calculated in the same way as for the concrete cone resistance.

The splitting of the concrete member during the anchor installation should be avoided by respecting the parameters, $c_{cr,sp}$ and $s_{cr,sp}$ given in the technical approval. The splitting resistance due to the anchorage loading can be calculated multiplying $N_{Rk,c}$ from Equation (8-26) with $\psi_{h,sp}$. The factor $\psi_{h,sp}$ takes into account the influence of the actual member thickness and can be calculated according to *Asmus (2007)*.

$$\psi_{h,sp} = \left(\frac{h}{h_{\min}}\right)^{2/3} \begin{cases} \le \left(\dfrac{h_{ef} + 1.5c_1}{h_{\min}}\right)^{2/3} \le 2.0 \\ \ge 1.0 \end{cases} \tag{8-28}$$

Furthermore, in the calculation of $A_{c,N}$ and $A^0_{c,N}$ the values $s_{cr,N}$ and $c_{cr,N}$ should be replaced by the values $s_{cr,sp}$ and $c_{cr,sp}$. $s_{cr,sp}$ and $c_{cr,sp}$ are the critical spacing and edge distance related to splitting failure and should be taken from the relevant technical approval.

8.2.5.2 Calculation of the anchorage mean shear resistance

The mean shear resistance, V_{Rm}, of the anchorage can be calculated assuming the anchorage shown in Figure 8-14b (or Figure 8-15b) loaded parallel to the edge. V_{Rm} is the smallest of the following resistances:

- Steel resistance, $V_{Rm,s,group}$,
- Concrete pryout resistance, $V_{Rm,cp}$, and
- Concrete edge resistance, $V_{Rm,c}$.

The shear steel resistance of a single anchor, $V_{Rm,s}$, shall be multiplied for the number of anchors in the group, n, to obtain the steel resistance of the group, $V_{Rm,s,group}$. A reduction factor of 0.8 should be applied to take into account the unequal anchors loading in groups with normal hole clearance according to *fib (2011)*, due to the brittleness of high strength steel usually used for post-installed anchors (*Fuchs, 1992*).

$$V_{Rm,s,group} = n \cdot V_{Rm,s} \tag{8-29}$$

The concrete pryout, $V_{R,cp}$, can be calculated according *fib (2011)* using the Equation (8-30).

$$V_{Rm,cp} = k_{cp} \cdot N_{Rm,c} \tag{8-30}$$

with:

k_{cp} = 1.0 or 2.0 for h_{ef} < 60 mm or h_{ef} ≥ 60 mm, respectively

$N_{Rm,c}$ = calculated according Equation (8-26)

Assuming that the presence of two edges does not influence negatively the anchorage behaviour (as shown in *Grosser, 2012*), a plane of symmetry parallel to the longitudinal axis of the beam can be used (Eq. (8-31). The resulting anchor group shown in Figure 8-18 can be considered for the verification of the concrete edge resistance, $V_{Rm,c}$, of the anchorage. $V_{Rm,c}$ can be calculated using the Equation (8-32) adopted by *fib (2011)*.

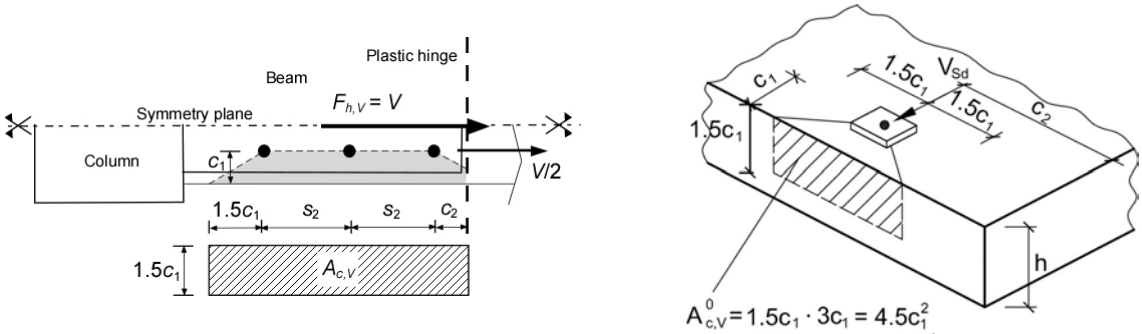

a) Anchorage considered to calculate $V_{Rm,c}$ b) Definition of $A^0_{c,V}$ (*fib, 2011*)

Figure 8-18: Anchor group considered for the determination of $V_{R,c}$

$$V / 2 \le V_{Rm,c} \rightarrow V \le 2V_{Rm,c} \tag{8-31}$$

$$V_{Rm,c} = V^0_{Rm,c} \cdot \psi_{A,V} \cdot \psi_{h,V} \cdot \psi_{s,V} \cdot \psi_{ec,V} \cdot \psi_{\alpha,V} \cdot \psi_{re,V} \tag{8-32}$$

with:

$$V^0_{Rm,c} = k_V \cdot d_{nom}^{\alpha} \cdot l_f^{\beta} \cdot \sqrt{f_{cm}} \cdot c_1^{1.5} \text{ (*Hofmann, 2005*)} \tag{8-32a}$$

where:

k_V = 2.3 or 3.2 for cracked and uncracked concrete, respectively. In this application the concrete should be conservatively considered cracked

α = $0.1(l_f / c_1)^{0.5}$

β = $0.1(d_{nom} / d_1)^{0.2}$

d_{nom} = outside diameter of the anchor ($d = d_{nom}$ for bolt type anchors)

l_f = influence length according to the relevant technical approval (usually $l_f = h_{ef}$ for anchor with constant diameter over the embedment depth)

c_1 = edge distance according to Figure 8-18b

$\psi_{A,V}$ = factor to take into account the geometric effects of spacing, member thickness and further edges

$$\psi_{A,V} = A_{c,V} \big/ A^0_{c,V} \tag{8-32b}$$

In this study $A_{c,V}$ and $A^0_{c,V}$ are calculated according to Figure 8-18a,b. The section, where the plastic hinge occurs, is conservatively considered equivalent to a free edge

$\psi_{h,V}$ = factor to take into account that the resistance does not decrease linearly with the member thickness as assumed by the ratio $A_{c,V}/A^0_{c,V}$

$$\psi_{h,V} = \sqrt{1.5c_1/h} \geq 1.0 \quad (8\text{-}32c)$$

$\psi_{s,V}$ = factor to take into account the influence of further edges on the distribution of stress in the concrete. This factor applies to the section where the plastic hinge occurs.

$$\psi_{s,V} = 0.7 + 0.3 \cdot c_2/1.5c_1 \leq 1.0 \quad (8\text{-}32d)$$

$\psi_{ec,V}$ = factor to take into account the effect of shear load acting on the anchorage with an eccentricity, e_V. This factor is assumed equal to 1.0 for this application.

$$\psi_{ec,V} = \frac{1}{1+2e_V/3c_1} \leq 1.0 \quad (8\text{-}32e)$$

$\psi_{\alpha,V}$ = factor to take into account the angle between the shear load applied and the direction to the free edge of the concrete member under consideration. In this case α_V = 90°. Several approaches have been recently proposed for the calculation of $\psi_{\alpha,V}$ to account for the increase of concrete edge resistance of an anchorage loaded toward the edge with an angle 0° < α_V ≤ 90° (with α_V = 0° or 90°if the shear load is directed perpendicular or parallel to the considered edge, respectively). According to ACI 318-08 Appendix D (*ACI 318, 2008*) $\psi_{90°,V}$ = 2.0. In the CEN TS (*CEN, 2009*) a value of 2.5 is used. In the fib (2011) $\psi_{90°,V}$ = 1.5, 2.0 or 2.5 for n_2 = 1, 2 or 3 is suggested (n_2 = 3 in Figure 8-18a). More detailed information about $\psi_{\alpha,V}$ please refer to *fib (2011)*.

$\psi_{re,V}$ = factor to take into account the positive effect of edge reinforcement that can be conservatively assumed equal to 1.0. The longitudinal and transverse reinforcement of the beam could increase the shear resistance acting as edge reinforcement of the anchorage since a beam bar diameter of d_b ≥ 12 mm is quite common also for pre 1970s lightly reinforced structures (condition according to *fib, 2011*). The second condition required by *fib (2011)* to apply $\psi_{re,V}$ = 1.4 is the presence of close spaced stirrups with s ≤ 100 mm and d_b ≥ 12 mm, which is usually not fulfilled in the considered building type.

8.2.5.3 Resistance to combined tension and shear load

If the approach shown in Figure 8-7 is adopted, the resistance of the anchorage to combined tension and shear has to be verified. In the case of seismic actions the Equation (8-33) should be used according to *fib (2011)* for all failure modes.

$$\frac{F_{h,V,t}}{V_{Rm}} + \frac{F_{h,N,t}}{N_{Rm}} \leq 1.0 \quad (8\text{-}33)$$

As discussed in Section 2.7.3 (see Figure 2-31, Figure 2-32) Equation (8-33) may lead to over-conservative results especially in cases, where the ratio $F_{h,v,t}/V_{Rm}$ is small in comparison to $F_{h,N,t}$ / N_{Rm}. Generally, this case occurs in this application as shown in Section 8.2.2 and in the following chapters. Further discussion is provided in Section 11.2.5.2.

8.3 Summary of the newly proposed retrofit solution

In this chapter the modification of the “Haunch Retrofit Solution” developed by *Pampanin et al. (2006)* by using post-installed anchors for the connection of diagonal haunches to an as-built 2D RC exterior beam-column joint has been proposed. It was discussed, how to evaluate the stiffness and strength of the anchors and the necessary modifications of the analytical assessment of the retrofit solution.

9 EXPERIMENTAL VALIDATION OF THE HAUNCH RETROFIT SOLUTION WITH POST-INSTALLED ANCHORS

The modification of the design method of the "Haunch Retrofit Solution" (HRS) to allow the use of post-installed anchors for the connection of the steel diagonals to the existing beam-column connection proposed in Chapter 8 was experimentally validated. In Sections 9.1 to 9.4 the experimental tests carried out in this study are presented and discussed. The measurements carried out during the experimental tests (i.e., force acting in the haunches as shown in Section 9.4.8) were used as input for the analytical evaluation of the eccentricity, e_N, of the axial load acting on the anchorage of the tensioned haunch (Section 9.4.9) and the calculation of the anchors stiffness (Section 9.4.10).

9.1 Test programme

The test programme shown in Table 9-1 was proposed in order to validate the assumptions of the assessment of the retrofitted joints discussed in Section 8.2.

The feasibility of using post-installed anchors for the optimisation of the HRS was investigated with two tests (2DG1 and 2DG2 shown in Figure 9-1a,b, respectively) carried out in the laboratory of the University of Canterbury (UC) (see *Genesio & Akgüzel, 2009*). In these tests the strength and the stiffness of the anchorage were designed to account for the possibility that the plastic hinge in the beam would occur in a section underneath the anchorage influencing negatively the load-displacement behaviour of the anchors. Epoxy based bonded anchors were chosen for this application, because they usually have a significantly stiffer behaviour under tension loading than mechanical anchor types as shown in Table 8-1 (Figure 9-2a). The specimens 2DG1 and 2DG2 had the same geometry and similar material properties as the as-built specimen "2D pre 1970s" (see Chapter 3). For both specimens haunches with an inclination $\alpha = 45°$ were chosen. In the first test (2DG1) the projected length of the haunches on the beam, *L',* was 480 mm and six bonded anchors were used for the connection with beam and column. In the second test specimen (2DG2), *L'* was equal to 350 mm and only four anchors were used for the connection (see Figure 9-3a,b). A constant column axial load, N_c = 110 kN was applied in both tests.

Five more tests on retrofitted beam-column joints were carried out in the laboratory of the Bhabha Atomic Research Centre (BARC) (see *Genesio & Sharma, 2010b*). The effect of the partial failure of the anchorage of the steel haunches on the retrofit solution was investigated (JT1-2 and JT1-3). To verify the possibility of applying this retrofit technique also in cases where no over design of the anchorage is feasible, a selective weakening strategy (*Kam, 2011*) was also investigated. To reduce the loading of the anchorage, the beam flexural

strength was reduced by cutting some of the longitudinal reinforcing bars in a cross section close to the end of the haunches. This weakening solution was validated with the specimen JT1-4. Two more tests (JT1-5 and JT1-6) were carried out to investigate the possibility of using mechanical instead of chemical anchors with the aim of reducing costs, time and effort in the installation of the haunches and to avoid faulty anchor installations (*Genesio et al., 2007* and *Grosser et al., 2011*). Concrete screws (Figure 9-2b) and bolt type expansion anchors were used (Figure 9-2c). The specimens JT1-2, JT1-3, JT1-4, JT1-5 and JT1-6 had the same geometry and similar material properties as JT1-1 (see Chapter 3) (see Figure 9-1c). For all the specimens tested at BARC the same haunch geometry with $\alpha = 45°$ and *L'* = 580 mm was used. Six anchors per each connection were used and no axial load in the column was applied (see Figure 9-3c).

Table 9-1: Test programme on retrofitted specimens

Specimen	f_c [MPa]	f_{ct} [a)] [MPa]	f_y [MPa]	Col. rein.	Beam rein. [b)]	L' [c)] [mm]	α [d)]	h_{ef} [mm]	Anchor Type
2DG1 [e)]	16.6	1.9	340	3+3	4 R10	480	45°	125	Epoxy
2DG2 [e)]	16.5	1.9		R10		350		125	Epoxy
JT1-2 [f)]	26.5	2.1	490	3+3 D20	2 D20 + 1D16	580	45°	150	Epoxy
JT1-3 [f)]	30.2	2.7						150	Epoxy
JT1-4 [f)]	33.6	3.1						150	Epoxy
JT1-5 [f)]	27.7	3.6						90	Screw
JT1-6 [f)]	23.3	3.3						115	Expansion

[a)] f_{ct} by splitting test; [b)] D = deformed bars; R = plain round bars (symmetrical reinforcement for top and bottom layer); [c)] Distance between the beam-column interface and the end of the haunch; [d)] Inclination's angle of the haunch; [e)] Tests carried out in the laboratory of the UC; [f)] Tests carried out in the laboratory of the BARC

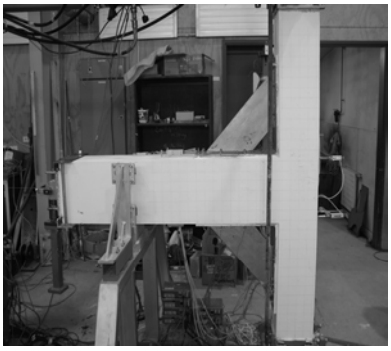

a) Haunches on 2/3 scale (specimen 2DG1)

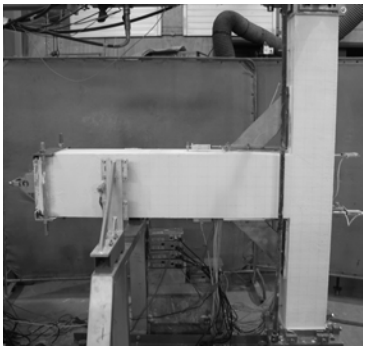

a) Haunches on 2/3 scale (specimen 2DG2)

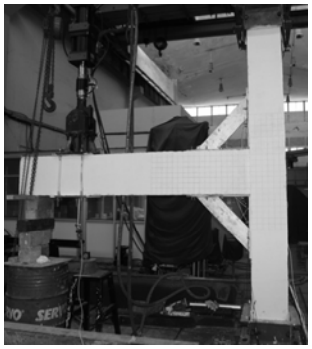

b) Haunches on full scale (specimen JT1-2)

Figure 9-1: Retrofitted specimens

a) Bonded anchor

b) Concrete screw

c) Expansion anchor

Figure 9-2: Post installed anchors used in the tests

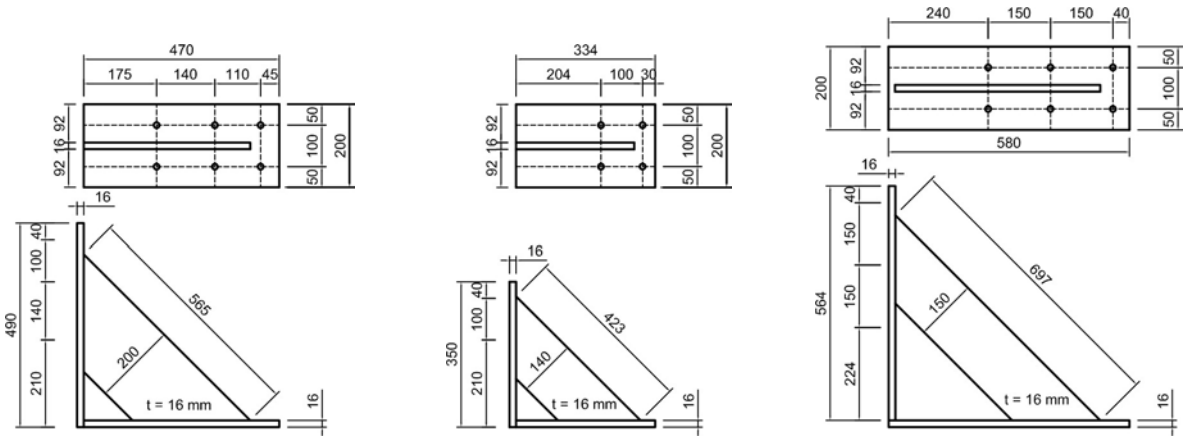

a) Haunch 2DG1 b) Haunch 2DG2 c) Haunches JT1-2, JT1-3, JT1-4, JT1-5, JT1-6

Figure 9-3: Dimensions of the haunches

9.2 Haunches installation

9.2.1 Installation sequence

The metallic haunches were installed following the steps shown in Figure 9-4:

STEP 1: Exact localisation of the reinforcement in the beam-column joint in order to avoid its cutting while drilling the holes (Figure 9-4a).

STEP 2: Cutting, drilling and welding of the steel plates constituting the haunches according to the design and after the verification of the feasibility done in STEP 1 (Figure 9-4b).

STEP 3: High strength mortar placed at the interface between beam/column and steel plates (thickness max 3 mm) to ensure the contact between surfaces of the haunches and specimen for a uniform load distribution (Figure 9-4c). In the case of not perfect orthogonality between beam and column the thickness of the mortar may be larger and this should be taken into account for the length of the anchors.

STEP 4: Placing of the steel diagonal on the joint and temporary fixing it in order to avoid voids in the interface (Figure 9-4d).

STEP 5: Installation of anchors according to instructions of the manufacturers (example with bonded anchors is shown in Figure 9-4): Drilling of the holes for the anchors through the holes in the steel anchor plates (Figure 9-4e), hole cleaning (Figure 9-4f), Mortar injections (Figure 9-4g) and insert of the anchors in the holes, application of torque moment (Figure 9-4h).

a) Localisation of reinforcement

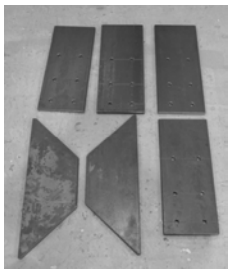

b) Cutting, Drilling and welding of the steel haunches

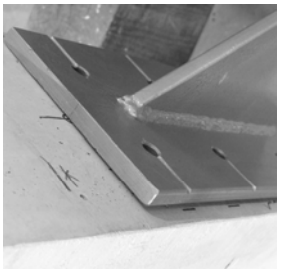

c) Preparation of concrete surfaces: grinding and placing of levelling mortar

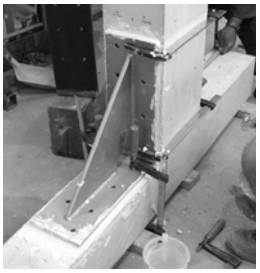

d) Temporary fixing of haunches

e) Holes drilling through the steel plates

f) Holes cleaning through mechanical brushing and vacuuming

g) Injection of epoxy mortar

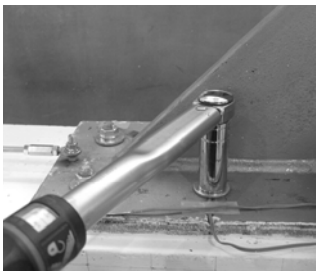

h) Application of torque moment

Figure 9-4: Installation sequence of metallic haunches with post-installed anchors

9.2.2 Anchors installation

The installation of the post-installed was carried out following the requirements and parameters of the relevant technical approvals. Hole clearances, which have a detrimental effect on the shear stiffness of the anchorage (see Figure 8-10a), were avoided. To achieve this goal bonded anchors were installed filling the gap between the threaded rods and the bore hole wall of the anchor plate with epoxy mortar. By using mechanical anchors (tests JT1-5 and JT1-6) a zero hole clearance could not be completely achieved, although the diameter of the holes in the steel plates was kept as close as possible to the anchor diameter.

9.3 Test setup and procedure

The setups, the testing procedures and loading protocols used for the tests of the retrofitted specimens at UC and BARC were the same as those used for the as-built specimens described in Section 3.3. In addition to the measurements taken during the tests on the as-built joints extra strain gauges were glued at different locations along the beam longitudinal bars to evaluate the distribution of the flexural moment on the beam, on the diagonal haunches (Figure 9-5a) and on the anchors to measure the axial strain were possible, i.e., bonded anchors (Figure 9-2a). It should be noted, however, that these measurements were not always reliable, mainly because of difficulty of installation of strain gauges on threaded rods embedded in epoxy mortar. The axial load acting in on the diagonal haunches could be

calculated according Equation (9-1) using the measurements schematically shown in Figure 9-5b.

$$F_h = \frac{(\varepsilon_1 + \varepsilon_2 + \varepsilon_3)}{3} \cdot w_d \cdot t_d \cdot E_s \quad (9\text{-}1)$$

with:
w_d = width of the haunch
t_d = thickness of the haunch
ε_1, ε_2 and ε_3 = strain measurements as shown in Figure 9-5

Furthermore, the readings of the strain gauges were used to estimate the eccentricity, e_N, (see Section 9.4.9) necessary for the verification of the resistance of the anchor group under axial load, $F_{h,N}$.

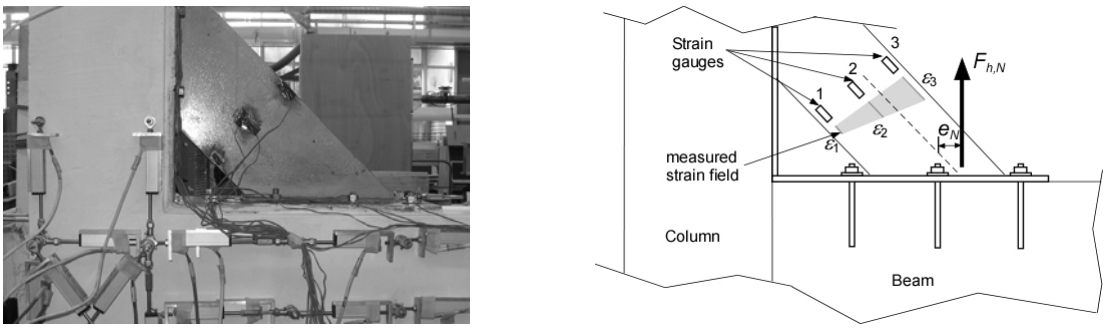

a) Strain gauges glued on diagonal haunch (2DG1) b) Schema for the evaluation of loading of the haunch

Figure 9-5: Instrumentation of the diagonal haunches

9.4 Results of the tests

In the following sections the results of the tests are presented and discussed. The efficiency of the retrofit solution in each test was evaluated by comparing the cracking pattern, hysteretic behaviour and joint shear distortion of retrofitted and as-built benchmark specimen. The analysis of the tensile and compressive forces in the haunches gave important information on the effective stiffness of the steel diagonal fixed with post-installed anchors to the existing structure and the loading of the anchorage. The effectiveness of the retrofit in the redistribution of the internal forces in the beam-column connection was further validated by analysing the moment decrease in the beam due to the effect of the haunch.

9.4.1 Test 2DG1

The behaviour of the specimen 2DG1 was characterised by a higher initial stiffness than the benchmark specimen “2D pre 1970s” (Figure 9-7a). The first flexural cracks occurred during the 0.1% top drift cycle in the cross section of the beam where the plastic hinge was expected to occur (Figure 9-6a). At the end of the 0.5% top drift cycle, yielding of the beam longitudinal bars was measured in both loading directions at approximately 24 kN column top lateral load (Figure 9-7a) and more flexural cracks in the beam were observed. Furthermore, one inclined beam shear crack in each loading direction occurred (Figure 9-6b). The strength of the specimen was approximately constant up to a top drift of 2.0% in both loading directions. The strength reduction observed in the specimen in the last part of the test was due to the buckling of the longitudinal beam bars, which were not adequately confined due to the large spacing of the shear reinforcement (Figure 9-6c). The beam flexural strength was

additionally reduced by the decrease of the static height of the cross section, because of the spalling of concrete cover (Figure 9-6c).

a) 0.5% b) 1.5% c) 3.0%

Figure 9-6: Test 2DG1 – Cracking patterns at increasing top drift levels

Both top and bottom parts of the column and the joint region remained uncracked during the entire test and its shear distortion was negligibly small (Figure 9-7b). In Figure 9-7b the ratio $p_t/\sqrt{f_c}$ is calculated assuming the as-built joint configuration for better comparability. The anchors used for the connection of metallic haunches exhibited a sufficient stiff behaviour and a negligible displacement was observed (0.1 to 0.5 mm). The plastic hinge was located at approximately 100 mm from the last row of anchors (Figure 9-6c). One flexural crack was observed in the cross section of the beam coincident with the middle row of anchors. However, the crack width was less than 0.3 mm during the entire test and did not significantly influence the load-displacement behaviour of the anchors. The force transferred by the metallic haunch in compression was higher than the force in tension (Figure 9-8a). Because of the difference of axial stiffness in tension and compression (see Section 8.2.2), a ratio $F_{d,c}/F_{d,t}$ ~ 1.5 in positive and negative loading directions was observed. These observations allowed the estimation of the haunch stiffness using the model proposed in Chapter 8 (see Section 9.4.10). The analysis of the strain gauge readings shown in Figure 9-8b displays the effectiveness of the haunches in reducing the beam flexural moment with decreasing distance from the column face.

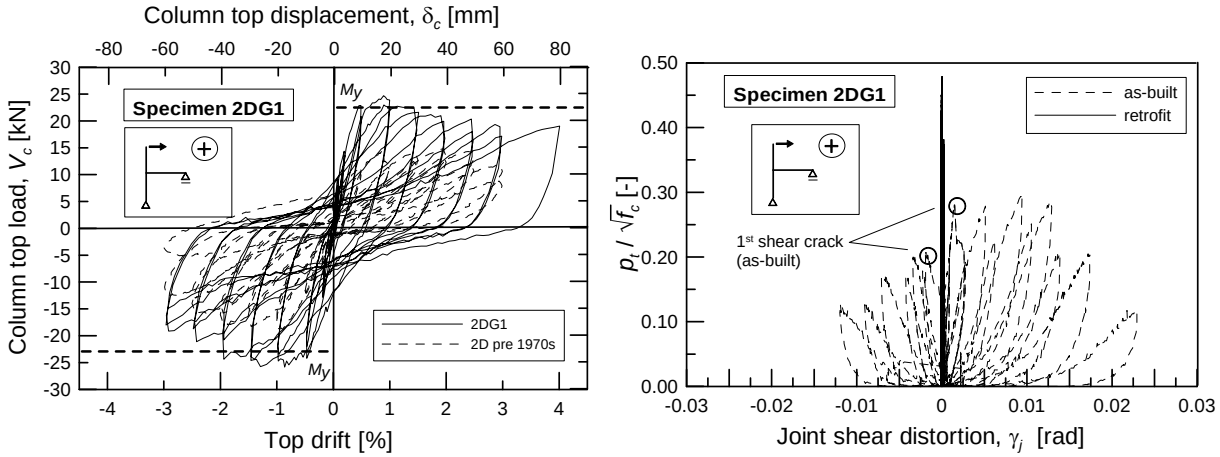

a) Hysteretic behaviour b) Joint shear distortion

Figure 9-7: Test 2DG1 – Load-deformation behaviour

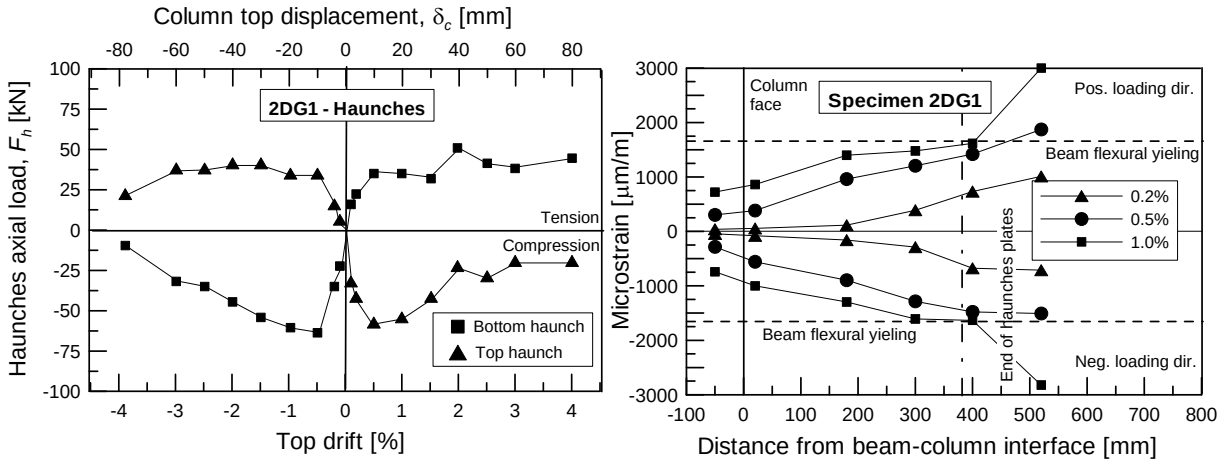

a) Haunches loading b) Bending moment in the beam

Figure 9-8: Test 2DG1 – Analysis of strain gauges readings

9.4.2 Test 2DG2

The test 2DG1 confirmed the feasibility of the retrofit solution. However, the formation of shear cracks in the beam is undesirable, because in a real situation the vertical static and seismic loads acting on the floors could induce a brittle failure of the beam. To reduce the shear load in the beam, the length of the haunch was reduced to *L'* = 350 mm for test 2DG2. Furthermore, 4 instead of 6 anchors were used for each connection of the steel haunches to beam and column. The first flexural cracks at the end of the anchor plate occurred during the 0.1% top drift cycle in the cross section of the beam where the plastic hinge was expected to occur (Figure 9-11a). In the further cycles only a few minor cracks in the beam were observed and the largest part of the deformation was concentrated in the first cracked section. The yielding of the longitudinal beam bars and the consequent formation of a plastic flexural hinge occurred in the positive and negative loading direction during the 1.0% top drift cycle at a column top load of approximately 20 kN (Figure 9-9a). Starting from the 2.5% top drift cycle, cracks in the joint region spalling of the concrete cover, due to the pressure of the compressed hooks against the beam surface, were observed (Figure 9-11b). The cracks indicated the loss of bond of the smooth reinforcing bars and consequent concentration of compression forces in the hooks. The column and the joint panel remained uncracked during the entire test. No significant joint shear deformation was measured (see Figure 9-9b). The joint strength was approximately constant up to 2.5% drift in the positive loading direction and started decreasing after the cracking of the concrete cover on the back side of the joint, while in the negative loading direction the strength degradation was negligible (Figure 9-9a). Also during this test buckling of the beam reinforcement in the vicinity of the plastic hinge was observed (Figure 9-11c). The analysis of the axial forces in the steel haunches showed a limited reduction of the loads taken up by the haunches in comparison with test 2DG1 with larger haunches (compare Figure 9-10a with Figure 9-8a). The malfunctioning of one strain gauge located on the bottom haunch did not allow a reliable analysis of the axial forces of the bottom haunch (see Figure 9-10a). Displacement of the anchorages of approximately 0.2-0.4 mm was observed. The retrofit solution was successful in reducing the beam flexural moment at the beam-column interface as shown by the analysis of the strain gauges glued on the beam reinforcing bars (Figure 9-10b).

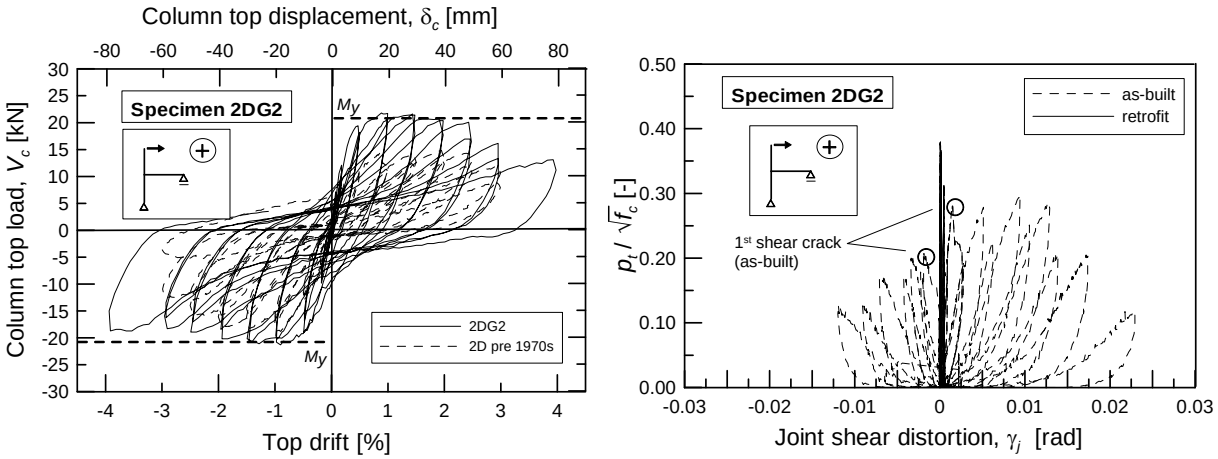

Figure 9-9: Test 2DG2 – Load-deformation behaviour

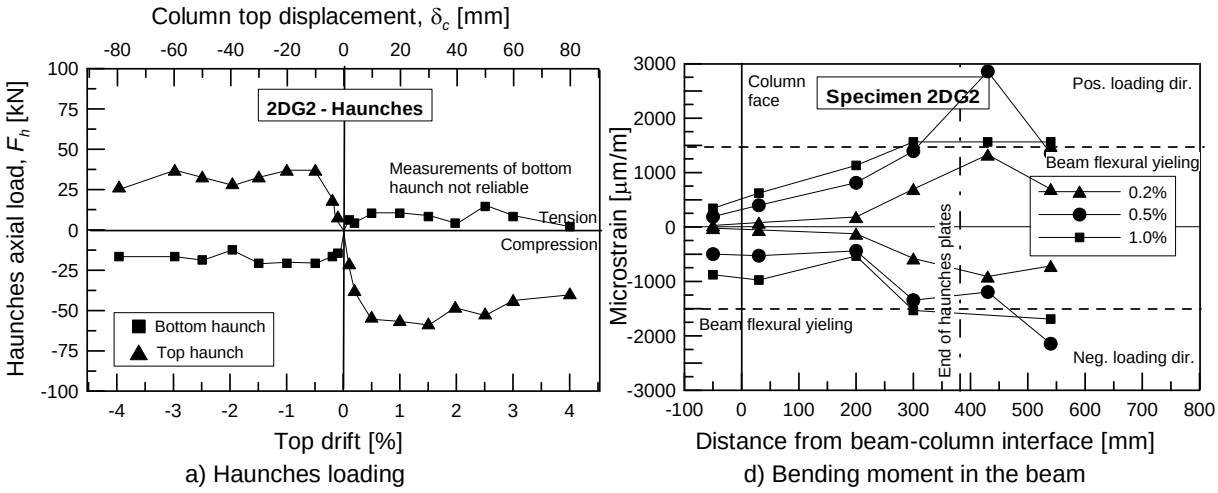

Figure 9-10: Test 2DG2 – Analysis of strain gauges readings

a) 1.0% b) 2.5% c) 4.0%

Figure 9-11: Test 2DG2 – Cracking patterns at increasing top drift levels

9.4.3 Test JT1-2

The test specimens JT1-2 was designed to reproduce more critical conditions for the anchorages of the steel haunches to beam and column in comparison to the previous tests. The tensioned anchorages were loaded up to approximately their ultimate strength to investigate the effect of a tensile anchorage failure on the overall behaviour of the specimen.

During the test the first flexural cracks in the beam occurred at the end of the haunches, similar as observed in the previous tests (until ±20 mm) (Figure 9-12a). With increasing top

drift level, the cracking of the specimen extended to the beam portion underneath the diagonal haunches (Figure 9-12b). Also in the column minor flexural cracks were observed. Starting from the cycle at 40 mm displacement, bond cracks occurred in the joint panel (Figure 9-12c).

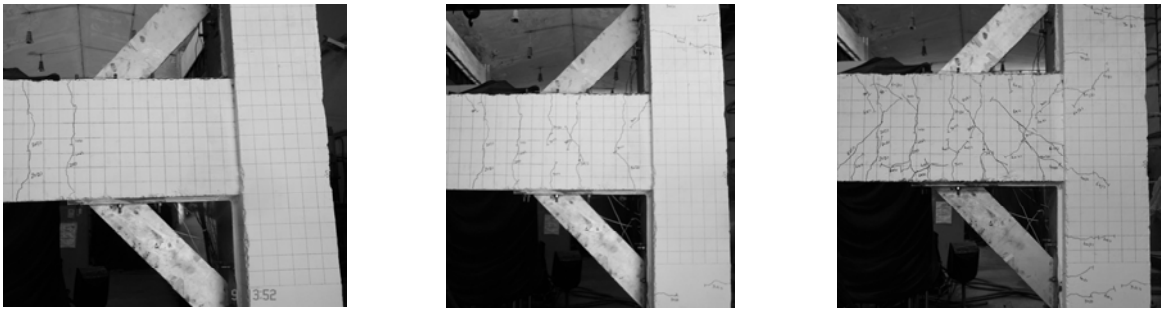

a) +20/II b) +30/II c) +70/I

Figure 9-12: Test JT1-2 – Cracking patterns at increasing beam end displacement levels

Yielding of the beam bars in the section at the end of the anchorage plates was recorded during the 1st 60 mm top drift cycle (Figure 9-13a). The test could not be completed because of the sliding of the column restraints. However, the target displacement of 70 mm could be reached in positive direction. No significant shear cracks were observed in the joint core and its deformation was much lower than those of the as-built specimen (Figure 9-13b). In Figure 9-14a the axial forces measured in the diagonal haunches are shown. The anchorage with post-installed anchors was loaded almost up to the ultimate strength (see Figure 9-30). However, no displacement that could indicate the loss of strength of the anchorage was observed during the test (Figure 9-12). The axial force measured in the haunches in compression was up to 1.7 larger than in tension. The analysis of the strain gauges on the beam bars confirmed an effectiveness of the retrofit similar to the previews tests (comparing Figure 9-14b with Figure 9-10b and Figure 9-8b). In the final part of the test (i.e., starting approximately during the ±60 mm cycle) minor shear cracks in the beam were observed (Figure 9-12c).

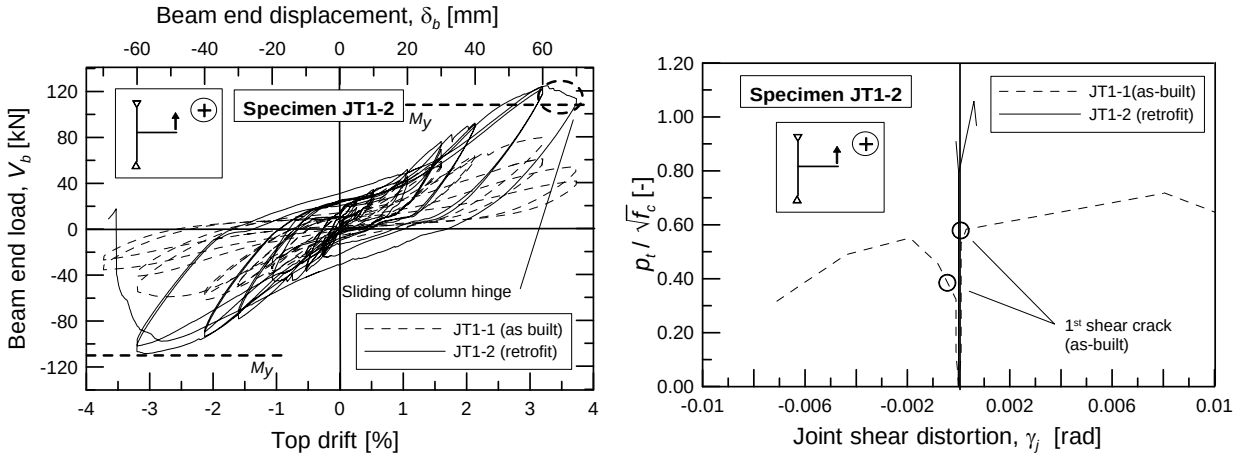

a) Hysteretic behaviour b) Joint shear distortion

Figure 9-13: Test JT1-2 - Load-deformation behaviour

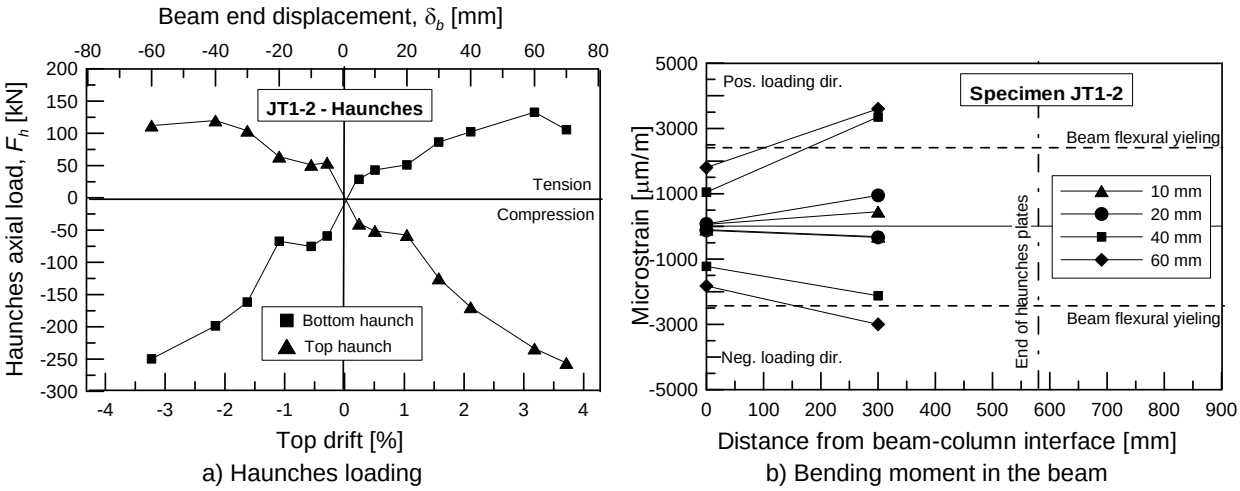

Figure 9-14: Test JT1-2 - Analysis of strain gauges readings

9.4.4 Test JT1-3

The test JT1-3 was a repetition of the JT1-2 using a slightly modified test setup to avoid any sliding of the restrains, when the specimen reached approximately its ultimate strength (see Figure 9-13a). The behaviour of the specimen JT1-3 was very similar to JT1-2 up to the 2nd cycle at 20 mm top drift (Figure 9-17a). During the 1st cycle at 30 mm a loss of stiffness in negative direction was observed (Figure 9-15a). The analysis of the readings of the strain gauges glued on the bonded anchors and on the steel diagonals shows that the capacity of the anchorage of the top haunch was most probably exceeded (see Figure 9-16a and Figure 9-30). At this stage of deformation the failure mode of the anchorage can be explained from the observation of the cracking patterns. The larger amount of cracks in the beam when compared to the column, leads to the assumption that the failure did occurr at the connection between beam and top haunch. This assumption was confirmed at higher drift levels, as shown in Figure 9-17b,c. In the positive loading direction the yielding of the beam longitudinal bars was reached at approximately 30 mm during the 40 mm beam end displacement cycle, while in the negative loading direction yielding was reached at approximately 50 mm of beam end vertical displacement, due loss of stiffness mentioned above. Observing the cracking pattern shown in Figure 9-17c, it appears that the row of anchors in the beam further away from the joints holding the top haunch started failing in pullout in combination with concrete cone failure. Such behaviour of the anchorage is undesirable; however, the global behaviour of the retrofitted specimen was significantly improved in comparison to the as-built specimen in terms of ultimate strength and ductility. The joint shear distortion (Figure 9-15b) exceeded the elastic limits, but it was much smaller than in the as-built specimen, since the width of the shear cracks in the core was not more than 0.3-0.5 mm. The final cracking pattern was characterised by many flexural cracks in beam and column and a few minor shear cracks in the joint region (Figure 9-17c). In this test, as well as in JT2-1, the plastic hinge was not clearly localised in one beam section (compare Figure 9-17 and Figure 9-12 with Figure 9-6 and Figure 9-11). This is due to the higher beam stiffness in comparison to the haunches for the specimens JT1-2 and JT1-3 than for 2DG1 and 2DG2 and the use of ribbed bars compared to of plain round bars in the tests carried out at UC and consequent reduction of the amount of cracks in the beam. From the analysis of the strains in the beam bars it can be seen that the retrofit solution was fully efficient up to a displacement of 40 mm (Figure 9-16b), i.e., only minor shear cracks in the joint were observed, as shown in Figure 9-17b. It

should be noted that the presence of moderate column axial load (n_c < 5%) would have been sufficient to avoid the joint shear cracking which occurred almost at ultimate load (see Figure 5-4 and Figure 9-15a).

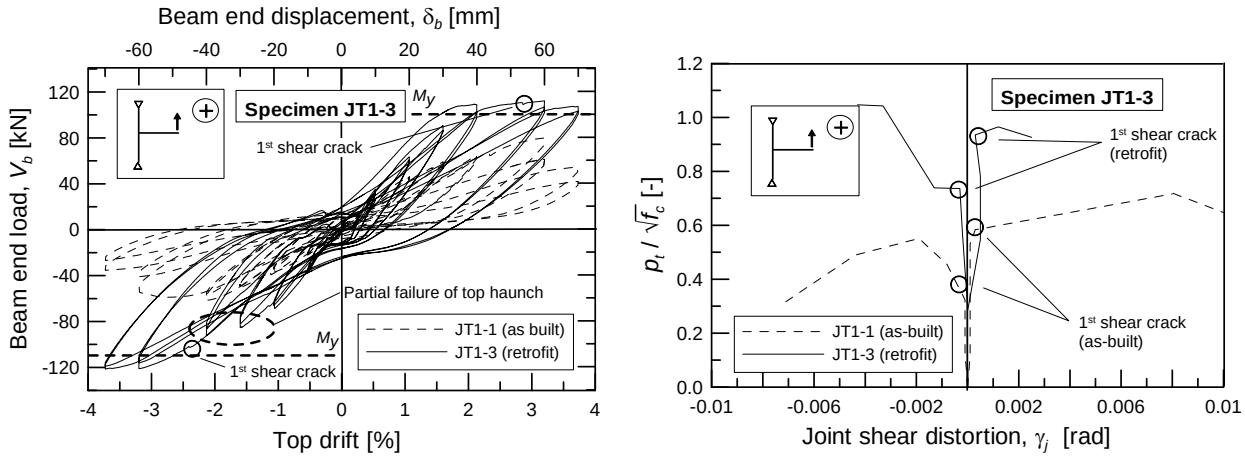

a) Hysteretic behaviour b) Joint shear distortion

Figure 9-15: Test JT1-3 – Load-deformation behaviour

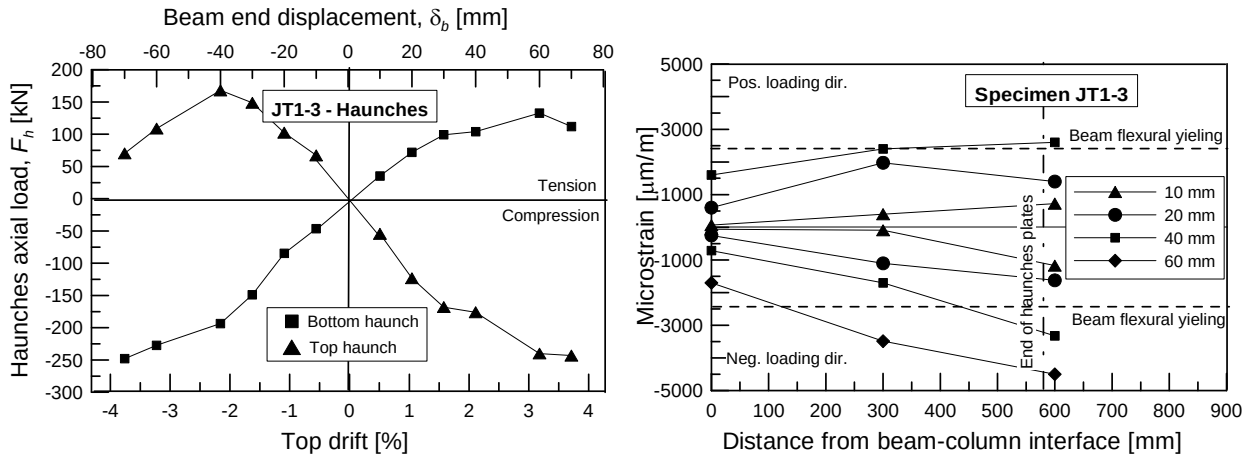

a) Haunches loading b) Bending moment in the beam

Figure 9-16: Test JT1-3 – Analysis of strain gauges readings

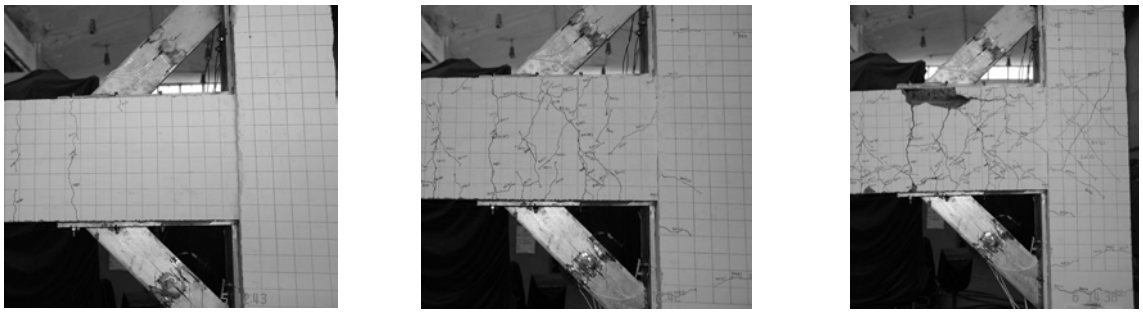

a) -10/II b) +40/II c) -70/II

Figure 9-17: Test JT1-3 – Cracking patterns at increasing beam end displacement levels

9.4.5 Test JT1-4

The test JT1-3 displayed the limit of the proposed “Haunch Retrofit Solution” (HRS). The required strength of the connection with post-installed anchors necessary to induce the formation of a flexural hinge in the beam exceeded the tensile anchorage capacity and

undesirable shear cracking of the joint occurred. A possible solution to these issues was proposed and validated with the test JT1-4. In Figure 9-18 the graphical representation of the design of the retrofit (analogous to Figure 8-4) for the tests JT1-3 and JT1-4 are shown. In the test JT1-3 (no weakening) the acceptable damage limit state of the joint was exceeded before the plastic hinge in the beam was formed. To protect the joint panel and achieving beam yielding, a reduction of the beam flexural strength was aimed. This leads to a reduction of the load on the anchorage and the horizontal shear stress in the core. The reduction of the beam flexural capacity (weakening) was achieved cutting one of the three longitudinal reinforcing bars of the beam (top and bottom layer) in a section at approximately 50 mm from the end of the anchor plates of the haunches. The beam flexural strength after the retrofit with weakening was lower than the joint shear strength and therewith a desirable hierrachy of strength was achieved. At the same time a strength increment in comparison to the as-built specimen was achieved. The target strength of the specimen JT1-4 was smaller than JT1-2 and JT1-3, but no failure of the anchorage occurred. Furthermore, a weak section for the formation of the plastic hinge was defined and the anchorage was protected from excessive concrete cracking.

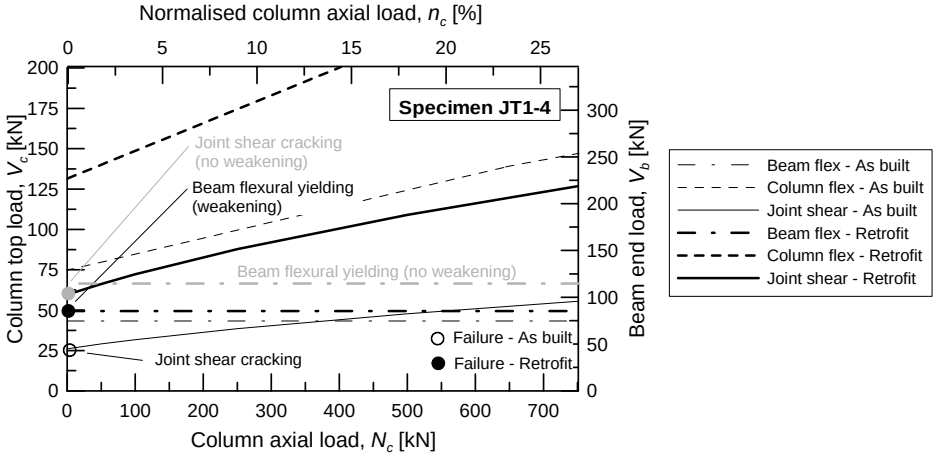

Figure 9-18: Hierarchy of strength before and after retrofit with weakening of the beam (shear limit states of beam and column omitted for simplicity)

The behaviour of the specimen JT1-4 was qualitatively similar to JT1-3. The yielding of the longitudinal beam bars started at approximately 50 mm and 40 mm in the positive and negative loading direction, respectively (Figure 9-19a). The corresponding beam shear load, V_b, was approximately 90 kN (more than 20 kN less than in the test JT1-3, due to the effect of the weakening). Conversely to the test JT1-4, the joint panel remained elastic during the entire test (comparing Figure 9-19b with Figure 9-15b) The axial loading of the haunches was successfully reduced from 125~150 kN (tests JT1-2 and JT1-3) to approximately 100 kN in the test JT1-4 (compare Figure 9-20a with Figure 9-16a and Figure 9-14a). During the test flexural cracks occurred in beam and column, while only minor cracks occurred in the joint region (Figure 9-21b). The ductility of the specimen was verified by increasing the top drift demand up to 8.0% with satisfactory results (Figure 9-19a and Figure 9-21c). Comparing the strain level of the beam bars at the column face measured in JT1-4 with values of the previous tests JT1-2 and JT1-3 (compare Figure 9-20b with Figure 9-16b and Figure 9-14b), it can be observed that in the test JT1-4 lower strains were measured, i.e., more efficient protection of the joint region by the haunches was achieved.

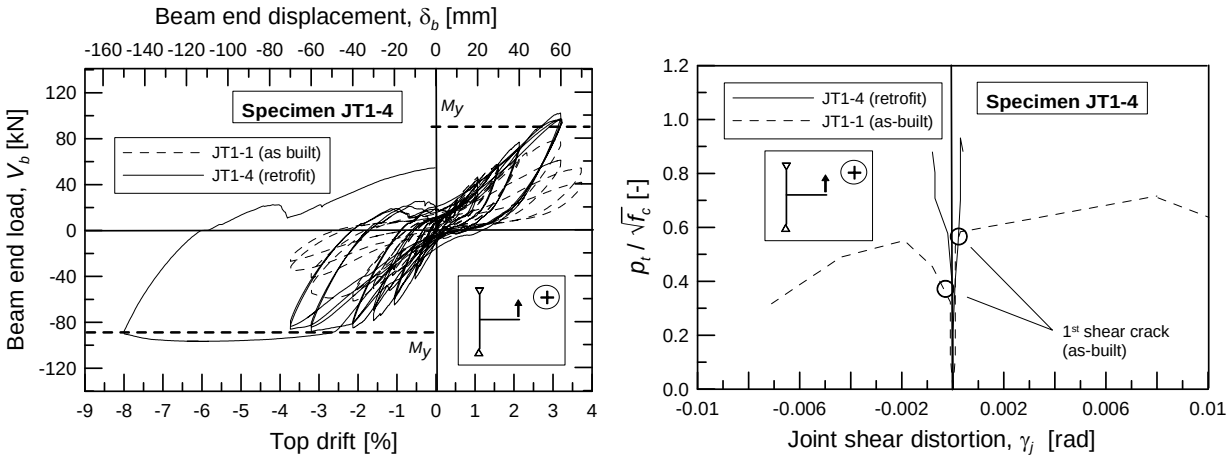

Figure 9-19: Test JT1-4 – Load-deformation behaviour

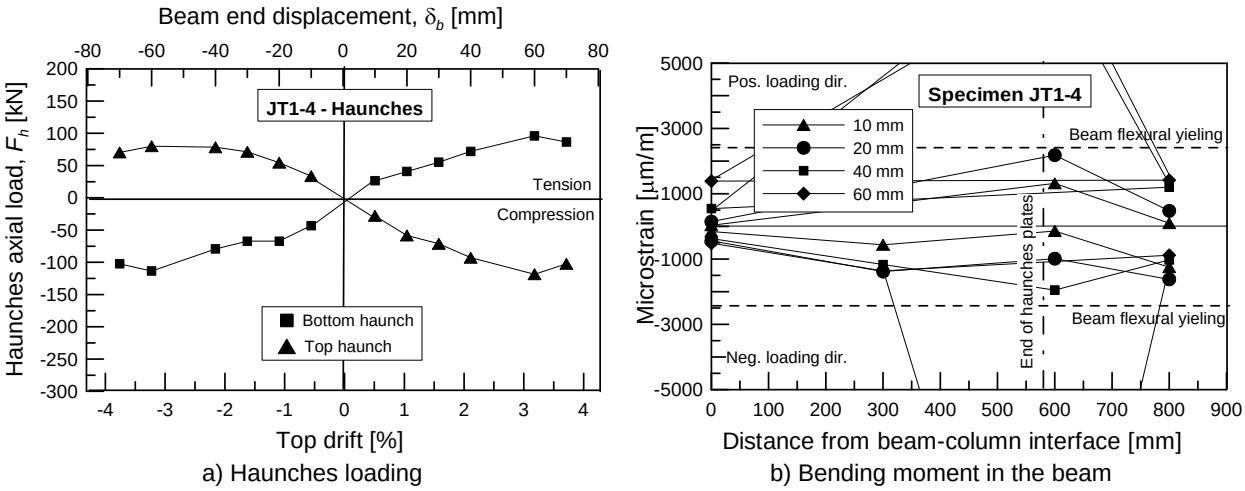

Figure 9-20: Test JT1-4 – Analysis of strain gauges readings

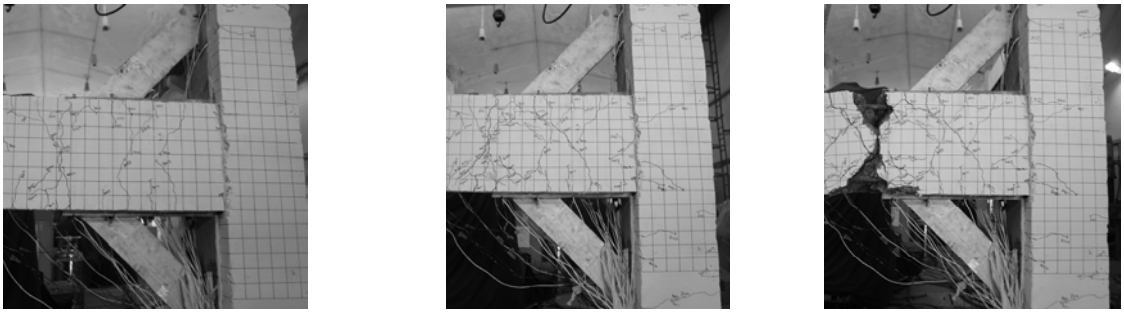

a) +30/II b) +60/II c) -150

Figure 9-21: Test JT1-4 – Cracking patterns at increasing beam end displacement levels

9.4.6 Test JT1-5

In the test JT1-5 concrete screws were used, instead of bonded anchors, for the connection of the steel haunches to beam and column. The effective embedment depth, h_{ef}, was reduced from 150 mm (tests JT1-2, JT1-3 and JT1-4) to 90 mm, because of the limits in the geometry of the product used. This difference in h_{ef} does not influence the resistance of the anchorage. However, the shorter embedment depth may increase the sensitivity of the anchorage to the negative effect of flexural cracking in beam and column. The other parameters of the anchorage (i.e., number and spacing of anchors) were as in JT1-2 and

JT1-3. Previous tests have shown that concrete screws generally exhibit a quite stiff behaviour in comparison to other mechanical anchors types, if loaded in tension in cracked concrete, which is typically followed by a brittle failure (*Hoehler, 2006* and *Genesio 2007c*). This behaviour of the concrete screws was also observed in this test. The specimen behaved similarly to the previous tests up to a displacement level of 30 mm, where the first cracks in the joint region occurred and a displacement of approximately 0.5 mm of the anchor plate from the column surface could be observed (Figure 9-22a). During the 40 mm cycles, cracks in the column occurred (both at top and bottom haunch), indicating a concrete cone failure of the anchorage (Figure 9-22b). In the further cycles, the width of flexural cracks in the beam decreased significantly and the deformation of the specimen started concentrating in the column and in the joint region (Figure 9-22c).

a) -30/I b) -40/I c) +70/II

Figure 9-22: Test JT1-5 – Cracking patterns at increasing beam end displacement levels

The overall hysteretic behaviour and joint shear deformation of the specimen were comparable to the as-built benchmark joint (Figure 9-23a,b). The analysis of the axial forces in the haunches showed the poor performance of the concrete screws, which failed at a load level of approximately 100 kN (Figure 9-24a). The lower load-carrying capacity in comparison to the bonded anchors was mainly due to the shorter h_{ef}, which made the anchors particularly sensitive to the flexural cracks in the beam-column connection (Figure 9-22c). Yielding of the beam bars could not be achieved (see Figure 9-24b). It should be noted that, in a practical application the concrete failure of the anchorage in the column is undesirable, because of the reduction of the cross section and consequent loss of compressive capacity of the column.

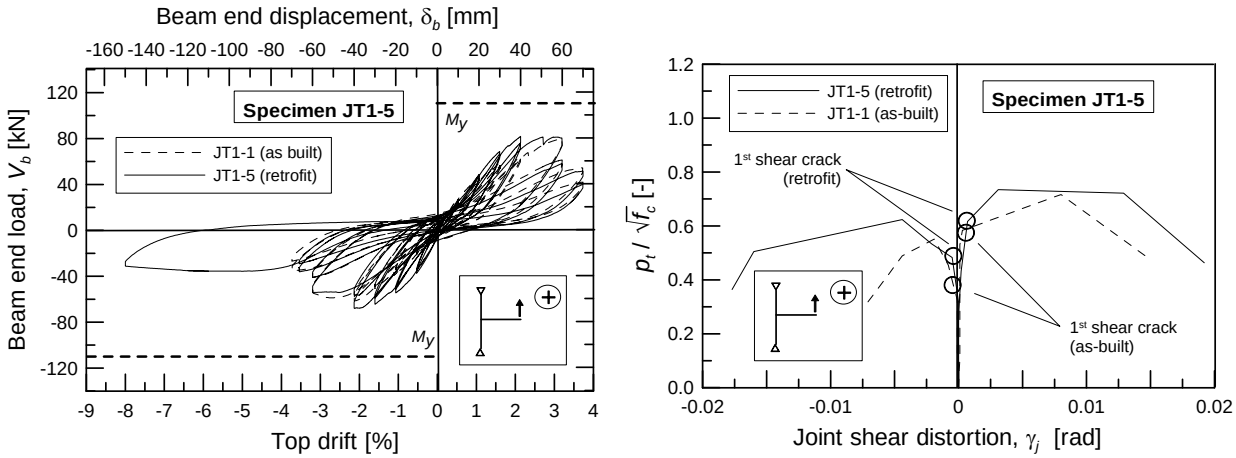

a) Hysteretic behaviour b) Joint shear distortion

Figure 9-23: Test JT1-5 – Load-deformation behaviour

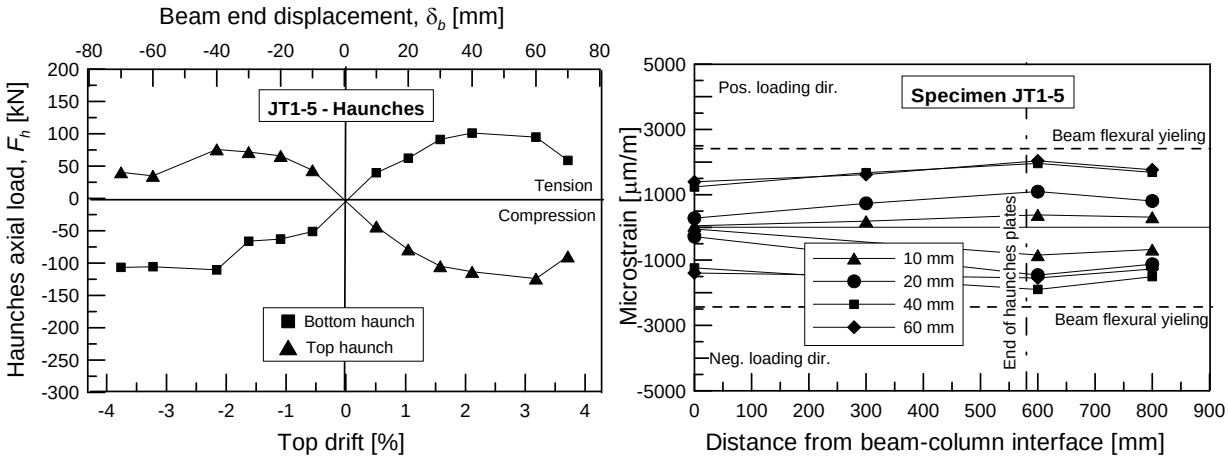

Figure 9-24: Test JT1-5 – Analysis of strain gauges readings

9.4.7 Test JT1-6

In the test JT1-6 the steel haunches were connected to beam and column using bolt type expansion anchors. The anchorages were designed to avoid a brittle concrete cone failure to reach a pseudo-ductile pull-through behaviour (*Hoehler, 2006* and *Genesio, 2007a,b*). Therefore, h_{ef} was increased from 85 mm (h_{ef} in accordance with the relevant technical approval) to 115 mm. It is widely acknowledged that this type of anchor exhibits a much lower stiffness than bonded anchors or concrete screws. Although damage of the specimen during the transportation from the construction site to the laboratory negatively influenced the hysteretic behaviour especially in negative loading direction (Figure 9-25a), some important information could be obtained from this test. The initial cracking pattern of the joint was very similar to the previews tests (Figure 9-25a). Minor shear cracks in the joint panel occurred starting from the 60 mm top drift cycle (Figure 9-25b).The joint shear distortion is shown in Figure 9-26b. The slip of the anchors gradually increased during the test up to approximately 5 mm (Figure 9-25c).

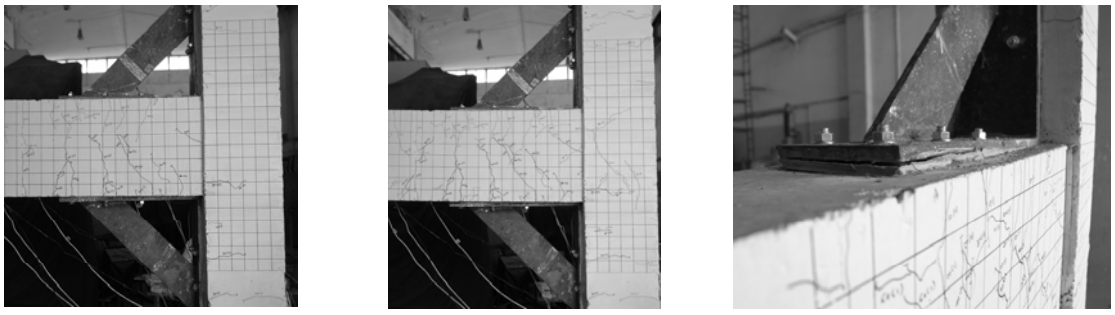

a) +30/II b) +60/I c) -60/I

Figure 9-25: Test JT1-6 – Cracking patterns at increasing beam end displacement levels

The yielding of the beam bars could be reached only in positive direction during the 60 mm cycle (Figure 9-26a). The flexible behaviour of the anchors was reflected also in the hysteretic loops which exhibited a lower energy dissipation and higher pinching than in the previous tests, as can be seen comparing Figure 9-26a with Figure 9-15a. The analysis of the axial forces in the haunches shown in Figure 9-27a is reliable for further considerations only for the bottom haunch for the reason mentioned above (damage during impostation). The poor stiffness of the haunches was also reflected by the fact that the moment reduction

in the beam (Figure 9-27) was not enough to protect the joint panel (see joint deformation in Figure 9-26b).

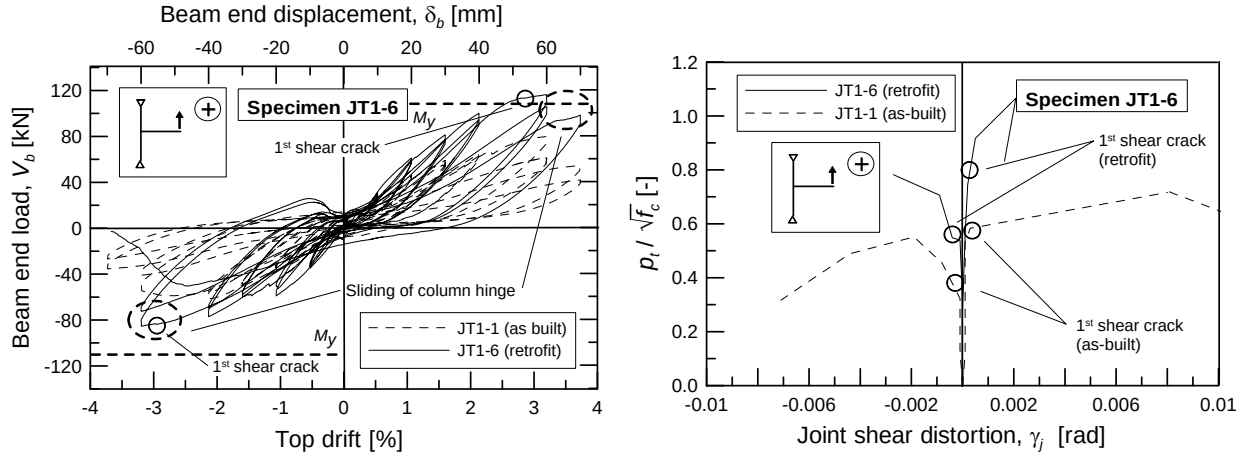

Figure 9-26: Test JT1-6 – Load-deformation behaviour

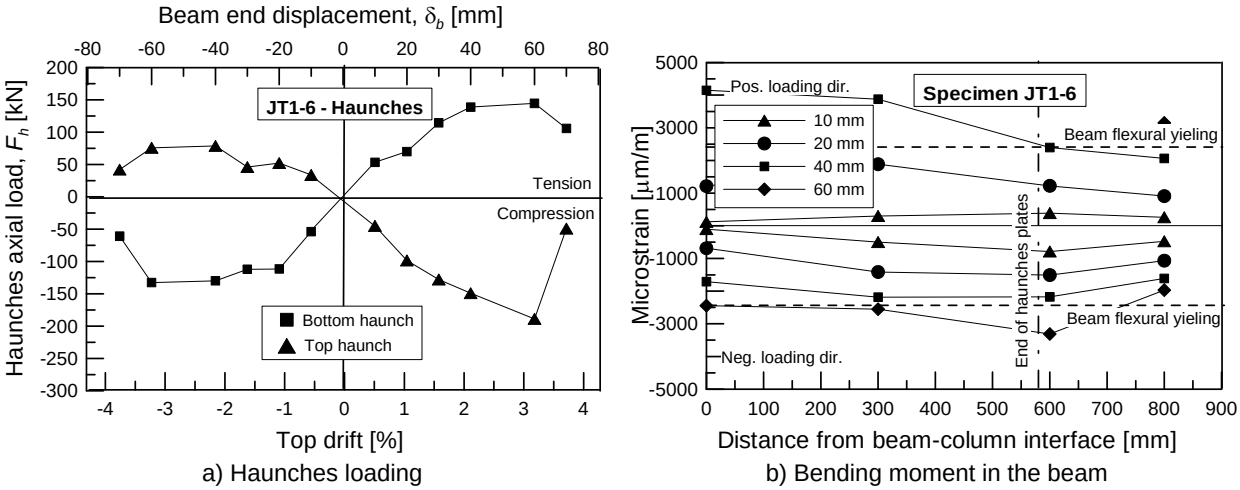

Figure 9-27: Test JT1-6 – Analysis of strain gauges readings

9.4.8 Evaluation of loading of the anchorage

The measurements of the axial strain in the anchors and diagonal haunches provided information on the strain distribution on the steel diagonals and location of the resultant force (i.e., eccentricity, e_N) transferred from the diagonal haunches into the anchorage. In Figure 9-28a,b,c measurements in the three anchor rows of the beam bottom anchorage of the specimen 2DG1 are shown as an example. Figure 9-28d shows the comparison between the sum of the anchor forces and the vertical component of the force measured in the haunch. The loading of the anchorage was estimated on the basis of the forces measured in the haunches (see results shown in Section 9.4.1 to 9.4.7 and analysis in Section 9.4.10). The readings of the strain gauges glued on the anchors were often not much reliable, because of multiple affecting parameters, e.g., shear actions on the anchor and significant failure rate of the strain gauges. For comparison anchor forces of one anchorage of specimens JT1-3 and JT1-4 are also shown (Figure 9-29). The readings of axial strain of the anchors provide useful indications on the activation of the anchorage, but not enough precision could be guaranteed for exact measurements. No measurement of the shear forces acting in the

anchors was possible with the available instrumentation. No measurement on concrete screws (test JT1-5) and expansion anchors (test JT1-6) were possible, because the torquing of the anchors would have damaged the wire of the strain gauge. A more detailed analysis of the loading of the anchorage was, therefore, carried out on the basis of the numerical simulations (see Chapter 10).

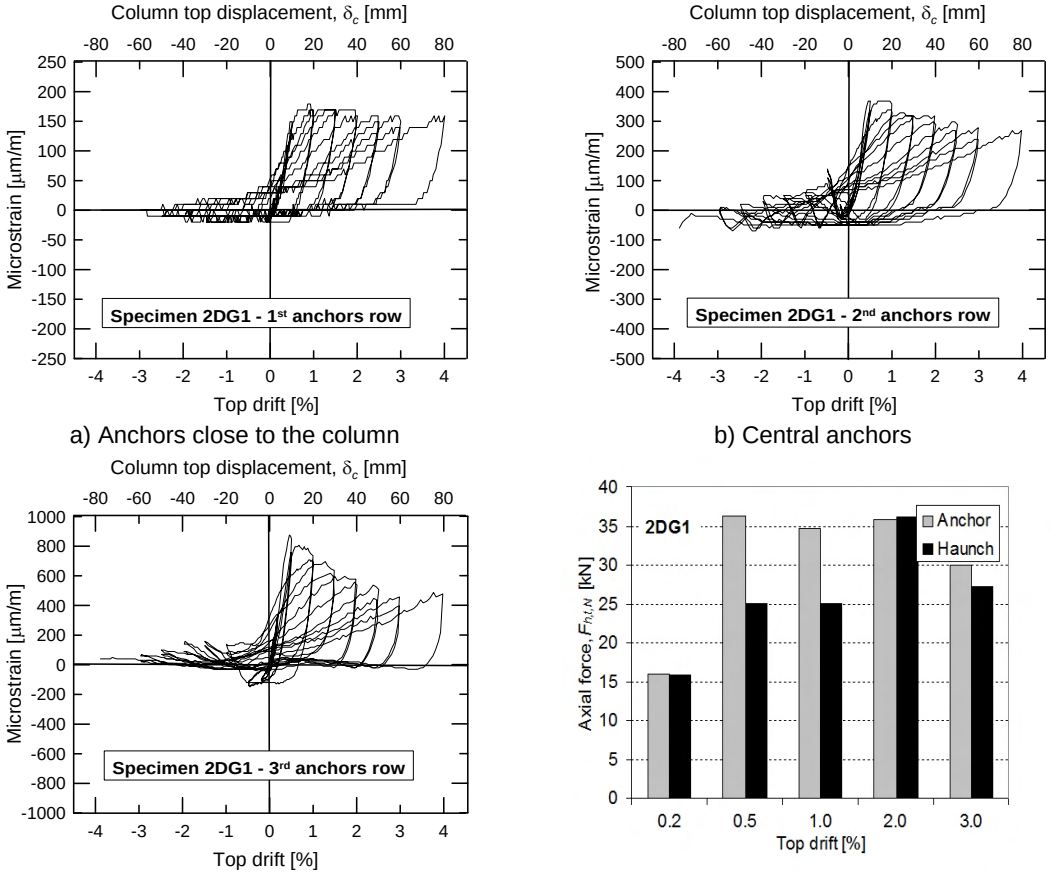

Figure 9-28: Measurements of anchors axial strains (anchorage on the bottom beam side of specimen 2DG1)

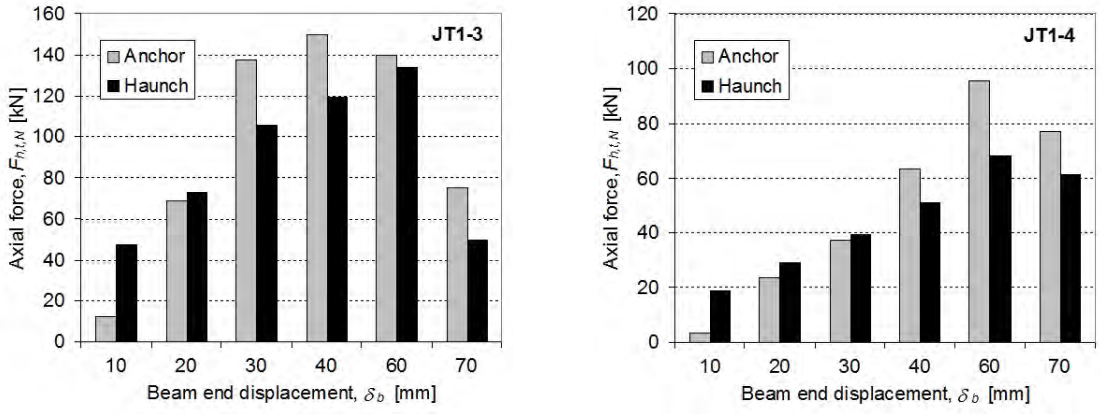

Figure 9-29: Comparison between forces in the anchors and in the steel diagonals

The tensile strengths of the anchorages calculated according to Section 8.2.5.1 (rows “calc res cracked/uncracked” in Figure 9-30) were compared to the forces on the anchors

estimated from the strain gauges readings carried out during the tests (rows “Exp pos” and “Exp neg” in Figure 9-30). In the tests 2DG1 and 2DG2 no failure of the anchorage was observed and the anchorage was located in uncracked concrete (see Figure 9-6 and Figure 9-11). The calculated resistance of the anchorage of the specimen JT1-4 assuming uncracked concrete exceeded approximately 30% the strength demand. The calculated resistance assuming cracked concrete is slightly larger than the acting tension loads. During the tests JT1-2, JT1-3 and JT1-6 the yielding of the beam bars occurred, but the formation of the plastic hinge was not completed. In the test JT1-5 the beam remained elastic. Therefore, the resistance of the anchorage was recalculated without assuming a free edge at the end of the steel plates of the haunches and assuming cracked concrete, which agrees with the experimental observations (“Mod. Calc”, in Figure 9-30). It should be noted that the concrete screws (JT1-5) failed at a lower load, because of the high sensitivity to concrete cracking of the screw anchors. The strength predictions agree in all cases reasonably well with the experimental results. The same comparison was carried out for the anchorage shear resistance of the compressed haunch. The calculation of the resistances was carried out according to Section 8.2.5.2. Figure 9-31 shows, consistently with the experimental results, that no failure was to be expected. In the calculation it was conservatively assumed that 50% of the shear force was taken up by friction.

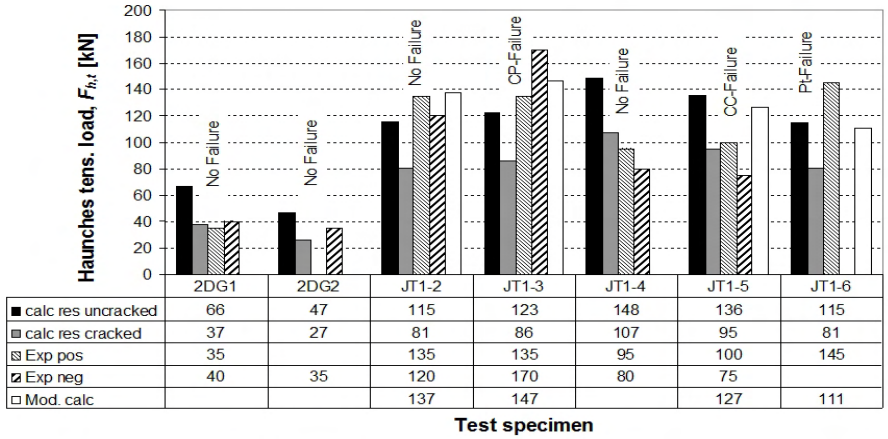

	2DG1	2DG2	JT1-2	JT1-3	JT1-4	JT1-5	JT1-6
calc res uncracked	66	47	115	123	148	136	115
calc res cracked	37	27	81	86	107	95	81
Exp pos	35		135	135	95	100	145
Exp neg	40	35	120	170	80	75	
Mod. calc			137	147		127	111

CP-Failure: combined concrete cone and pullout failure; CC-Failure: concrete cone failure; Pt-Failure: pull-through

Figure 9-30: Calculated anchorage tensile mean resistances vs. measured loads

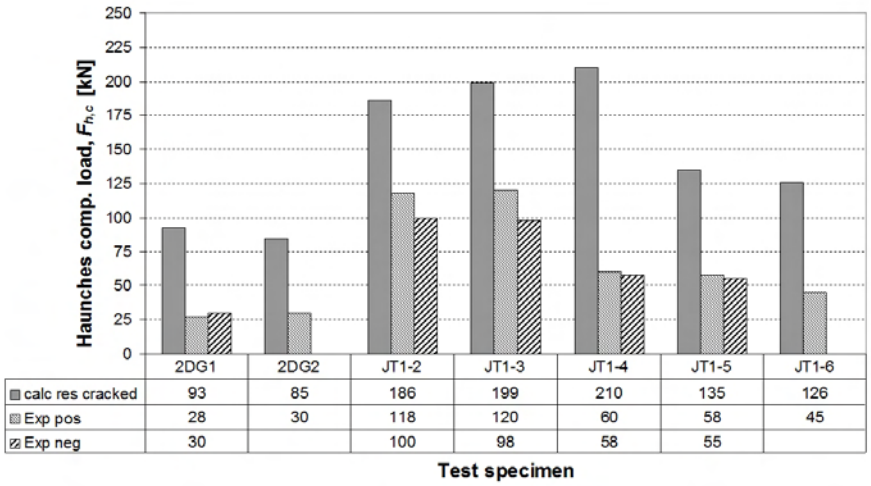

	2DG1	2DG2	JT1-2	JT1-3	JT1-4	JT1-5	JT1-6
calc res cracked	93	85	186	199	210	135	126
Exp pos	28	30	118	120	60	58	45
Exp neg	30		100	98	58	55	

Note: it is assumed that 50% of the shear force is taken up by friction

Figure 9-31: Calculated anchorage shear mean resistances vs. measured loads

9.4.9 Evaluation of eccentricity of the tension load on the anchorage

The evaluation of the eccentricity, e_N, of the resulting axial load acting on the anchorage was carried out on the basis of the strain gauges readings of the diagonal haunches. In Table 9-2 the measured eccentricities for all tested specimens are shown. The corresponding values $\psi_{ec,N}$ calculated according to Equation (8-26d) are also shown for each test and loading direction. All the tested specimens had similar $\psi_{ec,N}$ values ($\psi_{ec,N,m} = 0.92$, CV = 5.8%), although they exhibited different qualitative behaviours. $\psi_{ec,N} = 0.9$ can be used for the anchorage design for haunch connections with similar geometrical characteristics of the types used in this study (see Figure 9-3).

Table 9-2: Eccentricity e_N calculated according to strain gauges readings (tension loading)

	2DG1 [b)]	**2DG2** [b)]	**JT1-2** [b)]	**JT1-3** [b)]	**JT1-4** [b)]	**JT1-5** [b)]	**JT1-6** [b)]
Dist [a)] **[mm]**	66 / 66	- / 68	62 / 71	68 / 73	78 / 72	76 / 75	69 / 73
e_N **[mm]**	2 / 2	- / 51	32 / 20	24 / 17	9 / 18	13 / 14	22 / 17
$\psi_{ec,N}$ **[-]**	0.99 / 0.99	- / 0.79	0.86 / 0.91	0.89 / 0.92	0.95 / 0.92	0.94 / 0.93	0.89 / 0.92

[a)] Horizontal distance between the barycentre of the anchorage and the point of application of the resultant force of the haunch; [b)] Positive / negative loading direction

Note: all the values refers to the maximum measured tension load

9.4.10 Estimation of the haunches stiffness

During the experimental tests it was not possible to measure the stiffness of the single anchors, but the compressive and tensile forces acting on the diagonal haunches are known from the readings of the strain gauges on the diagonal haunches. The ratio between compression acting on the top (bottom) haunch and the tension acting on the bottom (top) haunch corresponds to the ratio between compressive ($K_{h,c}$) and tensile ($K_{h,t}$) stiffness of the haunches, $K_{h,c}/K_{h,t}$. Based on the assessment method for the retrofit solution presented in Section 8.2, the compressive and tensile stiffness of the haunches, $K_{h,c}$ and $K_{h,t}$, were calculated using the measured forces, $F_{h,t,max}$ and $F_{h,c}$, as input parameters, evaluated at the point of highest tensile forces of the entire loading history. In Table 9-3 the experimental evaluation of the ratio $K_{h,c}/K_{h,t}$ is shown. In all tests the ratio $K_{h,c}/K_{h,t}$ was larger than 1.0 and average, considering only the tests were the retrofit was successful (i.e., excluding the test JT1-5) $K_{h,c}/K_{h,t} = 1.46$ with CV = 14.3% was obtained. Considering only the tests with bonded anchors a mean value of $K_{h,c}/K_{h,t} = 1.57$ with CV = 11.8% was calculated. For the calculations shown in Table 9-3 the material properties were taken according to Table 9-1 and the effective inertial moments of beam and column (see (8-9a,b)) were taken according to the indications of *Paulay & Priestley (1992)*, moment curvature analysis and experimental observations.

Table 9-3: Experimental comparison between $K_{h,c}$ and $K_{h,t}$

Test	$F_{h,t,max}$ [a)] [kN]	$F_{h,c}$ [a)] [kN]	$K_{h,c}/K_{h,t}$ [-]	$K_{h,t}$ [b)] [kN/m]	$K_{h,c}$ [b)] [kN/mm]
2DG1 [c)]	35 / 40	55 / 60	1.57 / 1.50	95 / 120	145 / 180
2DG2 [c)]	- / 35	60 / -	-	-	-
JT1-2 [d)]	135 / 120	235 / 200	1.75 / 1.67	120 / 120	210 / 200
JT1-3 [d)]	135 / 170	240 / 195	1.78 / 1.15	160 / 200	285 / 230
JT1-4 [d)]	95 / 80	120 / 115	1.26 / 1.44	85 / 75	110 / 110
JT1-5 [d)]	100 / 75	115 / 110	1.15 / 1.47	115 / 110	135 / 170
JT1-6 [d)]	145 / -	190 / -	1.30 / -	135 / -	175 / -
		Average:	**1.46**		
		CV:	**14.3%**		

[a)] Positive / negative loading direction; [b)] Values calculated using the analytical model presented in Section 8.2 related to the maximum tension loading of the haunch; [c)] $\theta_b = 0.30$; $\theta_c = 0.80$; [d)] $\theta_b = 0.35$; $\theta_c = 0.40$

In Table 9-4 the tensile (k_N) and shear (k_V) stiffness of the anchors and the frictional stiffness of the steel plates (k_f) are assessed using the equations proposed in Chapter 8. If k_N is calculated according to Equation (8-13b) solving for $K_N = nk_N$ the resulting values are all compatible with the values according to the relevant ETA (European Technical Approval) and typical tensile stiffness values for bonded anchors (compare Table 8-1). If Equation (8-15) is applied to take into account the flexural deformation of beam and column and, therefore, the loading of the anchors in shear (see Figure 8-7) minor variations of the k_V values are established. A value of the shear stiffness, k_V, equal to 20 kN/mm was assumed. The significant variability of the values k_N (see Section 8.2.2.1) does not allow to evaluate the accuracy of the two approaches. Considering only the tests where bonded anchors were used, an average stiffness, $k_N = 36.7$ kN/mm using Equation (8-13a) (or 47.0 kN/mm using Equation (8-15)) with CV ~ 50% was obtained. This value represents the average of 18 anchorages. It should be noted that the coefficient of variation CV = 50% is significantly larger than the value of 10-15% indicated in Section 8.3.2.1 for bonded anchors. This difference is due to the complex loading history and concrete conditions (i.e., cracking), which occur in this application. Therefore, 20 kN/mm < k_N < 55 kN/mm using Equation (8-13a) (20 kN/mm < k_N < 70 kN/mm using Equation (8-15)) can be a realistic range of the anchor tensile stiffness for the considered anchor type and dimensions as well as the used loading protocol.

The evaluation of k_V is more uncertain, because it is related to the frictional coefficient, μ_f, and the frictional stiffness, k_f, through Equations (8-13b) and (8-14). In the analysis shown in Table 9-4 μ_f was assumed equal to 0.4 and the value of k_f was evaluated for plausible k_V values. On the basis of past experience (see Table 8-2) a value of k_V between 10 kN/mm and 30 kN/mm for M12 bonded anchors can be assumed. On the basis of these assumptions k_f values were calculated. The values of k_f for the tested specimen are within the range suggested by the investigations of *Tassios & Vintzileou (1987)* briefly described in Section 8.2.2. For the test 2DG1 a smaller contribution of the friction in comparison to the other tests was expected, because of the use of high strength gypsum instead of epoxy mortar, which has a higher gluing capacity between steel plates and concrete elements than gypsum. The analysis of 2DG1 indicates k_f ~ 5.0 kN/mm^3. For the tests JT1-2 and JT1-3 k_f was higher

(k_f = 7.5 ~ 15 kN/mm^3). The k_f value for the test JT1-4 is also approximately equal to 2.5 kN/mm^3. In the tests JT1-5 and JT1-6 large displacement of the anchorages were observed which could have had a detrimental effect on the friction in the subsequent half cycle. For the tests JT1-5 and JT1-6 k_f ~ 5.0 kN/mm^3 was calculated.

Table 9-4: Evaluation of anchor's axial (k_N) and shear (k_V and K_f) stiffness

Test	Tension		Shear	
	k_N [kN/mm] Eq. (8-13a) [a]	k_N [kN/mm] Eq. (8-15) [a]	k_V [kN/mm]	K_f [kN/mm^3]
			Eq. (8-13b) and (8-14)	
2DG1	25 / 32	29 / 41	25 / 33	5.0 / 5.0
2DG2	-	-	-	-
JT1-2	35 / 35	46 / 46	30 / 21	7.5 / 7.5
JT1-3	51 / 71	70 / 98	20 / 18	15.0 / 10.0
JT1-4	23 / 20	26 / 20	18 / 25	2.5 / 2.5
Average:	**36.7**	**47.0**		
CV:	**46%**	**55%**		
JT1-5	34 / 32	43 / 40	36 / 29	2.5 / 5.0
JT1-6	41 / -	55 / -	32.6 / -	5.0 / -

[a] Positive / negative loading direction

The tests with bonded anchors M12 with h_{ef} between 125 and 150 mm (2DG1, 2DG2, JT1-2, JT1-3 and JT1-4) are considered in the analysis shown in Table 9-5. The values obtained for k_N are in the same range of the values taken from the ETA (European Technical Approval). The stiffness value for short time loading in uncracked concrete according to the ETA of 188 kN/mm appears to be significantly higher than the highest value measured in the tests of 71 (or 98) kN/mm. In the tests at least some of the anchors were usually located in cracks and the cyclic loading also has a detrimental effect on the stiffness. Furthermore, it cannot be ignored that the real stiffness of the anchorage of the tensioned haunch may be negatively influenced by the shear stiffness of the anchors (Figure 8-7b and Equation (8-15)). The highest anchor stiffness to be used for the calculation of β_{max} should be, therefore, taken considering short term loading in cracked concrete. The values of k_V determined according to the ETA are similar to the values proposed in Table 8-2.

Table 9-5: Comparison between stiffness of bonded anchors analytical calculated from the tests measurements and values taken from ETA

	Tests [a]		Values from ETA		Values from test database [b]	
	min	max	min	max	min	max
k_N [kN/mm]	20 (20)	71 (98)	25 [c]	188 (112) [d]	35	75
k_V [kN/mm]	-	-	12.5	20	10	30

[a] Values according to Equations (8-13a) and (Equation (8-15)); [b] Values from Table 8-1 and Table 8-2 (cracked concrete is assumed); [c] Axial stiffness for long term loading in cracked concrete; [d] Axial stiffness for short term loading in uncracked (cracked) concrete

Table 9-6 shows the comparison of the stiffness, k_N and k_V of the investigated mechanical anchors (concrete screws and expansion anchors) calculated from the tests and taken from the available experience (ETA and databases summarised in Table 8-1 and Table 8-2). For both, concrete screw and expansion anchors, the stiffness values calculated from the tests results agree with the available experience. It should be noted that the measured axial

stiffness, k_N for expansion anchors is significantly larger than the ETA's values for cracked concrete. This value can be explained with the cyclic behaviour of anchors shown in Figure 8-9.

Table 9-6: Comparison between stiffness of mechanical anchors analytical calculated from the tests measurements and values taken from ETA

	Tests [a)]	Design values from ETA		Values from test database [b)]	
		min	max	min	max
Concrete screws					
k_N [kN/mm]	33 (42)	10 [c)]	40 (35) [d)]	10	30
k_V [kN/mm]	-	5.3	7.8	5	20
Expansion anchors					
k_N [kN/mm]	41 (55) [b)]	9.2 [c)]	55.7 (11.9) [d)]	-	-
k_V [kN/mm]	-	8.6	5.7	10	30

[a)] Values according to Equations (8-13a) and (Equation (8-15)); [b)] Values from Table 8-1 to Table 8-2 (cracked concrete is assumed); [c)] Axial stiffness for long term loading in cracked concrete; [d)] Axial stiffness for short term loading in uncracked (cracked) concrete

It should be noted that the minimum values of k_N and k_V from ETA contained in Table 9-5 and Table 9-6, respectively, are not physically consistent with the stiffness values measured in the tests, because they refer to sustained (i.e., long term) loading conditions, while the seismic loading is a typical short term action, i.e., no significant loading of the haunches occurs under static conditions.

9.5 Summary and discussion of the experimental tests

The tests presented in this chapter confirmed the feasibility of the proposed retrofit solution for 2D RC exterior beam column joints. A variety of qualitative behaviours of the retrofit solution could be reproduced.

- The tests 2DG1 and 2DG2 represent the optimal effect of the retrofit solution improving the joint performance with the formation of the plastic hinge in the beam and no cracking in the joint region. The anchors could guarantee a monolithic connection of the haunches with the beam-column connection. The anchorage was loaded in tension up to less than 70% of its ultimate strength.
- In test JT1-3 the anchorage was loaded in tension beyond the ultimate strength. The combined pullout and concrete cone failure of the last row of anchors of the top haunch influenced negatively the effect of the retrofit with a reduction of stiffness. However, the establishment of ductile failure mechanism of the specimen was still possible. The full protection of the joint region was not achieved, but the cracks observed under the haunches and in the core did not negatively influence the overall performance of the retrofitted beam-column connection.
- In the case that a performance such as 2DG1 or 2DG2 cannot be achieved, because the strength demand of the anchorage is close to the ultimate capacity and no over-design is feasible, a reduction of the target demand by reducing the beam flexural capacity of the beam is possible. The test JT1-4 confirmed the feasibility of this solution. The retrofitted specimen performed in a very ductile way and the load-carrying capacity of anchorage was guaranteed with a higher degree of safety than in the test JT1-3.

- In test JT1-5 a concrete cone failure of the brittle concrete screws was observed. The retrofitted specimen behaved similarly to the as-built specimen after the failure of the anchorages.
- In test JT1-6 the effect of using pseudo-ductile mechanical expansion anchors on the retrofit solution was investigated. The anchors exhibited significant slip, but did not fail allowing the increase of the strength of the specimen up to yielding of the beam bars. The use of this type of anchor, cheaper and easier to install than bonded anchors, could be more effective if combined with a weakening solution (see JT1-4) or in the case where an over design of the anchorage is needed (see 2DG1 and 2DG2).
- The beam yielding moment (associated with the steel yielding strength, f_y) appears to be the most accurate limit state to quantify the ultimate resistance of the retrofitted specimen, since in none of the tests with well-functioning retrofit the ultimate beam moment (associated with the steel ultimate strength, f_u) was reached.
- The tension forces acting on the anchorage measured in the tests are compatible with the strength calculated with the procedure explained in Section 8.2.5.1.
- The calculation of the tensile anchor stiffness using the forces during the tests and the analytical formulation proposed in Section 8.2.2.1 led to values which are compatible with the indications that can be obtained from the relevant technical approval.
- The frictional stiffness, K_f, acting parallel to the shear resistance of the anchors, was estimated to be within the range of values, which were also measured in the tests of *Tassios & Vintzileou (1987)*.
- The analysis of the measurements of the forces in the haunches carried out during the tests provided important information about the anchors stiffness (k_N, k_V and K_f) and the eccentricity, e_N, of the tensile loading acting on the anchorage.

10 NUMERICAL VALIDATION OF THE HAUNCH RETROFIT SOLUTION WITH POST-INSTALLED ANCHORS

The Finite Element (FE) model developed and verified in Chapter 4 for the simulation of the behaviour of as-built beam-column joints was used for the analysis of the retrofitted specimens. The modelling of the retrofit solution is explained in Section 10.1. Preliminarily, the plausibility of the results of the numerical simulations was verified by analysing the force distribution between steel plates and the beam-column joint (Section 10.2.1), the forces distribution in the anchor group (Section 10.2.2) and the sensitivity of the model to the simulation of different failure modes (Section 10.2.3). In Section 10.3 the simulation of the experimental tests of Chapter 9 is presented and discussed. Emphasis was given to the global behaviour of the retrofitted specimens and to the forces transferred by the haunches. The anchors stiffness values calculated in Section 9.4.10 were used as input parameter in the FE analyses. In Section 10.4 the numerical simulations were used to analyse the effect of parameters that could not be directly captured through experimental measurements such as the estimation of effective haunch length (Section 10.4.1). The parametric study was limited to the anchors stiffness, since the influence of other parameters which influence the assessment of the as-built and retrofitted beam-column connection is already well-known (Section 10.4.2). Finally, the design model of the retrofit solution proposed in Chapter 8 was verified comparing analytical and numerical results (Section 10.4.3). The main achievements of this study are summarised in Section 10.5.

10.1 Modelling strategy

For the numerical simulations of the retrofitted specimens the same models presented in Chapter 4 for the analysis of the as-built beam-column connections were used. Additionally, the connection of the diagonal haunches with the beam and the column with post installed anchors had to be modelled.

Extensive experience has been obtained in recent years in FE analysis of post-installed anchors loaded in tension and shear at the Institute of Construction Materials of the University of Stuttgart using the FE code MASA. Several three-dimensional (3D) models have been developed for different types of post-installed anchors and loading directions, e.g., *Küenzlen (2005)* for concrete screws in tension, *Appl (2009)* for bond anchors in tension and *Hofmann (2005)* for anchors under shear close to an edge. These experiences have shown that to realistically reproduce the load-displacement behaviour of anchors, the optimal mesh size for the portion of concrete around the anchor should be much smaller than the one used in this study (up to 5 mm instead of 20 mm).

In this work, the idea of a detailed modelling of the post-installed anchors was abandoned for the following reasons:

- The modelling of beam-column joints and anchorages is generally carried at different scale levels (i.e., different average mesh-size). A general reduction of the mesh-size (up to 5 mm) would enable an appropriate modelling of the anchors, but would lead to unacceptable time and resources consuming analyses. The use of the mesh-size generally adopted for the simulation of beam-column joints (approximately 20 mm) would lead to unacceptable approximations for the correct simulation of the load-displacement behaviour of the anchors.
- Due to the impossibility of carrying out reliable measurements during the tests the complete load-displacement behaviour of the single anchors in the tests is not known. Therefore, no reliable validation of the model would be possible.
- The principle aim of the FE analysis is not the simulation of the anchor behaviour, but the evaluation of the influence of the anchor stiffness on the retrofit solution proposed and the validation of the analytical model proposed in Section 8.2.
- The FE model for the beam-column connections developed in Chapter 4 is able to reproduce the mechanics of RC exterior joints distinguishing between different failure modes (e.g., joint shear cracking and beam flexural yielding) with sufficient accuracy and, therefore, there are no need and intention to modify it.

In Figure 10-1a,b a typical model of a retrofitted beam column joint including the discretisation of the metallic haunches is shown. On the basis of the above considerations, the anchors were modelled using non-linear springs, which can be calibrated to reproduce a certain load-displacement curve (Figure 10-1c). The non-linear springs implemented in MASA are able to transfer only tension loads. For this reason two springs are necessary for the simulation of the shear behaviour of the anchors (since the loading direction is not known a priori), while only one is required for the transfer of the tension load (Figure 10-1c). Because of the impossibility of defining a hysteretic behaviour of the non-linear springs, only monotonic simulations of the retrofitted beam-column joints were carried out.

The non-linear springs implemented in MASA are modelled by one-dimensional (1D) truss elements. By setting the length of the bar element to l = 1 mm and the cross section area to A = 1 mm^2, according to the Hooke's law, the stress-strain relations of the bar equals the load-displacement relation of the anchor. A given load-displacement curve of an anchor can be reproduced defining a polynomial path made of n segments. For the analyses carried out in this study, usually, two segments are defined to reproduce the secant stiffness of an anchor and the descending branch corresponding to its failure.

A thin contact layer was introduced between the concrete surface and the anchor plates (thickness, t = 1 mm). This layer allows the transfer of compression forces and friction, μ_f ($0.0 \leq \mu_f \leq 1.0$), and no tension forces (*Fichtner, 2005*). A frictional coefficient, $\mu_f = 0.4$ between steel and concrete was assumed in the analyses. It should be noted that the friction simulated in the FE analysis has a pure adhesive nature and the effect of roughness of material cannot realistically be taken into account, i.e., as soon as a gap between the contact surfaces opens, no friction can be mobilised. In reality, friction forces may be mobilised up to at least a gap of 1-3 mm, because of the irregular rupture surface of the grout layer. The

roughness of the surfaces can be indirectly taken into account using a value for the anchors shear stiffness, k_V, considering reference tests without a teflon sheet between the concrete surface and the steel fixture (see Section 8.2.2).

To assure the transfer of the tension and shear loads from the anchors into the base material, rows of stiff linear elastic steel elements with length equal to h_{ef} were defined (Figure 10-1b).

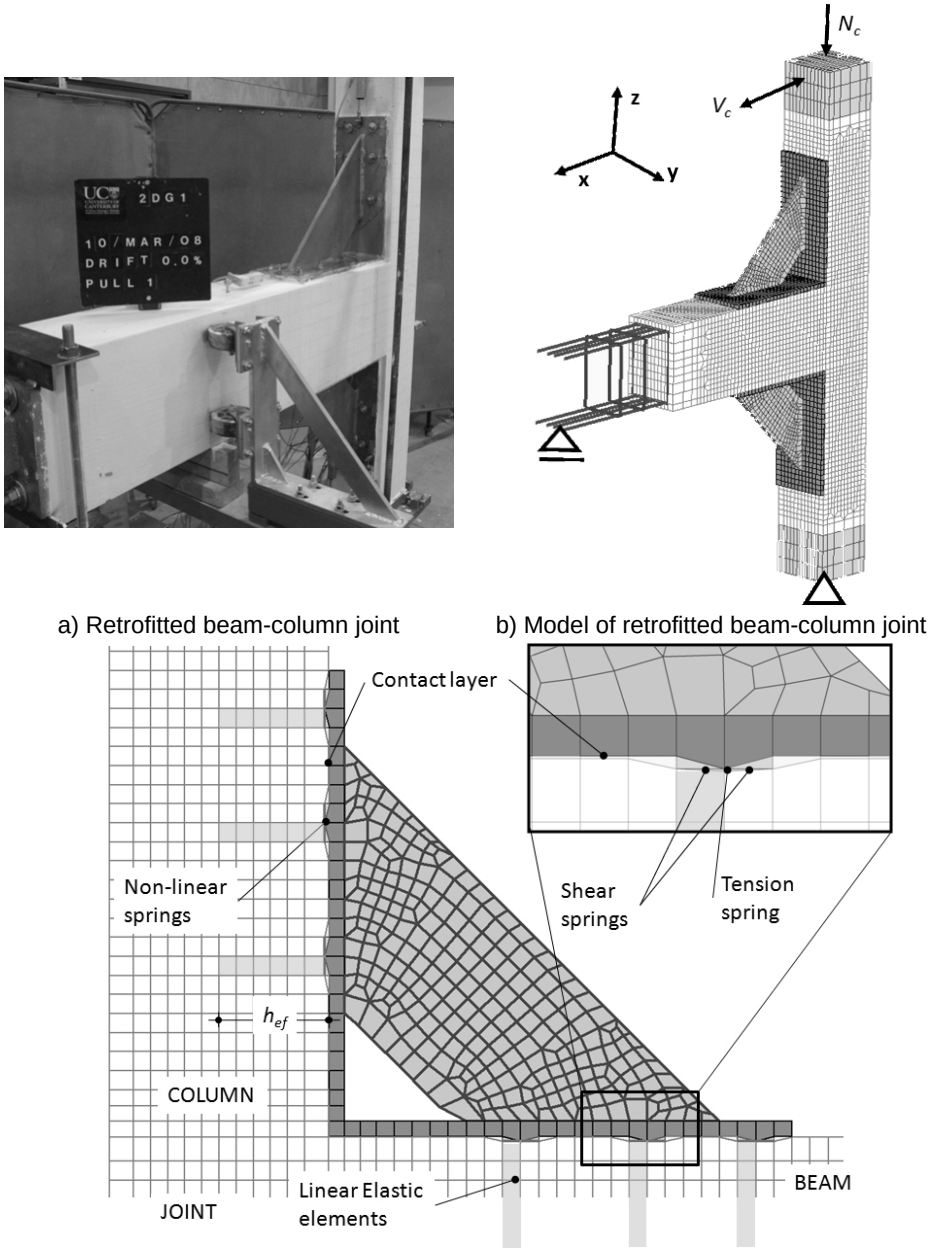

a) Retrofitted beam-column joint b) Model of retrofitted beam-column joint

c) detail of the anchorage of the steel haunches

Figure 10-1: Model of the specimen 2DG1

The modelling strategy adopted in this study allows the stiffness and strength of the anchors to be easily varied and thus the investigation of their effect on the retrofit solution. In contrast, different failure modes of anchors and the effect of the changes of stress-strain state of the base material (i.e., cracking of concrete) on the load-displacement characteristic cannot be realistically reproduced.

10.2 Evaluation of the modelling technique

10.2.1 Analysis of forces in the steel plate-concrete surface contact planes

As a first evaluation of the FE model, the distribution of forces on the contact surface between steel plates and concrete surfaces of beam and column were qualitatively analysed. The shear forces of the tensioned haunch were transmitted in beam and column in form of compression stresses in the corners of the anchor plates (Figure 10-2a) as predicted in the scheme shown in Figure 8-6 and Figure 8-7b. In the compressed haunch, the compression stresses were mainly located in the contact surface at the end of the anchor plates far from the joint panel (Figure 10-2b). With increasing displacement, the compressed area decreased (compare Figure 10-2b,c). This behaviour differed from the schematisation of Figure 8-6 and confirm the forces distribution shown in Figure 8-7a. This deformed configuration of compressed diagonal haunch did not allow the activation of the friction forces that are assumed in the analytical (Chapter 8) and experimental analysis of the anchorage (Chapter 9).

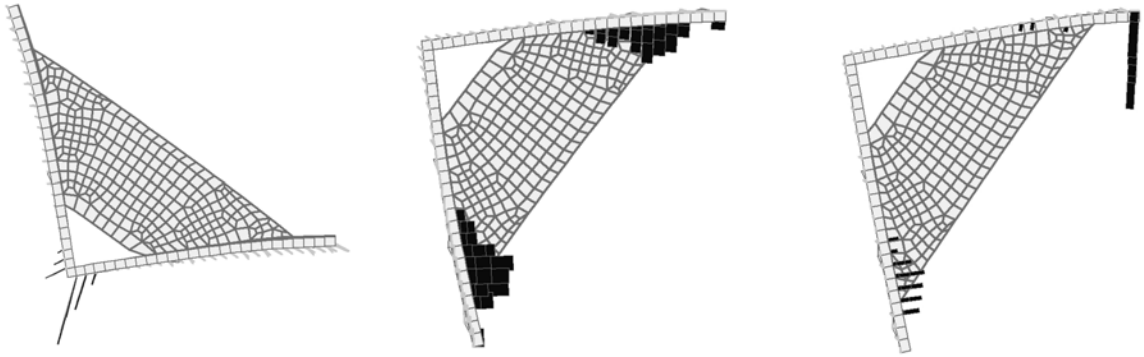

a) Tensioned haunch b) Compressed haunch (δ_c = 2 mm) c) Compressed haunch (δ_c = 20 mm)

Figure 10-2: Compression forces in the haunches-concrete contact surfaces (2DG1)

To overcome this limit of the FE simulation the shear stiffness of anchors, k_V, of the compressed haunch was doubled to implicitly account for the friction effect consistent with the observations made in Section 8.2.2. In the following sections the values of k_V of single anchors are given including the effect of stiffness for the compressed anchorage. This value is divided by two to obtain the shear stiffness of the anchors of the tensioned anchorage.

In Figure 10-3a,b the distributions of the principle stresses , σ_{11}, and σ_{33}, in the compressed and tensioned haunches are shown. The compression force transferred by the haunch was quite uniformly distributed under the steel plates in the column, while in the beam the compression forces were mostly concentred at the end of the steel plates (Figure 10-3a). This can be explained with the lower flexural deformation of the column in comparison to the beam. Similarly to the force distributions shown in Figure 8-7a, a compression field oriented approximately 45° to the beam and column axis was observed. The analysis of the tensile stresses shown in Figure 10-3b showed that the middle row of anchors was the most loaded, because the external row was disturbed, by the flexural cracking in the beam. Therefore, the load distribution in the anchors was different than observed in the experimental campaign, where the outer row of anchors was loaded more than the other two rows (see Figure 9-28).

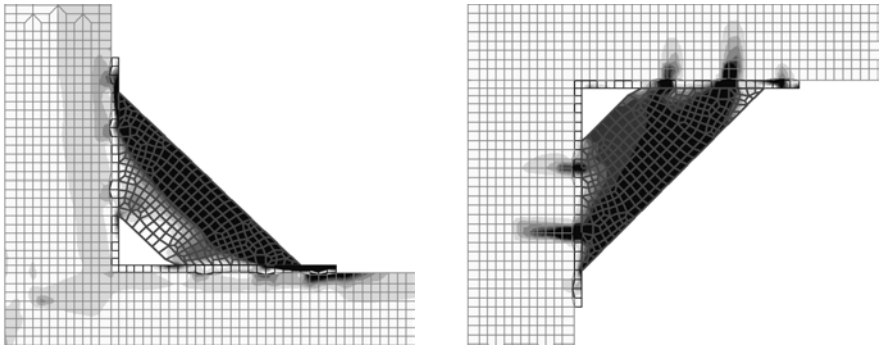

a) σ_{33} in the zone of compressed haunch b) σ_{11} in the zone of tensioned haunch

(Darker elements → higher σ_{33} and σ_{11} , respectively)

Figure 10-3: Distribution of stresses (2DG1)

The analysis of the distribution of the principle compressive and tensile stresses shown in Figure 10-4 for the specimen 2DG2 and Figure 10-5 for JT1-2, JT1-3 and JT1-4 indicate a similar behaviour as seen for specimen 2DG1.

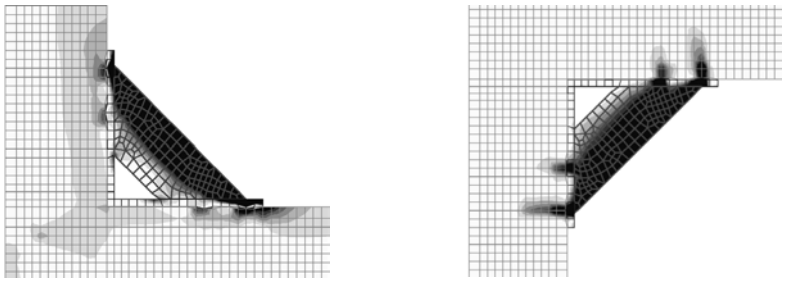

a) σ_{33} in the zone of compressed haunch b) σ_{11} in the zone of tensioned haunch

(Darker elements → higher σ_{33} and σ_{11} , respectively)

Figure 10-4: Distribution of stresses (2DG2)

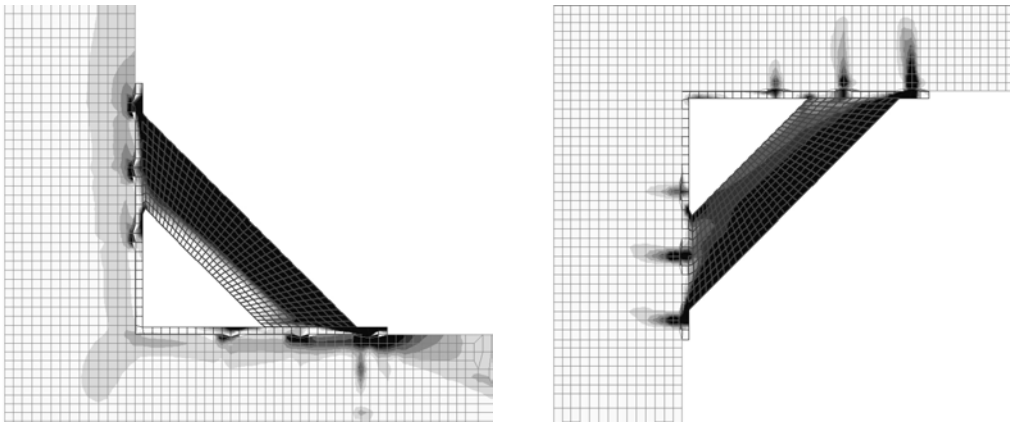

a) σ_{33} in the zone of compressed haunch b) σ_{11} in the zone of tensioned haunch

(Darker elements → higher σ_{33} and σ_{11}, respectively)

Figure 10-5: Distribution of stresses JT1-2, JT1-3 and JT1-4

10.2.2 Evaluation of forces in the anchors

In the experimental tests only limited data on the forces acting on the anchors could be collected (see Section 9.4.7). In this section the shear and tensile forces measured in the anchors in the FE simulations are analysed. Figure 10-6 shows the notation used for the anchor forces and the possible forces transfer mechanism between the haunch and the

beam-column connection as explained in Chapter 8 (repetition of Figure 8-6 and Figure 8-7 for clarity).

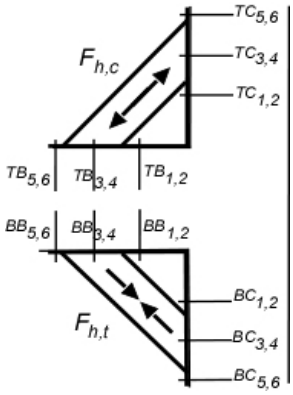

TB = Top Beam
BB = Bottom Beam
TC = Top Column
BC = Bottom Column

a) Notations

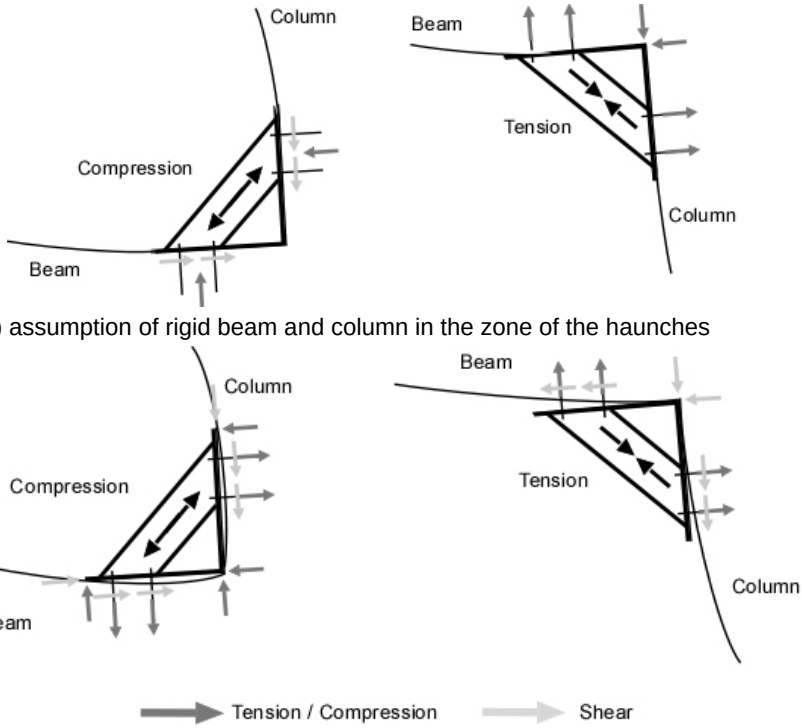

b) assumption of rigid beam and column in the zone of the haunches

c) assumption of flexible beam and column in the zone of the haunches

Figure 10-6: Notation used for anchors forces

From Figure 10-7 to Figure 10-10 the forces measured in the anchorages are expressed in [%], where 100% corresponds to the values measured in the haunches in tension or in compression. The following observations can be made:

- The anchorage of the tensioned haunch carries approximately the entire component of the force acting perpendicular to the concrete surface (see Figure 10-7a to Figure 10-10a left group of vertical bars);
- A significant portion of the shear force induced by the compressed haunch in the anchorage (20~50%) is not taken up by the anchors, but it is transmitted to beam and column by friction and/or mechanical interlocking (see Figure 10-7a to Figure 10-10a, right group of vertical bars);
- Figure 10-7b to Figure 10-10b show the behaviour of the anchorages following the assumption shown in Figure 10-6b. If the force distribution shown in Figure 10-6a is valid, the anchorage of the tensioned haunch would not carry any shear load and the anchorage of the compressed haunch would not carry any tension loading;
- The tension forces acting in the compressed anchorage appear to be negligible; and
- The shear forces acting in the tensioned anchorage should be conservatively taken into account in the design (50 to 100% of the tensile force), although no experimental verification is available yet.

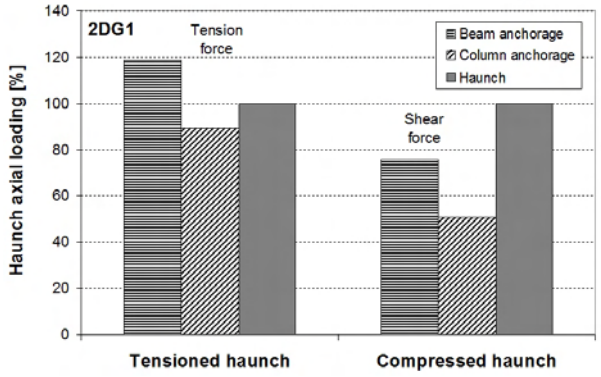

a) Comparison of forces measured in the haunches and in the anchorages

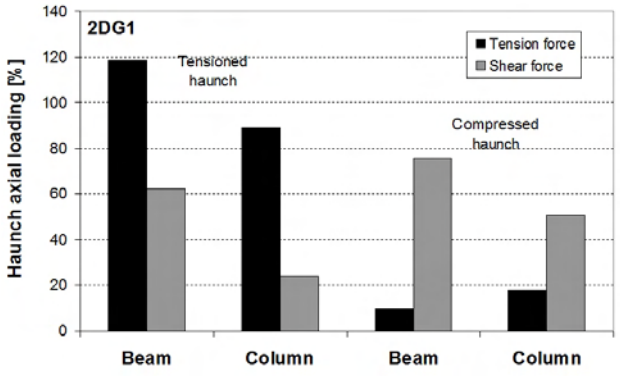

b) Comparison of tension / shear forces measured in the anchorages

Figure 10-7: Analysis of anchorage forces of specimen 2DG1

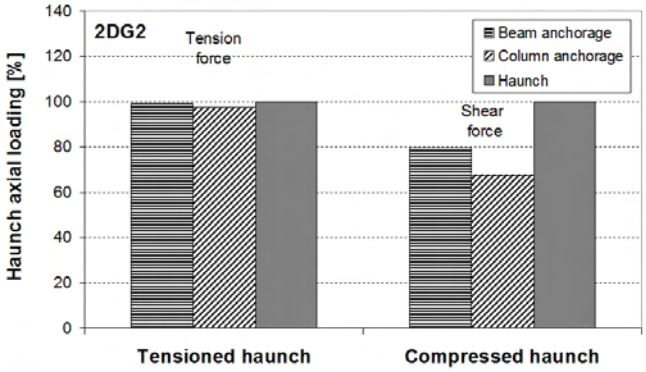

a) Comparison of forces measured in the haunches and in the anchorages

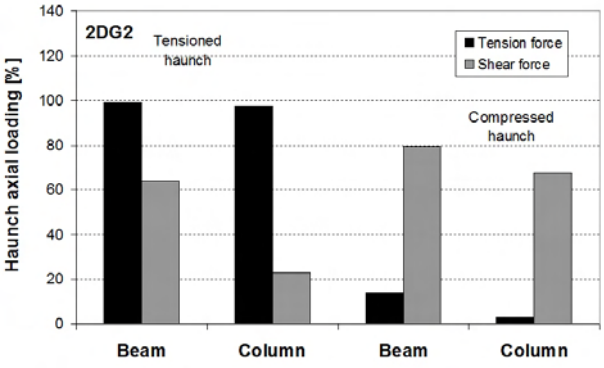

b) Comparison of tension / shear forces measured in the anchorages

Figure 10-8: Analysis of anchorage forces of specimen 2DG2

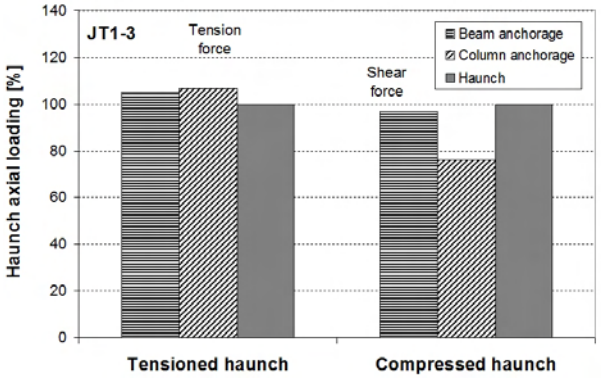

a) Comparison of forces measured in the haunches and in the anchorages

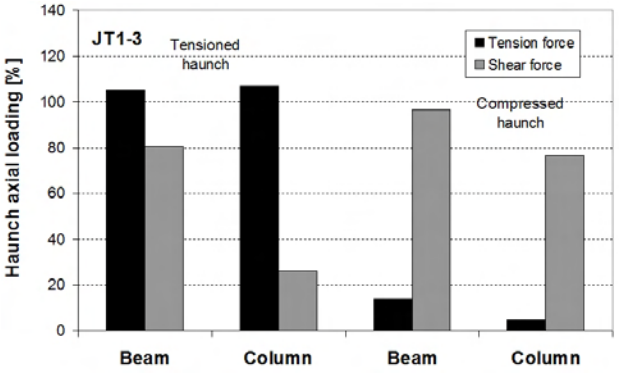

b) Comparison of tension / shear forces measured in the anchorages

Figure 10-9: Analysis of anchorage forces of specimen JT1-3

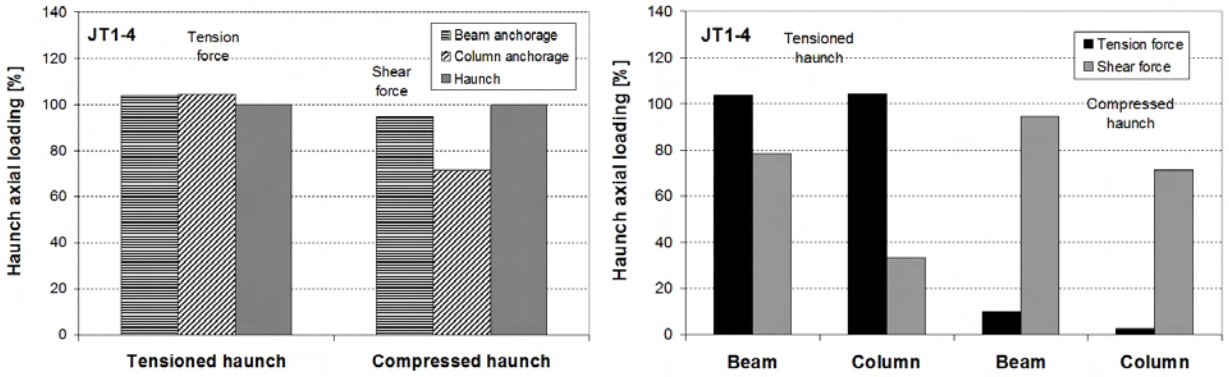

a) Comparison of forces measured in the haunches and in the anchorages

b) Comparison of tension / shear forces measured in the anchorages

Figure 10-10: Analysis of anchorage forces of specimen JT1-4

In Figure 10-11 the distribution of the tension and shear forces in the four anchorages of specimen JT1-4 are shown as example. Confirming the experimental results (Section 9.4.8) and the stress distribution in concrete of the FE analysis (Figure 10-5), with increase in distance from the joint panel the loading of the anchors increases.

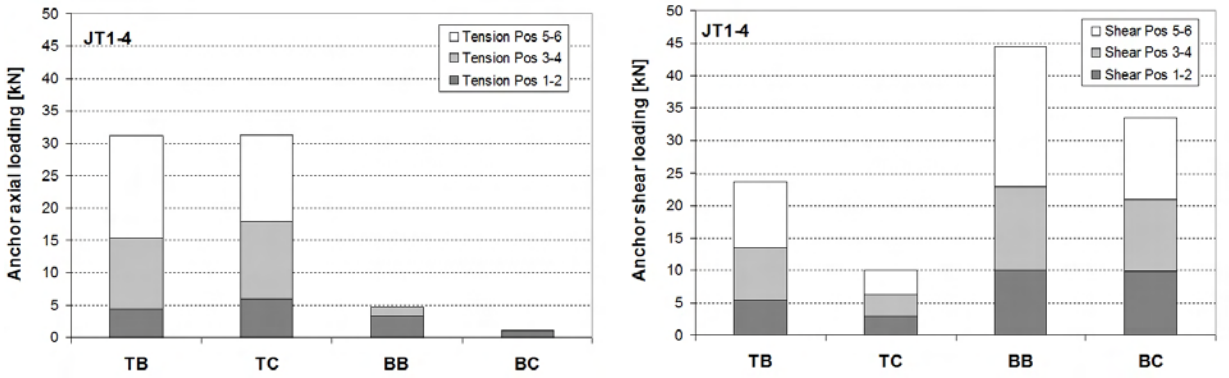

a) Tension forces

b) Shear forces

Figure 10-11: Anchors forces of specimen JT1-4 (notations of Figure 10-6a are used)

10.2.3 Evaluation of the FE model sensitivity

To evaluate the sensitivity of the numerical model to the input parameters (k_V and k_N), it was necessary to check its capability in reproducing different failure modes. In Figure 10-12 three runs with the model 2DG1 using different anchor shear and tensile stiffness are compared. Figure 10-12a,b,c show the increase of damage in the specimen outside of the targeted section for the formation of a plastic hinge in the beam with decreasing haunches stiffness ($K_h = K_{h,t} + K_{h,c}$). The reduction of global stiffness of the specimen which accompanies the decrease of the stiffness of the haunch connection can be seen in the load-displacement behaviour (Figure 10-12d). Using the forces measured in haunches ($F_{h,c}$ and $F_{h,t}$) as an input parameter for the calculation of the haunches stiffness, $K_h = K_{h,t} + K_{h,c}$, and subsequent determination of the β-factor (Figure 10-12e), it can be observed that for analysis 1 and 2 the joint was predicted to remain uncracked ($\beta > \beta_{min}$), while for the analysis 3, $\beta < \beta_{min}$, i.e., the shear cracking limit state of the joint was exceed, as confirmed in Figure 10-12c,d. The FE simulations confirm the analytical predictions.

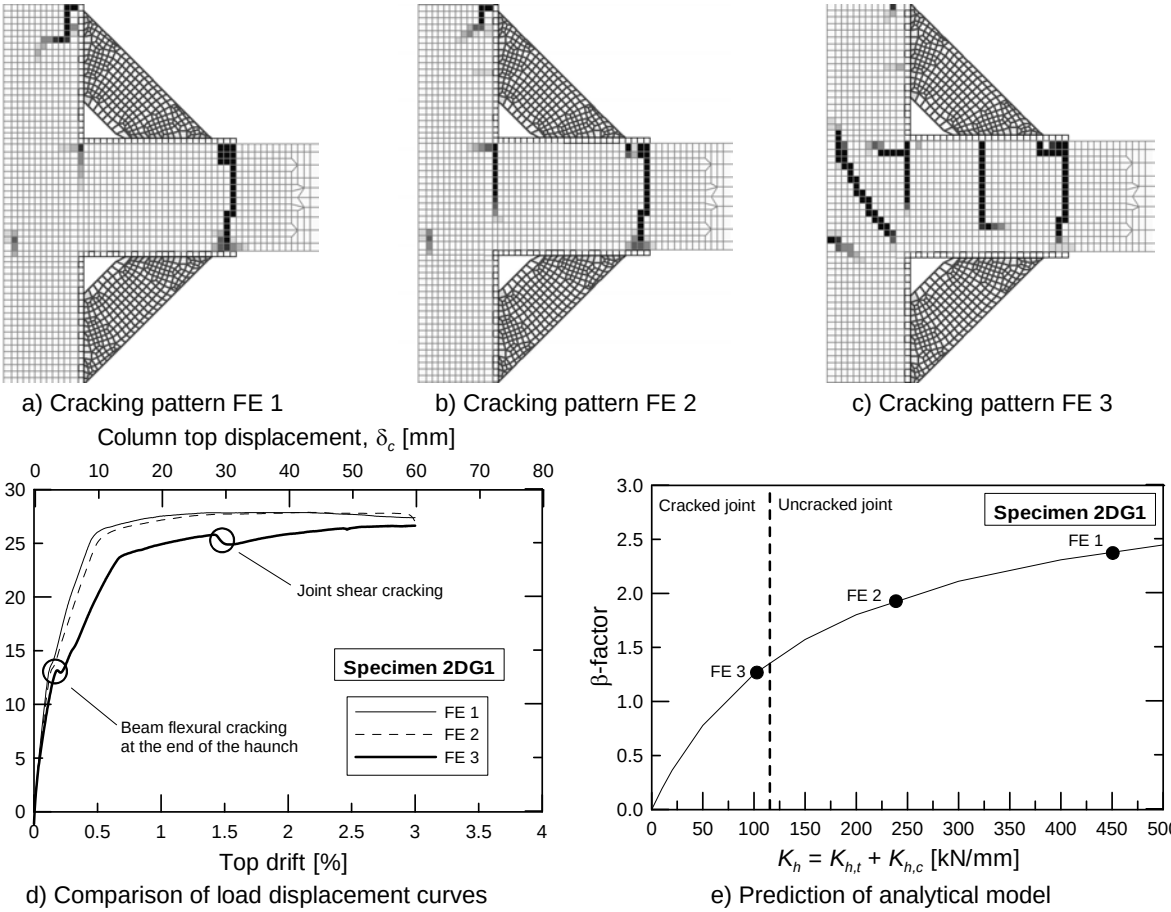

Figure 10-12: Evaluation of FE model sensitivity

10.3 Simulation of the experimental tests

10.3.1 Test 2DG1

The numerical simulation of the retrofitted specimen 2DG1 indicated the formation of a plastic hinge in the beam as displayed by the cracking pattern observed (Figure 10-13b), while the joint remains uncracked as also observed in the experimental test. The FE model behaved in ductile manner as shown in Figure 10-13a. The ultimate load measured in the test was overestimated by 15% and 10% by the numerical analysis in negative and positive loading direction, respectively. The simulation could not reproduce the strength decrease observed in the test due to concrete spalling and buckling of the longitudinal beam bars (see Figure 10-13a,b and Section 9.4.1).

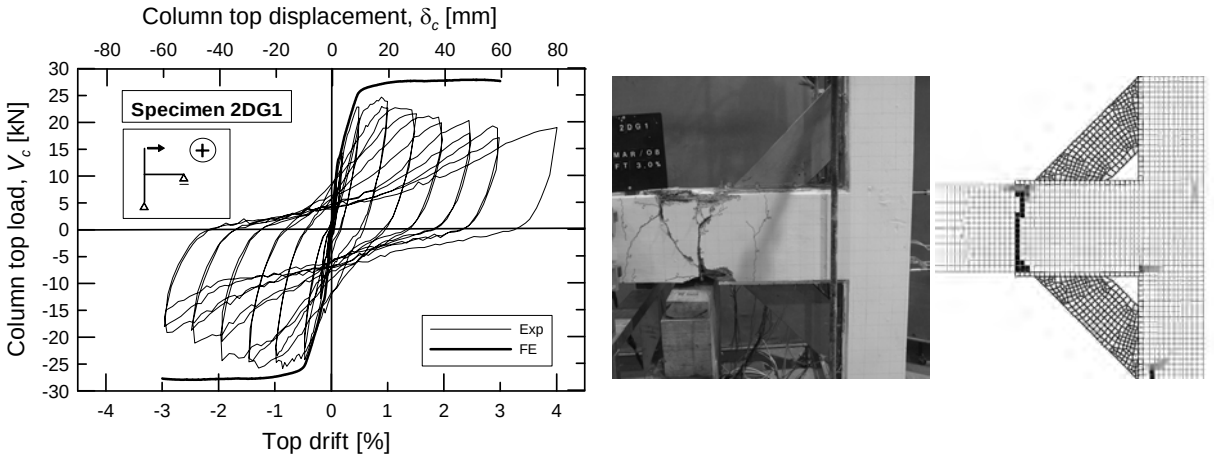

a) Comparison of hysteretic behaviour b) Comparison of cracking patterns

Figure 10-13: Simulation of specimen 2DG1

The evolution of the compressive (Figure 10-14a) and tensile (Figure 10-14b) forces inside the haunches measured in the specimen 2DG1 during the experimental investigations and numerical analysis are compared. The values of $k_V \sim 25$ kN/mm (in addition to the effect of friction with $k_f \sim 5$ kN/mm^3) and $k_N \sim 25$ kN/mm obtained from the analysis of the experimental tests (see Section 9.4.10) were confirmed by the numerical simulations with reasonable approximation ($k_N = 25$ kN/mm and $k_V = 50$ kN/mm were used in the FE analyses).

While comparing the experimental and numerical results shown in Figure 10-14a,b it should be kept in mind that at $F_{h,t,max}$ the column lateral load, V_c, measured in the FE analysis exceed the experimental observations by about 10% (see Figure 10-13a). Furthermore, the compression force, $F_{h,c}$, measured in the FE simulation diverges from the experimental value for increasing drift levels for the reasons mentioned above in the comparison of the load-displacement behaviour.

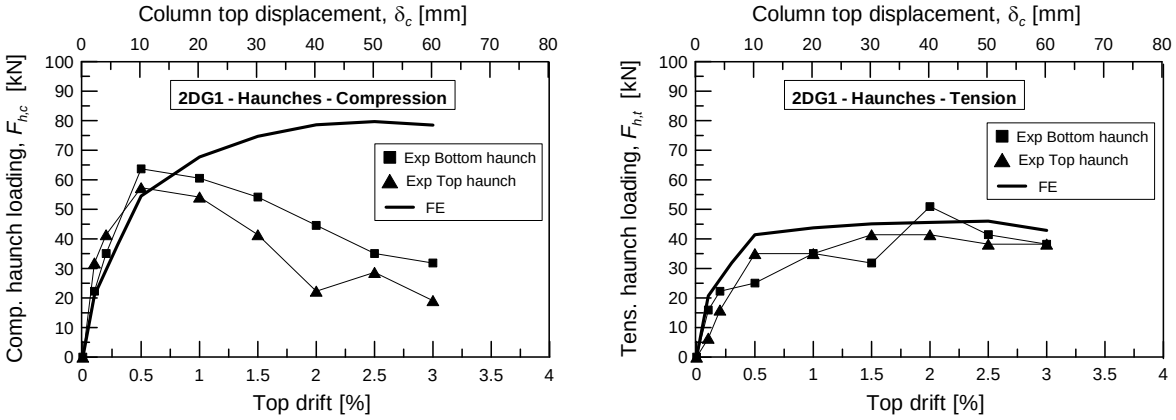

a) Comparison of compression forces b) Comparison of tension forces

Figure 10-14: Forces in the haunches – Comparison between FEA and experiment (2DG1)

10.3.2 Test 2DG2

As described in Section 9.4.2, the specimen 2DG2 had the same geometrical and material properties of 2DG1. Similarly to the specimen 2DG1, the experimental observations were reproduced fairly well. The beam flexural yielding was overestimated by approximately 10% when compared to the experimental test (Figure 10-15a). The cracking pattern observed in

the experiment, mainly characterised by the formation of the plastic hinge in the beam at the haunch, was also correctly reproduced by the FE simulation (Figure 10-15b). In both test and analysis cracks could be observed due to the push-pull action of the 180°-hooks on the concrete cover in the joint panel (Figure 10-15b).

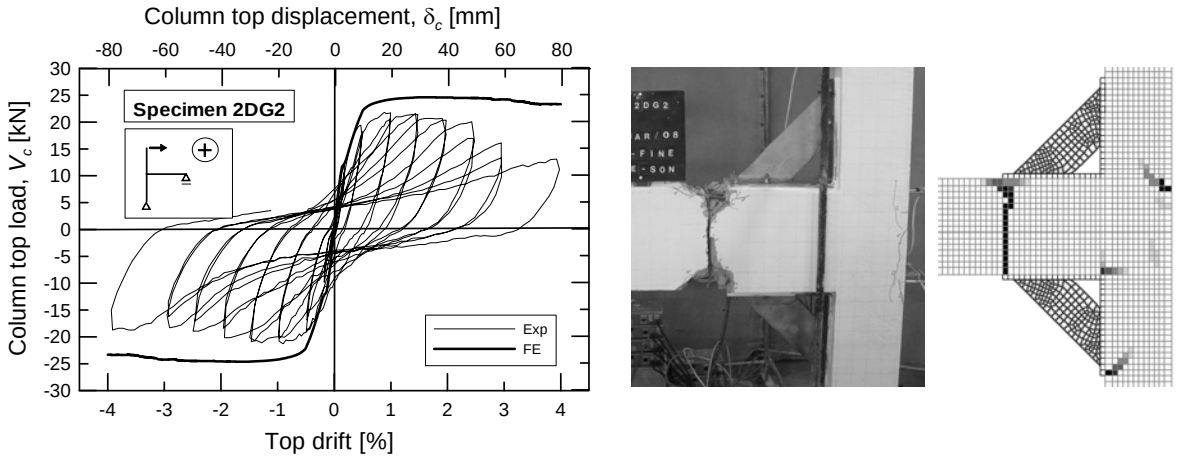

a) Comparison of hysteretic behaviour b) Comparison of cracking patterns

Figure 10-15: Simulation of specimen 2DG2

Assuming k_N = 25 kN/mm and k_V = 50 kN/mm for the numerical simulation, compressive (Figure 10-16a) and tensile (Figure 10-16b) forces in the haunches comparable to the experimental tests were obtained. The impossibility of simulating the buckling and slipping of the plain round reinforcing bars of the beam and the spalling of concrete are the main causes of the difference in the prediction of the compression forces in the haunch with increasing top drift. This difference is much less that for the specimen 2DG1 as can be seen also by comparing the hysteretic behaviours (Figure 10-13 and Figure 10-15) It should be noted that the backbone curves of the experimental measurement shown in Figure 10-16a,b refer to the negative load only.

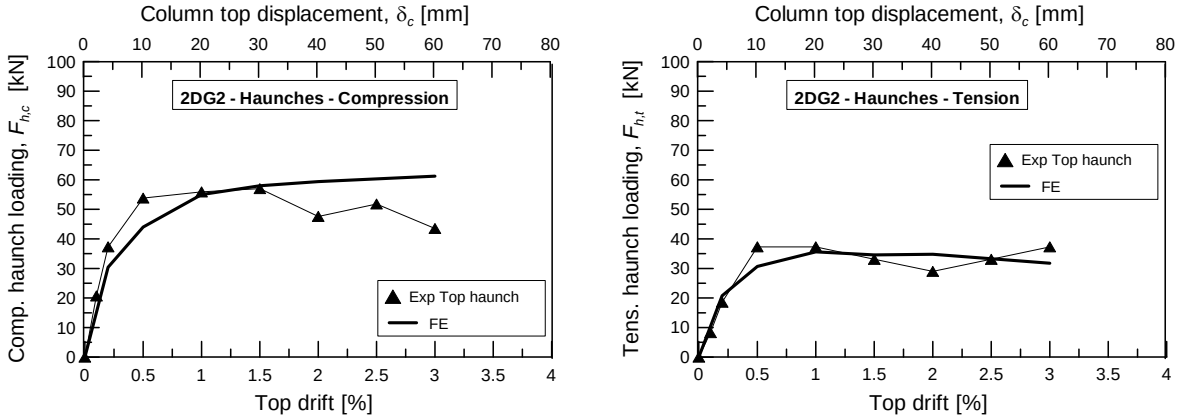

a) Comparison of compression forces b) Comparison of tension forces

Figure 10-16: Forces in the haunches – Comparison between FEA and experiment (2DG2)

10.3.3 Test JT1-2 and JT1-3

As explained in Chapter 9, the behaviour of the retrofitted specimens tested at BARC was more complex, because the anchorage was generally loaded up its ultimate strength. The non-linear behaviour of the anchors pre- and post-peak could not be simulated with sufficient accuracy. However, the FE analysis could reproduced fairly well the backbone curve of the

hysteretic behaviour indicating the flexural yielding of the beam (Figure 10-17a). A significantly higher initial stiffness, due to the idealisation of the boundary conditions; was predicted by the FE simulation. The comparison of the cracking patterns of experiments and numerical simulation also shows an acceptable agreement (Figure 10-17b). The FE simulation correctly predicted the formation of the flexural and shear cracks in the beam as well as the cracking of the joint core.

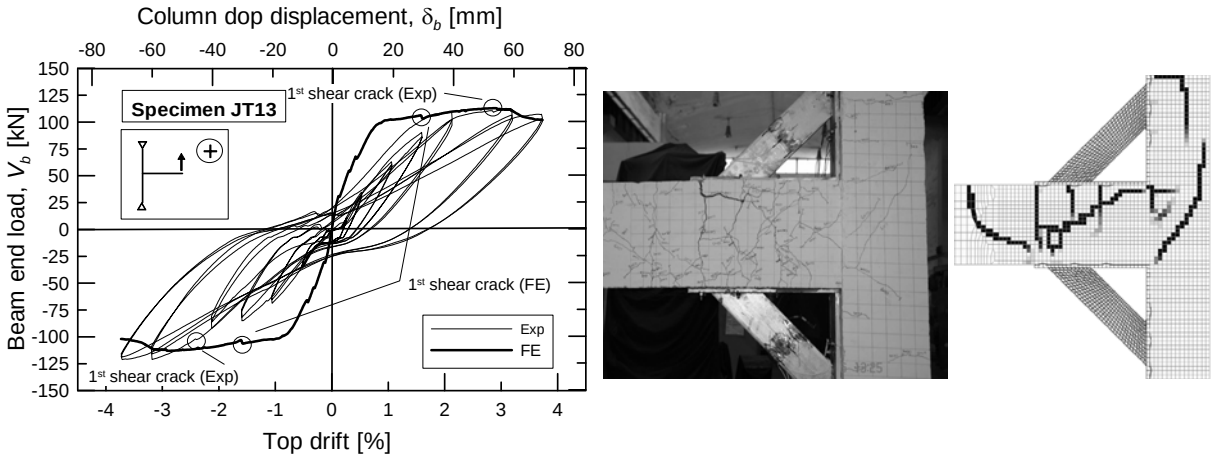

a) Comparison of hysteretic behaviour b) Comparison of cracking patterns

Figure 10-17: Simulation of specimen JT1-3

Figure 10-18 shows the comparison of the haunch forces in the test and in the FE analysis. The compression force predicted by the numerical simulation agrees acceptably with the forces measured in the tests JT1-2 and JT1-3 (Figure 10-18a). The analysis of the tension forces indicate that the failure of the anchorage occurred between 1.0% and 1.5% drift. In the experimental tests the failure was observed only in one loading direction for the specimen JT1-3 at approximately 2.0% drift (Figure 10-18b). This difference is mainly due to the higher initial stiffness of the FE analysis (see Figure 10-17a). The anchorage failure load at around 110 kN is significantly lower that the load measured in the tests (~ 170 kN), but similar to the analytical prediction shown in Figure 9-30 (123 kN in uncracked and 86 kN in cracked concrete). $k_N = k_V = 50$ kN/mm, consistently with the experimental measurements, were assumed.

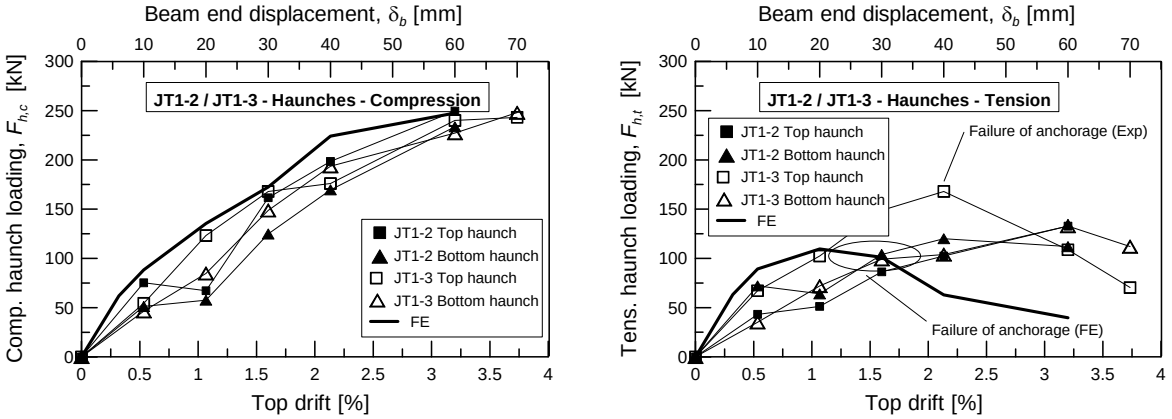

a) Comparison of compression forces b) Comparison of tension forces

Figure 10-18: Forces in the haunches – Comparison between FEA and experiment (Test JT1-3)

10.3.4 Test JT1-4

In test JT1-4 the beam flexural capacity was reduced adopting a weakening strategy (see Section 9.4.5). The anchors tensile stiffness was also reduced to k_N = 25 kN/mm, while k_V = 50 kN/mm was kept unchanged according to the stiffness values of Table 9-4. The ultimate strength of test JT1-4 was reproduced with sufficient accuracy (Figure 10-19a). However, the FE simulation indicated a much stiffer initial behaviour than the experimental backbone curve. The analysis of the principle tensile strains, ε_{11}, of concrete (cracks) showed that the joint panel remained uncracked up to the target displacement of 70 mm (approximately 3.7% drift) and also the other cracks are comparable to the experimental observations (Figure 10-19b). The differences in haunch compression and tension forces between experimental and FE analysis (Figure 10-20) are probably related to the stiffness difference in the load-displacement behaviour clearly visible in Figure 10-19a.

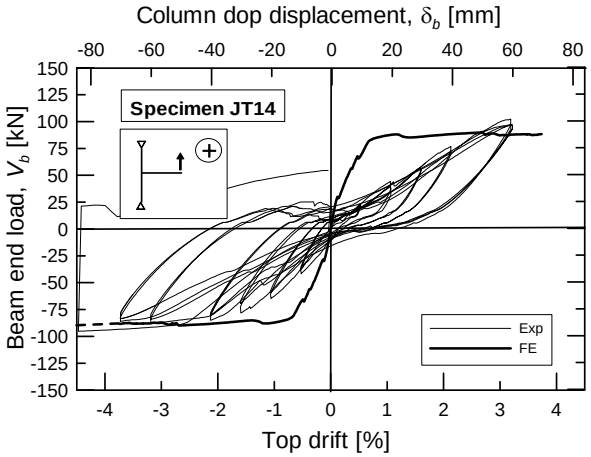

a) Hysteretic behaviour

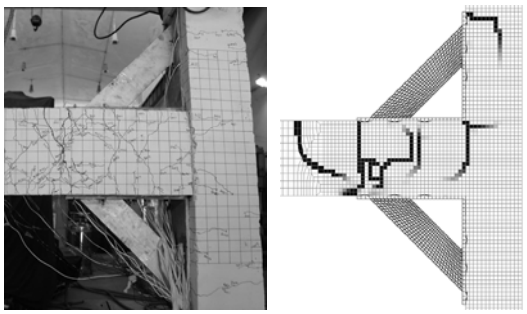

b) Comparison of cracking patterns

Figure 10-19: Simulation of specimen JT1-4

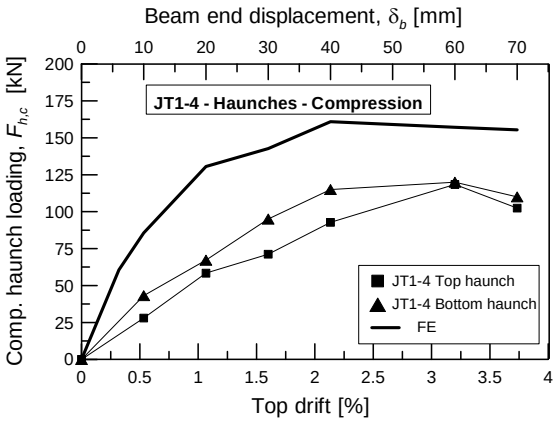

a) Comparison of compression forces

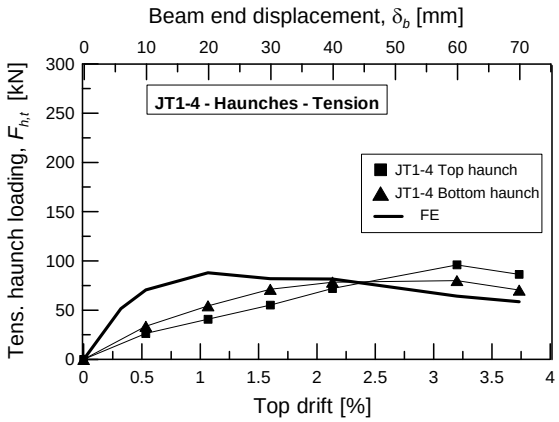

b) Comparison of tension forces

Figure 10-20: Forces in the haunches – Comparison between FEA and experiment (Test JT1-4)

10.4 Analysis of FE simulations

10.4.1 Evaluation of effective haunch length

In Section 8.2.1 the need to distinguish between the distance from the joint panel, where the plastic hinge in the beam should occur (*L'*) and the effective haunch length, i.e., distance of application of the resultant haunch forces, was addressed. The resultant tension action on the anchorage acts generally with an eccentricity, e_N = 10~50 mm from the barycentre of the

anchorage towards the outer side of the anchor plate. The numerical simulations showed that the largest fraction of the compression force (approximately, 30-40% of the shear and 80-100% of the axial components) are concentrated at the end of the anchor plate (distance *L'* from the joint panel). On the basis of these considerations, the resultant force of the two haunches is between 50 and 100 mm from the end of the anchor plate. Therefore, for the considered geometries of haunches and anchorages (see Figure 9-3) $L_{eff} = L'$ - 100 mm is conservatively assumed.

10.4.2 Evaluation of the influence of tensile and shear stiffness of the anchors

To evaluate the performance of the FE model, the shear (k_V) and tension (k_N) stiffness of the anchors were varied. The forces in the haunches obtained in the FE analysis of model 2DG1 are shown in Figure 10-21. According to the results plotted in Figure 10-21a, the variation of k_N significantly influences the strength demand in the anchorage. Figure 10-21b clearly shows that the variation of k_V of the anchors has only a secondary influence on the haunch tensile loading. On the basis of these observations, it can be argued that the tensile stiffness of the haunches is mainly influenced by k_N, i.e., Equation (8-13a) can be used instead of Equation (8-15) for the calculation of the tensile stiffness of the haunch, $K_{h,t}$.

k_N and k_V were varied within a very wide range ($25 \le k_N \le 100$ kN/mm and $10 \le k_V \le 50$ kN/mm). The ratio of the axial forces in the haunches $F_{h,c} / F_{h,t}$ varied between 1.36 and 1.70. $F_{h,c} / F_{h,t} = 1.36$ was obtained with $k_V / k_N = 0.5$ and $F_{h,c} / F_{h,t} = 1.70$ with $k_V / k_N = 2.0$. According to the indicative values for k_N and k_V provided in Chapter 8, a ratio $k_V / k_N \sim 1.0$ can be expected in the case that the anchorage under axial load does not exhibit total or partial failure during the test. This behaviour was observed in the experimental tests 2DG1, 2DG2 and JT1-4 and in these case the measured ratio $F_{h,c} / F_{h,t}$ was between 1.30 and 1.50. In the tests JT1-2 and JT1-3, where the anchorage under axial load reached the ultimate limit state (i.e., increasing contribution of compressed haunch with decreasing strength of the tensioned anchorage), the ratio $F_{h,c} / F_{h,t}$ was larger than 1.70.

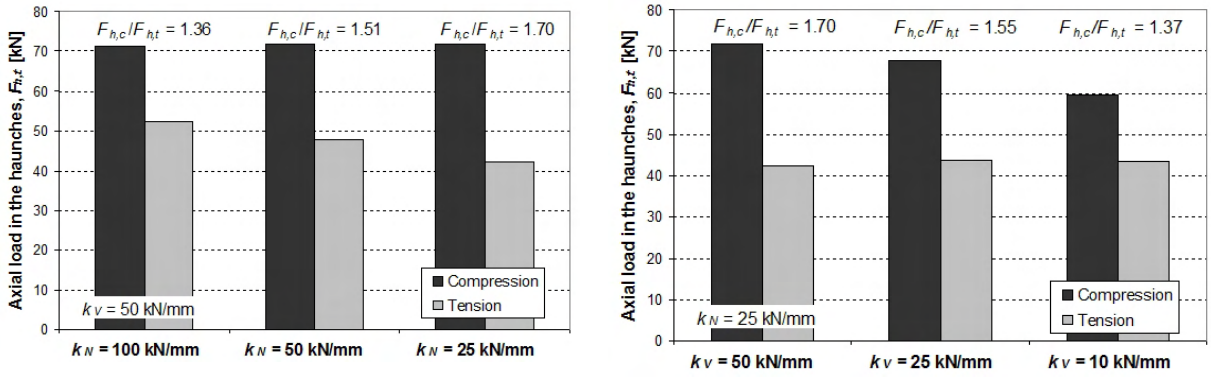

a) Variation of tensile stiffness b) Variation of shear stiffness

Figure 10-21: Variation of tensile and shear stiffness of the anchors (specimen 2DG1)

In Figure 10-22 the ratios $K_{h,c} / K_{h,t}$ (or equivalently $F_{h,c} / F_{h,t}$) obtained in the FE simulations carried out on the specimens 2DG1, 2DG2, JT1-2, JT1-3 and JT1-4 are plotted as a function of the ratio k_V / k_N. For comparison also the experimental results are shown. For all tests and FE simulations the stiffness values were measured at the load step where the highest value of $F_{h,t}$ was measured. The range of the ratio k_V / k_N ($0.2 \le k_V / k_N \le 2.0$) considered in the analysis was chosen according to the stiffness values calculated for bonded anchors on the

basis of the relevant ETA. It should be noted that in the evaluation of k_V from the experimental tests require the separation of the three components (anchor stiffness, friction and mechanical interlocking), this is generally not possible. Furthermore, the analysis does not take into account the influence of friction estimated in the experimental tests (see Table 9-4), which is considered as an increase of k_v. Therefore, $(k_V/k_N)_{Exp}$ is generally higher in the experiments than in the FE simulations. The ratio $K_{h,c} / K_{h,t}$ increases with increasing ratio k_V / k_N. $K_{h,c} / K_{h,t} = 1.5$ can be assumed as average, if the analyses where joint shear cracking occurred are excluded, and it can be used for design purposes. In tests, where the friction contribution is higher, the ratio $K_{h,c} / K_{h,t}$ increases and, hence the retrofit is more efficient ($K_{h,t} + K_{h,c}$ increases) and the axial loading of the anchorage decreases.

Using this simplification, i.e., $K_{h,c} / K_{h,t} = 1.5$, only the assumption of k_N is required, while the shear stiffness k_V and the frictional parameters (coefficient, μ_f, and stiffness, K_f) are implicitly taken into account, i.e., Equation (8-13a) only is required.

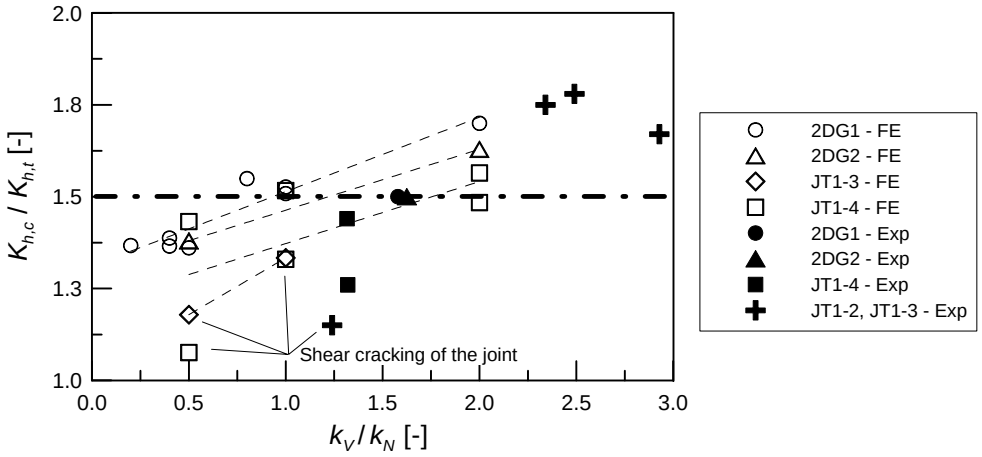

Figure 10-22: ratios $K_{h,c} / K_{h,t}$ vs k_V / k_N

10.4.3 Verification of the analytical model

In Figure 10-23 the comparison of haunch tensile loading, $K_{h,t}$, measured in the FE analyses and calculated with analytical model proposed in Chapter 8 is shown. The same ratio, $K_{h,c} / K_{h,t}$, as measured in the FE simulations, was assumed in the analytical model. On the basis of 19 simulations the ratio $F_{h,t,FE} / F_{h,t,Calc}$ was equal to 0.94 with CV = 10.4% (Figure 10-23a). Assuming a constant ratio $K_{h,c} / K_{h,t} = 1.5$ (grey points in Figure 10-23b), $F_{h,t,FE} / F_{h,t,Calc} = 0.96$ with CV = 9.0% was obtained. It should be noted that a ratio $F_{h,t,FE} / F_{h,t,Calc} < 1.0$ corresponds to a conservative design, because the calculated tension force acting on the haunch is overestimated and the strength demand on the anchorage under tension loading is higher. The same FE simulations evaluated in Figure 10-22 were considered for the verification of the analytical model.

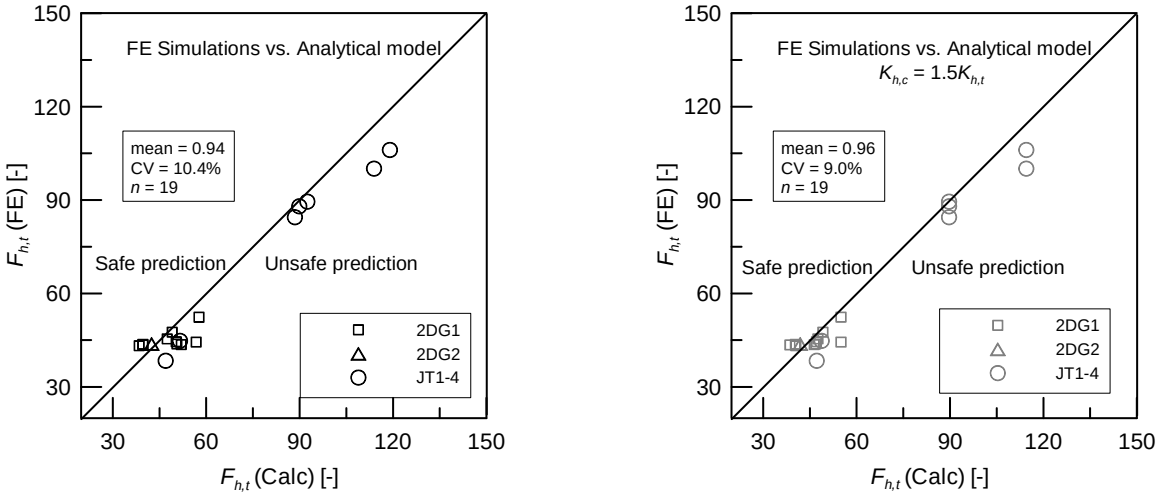

a) k_N and k_V as input for FE and Calculation b) $K_{h,c} = 1.5K_{h,t}$ in the analytical calculation

Figure 10-23: Comparison between FE simulations and analytical model

10.5 Summary of the results of the FE simulations

The main achievements of the FE simulations of the retrofitted beam-column joints can be summarised as follows:

- The limits of this modelling approach are related to the lack of accuracy in the modelling of the load-carrying mechanism of the anchors in concrete. The elements used to reproduce the load displacement behaviour of the anchors could not take into account the deformation (cracking) of the concrete elements.
- The numerical simulations allowed to get realistic overviews on the force transfer between diagonal haunch and the existing beam-column joint as well as load distribution in the anchors of the anchorage, which can be useful to refine the design of the anchorage. In particular the shear force carried by the tensioned anchorage should be additionally taken into account.
- The adopted modelling technique was suitable to simulate the behaviour of the retrofitted beam-column joints using as main input parameter the anchors stiffness (k_N and k_V) as proposed in the Chapters 8 and 9. With this approach the specimens 2DG1, 2DG2, JT1-3 and JT1-4 could be simulated with sufficient accuracy for practical purposes.
- On the basis of compressive and tensile stress distributions between anchor plates and beam/column an effective projected haunch length, $L_{eff} = L'$ - 100 mm is proposed for geometries similar to the tests carried out in this study.
- The ratio $K_{h,c} / K_{h,t}$ was evaluated varying the values of k_V and k_N and confirming the experimental observations. For design purpose $K_{h,c} / K_{h,t} = 1.5$ can be conservatively assumed (Figure 10-22).
- Lastly, the analytical model proposed in Chapter 8 was validated on the basis of the results of the FE simulations. The numerical and analytical predictions, expressed in terms of haunch tensile demand, $F_{h,t}$, agreed reasonable well (see Figure 10-23).

11 DESIGN OF THE PROPOSED SEISMIC RETROFIT SOLUTION

In this chapter, guidelines for the design of the Haunch Retrofit Solution (HRS) using post-installed anchors, i.e., safety concept (Section 11.1) and design method (Section 11.2) are given. The analytical assessement of the retrofit solution proposed in Chapter 8 has been verified and refined in Chapters 9 and 10. The assessment of the strength of the as-built as well as the retrofitted joint panel is carried out using the model presented in Chapter 6 within the assessment of the "hierarchy of Strength" of the beam-column joint discussed in Chapter 7. The verification of the safety concept based on *EC8-3 (2005)* and *fib (2011)* (similarly to CEN/TS 1992-4:2009 (*CEN, 2009*)) on the test specimens investigated in this study is discussed in Section 11.3.

The design method for the design of HRS proposed in this Chapter addresses only the type of plastic mechanism (brittle vs. ductile) to be established after the retrofit intervention. No quantification of the ductility level is given. Furthermore, no direct guidance is given for the cases, where a strength upgrade of the beam-column joints is required on the basis of a global analysis of the structure. As discussed in the previews chapters (Chapters 8 to 10), the HRS allows to utilise the beam flexural strength of a target section. If a larger strength is needed, a combination of the HRS with other strengthening techniques should be considered. This is not object of this study.

11.1 Design format

The design of the beam-column joint retrofit should follow the principles of "hierarchy of strength" described in Chapter 7 for the assessment of the as-built connection. To achieve a conservative seismic assessment and retrofit of the beam-column joint the following principles should be followed while establishing the hierarchy of strength of the structural elements constituting the connection (beam, column and joint):

- Overstrength of the reinforcement should be taken into account for the evaluation of desirable plastic mechanisms, i.e., beam flexural hinging;
- Characteristic strength should be considered for the evaluation of brittle plastic mechanisms, i.e., joint shear failure, column flexural hinging and shear failure of beam or column.

In practical applications, the concrete and reinforcement steel mechanical properties should be determined by testing of samples taken from the existing structure and/or using non-destructive techniques. For the new elements (steel diagonals and post-installed anchors), characteristic steel properties can be used.

The choice of the partial safety factors (PSF) for the verification of the retrofitted beam-column connection and the anchorage is related to the "Earthquake Design Level" and the required "Performance Level" of the building to be retrofitted. Considering "Performance Based Design" according to *EC8-3 (2005)* (similar to the matrix shown in Figure 1-3b), three Performance Levels can be associated to the behaviour of the joint retrofitted with HRS using post-installed anchors. In Table 11-1 a possible Performance Based Design concept of the retrofit is shown.

Table 11-1: Performance Levels of the retrofitted joint

Performance Level	Beam	Column	Joint	Anchorage
Damage Limitation	Cracked / Elastic	Uncracked	Uncracked	Ultimate LS [a)]
Significant Damage	Yielded	Cracked / Elastic	Uncracked	Ultimate LS [b)]
Near Collapse	Yielded	Cracked / Elastic	Cracked	Ultimate LS [b)]

[a)]: All rows of the anchorage should be considered; [b)]: The row of anchors closest to the plastic hinge is conservatively considered ineffective according to Figure 8-15 except in cases described in Section 11.2.5.3

The target "Performance Level" depends on the socio-economic importance of the building and the "Earthquake Design Level" (i.e., in EC8 "Hazard Levels") (frequent, occasional, rare, typically with return periods of 225, 475 and 2475 years, i.e., with a probability of exceedance of 20%, 10% and 2% in 50 years).

11.1.1 Assessment of as-built and retrofitted beam-column joint

In *EC8-3 (2005)* it is suggested to use the mean value properties of existing materials, as obtained from in-situ tests and other additional sources of information, after the "correction" with a confidence factor, CF_{KLi}, which is used instead of the γ_M-factors of *EC8-1 (2004)*. The verifications should be carried out using Equation (11-1):

$$S_d \leq R_d = \frac{R_k}{\gamma_{eq} \cdot CF_{KLi}} \tag{11-1}$$

with:

CF_{KLi} = Confidence Factor according to *EC8-3 (2005)*

S_d = design action. It corresponds to the strength of the weakest ductile plastic mechanism of the connection (i.e., beam flexural hinging)

= $R_m \cdot CF_{Kli}$ (Note that with increasing uncertainess on the materials ($CF_{Kli} > 1.0$), the design action increases)

R_m = Mean resistance of weakest ductile mechanism (e.g., beam flexural hinging)

R_d = design resistance of weakest brittle plastic mechanism (e.g., joint shear failure)

R_k = characteristic resistance of weakest brittle plastic mechanism (e.g., joint shear failure)

γ_{eq} = 1.0 for building of normal importance

> 1.0 for strategic building, according to the provisions of National Annexes of EC8

According to *EC8-3 (2005)*, the amount of available information (geometry and material properties) on the existing structure allows the definition of a Knowledge Level (KL1, KL2 and KL3 with increasing information) and the CF_{KLi} varies according to Table 11-2. In general, the

design of a local retrofit strategy requires an adequate Knowledge Level (i.e., KL2 or better KL3) of the as-built structure, because the behaviour of a retrofitted joint relies also on the strength of the other structural elements, e.g., the strength and ductility of the retrofitted beam-column joints depends significantly on the plastic hinging of the beam.

Table 11-2: Recommended partial safety factors for different KLs (*EC8-3, 2005*)

Knowledge Level (KL)	Confidence Factors (CF)
KL1: Limited knowledge	1.35
KL2: Normal knowledge	1.20
KL3: Full knowledge	1.00

11.1.2 Assessment of anchorage strength

For the design of the anchorage the indications of *fib (2011)* should be followed. For the seismic verification of different failure modes of the anchorage the anchorage resistance should be evaluated using Equation (11-2).

$$R_{d,eq} = \alpha_{eq} R_k / \gamma_M \tag{11-2}$$

with:

The factor α_{eq} takes in to account the non-uniform loading distribution in anchor groups arising from the different anchor stiffness. Furthermore, the cracking of the concrete under seismic conditions may be larger than in normal conditions.

According to *CEN (2009)*:

α_{eq} = 0.75 for concrete related failure modes

α_{eq} = 1.00 for steel failure modes

In this study the crack width in the base material of the anchorage is limited by the anchor plates and by the fact that the formation of the plastic hinge in the beam is targeted in a precise section (see Section 11.2.5.3). Therefore, α_{eq} = 1.00 for all failure modes is proposed for this application.

For γ_M the following values should be assumed:

Steel failure modes: $\gamma_{Ms} = 1.2 \frac{f_{uk}}{f_{yk}} \geq 1.4$ (11-3)

Concrete failure modes: $\gamma_{Mc} = \gamma_c \cdot \gamma_{inst} \cdot \gamma_{CV}$ (11-4)

with:

γ_c = CF_{KLi} for concrete according Section 11.1.1.

γ_{inst} = PSF taking into account the installation safety. It is product dependent and, therefore, it should be taken from the relevant technical approval. In general, γ_{inst} = 1.0, 1.2 and 1.4 for high, average and low installation safety, respectively, should be taken (*fib, 2011*). It is recommended to use a product with high installation safety (γ_{inst} = 1.0)

γ_{CV} = PSF taking into account the Coefficient of Variation, CV, of the considered failure mode.

= 1.0 for CV ≤ 15% and

= 1.0+(CV-15)·0.03 for 20% ≤ CV ≤ 15%.

If no more detailed information is available, the characteristic values of the resistances of the anchorage to different failure modes presented in Section 8.2.5 can be calculated from the average resistance using the Equations (11-5a,b).

$R_k = 0.75 \cdot R_m$ for concrete failure modes (CV ~ 15%) (11-5a)

$R_k = 0.85 \cdot R_m$ for steel failure modes (CV ~ 10%) (11-5b)

11.2 Design procedure

The design of the HRS using post-installed anchors for the connection of the steel haunch to the beam-column connection can be carried out according to the analytical model proposed by *Pampanin et al. (2006)* modified as explained in Section 8.2. The design should follow the scheme shown in Figure 11-1.

For a given beam-column joint which should be retrofitted beacause the equation (11-1) could not be satisfied or because, the strength of the connection does not satifies the requirements of the global seismic assessment of the structure, the parameters of the retrofit intervention, i.e., choice of the haunch geometry (length, L_h, and inclination, α) and anchorage (anchor type and group arrangement), should be assumed as preliminary step (Step 0). The lower and upper bound of the tensile and compressive stiffness can now be calculated (Step 1). The form of the curves schematically sketched in the diagrams of Step 2 depends on the as-built joint and haunch parameters. If both $K_{h,min}$ and $K_{h,max}$ correspond with the values β_{min} and β_{max} in the upper, and flatter, part of the K_h-β curve, the design of the retrofit is less sensitive to the variability of the stiffness of the anchorage. Alternatively, the verifications can be carried out using a single average value, β_m. Steps 3, 4 and 5 deal with the conditions which need to be fulfilled, i.e., shear action in the joints panel smaller than the avaiable resistance (Step 3), verification of the anchorage resistance (Step 4) and verification that the beam flexural yielding is the smallest resistance of the system and the shear failure of beam and column as well as column flexural yielding are avoided (Step 5). If one or more of these verifications is not satisfied new design parameters (Step 0) need to be chosen.

Further recommendations complementary to the design procedure described in Chapter 8 are discussed in the following sections.

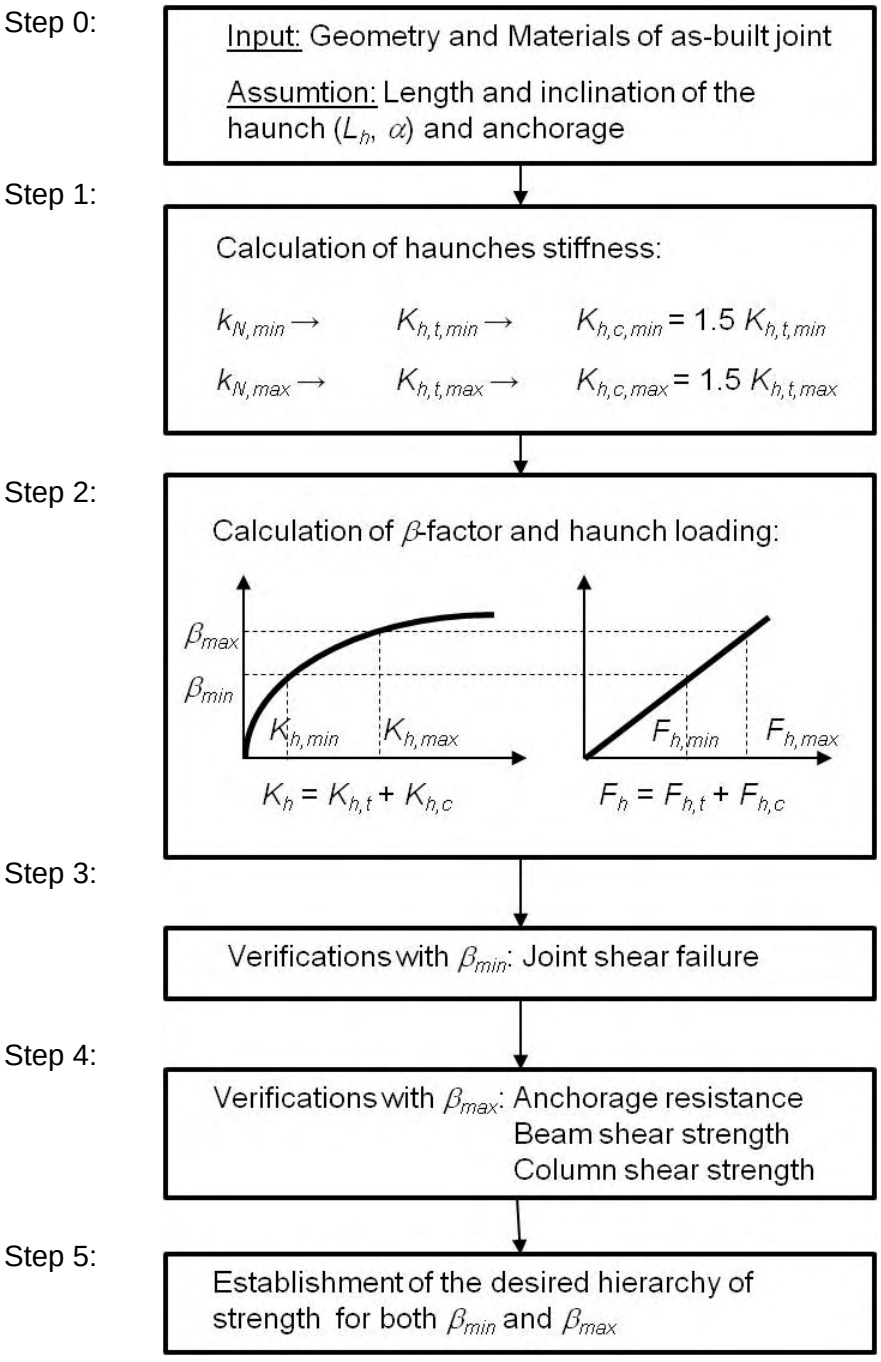

Assessment of as-built joint: Chapters 6 and 7, Appendix D as well as Section 11.2.1

Assumption of $k_{N,min}$ and $k_{N,max}$: Sections 8.2.2.1 and 11.2.2

Calculation of $K_{h,t}$ and $K_{h,c}$: Section 8.2.2, Eq. (8-13a) and Section 10.4.2

Calculation of β-factor: Section 8.2.1 and 11.2.3

Calculation of $F_{h,t}$ and $F_{h,c}$: Section 8.2.4, Eqs. (8-20) and (8-21)

Verification of joint shear resistance β_{min}: Sections 8.2 and 11.2.4

Verification of the anchorage with β_{max} (i.e., with $F_{h,t,max}$: and $F_{h,c,max}$): Sections 8.2.5 and 11.2.5.
Verification of beam and column shear strength

Verification of the desired hierarchy of strength: Sections 8.1, 8.2, 11.2.6 and Appendix F

Figure 11-1: Flowchart for the design of the HRS using post-installed anchors

11.2.1 Step 0: Assessment of the as-built beam-column joint and choice of the retrofit parameters

For the assessment of the as-built beam-column joints the flexural and shear resistance of beam and column can be evaluated according to the relevant standards. For the estimation of the joint shear strength, it is recommended to limit the principle tensile stress in the joint panel according to Equations (11-6) and (11-7a,b) validated in this study (see Chapters 5 and 6). The corresponding shear forces in beam and column can be evaluated using

Equations (7-3) to (7-7). The calculations of the hierarchy of strength of the as-built joints tested in this research work are shown in Appendix D.

1st joint shear cracking:

$$\frac{p_t}{\sqrt{f_c}} = \left[k_0 + k_1 \left(2 - \frac{h_b}{h_c} \right) \right] \cdot \alpha_{setup} \cdot \alpha_{5\%} \qquad (11\text{-}6)$$

Ultimate limit state:

$$\frac{p_t}{\sqrt{f_c}} = k_0 + k_1 \left(2 - \frac{h_b}{h_c} \right) + \left[\frac{(n_{c,0} - n_c)}{100} \cdot k_2 \cdot \rho_b \right] \cdot \alpha_y \cdot \alpha_{setup} \cdot \alpha_{5\%} \quad \text{for } n_c \le n_{c,0} \qquad (11\text{-}7a)$$

$$\frac{p_t}{\sqrt{f_c}} = \left[k_0 + k_1 \left(2 - \frac{h_b}{h_c} \right) \right] \cdot \alpha_{setup} \cdot \alpha_{5\%} \quad \text{for } n_c > n_{c,0} \qquad (11\text{-}7b)$$

with:

α_{setup} = 0.85

k_0, k_1, k_2, $\alpha_{5\%}$ according to Table 11-3

Table 11-3: Empirical coefficients of the assessment model and statistical evaluation

Anchorage Type	k_0 [-]	k_1 [-]	k_2 [-]	$n_{c,0}$ [%]	CV [a] [%]	$\alpha_{5\%}$ [a] [-]
1: def. bars, 90° bent in	0.15	0.30	1.2	20	18.0	0.7
2: def. bars, 90° bent out	0.20	0.00	0.9	10		
3: def bars, U-shaped	0.15	0.30	1.2	20		
4: def bars, 180° big hooks	0.15	0.30	1.2	20		
5: def bars, straight	0.15	0.30	1.2	20		
6: smooth bars, 180° hooks	0.10	0.30	1.2	10		

11.2.2 Step 1: Calculation of haunch stiffness

The evaluation of the tensile and compressive stiffness of the haunches constitutes a great source of uncertainty. A reliable analytical formulation cannot be proposed at this stage, because of the high scattering of the stiffness of post-installed anchors and of the conditions during the loading history of the retrofitted beam-column joint concerning the shear loading of the anchors. Therefore, the evaluation of the upper and lower bounds of the tensile stiffness of the anchors is proposed ($k_{N,max}$, $k_{N,min}$) as explained in the flow chart in Figure 11-1. The tensile stiffness of the haunch, $K_{h,t}$, can be determined using Equation (8-13a).

On the basis of the experimental and numerical investigations, it is suggested to assume $K_{h,c} = 1.5\, K_{h,t}$. The experimental and the FE analyses have shown that this ratio can be expected to occur in the case of a well-functioning retrofit for realistic values of shear and tensile stiffness of the anchors, material properties and geometry of beam-column connections similar to the tested specimens (see Chapter 9). This assumption allows the determination of the effectiveness of the retrofit solution (i.e., determination of the design stiffness of the haunches) starting just from the geometry of the haunch and the axial stiffness of the adopted anchor, k_N. This simplification is required due to the impossibility to make a reliable estimation of the shear stiffness of the anchorage, which is influenced by friction and mechanical interlocking between steel plates and concrete surfaces.

If epoxy based bonded anchors, similar to the anchors used in this study (M12 with h_{ef} = 125 ~ 150 mm) are employed, $k_{N,m}$ = 35 kN/mm can be assumed (instead of $k_{N,min}$ and $k_{N,max}$). These values are based on the tests presented in Chapter 9 and refer to realistic cyclic loading patterns of the anchorage and deformation of base material (i.e., cracking of beam and column).

In the absence of specific investigations, as a first approximation, the anchors stiffness can be taken from the relevant approval. If ETAs are used the following values can be used (Eqs. (11-8a,b):

$$k_{N,\max} = N/\delta_{N0} \text{ with } N \text{ in [kN] and } \delta_{N0} \text{ in [mm] (cracked concrete, short term loading)} \quad (11\text{-}8a)$$

$$k_{N,\min} = k_{N,\max}/4 \quad (11\text{-}8b)$$

As briefly discussed in Section 8.2.2.3 and experimentally shown (see Table 9-6), anchor types such as expansion anchors, characterised by low axial stiffness in cracked concrete, my exhibit significant higher stiffness under cyclic loading. To account for this anchor behaviour Equation (11-8c) is proposed, as a first indication, for bolt type expansion anchors:

$$k_{N,\max} = N/\delta_{N0} \text{ with } N \text{ in [kN] and } \delta_{N0} \text{ in [mm] evaluated in uncracked concrete} \quad (11\text{-}8c)$$

The stiffness values for prequalified anchors according to *ETAG 001 (1997)* and *AC 193 (ICC-ES, 2010)* are generally not comparable. The indications contained in this study are, therefore, valid only for ETAs.

11.2.3 Step 2: Calculation of β-factor and actions on the anchorages

The experimental (Chapter 9) and numerical (Chapter 10) investigations confirmed the validity of the recommendations of Section 8.2.1. According to the analysis of the FE simulations discussed in Section 10.4.1, $L_{eff} = L' - 100$ can be conservatively assumed for the calculation of the β-factor in the case of haunch geometries similar to those used in the study. The Equation (8-11) for the calculation of the factor β is repeated below for reason of clarity.

$$\beta = \frac{b}{a}\left(\frac{6Lh_b + 3ah_b + 6bL + 4ab + \frac{2I_b b^3}{I_c a H_c} + \frac{3I_b H L_b b^3}{2I_c a^2 H_c} + \frac{3I_b h_c H L_b b^2}{I_c a^2 H_c}}{3h_b + 6bh_b + 4b^2 + \underline{\underline{\frac{12E_c I_b}{(K_{h,c} + K_{h,t})a\cos^2\alpha}}} + \frac{6I_b b^2}{a^2 A_c} + \frac{2I_b h_c b^2}{I_c a} + \frac{3I_b h_c b^2}{I_c a^2} + \frac{3I_b h_c^2 b^3}{2I_c a^3}} \right) \quad (11\text{-}9)$$

with:

$K_{h,c}$ and $K_{h,t}$ in [N/mm]

a, b = effective projected length of the haunches on beam and column, respectively
= L_{eff} if the inclination angle of the haunches is α = 45°

L = $L_b - h_c - 2a$ (h_c = height of the cross section of the column)

H = $H_c - h_b - 2b$ (h_b = height of the cross section of the beam)

I_b, I_c = effective inertial moment of beam and column, respectively

11.2.4 Step 3: Verification of joint shear strength

For the design of the HRS the β-factor should be calculated according Equation (8-11) after the assumption of the haunch geometry and the anchorage.

After the calculation of β_{min} with $k_{N,min}$ (or alternatively β_m with $k_{N,m}$) the column shear corresponding to the joint shear strength can be determined with Equation (11-10).

$$V_{c,joint} = \frac{A_j \sqrt{p_t^2 - \left(p_t N_c / A_c\right)}}{\left(1 - \frac{\beta_{\min} H_c}{L_b \tan\alpha} - \frac{H_c \left(L_n - 2L'\right)}{j_b L_b}\left(1 + \frac{\left(1-\beta_{\min}\right)L'}{L}\right)\right)} \tag{11-10}$$

p_t = principle tensile stress in the joint panel corresponding to initial joint cracking calculated according to the model proposed in Chapter 6 (Equations (7-3) to (7-7)).

L_n = L_b-h_c

The column shear corresponding to the joint shear failure ($V_{c,joint}$) should satisify the Equation (11-1), i.e., it should be larger than the beam flexural hinging (ductile failure of the beam-column connection).

In general, it should be assured that the joint remains uncracked following the provisions of Section 11.2.1. However, some of the tests presented in Chapter 9 have shown that the joint shear cracking does not necessarily have a negative effect on the overall behaviour of the retrofitted joint as long as the anchorage of the haunches is fully efficient.

11.2.5 Step 4: Evaluation of the strength of the anchorage

The verification of the anchorage loaded in tension and shear should be carried out using the Equations (11-11a,b) and assuming the values $K_{N,max}$ and β_{max} (or alternatively $k_{N,m}$ and β_m). The design tensile and compressive forces in the diagonal haunches ($F_{Sd,h,t}$ and $F_{Sd,h,c}$, respectively) calculated with the Equations (11-11a,b) are related to the actions in the anchorage according to the Equation (11-11d) to (11-11g).

$$F_{Sd,h,t} = V_{Sd} \cdot \beta_{\max} \cdot \tan\alpha \frac{K_{h,t,\max}}{K_{h,c,\max} + K_{h,t,\max}} \tag{11-11a}$$

$$F_{Sd,h,c} = V_{Sd} \cdot \beta_{\max} \frac{K_{h,c,\max}}{K_{h,c,\max} + K_{h,t,\max}} \tag{11-11b}$$

with:

V_{Sd} = design shear force in the beam corresponding to the yielding moment in the target beam section after retrofitting, $M_{bm,y}$

= $V_{bm,y} \cdot CF_{KLi} \cdot \gamma_{eq}$

$V_{bm,y}$ = $M_{bm,y} / (L_b/2 - L')$ (11-11c)

$F_{Sd,h,t}$ = design tensile action in the diagonal haunch

$F_{Sd,h,c}$ = design compressive action in the diagonal haunch

The following forces act on the anchorage:

$N_{Sd,comp}$ = 0 (11-11d)

$V_{Sd,comp}$ = $F_{Sd,h,c} \cdot \cos\alpha$ (see also Section 11.2.5.1) (11-11e)

$N_{Sd,tens} = F_{Sd,h,t} \cdot \sin\alpha$ (11-11f)

$V_{Sd,tens} = F_{Sd,h,t} \cdot \cos\alpha$ (see also Section11.2.5.2) (11-11g)

The strength of the anchorage can be evaluated according to the *Design of anchorages in Concrete*" (*fib, 2011*) and the recommendations explained in Section 8.2.5. The applicability of such approach was confirmed by the experimental investigations (see Figure 9-30 and Figure 9-31 in Section 9.4.8). For all verifications the concrete should be conservatively considered as cracked.

11.2.5.1 Compressed anchorage

The anchorage of the compressed haunch should be designed to carry the shear component of the axial force of the haunch. Assuming $\mu_f = 0.4$ and $k_f = 5$ kN/mm^3 and $k_V = 20$ kN/mm and considering anchor plates with similar dimensions and inclination ($\alpha = 45°$) as in the tests presented in Chapter 9, the anchors should carry approximately 25-40% of the shear load acting in the diagonal haunch, $V_{Sd,comp}$. The rest of $V_{Sd,comp}$ is taken up by friction. For increasing values of the angle α of the haunces the friction contribution increases. The shear force to be resisted the anchorage, $V_{Rd,comp}$ is 50% of the shear action $V_{Sd,comp}$ according to Equation (11-12) for the verification of the compressed ancorage is generally conservative for $\alpha = 45°$.

$V_{Rd} \geq 0{,}5\ V_{Sd,comp}$ (11-12)

11.2.5.2 Tensioned anchorage

The anchorage of the tensioned haunch has to be designed to carry the tensile component of the axial force of the haunch. The FE analyses suggested that the anchors may have to carry shear load also when the anchorage is loaded in tension in a fraction of 60% to 90% of the tension loading (see Section 10.2.2). It is recommended to considered fraction of 75% of the shear load to the taken up by the anchorage in the design, if no reliable experimental results are available to support another assumption. As shown in Figure 2-31 and Figure 2-32, anchors loaded in combined tension and shear in cracked concrete are less sensitive to the negative effect of cracked concrete. For bonded anchors the negative effect of cracks is completely counterbalanced and the tensile load carrying capacity of the case of uncracked concrete can be reached (Figure 2-31a and Figure 2-32d). For expansion and undercut anchors this effect is less evident and only a negligible increase of approximately 10% can be obtained (Figure 2-31b and Figure 2-32a,b,c). For concrete screws no tests are known to be available, but it can be expected that they behave similarly to bonded anchors, because the load carrying mechanism is also distributed on the entire embedment depth. On the basis of the above considerations based on the experimental results of *Dieterle et al. (1990), Genesio (2007a)*, it may be conservative to carry out the following verifications to consider the interaction between tension and shear forces (Eq. (11-13) for bonded anchors and (11-14) for all other types of anchors).

$$\frac{N_{Rd}}{N_{Sd,tens}} + \frac{V_{Rd}}{0.75 \cdot V_{Sd,tens}} \leq 1.2 \qquad \text{(valid for bonded anchors only)} \qquad (11\text{-}13)$$

$$\frac{N_{Rd}}{N_{Sd,tens}} + \frac{V_{Rd}}{0.75 \cdot V_{Sd,tens}} \leq 1.0 \qquad \text{(valid for other anchor types)} \qquad (11\text{-}14)$$

with:

11.2.5.3 Anchorage vs. Plastic hinge

All the relevant design provisions (e.g., *fib, 2011*; *ACI 318-08 Appendix D*) cover the design of anchorage only if they a located outside of plastic hinges.

In most of the cases, it is not possible to exclude that the most external row of anchors is not located in the plastic hinge and hence its contribution to the global resistance of the anchorage should be conservatively neglected. As shown in the exemplary calculations for the specimens 2DG1 and JT1-2 in Appendix F, this assumption influences significantly the failure modes related to the number of anchors, *n* (i.e., steel failure in tension and shear and pullout failure), but it reduces only slightly (< 10% for the specimen 2DG1 and < 5% for the specimens JT1-2, JT1-3, JT1-4, JT1-5 and JT1-6, see Appendix F) the resistance to failure modes proportional to the projection of the concrete breakout body (i.e., concrete failure modes under tension and shear). Furthermore, if a smaller amount of anchors are considered to the effective, the stiffness $K_{h,t}$ decreases and this implies a reduction of the strength demand in the anchorage. Therefore, in most of the cases the verification of the retrofitted joint with most external row of anchors located in the plastic hinge is more decisive for the joint protection (β_{min}) than for the anchorage resistance as well as beam and column shear resistance (β_{max}).

Tests on beam-column joints having plain round bar reinforcement carried out in as-built as well as in retrofitted configurations within this research project and in other works (*Pampanin et al. 2002*; *Hertanto, 2005*; *Kam, 2011* and *Akgüzel, 2011*) have shown that flexural cracks in beams and columns usually occur in the cross section corresponding with the location of stirrups. The tests 2DG1 and 2DG2 indicated that the presence of bonded anchors generally does not change the location of the cracks (Figure 11-2). Therefore, if the last row of anchors is located at least 50 mm from the first stirrup after the end of the anchor plate, it may be assumed that it is active also after the formation of the plastic hinge.

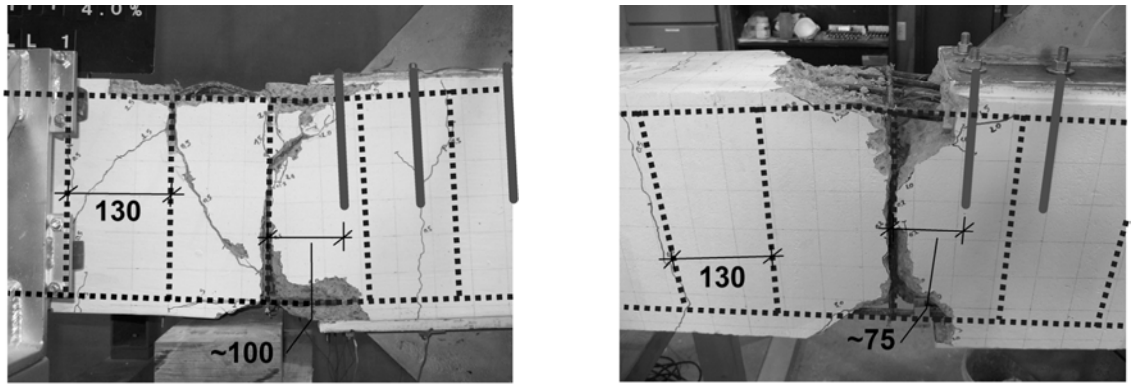

a) Test 2DG1 b) Test 2DG2

Figure 11-2: Plastic hinge in specimens with plain round bars (measures in mm)

If a weakening strategy is adopted as for the specimen JT1-4 (see Section 9.4.5), it may be assumed with reasonable safety that the plastic hinge forms far enough away from the anchors.

11.2.6 Step 5: Establishment of new hierarchy of strength

After determining the β-factor (i.e., β_{min} *and* β_{max}) and the verifying the strength of the anchorage, the new hierarchy of strength of the beam-column connection (see Figure 8-4) can be calculated using the formulas contained in Appendices E and F. A suitable hierarchy of strength is established if Equation (11-15) is satisfied, i.e., if the beam flexural hinging occurs at a lower load values than all britte failure modes. Note that while the joint shear strength should be calculated using β_{min}, the other brittle failure modes (column and beam shear failure) shall be determined using β_{max}.

$$M_{c,beam-hinge} \leq \min\left(\frac{M_{c,joint-shear}}{\gamma_1};\frac{M_{c,column-shear}}{\gamma_2};\frac{M_{c,column-hinge}}{\gamma_3};\frac{M_{c,beam-shear}}{\gamma_4}\right) \qquad (11\text{-}15)$$

The factors γ_i should be not smaller than 1.0, since they indicate the probability to avoid an undesired brittle plastic mechanism and should be largest for the most undesirable mechanism (e.g., column shear failure) and where uncertainty in the calculation is the highest, i.e., high variability and/or lack of information about the material properties.

The calculations of the hierarchy of strength of the retrofitted joints tested in this research work are shown in Appendix F.

11.2.7 Sources of uncertainness and recommendations

11.2.7.1 Effective inertial moments of beam and column

As explained in Section 8.1 the effective inertial moments of beam and column should be inserted in Equation (8-11) for the calculation of the β-factor. They are usually equal to a fraction of the theoretical values (coefficients θ_b and θ_c in Equations (8-9a,b)). θ_b and θ_c decrease with increasing cracking of the concrete members and the β-factor increases for decreasing values. In the assessment procedure of the retrofitted specimen it is suggested to use values of θ_b corresponding to the beam yielding. If no reliable data from analysis is available θ_c should be conservatively assumed close to 1.0, i.e., as assumed in *Paulay & Priestley (1992)* considering the largest expected axial load.

11.2.7.2 Protection of the column

The failure of the column is generally the most undesirable plastic mechanism of a beam-column connection. Therefore, its shear and flexural resistance should be the higher that the strength of the other elements (i.e., beam and joint panel). Additionally, it should be assured that a failure mode of the anchorage, which can reduce the strength of the column is excluded, i.e., concrete cone failure in tension (see test JT5-1, in Section 9.4.6) and concrete pryout or concrete edge failure in shear. If possible, it should be always assured that the anchorage of the haunches on the column sides have strengths larger than the anchorages on the beam.

11.2.7.3 Shear failure of the beam

During the testing of beam-column joints the vertical static loads acting on the beam are usually neglected. Their presence could have a negative effect on the plastic hinge, because of the lack of adequate shear reinforcement typical of substandard beam-column connections. To avoid an undesirable shear failure of the beam the geometry of the bottom haunch could be modified. The steel plate of the bottom anchorage could be extended to take up the vertical loads of the beam after the formation of the plastic hinge (see Figure 11-3).

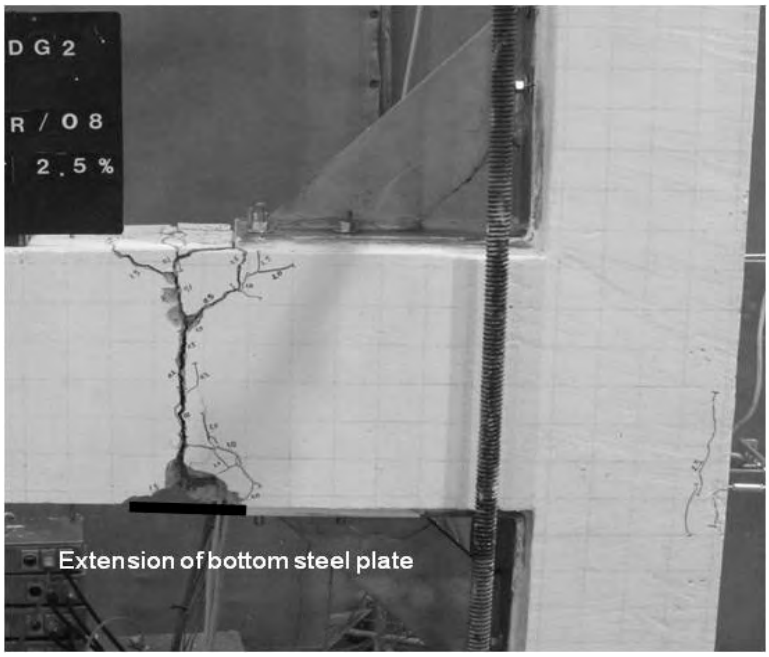

Figure 11-3: Possible constructive solution to allow the beam to carry the veritical loads after the formation of the plastic hinge by extending the bottom steel plate

11.2.7.4 Positioning of the anchorage to limit the eccentricity

Centring the barycentre of the anchorage in respect to the steel diagonal, the eccentricity, e_N, can be limited. Therefore, $\psi_{ec,N}$ can be approximately equal to 0.9 (see Sections 8.2.5.1 and 9.4.9). The factor $\psi_{ec,N}$ should be conservatively reduced to 0.8 in the evaluation of anchorage strength after failure of the most external row of anchors.

11.2.7.5 Choice of anchor type

The choice of the anchor type to be used in this retrofit technique plays a central role in the design of this retrofit solution. The experimental investigations carried out in this study have shown the good behaviour of bonded anchors, while the applicability of mechanical anchors should be further evaluated. However, stiffness and load carrying capacity should be sufficient evaluation parameters.

11.3 Verification of the analytical model

The analytical model for the design of the haunch retrofit solution schematically summarised in Figure 11-1 was verified analysing the experimental tests described in Chapter 9. In Figure 9-30 and Figure 9-31 the calculation of the experimental tests using the measured stiffness was shown. In Table 11-4 the comparison between experimental observations and analytical

prediction using the model schematically presented in the flow chart in Figure 11-1 is shown. For these calculations, the values of the material properties measured in the tests were used (i.e., average values). The detailed calculations are shown in Appendix F.

Table 11-4: Comparison between experimental tests and analytical model (global behaviour)

	Failure mode		$V_{c,max}$ [kN]	
Test	**Exp.**	**Calc.**	**Exp.** [a)]	**Calc.**
2DG1	B	B	24.7 / 25.9	24.7
2DG2	B	B	21.8 / 21.3	21.7
JT1-2	B	B + JS	72.3 / 62.8	66.7
JT1-3	B + JS	B + JS	65.1 / 70.5	66.7
JT1-4	B	B	59.4 / 51.1	49.5
JT1-5	JS	JS	47.2 / 39.4	- [b)]
JT1-6	B +JS	B + JS	67.6 / -	66.7

[a)] Positive / negative loading direction; [b)] The premature failure of the anchorage could not be analytically calculated (see Section 9.4.6); B = Beam hinging; JS = Joint shear cracking

In Table 11-5 the verification of the anchorage in the form of the ratio between acting axial load and tensile resistance of the anchorage is shown. Values of the ratio smaller than1.0 or 1.2 in the case of combined tension and shear for bond anchors indicate that the verification is fulfilled.

The PSF proposed in Section 11.1.2 for the calculation of anchorage strength were applied. It can be observed for the specimens were the anchorage did not fail (2DG1, 2DG2, JT1-4 and JT1-6) the ratio S/R (Action/Resistance) is between 1.0 and 1.6, while for the other specimens the ratio was larger than 2.5 (with the exception of the specimen JT1-5).

Table 11-5: Comparison between experimental tests and analytical model in terms of ratio anchorage loading / anchorage resistance

Test specimen	**Experimental observation: anchorage at the end of the test**	**Ratios between actions measured in the tests and characteristic design resistances** [a)]			
		Tension	**Shear (Tensioned haunch)**	**Combined tension and shear (tensioned haunch)**	**Shear (Compressed haunch)**
2DG1	No failure	0.77	0.29	**1.06**	**0.44**
2DG2	No failure	0.71	0.24	**0.96**	**0.55**
JT1-2	No failure	2.16	0.81	**2.97**	**0.86**
JT1-3	Partial failure [b)]	2.02	0.76	**2.78**	**0.86**
JT1-4	No failure	1.19	0.45	**1.64**	**0.63**
JT1-5	Failure	1.54	0.55	**2.09**	**0.84**
JT1-6	Partial failure	0.96	0.35	**1.30**	**0.52**

[a)] $\gamma_c = CF_{KL3} = 1.0$ (KL3); $\gamma_{inst} = 1.0$; $\gamma_{CV} = 1.0$; $\gamma_{eq} = 1.0$

[b)] Partial failure occurred in negative loading direction only

The results of the calculation of the tested specimens using the proposed design model and PSF shown in Table 11-5 highlighted that the model yields conservative results in respect to the experimental measurements of the tensile strength of the anchorage obtained. Two main uncertainess in the evaluation of the results shown in Table 11-5 should be kept in mind:

- the verification of anchor groups loaded by combined tension and shear under seismic loads (cyclic, dynamic loads) and conditions (opening and closing cracks in concrete) has not been extensively investigated yet. Therefore, the proposed verifications (Eq. (11-13) for bonded anchors and (11-14) for all other types of anchors) should to be considered a first approximation; and

- the assumption that the anchorage has to take up approximately 75% of the shear force of the tensioned haunch is based on the results of the numerical simulations only and no experimental confirmation is available yet.

As observed by *Fardis (2009)*, the *EC-8 (2005)* is the first of 58 EN-Eurocodes that deals with existing structures and it can be seen as an experiment. The harmonisation of assessment of existing structures and design of new elements, in this case anchorage according to *fib* (2011), was not deeply investigated yet.

12 SUMMARY AND OPEN QUESTIONS

12.1 Seismic assessment of beam-column joints

12.1.1 Summary

In the present study a shear strength model for substandard 2D RC exterior beam-column joints was developed. The model constitutes a refinement of the Priestley-Pampanin model (*Priestley, 1997*; *Pampanin et al. 2003*) to include the contribution of several parameters such as geometrical aspect ratio, h_b/h_c, and the beam reinforcement ratio, ρ_b, on the calculation of the joint shear strength. Furthermore, the effect of the column axial load, n_c, was related to different failure mechanisms (cracking of the tensile tie and crushing of the compressive strut), giving a physically plausible answer to one of the still open questions in the assessment of the joint shear strength.

The assessment model was developed on the basis of a large parametric study using the 3D non-linear FE code MASA. The modelling technique was verified on a set of experimental tests carried out in this study. The proposed model includes the definition of two limit states: initial joint shear cracking and ultimate strength, and it provides a quantification of the related joint shear deformation. The mechanical plausibility of the proposed model was verified analysing the stress and strain distribution in the joint panel. Its applicability in engineering practice was validated by comparing the model's joint shear strength predictions with a large experimental database.

To achieve a conservative seismic assessment in the framework of Capacity Assessment, the shear strength of the joint should be compared to the other possible failure modes of the beam-column connection. With this aim in mind, the procedure of establishment of internal hierarchy of strength can be used.

12.1.2 Open questions

This work highlighted the need of more research to further develop and verify the proposed shear strength model:

- A number of observations (i.e., joint shear degradation and effect of test setup), which are based on FE analyses only, need to be experimentally verified;
- The joint shear strength model takes into account the influence of beam and column reinforcement, but the effect of specific reinforcement configurations needs to be investigated, e.g., Multiple layer of reinforcement in beam and column reinforcement crossing the joint panel;
- Further experimental investigations and FE analyses are needed to extend the validity of the proposed model to different types of exterior joints that can realistically

represent conditions which occur in moment resisting frames more complex than simple 2D joints, i.e., effect of transverse beam, floor, behaviour of 3D corner joints, roof joint and interior joint in 2D and 3D configuration, aiming to assess them using a similar approach;

- The possibility to extend the model to “well designed” joints, i.e., containing different configurations of transverse reinforcement in the core should be evaluated;
- The influence of different lateral loading protocols (2D and 3D) and loading rate (i.e., dynamic loading) should be evaluated; and
- The results obtained on beam-column joints should be extended to a larger structural level, i.e., testing of RC frame to evaluate the effect of the joint behaviour on the global structural behaviour. Tests on 2D frames are ongoing in the framework of a subsequent research project (*Genesio et al., 2010b*).

12.2 Haunch Retrofit Solution using post-installed anchors

12.2.1 Summary

The “Haunch Retrofit Solution” (HRS) proposed by *Pampanin et al. (2006)* was optimised by connecting the diagonal haunch to both beam and column with post-installed anchors instead of using rods passing through floors and external walls of the building. The design method was accordingly modified to take into account the load-displacement behaviour of these anchors. The proposed solution was experimentally validated. Additionally, FE simulations were carried out to further verify the design model and better understand the experimental observations. Finally, a design model using the partial safety factors indicated by *EC8-3 (2005)* and *fib (2011)* was proposed and discussed.

12.2.2 Open questions

To allow the use of this seismic retrofit technique for practical applications further investigations are needed:

- The effect of application of diagonal haunches on different types of joints (e.g., corner, interior and roof joints) should be evaluated and, if necessary, the design method should be accordingly modified;
- The investigations of the proposed retrofit solution highlighted the need of a displacement oriented design of anchorages as amendment to the force oriented design methods available in the literature;
- Further experimental investigations are needed to better understand the interface problem in terms of shear stiffness between the steel fixtures of the anchorage and the concrete surface of beam and column;
- Experimental testing and numerical investigations on RC frames should be carried out to evaluate the effect of the proposed retrofit solution on the seismic response of full structures and to determine the need of retrofitting in terms of type and amount of joints that have to be considered for an optimal performance. Preliminary numerical investigations are contained in *Pampanin & Christopoulos (2003)*. Experimental and numerical investigations at full scale are ongoing as a continuation of this research project (*Genesio et al.*, *2010b*);

ZUSAMMENFASSUNG (GERMAN SUMMARY)

Kap. 1: Einleitung

Nach einer kurzen Einleitung über die historische Entwicklung der Kenntnisse der Menschheit über Erdbeben und erdbebensicheres Bauen wird in diesem Kapitel die Begründung dieses Forschungsvorhabens vorgestellt. Die Struktur und Gliederung der Arbeit werden außerdem dargestellt.

Kap. 2: Kenntnisstand: Analyse und Auswertung

In diesem Kapitel wird der zum Zeitpunkt der Untersuchungen vorhandene Kenntnisstand in den Bereichen, die relevant für dieses Forschungsvorhaben sind, vorgestellt und analysiert:

(1) seismisches Verhalten von zweidimensionalen (2D) Stahlbetonrahmenendknoten, die infolge der Ausbildung eines Schubmechanismus versagen;
(2) seismische Ertüchtigung von Stahlbetonrahmen und insbesondere Rahmenknoten;
(3) seismisches Verhalten von nachträglichen Befestigungsmitteln.

Im Teil (1) sind die wesentlichen Ergebnisse aus experimentellen Untersuchungen zusammengefasst, die weltweit im Laufe der letzten vier Jahrzehnte durchgeführt wurden. Diese Erkenntnisse wurden in einige Bemessungsmodelle eingearbeitet, aber es wurde noch kein Konsens in der Fachwelt gefunden. Die bisher vorgeschlagenen Bemessungsmodelle wurden präsentiert und verglichen. Um die Zielsetzung der seismischen Beurteilung von Stahlbetonrahmenknoten, die nicht nach den heutigen seismischen Bemessungsrichtlinien gebaut wurden, besser erfassen zu können, wurde die Entwicklung der Normen in den letzten fünfzig Jahren in einigen Ländern analysiert (USA, Japan, Neuseeland, Italien und Indien) und den Anforderungen der aktuellen seismisch orientierten Bemessungsrichtlinien gegenübergestellt.

Im Teil (2) wurden die Grundziele der seismischen Ertüchtigung von Bauwerken vorgestellt. Insbesondere wurden unterschiedliche Ertüchtigungsstrategien für Stahlbetonrahmenknoten analysiert, die im Laufe der letzten Jahrzehnte entwickelt wurden.

Im Teil (3) wurden einige Grundlagen des jetzigen Standes der Kenntnisse über das seismische Verhalten von nachträglichen Befestigungsmitteln kurz zusammengefasst. Mögliche Anwendungen von nachträglichen Befestigungsmitteln für seismische Ertüchtigungsmaßnahmen wurden als Beispiele vorgestellt.

Kap. 3: Experimente mit unverstärkten Rahmenknoten

Nach der Analyse der Versuche, die aus der Literatur zur Verfügung stehen, wurde der Bedarf nach weiteren experimentellen Untersuchungen festgestellt. Sechs Rahmenendknoten wurden getestet und so bemessen, dass die Knoten infolge eines Schubmechanismus versagt haben. Der Schwerpunkt der Untersuchungen wurde auf die folgenden Aspekte gelegt:

- Ermittlung des Knotenswiderstandes an zwei Grenzzuständen der Tragfähigkeit (erster Diagonalriss im Knotenbereich und Höchstlast);
- Messung der Knotenschubverzerrung;
- Vergleich der Schubtragfähigkeit von Knoten mit unterschiedlichen Verankerungsausführungen der Längsbewehrung des Riegels. Im Knotensbereich würde keine Schubbewehrung angeordnet.

Die meisten Modelle zur Berechnung der Knotensschubtragfähigkeit vernachlässigen i.d.R. den Einfluss von unterschiedlichen Verankerungsarten sowie den negativen Effekt der Anwendung von glatten Stäben. Darüber hinaus wird häufig die Tragfähigkeit von Knoten ohne Schubbewehrung überschätzt. Der Vergleich zwischen den experimentellen Ergebnissen und einigen analytischen Modellen zur Beurteilung der Schubtragfähigkeit von Rahmenknoten aus der Literatur zeigte, dass die meisten den Widerstand der getesteten Knoten deutlich überschätzten.

Das von *Priestley (1997)* und *Pampanin et al. (2003)* vorgeschlagene phänomenologische und semi-empirische Modell wurde für die Schätzung der Schubtragfähigkeit von Knoten ohne Schubbewehrung und unterschiedliche Bewehrungsausführungen entwickelt. Das Modell sieht vor, die Hauptzugspannungen im Knotenbereich statt der horizontalen Schubspannungen (wie die meisten Modelle) als Schädigungsindikator (Auftreten von Schubriss) im Knotensbereich zu nutzen. Damit wird der Einfluss der Normalkraft in der Stütze durch die Mohr'sche Theorie automatisch berücksichtigt. Das *Priestley-Pampanin* Modell zeigte eine brauchbare Übereinstimmung mit den durchgeführten Versuchen.

Folgende Schlussfolgerungen wurden anhand der experimentellen Untersuchungen gezogen:

- Rahmenknoten mit Verankerung der Riegelbewehrung im Knotenbereich anders als Typ 1 wiesen eine geringere Schubtragfähigkeit auf;
- die Knotenschubverzerrung, γ_j, wurde nur geringfügig von der Ausführung der Bewehrung beeinflusst; bei Entstehung des ersten Schubrisses, $\gamma_{j,crack}$ = 0.001 – 0.002 rad; bei Höchstlast, $\gamma_{j,peak}$ = 0.005 – 0.015 rad;
- die gesamte plastische Verformung eines Rahmenknotens tritt zu ca. 10%, 25% und 40% bei einer bezogenen Verschiebung von 1.0%, 2.0% und 3.5% im Knotenbereich auf;
- der Versuch JT1-5 zeigte, dass die Ausbildung eines duktilen plastischen Gelenkes im Balken nicht möglich ist, wenn der Knotenbereich bereits gerissen ist;
- das Bemessungsmodell *Priestley-Pampanin* kann die Knotenschubtragfähigkeit von Verbindungen ohne Schubbewehrung im Knotenbereich realistisch abschätzen.

Allerdings sollte der Einfluss von weiteren Parametern wie z.B. dem Schlankheitsgrad des Knotens berücksichtigt werden, die als Verhältnis h_b/h_c (Höhe des Riegelquerschnittes / Höhe des Stützenquerschnittes) ausgedrückt werden kann.

Kap. 4: FE Programm, Modellierung und Analysis

Das am Institut für Werkstoffe im Bauwesen der Universität Stuttgart entwickelte Finite Element (FE) Programm MASA wurde für die numerische Simulation des Schubverhaltens von Stahlbetonrahmenknoten eingesetzt. Für die Modellierung des Betons und die Erfassung von Rissentstehungs- und Schädigungsvorgänge wurde das „Microplane“ Modell verwendet. Die Bewehrung wurde mit eindimensionalen (1D) Stabelementen modelliert. Das Verbund-Schlupfverhalten zwischen Bewehrung und Beton wurde mit Hilfe eines diskreten Verbundelementes simuliert. Damit konnten Knoten mit gerippten und glatten Bewehrungsstäben simuliert werden.

Es wurde gezeigt, dass das FE Modell in der Lage ist, das mechanische Fachwerkmodell realistisch nachzubilden, das zum Schubversagen von Rahmenknoten führt. Es wurde folgendes beobachtet:

- das Auftreten des ersten Diagonalrisses im Knotenbereich entspricht dem Versagen der Zugstrebe;
- die Höchstlast des Rahmenknotens entspricht dem Versagen der Druckstrebe, wobei diese bereits durch den Diagonalriss geschwächt war;
- nach dieser Erläuterung des Schubverhaltens des Knotens wird der Einfluss der Normalkraft in der Stütze, N_c, erklärt. Diese Druckspannung entlastet die Zugstrebe (höhere Versagenslast, beim höheren N_c), aber diese kann sich ungünstig auf die Höchstlast auswirken, so dass die Druckstrebe mit höherem N_c stärker belastet wird.

Es wurde zusätzlich gezeigt, dass das FE Modell den Effekt von unterschiedlichen Bewehrungsausführungen (glatte und gerippte Stäbe mit unterschiedlichen Endhaken) und plastischen Mechanismen (Knotenschubversagen und Ausbildung eines plastischen Gelenkes im Riegel) simulieren kann. Die Verifizierung des numerischen Modells erfolgte durch die Nachrechnung von Versuchen aus der Literatur und durch eigene Versuche.

Kap. 5: Schubtragfähigkeitsmodell, basiert auf FE Untersuchungen

Aus der Grundlage einer numerischen Parameterstudie wurde ein neues Schubtragfähigkeitsmodell für Stahlbetonrahmenendknoten entwickelt, das auf dem Grundprinzip des Modells *Priestley-Pampanin* basiert. Folgende Erkenntnisse wurden aus der FE Studie gewonnen:

- Eine Zunahme der Knotenschubtragfähigkeit proportional mit $\sqrt{f_c}$ wurde für beide Grenzzustände der Tragfähigkeit bestätigt.
- Die Hauptzugspannung, p_t, bei Entstehung des ersten Schubrisses im Knotenbereich bleibt mit zunehmender Normallast in der Stütze konstant.

- Für niedrige normalisierte Werte der Axiallast in der Stütze, n_c, ist ein Anstieg der Knotenschubtragfähigkeit nach der Entstehung des ersten Schubrisses möglich. Diese Widerstandszunahme ist bis zu einem kritischen Wert $n_{c,0}$ begrenzt. Für $n_c \geq n_{c,0}$ ist keine Steigerung der Schubtragfähigkeit des Knotens nach der Entstehung des ersten Schubrisses mehr möglich. $n_{c,0}$ hängt maßgeblich von der Ausführung der Endhaken der Bewehrung des Riegels ab.
- Der Längsbewehrungsgrad der Stütze, ρ_c, hat einen kleinen positiven Einfluss auf die Last bei Entstehung des ersten Risses, aber nicht auf die Höchstlast.
- Der Längsbewehrungsgrad des Riegels, ρ_b, hat keinen Einfluss auf die Last bei Entstehung des ersten Risses, aber mit zunehmendem ρ_b steigt die Höchstlast. Dieser Effekt nimmt mit steigender Axiallast n_c ab.
- Die Schlankheit des Knotens, h_b/h_c, hat einen sehr starken Einfluss auf deren Schubtragfähigkeit. Mit zunehmendem h_b/h_c nimmt die Tragfähigkeit bei beiden Grenzzuständen ab. Dieses Verhalten wurde für alle Knotenausführungen mit Ausnahme von Endhaken 90°nach außen gebogen (Typ 2) beobachtet. Knoten mit Verankerung der Längsbewehrung des Riegels des Typs 2 werden von diesem Parameter nicht beeinflusst, weil die Inklination des Schubrisses nicht der geometrischen Diagonale des Knotens, im Gegensatz zu den anderen Verankerungsarten, folgt.
- Der Einfluss des Fließens der Riegelbewehrung auf die Knotenschubtragfähigkeit wurde untersucht und eine Abnahme des Verhältnisses $p_t/\sqrt{f_c}$ mit zunehmender Krümmungsduktilität, μ_ϕ, nach dem Prinzip von *Park (1997)* festgestellt.
- Die FE Simulationen zeigten, dass die Knotenschubverzerrung, γ_j, nur von der Knotenschlankheit, h_b/h_c, und der Axiallast in der Stütze, N_c (bzw. n_c), beeinflusst wird.

Folgende Grenzzustände der Schubtragfähigkeit eines 2D Rahmenknotens wurden vorgeschlagen:

Entstehung des ersten Schubrisses im Knotenbereich:

$$\frac{p_t}{\sqrt{f_c}} = k_0 + k_1\left(2 - \frac{h_b}{h_c}\right) \tag{1}$$

Höchstlast:

$$\frac{p_t}{\sqrt{f_c}} = k_0 + k_1\left(2 - \frac{h_b}{h_c}\right) + \frac{\left(n_{c,0} - n_c\right)}{100} \cdot k_2 \cdot \rho_b \qquad \text{für } n_c \leq n_{c,0} \tag{2a}$$

$$\frac{p_t}{\sqrt{f_c}} = k_0 + k_1\left(2 - \frac{h_b}{h_c}\right) \qquad \text{für } n_c > n_{c,0} \tag{2b}$$

Die Koeffizienten k_0, k_1, k_2 und $n_{c,0}$ hängen von der Ausführung der Verankerung der Riegellängsbewehrung im Knotenbereich ab und sind in Tabelle 1 aufgelistet.

Falls das Auftreten von Fließen der Riegellängsbewehrung und $n_c \leq n_{c,0}$ erwartet wird, können folgende Gleichungen eingesetzt werden:

$$\frac{p_t}{\sqrt{f_c}} = k_0 + k_1\left(2 - \frac{h_b}{h_c}\right) + \left[\frac{\left(n_{c,0} - n_c\right)}{100} \cdot k_2 \cdot \rho_b\right] \cdot \alpha_y \quad \text{für } n_c \le n_{c,0} \tag{3a}$$

mit: $\alpha_y = 1 - \mu_\phi / 6$ (3b)

Kap. 6: Vergleich zwischen Modell und Versuchesergebnissen

Zur Verifizierung wurde das auf der FE Studie basiertes Schubtragfähigkeitsmodell mit einer Datenbank von Versuchen verglichen. Um die Ergebnisse der Versuchsdatenbank miteinander vergleichen zu können, wurde der Effekt von unterschiedlichen Versuchsaufbauten numerisch untersucht. Es wurde gezeigt, dass das vorgeschlagene Modell den Effekt der untersuchten Parameter mit ausreichender Genauigkeit erfassen kann. Zusätzlich erlaubte dieser Vergleich eine statistische Bewertung des Modells.

Des Weiteren wurde das Modell auf andere Ausführungen der Bewehrung in Rahmenendknoten erweitert, die in der Ingenieurpraxis der letzten Jahrzehnte eine breite Anwendung gefunden hatten. Dazu zählen gerade Verankerungen und die 180°-Umlenkung der Riegelbewehrung.

In Tabelle 1 sind die empirischen Koeffizienten für die Gleichungen (1) bis (3) und die statistischen Bewertungen (Variationskoeffizient und 5%-Fraktile) dargestellt.

Tabelle 1: Empirische Koeffizienten für die Beurteilungsmethode der Schubtragfähigkeit von Rahmenendknoten und statistische Bewertung

Verankerung (Typ)	k_0 [-]	k_1 [-]	k_2 [-]	$n_{c,0}$ [%]	Anzahl der Versuche	$\frac{\left(p_t/\sqrt{f_c}\right)_{Exp}}{\left(p_t/\sqrt{f_c}\right)_{Calc}}$		CV [a] [%]	$\alpha_{5\%}$ [a] [-]
						1. Riss	Höchstlast		
1	0.15	0.30	1.2	20	32 / 64	1.00	0.99	14.1 / 17.1	0.73 / 0.68
2	0.20	0.00	0.9	10	7 / 20	1.16	1.00	15.5 / 15.4	0.75 / 0.70
3	0.15	0.30	1.2	20	12 / 16	1.04	1.02	26.7 / 24.0	0.48 / 0.41
4	0.15	0.30	1.2	20	8 / 8	0.96	1.05	12.3 / 10.5	0.69 / 0.80
5	0.15	0.30	1.2	20	6 / 6	1.03	1.00	27.3 / 23.9	0.45 / 0.44
6	0.10	0.30	1.2	10	11 / 13	1.00	1.02	21.8 / 16.3	0.54 / 0.66
Gesamt	-	-	-	-	76 / 127	1.02	1.01	18.2 / 17.6	0.68 / 0.71

[a] Erster Schubriss / Höchstlast

Kap. 7: Seismische Beurteilung von Stahlbeton Rahmenendknoten

Die Beurteilung der Schubtragfähigkeit des Rahmenknotens wird als Teil eines Gesamtkonzeptes für die seismische Beurteilung von Stahlbetonrahmen betrachtet. Durch die Ermittlung von möglichen Versagensarten und von dazugehörigen Traglasten können die Tragfähigkeit und Duktilität eines Rahmenknotens ermittelt werden. Für eine bessere Übersichtlichkeit der so genannten „Widerstandshierarchie“ wurde eine grafische Darstellung durch ein Diagramm M_c (Biegemoment in dem Stützen/Knoten-Grenzquerschnitt) vs. N_c (Axiallast in der Stütze) von *Pampanin (2006)* vorgeschlagen (siehe Bild 1).

Vorschläge und Empfehlungen für eine sichere seismische Beurteilung von Stahlbetonrahmenendknoten sind in diesem Kapitel gemacht.

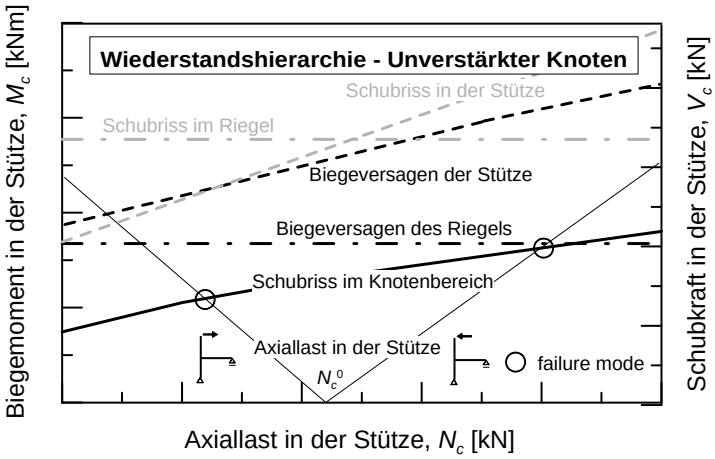

Bild 1: Schematische Darstellung der Widerstandshierarchie eines Rahmenknotens

Die seismische Beurteilung von Stahlbetonrahmenknoten, die nicht nach den modernen seismisch orientierten Bemessungsrichtlinien (keine Kapazitätsbemessung und mangelhafte Ausführung der Bewehrung) erfolgte, sollte den folgenden Prinzipien folgen:

- Für die Beurteilung von duktilen plastischen Mechanismen (z.B. Ausbildung eines Fliessgelenkes im Riegel) soll der Effekt der Überfestigkeit des Bewehrungsstahls berücksichtigt werden.
- Charakteristische Widerstandswerte sollten wiederum für die Versagensmechanismen mit geringem Verformungsvermögen (z.B. Biegeversagen der Stütze und Schubversagen von Riegel, Stütze oder Knoten) eingesetzt werden.
- Die Entstehung des ersten Schubrisses sollte als Grenzzustand der Knotenschubtragfähigkeit eingesetzt werden, um ein sprödes Versagen auszuschließen.
- Die Schubtragfähigkeiten von Riegel und Balken sollten nur aus dem Beitrag vom Beton hergeleitet werden, wenn der Abstand und die Ausführung der Schubbewehrung (Bügel) nicht den Anforderungen der modernsten Bemessungsrichtlinien entsprechen.

Kap. 8: Ertüchtigung mit Stahldiagonalen befestigt mit Dübeln: Konzept und Bemessung

Eine Ertüchtigungsmaßnahme, die an der University of Canterbury (Neuseeland) entwickelt wurde, die so genannte „Haunch Retrofit Solution“, wurde in dieser Studie berücksichtigt (Bild 2a). Diese Maßnahme zielt darauf ab, den Widerstand des Knotens zu erhöhen und die Widerstandshierarchie der Elemente des Knotens zu ändern, um ein sprödes Versagen zu vermeiden. Die Verstärkungsmaßnahme sieht vor, Diagonalen aus Stahl in den Ecken des Rahmenknotens einzusetzen. Bei entsprechender Bemessung der Stahldiagonalen werden die Kräfte teilweise um den Rahmenknoten herum geleitet, wodurch dieser geschützt wird und nicht versagen soll. Ziel ist die Schaffung einer Konstruktion mit einem duktilen

plastischen Mechanismus durch Auftreten eines plastischen Gelenkes im Rahmenriegel am Ende der Verstärkung. Dabei muss ausgeschlossen werden, dass die Verringerung der Schubschlankheit von Riegel und Stütze zu einer Überschreitung des Schubwiderstandes dieser Elemente führt.

Die Stahlplatten, die zur Aufnahme der Stahldiagonalen dienen, wurden mit durchgehenden Gewindestangen gegen den Stahlbetonrahmen gepresst, und so wurden die auftretenden Querkräfte schlupffrei durch Reibung in den Rahmenriegel eingeleitet (Bild 2a). In der Praxis wird eine Verankerung über Dübel gewünscht, weil dann der Aufwand für die Verstärkung reduziert wird und kein Bohren durch Decken und Wände erforderlich ist (Bild 2b).

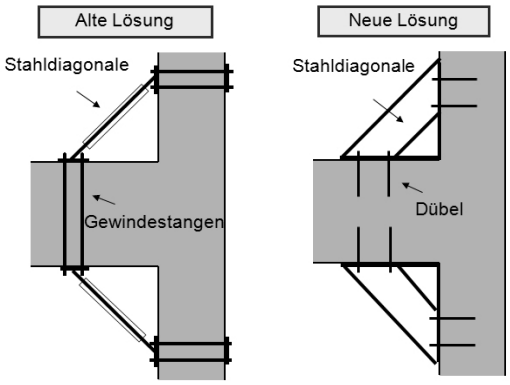

a) Alte Lösung b) Neue Lösung

Bild 2: Seismische Ertüchtigungsmaßnahme mit Stahldiagonalen

Diese neue Lösung wurde in diesem Kapitel theoretisch untersucht. Insbesondere wurden die folgenden Aspekte analysiert:

- Einbeziehung der Steifigkeit der Befestigung in der Ermittlung der Steifigkeit der Verstärkungsdiagonale, die maßgebend für die Wirksamkeit der Ertüchtigungsmaßnahme ist;
- Bemessung der Befestigung, die die Axiallasten der Stahldiagonalen in schmale Bauteile (Riegel und Stütze) und in unmittelbare Nähe eines plastischen Gelenkes (im Riegel) übertragen soll.

Die analytische Methode, die zur Bemessung dieser Ertüchtigungsmaßnahme an der University of Canterbury entwickelt wurde, wurde modifiziert, um die oben genannten Aspekte berücksichtigen zu können. Zur Wirksamkeit der Befestigung spielt neben der Steifigkeit der Befestigung die Reibung der gedruckten Ankerplatte auf Riegel- und Stützenoberfläche eine große Rolle.

Kap. 9: Experimentelle Verifizierung der Ertüchtigungsmaßnahme

Zur Verifizierung des im Kapitel 8 vorgeschlagenen Bemessungskonzeptes für die Ertüchtigung von Stahlbetonrahmenknoten durch zwei Stahldiagonalen, die mit Dübeln an das Bauteil befestigt sind, wurden sieben Versuche durchgeführt. Ziel der Versuche war:

- Überprüfung der Machbarkeit der vorgeschlagenen Ertüchtigungsmaßnahme;

- Bewertung des Effektes eines partiellen bzw. totalen Versagens der Befestigung;
- Untersuchung der Möglichkeit der Kombination der Ertüchtigungsmaßnahme mit einer Schwächung der Biegetragfähigkeit des Balkens, um eine Reduzierung der Belastung der Befestigung zur erzielen;
- Untersuchung der Anwendbarkeit von unterschiedlichen Dübeltypen;
- Messung der Kräfte in den Stahldiagonalen und Abschätzung der Zug- und Schubsteifigkeit der Befestigung, um die Gültigkeit des Bemessungsansatzes zur überprüfen.

In den durchgeführten Versuchen wurde folgendes beobachtet:

- Die Machbarkeit der Ertüchtigungslösung wurde mit den Versuchen 2DG1 und 2DG2 bestätigt. In diesen Versuchen wurde die Befestigung mit Verbunddübeln realisiert.
- Mit den Versuchen JT1-2 und JT1-3 wurde der Effekt einer Überlastung der Befestigung mit Verbunddübeln untersucht. Von insgesamt acht Befestigungen (vier pro Prüfkörper), versagte nur eine Befestigung, aber ohne einen totalen Verlust ihrer Tragfähigkeit. Der negative Effekt auf die Wirksamkeit der Verstärkung war nicht von großer Bedeutung. Sie Steifigkeit des Prüfkörpers nahm leicht ab, aber die Tragfähigkeit wurde nicht geschwächt.
- Weitere Versuche wurden durchgeführt, um die Anwendbarkeit von mechanischen Dübeln für die Befestigung der Stahldiagonale zu überprüfen. Die Anwendung von Betonschrauben (Versuch JT1-5) hat zu einem spröden Versagen der Befestigung und anschließendem Versagen des Rahmenknotens geführt. Die Befestigung mit Spreizdübeln des Bolzentyps zeigt eine bessere Wirksamkeit (Versuch JT1-6). Obwohl das große Schlupfen der Dübel zur Schädigung im Knotenbereich geführt hat, konnte das pseudoduktile Verhalten der Befestigung, das spröde Versagen des Prüfkörpers verhindern.
- Durch die Abschätzung der Kräfteverteilung in den Dübeln der Befestigung und durch Abschätzung der Belastung der Befestigungen und durch die Ermittlung der Druck- und Zugsteifigkeit der Stahldiagonalen und Bewertung der analytischen Formeln, die im Kapitel 8 vorgeschlagen wurden, wurde bestätigt, dass die Reibung zwischen den gedrückten Ankerplatten in der Riegel- und Stützenoberfläche eine große Rolle für die Wirksamkeit der Verstärkung spielt. Eine Entkopplung der Beiträge von Dübeln unter Schubbelastung und Reibung war allerdings nicht möglich, da hierfür keine Messungen durchgeführt werden konnten. Für die getestete Befestigungskonfigurationen zeigte sich im Durchschnitt ein Verhältnis zwischen Drucksteifigkeit, $K_{h,c}$, und Zugsteifigkeit, $K_{h,t}$, der mit Dübeln befestigten Stahldiagonalen, $K_{h,c}/K_{h,t} \sim 1.5$.

Kap. 10: Numerische Verifizierung der Ertüchtigungsmaßnahme

Das FE-Modell zur Simulation des seismischen Verhaltens von Rahmenknoten (siehe Kapitel 4) wurde erweitert, um das Verhalten der Rahmenknoten nach der Verstärkung nachbilden zu können. Die Dübel wurden mit nichtlinearen Federn simuliert. Damit konnte der Effekt der Variation der Steifigkeit der Befestigung auf die Ertüchtigungsmaßnahme

untersucht werden. Auf Grund dieser Vereinfachung in der Modellierung der Befestigung, konnte das Versagen der Befestigung allerdings nicht ausreichend realistisch simuliert werden.

Trotz dieser Vereinfachung, die für die Modellierung der Verstärkung getroffen wurde, konnten die experimentellen Versuche mit ausreichend Genauigkeit nachgerechnet werden. Voraussetzung hierfür ist, dass für die Zug- (k_N) und Schubsteifigkeit (k_V) der Dübeln die Werte eingesetzt wurden, die aus den Versuchen ermittelt wurden.

Zug- und Schubsteifigkeit der Dübel wurden im realistischen Bereich variiert, um deren Einfluss auf die Wirksamkeit der Befestigung zu untersuchen. Es wurde bestätigt, dass ein Verhältnis $K_{h,c}/K_{h,t} \sim 1.5$ in der Bemessung angenommen werden kann. Damit ist nur der Wert k_N als Eingabeparameter erforderlich. Die Übereinstimmung zwischen numerischen und analytischen Ergebnissen war ausreichend genau.

Kap. 11: Bemessung der Ertüchtigungsmaßnahme

In diesem Kapitel werden die Erkenntnisse aus den analytischen (Kapitel 8), experimentellen (Kapitel 9) und numerischen (Kapitel 10) Untersuchungen in einem Bemessungsverfahren als Flussdiagramm zusammengeführt. Die einzelnen Schritte zur Verstärkung der Stahlbetonrahmenendknoten werden erläutert und diskutiert.

Des Weiteren wurde ein Sicherheitskonzept in Anlehnung an dem *EC8-3 (2005)* für die Beurteilung des Rahmenknotens vor und nach der Verstärkung und *fib (2011)* für die Bemessung der Befestigung mit Dübeln vorgeschlagen.

Kap. 12: Zusammenfassung und Ausblick

Schließlich werden die wesentlichen Ergebnisse der Forschungsarbeit zusammengefasst, und es werden Perspektiven für die Weiterführung des Forschungsvorhabens vorgestellt.

Das Modell zur Beurteilung der Schubtragfähigkeit von Stahlbetonrahmenendknoten sollte erweitert werden. Dabei sollten folgende Punkte untersucht werden:

- Erweiterung des Modells zur Berücksichtigung von Schubbewehrung im Knotenbereich;
- Erweiterung des Modells auf andere Knotengeometrien (2D und 3D Innen- und Eckknoten) und Einfluss von angrenzenden Bauteilen (Riegel und Decken);
- dynamische Untersuchungen an 2D und 3D Stahlbetonrahmen, um den Effekt des Knotenschubversagens auf das gesamte Tragwerk beurteilen zu können.

Für eine genauere und wirtschaftlichere Bemessung der vorgeschlagenen Ertüchtigungsmaßnahmen sollten einige Aspekte geklärt und untersucht werden:

- genauere Informationen über die Steifigkeit von Dübeln sind notwendig;

- eine rechnerische Entkopplung von Schub- und Reibesteifigkeit auf der Grundlage von experimentellen Ergebnissen soll angestrebt werden;
- dynamische Untersuchungen an 2D und 3D Stahlbetonrahmen, um den Effekt der Ertüchtigungsmaßnahmen auf das gesamte Tragwerk beurteilen zu können, bzw. um zu ermitteln, wie viele und welche Knoten verstärkt werden sollten.

LITERATURE

A

Aboutaha et al. (1994): Aboutaha R.S.; Engelhardt, M.D.; Jirsa, J.O.; Kreger, M.E.: Seismic retrofit of R/C columns with inadequate lap splices. In: Baker, N.C.; Goodno, B.J. (Eds.): *Structures Congress XII, Proceedings of the Papers, Atlanta, GA, April 24-28, 1994*. New York, NY: ASCE, 1994, pp. 1502-1507

Abrams (1987): Abrams, D. P.: Scale Relations for Reinforced Concrete Beam-Column Joints. In: *ACI Structural Journal* 84 (1987), No. 6, pp. 502-512

ACI 318 (1951): ACI 318-51: *Building code requirements for reinforced concrete*. Detroit, MI: American Concrete Institute (ACI), 1951

ACI 318 (1963): ACI 318-63: *Building code requirements for reinforced concrete*. Detroit, MI: American Concrete Institute (ACI), 1963

ACI 318 (1971): ACI 318-71: *Building code requirements for reinforced concrete (ACI 318-71) and commentary (ACI 318R-71)*. Detroit, MI: American Concrete Institute (ACI), 1971

ACI 318 (1977): ACI 318-77: *Building code requirements for reinforced concrete (ACI 318-77) and commentary (ACI 318R-77)*. Detroit, MI: American Concrete Institute (ACI), 1977

ACI 318 (1983): American Concrete Institute (ACI): *Building code requirements for structural concrete (ACI 318-83) and commentary (ACI 318R-83)*. Farmington Hills, MI: ACI, 1983

ACI 318 (2002): ACI 318-02: *Building code requirements for structural concrete (ACI 318-02) and commentary (ACI 318R-02)*. Farmington Hills, MI: American Concrete Institute (ACI), 2002

ACI 318 (2008): ACI 318-08: *Building code requirements for structural concrete (ACI 318-08) and commentary (ACI 318R-08)*. Farmington Hills, MI: American Concrete Institute (ACI), 2008

ACI 352 (1976): ACI 352-76: *Recommendations for design of beam-column joints in monolithic reinforced concrete structures*. Detroit, MI: American Concrete Institute (ACI), 1976

ACI 355.2 (2007): ACI 355.2-07: *Qualification of post-installed mechanical anchors in concrete and commentary*. Farmington Hills, MI: American Concrete Institute (ACI), 2007

ACI 374 (2005): ACI 374.1-05: *Acceptance criteria for Moment Frames Based on Structural Testing and Commentary*. Farmington Hills, MI: American Concrete Institute (ACI), 2005

AIJ (1982): *Standard for Structural Calculation of Reinforced Concrete Structures*. Tokyo: Architecture Institute of Japan (AIJ), 1982. (In Japanese)

Akgüzel (2011): Akgüzel U.: *Seismic Performance of FRP Retrofitted Exterior RC Beam-Column Joints under Varying Axial and Bidirectional Loading.* Christchurch, University of Canterbury, PhD thesis, 2011

Akiyama et al. (2007): Akiyama, T.; Yamamoto, Y.; Ariki, K.; Kado, Y.: Seismic strengthening of school building damaged by 2004, Niigata-Chuetsu Earthquake. In: Eligehausen, R.; Fuchs, W.; Genesio, G.; Grosser, P. (Eds.): *Connections between Steel and Concrete: Stuttgart, Germany, September 4th - 7th, 2007, Vol. 2.* Stuttgart: Ibidem, 2007, pp. 771-781

Alath & Kunnath (1995): Alath, S.; Kunnath, S. K.: Modeling inelastic shear deformations in RC beam-column joints. In: Stein, S. (Ed.): *Engineering Mechanics: Proceedings of 10th Conference, University of Colorado at Boulder, May 21-24, 1995.* New York NY: ASCE, 1995, pp. 822-825

Alcocer & Jirsa (1993): Alcocer, S.M.; Jirsa, J.O.: Strength of RC Framed Connections Rehabilitation by Jacketing. In: *ACI Structural Journal* 90 (1993), No. 3, pp. 249-261

Altoontash (2004): Altoontash, A.: *Simulation and damage models for performance assessment of reinforced concrete beam-column joints*. Stanford, CA, University, PhD Thesis, 2004

Anderson & Meinheit (2006): Anderson, N. S.; Meinheit, D. F.: *Design Criteria for Headed Stud Groups in Shear*: *Final Report*. Northbrook, IL: Wiss., Janney, Elstner Associates, Inc., 2006. Report No. WJE 1996.0002

Antonopoulos & Triantafillou (2003): Antonopoulos, C. P.; Triantafillou, T. C.: Experimental Investigation of FRP-Strengthened RC Beam-Column Joints. In: *Journal of Composites for Construction* 7 (2003), No. 1, pp. 39-49

Appl. (2009): Appl., J.: *Tragverhalten von Verbunddübeln unter Zugbelastung (Load-carrying behavior of bonded anchors under tension loading)*. Stuttgart, University, PhD Thesis, 2009 (Oral defense 19.12.2008). (In German)

ASCE 41 (2007): ASCE Standard 41: *Seismic rehabilitation of existing buildings.* Reston, VA: American Society of Civil Engineers (ASCE), 2007

Asmus (2007): Asmus, J.: Design Method for Splitting Failure of Fastenings. In: Eligehausen, R.; Fuchs, W.; Genesio, G.; Grosser, P. (Eds.): *Connections between Steel and Concrete: Stuttgart, Germany, September 4th - 7th, 2007, Vol. 1.* Stuttgart: Ibidem, 2007, pp. 505-517

B

Baglin & Scott (2000): Baglin, P. S.; Scott, R. H.: Finite Element Modeling of Reinforced Concrete Beam-Column Connections. In: *ACI Structural Journal* 97 (2000), No. 6, pp. 886-894

Bakir & Boduroğlu (2002): Bakir, P. G.; Boduroğlu, H. M.: A new design equation for predicting the joint shear strength of monotonically loaded exterior beam-column joints. In: *Engineering Structures* 24 (2002), No. 8, pp. 1105-1117

Banon et al. (1981): Banon, H.; Biggs, J. M.; and Irvine, H. M.: Seismic Damage in Reinforced Concrete Frames. In: *ASCE Journal of the Structural Division* 107 (1981), No. 9, pp. 1713-1729

Bažant & Prat (1988): Bažant Z. P.; Pratt, P. C.: Microplane model for brittle-plastic material, -parts I and II. In: *ASCE Journal of Engineering Mechanics* 116 (1988), No. 11, pp. 2485-2504

Bažant (1984): Bažant Z. P.: Microplane Model for Strain- Controlled Inelastic Behavior. In: Desai, C.S.; Gallagher, R.H. (Eds.): *Mechanics of Engineering Materials.* London: Wiley, 1984, Chapter 3, pp. 45-59

Bažant & Cedolin (1979): Bažant, Z. P.; Cedolin, L.: Blunt crack band propagation in finite element analysis. In: *ASCE Journal of Engineering Mechanics* 105 (1979), No. 2, pp. 297-315

Bažant & Oh (1983): Bažant, Z. P.; Oh, B.-H: Crack Band Theory for Fracture of Concrete. In: *Materials and Structures* 16 (1983), No. 93, pp. 155-177

Bažant & Ožbolt (1990): Bažant, Z. P.; Ožbolt, J.: Nonlocal microplane model for fracture, damage and size effect in structures. In: *ASCE Journal of Engineering Mechanics* 116 (1990), No. 11, pp. 2485-2504

Bedirhanoglu et al. (2010): Bedirhanoglu, I.; Ilki, A.; Pujol, S.; Kumbasar, N.: Behavior of Deficient Joints with Plain Bars and Low-Strength Concrete. In: *ACI Structural Journal* 107 (2010), No. 3, pp. 300-310

Biddah & Ghobarah (1999): Biddah, A.; Ghobarah, A.: Modelling of shear deformation and bond slip in reinforced concrete joints. In: *Structural Engineering and Mechanics* 7 (1999), No. 4, pp. 413-432

Braga et al. (2001a): Braga, F. De Carlo, G.; Gigliotti, R.; Laterza, M.; Nigro, D.: Meccanismi di risposta di nodi trave-pilastro in c.a. di strutture non antisismiche (Response mechanisms of RC beam-column joints in non-seismic resistant structures). In: ANIDIS (Ed.): *X Congresso Nazionale L'Ingegneria Sismica in Italia, Potenza-Matera, Sept. 9-13, Italy.* Potenza: Lamisco, 2001. (In Italian)

Braga et al. (2001b): Braga, F. De Carlo, G.; Gigliotti, R.; Laterza, M.: Modellazione dell'aderenza nei meccanismi di risposta di nodi trave-pilastro in c.a. in presenza di armature lisce (Modeling of the bond-slip behavior in the response mecanisms of RC beam-coloumn joints with plain round bars). In: ANIDIS (Ed.): *X Congresso Nazionale L'Ingegneria Sismica in Italia, Potenza-Matera, Sept. 9-13, Italy.* Potenza: Lamisco, 2001. (In Italian)

BS 8110 (1985): BS 8110:1985: *Structural use of concrete*. London: British Standard Institution, 1985

C

Calvi et al. (2002): Calvi, G. M.; Magenes, G.; Pampanin, S.: Relevance of beam-column damage and collapse in RC frame assessment. In: *Journal of Earthquake Engineering* 6 (2002), No. S1, pp. 75-100

Calvi (2010): Calvi, G. M.: Engineers Understanding of Earthquakes Demands and Structures Response. In: Garevski, M.; Ansal, A. (Eds.): *Earthquake Engineering in Europe*. Dordrecht: Springer, 2010 (Geotechnical, Geological and Earthquake Engineering; 17), pp. 223-247

CEB (1993): Comité Euro-International du Béton (CEB): *CEB-FIP Model Code 1990*. London: Telford, 1993. (Bulletin d'Information; 213/214)

CEB (1995): Comité Euro-International du Béton (CEB): *Fastenings for seismic retrofitting*. Lausanne: CEB, 1995. (Bulletin d'Information; 226), pp. 147-217

Celik & Ellingwood (2008): Celik, O. C.; Ellingwood, B. R.: Modeling Beam-Column Joints in Fragility Assessment of Gravity Load Designed Reinforced Concrete Frames. In: *Journal of Earthquake Engineering* 12 (2008), No. 3, pp. 357-381

CEN (2009): CEN/TS 1992-4:2009 *Design of fastenings for use in concrete*. Brussels: Comité Européen de Normalisation (CEN), 2009

Chaimahawan & Pimanmas (2009): Chaimahawan, P.; Pimanmas, A.: Seismic retrofit of substandard beam-column joint by planar joint expansion. In: *Materials and Structures* 42 (2009), No. 4, pp. 443-459

Chen (2006): Chen, T.-H.: *Development of a low invasive seismic retrofit solution for under-designed frame systems based on a metallic haunch.* Christchurch, University of Canterbury, MS Thesis, 2006

Clyde et al. (2000): Clyde, C.; Pantelides, C. P.; Reaveley, L. D.: *Performance-Based Evaluation of Exterior Reinforced Concrete Building Joints for Seismic Excitation*. Berkeley, CA: University of California, 2000. PEER Report 2000/05

D

Decanini et al. (2010): Decanini, L.D.; Liberatore, L.; Mollaioli, F.: Damage Suffered by RC Buildings During the 2009 L'Aquila Earthquake, a General Overview and a Case Study. In: Garevski, M. (Ed.): *14th European Conference on Earthquake Engineering, Aug 30-Sept 3, 2010, Ohrid, Macedonia: Proceedings*. Skopje: Macedonian Association for Earthquake Engineering, 2010, CD-Rom

Dieterle et al. (1990): Dieterle, H.; Bozenhardt, A.; Hirth, W.; Opitz, V.: *Tragverhalten von Dübeln in Parallelrissen unter Schrägzugbeanspruchung (Load-bearing behaviour of anchors in uni-axial cracks under combined tension and shear loading.* Stuttgart: IWB, Universität Stuttgart, 1990. Report No. 1/45-89/19. (In German, not published)

Dragoni (2005): Dragoni, M.: *Terrae Motus – La sismologia da Eratostane allo tsunami di Sumatra (Terrae Motus – The seismology from Eratostane to the tsunami of Sumatra)*. Torino: Utet libreria, 2005. (In Italian)

DM (1972): Decreto Ministeriale LL. PP: n. 9161 30/05/1972: *Norme tecniche per il calcolo, l'esecuzione e il collaudo delle strutture in conglomerato cementizio armato normale e precompresso e per le strutture metalliche* (*Technical standards for the design, construction and approval of reinforced concrete, prestressed concrete and metallic structures*). Roma: Ministero dei Lavori Pubblici, 1972. (In Italian)

DM (1984): Decreto Ministeriale LL. PP. 14/07/1984: *Norme tecniche per le costruzioni in zone sismiche* (*Technical standards for the constrution in seismic areas)*. Roma: Ministero dei Lavori Pubblici, 1984. (In Italian)

DM (1992): Decreto Ministeriale LL. PP. 14/02/1992: *Norme tecniche per l'esecuzione delle opere in c.a. normale e precompresso e per le strutture metalliche* (*Technical standards for reinforced concrete, prestressed concrete and metallic structures*). Roma: Ministero dei Lavori Pubblici, 1992. (In Italian)

DM (1996): Decreto Ministeriale LL. PP. 16/01/1996: *Norme tecniche per le costruzioni in zone sismiche* (*Technical standards for the constrution in seismic areas)*. Roma: Ministero dei Lavori Pubblici, 1996. (In Italian)

E

EC2 (1992): EN 1992-1-1:1992: *Eurocode 2: Design of concrete structures. Part 1-1: General rules and rules for buildings and civil engineering structures.* Brussels: Comité Européen de Normalisation (CEN), 1992

EC3 (2005): EN 1993:2005: *Eurocode 3: Design of Steel Structures.* Brussels: Comité Européen de Normalisation (CEN), 2005

EC8-1 (2004): EN 1998-1:2004: *Eurocode 8: Design of structures for earthquake resistance. Part 1: General rules, seismic actions and rules for buildings*. Brussels: Comité Européen de Normalisation (CEN), 2002

EC8-3 (2005): EN 1998-3:2005: *Eurocode 8: Design of structures for earthquake resistance. Part 3: Strengthening and repair of buildings.* Brussels: Comité Européen de Normalisation (CEN), 2005

Eligehausen et al. (1983): Eligehausen, R.; Popov, E. P.; Bertero, V. V.: *Local bond-stress relationships on deformed bars under generalized excitation.* Berkeley, CA: EERC, Univ. of California. Report No. UCB/EERC 83/23

Eligehausen & Balogh (1995): Eligehausen, R.; Balogh, T.: Behavior of fasteners loaded in tension in cracked reinforced concrete. In: *ACI Structural Journal* 92 (1995), No. 3, pp. 365-379

Eligehausen et al. (2006a): Eligehausen, R.; Mallée, R.; Silva, J.: *Anchorage in Concrete Construction*. Berlin: Ernst & Sohn, 2006

Eligehausen et al. (2006b): Eligehausen, R.; Ožbolt, J.; Genesio, G.; Hoehler, M. S.; Pampanin, S.: Three-dimensional Modelling of Poorly Detailed RC Frame Joints. In: Brabhaharan, P.; Deam, B. (Eds.): *Remembering Napier 1931: Building on 75 years of earthquake engineering in New Zealand, Conference 2006, 10-12 March, Napier, New Zealand*. Wellington: NZSEE, 2006, CD-Rom, Paper No. 23

Eligehausen et al. (2009): Eligehausen, R.; Genesio, G.; Ožbolt, J.; Pampanin, S.: 3D Analysis of Seismic Response of RC Beam-Column Exterior Joints before and after Retrofit. In: Alexander, M.G.; Beushausen, H.-D.; Dehn, F.; Moyo, P. (Eds.): *Concrete Repair Rehabilitation and Retrofitting II: Proceedings of the 2nd Conference; Cape Town, South Africa, November 24-26, 2008*. London: Taylor & Francis, 2009, pp. 407-408

Elmorsi et al. (2000): Elmorsi, M.; Kianoush, M. R.; Tso, W. K.: Modeling bond-slip deformations in reinforced concrete beam-column joints. In: *Canadian Journal of Civil Engineering*. 27 (2000), No. 3, pp. 490-505

Elwood & Moehle (2005): Elwood, K.; Moehle, J. P.: Drift capacity model for shear-damaged columns. In: *ACI Structural Journal* 102 (2005), No. 4, pp. 578-587

Engindeniz et al. (2005): Engindeniz, M.; Kahn, L. F.; Zureick, A.-H.: Repair and strengthening of Reinforced Concrete Beam-Column Joints: State of the Art. In: *ACI Structural Journal* 102 (2005), No. 2, pp. 187-197

EOTA (1997): ETAG 001 (1997): *Guideline for European Technical Approval of Metal Anchors for Use in Concrete (+Amendments)*. Brussels: European Organisation for Technical Approvals (EOTA), 1997

F

Fardis (2009): M. N. Fardis: *Seismic Design, Assessment and Retrofitting of Concrete Buildings according to EN-Eurocode 8*. Dordrecht: Springer, 209 (Geotechnical, Geological and Earthquake Engineering; 8)

Fabbrocino et al. (2002): Fabbrocino. G.; Verderame G. M.; Manfredi, G.: Experimental behaviour of anchored smooth rebars in old type reinforced concrete buildings. In: *12th European Conference on Earthquake Engineering, 9-13 September 2002, London*. Oxford: Elsevier, 2002, CD-Rom, Paper No. 393

Fabbrocino et al. (2005): Fabbrocino, G.; Verderame G. M.; Manfredi, G.: Experimental behaviour of anchored smooth rebars in old type reinforced concrete buildings. In: *Engineering Structures* 27 (2005), No. 10, pp. 1575-1585

FEMA 273 (1997): FEMA 273: *NEHRP Guidelines for the Seismic Rehabilitation of Buildings*. Washington, DC: Federal Emergency Management Agency, 1997

FEMA 356 (2000): FEMA 356: *Prestandard and Commentary for the Seismic Rehabilitation of Buildings*. Washington, DC: Federal Emergency Management Agency, 2000

FEMA 547 (2006): FEMA 547: *Techniques for the Seismic Rehabilitation of Existing Buildings.* Washington, DC: Federal Emergency Management Agency, 2006

fib (2003): International Federation of Structural Concrete (fib): *Seismic assessment and retrofit of reinforced concrete buildings*. Lausanne: fib, 2003. (fib bulletin; 24)

fib (2011): International Federation of Structural Concrete (fib): *Design of Anchorages in Concrete*. Lausanne: fib, 2011. (fib bulletin; 58)

Fichtner (2005): Fichtner, S.: *Implementierung einer Kontaktschicht mit Reibeigenschaften für kleine Verformungen in das Programm MASA (Implementation of a contact layer with friction's properties for small deformations in the program MASA*. Stuttgart: IWB, Universität Stuttgart. Report No. HT 141/01-04/8. (In German, not published)

Fichtner (2011): Fichtner, S.: *Untersuchungen zum Tragverhalten von Gruppenbefestigungen unter Berücksichtigung der Ankerplattendicke und einer Mörtelschicht (Investigations on the load-carrying behaviour of anchor groups considering the effect of fixture thickness and mortar layer).* Stuttgart, University, PhD Thesis, 2011. (In German)

Filiatrault & Lebrun (1996): Filiatrault, A.; Lebrun, I.: Seismic Rehabilitation of Reinforced Concrete Joints by Epoxy Pressure Injection Technique. In: Sabnis, G.M.; Shroff, A.C.; Kahn, L.F. (Eds.): *Seismic rehabilitation of concrete structures*. Farmington Hills, MI: ACI, 1996. (ACI Special Publication; 160), pp. 73-92

Fillipou et al. (1983): Fillipou, F. C.; Popov, E. P.; Bertero, V. V.: *Effects of bond deterioration on hysteretic behaviour of reinforced concrete joints.* Berkeley, CA: EERC, Univ. of California. Report No. UCB/EERC 83/19

Fillipou & Issa (1988): Fillipou, F. C.; Issa, A.: *Nonlinear analysis of reinforced concrete frames under cyclic load reversals.* Berkeley, CA: EERC, Univ. of California. Report No. UCB/EERC-88/12

Fischer (1995): Fischer, L.: Bestimmung des 5% - Quantils im Zuge der Bauwerksprüfung – Bezugnahme auf DIN-Normen und Eurocodes (Evaluation of 5% - Quantile in the course of Structural Inspection. Reference to DIN-Standards and EURO-Codes). In: *Bautechnik* 72 (1995), No. 11, pp. 712-722

Fuchs (1992): Fuchs, W.: *Tragverhalten von Befestigungen unter Querlasten in ungerissenem Beton (Load-bearing behaviour of fastenings under shear loading in uncracked concrete)*. Berlin: Beuth, 1992. (Deutscher Ausschuss für Stahlbeton ; 424). (In German)

Fuchs et al. (1995): Fuchs, W.; Eligehausen, R.; Breen, J. E.: Concrete Capacity Design (CCD) approach for fastening to concrete. In: *ACI Structural Journal* 92 (1995), No. 1, pp. 73-94

Fujikake et al. (2003): Fujikake, K.; Nakayama, J. Sato, H., Mindess, S.; Ishibashi, T.: Chemically bonded anchors subjected to rapid pullout loading. In: *ACI Materials Journal* 100 (2003), No. 3, pp. 246-252

G

Genesio (2007a): Genesio, G.: *Tragverhalten von Befestigungen unter Schrägzugbeanspruchung im gerissenen Beton (w = 0.8 mm) (Load-bearing behaviour of fasteners under combined tension and shear in cracked concrete) – Series C1.* Stuttgart: IWB, University of Stuttgart, 2007. Test Report No. WS 212/17-07/06. (In German, not published)

Genesio (2007b): Genesio, G.: *Tragverhalten von Befestigungen unter wechselnder Querzugbeanspruchung im gerissenen Beton (w = 0.8 mm) (Load-bearing behaviour of fasteners under alternating shear loading in cracked concrete) – Series C2.* Stuttgart: IWB, University of Stuttgart, 2007. Test Report No. WS 212/19-07/08. (In German, not published)

Genesio (2007c): Genesio, G.: *Zugbeanspruchte Befestigungsmittel im sich öffnenden und schließenden Rissen (Tensioned fasteners in opening and closing cracks) – Series B3.* Stuttgart: IWB, University of Stuttgart, 2007. Test report No. WS 212/18-07/07. (In German, not published)

Genesio et al. (2007): Genesio, G., Periškić, G.; Schmid K.; Appl, J.; Eligehausen, R.: Requirements of Technical Approvals versus practice (Bonded Anchors and Post-installed Rebars). In: Eligehausen, R.; Fuchs, W.; Genesio, W.; Grosser, P. (Eds.): *Connections between Steel and Concrete: Stuttgart, Germany, September 4th - 7th, 2007, Vol. 1.* Stuttgart: Ibidem, 2007, pp.75-84

Genesio & Eligehausen (2008): Genesio, G.; Eligehausen, R.: Seismic Assessment and Retrofit of Poor Detailed Reinforced Concrete Exterior Beam-Column Joints. In: *Earthquake Engineering for Sustainable Structures: Proceedings of the IIT-TU9 Workshop, Nov 29 – Dec 2, 2008, Chennai, India*. Madras: Indian Institute of Technology, 2008

Genesio & Akgüzel (2009): Genesio, G.; Akgüzel, U.: *Seismic retrofit for reinforced concrete exterior beam-column joints using a fully fastened metallic haunch solution, Part 1: Feasibility study.* Stuttgart: IWB, University of Stuttgart, 2009. Test Report No. WS 212/23 - 09/02. (Not published)

Genesio & Sharma (2010a): Genesio, G.; Sharma, A.: *Seismic retrofit solution for reinforced concrete exterior beam-column joints using a fully fastened haunch - Part 2-1: As-built joints.* Stuttgart: IWB, University ot Stuttgart, 2010. Test Report No. WS 221/07 - 10/01. (Not published)

Genesio & Sharma (2010b): Genesio, G.; Sharma, A.: *Seismic retrofit solution for reinforced concrete exterior beam-column joints using a fully fastened haunch - Part 2-2: Retrofitted joints.* Stuttgart: IWB, University of Stuttgart, 2010. Test Report No. WS 221/08 - 10/02. (Not published)

Genesio et al. (2010a): Genesio, G.; Sharma, A.; Eligehausen, R.; Pampanin, S.: Experimental and Numerical Study towards a Deformation-Based Seismic Assessment of Substandard Exterior R.C. Beam-Column Joints. In: Oh, B.H.; Choi, O.C.; Chung, L. (Eds.): *Proceedings of the 7th Int. Conf. on Fracture Mechanics of Concrete and Concrete Structures (FRAMCOS-7), Jeju, Korea, May, 23-28, 2010*. Seoul: Korea Concrete Institute 2010

Genesio et al. (2010b): Genesio, G.; Sharma, A.; Eligehausen, R.; Pampanin, S.; Reddy, G. R.: Development of seismic retrofit technique of rc frame using fully fastened haunch elements: static to dynamic testing. In: Kumar, A. (Ed.): *Earthquake Engineering: Proc. Of the 14th Symposium*, Roorkee, India, Dec 17-19. 2010. New Delhi: Elite Pub. House, 2010

Gergely et al. (2000): Gergely, J.; Pantelides, C. P.; Reaveley, L. D.: Shear Strengthening of RCT-Joints Using CFRP Composites. In: *Journal of Composites for Construction* 4 (2000), No. 2, pp. 56-64

Ghobarah et al. (1997): Ghobarah, A.; Aziz, T.S.; Biddah, A.: Rehabilitation of Reinforced Concrete Frame Connections using Corrugated Steel Jacketing. In: *ACI Structural Journal* 94 (1997), No. 3, pp. 283–294

Ghobarah & Said (2001): Ghobarah, A.; Said, A.: Seismic rehabilitation of beam-column joints using FRP laminates. In: *Journal of Earthquake Engineering* 5 (2001), No. 1, pp. 113-129

Grosser et al. (2011): Grosser, P.; Fuchs, W.; Eligehausen, R.: A Field Study of Adhesive Anchor Installations. In: *Concrete International* 33 (2011), No. 1, pp. 57-63

Grosser (2012): Grosser, P.: *Load-bearing behavior and design of anchorage subjected to shear and torsion loading in uncracked concrete*. Stuttgart, University, PhD Thesis, 2006. (In preparation)

Guillet (2011): Guillet, T.: Behavior of Metal Anchors under Combined Tension and Shear Cyclic Loads. In: *ACI Structural Journal* 108 (2011), No. 3m pp. 315-323

Guillet & David (2007): Guillet, T.; David, E.: A new seismic test for metal anchors. In: Eligehausen, R.; Fuchs, W.; Genesio, G.; Grosser, P. (Eds.): *Connections between Steel and Concrete: Stuttgart, Germany, September 4th - 7th, 2007, Vol. 1.* Stuttgart: Ibidem, 2007, pp.677-686

H

Hakuto et al. (2000): Hakuto, S.; Park, R.; Tanaka, H.: Seismic Load Tests on Interior and Exterior Beam-Column Joints with Substandard Reinforcing Details. In: *ACI Structural Journal* 97 (2000), No. 1, pp. 11-25

Hamil (2000): Hamil, S. J.: *Reinforced Concrete Beam-Column Connection Behaviour*. Durham, University, PhD Thesis, 2000

Hanson & Connor (1967): Hanson, N. W.; Connor, H. W.: Seismic Resistance of Reinforced Concrete Beam-Column Joints. In: *ASCE Journal of the Structural Division* 93 (1967), No. 5, pp. 533-560

Hattori & Yamamoto (2007): Hattori, Y.; Yamamoto, Y.: Shear transfer mechanism to bonded anchors for exterior seismic retrofitting". In: Eligehausen, R.; Fuchs, W.; Genesio, G.; Grosser, P. (Eds.): *Connections between Steel and Concrete: Stuttgart, Germany, September 4th - 7th, 2007, Vol. 2.* Stuttgart: Ibidem, 2007, pp. 759-769

Hegger et al. (2002): Hegger, J.; Roeser, W.: *Die Bemessung und Konstruktion von Rahmenknoten – Grundlagen und Beispiele gemäß DIN 1045-1 (The design and detailing of beam-column joints – Background and examples according to DIN 1045-1)*. Berlin: Beuth, 2003. (Deutscher Ausschuss für Stahlbeton ; 532). (In German)

Hegger et al. (2003): Hegger, J; Sherif, A.; Roeser, W.: Nonseismic Design of Beam-Column Joints. In: *ACI Structural Journal* 100 (2003), No. 5, pp. 654-664

Hegger et al. (2004): Hegger, J; Sherif, A.; Roeser, W.: Nonlinear Finite Element Analysis of Reinforced Concrete Beam-Connections. In: *ACI Structural Journal* 101 (2004), No. 5, pp. 604-614

Hertanto (2005): Hertanto, E.: *Seismic assessment of pre-1970s reinforced concrete structures*. Christchurch, University of Canterbury, MS Thesis, 2005

Hoehler (2006): Hoehler, M. S.: *Behavior and Testing of Fastenings to Concrete for Use in Seismic Applications*. Stuttgart, University, PhD Thesis, 2006

Hoehler & Ožbolt (2001): Hoehler, M. S.; Ožbolt, J.: Three-Dimensional Cyclic Analysis of Reinforced Concrete Members Using the Microplane Model. In: *Otto Graf Journal* 12 (2001), pp. 93-113

Hoehler & Stanton (2006): Hoehler, M. S.; Stanton, J. F.: Simple Phenomenological Model for Reinforcing Steel under Arbitrary Load. In: *ASCE Journal of Structural Engineering* 132 (2006), No. 7, pp. 1061-1069

Hoekstra (1977): Hoekstra, A. S.: *De invloed van de wapeningsdetaillering op het gedrag van de doorgaande-kolom-balkverbinding* (*The influence of the reinforcement detailing the behavior of the continuous beam-column connection*). Delft: TH Delft, 1977. Report. (In Dutch)

Hofmann (2005): Hofmann, J.: *Tragverhalten und Bemessung von Befestigungen unter beliebiger Querbelastung in ungerissenem Beton (Load carrying behaviour and design of fasteners under shear loading in an arbitrary angle to the edge"*. Stuttgart, University, PhD Thesis, 2005. (Oral defense: 04.10.2004, in German)

Hollings (1969): Hollings, J. P.: Reinforced Concrete Seismic Design. In: *Bulletin of the New Zealand National Society for Earthquake Engineering*. 2 (1969), No. 3, pp. 217-250

Hwang & Lee (1999): Hwang, S. J. and Lee, H. J.: Analytical Model for Predicting Shear Strength of Exterior RC Beam-Column Joints for Seismic Resistance. In: *ACI Structural Journal 96* (1999), No. 5, pp. 846-857

I

ICC-ES (2009): AC308-09: *Acceptance criteria for post-installed adhesive anchors in concrete elements*. Whittier, CA: International Code Council-Evaluation Service (ICC-ES), 2009

ICC-ES (2010): AC193-10: *Acceptance criteria for mechanical anchors in concrete elements*. Whittier, CA: International Code Council-Evaluation Service (ICC-ES), 2010

IS 456 (1978): IS 456:1978: *Plain and Reinforced Concrete – Code of Practice*. New Delhi: Bureau of Indian Standards, 1978

IS 1893 (1975): IS 1893:1975: *Criteria for Earthquake resistant Design of Structures*. New Delhi: Bureau of Indian Standards, 1975

IS 1893 (2002): IS 1893-1:2002: *Criteria for Earthquake resistant Design of Structures, Part 1: General Provisions and Buildings*. New Delhi: Bureau of Indian Standards, 2002

IS 4326 (1976): IS 4326:1976: *Code of Practice for Earthquake Resistant Design and Construction*. New Delhi: Bureau of Indian Standards, 1976

IS 13920 (1993): IS 13920:993: *Ductile Detailing of Reinforced Concrete Structures Subjected to Seismic Forces — Codes of Practice*. New Delhi: Bureau of Indian Standards, 1993

J

Jirsa & Marques (1972): Jirsa, O. J.; Marques, J. L. G.: *A study of hooked bar anchorages in beam-column joints*. Austin, TX: University of Texas, 1972. Final Report - Reinforced Concrete Research Council, Project 33

JBPA (1990): JBPA/Japan Building Disaster Prevention Association: *Guideline for application of seismic evaluation and retrofitting design of existing reinforced concrete buildings*. Tokyo: JBPA, 1990. (In Japanese)

K

Kam et al. (2010): Kam, W.Y.; Quintana Gallo, P.; Akgüzel, U.; Pampanin, S.: *Influence of slab on the seismic response of sub-standard detailed exterior reinforced concrete beam column joints*. In: Proc. of the 9th U.S. National and 10th Canadian Conference on Earthquake Engineering: Reaching Beyond Borders, Jul 25-29, 2010, Toronto, Canada. Oakland, CA: EERI, 2010, CD-Rom

Kam (2011): Kam, W.Y.: *Selective weakening and post-tensioning for the seismic retrofit of non ductile R.C. frames.* Christchurch, University of Canterbury, PhD Thesis, 2011

Kanada et al. (1985): Kanada, K.; Fujii, S; Morita, S.: *Effect of Joint Shear Reinforcement on Behaviors of Exterior Beam-Column Joints under Reversed Cyclic Loading*, In: Design of Reinforced Beam-Column-Joints: 2nd U.S. – N.Z. – Japan Seminar, Tokyo. Tokyo: University, Dept. of Architecture, 1985

Karayannis et al. (2008): Karayannis, C. G.; Chaliori, C. E.; Sirkelis, G. M.: Local retrofit of exterior RC beam-column joints using this RC jackets – An experimental study. In: *Earthquake Engineering and Structural Dynamics* 37 (2008), No. 5, pp. 727-746

Kuang & Wong (2006): Kuang, J. S.; Wong, H. F.: Effects of beam bar anchorage on beam-column joint behaviour. In: *Structures & Buildings* 159 (2006), No. 2, pp. 115-124

Kunnath at al. (1995a): Kunnath, S. K.; Hoffmann, G.; Reinhorn, A. M.; Mander, J. B.: Gravity-load-designed reinforced concrete buildings — Part I: Seismic evaluation of existing construction. In: *ACI Structural Journal* 92 (1995), No. 3, pp. 343–354

Kunnath at al. (1995b): Kunnath, S. K.; Hoffmann, G.; Reinhorn, A. M.; Mander, J. B.: Gravity load-designed reinforced concrete buildings — Part II: Evaluation of detailing enhancements. In: *ACI Structural Journal*. 92 (1995), No. 4, pp. 470–478

Küenzlen (2005): Küenzlen, J.: *Tragverhalten von Schraubdübeln unter statische Zugbelastung (Load-bearing behavior of screw anchors under static tension load)*. Stuttgart, University, PhD Thesis, 2005. (Oral defense: 06.04.2004, in German)

Kurose (1987): Kurose, Y.: *Recent studies on reinforced concrete beam-column joints in Japan*. Austin, TX: University of Texas, 1987. PMFSEL Report No. 87-8

L

Le-Trung et al. (2010): Le-Trung, K.; Lee, K.; Lee, J.; Lee, H.; Woo, S.: Experimental study of RC beam-column joints strengthened using CRFP composites. In: *Composites: Part B* 41 (2010), No. 1, pp. 76-85

Lettow (2006): Lettow, S.: Ein Verbundelement für nichtlineare Finite Element Analysen – Anwendung auf Übergreifungsstöße (Bond Element for nonlinear Finite Element Analysis - Application to Lap Splices), University of Stuttgart, PhD Thesis, 2006 (Oral defense: 18.01.2006, in German)

Lima et al. (2010): Lima, C.; Faella, C.; Martinelli, E.: Validation of Capacity Models for Monotonic and Cyclic Behaviour of RC Beam-to-Column Joints. In: Garevski, M. (Ed.): *14th European Conference on Earthquake Engineering, Aug 30-Sept 3, 2010, Ohrid, Macedonia; Proceedings*. Skopje: Macedonian Association for Earthquake Engineering, 2010, CD-Rom

Liu & Park (2001): Liu, A.; Park, R.: Seismic behaviour and retrofit of pre-1970's as-built exterior beam-column joints reinforced by plain round bars. In: *Bulletin of the New Zealand Society for Earthquake Engineering* 34 (2001), No. 1, pp. 68-81

Liu (2006): Liu, C.: *Seismic behaviour of beam-column joint subassemblies reinforced with steel fibres.* Christchurch, University of Canterbury, MS Thesis, 2006

Lopez & Nanni (2006): Lopez A, Nanni A.: *Field evaluation and monitoring of five reinforced concrete bridges*. In: *Concrete international* 28 (2006), No. 1, pp. 74-80

Lowes & Altoonash (2003): Lowes, l.; Altoonash, A.: Modeling Reinforced-Concrete Beam-Column Joints Subjected to Cyclic Loading. In: *Journal of Structural Engineering* 129 (2003), No. 12, pp. 1686-1697

M

Mahajan, M. (2009): Mahajan, M. A.: *Evaluation of shear strength and effective width of reinforced concrete exterior beam–column joints*. Chennai, IIT Madras, PhD Thesis, 2009

Mahajan et al. (2010): Mahajan, M. A.; Genesio, G.; Eligehausen, R.: *Numerical study on Interaction of Failure modes of Substandard Exterior RC Beam-Column Joints.* Stuttgart: IWB, Universität Stuttgart, 2010. Research Report No. E10/15-BFT/15. (Not published)

Mahrenholtz et al. (2010): Mahrenholtz, C.; Eligehausen, R.; Sharma, A.: Behavior of post-installed concrete undercut anchors subjected to high loading rate and crack cycling frequency. In: *Proc. of the 9th U.S. National and 10th Canadian Conference on Earthquake Engineering: Reaching Beyond Borders, Jul 25-29, 2010, Toronto, Canada*. Oakland, CA: EERI, 2010, CD-Rom

Mahrenholtz (2011): Mahrenholtz, P.: *Anchor ductility – Development of ductility parameters and evaluation of data base.* Test report HS III/08-11/02, University Stuttgart. (not published)

Mayer & Eligehausen (1984): Mayer, B.; Eligehausen, R.: Ankergruppen mit Dübeln in der Betonzugzone (Groups of anchors in the concrete tensile zone). In: *Werkstoff und Konstruktion, Prof. Dr.-Ing. Gallus Rehm zum 60. Geburtstag*. Stuttgart: IWB, University of Stuttgart, 1984, pp. 167-180 (in German)

Megget (2006): Megget, L. M.: From brittle to ductile: 75 years of seismic design in New Zealand. In: Brabhaharan, P.; Deam, B. (Eds.): *Remembering Napier 1931: Building on 75 years of earthquake engineering in New Zealand, Conference 2006, 10-12 March, Napier, New Zealand*. Wellington: NZSEE, 2006, CD-Rom, Paper No. 01

Minami & Nishimura (1985): Minami, K.; Nishimura, Y.: Anchorage Strength of Bent Bar in Exterior Joints. In: Design of Reinforced Beam-Column-Joints: 2nd U.S. – N.Z. – Japan Seminar, Tokyo. Tokyo: University, Dept. of Architecture, 1985

Morita & Fuji (1984): Morita S.; Fuji, S.: Interactive Decay of Bent-Bar Anchorage and Joint-Shear Capacity at Exterior Beam-Column Joints under Reversed Cyclic Loading. In: *Design of Reinforced Beam-Column Joints: 1st U.S. – N.Z. Japan Seminar, Monterey, USA, 1984*

Mukherjee & Joshi (2005): Mukherjee, A., and Joshi, M.: FRPC Reinforced Concrete Beam–Column Joints under Cyclic Excitation. In: *Composite Structures* 70 (2005), No. 2, pp. 185-199

Murty et al. (2003): Murty, C. V. R.; Durgesh, C. R.; Bajpai, K. K.; Jain, S. K.: Effectiveness of Reinforcement Details in Exterior Reinforced Concrete Beam-Column Joints for Earthquake Resistance. In*: ACI Structural Journal* 100 (2003), No. 2, pp. 149-156

N

Nilsson (1973): Nilsson, I. H. E.: *Reinforced concrete corners and joints subjected to bending moment*. Stockholm: National Swedish Building Research, 1973. (Document ; D7,1973)

Nishimura & Minami (1988): Nishimura, Y.; Minami, K.: Anchorage behavior of bent bar in exterior beam-column joints under seismic loading. In: *Proceedings of 9th World Conference on Earthquake Engineering, Aug 2-9, 1988, Tokyo-Kyoto, Japan, Vol. 4*. Tokyo: Japan Association for Earthquake Engineering, 1988, pp. 639-644

Nuti & Santini (2008): Nuti, C.; Santini, S.: Fastening technique in seismic areas: A critical review. In: Walraven, J.C.; Stoelhorst, D. (Eds.): *Tailor made concrete structures: new solutions for our society; proceedings of the international FIB Symposium 2008, Amsterdam, The Netherlands, 19-21 May 2008*. Boca Raton, FL: CRC Press, pp. 899-905

NZS (1955): NZS 95:1955: *New Zealand Standard – Model Building By-Laws. Part IV and V.* Wellington: New Zealand Standard Institute, 1955

NZS (1972): NZS 3101:1972: *Design of Concrete Structures*. Wellington: New Zealand Standard Institute, 1972

NZS (1976): NZS 4203:1976: *Code of practice for General Structural Design and Design Loadings for Buildings.* Wellington: New Zealand Standard Institute, 1976

NZS (1982): NZS 3101:1982: *Design of Concrete Structures*. Wellington: New Zealand Standard Institute, 1982

NZS (1995): NZS 3101:1995: *Design of Concrete Structures*. Wellington: New Zealand Standard Institute, 1995

O

OM 3274 (2003): Ordinanza del Presidente del Consiglio dei Ministri 3274, 20/03/2003: *Primi elementi in materia di criteri generali per la classificazione sismica del territorio nazionale e di normative tecniche per le costruzioni in zona sismica (First elements of general criteria concerning the seismic classification of the National territory and tecnical requirements for the constructions in seismic areas).* Roma: Consiglio dei Ministri. (In Italian)

Ortiz (1993): Ortiz, I. R.: *Strut-and-Tie Modeling of Reinforced Concrete Short Beams and Beam-Column Joints*. London, University of Westminster, PhD Thesis, 1993

Otani (1974): Otani, S.: Inelastic analysis of RC frame structures. In: *ASCE Journal of Structural Division* 100 (1974), No. 7, pp. 1433-1449

Ožbolt (1998): Ožbolt, J.: *Manual for MASA 3 – Finite Element Program for 3D Nonlinear Analysis of Concrete and Reinforced Concrete Structures.* Stuttgart: IWB, University of Stuttgart, 1998

Ožbolt & Bazant (1992): Ožbolt, J.; Bazant Z. P.: Microplane Model for Cyclic Triaxial Behavior of Concrete. In: *ASCE Journal of Engineering Mechanics* 118 (1992), No. 7, pp. 1365-1386

Ožbolt & Bazant (1996): Ožbolt, J.; Bazant Z. P.: Numerical smeared fracture analysis: Nonlocal microcrack interaction approach. In: *International Journal for Numerical Methods in Engineering* 39 (1996), No. 4, pp. 635-661.

Ožbolt et al. (1998): Ožbolt, J.; Li, Y.; Eligehausen, R.: 3D-Analyse von Balken-Stützen-Verbindungen aus Normal und hochfestem Beton unter zyklischer Beanspruchung (Three-dimensional analysis of beam-column connections of normal and high strength concrete under cyclic loading). In: *Beton- und Stahlbetonbau* 93 (1998), No 4, pp. 91-97. (In German)

Ožbolt et al. (1999): Ožbolt, J.; Mayer, U.; Vocke, H.: Smeared Fracture FE-Analysis of Reinforced Concrete Structures – Theory and Examples. In: Shing, P.B.; Tanabe, T. (Eds.): *Modeling of Inelastic Behavior of RC Structures.* Reston, VA : ASCE, 1999, pp. 234-256

Ožbolt et al. (2001): Ožbolt, J.; Li, Y-J.; Kožar, I.: Microplane Model for Concrete with Relaxed Kinematic Constraint. In: *International Journal of Solid and Structures* 38 (2001), No. 16, pp. 2683-2711

Ožbolt et al. (2002): Ožbolt, J.; Lettow, S.; Kožar, I.: Discrete Bond Element for 3D Finite Element Analysis of Reinforced Concrete Structures. In: Balazs, G.L.; Bartos, P.J.M.; Cairns, J.; Borosnyói, A. (Eds.): *Bond in Concrete – from Research to Standards: Proceedings of the 3rd International Symposium: Budapest, Hungary, 20-22 November, 2002*. Budapest: Publ. Comp. of Budapest Univ. of Technology and Economics, 2002, pp. 9-19

P

Pampanin et al. (2002): Pampanin, S.; Calvi, G. M.; Moratti, M.: *Seismic Behaviour of R.C. Beam-Column Joints Design for Gravity Loads*. In: *12th European Conference on Earthquake Engineering, 9-13 September 2002, London*. Oxford: Elsevier, 2002, CD-Rom, Paper No. 726

Pampanin & Christopoulos (2003): Pampanin, S.; Christopoulos, C.: Non-invasive Retrofit of Existing RC Frames Designed for Gravity Loads only. In: *Concrete Structures in Seismic Regions: fib 2003 Symposium, May 6-8, Athens, Greece.* Athens: Technical Chamber of Greece, 2003, Paper No. 170

Pampanin et al. (2003): Pampanin, S.; Magenes, G.; Carr, A.: Modeling of Shear hinge Mechanism in Poorly Detailed RC Beam Column Joints In: *Concrete Structures in Seismic Regions: fib 2003 Symposium, May 6-8, Athens, Greece. Athens:* Technical Chamber of Greece, 2003, Paper No.171

Pampanin (2006): Pampanin, S.: Controversial aspects in seismic assessment and retrofit of structures in modern times: understanding and implementing lessons from ancient heritage. In: *Bulletin of New Zealand Society for Earthquake Engineering* 39 (2006), No. 2, pp. 120-133

Pampanin et al. (2006): Pampanin, S.; Christopoulos, C.; Chen, T.-H.: Development and validation of a metallic haunch seismic retrofit solution for existing under-designed RC frame buildings. In: *Earthquake Engineering and Structural Dynamics* 35 (2006), No. 14, pp. 1739-1766

Pampanin et al. (2007): Pampanin, S.; Bolognini, D.; Pavese, A.: Performance-Based Seismic Retrofit Strategy for Existing Reinforced Concrete Frame Systems Using Fiber-Reinforced Polymer Composites. In: *Journal of Composites for Construction* 11 (2007), No. 2, pp. 211-226

Pantelides et al. (2002): Pantelides, C. P.; Hansen, J. Nadauld, J.; Reaveley, L. D.: *Assessment of Reinforced Concrete Building Exterior Joints with Substandard Details*. Berkeley, CA: University of California. PEER Report 2002/18

Park (1997): Park, R.: A static force-based procedure for the seismic assessment of existing reinforced concrete moment resisting frames. In: *Bulletin of the New Zealand National Society for Earthquake Engineering* 30 (1997), No. 3 pp. 213-226

Park & Mosalam (2009): Park, S.; Mosalam, K. M.: *Shear Strength Models of Exterior Beam-Column Joints without Transverse Reinforcement*. Berkeley, CA: University of California, 2009. PEER Report 2009/106

Parker & Bullmann (1997): Parker, D. E.; Bullmann, P. J. M.: Shear strength within reinforced concrete beam-column joints. In: *The Structural Engineer* 75 (1997), No. 4, pp. 53-57

Paulay et al. (1978): Paulay, T.; Park, R.; Priestley, M. N. J.: Reinforced Concrete Beam-Column Joints under Seismic Actions. In: *ACI Journal* 75 (1978), No. 11, pp. 585-593

Paulay (1989): Paulay, T.: Equilibrium Criteria for Reinforced Concrete Beam-Column Joints. In: *ACI Structural Journal* 86 (1989), No. 6, pp. 635-643

Paulay & Priestley (1992): Paulay, T.; Priestley, M. J. N.: *Seismic Design of Reinforced Concrete and Masonry Buildings*. New York, NY: Wiley, 1992

Pinc et al. (1977): Pinc, R. L.; Watkins, M. D.; Jirsa, J. O.: *Strength of hooked bar anchorages in beam-column joints*. Austin, TX: University of Texas, 1977. CESRL Report No. 77-3

Pijaudier-Cabot & Bažant (1987): Pijaudier-Cabot, G.; Bažant Z. P.: Nonlocal Damage Theory. In: *ASCE Journal of Engineering Mechanics* 113 (1987), No. 10, pp. 1512-1533

Priestley et al. (1994): Priestley, M. N. J.; Verma R.; Xiao, Y.: Seismic shear strength of reinforced concrete columns. In: *ASCE Journal of Structural Engineering* 120 (1994), No. 8, pp. 2310-2329

Priestley (1997): Priestley, M. N. J.: Displacement-Based Seismic Assessment of Reinforced Concrete Buildings. In: *Journal of Earthquake Engineering* 1 (1997), No. 1, pp. 157-192

Priestley et al. (2007): Priestley, M. J. N.; Calvi, G. M.; Kowalsky M. J.: *Displacement-Based Seismic Design of Structures*. Pavia: IUSS Press, 2007

Pregartner & Asmus (2007): Pregartner, T.; Asmus, J.: *Load Bearing Behaviour of Bonded Expansion Anchors*. In: Eligehausen, R.; Fuchs, W.; Genesio, G.; Grosser, P. (Eds.): *Connections between Steel and Concrete: Stuttgart, Germany, September 4th - 7th, 2007, Vol. 1.* Stuttgart: Ibidem, 2007, pp. 341-352

R

Rabbat & Russel (1985): Rabbat, B. G.; Russel, H. G.: Friction Coefficient of Steel on Concrete or Grout. In: *ASCE Journal of Structural Engineering* 111 (1985), No. 3, pp. 505-515

Regio Decreto (1939): Regio Decreto 16 Novembre-XVIII, n. 2228, 1993. (In Italian)

Remmel (1994): Remmel, G.: *Zum Zug- und Schubtragverhalten von Bauteilen aus hochfestem Beton (Tension and shear behaviour of building components made from high strength concrete)*. Berlin: Beuth, 1994. Deutscher Ausschuss für Stahlbeton; 444. (In German)

Response (2001): Bentz, E.: *Response 2000 – User's manual*. Toronto: University of Toronto, 2001

RILEM (1982): RILEM: *Recommendation RC 5, Bond test for reinforcement steel, 1. Beam-test*. 2nd Edition. Bagneux: RILEM, 1982

Russo & Somma (2006): Russo, G.; Somma, G.: Shear Strength of Exterior Beam-Column Joints under Seismic Loading. In: *Proceedings of the 2nd fib Congress, Jun 5-8, 2006, Naples, Italy*. Napoli: fib Italia, 2006, Paper No. 9-38

S

SEAOC (1966): Structural Engineers Association of California: *Recommended lateral force requirements and commentary.* Sacramento, CA: SEAOC, 1966

SEAOC (1973): Structural Engineers Association of California: *Recommended lateral force requirements and commentary.* Sacramento, CA: SEAOC, 1973

SEAOC (1995): Structural Engineers Association of California*: A framework for performance-based seismic engineering*. Sacramento, CA: SEAOC, 1995. Vision 2000 Committee Report

Sagbas (2007): Sagbas, G.: *Nonlinear Finite Element Analysis of Beam-Column Subassemblies*. Toronto, University of Toronto, MS Thesis, 2007

Said & Nehdi (2001): Said, A.; Nehdi, M.: Rehabilitation of RC frame joints using local steel bracing. In: *Structure and Infrastructure Engineering* 4 (2001), No. 6, pp. 431-447

Santarella (1957): Santarella, L.: *Il cemento armato* (*The reinforced concrete*), *Vol 2.* Milan: Hoepli, 1957 (In Italian)

Sarsam & Phipps (1985): Sarsam, K. F.; Phipps, M. E.: The shear design of in situ reinforced concrete beam-column joints subjected to monotonic loading. In: *Magazine of Concrete Research* 37 (1985), No. 130, pp. 16-28

Sasmal (2009): Sasmal, S.: *Performance Evaluation and Strengthening of Deficient Beam-Column Sub-assemblages under Cyclic Loading*. Stuttgart, Universität, PhD Thesis, 2009

Sawabe & Okuzawa (1984): Sawabe Y, Okuzawa K.: *Studies on seismic retrofitting of existing reinforced concrete frames using post-cast shear walls*. Tokyo: Aoyama Lab., University of Tokyo, 1984 (In Japanese)

Scott (1992): Scott, R. H.: The effects of detailing on RC beam/column connection behaviour. In: *The Structural Engineer* 70 (1992), No. 18, pp. 318-324

Scott et al. (1994): Scott, R. H.; Feltham, I.; Whittle R. T.: Reinforced concrete beam-column connections and BS 8110. In: *The Structural Engineer 72* (1994), No. 4, pp. 55-60

Scott (1996): Scott, R. H.: Intrinsic mechanism in reinforced concrete beam-column connection behaviour. In: *ACI Structural Journal* 93 (1996), No. 3, pp. 336-346

Sezen & Moehle (2004): Sezen, H.; Moehle, J. P.: Shear strength for lightly reinforced column. In: *ASCE Journal of Structural Engineering* 103 (2004), No. 11, pp. 1692-1703

Sharma et al. (2009): Sharma, A.; Genesio, G.; Reddy, G.R.; Eligehausen, R.: Nonlinear dynamic analysis using microplane model for concrete and bond slip model for prediction of behavior of nonseismically detailed RCC beam-column joints. In: *Journal of Structural Engineering* 36 (2009), No. 4, pp. 250-257

Sharma et al. (2011): Sharma, A.; Eligehausen, R.; Reddy, G.R.: A new model to simulate joint shear behavior of poorly detailed beam–column connections in RC structures under seismic loads, part I: exterior joints. In: *Engineering Structures* 33 (2011), Nr. 3, pp. 1034-1051

Shin & LaFave (2004): Shin, M.; LaFave, J. M.: Modeling of cyclic joint shear deformation contribution in RC beam-column connection to overall frame behavior. In: *Structural Engineering and Mechanics* 18 (2004), No. 5, pp. 645-669

Shiohara (2004): Shiohara, H.: Quadruple flexural resistance in r/c beam-column joints. In: *13th World Conference on Earthquake Engineering, Conference Proceedings, August 1-6, 2004*. Vancouver: Canadian Association for Earthquake Engineering, Paper No. 491

Simons (2007): Simons, I. N.: V*erbundverhalten von eingemörtelten Bewehrungsstäben unter zyklischer Beanspruchung (Bond behaviour of post-installed reinforcing bars under cyclic loading)*. Stuttgart, Universität, PhD Thesis, 2007. (In German)

Silva (2007): Silva, J. F.: Open Questions in the Field of Anchorage to Concrete. In: *Beton- und Stahlbetonbau* 102 (2007), No. S1, pp. 2-6

Silva & Hoehler (2007): Silva, J. F.; Hoehler, M. S.: Seismic design provisions for anchors in the U.S. In: Eligehausen, R.; Fuchs, W.; Genesio, G.; Grosser, P. (Eds.): *Connections between Steel and Concrete: Stuttgart, Germany, September 4th - 7th, 2007, Vol. 1.* Stuttgart: Ibidem, 2007, pp.667-676

SP 22 (1982): Indian Standard SP 22:1982: *Explanatory Handbook on Codes for Earthquake Engineering IS:1893-1975 and IS:4326-1976*. New Delhi: Bureau of Indian Standards, 1982

SP 34 (1987): Indian Standard SP 34:1987: *Handbook of Concrete Reinforcing and Detailing*. New Delhi: Bureau of Indian Standards, 1987

T

Takeda et al. (1970): Takeda, T.; Sozen, M. A.; Nielsen, N. N.: Reinforced concrete response to simulated earthquakes. In: *ASCE Journal of Structural Engineering Division* 96 (1970), No. 12, pp. 2257-2273

Tassios & Vintzileou (1987): Tassios, T. P.; Vintzileou, E. N.: Concrete-to-Concrete Friction. In: *ASCE Journal of Structural Engineering* 113 (1987), No. 4, pp. 832-849

Taylor (1938): Taylor, G. I.: Plastic Strain in Metals. In: *Journal of the Institute of Metals* 62 (1938), pp. 307-324

Taylor (1974): Taylor, H. P. J.: T*he behaviour of in situ concrete beam-column joints*. London: Cement and Concrete Association, 1974. Technical Report

Taylor & Clarke (1976): Taylor, H. P. J.; Clarke, J. L.: Some detailing problems in concrete frame structures. In: *The Structural Engineer* 54 (1976), No. 1, pp. 19-32

Tsonos (2007): Tsonos, A. G.: Strength and Ductility of Cast-In-Place Beam-Column Joints. In: *ACI Structural Journal* 104 (2007), No. 4, pp. 468-478

Tsonos (1999): Tsonos, A. G.: Lateral Load Response of Strengthened RC Beam-to-Column Joint. In: *ACI Structural Journal* 96 (1999), No. 1, pp. 46–56

U

UNIDO (1983): United Nations Industrial Development Organization: *Repair and Strengthening of Reinforced Concrete, Stone and Brick-Masonry Buildings*. Vienna: UNIDO, 1983. UNDP / UNIDO Project RER/79/015. (Building Construction under Seismic Conditions in the Balkan Regions; 5)

V

Vecchio & Collins (1986): Vecchio, F. J.; Collins, M. P.: The modified-compression field theory for reinforced-concrete elements subjected to shear. In: *Journal of the ACI* 83 (1986) No. 2, pp. 219-231

Vecchio (2000): Vecchio, F. J.: The Disturbed Stress Field Model for Reinforced Concrete Formulation. In: *ASCE Journal of Structural Engineering* 126 (2000), No.9, pp. 1070-1077

Vollum (1998): Vollum, R. L.: *Design and Analysis of Exterior Beam Column Connections*. London, University of London, PhD Thesis, 1998

Vollum & Newmann (1999): Vollum, R. L.; Newmann, J. B.: The design of external reinforced concrete beam-column joints. In: *The Structural Engineer* 77 (1999), No. 23-24, pp. 21-27

Verderame et al. (2001): Verderame, G. M.; Stella, A.; Cosenza, E.: Le proprietà meccaniche degli acciai impiegati nelle strutture in c.a. realizzate negli anni ’60 (The mechanical properties of the steel used in RC structures in the 1960s). In: ANIDIS (Ed.): *X Congresso Nazionale L’Ingegneria Sismica in Italia, Potenza-Matera, Sept. 9-13, Italy.* Potenza: Lamisco, 2001. (In Italian)

W

Wolinski et al. (1987): Wolinski, D. A.; Hordijk, S.; Reinhardt, H.W., Cornelissen, H.A.W.: Influence of Aggregate Size on Fracture Mechanics Parameters of Concrete. In: *International Journal Cement Composites and Lightweight Concrete* 9 (1987), No. 2, pp. 95-103

Wong (2005): Wong, H. F.: *Shear Strength and Seismic Performance of Non-Seismically Designed RC Beam-Column Joints*. Hong Kong, University of Science and Technology, PhD Thesis, 2005

Wong & Kuang (2008): Wong, H. F.; Kuang, J. S.: Effects of beam-column depth ratio on joint seismic behaviour. In: *Structures and Buildings* 161 (2008); No. 2, pp. 91-101

Y

Youssef & Ghobarah (2001): Youssef, M.; Ghobarah, A.: Modelling of RC Beam-Column Joints and Structural Walls. In: Journal of Earthquake Engineering 5 (2001), No. 1, pp. 93-111

Yu et al. (2000): Yu, Q.-S.; Uang, C.-M.; Gross, J.: Seismic Rehabilitation Design of Steel Moment Connection with Welded Haunch. In: *ASCE Journal of Structural Engineering* 126 (2000), No. 1, pp. 69-78

Z

Zhang & Jirsa (1982): Zhang, L.; Jirsa, J.O.: *A Study of the Shear Behavior of RC Beam-Column Joints*. Austin, TX: University of Texas, 1982. PMFSEL Report No. 82-1

APPENDIX A: JOINT SHEAR STRENGTH MODELS

Empirical Models

Sarsam & Phipps (1985)
Based on test results Sarsam and Phipps developed a model for the estimation of the shear strength of beam-column joints taking into account the effect of various parameters, i.e., joint aspect ratio, amount of column reinforcement and column axial load. The limit states proposed are given in Equations (A-1) and (A-2):

$$v_{jc,cr} = 2.03 \cdot \left(f_{cc} \cdot \rho_c \cdot h_c / h_b\right)^{0.33} \left(1 + 0.29 \cdot N_c / A_c\right)^{0.5} \text{ (first diagonal crack)} \quad \text{(A-1)}$$

$$v_{jc} = 5.08 \cdot \left(f_{cc} \cdot \rho_c\right)^{0.33} \left(h_c / h_b\right)^{1.33} \left(1 + 0.29 \cdot N_c / A_c\right)^{0.5} \text{ (ultimate strength)} \quad \text{(A-2)}$$

The ultimate strength of the joint can be increased by the presence of stirrups by an additive element according to Equation (A-3):

$$V_{js} = 0.87 \cdot A_{js} \cdot f_y \text{ (ultimate strength)} \quad \text{(A-3)}$$

Vollum & Newman (1999)
Vollum and Newman believed in the impossibility to develop a realistic Strut-And-Tie model, due to the complexity of defining the joint dimension and equivalent strut width. Therefore, they proposed and empirical formula to calculate the ultimate joint shear strength including the effect of joint aspect ratio, anchorage configuration and transverse reinforcement (Eq. (A-4)).

$$v_j = v_{jc} + A_{js} \cdot f_y \quad \text{(A-4)}$$

with:

$$v_{jc} = 0.642 \cdot \beta \cdot \left[1 + 0.552 \cdot \left(2 - h_b / h_c\right)\right] \cdot \sqrt{f_c} \quad \text{(A-4a)}$$

with:
β = 1.0 and 0.9 for anchorage Type 1 and 3, respectively

Bakir & Boduroğlu (2002)
An empirical model by regression of published test data was developed by Bakir and Boduroğlu. This model takes into account parameters such as the amount of beam reinforcement and the aspect ratio, but it neglects the effect of the column axial load. It also distinguishes between anchorage of the beam bars Types 1 and 4. The ultimate limit state for the joint shear strength proposed by Bakir and Boduroğlu is given in Equation (A-5):

$$v_{jc} = \frac{0.71 \cdot \beta \cdot \gamma \cdot \left(\frac{100 \cdot A_{sb}}{w_b \cdot (h_b - c)} \right)^{0.4289}}{(h_b / h_c)^{0.61}} \sqrt{f_c} \quad \text{(A-5)}$$

with:
β = 1.0 and 0.85 for anchorage type 1 and 4, respectively and γ = 1.37 if inclined bars in the joint are provided and 1.0 if not

If transverse reinforcement is present, an additive contribution to the joint shear strength should be considered according to Equation (A-6).

$$v_{js} = \frac{\alpha \cdot A_{js} \cdot f_y}{b_j \cdot h_j \cdot \sqrt{f_c}} \quad \text{(A-6)}$$

with:
β = 0.37, 0.6 and 0.66 for high, medium and low amount of stirrups, respectively

Hegger at al. (2003)
The model proposed in *Vollum & Newman (1999)* was critically analysed and further developed on the basis of new experimental tests by Hegger. The influence of concrete compression strength was estimated with the cubic root in order to better take into account the influences of high strength concrete. The Equation (A-7), which includes also the influence of the amount of column reinforcement, was proposed:

$$v_{jc} = \alpha_1 \cdot \left(1.2 - 0.3 \cdot \frac{h_b}{h_c} \right) \cdot \left(1.0 + \frac{\rho_c - 0.5}{7.5} \right) \cdot 2\sqrt[3]{f_c} \quad \text{(A-7)}$$

with:
α_1 = 0.95 and 0.85 for anchorage Type 1 and 3, respectively. The Equation (A-7) is valid for: $0.75 \le h_b / h_c \le 2$ and $20 \le f_c \le 100$ MPa

The presence of stirrups or hairpins in the joint enhances the joint shear strength according to Equation (A-8):

$$v_j = \alpha_1 \cdot \min \begin{cases} \gamma_1 \cdot (v_c + \alpha_2 \cdot A_{js} \cdot f_y) \\ 2 \cdot v_c \\ \gamma_3 \cdot \gamma_4 \cdot 0.25 \cdot f_c \end{cases} \quad \text{(A-8)}$$

with:

γ_1 = 1.1 or 1.0	with or without diagonal reinforcement, respectively
γ_2 = 1.2 or 1.0	with or without anchorage with steel plate, respectively
$\gamma_3 = 1.5(1\text{-}0.8N_c/(A_c f_c)) \le 1.0$	influence of axial load in the column
$\gamma_4 = 1.9\text{-}0.6h_b/h_c \le 1.0$	influence of the joint slenderness ratio

α_2 = represents the efficiency of the transverse reinforcement as a function of its form

hairpins or hoops) and of the anchorage of the beam bars (90° or 180°) and it varies between 0.5 and 0.7 according to Table A 1.

Table A 1: coefficient α_2

Anchorage Type	Hairpins	Closed stirrups
1	0.7	0.6
3	0.6	0.5

Mahajan (2009)

The model proposed by Mahajan was calibrated on two experimental tests and the influence of different parameters was evaluated with numerical simulations. The Equation (A-9) offers an estimation of the joint shear ultimate strength including the effect of eccentricity between beam and column and reducing factor to account for cyclic loading.

$$V_{jc} = \gamma_1 \cdot \gamma_2 \cdot \cos\theta \cdot \left(2.5\sqrt{f_c} - 5.5\right) \cdot \left(0.03\sqrt{\frac{\rho_s \cdot f_{ys}}{f_c}} + 1.0\right) \cdot h_c \cdot w_{je} \qquad \text{(A-9)}$$

with:

γ_1 accounting for the positive effect of axial load in the column and can be calculated according to Equation (A-9a$_1$,a$_2$);

$$\gamma_1 = 1 + 1.1\frac{N_c}{A_c \cdot f_c} \qquad \text{for } N_c/A_c f_c \le 0.3 \qquad \text{(A-9a}_1\text{)}$$

$$\gamma_1 = 1.33 \qquad \text{for } N_c/A_c f_c > 0.3 \qquad \text{(A-9a}_1\text{)}$$

γ_2 = 1, and 0.75 for monotonic and cyclic loading respectively; θ = arctan(h_b / h_c) and w_{je} according Equation (A-9b):

$$w_{je} = w_b \cdot \left[1.1 \cdot \left(1 - \frac{w_b}{w_c}\right) - \left[0.75\frac{(e/w_b)}{(h_b/h_c)}\right]\right] \qquad \text{(A-9b)}$$

The confining effect of the joint transverse reinforcement is taken into account by Equation (A-9). The fraction of shear stress taken by the hoops in the joint can be evaluated with Equation (A-9c).

$$v_{js} = A_{js,eff} \cdot f_{ys} = \alpha_1 \cdot A_{js} \cdot f_{ys} \qquad \text{(A-9c)}$$

with:

α_1 being a function of the yield strength of the joint hoops, f_{ys}, expressed in terms of the tie index ω_s

$$\omega_s = \frac{A_s \cdot f_{ys}}{w_j \cdot h_c \cdot f_c} \qquad \text{(A-9c}_1\text{)}$$

for f_{ys} = 250 MPa

$$\begin{cases} 0 < \omega_s < 4 \rightarrow \alpha_1 = 0.70 + 0.15\omega_s \\ 4 < \omega_s < 8 \rightarrow \alpha_1 = 0.1 \end{cases} \qquad \text{(A-9c}_2\text{)}$$

for f_{ys} = 415 MPa $\quad \begin{cases} 0 < \omega_s < 7 \rightarrow \alpha_1 = 0.87 + 0.11\omega_s \\ 7 < \omega_s < 24 \rightarrow \alpha_1 = 0.1 \end{cases}$ (A-9c$_3$)

The formulation proposed by Mahajan is valid for 25 ≤ f_c ≤ 80 MPa and 0 ≤ $p_s f_s / f_c$ ≤ 66

Strut And Tie (SAT) Models

Nilsson (1973)

The joint shear strength was assessed by Nilsson by determining the bending moment in the beam at which diagonal tension crack occurs, which is expressed in Equation (A-10):

$$M_b = \frac{4}{3 \cdot \sqrt{5}} \cdot 0.8 \cdot z_b \cdot w_b \cdot l_{dc} \cdot f_{ct} \qquad \text{(A-10)}$$

with:

l_{dc} = length of the tensile crack

Hoekstra (1977)

The determination of the shear strength at which the diagonal tension crack occurs was proposed according to Equation (A-11) assuming the failure of the tension truss:

$$\tau_{cr} = \frac{0.65 \cdot f_{ct} + \sigma_{Nb}}{\tan \alpha} \qquad \text{(A-11)}$$

with:

σ_{Nb} = axial stress in the beam and α = inclination angle of the diagonal crack

Zhang & Jirsa (1982)

Based on the statistical analysis of a large database of monotonic and cyclic tests, Zhang and Jirsa derived a model for the estimation of the JS and BJ failure modes. The model takes into account the effect of several parameters including: the concrete strength, the column axial load, the transverse reinforcement ratio, the joint aspect ratio and the presence of lateral beams. For monotonic loading the joint shear strength is given by Equations (A-12a) and (A-12b).

$$Q_m = k \cdot \zeta \cdot \gamma \cdot f_c \cdot w_c \cdot \sqrt{a_c + a_b} \cdot \cos\theta \qquad \text{for JS failure mode} \qquad \text{(A-12a)}$$

$$Q_m = k \cdot \zeta \cdot \gamma \cdot f_c \cdot w_c \cdot a_c \cdot \cos\theta \qquad \text{for BJ failure mode} \qquad \text{(A-12b)}$$

with:

ζ = factor representing the effect of volumetric transverse reinforcement, ρ_s according to Equation (A-13a)

γ = factor representing the effect of the later beams according to Equation (A-13b)

θ = factor representing the angle of the inclination of the strut according to Equation (A-13c,d)

$$\zeta = 0.95 + 4.5 \cdot \rho_s \le 1.20 \text{ and } 0.01 \le \rho_s \le 0.06 \qquad \text{(A-13a)}$$

$$\gamma = 0.85 + 0.30 \frac{W_L}{h_c} \text{ and } 0.5 \le \frac{W_L}{h_c} \le 1.0 \qquad \text{(A-13b)}$$

with:
W_L = width of the lateral beam

$$\theta = \arctan\left(\frac{h_b - 2/3 \cdot a_b}{h_c - 2/3 \cdot a_c}\right) \text{ with JS failure mode} \quad \text{(A-13c)}$$

$$\theta = \arctan\left(\frac{h_b}{h_c - 2/3 \cdot a_c}\right) \text{ with BJ failure mode} \quad \text{(A-13d)}$$

with:
a_b and a_c being the depth of the compression zone in beam and column, respectively

In the case of cyclic loading the Equations (A-12a,b) have to be multiplied by the factor η, which is determined by Equation (A-14):

$$Q_c = \eta \cdot Q_m \text{ with } \eta = \begin{cases} 1.0 - 4.0\,\delta_b / L_b \\ 0.83 - 4.0\,\delta_b / L_b \end{cases} \quad \text{(A-14)}$$

Ortiz (1993)
In the SAT model proposed by Ortiz the concrete strut is assumed to fail according to the criteria proposed by the FIP-CEB Model Code 1990 (*CEB, 1993*). The failure of the compressive strut is expressed by Equation (A-15):

$$D/(w_i \cdot w_c) = \sigma_d = 0.6 f_c \cdot (1 - f_c/250) \quad \text{(A-15)}$$

with: w_i = width of the strut at the iteration *i*

A solution utilising an iterative procedure is needed because the geometry of the compression strut depends on the applied loading, since it is given by the forces in beam and column. The graphic visualisation of the strut is shown in Figure A 1.

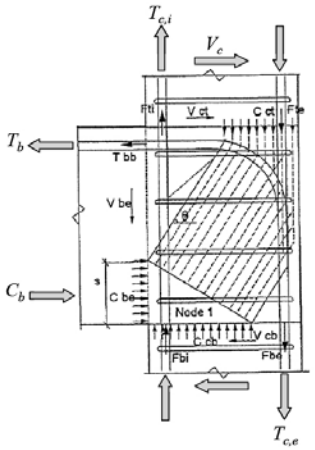

Figure A 1: Free body diagram of joint (*Ortiz, 1993*)

FEMA 273 (1997)
According to *FEMA 273 (1997)* the ultimate joint shear capacity can be expressed according to Equation (A-16):

$$V_j = \lambda_{FEMA} \cdot \Gamma \sqrt{f_c} \cdot A_j \quad \text{(A-16)}$$

with:

λ_{FEMA} = 0.75 and 1.0 for lightweight and normal weight concrete, respectively

Γ = 6 [psi$^{0.5}$] for exterior joints with ρ_j < 0.003

Parker & Bullman (1997)

According to the model proposed by Parker and Bullman the shear force resisted by the concrete is limited by the resistance of the compression strut (Figure A 2), which is expressed by the equation (A-17):

$$v_j = \alpha \cdot \upsilon \cdot f_{cc} \tag{A-17}$$

with:

$$\alpha = \left(1 - \arctan\frac{a_v}{h_c}\right) \Big/ \left(\arctan\frac{a_v}{h_c} + 1 \Big/ \arctan\frac{a_v}{h_c}\right) \tag{A-17b}$$

$$\upsilon = 0.56 - f_{cc}/310 < 0.40 \tag{A-17c}$$

a_v defined according Figure A 2

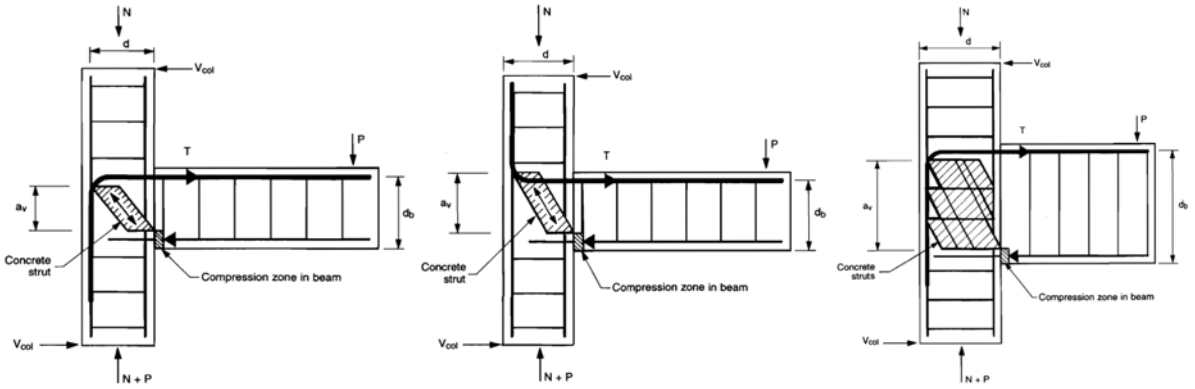

a) Anchorage Type 1 b) Anchorage Type 2 c) Anchorage Type 1 and trans. rein.

Figure A 2: Representation of the concrete strut for different joint configurations *(Parker & Bullman, 1997)*

Vollum (1998)

According to the model proposed by Vollum joint shear failure occurs when the maximum diagonal stress at the top node reaches the cracked concrete. The maximum stress and tensile strain are determined by Equation (A-18*)*.

$$\sigma_d = \lambda \cdot f_c \left[2\left(\frac{\varepsilon_2}{\varepsilon_0}\right) - \left(\frac{\varepsilon_2}{\varepsilon_0}\right)^2\right] \tag{A-18}$$

with:

$$\lambda = \frac{1}{0.8 - 0.34 \cdot \varepsilon_1/\varepsilon_0} \text{ and } \varepsilon_1 = \varepsilon_h + \left(\varepsilon_h - \varepsilon_1\right)\cot^2\theta$$

ε_1 and ε_2 are principle tensile and compressive strain, respectively; ε_0 is the maximum compressive (negative) strain in the diagonal strut assumed to be -0.002% and ε_h is the

tensile strain in the transverse direction. The coefficient *k* depends of the level of axial load in the column (Figure A 3a,b).

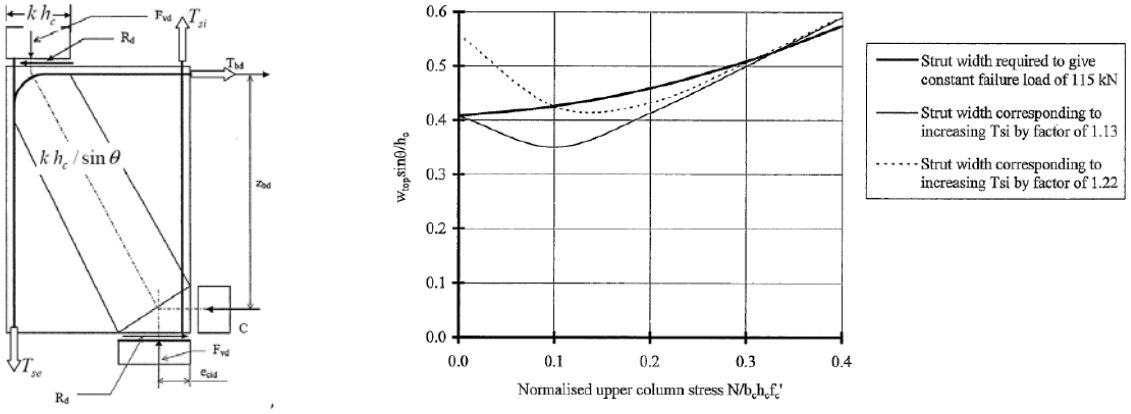

a) Free body diagram b) Calibration of the coefficient *k*

Figure A 3: Joint shear strength model by *Vollum (1998)*

Hwang & Lee (1999)

A softened SAT model was proposed by Hwang & Lee. According to this model the shear in the joint is transferred by three mechanisms: (i) diagonal strut mechanism, (ii) horizontal mechanism and (iii) vertical mechanism (see Figure A 4). The fraction of the components shown in Equation ((A-19) depends on the aspect ratio of the joint.

$$V_{jh} = D \cdot \cos\theta + F_h + F_v \cdot \cot\theta \qquad \text{(A-19)}$$

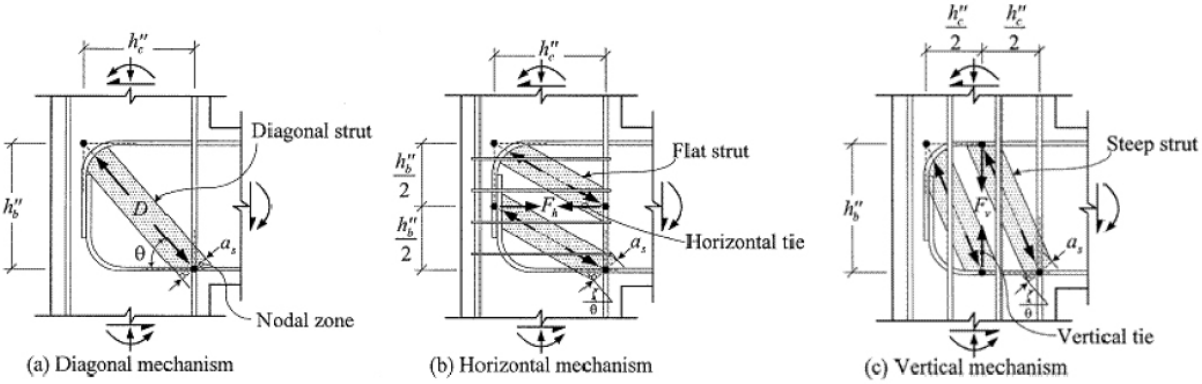

Figure A 4: Joint shear resisting mechanism proposed by *Hwang & Lee (1999)*

The solution of the problem can be obtained only through an iterative process and it was formulated for the failure of the concrete strut in the following cases:

- No yielding of reinforcement
- Yielding of joint hoops precedes the yielding of vertical reinforcement
- Yielding of vertical reinforcement precedes the yielding of joint hoops
- Yielding of hoops only
- Yielding of vertical reinforcement only

Park & Mosalam (2009)

Park and Mosalam developed a model to evaluate the shear strength of joints without shear reinforcement. The model assumes that the joint shear strength is resisted by two diagonal

struts (see Figure A 5). The major strut (ST1) is developed by the 90°-hook of the beam reinforcement (only anchorage Type 1 is taken into consideration). The minor strut (ST2) is developed by the bond of the concrete surrounding the beam reinforcement (only deformed bars are considered). The contribution of ST1 is considered negligible as long as ST2 is able to resist the entire horizontal shear force.

The shear force of the struts ST1 and ST2 can be expressed according Equation (A-20a,b):

$$V_{jh,ST1} = \alpha V_{jh} \tag{A-20a}$$

$$V_{jh,ST2} = (1-\alpha) V_{jh} \tag{A-20b}$$

with:

$$\alpha = \frac{H_c}{H_c - 0.85 h_b} \left(1 - \frac{4}{d_b} \frac{\int_0^h \mu(f_y)\, dx}{f_y} \right)$$

and $\mu(f_y)$ = is the bond stress distribution along the beam bar

The joint shear failure is defined by the failure of the strut ST1 according to Equation (A-21)

$$v_{jh,ST1,\max} = c \frac{\cos\theta \cdot \sqrt{f_c}}{1.31 + 0.085 \left(\frac{h_b}{h_c} \right)} \text{ and } c = \frac{\cos(0.83)}{1.31 + 0.085 \cdot 1.1} \tag{A-21}$$

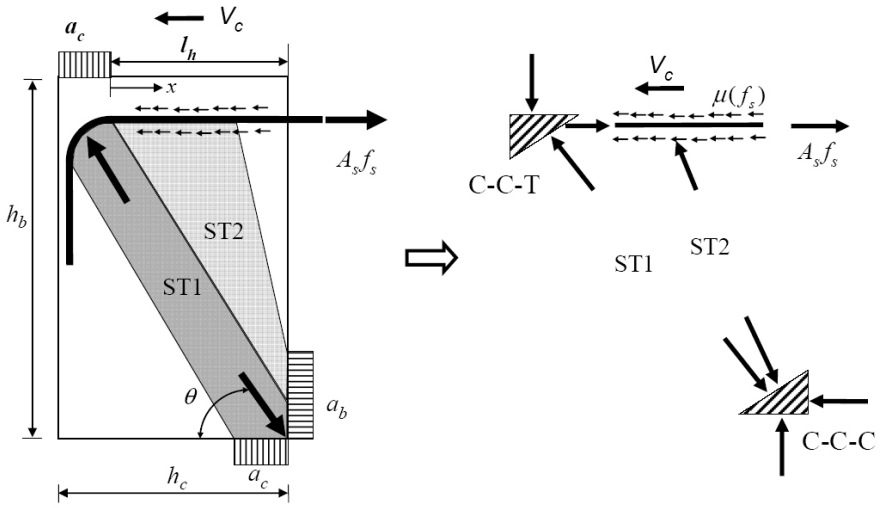

Figure A 5: Joint shear (*Park & Mosalam, 2009*)

Park and Mosalam also proposed a semi-empirical model that does not consider the contribution of the strut ST2. The joint shear strength can be calculated according to the following steps:

- Input of joint geometry and materials
- Determine Y_{min} and Y_{max} as shown in Figure A 6

- Calculate the beam reinforcement index (Eq. (A-22))

$$\frac{V_{jh}}{b_j \cdot h_c \sqrt{f_c}} \approx \left(\frac{A_s f_y}{b_j \cdot h_c \sqrt{f_c}} \right) \cdot \left(1 - 0.85 \frac{h_b}{H_c} \right) \quad \text{(A-22)}$$

- Check if the beam reinforcement index is located between X1 and X2, if so interpolate the corresponding overstrength as shown in Figure A 6
- Calculate the joint shear strength with Equation (A-23)

$$\frac{V_{jh}}{b_j \cdot h_c \sqrt{f_c}} \begin{cases} = \Phi \cdot \left(\frac{A_s f_y}{b_j \cdot h_c \sqrt{f_c}} \right) \cdot \left(1 - 0.85 \frac{h_b}{H_c} \right) \geq a_{\min} \frac{\cos\theta}{1.31 + 0.085 \left(h_b / h_c \right)} \\ \leq a_{\max} \frac{\cos\theta}{1.31 + 0.085 \left(h_b / h_c \right)} \end{cases} \quad \text{(A-23)}$$

with:

Φ = 1.0 to 1.25 overstrength factor for reinforcing steel

a_{min} = 21.1 mm

a_{max} = 48.5 mm

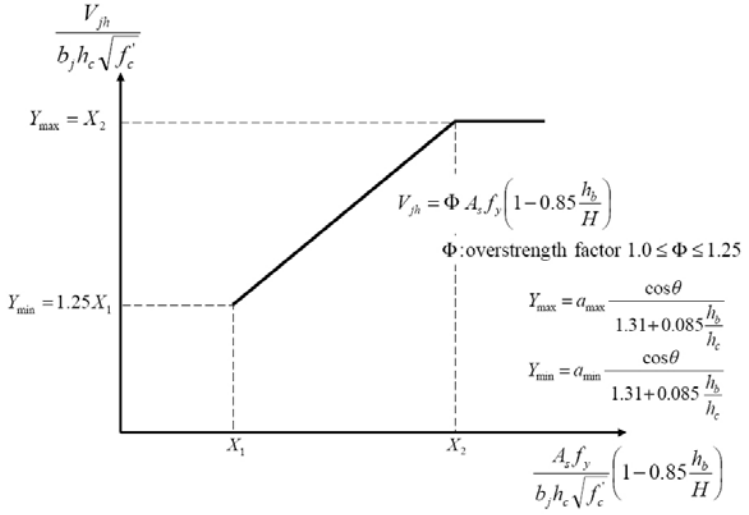

Figure A 6: Illustration of the semi-empirical model proposed by *Park & Mosalam (2009)*

Average plane stress models

Taylor (1974)

In order to guarantee that the joint is able to transfer the shear forces between the framing members two equations, for serviceability limit state (Eq. (A-24)) and ultimate limit state (Eq. (A-25)) were proposed.

$$v_{j,cr} = 0.67 \cdot \sqrt{f_{ct}^2 + f_a \cdot f_{ct}} \text{ (Diagonal cracking)} \quad \text{(A-24)}$$

$$\rho_b = \left(3 + \frac{2 \cdot h_c}{z_b} \right) \cdot \frac{b_c \cdot h_c}{b_b \cdot h_b} \cdot \frac{\beta \cdot v_c}{0.87 \cdot f_y} \text{ (Peak load)} \quad \text{(A-25)}$$

β is a factor which takes into account the redistribution of the beam moment in the column. The serviceability limit state is determined with a principal stress analysis considering the concrete tensile strength and column axial load. The ultimate limit state is given by an

equation, which limits the beam steel percentage in order to avoid the joint shear failure. In none of the limit states the influence of different beam bar anchorage detailing is taken into account.

Scott et al. (1994)
It was recognised by Scott *at al.* that a SAT model would be the most rigorous procedure to analyse the shear behaviour of a joint. However, it is very difficult to implement in normal design, because of the difficulty in determining the dimensions and inclination of the strut and the tie. In the model proposed by Scott *et al.* a formulation for the shear stress corresponding to the crushing of the joint is proposed (Eq. (A-26))

$$v_j = 2\sqrt{f_{cc}} \Big/ \left(j_b / j_c + j_c / j_b \right) \tag{A-26}$$

Hamil (2000)
On the base of experimental and numerical simulations limits for the formation of first diagonal cracking (Eq. (A-27)) and ultimate capacity (Eq. (A-28)) were proposed.

$$v_{jh,cr} = v_c \cdot \sqrt{1 + \frac{N_c}{h_c \cdot w_c \cdot v_c}} \text{ (Diagonal cracking)} \tag{A-27}$$

with:
v_c = design concrete shear stress for a reinforced concrete section according to *BS 8110 (1985)* Table 3.9.

$$v_{jh,u} = \alpha \cdot \beta \cdot \sqrt{f_c} \text{ (Peak load)} \tag{A-28}$$

with:
α = 1 and 0.83 for anchorage Types 1 and 3, respectively

$\beta = 0.25 \cdot \left(5.4 - \frac{h_b}{h_c} \right)$ is a reduction factor to take into account the aspect ratio

(valid for $1.4 \le \frac{h_b}{h_c} \le 2.0$)

Priestley (1997) and Pampanin et al. (2003)
Priestley proposed a formulation of the joint principle compression (p_c) and tension (p_t) stresses evaluated according to Mohr's circle theory in order to account for the contribution of the axial load on the column (Eq. (A-29)).

$$p_{c,t} = \frac{f_a}{2} \pm \sqrt{\left(\frac{f_a}{2} \right)^2 + v_{jh}^2} \tag{A-29}$$

On the base of experimental observations the lower limit of p_t for the joint diagonal cracking was proposed as $0.29\sqrt{f_c}$. Furthermore, it was observed that for joint with anchorage Type 2 the failure initiates at this principle tension level. For joints with anchorage Type 1 higher principle tension stresses up to $0.42\sqrt{f_c}$ are possible. Pampanin *et al.* extended the validity of the model for joints with plain round bars and 180°-hooks (anchorage type 6) proposing a

limit of $0.20\sqrt{f_c}$ for joint diagonal cracking. A strength degradation model was proposed as function of the shear deformation and interstorey drift (Figure A 7).

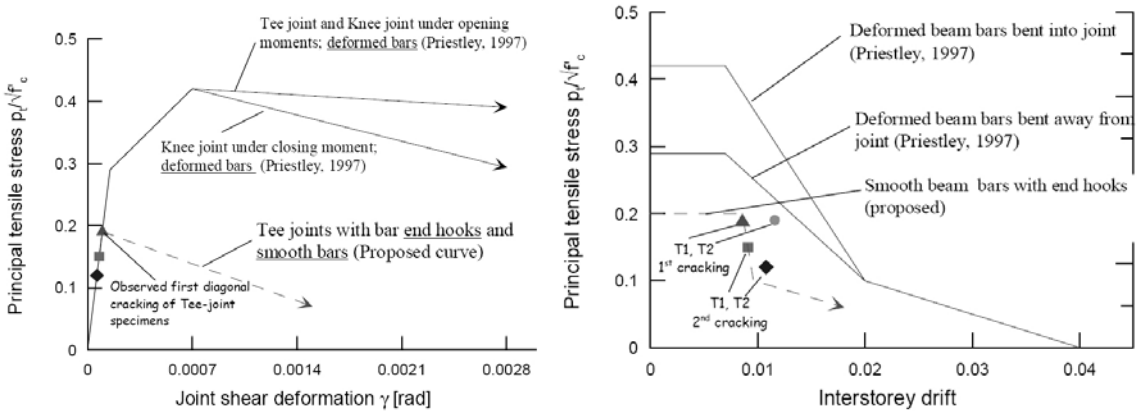

Figure A 7: Shear degradation curves for RC joints (*Priestley, 1997* and *Pampanin et al., 2003*)

Wong (2005)

Wong proposed a shear strength model for exterior joints, named "Modified Rotating-Angle-Softened-Truss Model" (MRA-STM), based on a proposed compatibility equation. The model considers the influence of the aspect ratio. It is also extended to consider the joint shear degradation in terms of displacement ductility by reducing the effective stress in the core. More information can be found in *Wong (2005)*.

Somma & Russo (2006)

Somma and Russo proposed a model, which takes into account three contributions to the joint shear strength:

- Axial force in the concrete strut, $v_{R,jh,c}$, according to Equation (A-30);
- Shear strength provided by the longitudinal reinforcement in the beam, $v_{R,jh,l}$, according to Equation (A-31); and
- Contribution of horizontal stirrups into the joint, $v_{R,jh,h}$, according to Equation (A-32).

$$v_{R,jh,c} = \bar{p}_t \sqrt{1 + \frac{|\sigma_a - \sigma_v|}{\bar{p}_t}} \tag{A-30}$$

$$v_{R,jh,l} = \frac{k_1 \cdot A_{sb} \cdot f_y}{A_j} \tag{A-31}$$

$$v_{R,jh,h} = \frac{k_h \cdot A_{sj} \cdot f_y}{A_j} \tag{A-32}$$

with:

$\bar{p}_t$ = principal stress derived by assuming $\sigma_v = f_c$

σ_a =vertical stress due to axial load in the column

σ_v = vertical stress due column longitudinal reinforcement

k_1 and k_h are experimentally calibrated coefficients

Tsonos (2007)

This model is based on the assumption of a fifth degree polynomial formulation for the biaxial concrete strength curve. It is assumed that the summation of vertical and horizontal forces equals the vertical and horizontal shear force as follows:

$$D_{cy} + \left(T_1 + T_2 + \ldots\right) = D_{cy} + D_{sy} = V_{jv} \tag{A-33}$$

$$D_{cx} + \left(D_{1x} + D_{2x} + \ldots\right) = D_{cx} + D_{sx} = V_{jh} \tag{A-34}$$

D_{cy} and D_{cx} are, respectively, the horizontal and vertical components of the compression force induced by the diagonal strut mechanism; T_i are the tension forces acting in the column longitudinal bars and D_{ix} are the components of the compression force induced by the truss mechanism (see Figure A 8).

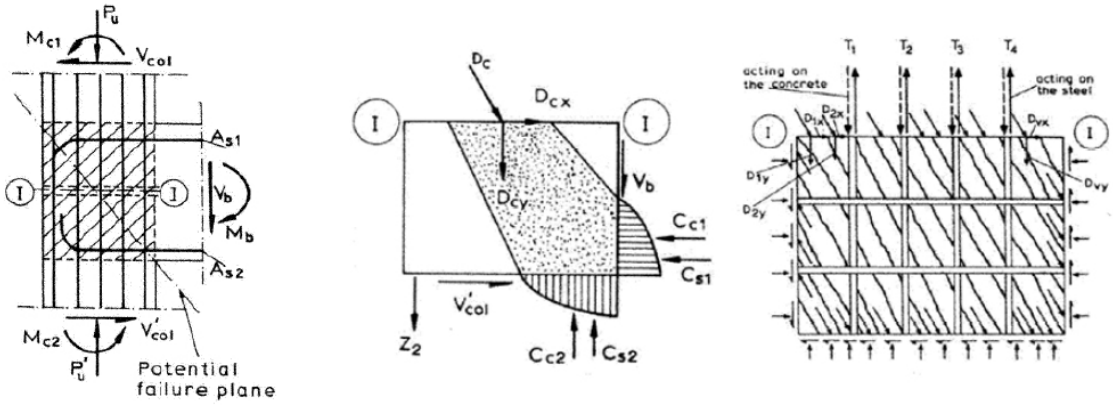

(a) Exterior beam-column joint (b) Diagonal strut mechanism (c) Truss mechanism

Figure A 8: Equilibrium of exterior beam-column joint (*Tsonos, 2007)*

The vertical axial compressive stress, σ, and the horizontal shear stress, v_{jh}, are calculated using Equations (A-35a,b), respectively.

$$\sigma = \frac{D_{cy} + D_{sy}}{w_c \cdot h_c} = \frac{V_{jv}}{w_c \cdot h_c} \tag{A-35a}$$

$$v_{jh} = \frac{V_{jh}}{w_c \cdot h_c} \tag{A-35b}$$

$$\sigma = \frac{V_{jv}}{V_{jh}} v_{jh} = \frac{h_b}{h_c} v_{jh} \tag{A-35c}$$

The principle compressive and tensile stresses are calculated according to the Mohr's circle theory by:

$$\sigma_{1,2} = \frac{\sigma}{2} \pm \frac{\sigma}{2}\sqrt{1 + 4\left(v_{jh}/\sigma\right)^2} \tag{A-36}$$

The joint shear strength can be calculated assuming:

$$-10\frac{\sigma_1}{f_c} + \left(\frac{\sigma_2}{f_c}\right)^2 = 1 \tag{A-37}$$

the model considers the effect of confinement of concrete due to the joint transverse reinforcement (Eq. (A-38)) and v_{jh} is assumed to be proportional to $\sqrt{f_c}$ (Eq. (A-39)).

$$f_c = \left(1 + \frac{\rho_s \cdot f_{ys}}{f_c'}\right) f_c' \tag{A-38}$$

$$v_{jh} = \gamma \cdot \sqrt{f_c} \tag{A-39}$$

Substituting the Equation (A-38) and (A-39) in Equation (A-37) the joint shear strength can be calculated.

Other models

Shiohara (2004)

In the model developed by Shiohara the joint shear failure of beam-column joints is limited by the quadruple flexural resistance. The joint shear deformation in assumed to be primarily due to the rotation of the four triangular concrete segments and the crack opening. Therefore, four sets of flexural resisting action are identified in the moment resistance of the beam-column connection (see Figure A 9a,b). The model considers two sets of critical sections associated with two independent deformation modes, called J-mode and B-mode (see Figure A 9d,e). The two modes (J-mode and B-mode) usually give different values of the joint strength, because of the difference in choice of the critical sections. The smaller value of strength is interpreted as the real strength and its mode is the dominant plastic mechanism. The joint strength can be calculated considering the forces shown in Figure A 9d,e and applying the following principles:

- Equilibrium should be satisfied in every critical section;
- Stress resultants should not exceed the material strength (concrete tensile and compressive strength, yielding strength of reinforcing bars and bond stress); and
- Diagonal cracks occur in two directions due to cyclic loading in the beam-column joint (cyclic loading is assumed).

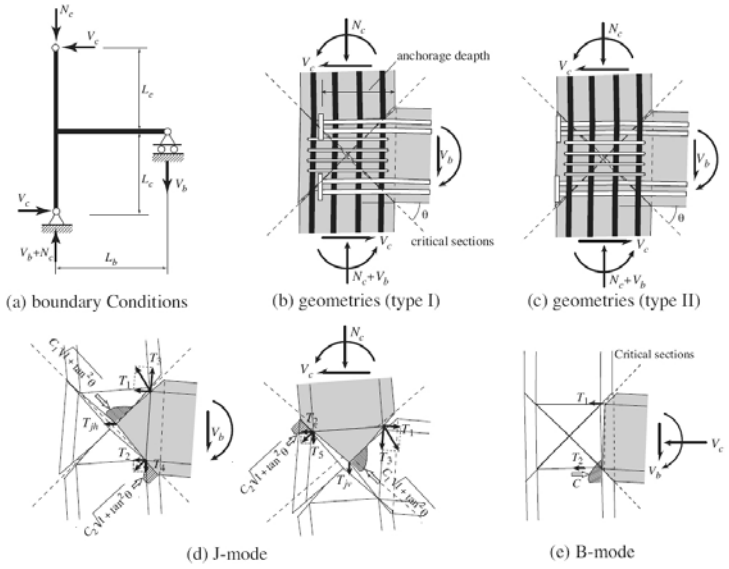

Figure A 9: Quadruple flexural resistance of exterior beam-column joint (*Shiohara, 2004*)

APPENDIX B: EXPERIMENTAL DATABASE

In this database only beam-column joints without transverse reinforcement in the core and failing in shear (in at least one of the loading directions in the case of cyclic loading) were included. Additionally following types of tests available in the literature are included:

- joints exhibiting a BJ-Mode;
- joints with transverse reinforcement in the core and information on the initial joint shear cracking; and
- joints with beam bars anchorage in the core shorter than the column depth.

Tests with deficient documentation in order to establish their reliability were also not taken into consideration in the statistical evaluation of the joint shear strength model proposed in Chapter 6.

Reinforcement Types

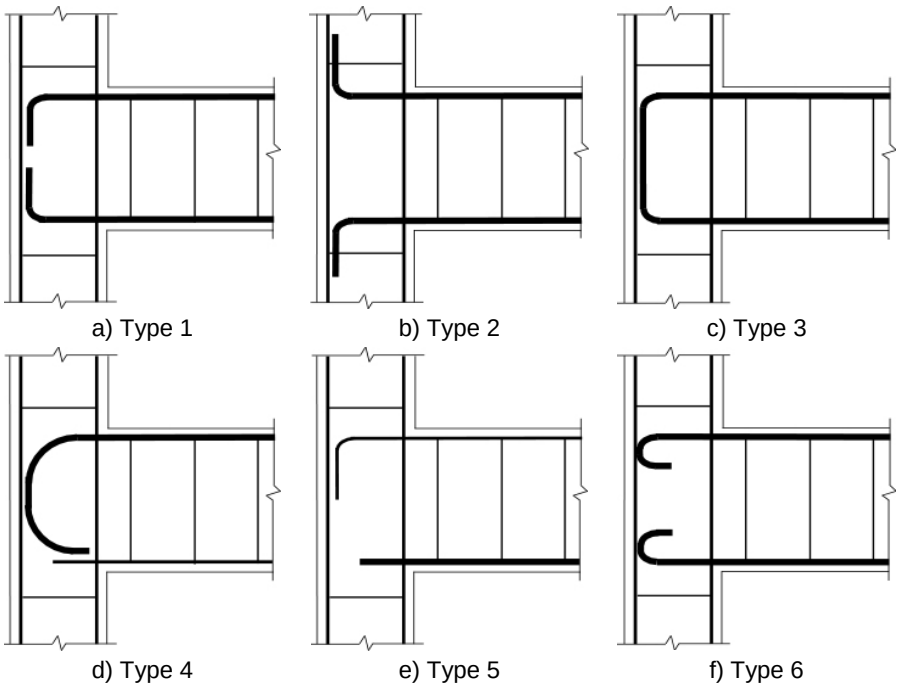

Figure B 1: Definition of anchorage Types

Reference		Loading		Materials					Geometry			Results (pos / neg loading direction for cyclic loading)						
No.	1st Author (year) / Specimen	Type	Axial Load [%]	Anchorage Top / bottom	f_c / f_{ct} [MPa]	f_y [MPa]	ρ_b / ρ'_b [%]	ρ_c [%]	H_c / L_b/2 [mm]	h_c x w_c [mm]	h_b x w_b [mm]	Failure mode	$V_{b,\,crack}$ [kN]	$\gamma_{j,crack}$ [rad]	$Drift_{crack}$ [%]	$V_{b,\,peak}$ [kN]	$\gamma_{j,peak}$ [rad]	$Drift_{peak}$ [%]
1	Nilsson (1973) / T1	mono	0	2 / 2	30.2 / 2.1	405	1.68 / 1.68	2.71	1900 / 1500	200 x 200	200 x 200	- / JS	- / 5.9	-	-	- / 9.8	-	-
2	Nilsson (1973) / T15	mono	0	2 / 2	29.6 / 2.5	679	0.65 / 0.65	0.45	1900 / 1500	200 x 200	200 x 200	- / JS	- / 4.9	-	-	- / 6.8	-	-
3	Nilsson (1973) / T11	mono	0	2 / 2	29.6 / 2.7	665	1.30 / 1.30	0.90	1900 / 1500	200 x 200	200 x 200	- / JS	- / 7.6	-	-	- / 7.8	-	-
4	Nilsson (1973) / T14	Mono	0	5 / 5	25.5 / 2.3	644	0.65 / 0.65	0.45	1900 / 1500	200 x 200	200 x 200	- / JS	- / 7.8	-	-	- / 9.8	-	-
5	Taylor (1974) / P2/41/24A	mono	32.9	1 / -	37.2 / -	460	2.20 / 2.20	2.33	1600 / 570	140 x 140	200 x 100	JS / -	32.9 / -	-	-	50.5 / -	-	-
6	Taylor (1974) / A3/41/13	mono	34.0	1 / -	36.0 / -	460	1.29 / 2.20	2.33	1600 / 570	140 x 140	200 x 100	JS / -	37.4 / -	-	-	44.8 / -	-	-
7	Taylor (1974) / D3/41/13	mono	6.6	1 / -	46.3 / -	460	1.29 / 2.20	2.33	1600 / 570	140 x 140	200 x 100	JS / -	25.7 / -	-	-	32.6 / -	-	-
8	Taylor (1974) / D3/41/09	mono	9.0	1 / -	34.0 / -	460	1.29 / 2.20	2.33	1600 / 570	140 x 140	200 x 100	JS / -	32.7 / -	-	-	28.8 / -	-	-
9	Taylor (1974) / E3/41/24c	mono	36.8	1 / -	33.3 / -	460	2.20 / 2.20	2.33	1600 / 570	140 x 140	200 x 100	JS / -	32.4 / -	-	-	32.7 / -	-	-
10	Taylor (1974) / C3/41/24x	mono	30.3	2 / -	40.4 / -	460	2.20 / 2.20	2.33	1600 / 570	140 x 140	200 x 100	JS / -	29.2 / -	-	-	32.6 / -	-	-
11	Hoekstra (1977) / 1001	mono	18.7	- / 4	19.3 / -	458	0.55 / 0.55	1.13	2000 / 600	200 x 150	300 x 150	- / JS	-	-	-	- / 55.0	-	-
12	Hoekstra (1977) / 1402	mono	32.3	- / 4	19.3 / -	400	1.11 / 1.11	2.33	2000 / 600	200 x 150	300 x 150	- / JS	-	-	-	- / 65.0	-	-
13	Hoekstra (1977) / 1003	mono	14.6	- / 4	24.6 / -	458	0.55 / 0.55	1.13	2000 / 600	200 x 150	300 x 150	- / JS	-	-	-	- / 69.0	-	-
14	Hoekstra (1977) / 1404	mono	25.3	- / 4	24.6 / -	400	1.11 / 1.11	2.33	2000 / 600	200 x 150	300 x 150	- / JS	-	-	-	- / 75.0	-	-
15	Hoekstra (1977) / 1005	mono	9.6	- / 4	37.5 / -	458	0.55 / 0.55	1.13	2000 / 600	200 x 150	300 x 150	- / JS	-	-	-	- / 68.0	-	-
16	Hoekstra (1977) / 1406	mono	16.6	- / 4	37.5 / -	400	1.11 / 1.11	2.33	2000 / 600	200 x 150	300 x 150	- / JS	-	-	-	- / 90.0	-	-
17	Hoekstra (1977) / 1007	mono	14.5	- / 1	24.9 / -	458	0.55 / 0.55	1.13	2000 / 600	200 x 150	300 x 150	- / JS	-	-	-	- / 63.0	-	-
18	Hoekstra (1977) / 1408	mono	6.2	- / 1	24.9 / -	400	1.11 / 1.11	2.33	2000 / 600	200 x 150	300 x 150	- / JS	-	-	-	- / 68.0	-	-
19	Hoekstra (1977) / 1615	mono	47.4	- / 4	21.5 / -	465	1.37 / 1.37	3.48	2000 / 600	200 x 150	300 x 150	- / JS	-	-	-	- / 74.0	-	-
20	Hoekstra (1977) / 1616	mono	47.4	- / 4	21.5 / -	465	1.37 / 1.37	3.48	2000 / 600	200 x 150	300 x 150	- / JS	-	-	-	- / 78.0	-	-
21	Morita (1984) / U40L	cyclic	0	1 / 1	24.8 / -	395	1.28 / 1.28	1.46	1500 / 900	300 x 300	380 x 260	JS / JS	-	-	-	130.0 / 130.0	-	-
22	Sarsam (1985) / EX 1	mono	17.3	0 / 1	56.3 / -	517	1.00 / 1.00	1.50	1530 / 1524	205 / 150	305 x 150	- / JS	- / 29.6	-	-	- / 41.6	-	-
23	Sarsam (1985) / EX 2	mono	18.1	0 / 1	53.9 / -	517	1.00 / 1.00	1.50	1530 / 1524	205 / 150	305 x 150	- / JS	- / 29.2	-	-	- / 39.2	-	-
24	Sarsam (1985) / EX 3	mono	23.6	0 / 1	41.3 / -	517	1.00 / 1.00	1.50	1530 / 1524	205 / 150	305 x 150	- / JS	- / 26.3	-	-	- / 84.9	-	-
25	Sarsam (1985) / EX 4	mono	19.8	0 / 1	49.3 / -	517	1.00 / 1.00	1.50	1530 / 1524	205 / 150	305 x 150	- / JS	- / 26.7	-	-	- / 66.8	-	-
26	Sarsam (1985) / EX 5	mono	20.1	0 / 1	48.5 / -	517	1.00 / 1.00	1.50	1530 / 1524	205 / 150	305 x 150	- / JS	- / 28.8	-	-	- / 39.2	-	-
27	Blakie (1988) / Ext.	cyclic	0	1 / 1	25.7 / -	320	2.10 / 2.10	0.45	3658 / 2130	460 / 500	625 / 400	JS / JS	-	-	-	210.0 / 260.0	-	-
28	Nishimura (1988) / A4	mono	0	1 / -	30.5 / 3.1	350	0.83 / 0.83	0.48	1500 / 1025	250 x 250	300 x 180	BJ / -	-	-	-	36.9 / -	-	-
29	Nishimura (1988) / A5	mono	0	1 / -	36.9 / 3.4	350	0.83 / 0.83	0.48	1500 / 1025	250 x 250	300 x 180	BJ / -	-	-	-	38.7 / -	-	-
30	Nishimura (1988) / U4	mono	0	2 / -	30.5 / -	350	0.83 / 0.83	0.48	1500 / 1025	250 x 250	300 x 180	JS / -	-	-	-	21.6 /	-	-
31	Nishimura (1988) / U5	mono	0	2 / -	36.9 / -	350	0.83 / 0.83	0.48	1500 / 1025	250 x 250	300 x 180	JS / -	-	-	-	25.2 /	-	-

Reference		Loading		Materials					Geometry			Results (pos / neg loading direction for cyclic loading)						
No.	1st Author (year) / Specimen	Type	Axial Load [%]	Anchorage Top / bottom	f_c / f_{ct} [MPa]	f_y [MPa]	ρ_b / ρ'_b [%]	ρ_c [%]	H_c / L_b/2 [mm]	h_c x w_c [mm]	h_b x w_b [mm]	Failure mode	$V_{b,\,crack}$ [kN]	$\gamma_{i,crack}$ [rad]	$Drift_{crack}$ [%]	$V_{b,\,peak}$ [kN]	$\gamma_{i,peak}$ [rad]	$Drift_{peak}$ [%]
32	Nishimura (1988) / A41N	mono	10	1 / -	25.2 / 3.5	350	0.83 / 0.83	0.48	1500 / 1025	250 x 250	300 x 180	BJ / -	-	-	-	51.3 / -	-	-
33	Nishimura (1988) / U41N	mono	10	2 / -	25.2 / 3.5	350	0.83 / 0.83	0.48	1500 / 1025	250 x 250	300 x 180	JS / -	-	-	-	34.1 / -	-	-
34	Nishimura (1988) / U42N	mono	20	2 / -	25.9 / 2.2	350	0.83 / 0.83	0.48	1500 / 1025	250 x 250	300 x 180	BJ / -	-	-	-	43.5 / -	-	-
35	Nishimura (1988) / U4A	mono	0	2 / -	29.6 / 2.8	350	0.83 / 0.83	0.48	1500 / 1025	250 x 250	300 x 180	JS / -	-	-	-	27.9 / -	-	-
36	Nishimura (1988) / A2	mono	0	1 / -	36.9 / 3.4	350	0.83 / 0.83	0.48	1500 / 1025	250 x 250	300 x 180	JS / -	-	-	-	17.0 / -	-	-
37	Nishimura (1988) / A3	mono	0	1 / -	36.9 / 3.4	350	0.83 / 0.83	0.48	1500 / 1025	250 x 250	300 x 180	JS / -	-	-	-	28.4 / -	-	-
38	Nishimura (1988) / A21N	mono	10	1 / -	25.2 / 3.5	350	0.83 / 0.83	0.48	1500 / 1025	250 x 250	300 x 180	JS / -	-	-	-	27.0 / -		
39	Nishimura (1988) / A22N	mono	20	1 / -	25.0 / 2.2	350	0.83 / 0.83	0.48	1500 / 1025	250 x 250	300 x 180	JS / -	-	-	-	37.6 / -	-	-
40	Nishimura (1988) / U2	mono	0	2 / -	35.6 / 2.4	350	0.83 / 0.83	0.48	1500 / 1025	250 x 250	300 x 180	JS / -	-	-	-	19.8 / -	-	-
41	Nishimura (1988) / U3	mono	0	2 / -	35.3 / 3.4	350	0.83 / 0.83	0.48	1500 / 1025	250 x 250	300 x 180	JS / -	-	-	-	23.9 / -	-	-
42	Nishimura (1988) / U21N	mono	10	2 / -	25.5 / 3.5	350	0.83 / 0.83	0.48	1500 / 1025	250 x 250	300 x 180	JS / -	-	-	-	23.2 / -	-	-
43	Nishimura (1988) / U22N	mono	20	2 / -	25.9 / 2.2	350	0.83 / 0.83	0.48	1500 / 1025	250 x 250	300 x 180	JS / -	-	-	-	24.4 / -	-	-
44	Ortiz (1993) / BCJ1	mono	0	- / 1	34.0 / -	600	1.11 / 1.11	1.15	2000 / 1200	300 x 300	400 x 200	- / JS	-	-	-	- / 118.0	-	-
45	Ortiz (1993) / BCJ3	mono	0	- / 1	33.0 / -	600	1.11 / 1.11	1.15	2000 / 1200	300 x 300	400 x 200	- / JS	-	-	-	- / 128.0	-	-
46	Ortiz (1993) / BCJ5	mono	0	- / 1	38.0 / -	600	1.11 / 1.11	1.91	2000 / 1200	300 x 300	400 x 200	- / JS	-	-	-	- / 115.0	-	-
47	Ortiz (1993) / BCJ6	mono	0	- / 1	35.0 / -	600	1.11 / 1.11	1.91	2000 / 1200	300 x 300	400 x 200	- / JS	-	-	-	- / 115.0	-	-
48	Scott (1996) / C1	mono	33.6	- / 1	36.4 / 2.5	500	1.14 / 1.14	2.23	1500 / 825	150 x 150	210 x 110	- / BJ	- / 17.1	-	-	- / 26.2	-	-
49	Scott (1996) / C1A	mono	27.8	- / 1	44.0 / 2.7	500	1.14 / 1.14	2.23	1500 / 825	150 x 150	210 x 110	- / BJ	- / 19.0	-	-	- / 26.8	-	-
50	Scott (1996) / C1AL	mono	7.4	- / 1	30.2 / 2.1	500	1.14 / 1.14	2.23	1500 / 825	150 x 150	210 x 110	- / JS	- / 11.0	-	-	- / 22.0	-	-
51	Scott (1996) / C2	mono	26.8	- / 2	45.6 / 3.2	500	1.14 / 1.14	2.23	1500 / 825	150 x 150	210 x 110	- / JS	- / 18.9	-	-	- / 21.5	-	-
52	Scott (1996) / C3	mono	37.4	3 / 3	32.7 / 3.1	500	1.14 / 1.14	2.23	1500 / 825	150 x 150	210 x 110	- / BJ	- / 19.9	-	-	- / 25.9	-	-
53	Scott (1996) / C3L	mono	6.9	3 / 3	32.2 / 2.6	500	1.14 / 1.14	2.23	1500 / 825	150 x 150	210 x 110	- / JS	- / 12.5	-	-	- / 21.6	-	-
54	Scott (1996) / C4	mono	32.2	- / 1	37.9 / 3.2	500	2.03 / 2.03	2.23	1500 / 825	150 x 150	210 x 110	- / JS	- / 18.8	-	-	- / 29.7	-	-
55	Scott (1996) / C4A	mono	30.1	- / 1	40.6 / 3.0	500	2.03 / 2.03	2.23	1500 / 825	150 x 150	210 x 110	- / JS	- / 18.8	-	-	- / 31.8	-	-
56	Scott (1996) / C4AL	mono	6.9	- / 1	32.4 / 2.4	500	2.03 / 2.03	2.23	1500 / 825	150 x 150	210 x 110	- / JS	- / 12.1	-	-	- / 28.3	-	-
57	Scott (1996) / C5	mono	40.9	- / 2	29.9 / 2.8	500	2.03 / 2.03	2.23	1500 / 825	150 x 150	210 x 110	- / JS	- / 9.7	-	-	- / 13.8	-	-
58	Scott (1996) / C6	mono	33.7	3 / 3	36.3 / 2.6	500	2.03 / 2.03	2.23	1500 / 825	150 x 150	210 x 110	- / JS	- / 14.8	-	-	- / 21.8	-	-
59	Scott (1996) / C6L	mono	5.3	3 / 3	42.1 / 2.8	500	2.03 / 2.03	2.23	1500 / 825	150 x 150	210 x 110	- / JS	- / 14.8	-	-	- / 26.0	-	-
60	Scott (1996) / C7	mono	38.3	- / 1	31.9 / 3.0	500	1.35 / 1.35	2.23	1500 / 825	150 x 150	300 x 110	- / JS	- / 22.2	-	-	- / 32.0	-	-
61	Scott (1996) / C8	mono	30.0	- / 2	40.8 / 3.4	500	1.35 / 1.35	2.23	1500 / 825	150 x 150	300 x 110	- / JS	- / 26.2	-	-	- / 27.3	-	-
62	Scott (1996) / C9	mono	37.5	3 / 3	32.6 / 3.0	500	1.35 / 1.35	2.23	1500 / 825	150 x 150	300 x 110	- / JS	- / 22.9	-	-	- / 27.9	-	-
63	Parker (1997) / 4a	mono	0	- / 1	39.2 / -	570	0.88 / 0.88	0.55	2000 / 1000	300 x 300	500 x 250	- / JS	-	-	-	- / 118	-	-
64	Parker (1997) / 4b	mono	8.5	- / 1	39.2 /	570	0.88 / 0.88	0.55	2000 / 1000	300 x 300	500 x 250	- / JS	-	-	-	- / 138	-	-

Reference		Loading		Materials					Geometry			Results (pos / neg loading direction for cyclic loading)						
No.	1st Author (year) / Specimen	Type	Axial Load [%]	Anchorage Top / bottom	f_c / f_{ct} [MPa]	f_y [MPa]	ρ_b / ρ'_b [%]	ρ_c [%]	H_c / L_b/2 [mm]	h_c x w_c [mm]	h_b x w_b [mm]	Failure mode	$V_{b,\,crack}$ [kN]	$\gamma_{i,crack}$ [rad]	$Drift_{crack}$ [%]	$V_{b,\,peak}$ [kN]	$\gamma_{i,peak}$ [rad]	$Drift_{peak}$ [%]
65	Parker (1997) / 4c	mono	17.2	- / 1	36.8 /	570	0.88 / 0.88	0.55	2000 / 1000	300 x 300	500 x 250	- / JS	-	-	-	- / 170	-	-
66	Parker (1997) / 4d	mono	0	- / 1	39.2 /	570	0.88 / 0.88	2.19	2000 / 1000	300 x 300	500 x 250	- / JS	-	-	-	- / 150	-	-
67	Parker (1997) / 4e	mono	8.3	- / 1	40.3 /	570	0.88 / 0.88	2.19	2000 / 1000	300 x 300	500 x 250	- / JS	-	-	-	- / 160	-	-
68	Parker (1997) / 4f	mono	16.8	- / 1	37.8 /	570	0.88 / 0.88	2.19	2000 / 1000	300 x 300	500 x 250	- / JS	-	-	-	- / 183	-	-
69	Clyde (2000) / #2	cyclic	10.0	1 / 1	46.2 / -	450	2.30 / 2.30	1.21	2570 / 1499	457 / 305	406 / 305	JS / JS	- / 187.0	- / 0.001	- / 0.9	245.0 / 290.0	- / 0.007	- / 1.9
70	Clyde (2000) / #4	cyclic	25.0	1 / 1	41.0 /	450	2.30 / 2.30	1.21	2570 / 1499	457 / 305	406 / 305	JS / JS	- / 227.0	- / 0.001	- / 0.5	260.0 / 295.0	- / 0.014	- / 0.7
71	Clyde (2000) / #5	cyclic	25.0	1 / 1	37.0 /	450	2.30 / 2.30	1.21	2570 / 1499	457 / 305	406 / 305	JS / JS	- / 209.0	- / 0.002	- / 0.5	260.0 / 260.0	- / 0.017	- / 1.7
72	Clyde (2000) / #6	cyclic	10.0	1 / 1	40.1 /	450	2.30 / 2.30	1.21	2570 / 1499	457 / 305	406 / 305	JS / JS	- / 182.0	- / 0.001	- / 0.6	235.0 / 275.0	- / 0.019	- / 1.9
73	Hakuto (2000) / O7	cyclic	0	2 / 2	31.0 / -	308	0.66 / 0.98	0.47	3200 / 1905	460 x 460	500 x 300	JS / JS	67.2 / 75.6	0.001 / -	0.5 / 1.0	67.2 / 75.6	0.004 /	0.5 / 1.0
74	Hamil (2000) / C4ALN0	mono	5.7	1 / 1	38.8 / 2.7	500	2.03 / 2.03	2.23	1750 / 825	150 x 150	210 x 110	- / JS	- / 13.2	-	-	- / 26.5	-	-
75	Hamil (2000) / C4ALN1	mono	5.3	1 / 1	41.9 / 3.2	500	2.03 / 2.03	2.23	1750 / 825	150 x 150	210 x 110	- / JS	- / 18.7	-	-	- / 33.5	-	-
76	Hamil (2000) / C4ALN3	mono	5.8	1 / 1	38.0 / 2.9	500	2.03 / 2.03	2.23	1750 / 825	150 x 150	210 x 110	- / JS	- / 15.7	-	-	- / 33.2	-	-
77	Hamil (2000) / C4ALN5	mono	4.8	1 / 1	46.6 / 3.2	500	2.03 / 2.03	2.23	1750 / 825	150 x 150	210 x 110	- / JS	- / 16.1	-	-	- / 39.5	-	-
78	Hamil (2000) / C6LN0	mono	4.7	3 / 3	47.4 / 3.4	500	2.03 / 2.03	2.23	1750 / 825	150 x 150	210 x 110	- / JS	- / 18.5	-	-	- / 23.9	-	-
79	Hamil (2000) / C6N0	mono	4.9	3 /3	47.4 / 3.3	500	2.03 / 2.03	2.23	1750 / 825	150 x 150	210 x 110	- / JS	-	-	-	- / 24.6	-	-
80	Hamil (2000) / C6LN1	mono	4.9	3 / 3	45.0 / 3.2	500	2.03 / 2.03	2.23	1750 / 825	150 x 150	210 x 110	- / JS	- / 18.1	-	-	- / 27.5	-	-
81	Hamil (2000) / C6LN3	mono	4.9	3 / 3	45.0 / 3.2	500	2.03 / 2.03	2.23	1750 / 825	150 x 150	210 x 110	- / JS	- / 17.8	-	-	- / 28.7	-	-
82	Hamil (2000) / C6LN5	mono	6.7	3 / 3	33.4 / 2.7	500	2.03 / 2.03	2.23	1750 / 825	150 x 150	210 x 110	- / JS	- / 14.7	-	-	- / 33.9	-	-
83	Hamil (2000) / C7LN0	mono	6.3	- / 1	35.0 / 2.6	500	1.35 / 1.35	2.23	1750 / 825	150 x 150	300 x 110	- / JS	- / 23.5	-	-	- / 35.7	-	-
84	Hamil (2000) / C9LN0	mono	6.3	3 / 3	35.0 / 3.4	500	1.35 / 1.35	2.23	1750 / 825	150 x 150	300 x 110	- / JS	- / 19.6	-	-	- / 33.3	-	-
85	Braga (2001a) / T23-1	cyclic	17.2	6 / 6	17.4 /	-	0.51 / 0.51	0.67	2000 / 1500	200 x 200	330 x 200	JS / JS	-	-	-	15.3 / 18.1	-	2.5 / 2.5
86	Ghobarah (2001) / T1	cyclic	19.5	1 / 1	30.8 / -	425	1.27 / 1.27	0.96	2750 / 2070	400 x 250	400 x 250	BJ / BJ	-	-	-	116.8 / 218.4	-	-
87	Pampanin (2002) / T1	cyclic	10.0	6 / 6	23.9 / -	345	0.54 / 0.54	0.43	2330 / 1600	200 x 200	330 x 200	JS / JS	14.6 / 16.8	0.001 / -	0.9 / 0.9	14.6 / 16.8	0.005 / -	0.9 / 0.9
88	Pampanin (2002) / T2	cyclic	25.0	6 / 6	23.9 / -	345	0.35 / 0.35	0.43	2330 / 1600	200 x 200	330 x 200	JS / BJ	12.3 / 16.0	0.001 / -	1.1 / 1.1	12.3 / 16.0	-	1.1 / 1.1
89	Pantelides (2002) / TU1	cyclic	10.0	5 / 4	33.1 / -	455	1.71 / 1.71	1.36	3900 / 1703	406 / 406	406 x 406	JS / JS	81.7 / 134.4	0.002 / 0.001	0.75 / 0.75	92.3 / 192.2	0.010 / 004	1.5 / 1.5
90	Pantelides (2002) / TU2	cyclic	25.0	5 / 4	30.2 / -	455	1.71 / 1.71	1.36	3900 / 1703	406 / 406	406 x 406	JS / JS	101.8 / 126.1	0.001 / 0.001	0.75 / 0.75	125.8 / 189.9	0.007 / 0.005	1.5 / 1.5
91	Pantelides (2002) / TU3	cyclic	10.0	5 / 4	34.0 / -	455	1.71 / 1.71	1.36	3900 / 1703	406 / 406	406 x 406	JS / JS	123.3 / 113.8	0.001 / 0.001	0.75 / 0.75	187.5 / 184.2	0.010 / 0.009	2.0 / 2.0
92	Pantelides (2002) / TU4	cyclic	25.0	5 / 4	31.6 / -	455	1.71 / 1.71	1.36	3900 / 1703	406 / 406	406 x 406	JS / JS	105.9 / 127.9	0.001 / 0.001	1.0 / 0.75	211.4 / 301.2	0.008 / 0.009	2.0 / 2.0
93	Pantelides (2002) / TU5	cyclic	10.0	4 / 4	31.7 / -	455	1.71 / 1.71	1.36	3900 / 1703	406 / 406	406 x 406	JS / JS	104.9 / 93.1	0.001 / 0.001	0.75 / 0.75	170.0 / 291.0	0.008 / 0.008	2.0 / 2.0
94	Pantelides (2002) / TU6	cyclic	25.0	4 / 4	31.0 / -	455	1.71 / 1.71	1.36	3900 / 1703	406 / 406	406 x 406	JS / JS	136.1 / 134.4	0.001 / 0.001	1.0 / 1.0	192.0 / 296.4	0.007 / 0.008	2.0 / 2.0
95	Antonopoulos (2003) / C1	cyclic	5.9	1 / 1	19.5 / -	585	0.87 / 0.87	0.93	1500 / 1100	200 x 200	300 x 200	JS / JS	-	-	-	31.3 / 27.1	-	-
96	Antonopoulos (2003) / C2	cyclic	4.9	1 / 1	23.7 / -	585	0.87 / 0.87	0.93	1500 / 1100	200 x 200	300 x 200	JS / JS	-	-	-	30.8 / 31.1	-	-
97	Antonopoulos (2003)/S-C	cyclic	6.0	1 / 1	19.3 / -	585	0.87 / 0.87	0.93	1500 / 1100	200 x 200	300 x 200	JS / JS	-	-	-	33.3 / 32.2	-	-

Reference		Loading		Materials					Geometry			Results (pos / neg loading direction for cyclic loading)						
No.	1st Author (year) / Specimen	Type	Axial Load [%]	Anchorage Top / bottom	f_c / f_{ct} [MPa]	f_y [MPa]	ρ_b / ρ'_b [%]	ρ_c [%]	H_c / L_b/2 [mm]	h_c x w_c [mm]	h_b x w_b [mm]	Failure mode	$V_{b,\,crack}$ [kN]	$\gamma_{i,crack}$ [rad]	$Drift_{crack}$ [%]	$V_{b,\,peak}$ [kN]	$\gamma_{i,peak}$ [rad]	$Drift_{peak}$ [%]
98	Hertanto (2005) / TDP1	cyclic	var.	6 / 6	22.9 / -	348	0.26 / 0.51	0.50	2000 / 1525	230 x 230	330 x 200	BJ / JS	- / 21.0	- / 0.001	- / 1.25	11.8 / 21.0	- / 0.001	- / 1.3
100	Hertanto (2005) / TDD2	cyclic	var.	1 / 1	24.7 / -	354	0.51 / 0.77	0.50	2000 / 1525	230 x 230	330 x 200	JS / JS	20.9 / 27.5	0.003 / 0.003	0.5 / 0.5	21.6 / 30.2	0.005 / 0.007	1.0 / 1.0
101	Hertanto (2005) / TDP2	cyclic	var.	6 / 6	25.0 / -	333	0.51 / 0.51	0.50	2000 / 1525	230 x 230	330 x 200	JS / JS	16.3 / 21.0	0.001 / 0.001	0.5 / 0.7	19.2 / 21.8	0.006 / 0.005	2.0 / 1.5
102	Kuang (2006) / BS-L	cyclic	16.2	1 / 1	30.9 / -	520	0.92 / 0.92	1.34	3000 / 1500	300 x 300	450 x 260	JS / JS	-	-	-	100.9 / 90.2	-	1.3 / 1.7
103	Kuang (2006) / BS-OL	cyclic	16.2	2 / 2	30.9 / -	520	0.92 / 0.92	1.34	3000 / 1500	300 x 300	450 x 260	JS / JS	-	-	-	68.9 / 70.1	-	0.7 / 0.7
104	Kuang (2006) / BS-LL	cyclic	11.9	1 / 2	42.1 / -	520	0.92 / 0.92	1.34	3000 / 1500	300 x 300	450 x 260	JS / JS	-	-	-	127.5 / 83.5	-	1.3 / 0.7
105	Kuang (2006) / BS-U	cyclic	16.1	3 / 3	31.0 / -	520	0.92 / 0.92	1.34	3000 / 1500	300 x 300	450 x 260	JS / JS	-	-	-	96.2 / 109.1	-	1.3 / 1.3
106	Kuang (2006) / BS-L-LS	cyclic	15.8	1 / 1	31.6 / -	520	0.92 / 0.92	1.34	3000 / 1500	300 x 300	450 x 260	JS / JS	-	-	-	110.2 / 86.8	-	1.3 / 1.3
107	Liu (2006) / RC1	cyclic	7.3	1 / 1	19.4 / -	324	0.77 / 0.77	0.50	2000 / 1525	230 x 230	330 x 200	JS / JS	27.5 / 29.7	0.001 / 0.001	0.6 / 0.7	27.5 / 29.7	0.001 / 0.001	0.6 / 0.7
108	Karayannis (2008) / A0	cyclic	5.0	1 / 1	31.6 / -	580	0.28 / 0.28	0.42	1500 / 1100	200 x 200	300 x 200	JS / JS	-	-	-	29.0 / 29.0	-	-
109	Karayannis (2008) / B0	cyclic	5.0	1 / 1	31.6 / -	580	0.28 / 0.28	0.42	1500 / 1100	200 x 200	300 x 200	JS / JS	-	-	-	95.5 / 95.5	-	-
110	Karayannis (2008) / C0	cyclic	5.0	1 / 1	31.6 / -	580	0.83 / 0.83	1.36	1500 / 1100	300 x 200	300 x 200	JS / JS	-	-	-	91.0 / 91.0	-	-
111	Wong (2008) / BS-L-V2	cyclic	14.7	1 / 1	34.1 / -	520	1.48 / 1.48	1.34	3000 / 1500	300 x 300	450 x 260	JS / JS	-	-	-	95.0 / 127.0	-	1.7 / 1.3
112	Wong (2008) / BS-L-V4	cyclic	16.2	1 / 1	30.9 / -	520	0.92 / 0.92	1.34	3000 / 1500	300 x 300	450 x 260	JS / JS	-	-	-	95.0 / 128.8	-	1.7 / 1.3
113	Wong (2008) / BS-L-H1	cyclic	13.7	1 / 1	36.4 / -	520	0.66 / 0.66	1.34	3000 / 1500	300 x 300	300 x 260	JS / JS	-	-	-	90.0 / 124.5	-	1.7 / 1.3
114	Wong (2008) / BS-L-300	cyclic	17.7	1 / 1	28.3 / -	520	1.48 / 1.48	1.34	3000 / 1500	300 x 300	450 x 260	JS / BJ	-	-	-	80.0 / 95.4	-	1.7 / 3.3
115	Wong (2008) / BS-L-450	cyclic	15.0	1 / 1	33.3 / -	520	0.92 / 0.92	1.34	3000 / 1500	300 x 300	450 x 260	JS / JS	-	-	-	95.9 / 100.9	-	1.7 / 1.3
116	Wong (2008) / BS-L-600	cyclic	11.9	1 / 1	42.1 /	520	0.66 / 0.66	1.34	3000 / 1500	300 x 300	600 x 260	JS / JS	-	-	-	95.0 / 132.7	-	0.7 / 1.3
117	Genesio (2009) / 2D1	cyclic	var.	6 / 6	17.7 / 1.8	430	0.45 / 0.45	0.50	2000 / 1525	230 x 230	330 x 230	JS / JS	18.8 / 24.8	0.002 / 0.002	0.5 / 1.0	19.5 / 24.8	0.01 / 0.003	2.0 / 1.0
118	Le-Trung (2009) / NS	cyclic	0	2 / 1	36.5 / 3.8	324	1.27 / 0.95	0.93	1100 / 1350	167 x 167	200 x 134	JS / BJ	-	-	-	8.5 / 16.0	-	-
119	Genesio (2010) / JT1-1	cyclic	0	1 / 1	25.4 / -	560	0.77 / 0.77	1.04	3230 / 1875	300 x 350	400 x 300	JS / JS	67.6 / 39.3	0.002 / 0.001	2.3 / 1.1	79.9 / 61.5	0.005 / 0.004	3.2 / 2.1
120	Genesio (2010) / JT2-1	cyclic	0	6 / 6	24.4 / 3.5	350	0.77 / 0.77	1.04	3230 / 1875	300 x 350	400 x 300	JS / JS	28.5 / 28.6	0.002 / 0.001	0.9 / 0.8	41.5 / 39.1	0.008 / 0.009	3.2 / 2.1
121	Genesio (2010) / JT3-1	cyclic	0	5 / 1	27.5 / -	560	0.77 / 0.77	1.04	3230 / 1875	300 x 350	400 x 300	JS / JS	25.5 / 40.9	0.001 / 0.001	0.9 / 1.1	380.0 / 53.5	0.009 / 0.04	3.1 / 2.3
122	Genesio (2010) / JT4-1	cyclic	0	2 / 1	28.2 / 3.0	560	0.77 / 0.77	1.04	3230 / 1875	300 x 350	400 x 300	JS / JS	26.1 / 46.6	0.001 / 0.003	0.7 / 1.5	45.0 / 56.8	0.014 / 0.007	3.2 / 2.1
123	Genesio (2010) / JT5-1	cyclic	0	1 / 1	24.6 / 3.4	540	0.42 / 0.42	1.04	3230 / 1875	300 x 350	400 x 300	BJ / BJ	50.2 / 35.7	0.001 / 0.001	1.6 / 1.2	51.0 / 39.5	0.003 / 0.009	2.1 / 2.1

APPENDIX C: NUMERICAL RESULTS

The Geometry of the specimens used in this parametric study is the same of the specimens tested by *Genesio & Akgüzel (2009)* (NZ1), *Hertanto (2005)* (NZ2) and *Genesio & Sharma (2010a)* (IND). In Figure C 1a,b,c the geometry and the test setup of the specimens types NZ1, NZ2 and IND are respectively shown.

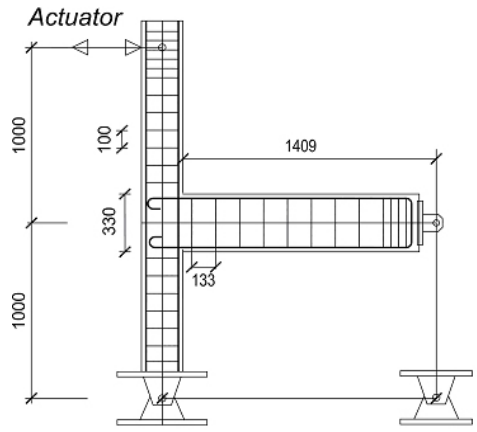

a) Test setup NZ1 (*Genesio & Akgüzel, 2009*)

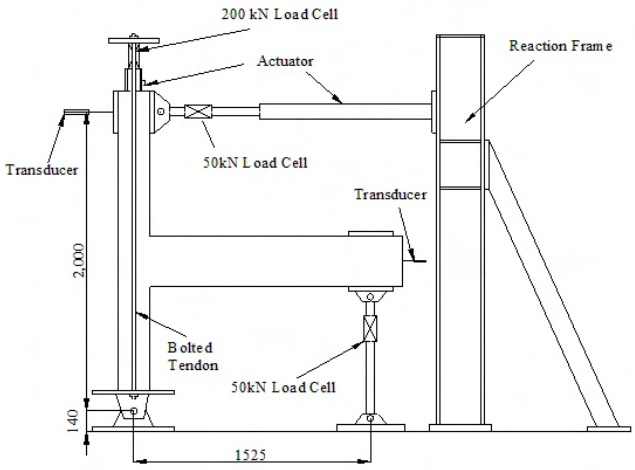

b) Test setup NZ2 (*Hertanto, 2005*)

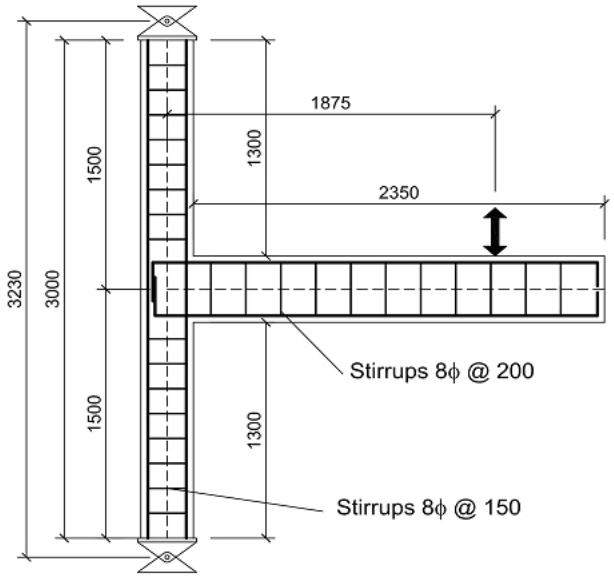

c) Test setup IND (*Genesio & Sharma, 2010*)

Figure C 1: Test setups of the experimental tests used as benchmark for the numerical simulation

Summary of material parameters used in the FE simulations

Table C-1: Macroscopic properties of concrete

f_c [MPa]	f_{ct} [MPa]	E_c [GPa]	G_F [N/mm]
12.0	1.6	21.7	0.060
17.7	1.8	24.7	0.070
20.0	2.2	25.8	0.070
24.0	2.5	27.4	0.070
28.0	2.8	28.8	0.075
30.0	2.9	29.5	0.080
33.0	3.1	30.5	0.080
38.0	3.4	31.9	0.085
40.0	3.5	32.1	0.085
43.0	3.7	33.3	0.090
50.0	4.0	34.5	0.095

Table C-2: Bond stress-slip-relationship for deformed bars with varying f_c (*Lettow, 2006*)

	f_c [MPa]	k_{sec} [N/mm^3]	$k_1 = k_{unload}$ [N/mm^3]	k_2 [N/mm^3]	s_2 [mm]	s_3 [mm]	τ_f [MPa]	τ_m [MPa]
D16	20	14.2	34.1	0.9	1.5	10.0	4.7	7.1
	28	16.0	38.5	1.0	1.5	10.0	5.6	8.4
	38	18.3	44.0	1.1	1.5	10.0	6.5	9.8
	48	20.6	49.5	1.2	1.5	10.0	7.3	11.0
D20	20	14.8	37	0.7	1.5	12.0	5.0	7.5
	28	16.6	41.6	0.8	1.5	12.0	5.9	8.8
	38	18.9	47.4	0.9	1.5	12.0	6.9	10.3
	48	21.2	53.1	1.1	1.5	12.0	7.7	11.6

Table C-3: Bond stress-slip relationship for deformed bars with varying bar dia. (*Lettow, 2006*)

	k_{sec} [N/mm^3]	$k_1 = k_{unload}$ [N/mm^3]	k_2 [N/mm^3]	s_2 [mm]	s_3 [mm]	τ_f [MPa]	τ_m [MPa]
D12	14.8	32.6	1.2	1.5	8.5	5.0	7.6
D16	16.0	38.5	1.0	1.5	10.0	5.8	8.4
D20	16.6	41.6	0.8	1.5	12.0	5.9	8.8
D25	17.2	44.8	0.7	1.5	14.0	6.2	9.3

f_c = 28.0 MPa

Table C-4: Bond stress-slip-relationship for plain round bars with varying bar diameter

	k_{sec} [N/mm^3]	$k_1 = k_{unload}$ [N/mm^3]	k_2 [N/mm^3]	s_2 [mm]	s_3 [mm]	τ_f [MPa]	τ_m [MPa]
R10	80	100	10	0.10	1.00	0.50	0.50
R12 [a)]	80	100	10	0.10	1.00	0.60	0.60
R14	40	50	10	0.20	2.00	0.80	0.70
R16 [a)]	10	30	5	0.30	2.50	1.10	0.90
R20	8	20	5	0.70	3.50	1.60	1.20
R25	8	20	3	0.70	3.50	1.60	1.20

[a)] Values calibrated using the tests by *Fabbrocino et al. (2002)*

List of FE simulations (as-built beam-column joints)

FE simulations of as-built beam-column joints with test setup NZ1																		
No.	**Name**	**Load**	**Rein. Type**	n_c **[%]**	f_c' **[MPa]**	f_{ct} **[MPa]**	E_c **[GPa]**	G_f **[Nm]**	f_y **[MPa]**	E_s **[GPa]**	h_b / h_c **[-]**	ρ_b **[%]**	ρ_c **[%]**	**Failure mode**	$\gamma_{j,crack}$ **[rad]**	$\gamma_{j,peak}$ **[rad]**	$V_{c,crack}$ **[kN]**	$V_{c,peak}$ **[kN]**
1	1_2D	Cyclic	6	Var.	17.7	1.8	24.7	0.070	430	200	1.43	0.45	0.50	JS	0.000	0.000	13.2 / 13.2	18.0 / 18.0
2	2_2D	Mono	6	Var.	17.7	1.8	24.7	0.070	430	200	1.43	0.45	0.50	JS	0.000	0.000	14.5	15.0
3	3_2D	Mono	6	12	17.7	1.8	24.7	0.070	430	200	1.43	0.45	0.50	JS	0.000	0.000	18.1	18.1
4	4_2D	Mono	6	24	17.7	1.8	24.7	0.070	430	200	1.43	0.45	0.50	JS-P	0.000	0.000	22.4	22.4
5	5_2D	Mono	6	6	17.7	1.8	24.7	0.070	430	200	1.43	0.45	0.50	JS	0.000	0.000	14.2	14.9
6	6_2D	Mono	6	6	17.7	1.8	24.7	0.070	430	200	1.43	0.45	0.50	JS	0.000	0.000	9.6	11.6
7	13_2D	Mono	6	12	17.7	1.8	24.7	0.070	430	200	1.43	0.64	0.50	JS	0.000	0.000	18.1	18.1
8	14_2D	Mono	6	12	17.7	1.8	24.7	0.070	430	200	1.43	0.88	0.50	JS	0.000	0.000	19.5	19.5
9	15_2D	Mono	6	12	17.7	1.8	24.7	0.070	430	200	1.43	1.15	0.50	JS	0.000	0.000	19.3	19.3
10	16_2D	Mono	6	12	17.7	1.8	24.7	0.070	430	200	1.43	1.79	0.50	JS	0.000	0.000	19.1	19.1
11	17_2D	Mono	6	12	17.7	1.8	24.7	0.070	430	200	1.43	0.29	0.50	JS	0.000	0.000	17.0	17.0
12	18_2D	Mono	6	12	17.7	1.8	24.7	0.070	430	200	1.43	0.45	0.72	JS	0.000	0.000	19.9	19.9
13	19_2D	Mono	6	12	17.7	1.8	24.7	0.070	430	200	1.43	0.45	1.31	JS	0.000	0.000	20.2	20.2
15	20_2D	Mono	6	12	17.7	1.8	24.7	0.070	430	200	1.43	0.45	1.71	JS	0.000	0.000	19.9	19.9
14	21_2D	Mono	6	12	17.7	1.8	24.7	0.070	430	200	1.43	0.45	2.66	JS	0.000	0.000	19.6	19.6
15	22_2D	Mono	6	12	17.7	1.8	24.7	0.070	430	200	1.43	0.45	0.42	JS	0.000	0.000	16.2	16.2
16	24_2D	Mono	6	18	17.7	1.8	24.7	0.070	1000	200	1.43	0.45	0.50	JS	0.000	0.000	21.3	21.3
17	25_2D	Mono	6	36	17.7	1.8	24.7	0.070	1000	200	1.43	0.45	0.50	JS-P	0.000	0.000	24.3	24.3
18	30_2D	Mono	6	8	12.0	1.6	21.7	0.060	430	200	1.43	0.45	0.50	JS	0.000	0.000	13.3	13.3
19	31_2D	Mono	6	3	28.0	2.8	28.8	0.075	430	200	1.43	0.45	0.50	JS	0.000	0.000	17.6	17.6
20	32_2D	Mono	6	4	33.0	3.1	30.5	0.080	430	200	1.43	0.45	0.50	JS	0.000	0.000	18.8	18.8
21	33_2D	Mono	6	5	38.0	3.4	31.9	0.085	430	200	1.43	0.45	0.50	JS	0.000	0.000	19.8	19.8
22	34_2D	Mono	6	5	43.0	3.7	33.3	0.090	430	200	1.43	0.45	0.50	JS	0.000	0.000	20.0	20.0
23	35_2D	Mono	6	3	24.0	2.5	27.4	0.070	430	200	1.43	0.45	0.50	JS	0.000	0.000	17.2	17.2
24	39_2D	Mono	6	2	17.7	1.8	24.7	0.070	430	200	1.43	0.45	0.50	JS	0.000	0.000	14.7	14.7
25	40_2D	Mono	6	11	17.7	1.3	24.7	0.070	430	200	1.43	0.45	0.50	JS	0.000	0.000	16.6	16.6
26	41_2D	Mono	6	11	17.7	2.3	24.7	0.070	430	200	1.43	0.45	0.50	JS	0.000	0.000	18.5	18.5
27	42_2D	Mono	6	11	17.7	1.8	21.0	0.070	430	200	1.43	0.45	0.50	JS	0.000	0.000	18.0	18.0

FE simulations of as-built beam-column joints with test setup NZ1																		
No.	**Name**	**Load**	**Rein. Type**	n_c [%]	f_c' [MPa]	f_{ct} [MPa]	E_c [GPa]	G_f [Nm]	f_y [MPa]	E_s [GPa]	h_b / h_c [-]	ρ_b [%]	ρ_c [%]	**Failure mode**	$\gamma_{j,crack}$ [rad]	$\gamma_{j,peak}$ [rad]	$V_{c,crack}$ [kN]	$V_{c,peak}$ [kN]
28	43_2D	Mono	6	11	17.7	1.8	28.0	0.070	430	200	1.43	0.45	0.50	JS	0.000	0.000	18.3	18.3
29	44_2D	Mono	6	11	17.7	1.8	24.7	0.050	430	200	1.43	0.45	0.50	JS	0.000	0.000	22.2	22.2
30	45_2D	Mono	6	11	17.7	1.8	24.7	0.090	430	200	1.43	0.45	0.50	JS	0.000	0.000	25.6	25.6
31	46_2D	Mono	6	11	17.7	1.8	24.7	0.070	430	200	1.43	0.45	0.50	JS	0.000	0.000	12.0	12.0
32	47_2D	Mono	6	11	17.7	1.8	24.7	0.070	430	200	1.43	0.45	0.50	JS	0.000	0.000	21.0	21.0
33	48_2D	Mono	6	11	17.7	1.8	24.7	0.070	430	200	1.43	0.45	0.50	JS	0.000	0.000	18.5	18.5
34	49_2D	Mono	6	11	17.7	1.8	24.7	0.070	430	200	1.43	0.45	0.50	JS	0.000	0.000	18.4	18.4
35	1_2D_1ar	Mono	6	11	17.7	1.8	24.7	0.070	430	200	1.00	0.45	0.50	P	0.000	0.000	11.4	11.4
36	1_2D_125ar	Mono	6	11	17.7	1.8	24.7	0.070	430	200	1.25	0.45	0.50	JS	0.000	0.000	17.8	17.8
37	1_2D_175ar	Mono	6	11	17.7	1.8	24.7	0.070	430	200	1.75	0.45	0.50	JS	0.000	0.000	20.0	20.0
38	1_2D_2ar	Mono	6	11	17.7	1.8	24.7	0.070	430	200	2.00	0.45	0.50	JS	0.000	0.000	21.8	21.8
39	2D_bent_in	Mono	1	11	17.7	1.8	24.7	0.070	430	200	1.43	0.45	0.50	JS	n.a.	n.a.	-	24.1
40	2D_bent_125ar	Mono	1	11	17.7	1.8	24.7	0.070	700	200	1.25	0.45	0.50	JS	n.a.	n.a.	-	21.2
41	2D_bent_in_175ar	Mono	1	11	17.7	1.8	24.7	0.070	430	200	1.57	0.45	0.50	JS	n.a.	n.a.	-	25.5
42	2D_bent_in_2ar	Mono	1	11	17.7	1.8	24.7	0.070	430	200	2.00	0.45	0.50	JS	n.a.	n.a.	-	27.9
43	2D_bent_out	Mono	2	11	17.7	1.8	24.7	0.070	430	200	1.43	0.45	0.50	JS	n.a.	n.a.	-	16.1
44	2D_bent_out_1ar	Mono	2	11	17.7	1.8	24.7	0.070	700	200	1.00	0.45	0.50	JS	n.a.	n.a.		13.2
45	2D_bent_out_125ar	Mono	2	11	17.7	1.8	24.7	0.070	700	200	1.25	0.45	0.50	JS	n.a.	n.a.	-	15.1
46	2D_bent_out_175ar	Mono	2	11	17.7	1.8	24.7	0.070	430	200	1.75	0.45	0.50	JS	n.a.	n.a.	-	24.7
47	2D_bent_out_2ar	Mono	2	11	17.7	1.8	24.7	0.070	430	200	2.00	0.45	0.50	JS	n.a.	n.a.	-	29.5

FE simulations of as-built beam-column joints with test setup NZ2																	
No.	**Name**	**Load**	**Rein.**	n_c **[%]**	f_c' **[MPa]**	f_{ct} **[MPa]**	E_c **[GPa]**	G_f **[Nm]**	f_y **[MPa]**	E_s **[GPa]**	h_b / h_c **[-]**	ρ_b **[%]**	ρ_c **[%]**	**Failure mode**	$\gamma_{j,crack}$ **[rad]**	$\gamma_{j,peak}$ **[rad]**	$V_{c,crack}$ **[kN]**	$V_{c,peak}$ **[kN]**
1	TDP2	Cyclic	6	Var.	25.0	2.5	25.0	0.070	340	200	1.43	0.51	0.50	JS	n.a.	n.a.	18.0 / 13.7	18.0 / 16.2
2	TDP2-bond [a)]	mono	6	Var.	25.0	2.5	25.0	0.070	340	200	1.43	0.51	0.50	JS	n.a.	n.a.	21.1	21.1
3	TDP2-no-bond [a)]	mono	6	Var.	25.0	2.5	25.0	0.070	340	200	1.43	0.51	0.50	B	n.a.	n.a.	-	19.8
4	TDD1	Cyclic	1	Var.	23.3	2.3	25.0	0.070	340	200	1.43	0.51 / 0.26	0.50	B	n.a.	n.a.	- / -	17.7 / 10.8
5	TDD2	Cyclic	1	Var.	24.6	2.4	25.0	0.070	340	200	1.43	0.51 / 0.77	0.50	JS	n.a.	n.a.	18.8 / 18.0	23.7 / 18.8
6	1_TDD2	Mono	1	Var.	24.6	2.4	25.0	0.070	340	200	1.43	0.51 / 0.77	0.50	JS	n.a.	n.a.	-	27.2
7	1_TDD2_125ar	Mono	1	5.8	24.6	2.4	25.0	0.070	700	200	1.25	0.51 / 0.77	0.50	JS	n.a.	n.a.	-	26.7
9	1_TDD2_175ar	Mono	1	5.8	24.6	2.4	25.0	0.070	340	200	1.75	0.51 / 0.77	0.50	JS	n.a.	n.a.	-	28.6
10	1_TDD2_2ar	Mono	1	5.8	24.6	2.4	25.0	0.070	340	200	2.00	0.51 / 0.77	0.50	JS	n.a.	n.a.	-	28.1

[a)] Analysis carried out with different model than No. 1

FE simulations of as-built beam-column joints with test setup IND																		
No.	**Name**	**Load**	**Rein.**	n_c **[%]**	f_c' **[MPa]**	f_{ct} **[MPa]**	E_c **[GPa]**	G_f **[Nm]**	f_y **[MPa]**	E_s **[GPa]**	h_b / h_c **[-]**	ρ_b **[%]**	ρ_c **[%]**	**Failure mode**	$\gamma_{j,crack}$ **[rad]**	$\gamma_{j,peak}$ **[rad]**	$V_{b,crack}$ **[kN]**	$V_{b,peak}$ **[kN]**
1	2_1_JT_b	Mono	1	0	29.0	2.8	28.5	0.075	552	200	1.33	0.77	1.04	JS	0.0018	0.0047	45.0	57.5
2	2_1_JT_cycl	Cyclic	1	0	29.0	2.8	28.5	0.075	552	200	1.33	0.77	1.04	JS	n.a.	n.a.	44.4 / 44.5	52.9 / 52.3
3	JT2_test	Mono	6	0	24.4	2.3	25.0	0.07	312	200	1.33	0.77	1.04	JS	0.0015	0.0079	32.8	44.9
4	JT2_test_cyclic	Cyclic	6	0	24.4	2.3	25.0	0.07	312	200	1.33	0.77	1.04	JS	n.a.	n.a.	31.5 / 32.8	39.4 / 43.1
5	JT2_test_20fc	Mono	6	0	20.0	2.2	25.8	0.07	312	200	1.33	0.77	1.04	JS	0.0016	0.0066	31.9	42.0
6	JT2_test_30fc	Mono	6	0	30.0	2.9	29.5	0.08	312	200	1.33	0.77	1.04	JS	0.0016	0.0075	38.7	50.9
7	JT2_test_40fc	Mono	6	0	40.0	3.5	32.1	0.085	312	200	1.33	0.77	1.04	JS	0.0016	0.0067	42.4	59.2
8	JT2_test_50fc	Mono	6	0	50.0	4.0	34.5	0.095	312	200	1.33	0.77	1.04	JS	0.0015	0.0063	45.6	61.9
9	JT2_16b	Mono	6	0	24.4	2.3	25.0	0.07	312	200	1.33	0.56	1.04	JS	0.0010	0.0074	33.1	43.1
10	JT2_25b	Mono	6	0	24.4	2.3	25.0	0.07	312	200	1.33	1.36	1.04	JS	0.0016	0.0086	33.1	49.4
11	JT2_25_4b	Mono	6	0	24.4	2.3	25.0	0.07	312	200	1.33	1.82	1.04	JS	0.0012	0.0095	33.6	53.0
12	JT2_12c	Mono	6	0	24.4	2.3	25.0	0.07	312	200	1.33	0.77	0.37	JS	0.0010	0.0078	27.8	45.4
13	JT2_16c	Mono	6	0	24.4	2.3	25.0	0.07	312	200	1.33	0.77	0.66	JS	0.0016	0.0079	31.6	44.4
15	JT2_25c	Mono	6	0	24.4	2.3	25.0	0.07	312	200	1.33	0.77	1.62	JS	0.0010	0.0059	34.2	44.5
14	JT2_25_4c	Mono	6	0	24.4	2.3	25.0	0.07	312	200	1.33	0.77	2.16	JS	0.0014	0.0074	38.0	44.9
15	JT2_350ar	Mono	6	0	24.4	2.3	25.0	0.07	312	200	1.17	0.77	1.04	JS	0.0017	0.0058	26.8	39.4
16	JT2_500ar	Mono	6	0	24.4	2.3	25.0	0.07	312	200	1.67	0.77	1.04	JS	0.0013	0.0102	25.7	40.8
17	JT2_600ar	Mono	6	0	24.4	2.3	25.0	0.07	312	200	2.00	0.77	1.04	JS	0.0021	0.0111	30.0	45.4
18	JT2_roll_0N	Mono	6	0	24.4	2.3	25.0	0.07	312	200	1.33	0.77	1.04	JS	0.0019	0.0064	36.1	43.2
19	JT2_roll_150N	Mono	6	5.9	24.4	2.3	25.0	0.07	312	200	1.33	0.77	1.04	JS	0.0029	0.0082	44.5	50.5
20	JT2_roll_300N	Mono	6	11.7	24.4	2.3	25.0	0.07	312	200	1.33	0.77	1.04	JS	0.0040	0.0098	53.5	57.0
21	JT2_roll_450N	Mono	6	17.6	24.4	2.3	25.0	0.07	312	200	1.33	0.77	1.04	JS	0.0057	0.0057	65.5	66.0
22	JT2_roll_600N	Mono	6	23.4	24.4	2.3	25.0	0.07	312	200	1.33	0.77	1.04	JS	0.0059	0.0059	74.2	74.2
23	JT2_roll_900N	Mono	6	35.1	24.4	2.3	25.0	0.07	312	200	1.33	0.77	1.04	JS	0.0074	0.0074	86.7	86.7
24	JT2_roll_1200N	Mono	6	46.8	24.4	2.3	25.0	0.07	312	200	1.33	0.77	1.04	JS	0.0079	0.0079	94.7	94.7
25	JT4_2test	Mono	2	0	28.2	3.0	28.5	0.075	552	200	1.33	0.77	1.04	JS	0.0014	0.0098	33.0	44.6
26	JT4_2test_neg	Mono	1	0	28.2	3.0	28.5	0.075	552	200	1.33	0.77	1.04	JS	0.0023	0.0088	44.0	61.0
27	JT4_test_cyclic	Cyclic	2 / 1	0	28.2	3.0	28.5	0.075	552	200	1.33	0.77	1.04	JS	n.a.	n.a.	32.6 / 40.8	43.3 / 58.1

FE simulations of as-built beam-column joints with test setup IND																		
No.	**Name**	**Load**	**Rein.**	n_c [%]	f_c' [MPa]	f_{ct} [MPa]	E_c [GPa]	G_f [Nm]	f_y [MPa]	E_s [GPa]	h_b / h_c [-]	ρ_b [%]	ρ_c [%]	**Failure mode**	$\gamma_{j,crack}$ [rad]	$\gamma_{j,peak}$ [rad]	$V_{b,crack}$ [kN]	$V_{b,peak}$ [kN]
28	JT4_20fc	Mono	2	0	20.0	2.2	25.8	0.070	552	200	1.33	0.77	1.04	JS	0.0014	0.0110	28.0	37.4
29	JT4_20fc_neg	Mono	1	0	20.0	2.2	25.8	0.070	552	200	1.33	0.77	1.04	JS	0.0022	0.0106	37.0	51.6
30	JT4_40fc	Mono	2	0	40	3.5	31.1	0.085	552	200	1.33	0.77	1.04	JS	0.0015	0.0115	39.2	56.1
31	JT4_40fc_neg	Mono	1	0	40	3.5	31.1	0.085	552	200	1.33	0.77	1.04	JS	0,0023	0,0079	51.8	76.6
32	JT4_50fc	Mono	2	0	50	4.0	34.5	0.095	552	200	1.33	0.77	1.04	JS	0.0015	0.0126	44.3	65.8
33	JT4_50_fc_neg	Mono	1	0	50	4.0	34.5	0.095	800	200	1.33	0.77	1.04	JS	0.0024	0.0082	90.7	58.9
34	JT4_16b	Mono	2	0	28.2	3.0	28.5	0.075	552	200	1.33	0.56	1.04	JS	0.0013	0.0114	32.5	43.8
35	JT16b_neg	Mono	1	0	28.2	3.0	28.5	0.075	552	200	1.33	0.56	1.04	JS	0.0017	0.0082	43.0	59.4
36	JT4_25b	Mono	2	0	28.2	3.0	28.5	0.075	552	200	1.33	1.36	1.04	JS	0.0011	0.0074	34.6	47.7
37	JT4_25b_neg	Mono	1	0	28.2	3.0	28.5	0.075	552	200	1.33	1.36	1.04	JS	0.0018	0.0084	46.8	67.2
38	JT4_25_4b	Mono	2	0	28.2	3.0	28.5	0.075	552	200	1.33	1.82	1.04	JS	0.0015	0.0109	35.4	50.6
39	JT4_25_4b_neg	Mono	1	0	28.2	3.0	28.5	0.075	552	200	1.33	1.82	1.04	JS	0.0014	0.0110	73.2	46.3
40	JT4_12c	Mono	2	0	28.2	3.0	28.5	0.075	552	200	1.33	0.77	0.37	JS	0,0011	0,0097	31.0	44.8
41	JT4_12c_neg	Mono	1	0	28.2	3.0	28.5	0.075	552	200	1.33	0.77	0.37	JS	0,0028	0,0107	38.5	64.1
42	JT4_16c	Mono	2	0	28.2	3.0	28.5	0.075	552	200	1.33	0.77	0.66	JS	0.0015	0.0092	32.3	43.2
43	JT4_16c_neg	Mono	1	0	28.2	3.0	28.5	0.075	552	200	1.33	0.77	0.66	JS	0,0025	0,0089	40.9	61.7
44	JT4_25c	Mono	2	0	28.2	3.0	28.5	0.075	552	200	1.33	0.77	1.62	JS	0.0013	0.0110	38.0	47.0
45	JT4_25c_neg	Mono	1	0	28.2	3.0	28.5	0.075	552	200	1.33	0.77	1.62	JS	0,0021	0,0083	49.3	59.8
46	JT4_25_4c	Mono	2	0	28.2	3.0	28.5	0.075	552	200	1.33	0.77	2.16	JS	0.0011	0.0113	36.1	46.1
47	JT4_25_4c_neg	Mono	1	0	28.2	3.0	28.5	0.075	552	200	1.33	0.77	2.16	JS	0.0015	0.0076	47.2	62.2
48	JT4_roller_0N	Mono	2	0	28.2	3.0	28.5	0.075	552	200	1.33	0.77	1.04	JS	0.0018	0.0120	30.6	46.4
49	JT4_roller_150N	Mono	2	5.1	28.2	3.0	28.5	0.075	552	200	1.33	0.77	1.04	JS	0.0030	0.0110	46.1	48.5
50	JT4_roller_300N	Mono	2	10.1	28.2	3.0	28.5	0.075	552	200	1.33	0.77	1.04	JS	0.0045	0.0045	57.0	57.0
51	JT4_roller_450N	Mono	2	15.2	28.2	3.0	28.5	0.075	552	200	1.33	0.77	1.04	JS	0.0055	0.0055	71.2	71.2
52	JT4_roller_600N	Mono	2	20.2	28.2	3.0	28.5	0.075	800	200	1.33	0.77	1.04	JS	0.0064	0.0064	78.9	78.9
53	JT4_roller_900N	Mono	2	30.4	28.2	3.0	28.5	0.075	800	200	1.33	0.77	1.04	JS	0.0070	0.0070	94.0	94.0
54	JT4_roller_1200N	Mono	2	40.5	28.2	3.0	28.5	0.075	800	200	1.33	0.77	1.04	JS	n.a.	n.a.	108.2	108.2
55	JT4_roller_0N_neg	Mono	1	0.0	28.2	3.0	28.5	0.075	552	200	1.33	0.77	1.04	JS	0.0023	0.0085	43.2	60.8
56	JT4_roller_150N_neg	Mono	1	5.1	28.2	3.0	28.5	0.075	552	200	1.33	0.77	1.04	JS	0.0056	0.0100	60.8	69.6
57	JT4_roller_300_neg	Mono	1	10.1	28.2	3.0	28.5	0.075	800	200	1.33	0.77	1.04	JS	0.0070	0.0109	71.0	82.1

FE simulations of as-built beam-column joints with test setup IND																		
No.	**Name**	**Load**	**Rein.**	n_c [%]	f_c' [MPa]	f_{ct} [MPa]	E_c [GPa]	G_f [Nm]	f_y [MPa]	E_s [GPa]	h_b / h_c [-]	ρ_b [%]	ρ_c [%]	**Failure mode**	$\gamma_{j,crack}$ [rad]	$\gamma_{j,peak}$ [rad]	$V_{b,crack}$ [kN]	$V_{b,peak}$ [kN]
58	JT4_roller_450_neg	Mono	1	15.2	28.2	3.0	28.5	0.075	800	200	1.33	0.77	1.04	JS	0.0080	0.0080	82.3	82.3
59	JT4_roller_600_neg	Mono	1	20.2	28.2	3.0	28.5	0.075	800	200	1.33	0.77	1.04	JS	0.0084	0.0084	87.1	87.1
60	JT4_roller_900N_neg	Mono	1	30.4	28.2	3.0	28.5	0.075	800	200	1.33	0.77	1.04	JS	0.0096	0.0096	98.5	98.5
61	JT4_roller_1200N_neg	Mono	1	40.5	28.2	3.0	28.5	0.075	800	200	1.33	0.77	1.04	JS	0.0107	0.0107	108.3	108.3
62	JT4_350ar	Mono	2	0	28.2	3.0	28.5	0.075	552	200	1.17	0.77	1.04	JS	0.0010	0.0094	28.6	39.3
63	JT4_350ar_neg	Mono	1	0	28.2	3.0	28.5	0.075	552	200	1.17	0.77	1.04	JS	0.0022	0.0061	39.9	54.6
64	JT4_500ar	Mono	2	0	28.2	3.0	28.5	800	552	200	1.67	0.77	1.04	JS	0.0019	0.0107	44.7	61.4
65	JT4_500ar_neg	Mono	1	0	28.2	3.0	28.5	0.075	800	200	1.67	0.77	1.04	JS	0.0023	0.0120	52.8	80.4
66	JT4_600ar	Mono	2	0	28.2	3.0	28.5	0.075	800	200	2.00	0.77	1.04	JS	0.0053	0.0169	46.0	74.5
67	JT4_600ar_neg	Mono	1	0	28.2	3.0	28.5	0.075	800	200	2.00	0.77	1.04	JS	0.0029	0.0138	59.8	93.4
68	JT4_fix_neg	Mono	1	0	28.2	3.0	28.5	0.075	552	200	1.33	0.77	1.04	JS	0.0013	0.0065	48.7	69.2
69	JT4_fix	Mono	2	0	28.2	3.0	28.5	0.075	552	200	1.33	0.77	1.04	JS	0.0011	0.0091	36.3	53.5
70	JT1_4_neg_3BJ	Mono	1	0	28.2	3.0	28.5	0.075	300	200	1.33	0.77	1.04	BJ1	0.0023	0.0072	44.0	51.6
71	JT1_4_neg_2B	Mono	1	0	28.2	3.0	28.5	0.075	200	200	1.33	0.77	1.04	BJ2	0.0022	0.0036	42.0	42.0
72	JT4_neg_beam	Mono	1	0	28.2	3.0	28.5	0.075	350	200	1.33	0.47	1.04	B	0.0014	0.0014	-	39.0
73	JT5_test	Mono	1	0	24.6	3.4	25.0	0.074	540	200	1.33	0.47	1.79	BJ 1	0.0017	0.0043	45.5	47.6
74	JT5_test_cycl	Cyclic	1	0	24.6	3.4	25.0	0.074	540	200	1.33	0.47	1.79	BJ 1	n.a.	n.a.	45.2 / 45.9	47.4 / 46.9
75	m7	Mono	1	0	29.0	2.8	28.5	0.075	552	200	1.33	0.45	1.79	BJ 1	0.0011	0.0049	47.4	52.5
76	m8	Mono	1	0	29.0	2.8	28.5	0.075	552	200	1.33	0.48	1.79	BJ 1	0.0010	0.0048	46.5	54.5
77	m18	Mono	1	0	60.0	4.0	41.0	0.110	552	200	1.33	0.48	1.79	BJ 2	0.0009	0.0039	63.2	65.4
78	m19	Mono	1	0	60.0	4.0	41.0	0.110	552	200	1.33	0.56	1.79	BJ 1	0.0008	0.0035	64.6	72.6
79	m21	Mono	1	0	60.0	4.0	41.0	0.110	552	200	1.33	0.65	1.79	BJ 1	0.0009	0.0044	63.5	81.3
80	m22	Mono	1	0	60.0	4.0	41.0	0.110	552	200	1.33	0.69	1.79	BJ 1	0.0008	0.0044	61.7	82.8
81	m23	Mono	1	0	60.0	4.0	41.0	0.110	552	200	1.33	0.77	1.79	BJ 1	0.0010	0.0047	63.8	90.4
82	m25	Mono	1	0	29.0	2.8	28.5	0.075	552	200	1.33	0.31	0.45	BJ 1	0.0011	0.0050	35.3	43.4
83	m26	Mono	1	0	29.0	2.8	28.5	0.075	552	200	1.33	0.31	0.65	BJ 1	0.0011	0.0046	38.1	43.1
84	m27	Mono	1	0	29.0	2.8	28.5	0.075	552	200	1.33	0.31	1.15	BJ 2	0.0010	0.0045	41.8	43.1
85	m29	Mono	1	0	29.0	2.8	28.5	0.075	552	200	1.33	0.45	2.81	BJ 1	0.0009	0.0048	50.5	51.5
86	m30	Mono	1	0	29.0	2.8	28.5	0.075	552	200	1.33	0.45	1.15	BJ 1	0.0010	0.0048	42.2	53.5
87	m31	Mono	1	0	29.0	2.8	28.5	0.075	552	200	1.33	0.45	0.65	BJ 1	0.0011	0.0046	38.9	52.0

FE simulations of as-built beam-column joints with test setup IND																		
No.	**Name**	**Load**	**Rein.**	n_c [%]	f_c' [MPa]	f_{ct} [MPa]	E_c [GPa]	G_f [Nm]	f_y [MPa]	E_s [GPa]	h_b / h_c [-]	ρ_b [%]	ρ_c [%]	**Failure mode**	$\gamma_{j,crack}$ [rad]	$\gamma_{j,peak}$ [rad]	$V_{b,crack}$ [kN]	$V_{b,peak}$ [kN]
88	m32	Mono	1	0	29.0	2.8	28.5	0.075	552	200	1.33	0.45	0.45	BJ 1	0.0011	0.0049	36.0	53.0
89	m34	Mono	1	0	60.0	4.0	41.0	0.110	552	200	1.33	0.45	0.45	BJ 1	0.0010	0.0042	46.2	62.8
90	m35	Mono	1	0	60.0	4.0	41.0	0.110	552	200	1.33	0.45	0.65	BJ 1	0.0010	0.0038	51.4	61.5
91	m36	Mono	1	0	60.0	4.0	41.0	0.110	552	200	1.33	0.45	1.15	BJ 1	0.0009	0.0036	57.1	61.5
92	m38	Mono	1	0	29.0	2.8	28.5	0.075	552	200	1.33	0.65	2.81	BJ 1	0.0009	0.0044	71.8	80.7
93	m39	Mono	1	0	29.0	2.8	28.5	0.075	552	200	1.33	0.65	1.15	BJ 1	0.0010	0.0041	60.9	78.1
94	m40	Mono	1	0	60.0	4.0	41.0	0.110	552	200	1.33	0.65	0.65	BJ 1	0.0010	0.0045	52.8	79.4
95	m41	Mono	1	0	60.0	4.0	41.0	0.110	552	200	1.33	0.77	0.45	BJ 1	0.0010	0.0046	48.7	80.5
96	m47	Mono	1	0	29.0	2.8	28.5	0.075	250	200	1.33	0.77	1.79	BJ 2	0.0009	0.0046	45.9	47.2
97	m48	Mono	1	0	29.0	2.8	28.5	0.075	300	200	1.33	0.77	1.79	BJ 1	0.0010	0.0046	46.6	52.4
98	m49	Mono	1	0	29.0	2.8	28.5	0.075	400	200	1.33	0.77	1.79	BJ 1	0.0010	0.0047	46.8	61.5
99	JT2_10BJ	Mono	6	0	30.0	2.9	29.5	0.075	310	200	1.33	0.77	1.04	BJ 1	n.a.	n.a.	37.6	47.9
100	JT2_11BJ	Mono	6	0	30.0	2.9	29.5	0.075	270	200	1.33	0.77	1.04	BJ 1	n.a.	n.a.	37.6	44.8
101	JT2_20BJ	Mono	6	0	24.4	2.3	25.0	0.070	270	200	1.33	0.77	1.04	BJ 1	n.a.	n.a.	32.8	41.8
102	JT2_30BJ	Mono	6	0	24.4	2.3	25.0	0.070	310	200	1.33	0.66	1.04	BJ 1	n.a.	n.a.	32.2	40.9
103	JT4_10BJ	Mono	2	0	50.0	4.0	34.5	0.095	420	200	1.33	0.77	1.04	BJ 1	n.a.	n.a.	45.2	53.9
104	JT4_20BJ	Mono	2	0	28.0	2.2	28.5	0.075	270	200	1.33	0.77	1.04	BJ 1	n.a.	n.a.	33.0	37.4
105	JT4_30BJ	Mono	2	0	28.0	2.2	28.5	0.075	552	200	1.33	0.37	1.04	BJ 1	n.a.	n.a.	32.2	36.1
106	JT4_40BJ	Mono	2	0	28.0	2.2	28.5	0.075	270	200	1.33	0.67	1.04	BJ 1	n.a.	n.a.	32.8	35.0
107	JT4_r_0N_neg_4_25b	Mono	2	0	28.2	3.0	28.5	0.075	552	200	1.33	1.82	1.04	JS	n.a.	n.a.	47.8	72.7
108	JT4_r_300N_neg_4_25b	Mono	2	10.1	28.2	3.0	28.5	0.075	552	200	1.33	1.82	1.04	JS	n.a.	n.a.	69.7	85.6
109	JT4_r_600N_neg_4_25b	Mono	2	20.2	28.2	3.0	28.5	0.075	800	200	1.33	1.82	1.04	JS	n.a.	n.a.	85.5	86.6
110	JT4_r_0N_4_25b	Mono	2	0	28.2	3.0	28.5	0.075	552	200	1.33	1.82	1.04	JS	n.a.	n.a.	30.4	51.1
111	JT4_r_150N_4_25b	Mono	2	5.1	28.2	3.0	28.5	0.075	552	200	1.33	1.82	1.04	JS	n.a.	n.a.	46.2	50.6
112	JT4_r_300N_4_25b	Mono	2	10.1	28.2	3.0	28.5	0.075	552	200	1.33	1.82	1.04	JS	n.a.	n.a.	56.3	61.1
113	JT4_r_450N_4_25b	Mono	2	15.2	28.2	3.0	28.5	0.075	800	200	1.33	1.82	1.04	JS	n.a.	n.a.	70.4	70.4
114	JT2_r_0N_4_25b	Mono	6	0	24.4	2.3	25.0	0.07	312	200	1.33	1.82	1.04	JS	n.a.	n.a.	36.5	55.5
115	JT2_r_150N_4_25b	Mono	6	5.9	24.4	2.3	25.0	0.07	312	200	1.33	1.82	1.04	JS	n.a.	n.a.	43.4	56.2
116	JT2_r_300N_4_25b	Mono	6	11.7	24.4	2.3	25.0	0.07	312	200	1.33	1.82	1.04	JS	n.a.	n.a.	56.7	60.0
117	JT2_r_450N_4_25b	Mono	6	17.6	24.4	2.3	25.0	0.07	312	200	1.33	1.82	1.04	JS	n.a.	n.a.	67.3	67.5

FE simulations of as-built beam-column joints with test setup IND																		
No.	**Name**	**Load**	**Rein.**	n_c **[%]**	f_c' **[MPa]**	f_{ct} **[MPa]**	E_c **[GPa]**	G_f **[Nm]**	f_y **[MPa]**	E_s **[GPa]**	h_b / h_c **[-]**	ρ_b **[%]**	ρ_c **[%]**	**Failure mode**	$\gamma_{j,crack}$ **[rad]**	$\gamma_{j,peak}$ **[rad]**	$V_{b,crack}$ **[kN]**	$V_{b,peak}$ **[kN]**
118	JT2_r_600N_4_25b	Mono	6	23.4	24.4	2.3	25.0	0.07	312	200	1.33	1.82	1.04	JS	n.a.	n.a.	74.7	74.7

List of FE simulations (retrofitted beam-column joints)

The material and geometrical properties which are not listed in the following tables were taken as in the experimental tests for all simulations.

FE simulations of retrofitted beam-column joints with test setup NZ1																	
No.	**Name**	**Load**	n_c **[%]**	f_c' **[MPa]**	f_{ct} **[MPa]**	E_c **[GPa]**	G_f **[Nm]**	**No. of anchors [-]**	**Haunch** E_s **[GPa]**	**Haunch,** A_s **[mm²]**	**Failure mode**	$V_{c,crack}$ **[kN]**	$V_{c,peak}$ **[kN]**	$F_{h,t,max}$ **[kN]**	$F_{h,c}$ **[kN]**	k_N **[kN/mm]**	k_V **[kN/mm]**
1	2DG1_100_50	mono	12.5	16.6	1.9	24.0	0.065	6	200	16 x 200	B	-	27.9	52.4	71.3	100	50
2	2DG1_50_50	mono	12.5	16.6	1.9	24.0	0.065	6	200	16 x 200	B	-	28.0	47.6	71.8	50	50
3	2DG1_25_50	mono	12.5	16.6	1.9	24.0	0.065	6	200	16 x 200	B	-	28.0	42.3	71.9	25	50
4	2DG1_25_25	mono	12.5	16.6	1.9	24.0	0.065	6	200	16 x 200	B	-	27.9	43.7	67.7	25	25
5	2DG1_25_10	mono	12.5	16.6	1.9	24.0	0.065	6	200	16 x 200	BJ	26.3	26.7	43.5	59.4	25	10
6	2DG1_100_20	mono	12.5	16.6	1.9	24.0	0.065	6	200	16 x 200	B	-	27.7	44.4	61.4	100	20
7	2DG1_50_20	mono	12.5	16.6	1.9	24.0	0.065	6	200	16 x 200	B	-	26.8	44.5	61.8	50	20
8	2DG1_50_20_50c	mono	12.5	16.6	1.9	24.0	0.065	6	50	16 x 200	B	-	26.4	43.6	49.2	50	20
9	2DG1_50_20_100c	mono	12.5	16.6	1.9	24.0	0.065	6	100	16 x 200	B	-	26.7	43.8	55.0	50	20
10	2DG1_50_20_400c	mono	12.5	16.6	1.9	24.0	0.065	6	400	16 x 200	B	-	27.1	45.4	68.5	50	20
11	2DG1_50_20_50t	mono	12.5	16.6	1.9	24.0	0.065	6	50	16 x 200	B	-	27.0	43.8	62.8	50	20
12	2DG1_50_20_400t	mono	12.5	16.6	1.9	24.0	0.065	6	400	16 x 200	B	-	27.1	45.4	68.9	50	20
13	2DG1_5_5	mono	12.5	16.6	1.9	24.0	0.065	6	200	16 x 200	BJ	25.8	26.6	24.6	39.8	5	5
14	2DG2_25_50	mono	12.6	16.5	1.9	24.0	0.065	4	200	16 x 140	B	-	24.6	35.6	55.0	25	50
15	2DG2_50_50	mono	12.6	16.5	1.9	24.0	0.065	4	200	16 x 140	B	-	24.2	40.8	54.4	50	50
16	2DG2_100_50	mono	12.6	16.5	1.9	24.0	0.065	4	200	16 x 140	B	-	23.8	38.4	53.0	100	50

FE simulations of retrofitted beam-column joints with test setup IND																
No.	**Name**	**Load**	**Axial Load [%]**	**f_c' [MPa]**	**f_{ct} [MPa]**	**E_c [GPa]**	**G_f [Nm]**	**f_y [MPa]**	**ρ_b [%]**	**ρ_c [%]**	**Failure mode**	**$V_{c,crack}$ [kN]**	**$V_{c,peak}$ [kN]**	**$F_{h,t,max}$ [kN]**	**$F_{h,c}$ [kN]**	**k_N [kN/mm]**	**k_V [kN/mm]**
1	JT13_50_50	mono	0	30.2	2.7	28.5	0.075	490	0.76	1.04	BJ	106.1	113.0	109.6	135.5	50	50
2	JT13_100_50	mono	0	30.2	2.7	28.5	0.075	490	0.76	1.04	BJ	107.4	113.1	123.1	145.8	100	50
3	JT13_50_5025	mono	0	30.2	2.7	28.5	0.075	490	0.76	1.04	BJ	106.6	112.5	113.9	142.1	50	50
4	JT13_25_50	mono	0	30.2	2.7	28.5	0.075	490	0.76	1.04	BJ	106.3	112.6	129.7	133.4	25	50
5	JT14_25_5025	mono	0	33.6	3.1	28.5	0.080	490	0.58	1.04	B	-	89.9	84.5	132.2	50	50
6	JT14_25_50	mono	0	33.6	3.1	28.5	0.080	490	0.58	1.04	B	-	89.9	88.0	130.6	25	50
7	JT14_50_50	mono	0	33.6	3.1	28.5	0.080	490	0.58	1.04	B	-	88.4	100.1	151.8	50	50
8	JT14_100_50	mono	0	33.6	3.1	28.5	0.080	490	0.58	1.04	B	-	90.1	90.2	128.9	100	50
9	JT14_25_25	mono	0	33.6	3.1	28.5	0.080	490	0.58	1.04	B	-	90.1	89.5	119.8	25	25
10	JT4_50_25	mono	0	33.6	3.1	28.5	0.080	490	0.58	1.04	B	-	89.1	106.1	143.1	50	25

APPENDIX D: SEISMIC ASSESSMENT OF 2D RC EXTERIOR JOINTS

In this Appendix the as-built specimens tested in this study are analysed using the assessment procedure proposed in Chapters 7. The equations used are written only for the test specimen "2D pre 1970s", while for the other specimens only the results are shown.

Test 2D pre 1970s

Table D 1: Geometry of the specimen "2D pre 1970s"

Beam		**Column**		**Joint**	
$L_b/2$ =	1524 mm	H_c =	2000 mm	w_j =	230 mm
h_b =	330 mm	h_c =	230 mm	h_j =	230 mm
w_b =	230 mm	w_c =	230 mm	Anchorage	Type 6
Long. rein.	4+4 R10	Long. rein.	3+3 R10	Shear rein.	-
Shear rein.	R6 / 133 mm	Shear rein.	R6 / 100 mm		
c =	25 mm				

Table D 2: Material properties of the specimen "2D pre 1970s"

Concrete		**Rein. Steel**		
f_c =	17.7 MPa	R10	f_y =	430 MPa
f_{ct} =	1.8 MPa		f_u =	527 MPa
			E_s =	201 GPa
		R6	f_y =	397 MPa
			f_u =	452 MPa
			E_s =	196 GPa

Beam and flexural strength

$$M_{c,beam-hinge} = A_s \cdot f_y \cdot j_b \cdot \frac{2L_b}{H_c}\frac{(H_c - h_b)}{(L_b - h_c)} =$$

$$M_{c,beam-hinge} = \left[314 \cdot 430 \cdot 0.9(330-25) \cdot \frac{1524}{2000}\frac{(2000-330)}{(2 \cdot 1524 - 230)}\right] \Big/ 1000 = 16.7 \text{ kNm}$$

$M_{c,column-hinge} =$ … see diagram of hierarchy of strength

The flexural strength of the column can be plotted as function of N_c carrying out a moment-curvature analysis or alternatively plotting a line passing through the following points, which can be easily determined per hand calculation:

Point 1: Pure tension
Point 2: $N_c = 0$
Point 3: $f_s = f_y$
Point 4: $\varepsilon_s = 0.01$ and $\varepsilon_{cu} = 0.0035$
Point 5: $\varepsilon_s = 0$ and $\varepsilon_{cu} = 0.0035$
Point 6: Pure compression

Beam and column shear strength

$$M_{c,beam-shear} = \frac{H_c}{L_b}\left(H_c - h_b\right)\cdot V_{R,c,beam}$$

$$M_{c,beam-shear} = \frac{2000}{2\cdot 1524}\frac{\left(2000-330\right)\cdot 25.4}{1000} = 27.8\,\text{kNm}$$

with:

$$V_{R,c,beam} = \left[0.1\cdot\eta_1\cdot\kappa\cdot\left(100\cdot\rho_b\cdot f_c\right)^{1/3} - 0.12\cdot f_{a,b}\right]\cdot w_b\cdot\left(h_b - c\right) =$$

$$V_{R,c,beam} = \left[0.1\cdot 1.0\cdot\left(1+\sqrt{200/\left(330-25\right)}\right)\cdot\left(0.45\cdot 17.7\right)^{1/3}\right]\cdot\frac{230\cdot\left(330-25\right)}{1000} = 25.4\,\text{kN}$$

η_1 = 1.0 for normal concrete
$f_{a,b}$ = axial stress in the beam, usually equal to zero
$\kappa = 1+\sqrt{200/\left(h_b - c\right)}$

$$M_{c,column-shear} = \frac{\left(H_c - h_b\right)}{2}V_{R,c,column} = \frac{\left(2000-330\right)}{2\cdot 1000}23.9 = 20.0\,\text{kNm}$$

with:

$$V_{R,c,column} = \left[0.1\cdot\eta_1\cdot\kappa\cdot\left(100\cdot\rho_c\cdot f_c\right)^{1/3} - 0.12\cdot f_{a,c}\right]\cdot w_c\cdot\left(h_c - c\right) =$$

$V_{R,c,column}$ = …see diagram of hierarchy of strength

$f_{a,c}$ = axial stress in the column

Joint shear strength

$$M_{c,joint-shear} = \frac{V_{jh}\cdot\left(H_c - h_b\right)/2}{\left[\frac{H_c}{j_b}\left(1-\frac{h_c}{L_b}\right)-1\right]} =$$

$$M_{c,joint-shear} = \frac{74.1\cdot\left(2000-330\right)/\left(2\cdot 1000\right)}{\left[\frac{2000}{0.9\left(330-25\right)}\left(1-\frac{230}{2\cdot 1524}\right)-1\right]} = 10.8\,\text{kNm (decreasing } N_c\text{)}$$

$$M_{c,joint-shear} = \frac{111.9 \cdot (2000-330)/(2 \cdot 1000)}{\left[\frac{2000}{0.9(330-25)}\left(1-\frac{230}{2 \cdot 1524}\right)-1\right]} = 16.3\,\text{kNm (increasing } N_c\text{)}$$

with:

$$V_{jh} = w_j \cdot h_j \sqrt{p_t^2 - p_t \cdot f_{a,c} + 2f_{a,c}} = \frac{230 \cdot 230\sqrt{1.13^2 - 1.13 \cdot 0.79 + 2 \cdot 0.79}}{1000} = 74.1\text{kN}$$

(decreasing N_c)

$$V_{jh} = \frac{230 \cdot 230\sqrt{1.13^2 - 1.13 \cdot 3.68 + 2 \cdot 3.68}}{1000} = 111.9\,\text{kN}$$

(increasing N_c)

$$p_t = k\sqrt{f_c} = \left[k_0 + k_1(2 - h_b/h_c)\right]\sqrt{f_c} = \left[0.1 + 0.3(2 - 330/230)\right]\sqrt{17.7} = 1.13\,\text{MPa}$$

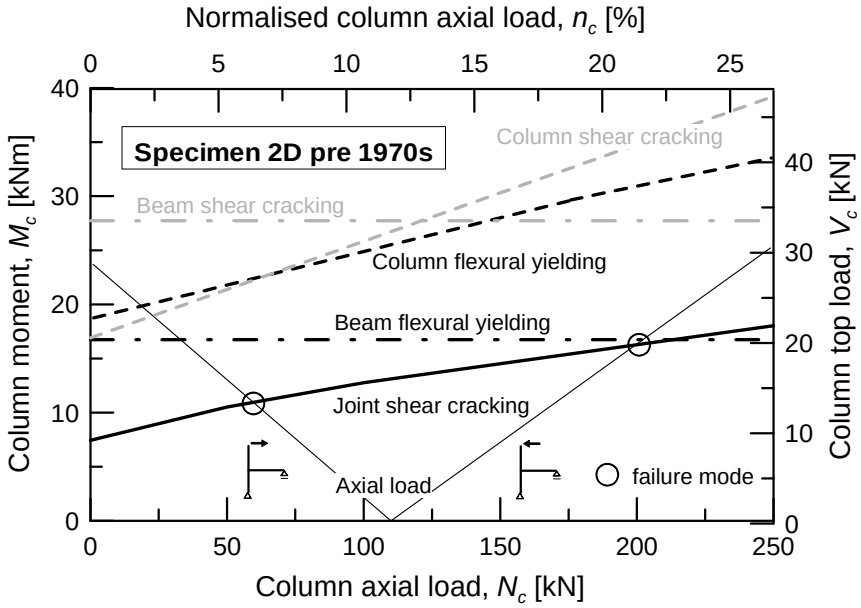

Figure D 1 : Hierarchy of strength of specimen „2D pre 1970s“

Test JT1-1

Table D 3: Geometry of the specimen JT1-1

Beam		**Column**		**Joint**	
$L_b/2$ =	1875 mm	H_c =	3230 mm	w_j =	350 mm
h_b =	400 mm	h_c =	300 mm	h_j =	300mm
w_b =	300 mm	w_c =	350 mm	Anchorage	Type 1
Long. rein.	2 D20 + 1D16 [a)]	Long. rein.	3+3 D20	Shear rein.	-
Shear rein.	D8 / 200 mm	Shear rein.	D8 / 150 mm		
c =	40 mm				

[a)] Symmetrical reinforcement top and bottom layer

Table D 4: Material properties of the specimen JT1-1

Concrete		**Rein. Steel**								
f_c =	25.4 MPa	D20	f_y =	552 MPa	D16	f_y =	558 MPa	D8	f_y =	548 MPa
f_{ct} =	n.a.		f_u =	672 MPa		f_u =	688 MPa		f_u =	652 MPa
			E_s =	200 GPa		E_s =	200 GPa		E_s =	200 GPa

$M_{c,beam\text{-}hinge}$ = 71.5 kNm
$M_{c,beam\text{-}shear}$ = 123.6 kNm
$M_{c,column\text{-}hinge}$ = 123.4 kNm (N_c = 0)
$M_{c,column\text{-}shear}$ = 86.4 kNm (N_c = 0)
$M_{c,joint\text{-}shear\ crack}$ = 32.1 kNm (N_c = 0)
$M_{c,joint\text{-}shear\ peak}$ = 48.3 kNm (N_c = 0)

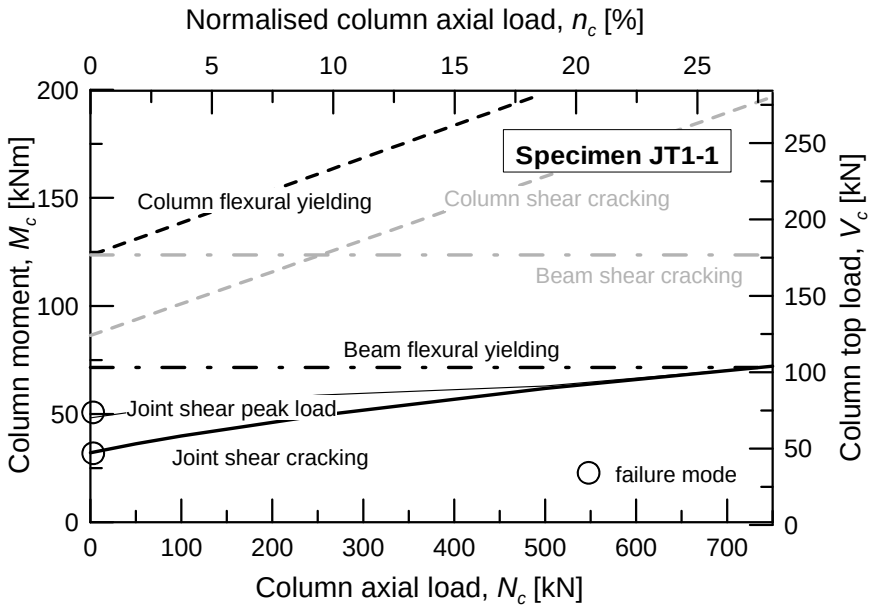

Figure D 2: Hierarchy of strength of specimen JT1-1

Test JT2-1

Table D 5: Geometry of the specimen JT2-1

Beam		**Column**		**Joint**	
$L_b/2$ =	1875 mm	H_c =	3230 mm	w_j =	350 mm
h_b =	400 mm	h_c =	300 mm	h_j =	300mm
w_b =	300 mm	w_c =	350 mm	Anchorage	Type 6
Long. rein.	2 R20 + 1R16 [a)]	Long. Rein.	3+3 R20	Shear rein.	-
Shear rein.	R8 / 200 mm	Shear rein.	R8 / 150 mm		
c =	40 mm				

[a)] Symmetrical reinforcement top and bottom layer

Table D 6: Material properties of the specimen JT2-1

Concrete		**Rein. Steel**								
f_c =	24.4 MPa	R20	f_y =	308 MPa	R16	f_y =	312 MPa	R8	f_y =	301 MPa
f_{ct} =	3.5 MPa		f_u =	382 MPa		f_u =	478 MPa		f_u =	485 MPa
			E_s =	200 GPa		E_s =	200 GPa		E_s =	200 GPa

$M_{c,beam\text{-}hinge}$ = 39.6 kNm
$M_{c,beam\text{-}shear}$ = 123.6 kNm
$M_{c,column\text{-}hinge}$ = 123.4 kNm (N_c = 0)
$M_{c,column\text{-}shear}$ = 85.3 kNm (N_c = 0)
$M_{c,joint\text{-}shear\ crack}$ = 27.0 kNm (N_c = 0)
$M_{c,joint\text{-}shear\ peak}$ = 35.4 kNm (N_c = 0)

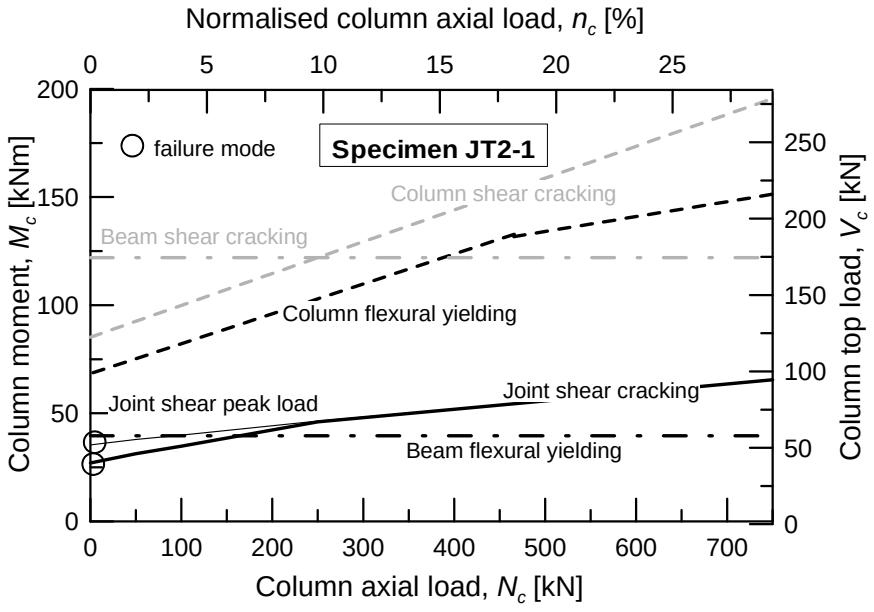

Figure D 3: Hierarchy of strength of specimen JT2-1

Test JT3-1

Table D 7: Geometry of the specimen JT3-1

Beam		**Column**		**Joint**	
$L_b/2$ =	1875 mm	H_c =	3230 mm	w_j =	350 mm
h_b =	400 mm	h_c =	300 mm	h_j =	300mm
w_b =	300 mm	w_c =	350 mm	Anchorage	Type 5-1 [b)]
Long. rein.	2 R20 + 1R16 [a)]	Long. rein.	3+3 R20	Shear rein.	-
Shear rein.	R8 / 200 mm	Shear rein.	R8 / 150 mm		
c =	40 mm				

[a)] Symmetrical reinforcement top and bottom layer

[b)] bottom – top layer of beam reinforcement

Table D 8: Material properties of the specimen JT3-1

Concrete		**Rein. Steel**
f_c =	27.5 MPa	See specimen JT1-1 (Table D 4)
f_{ct} =	n.a.	

$M_{c,beam\text{-}hinge}$ = 71.5 kNm
$M_{c,beam\text{-}shear}$ = 126.9 kNm
$M_{c,column\text{-}hinge}$ = 123.4 kNm (N_c = 0)
$M_{c,column\text{-}shear}$ = 88.7 kNm (N_c = 0)
$M_{c,joint\text{-}shear\ crack,1}$ = 33.5 kNm (N_c = 0)
$M_{c,joint\text{-}shear\ crack,5}$ = 21.2 kNm (N_c = 0)

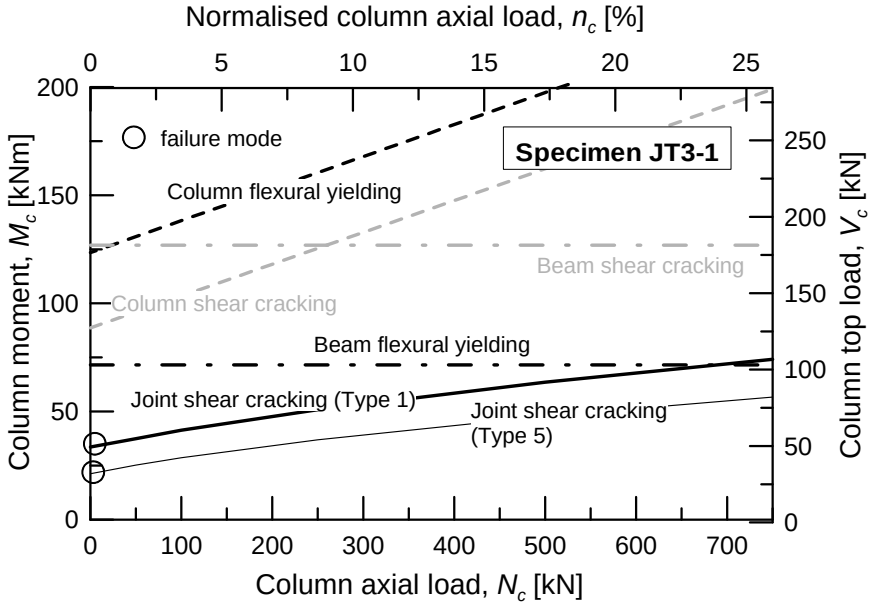

Figure D 4: Hierarchy of strength of specimen JT3-1

Test JT4-1

Table D 9: Geometry of the specimen JT4-1

Beam		**Column**		**Joint**	
$L_b/2$ =	1875 mm	H_c =	3230 mm	w_j =	350 mm
h_b =	400 mm	h_c =	300 mm	h_j =	300mm
w_b =	300 mm	w_c =	350 mm	Anchorage	Type 2-1 [b)]
Long. rein.	2 D20 + 1D16 [a)]	Long. rein.	3+3 D20	Shear rein.	-
Shear rein.	D8 / 200 mm	Shear rein.	D8 / 150 mm		
c =	40 mm				

[a)] Symmetrical reinforcement top and bottom layer

[b)] bottom – top layer of beam reinforcement

Table D 10: Material properties of the specimen JT4-1

Concrete		**Rein. Steel**
f_c =	28.2 MPa	See specimen JT1-1 (Table D 4)
f_{ct} =	3.0 MPa	

$M_{c,beam\text{-}hinge}$ = 71.5 kNm
$M_{c,beam\text{-}shear}$ = 128.0 kNm
$M_{c,column\text{-}hinge}$ = 123.4 kNm (N_c = 0)
$M_{c,column\text{-}shear}$ = 89.4 kNm(N_c = 0)
$M_{c,joint\text{-}shear\ crack,1}$ = 33.8 kNm (N_c = 0)
$M_{c,joint\text{-}shear\ crack,2}$ = 19.2 kNm (N_c = 0)

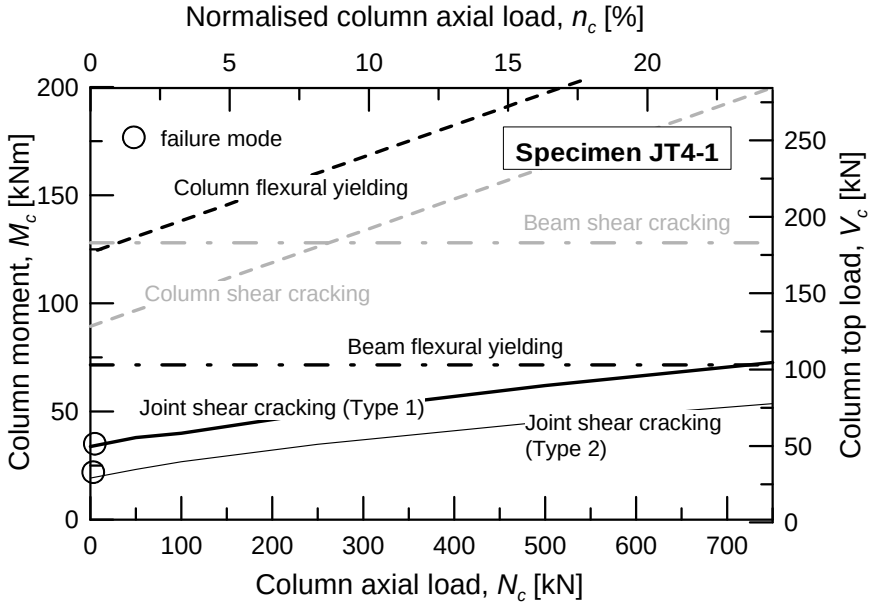

Figure D 5: Hierarchy of strength of specimen JT4-1

Test JT5-1

Table D 11: Geometry of the specimen JT5-1

Beam		**Column**		**Joint**	
$L_b/2$ =	1875 mm	H_c =	3230 mm	w_j =	350 mm
h_b =	400 mm	h_c =	300 mm	h_j =	300mm
w_b =	300 mm	w_c =	350 mm	Anchorage	Type 1
Long. rein.	4+4 D12 [a)]	Long. rein.	3+3 D20	Shear rein.	-
Shear rein.	D8 / 200 mm	Shear rein.	D8 / 150 mm		
c =	40 mm				
[a)] bottom – top layer of beam reinforcement					

Table D 12: Material properties of the specimen JT5-1

Concrete		**Rein. Steel**								
f_c =	24.6 MPa	D20	f_y =	519 MPa	D16	f_y =	543 MPa	D8	f_y =	530 MPa
f_{ct} =	3.4 MPa		f_u =	632 MPa		f_u =	640 MPa		f_u =	633 MPa
			E_s =	200 GPa		E_s =	200 GPa		E_s =	200 GPa

$M_{c,beam\text{-}hinge}$ = 37.7 kNm
$M_{c,beam\text{-}shear}$ = 100.0 kNm
$M_{c,column\text{-}hinge}$ = 114.6 kNm (N_c = 0)
$M_{c,column\text{-}shear}$ = 85.4 kNm (N_c = 0)
$M_{c,joint\text{-}shear\ crack}$ = 31.7 kNm (N_c = 0)
$M_{c,joint\text{-}shear\ peak}$ = 40.8 kNm (N_c = 0)

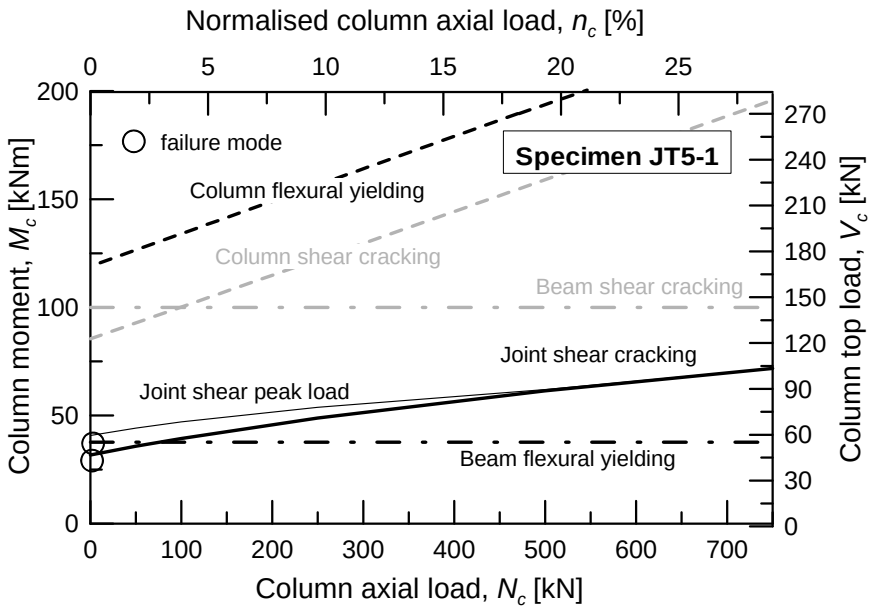

Figure D 6: Hierarchy of strength of specimen JT5-1

APPENDIX E: DESIGN OF HAUNCH RETROFIT SOLUTION

The design model for the Haunch Retrofit Solution (HRS) presented in this Appendix is taken from the work of *Yu et al. (2000)* and *Chen (2006)*.

Yu *et al.* proposed, on the basis of one welded haunch on the bottom of the beam, the analytical method to derive the β-factor. The β-factor is derived with the deformation compatibility theory of the model of the steel moment connection shown in Figure E 1. The horizontal (u_b) and vertical (v_b) component of the beam deformation at the haunch tip (Point B, in Figure E 2a) that is influenced by the haunch stiffness K_d and it can be calculated for a given shear, V_{pb} force acting at the beam end. The beam bending moment in the haunch region can be expressed at a location x (with x = 0 at the beam-column interface and $x = a$ at the point B as shown in Figure E 2a) according to Equation (E-1).

$$M(x) = (L'/2 + x)V_{pd} - x\left(\beta \cdot V_{pd} / \tan\theta\right) \cdot d/2 \tag{E-1}$$

The compressive stress in the beam bottom flange is given by the contributions of the bending moment and of the axial force (βV_{pd} / tanα in Figure E 2a,b) according to Equation (E-2).

$$\sigma(x) = \frac{(L'/2 + x)V_{pd}}{I_b}\frac{d}{2} - \frac{x\left(\beta \cdot V_{pd}\right)}{I_b}\frac{d}{2} - \frac{x\left(\beta \cdot V_{pd} / \tan\theta\right)}{I_b}\left(\frac{d}{2}\right)^2 - \frac{\beta \cdot V_{pd} / \tan\alpha}{A_b} \tag{E-2}$$

The horizontal component, u_b, of the beam deformation at the haunch tip is equal to the axial shortening of the beam bottom flange in the haunch region (Eq. (E-3)).

$$u_b = \int_0^a \frac{\sigma(x)}{E_s} dx = \left(\frac{L'/d - \beta \tan\theta}{E_s I_b}\left(\frac{d}{2}\right)^2 a + \frac{(1-\beta)a^2}{2E_s I_b}\frac{d}{2} - \frac{\beta a \tan\theta}{E_s I_b} \right) \cdot V_{pd} \tag{E-3}$$

The moment area method is used to estimate the vertical component, v_b, of the beam deformation at the haunch tip (Eqn. (E-4)).

$$v_b = \int_0^a \frac{xM(x)}{E_s I_b} dx = \left(\frac{L'/d - \beta \tan\theta}{E_s I_b}\frac{d}{4}a^2 + \frac{(1-\beta)a^3}{3E_s I_b} \right) \cdot V_{pd} \tag{E-4}$$

On the basis of the above calculations and being a and b the projections of the original length of the haunch, L_h, on beam and column, respectively, the shortening of the haunch, d_h, can be determined according to Equation (E-5).

$$\delta_h = \sqrt{\left(a-u_b\right)^2+\left(b-v_b\right)^2} - L_h \approx u_b\cos\theta + v_b\sin\theta$$
$$L_h = \sqrt{a^2+b^2} \qquad \text{(E-5)}$$

Inserting Equations (E-3) and (E-4) in Equation (E-5) and solving it as function of β, the Equation can be obtained (E-6).

$$\beta = \frac{b}{a}\left(\frac{3L'd+3ad+3bL'+4ab}{3d^2+6bd+4b^2+\frac{12I_b}{A_b}+\frac{12I_b}{A_h\cos^3\theta}}\right) \qquad \text{(E-6)}$$

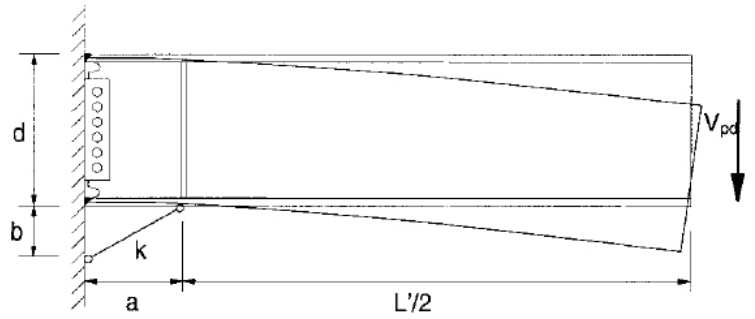

Figure E 1: Simplified model of welded haunch connection

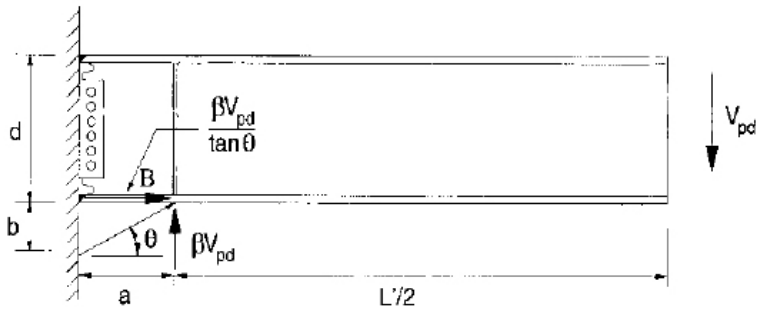

a) Free body diagram of the beam

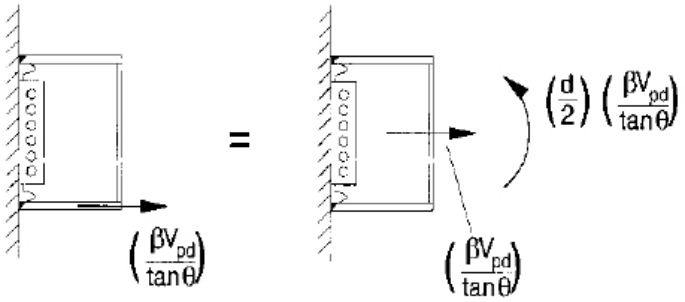

b) Eccentric force due to strut action

Figure E 2: Actions on the beam

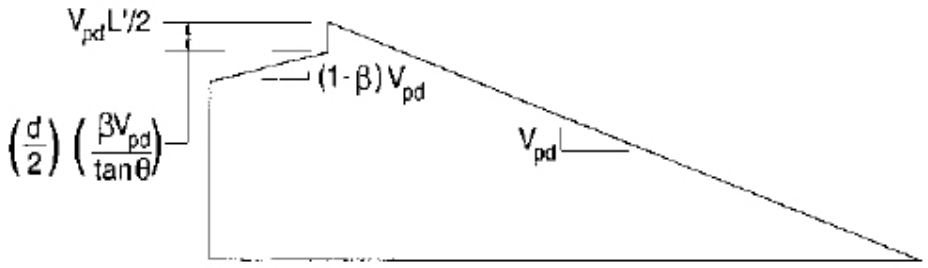

Figure E 3: Reduction of bending moment due to eccentric force

The Equation (E-6) was modified by *Pampanin & Christopoulos (2003)* in order to take into account the presence of two symmetrical haunches (top and bottom). The new formulation is given in Equation (E-7) using the notation adopted in this work.

$$\beta = \frac{b}{a}\left(\frac{6Lh_b + 3ah_b + 6bL + 4ab}{3h_b + 6bh_b + 4b^2 + \dfrac{12E_cI_b}{2K_d a\cos^2\alpha}}\right) \tag{E-7}$$

with:
$L = L_b - h_c - 2a$

Chen (2006) proposed a further formulation of the β-factor, in order to take additionally into account the contribution of column (terms in […]) and joint (terms in {…}) deformation (Eq. (E-8)).

$$\beta = \frac{b}{a}\left(\frac{\begin{array}{l}6Lh_b + 3ah_b + 6bL + 4ab + \left[\dfrac{2I_bb^3}{I_caH_c} + \dfrac{3I_bHL_bb^3}{2I_ca^2H_c} + \dfrac{3I_bh_cHL_bb^2}{I_ca^2H_c}\right] + \\ + \left\{\dfrac{12E_cI_b}{K_ja}\left(b + \dfrac{h_b}{2}\right)\left(a + \dfrac{h_c}{2} + L\right)\right\}\end{array}}{\begin{array}{l}3h_b + 6bh_b + 4b^2 + \dfrac{12E_cI_b}{2K_d a\cos^2\alpha} + \left[\dfrac{6I_bb^2}{a^2A_c} + \dfrac{2I_bh_cb^2}{I_ca} + \dfrac{3I_bh_cb^2}{I_ca^2} + \dfrac{3I_bh_c^2b^3}{2I_ca^3}\right] + \\ + \left\{\dfrac{12E_cI_bb}{K_ja}\left(b + \dfrac{h_c}{2}\right)\left(1 + \dfrac{h_b}{2b} + \dfrac{h_c}{2a}\right)\right\}\end{array}}\right) \tag{E-8}$$

with:
$H = H_c - h_b - 2b$
K_j = Joint rotational stiffness according to Equation (E-8a)

$$K_j = G_c\left(\frac{j_bH_c}{H_c - j_b}A_c\right) \tag{E-8a}$$

The numerical simulation and their experimental validation carried out by *Pampanin et al. (2006)* showed that the consideration of the column deformation is necessary to realistically evaluate the effect of the haunch on the beam-column connection. The influence of the joint deformation may be neglected in this concern (see Figure E 4).

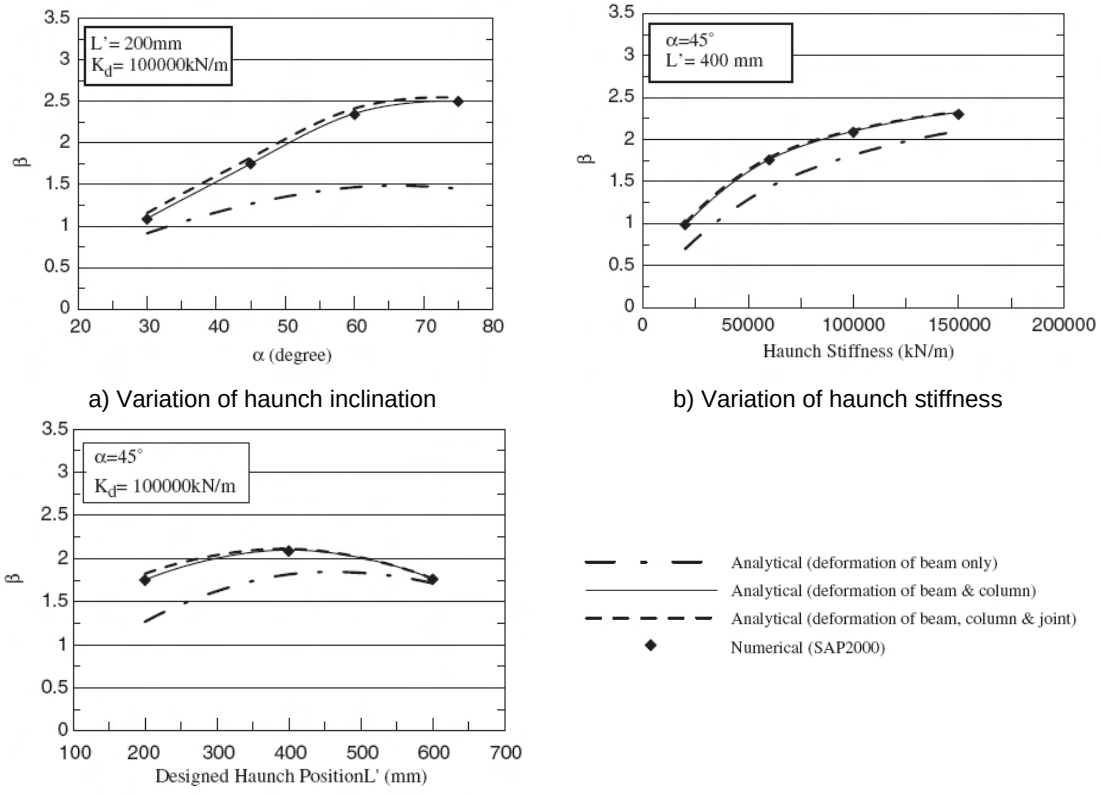

a) Variation of haunch inclination

b) Variation of haunch stiffness

c) Variation of haunch length

Figure E 4: Comparison between alternative formulations of the haunch β-factor when accounting for deformation contribution of beam, column and/or joint elements (*Pampanin et al., 2006*)

After the determination of β-factor all the forces acting on the beam-column joints are known (see Figure E 5 and Figure E 6).

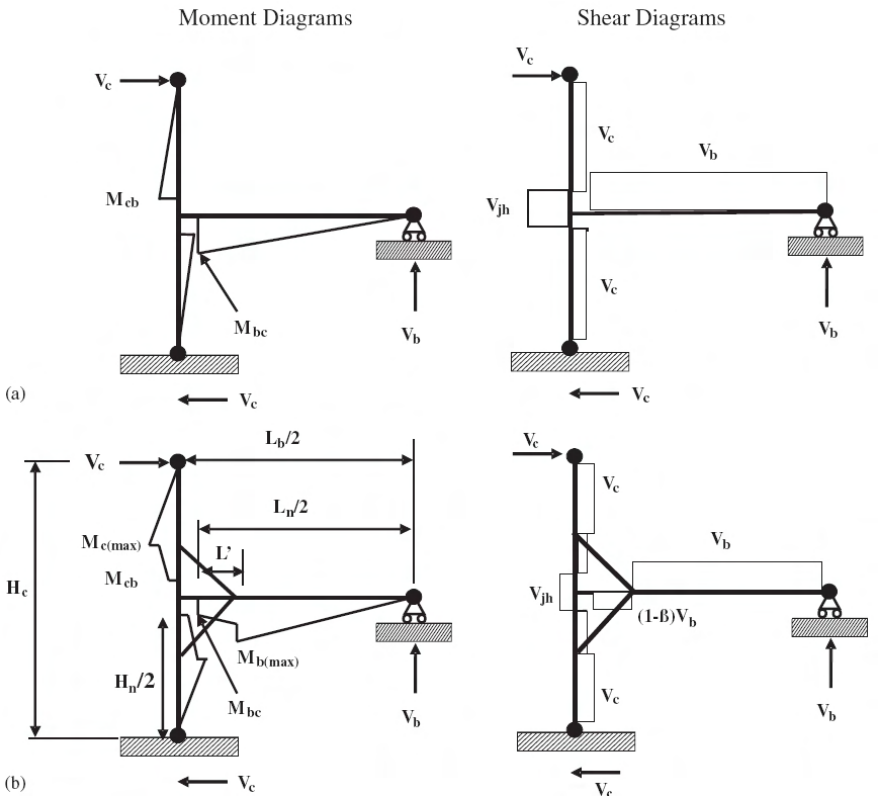

Figure E 5: Moment and shear diagrams of exterior joint: (a) as-built joint; (b) joint retrofitted with two diagonal haunches (*Pampanin et al., 2006*)

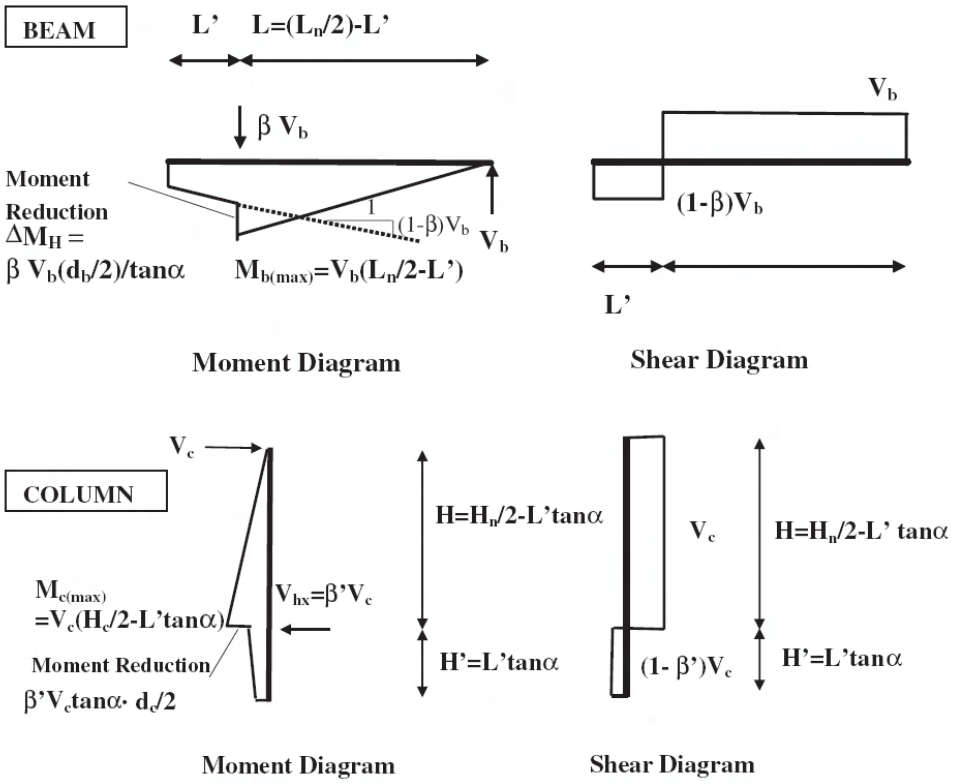

Figure E 6: Moment and shear diagrams in the beam and column after retrofitting with two diagonal haunches (*Chen, 2006*)

The design of the HRS follows an iterative step-by-step procedure:

Step 1: Preliminary choice of the haunch parameters (α, L_h and K_d)

Step 2: Determination of the β-factor according to Equation (E-8)

Step 3: Definition of acceptable damage / limit state in the joint

The horizontal shear force acting in the joint is defined by Equation (E-9)

$$V_{jh} = \frac{M_{bc}}{j_b} - \left(V_c - V_{hx}\right) \tag{E-9}$$

with:

$$M_{bc} = M_{b,\max}\left[1 - \frac{\beta h_b}{2L'\tan\alpha} + \frac{(1-\beta)L'}{L}\right] \tag{E-9a}$$

$$M_{b,\max} = V_b \cdot \left(\frac{L_b}{2} - \frac{h_c}{2} - L'\right) \tag{E-9b}$$

$$V_b = V_c \cdot \frac{L_b H}{L H_c} \tag{E-9c}$$

$$V_{hx} = \frac{2\beta V_c H_c}{3\tan\alpha\left(L_n + h_c\right)} \tag{E-9d}$$

By substitution of Equations (E-9a) to (E-9d) into Equation (E-9) the interstorey shear V_c corresponding to the considered limit state of the joint panel can be written as:

$$\bar{V}_{c,joint} = \frac{A_j\sqrt{p_t^2 - \left(p_t N_c / A_c\right)}}{\left(1 - \frac{\beta H_c}{\left(L_n + d_c\right)\tan\alpha} - \frac{H_c\left(L_n - 2L'\right)}{j_b\left(L_n + d_c\right)}\left(1 - \frac{\beta h_b}{2L\tan\alpha} + \frac{(1-\beta)L'}{L}\right)\right)} \tag{E-10}$$

where, the numerator represents the joint shear force $V_{jh} = A_j\sqrt{p_t^2 - \left(p_t N_c / A_c\right)}$

Step 4: Estimation of the required interstorey shear to force the development of a plastic hinge in the beam:

$$\bar{V}_{c,beam-hinge} = M_{by}\frac{\left(1 + \left(h_c + 2L'\right)/\left(L_n - 2L'\right)\right)}{H_c} \tag{E-11}$$

Step 5: Estimation of the interstorey shear corresponding to the development of a plastic hinge in the column:

$$\bar{V}_{c,column-hinge} = \frac{M_{cy}}{\left(H_c/2 - h_b/2 - L'\tan\alpha\right)} \tag{E-12}$$

Step 6: Estimation of the interstorey shear corresponding to the shear failure of the beam

If $\beta < 2 \rightarrow \overline{V}_{c,beam-shear} = \dfrac{\overline{V_b} \cdot L_b}{2 \cdot H_c}$ (E-13a)

If $\beta \geq 2 \rightarrow \overline{V}_{c,beam-shear} = \dfrac{\overline{V_b} \cdot L_b}{2 \cdot H_c \left(\beta - 1\right)}$ (E-13b)

with $\overline{V_b}$ = beam shear strength calculated according to the relevant code of practice

Step 7: Estimation of the interstorey shear corresponding to the shear failure of the column

If $\beta' < 2 \rightarrow \overline{V}_{c,column-shear} = \overline{V_c}$ (E-14a)

If $\beta' \geq 2 \rightarrow \overline{V}_{c,column-shear} = \overline{V_c}\left(\dfrac{\beta \cdot H_c}{\tan\alpha \cdot L_b} - 1\right)$ (E-14b)

with $\overline{V_b}$ = column shear strength calculated according to the relevant code of practice

Step 8: Verification of the achievement of the desired hierarchy of strength in the beam-column connection and related safety factors γ_1, γ_2, γ_3 and γ_4.

$$V_{c,beam-hinge} \leq \min\left\{\frac{V_{c,joint-shear}}{\gamma_1}; \frac{V_{c,column-shear}}{\gamma_2}; \frac{V_{c,column-hinge}}{\gamma_3}; \frac{V_{c,beam-shear}}{\gamma_4}\right\} \quad \text{(E-15)}$$

Iteration: If the verification at Step 7 is not fulfilled, a new set of design parameters has to be chosen (Step 1) and the Steps 2 to 6 should be repeated.

APPENDIX F: HAUNCH RETROFIT SOLUTION WITH POST-INSTALLED ANCHORS

In this Appendix the retrofitted specimens tested in this study are analysed using the assessment procedure and the retrofit design proposed in Chapters 7 and 11, respectively. The design format proposed in Section 11.1 is not applied and all the verifications were carried out using measured average values for the material properties.

Test 2DG1

Table F 1: Geometry of the specimen 2DG1

Beam		**Column**		**Joint**	
$L_b/2$ =	1524 mm	H_c =	2000 mm	w_j =	230 mm
h_b =	330 mm	h_c =	230 mm	h_j =	230 mm
w_b =	230 mm	w_c =	230 mm	Anchorage	Type 6
Long. rein.	4+4 R10	Long. Rein.	3+3 D10	Shear rein.	-
Shear rein.	D6 / 133 mm	Shear rein.	D6 / 100 mm		
c =	25 mm				

Table F 2: Material properties of the specimen 2DG1

Concrete		**Rein. Steel**					
f_c =	16.6 MPa	R10	f_y =	338 MPa	R6	f_y =	345 MPa
f_{ct} =	1.9 MPa		f_u =	449 MPa		f_u =	426 MPa
			E_s =	200 GPa		E_s =	n.a.
			H_s =	n.a.		H_s =	n.a.

Assessment of as-built joint

See Section 7 and assessment of specimen “2D pre 1970s” in Appendix D.

Choice of haunches dimensions and anchorage

See Chapter 9 for more details.

Table F 3: Design parameters of the retrofit (2DG1)

Haunch			
L_h =	679 mm	E_s =	200 GPa
$L_{h,eff}$ ~	380 mm	$L' = L_h \cos\alpha$ =	480 mm
A_d =	16x200 mm^2	$K_d = E_s A_d / L_h$ ~	1000 kN/mm
α =	45°		
Anchorage			
Anchor type:	Bonded anchors	c_1 =	65 mm
n =	6	$c_{2,1}$ =	187.5 mm
h_{ef} =	125 mm	$c_{2,2}$ ~	50 mm
d_{nom} =	12 mm	s_1 =	100 mm
Steel 5.6, f_{yk} = 300 MPa, f_u = 500 Mpa		$s_{2,1}$ =	140 mm
		$s_{2,2}$ =	110 mm

Assessment of retrofitted joint

$k_{N,m}$ = 35 kN/mm (see Sections 9.4.10 and 11.2.2)

PLASTIC HINGE IN FAVOURABLE LOCATION (see Figure 8-14)

$$K_{h,t} = 1 \Big/ \left(\frac{2 \cdot \sin\alpha}{n k_N} + \frac{1}{K_d} \right)$$

$$K_{h,t\,\mathrm{m}} = 1 \Big/ \left(\frac{2 \cdot \sin 45°}{6 \cdot 35} + \frac{1}{1000} \right) = \underline{\mathbf{129\ kN/mm}}$$

$$K_{h,c,\mathrm{m}} = 1.5 \cdot K_{h,t,\mathrm{m}} = \underline{\mathbf{194\ kN/mm}}$$

β_m = **2.165** (θ_b = 0.30; θ_c = 0.80)

$$\bar{V}_{c,beam-hinge} = M_{by} \frac{\left(1 + \left(h_c + 2L'\right) / \left(L_n - 2L'\right)\right)}{H_c} = \underline{\mathbf{23.9\ kN}}$$

$$\bar{V}_{c,column-hinge} = \frac{M_{cy}}{\left(H_c/2 - h_b/2 - L' \tan\alpha\right)} = \underline{\mathbf{78.5\ kN}}\ (N_c = 110\ \mathrm{kN})$$

$$\bar{V}_{b,beam-shear} = \frac{A_s \cdot f_y \cdot \left(h_b - c\right)}{s} = \frac{56.52 \cdot 345 \cdot \left(330 - 25\right)}{133 \cdot 1000} = 44.7\ \mathrm{kN}$$

$$\beta > 2 \rightarrow \bar{V}_{c,beam-shear} = \frac{V_{b,beam-shear} \cdot L_b}{2 \cdot H_c \left(\beta - 1\right)} = \frac{44.7 \cdot 2 \cdot 1524}{2 \cdot 2000 \cdot \left(2.247 - 1\right)} = \underline{\mathbf{27.3\ kN}}$$

$V_{c,column\text{-}shear}$ = **31.6 kN**

$$\bar{V}_{c,joint} = \frac{A_j\sqrt{p_t^2 - (p_t N_c / A_c)}}{\left(1 - \frac{\beta_{min} H_c}{(L_n + d_c)\tan\alpha} - \frac{H_c(L_n - 2L')}{j_b(L_n + d_c)}\left(1 + \frac{(1-\beta)L'}{L}\right)\right)} = \underline{\mathbf{36.0\ kN}}\ (N_c = 110\ kN)$$

with: $p_t = k\sqrt{f_c} = \left[k_0 + k_1(2 - h_b/h_c)\right]\sqrt{f_c} = \left[0.1 + 0.3(2 - 330/230)\right]\sqrt{16.6} = 1.10$ MPa

Hierarchy of strength (β = 2.165)

Sequence	Event
1	$V_{c,beam\text{-}hinge}$ = 23.9 kN
3	$V_{c,beam\text{-}ultimate}$ = 31.7 kN
2	$V_{c,beam\text{-}shear}$ = 27.3 kN
6	$V_{c,column\text{-}hinge}$ = 47.4 kN (N_c = 110 kN)
7	$V_{c,column\text{-}ultimate}$ = 63.0 kN (N_c = 110 kN)
4	$V_{c,column\text{-}shear}$ = 31.6 kN (N_c = 110 kN)
5	$V_{c,joint\text{-}shear\ crack}$ = 36.0 (N_c = 110 kN)

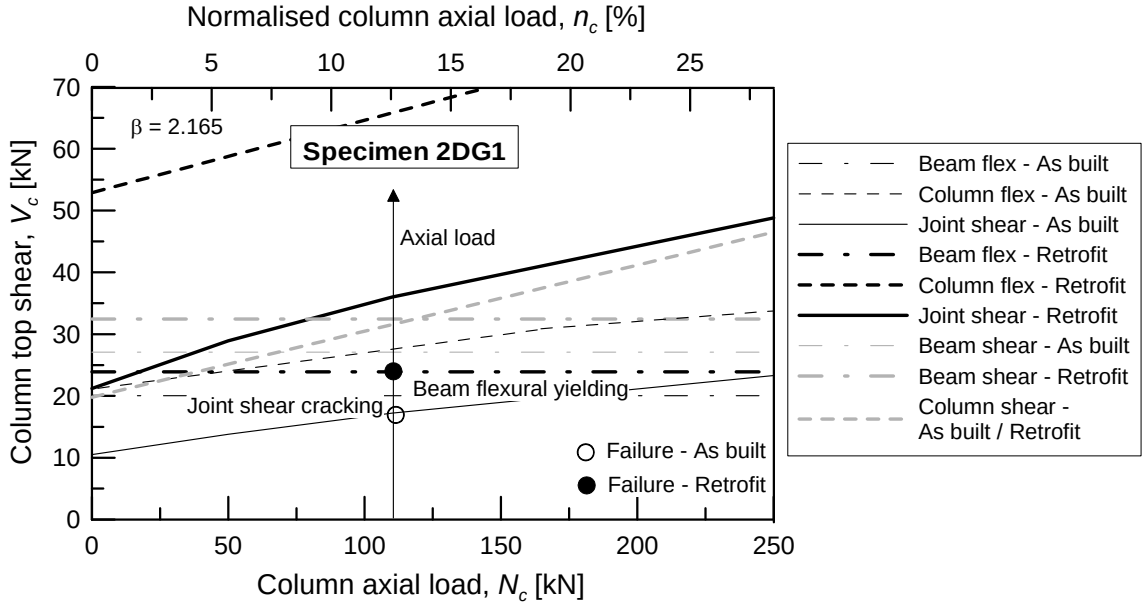

Figure F 1: Hierarchy of strength for β_m (2DG1)

PLASTIC HINGE IN UNFAVOURABLE LOCATION (see Figure 8-15)

$$K_{h,tm} = 1\Big/\left(\frac{2\cdot\sin 45°}{4\cdot 35} + \frac{1}{1000}\right) = \underline{\mathbf{90\ kN/mm}}$$

$$K_{h,c,m} = 1.5\cdot K_{h,t,m} = \underline{\mathbf{135\ kN/mm}}$$

β_m = **1.896** (θ_b = 0.30; θ_c = 0.80)

Further verifications are not shown for this case, because it is not occurred in the experimental test. Only the verification of the anchorage is exemplary shown in the following section.

Verification of the anchorage

PLASTIC HINGE IN FAVOURABLE LOCATION (see Figure 8-14)

Design actions

$$F_{h,\max} = \frac{\beta \cdot V_{b,y}}{\cos\alpha} = \frac{2.165 \cdot 31.4}{\cos 45°} = 96.1 \text{ kN}$$

$$F_{h,c} = F_h \frac{K_{h,c,\mathrm{m}}}{K_{h,c,\mathrm{m}} + K_{h,t,\mathrm{m}}} = 96.1 \frac{194}{129 + 194} = 57.7 \text{ kN}$$

$$F_{h,t} = F_h \frac{K_{h,t,\mathrm{m}}}{K_{h,c,\mathrm{m}} + K_{h,t,\mathrm{m}}} = 96.1 \frac{129}{194 + 129} = 38.4 \text{ kN}$$

$F_{h,N,t} = F_{h,t} \cdot \sin\alpha = 38.4 \cdot \sin 45° =$ **27.2 kN** (axial loading on the anchorage)

$F_{h,V,c} = F_{h,c} \cdot \cos\alpha = 57.7 \cdot \cos 45° =$ **40.8 kN** (shear loading on the anchorage)

TENSILE RESISTANCE

The anchorage configuration shown in Figure 8-16a is considered.

$$N_R = \min\left\{N_{R,s}; N_{R,p}; N_{R,c}; N_{R,sp}\right\}$$

Steel resistance

$$N_{R,s,grop} = n \cdot N_{R,s} = n \cdot A_{s,eff} \cdot f_u = \frac{6 \cdot 84.3 \cdot 500}{1000} = \mathbf{252.9\ kN}$$

Concrete cone resistance

$$N_{R,c} = N^0_{R,c} \cdot \psi_{A,N} \cdot \psi_{s,N} \cdot \psi_{ec,N} \cdot \psi_{re,N}$$

$$N^0_{R,c} = k_{N.uncr} \cdot \sqrt{f_c} \cdot h_{ef}^{1.5} = \frac{14.7 \cdot \sqrt{16.6} \cdot 125^{1.5}}{1000} = 83.7 \text{ kN (uncracked concrete)}$$

$$N^0_{R,c} = k_{N,cr} \cdot \sqrt{f_c} \cdot h_{ef}^{1.5} = \frac{10.3 \cdot \sqrt{16.6} \cdot 125^{1.5}}{1000} 58.6 \text{ kN (cracked concrete)}$$

$c_{cr} = 1.5h_{ef}$, $s_{cr} = 2c_{cr}$

$$\psi_{A,N} = \frac{A_{c,N}}{A^0_{c,N}} = \frac{(2c_1 + s_1)(c_{2,1} + s_{2,1} + s_{2,2} + c_{2,2})}{9h_{ef}^2} =$$

$$= \frac{(2 \cdot 65 + 100)(187.5 + 140 + 110 + 50)}{9 \cdot 125^2} = 0.80$$

$$\psi_{s,N} = 0.7 + 0.3\frac{\min\{c_1, c_{2,1}, c_{2,2}\}}{c_{cr,N}} = 0.7 + 0.3\frac{50}{1.5 \cdot 125} = 0.78$$

$\psi_{ec,N} = 0.9$ (assumption according to Section 9.4.9)

$\psi_{re,N} = 1.0$

$N_{R,c} = 83.7 \cdot 0.80 \cdot 0.78 \cdot 0.9 \cdot 1.0 =$ **47.0 kN** (uncracked concrete is assumed)

$N_{R,c} = 58.6 \cdot 0.80 \cdot 0.78 \cdot 0.9 \cdot 1.0 =$ **32.9 kN** (cracked concrete is assumed)

Combined concrete cone and pullout resistance

$$N_{R,p} = N^0_{R,p} \cdot \psi_{A,Np} \cdot \psi_{s,Np} \cdot \psi_{g,Np} \cdot \psi_{ec,Np} \cdot \psi_{re,Np}$$

$$N^0_{R,p} = \tau_{Rm,uncr} \cdot \pi \cdot d \cdot h_{ef} = \frac{21.3 \cdot 3.14 \cdot 12 \cdot 125}{1000} = 100.5 \text{ kN (uncracked concrete)}$$

$$N^0_{R,p} = \tau_{Rm,cr} \cdot \pi \cdot d \cdot h_{ef} = \frac{10.0 \cdot 3.14 \cdot 12 \cdot 125}{1000} = 47.1 \text{kN (cracked concrete)}$$

The values of $\tau_{Rk,uncr}$ and $\tau_{Rk,cr}$ taken from the relevant technical approval assuming Temperature Range I (short term loading -40°C to +40°C and long term loading +24°C) according to ETAG 001, Part 5 (*EOTA, 1997*). $\tau_{Rm,cr} = \tau_{Rk,cr} / 0.75$

$$s_{cr,Np} = 20d\sqrt{\frac{\tau_{Rm,uncr}}{7.5}} = 20 \cdot 12\sqrt{\frac{21.3}{7.5}} = 405 \le 3h_{ef} = 375 \text{ mm}$$

$$\psi_{A,Np} = \frac{A_{c,Np}}{A^0_{c,Np}} = \frac{(2c_1 + s_1)(c_{2,1} + s_{2,1} + s_{2,2} + c_{2,2})}{(s_{cr,Np})^2} =$$

$$= \frac{(2 \cdot 65 + 100)(187.5 + 140 + 110 + 50)}{375^2} = 0.80$$

$$\psi_{s,Np} = 0.7 + 0.3\frac{\min\{c_1, c_{2,1}, c_{2,2}\}}{c_{cr,Np}} = 0.7 + 0.3\frac{50}{187.5} = 0.78$$

$$\psi_{g,Np} = \psi^0_{g,Np} + \sqrt{\left(\frac{(s_1 + s_{2,1} + s_{2,2})/3}{s_{cr,Np}}\right)}\left(\psi^0_{g,Np} - 1\right) \ge 1.0$$

with:

$$\psi^0_{g,Np} = \sqrt{n} - \left(\sqrt{n} - 1\right)\left(\frac{\tau_{Rm,uncr}}{\max \tau_{R,uncr}}\right)^{1.5} \ge 1.0 \text{ (uncracked concrete)}$$

$$\psi^0_{g,Np} = \sqrt{n} - \left(\sqrt{n} - 1\right)\left(\frac{\tau_{Rm,cr}}{\max \tau_{R,cr}}\right)^{1.5} \geq 1.0 \text{ (cracked concrete)}$$

$$\max \tau_{R,uncr} = \frac{11.0}{\pi \cdot d}\sqrt{h_{ef} \cdot f_c} = \frac{11.0}{3.14 \cdot 12}\sqrt{125 \cdot 16.5} = 13.3 \text{ MPa}$$

$$\max \tau_{R,cr} = \frac{7.7}{\pi \cdot d}\sqrt{h_{ef} \cdot f_c} = 9.3 \text{ MPa}$$

$$\psi^0_{g,Np} = \sqrt{6} - \left(\sqrt{6} - 1\right)\left(\frac{21.3}{13.3}\right)^{1.5} = -0.5 \rightarrow 1.0 \text{ (uncracked concrete)}$$

$$\psi^0_{g,Np} = \sqrt{6} - \left(\sqrt{6} - 1\right)\left(\frac{10.0}{9.3}\right)^{1.5} = 0.83 \rightarrow 1.0 \text{ (cracked concrete)}$$

$$\psi_{g,Np} = 1.0 \text{ (uncracked and cracked concrete)}$$

$$\psi_{ec,Np} = \psi_{ec,N} \approx 0.9 \text{ (assumption according to Section 9.4.9)}$$

$$\psi_{re,Np} = \psi_{re,N} = 1.0$$

$$N_{R,p} = 100.5 \cdot 0.80 \cdot 0.78 \cdot 1.0 \cdot 0.9 \cdot 1.0 = \textbf{56.2 kN} \text{ (uncracked concrete)}$$

$$N_{R,p} = 47.1 \cdot 0.80 \cdot 0.78 \cdot 1.00 \cdot 0.9 \cdot 1.0 = \textbf{26.5 kN} \text{ (cracked concrete)}$$

Splitting resistance

Splitting during installation can be avoided respecting c_{min} and s_{min} indicated in the relevant technical approval.

h / h_{ef} = 2.64 → $c_{cr,Nsp} = h_{ef}$ = 125 < $c_{cr,N}$ → verification for splitting resistance is not required

SHEAR RESISTANCE

The anchorage configuration shown in Figure 8-18a is considered.

$$V_R = \min\left\{V_{R,s}; V_{R,cp}; V_{R,c}\right\}$$

Steel resistance

$$V_{R,s} = n \cdot \alpha \cdot A_{s,eff} \cdot f_u = \frac{6 \cdot 0.5 \cdot 84.3 \cdot 500}{1000} = \textbf{126.5 kN}$$

Concrete pryout resistance

$$V_{R,cp} = k_{cp} \cdot N_{R,c}$$

$$V_{R,cp} = 2.0 \cdot 47.0 = \textbf{94.0 kN}$$

$$V_{R,cp} = k_{cp} \cdot N_{R,c} = 2.0 \cdot 32.9 = \textbf{65.8 kN}$$

Concrete edge resistance

$$V_{R,c} = V_{R,c}^{0} \cdot \psi_{A,V} \cdot \psi_{h,V} \cdot \psi_{s,V} \cdot \psi_{ec,V} \cdot \psi_{\alpha,V} \cdot \psi_{re,V}$$

$$V_{R,c}^{0} = k_V \cdot d_{nom}^{\alpha} \cdot l_f^{\beta} \cdot c_1^{1.5} \sqrt{f_c}$$

k_V = 2.3 and 3.2 for cracked and uncracked concrete, respectively

$$\alpha = 0.1 \cdot \left(l_f / c_1\right)^{0.5} = 0.1 \cdot \left(125/65\right)^{0.5} = 0.14$$

$$\beta = 0.1 \cdot \left(d_{nom} / c_1\right)^{0.2} = 0.1 \cdot \left(12/65\right)^{0.2} = 0.07$$

$$V_{R,c}^{0} = \frac{3.2 \cdot 12^{0.14} \cdot 125^{0.07} \cdot 65^{1.5} \sqrt{16.6}}{1000} = 13.6 \text{ kN (uncracked concrete)}$$

$$V_{R,c}^{0} = \frac{2.3 \cdot 12^{0.14} \cdot 125^{0.07} \cdot 65^{1.5} \sqrt{16.6}}{1000} = 9.5 \text{ kN (cracked concrete)}$$

$$\psi_{A,V} = \frac{A_{c,V}}{A_{c,V}^{0}} = \frac{1.5c_1 \cdot \left(1.5c_1 + s_{2,1} + s_{2,2} + c_{2,2}\right)}{4.5c_1^2}$$

$$\psi_{A,V} = \frac{1.5 \cdot 65 \cdot \left(1.5 \cdot 65 + 140 + 110 + 50\right)}{4.5 \cdot 65^2} = 2.04$$

$$\psi_{h,V} = \sqrt{1.5c_1 / h} = 0.54 \rightarrow 1.0$$

$$\psi_{s,V} = 0.7 + 0.3 \frac{c_2}{1.5c_1} = 0.7 + 0.3 \frac{50}{1.5 \cdot 65} = 0.85$$

$$\psi_{ec,V} = 1.0$$

$\psi_{\alpha,V} = 2.5$ (3 rows of anchors perpendicular to the loading direction, see *fib, 2011*)

$$\psi_{re,V} = 1.0$$

$V_{R,c} = 13.6 \cdot 2.04 \cdot 1.0 \cdot 0.85 \cdot 1.0 \cdot 2.5 \cdot 1.0 = 59.0 \rightarrow$ **117.9 kN** (uncracked concrete)

$V_{R,c} = 9.5 \cdot 2.04 \cdot 1.0 \cdot 0.85 \cdot 1.0 \cdot 2.5 \cdot 1.0 = 41.2 \rightarrow$ **82.4 kN** (uncracked concrete)

CALCULATION OF TENSILE AND SHEAR RESISTANCE (n = 6)

Table F 4: Verification of the anchorage (2DG1, *n* = 6)

Tension			**Shear**		
	uncracked	**cracked**		**uncracked**	**cracked**
$N_{R,s}$ =	252.9 kN		$V_{R,s}$ =	126.5 kN	
$N_{R,c}$ =	**47.0 kN**	32.9 kN	$V_{R,cp}$ =	**94.0 kN**	**65.8 kN**
$N_{R,p}$ =	56.2 kN	**26.5 kN**	$V_{R,c}$ =	117.9 kN	82.4 kN
N_S =	27.2 kN [a)]		V_S =	40.8 kN [a)]	

[a)] calculated at beam flexural yielding

Tensioned anchorage: Combined tension and shear

27.2 / 47.0 + 27.2*0.75 / 94.0 = 0.58 + 0.22 = 0.78 < 1.2 OK!

Compressed anchorage: Shear

40.8*0.5 / 94.0 = 0.22 < 1.0 OK!

PLASTIC HINGE IN UNFAVOURABLE LOCATION (see Figure 8-15)

DESIGN ACTIONS

$$F_h = \frac{\beta \cdot V_{b,y}}{\cos\alpha} = \frac{1.896 \cdot 31.4}{\cos 45°} = 84.2 \text{ kN}$$

$$F_{h,c} = F_h \frac{K_{h,c,\text{m}}}{K_{h,c,\text{m}} + K_{h,t,\text{m}}} = 84.2 \frac{135}{90 + 135} = 50.5 \text{ kN}$$

$$F_{h,t,\max} = F_{h,\max} \frac{K_{h,t,\max}}{K_{h,c,\max} + K_{h,t,\max}} = 84.2 \frac{90}{135 + 90} = 33.7 \text{ kN}$$

$F_{h,N,t} = F_{h,t} \cdot \sin\alpha = 33.7 \cdot \sin 45° =$ **23.9 kN** (axial loading of the anchorage)

$F_{h,V,c} = F_{h,c} \cdot \cos\alpha = 50.5 \cdot \cos 45° =$ **35.9 kN** (shear loading of the anchorage)

TENSILE RESISTANCE

Steel resistance

$$N_{R,s,grop} = n \cdot N_{R,s} = n \cdot A_{s,eff} \cdot f_y = \frac{4 \cdot 84.3 \cdot 500}{1000} = \mathbf{168.6 \text{ kN}}$$

Concrete cone resistance

$N^0_{R,c} = 83.7$ kN (uncracked concrete)

$N_{R,c}^0 = 58.6\,\text{kN}$ (cracked concrete)

$$\psi_{A,N} = \frac{A_{c,N}}{A_{c,N}^0} = \frac{(2c_1 + s_1)(c_{2,1} + s_{2,1} + s_{2,2})}{9h_{ef}^2} =$$

$$= \frac{(2 \cdot 65 + 100)(187.5 + 140 + 110)}{9 \cdot 125^2} = 0.72$$

$$\psi_{s,N} = 0.7 + 0.3\frac{\min\{c_1, c_{2,1}\}}{c_{cr,N}} = 0.7 + 0.3\frac{65}{1.5 \cdot 125} = 0.80$$

$\psi_{ec,N} = 0.8$ (assumption, increase of eccentricity according to Figure 8-17c)

$\psi_{re,N} = 1.0$

$N_{R,c} = 83.7 \cdot 0.72 \cdot 0.80 \cdot 0.8 \cdot 1.0 =$ **38.6 kN** (uncracked concrete is assumed)

$N_{R,c} = 58.6 \cdot 0.72 \cdot 0.80 \cdot 0.8 \cdot 1.0 =$ **27.0 kN** (cracked concrete is assumed)

Combined concrete cone and pullout resistance

$N_{R,p}^0 = 100.5\,\text{kN}$ (uncracked concrete)

$N_{R,p}^0 = 47.1\,\text{kN}$ (cracked concrete)

$s_{cr,Np} = 375\,\text{mm}$

$$\psi_{A,Np} = \frac{(2c_1 + s_1)(c_{2,1} + s_{2,1} + s_{2,2})}{(s_{cr,Np})^2} =$$

$$= \frac{(2 \cdot 65 + 100)(187.5 + 140 + 110)}{375^2} = 0.72$$

$$\psi_{s,Np} = 0.7 + 0.3\frac{\min\{c_1, c_{2,1}, s_{2,2}\}}{c_{cr,Np}} = 0.7 + 0.3\frac{65}{187.5} = 0.80$$

$$\psi_{g,Np} = \psi_{g,Np}^0 + \sqrt{\left(\frac{(s_1 + s_{2,1})/2}{s_{cr,Np}}\right)}\left(\psi_{g,Np}^0 - 1\right) \geq 1.0$$

with:

$\max \tau_{R,uncr} = 13.3\,\text{MPa}$

$\max \tau_{R,cr} = 9.3\,\text{MPa}$

$$\psi_{g,Np}^0 = \sqrt{4} - \left(\sqrt{4} - 1\right)\left(\frac{21.3}{13.3}\right)^{1.5} = -0.1 \rightarrow 1.0 \text{ (uncracked concrete)}$$

$$\psi^0_{g,Np} = \sqrt{4} - \left(\sqrt{4} - 1\right)\left(\frac{10.0}{9.3}\right)^{1.5} = 0.90 \rightarrow 1.00 \text{ (cracked concrete)}$$

$\psi_{g,Np} = 1.0$ (uncracked and cracked concrete)

$\psi_{ec,Np} = \psi_{ec,N} = 0.8$

$\psi_{re,Np} = \psi_{re,N} = 1.0$

$N_{R,p} = 100.5 \cdot 0.72 \cdot 0.80 \cdot 1.0 \cdot 0.8 \cdot 1.0 =$ **45.4 kN** (uncracked concrete)

$N_{R,p} = 47.1 \cdot 0.72 \cdot 0.80 \cdot 1.00 \cdot 0.8 \cdot 1.0 =$ **21.7 kN** (cracked concrete)

Splitting resistance

$h / h_{ef} = 2.64 \rightarrow c_{cr,Nsp} = h_{ef} = 125 < c_{cr,N} \rightarrow$ verification for splitting resistance is not required

SHEAR RESISTANCE

$$V_R = \min\left\{V_{R,s}; V_{R,cp}; V_{R,c}\right\}$$

Steel resistance

$$V_{R,s} = n \cdot \alpha \cdot A_{s,eff} \cdot f_u = \frac{4 \cdot 0.5 \cdot 84.3 \cdot 500}{1000} = \textbf{84.3 kN}$$

Concrete pryout resistance

$V_{R,cp} = k_{cp} \cdot N_{R,c}$

$V_{R,cp} = 2.0 \cdot 42.0 =$ **84 .0 kN**

$V_{R,cp} = k_{cp} \cdot N_{R,c} = 2.0 \cdot 29.5 =$ **59.0 kN**

Concrete edge resistance

$V^0_{R,c} = 13.6$ kN (uncracked concrete)

$V^0_{R,c} = 9.5$ kN (cracked concrete)

$$\psi_{A,V} = \frac{A_{c,V}}{A^0_{c,V}} = \frac{1.5c_1 \cdot \left(3c_1 + s_{2,1}\right)}{4.5c_1^2}$$

$$\psi_{A,V} = \frac{1.5 \cdot 65 \cdot \left(3.0 \cdot 65 + 140\right)}{4.5 \cdot 65^2} = 1.72$$

$$\psi_{h,V} = \sqrt{1.5c_1 / h} = 0.54 \rightarrow 1.0$$

$$\psi_{s,V} = 0.7 + 0.3\frac{s_{2,2}}{1.5c_1} = 0.7 + 0.3\frac{110}{1.5 \cdot 65} = 1.04 \rightarrow 1.0$$

$\psi_{ec,V} = 1.0$

$\psi_{\alpha,V} = 2.0$ (2 rows of anchors perpendicular to the loading direction, see *fib, 2011*)

$\psi_{re,V} = 1.0$

$V_{R,c} = 13.6 \cdot 1.72 \cdot 1.0 \cdot 1.0 \cdot 1.0 \cdot 2.0 \cdot 1.0 = 46.8 \rightarrow$ **93.6 kN**

$V_{R,c} = 9.5 \cdot 1.72 \cdot 1.0 \cdot 1.0 \cdot 1.0 \cdot 2.0 \cdot 1.0 = 32.7 \rightarrow$ **65.4 kN**

CALCULATION OF TENSILE AND SHEAR RESISTANCE (n = 4)

Table F 5: Verification of the anchorage (2DG1, *n* = 4)

Tension			**Shear**		
	uncracked	**cracked**		**uncracked**	**cracked**
$N_{R,s}$ =	168.6 kN		$V_{R,s}$ =	84.3 kN	
$N_{R,c}$ =	**38.6 kN**	27.0 kN	$V_{R,cp}$ =	**84.0 kN**	**59.0 kN**
$N_{R,p}$ =	45.4 kN	**21.7 kN**	$V_{R,c}$ =	93.6 kN	65.4 kN
N_S =	23.8kN [a)]		V_S =	35.7 kN [a)]	

[a)] Calculated at beam flexural yielding

Tensioned anchorage: Combined tension and shear

23.8 / 38.6 + 23.8*0.75 / 84.0 = 0.62 + 0.21 = 0.83 < 1.2 OK!

Compressed anchorage: Shear

35.7*0.5 / 84.0 = 0.21 < 1.0 OK!

Test 2DG2

Table F 6: Geometry of the specimen 2DG2

Beam		**Column**		**Joint**	
$L_b/2$ =	1524 mm	H_c =	2000 mm	w_j =	230 mm
h_b =	330 mm	h_c =	230 mm	h_j =	230 mm
w_b =	230 mm	w_c =	230 mm	Anchorage	Type 6
Long. rein.	4+4 R10	Long. Rein.	3+3 D10	Shear rein.	-
Shear rein.	D6 / 133 mm	Shear rein.	D6 / 100 mm		
c =	25 mm				

Table F 7: Material properties of the specimen 2DG2

Concrete		**Rein. Steel**
f_c =	16.5 MPa	See specimen 2DG1 (Table F 2)
f_{ct} =	1.9 MPa	

Assessment of as-built joint

See Section 7 and assessment of specimen “2D pre 1970s” in Appendix D.

Choice of haunches dimensions and anchorage

See Chapter 9 for more details.

Table F 8: Design parameters of the haunches (2DG2)

Haunch			
L_h =	495 mm	E_s =	200 GPa
$L_{h,eff}$ ~	250 mm	$L' = L_h \cos\alpha$ =	350 mm
A_d =	16x140 mm^2	$K_d = E_s A_d / L_h$ ~	1050 kN/mm
α =	45°		
Anchorage			
Anchor Type	Bonded anchors	c_1 =	65 mm
n =	4	c_2 ~	50 mm
h_{ef} =	125 mm	s_1 =	100 mm
d_{nom} =	12 mm	s_2 =	100 mm
Steel 5.6, f_{yk} = 300 MPa, f_u = 500 Mpa			

Assessment of retrofitted joint

$k_{N,m}$ = 35 kN/mm (see Sections 9.4.10 and 11.2.2)

$$K_{h,t\mathrm{m}} = 1 \Big/ \left(\frac{2 \cdot \sin 45°}{4 \cdot 35} + \frac{1}{1050} \right) = \mathbf{90\ kN/mm}$$

$$K_{h,c,\mathrm{m}} = 1.5 \cdot K_{h,t,\mathrm{m}} = \mathbf{135\ kN/mm}$$

β_m = **1.619** (θ_b = 0.30; θ_c = 0.80)

Hierarchy of strength (β = 1.619)

Sequence	Event
1	$V_{c,beam\text{-}hinge}$ = 21.0 kN
3	$V_{c,beam\text{-}ultimate}$ = 27.9 kN
5	$V_{c,beam\text{-}shear}$ = 34.07 kN*
6	$V_{c,column\text{-}hinge}$ = 47.4 kN (N_c = 110 kN)
7	$V_{c,column\text{-}ultimate}$ = 63.0 kN (N_c = 110 kN)
4	$V_{c,column\text{-}shear}$ = 31.6 kN (N_c = 110 kN)
2	$V_{c,joint\text{-}shear\ crack}$ = 22.6 (N_c = 110 kN)

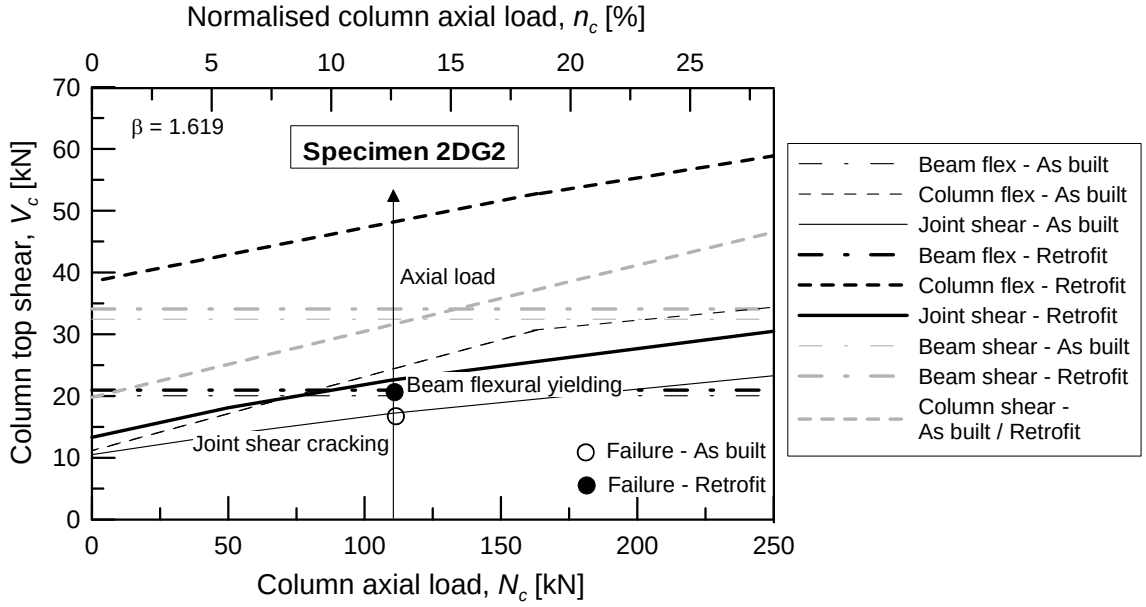

Figure F 2: Hierarchy of strength for β_m (2DG2)

DESIGN ACTIONS

See Calculations for specimen 2DG1.

CALCULATION OF TENSILE AND SHEAR RESISTANCE (n = 4)

Table F 9: Verification of the anchorage (2DG2, *n* = 4)

Tension			**Shear**		
	uncracked	**cracked**		**uncracked**	**cracked**
$N_{R,s}$ =	168.3 kN		$V_{R,s}$ =	84.2 kN	
$N_{R,c}$ =	**33.3 kN**	23.3 kN	$V_{R,cp}$ =	**66.6 kN**	**46.7 kN**
$N_{R,p}$ =	41.1 kN	**18.8 kN**	$V_{R,c}$ =	83.9 kN	60.3 kN
N_S =	17.9 kN [a)]		V_S =	26.8 kN [a)]	

[a)] Calculated at beam flexural yielding

Tensioned anchorage: Combined tension and shear

17.9 / 33.3 + 17.9*0.75 / 66.6 = 0.54 + 0.20 = 0.74 < 1.2 OK!

Compressed anchorage: Shear

26.8*0.5 / 66.6 = 0.20 < 1.0 OK!

Test JT1-2

Table F 10: Geometry of the specimens JT1-2

Beam		**Column**		**Joint**	
$L_b/2$ =	1875 mm	H_c =	3230 mm	w_j =	350 mm
h_b =	400 mm	h_c =	300 mm	h_j =	300mm
w_b =	300 mm	w_c =	350 mm	Anchorage	Type 1
Long. rein.	2 D20 + 1D16 [a)]	Long. Rein.	3+3 D20	Shear rein.	-
Shear rein.	D8 / 200 mm	Shear rein.	D8 / 150 mm		
c =	40 mm				

[a)] Symmetrical reinforcement top and bottom layer

Table F 11: Material properties of the specimen JT1-2

Concrete		**Rein. Steel**								
f_c =	26.5 MPa	D20	f_y =	501 MPa	D16	f_y =	478 MPa	D8	f_y =	548 MPa
f_{ct} =	2.1 MPa		f_u =	575 MPa		f_u =	590 MPa		f_u =	652 MPa
			E_s =	220 GPa		E_s =	209 GPa		E_s =	n.a.
			H_s =	1.3 GPa		H_s =	2.4 GPa		H_s =	n.a.

Assessment of as-built joint

See Section 7 and assessment of specimen JT1-1 in Appendix D.

Choice of haunches dimensions and anchorage

See Chapter 9 for more details.

Table F 12: Design parameters of the haunches (JT1-2)

Haunch			
L_h =	820 mm	E_s =	200 GPa
$L_{h,eff}$ ~	480 mm	$L' = L_h \cos\alpha$ =	580 mm
A_d =	16x150 mm^2	$K_d = E_s A_d / L_h$ ~	600 kN/mm
α =	45°		
Anchorage			
Anchor Type	Bonded anchors	c_1 =	100 mm
n =	6	c_2 ~	50 mm
h_{ef} =	150 mm	s_1 =	100 mm
d_{nom} =	12 mm	s_2 =	150 mm
Steel 8.8, f_{yk} = 640 MPa, f_{uk} = 800 Mpa			

Assessment of retrofitted joint

$k_{N,m}$ = 35 kN/mm (see Sections 9.4.10 and 11.2.2)

$$K_{h,t\min} = 1 \Big/ \left(\frac{2 \cdot \sin 45°}{6 \cdot 35} + \frac{1}{600} \right) = \underline{\mathbf{119\ kN/mm}}$$

$$K_{h,c,m} = 1.5 \cdot K_{h,t,m} = \underline{\mathbf{179\ kN/mm}}$$

β_m = **2.006** (θ_b = 0.35; θ_c = 0.40)

Hierarchy of strength (β = 2.006)

Sequence	Event
4	$V_{c,beam\text{-}hinge}$ = 66.7 kN
5	$V_{c,beam\text{-}ultimate}$ = 78.7 kN
2	$V_{c,beam\text{-}shear}$ = 57.7 kN [a)]
7	$V_{c,column\text{-}hinge}$ = 129.4 kN (N_c = 0)
8	$V_{c,column\text{-}ultimate}$ = 152.7 kN (N_c = 0)
3	$V_{c,column\text{-}shear}$ = 61.9 kN (N_c = 0) [a)]
1	$V_{c,joint\text{-}shear\ crack}$ = 44.6 kN (N_c = 0)
6	$V_{c,joint\text{-}shear\ peak\ load}$ = 67.9 kN (N_c = 0)

[a)] Shear cracking

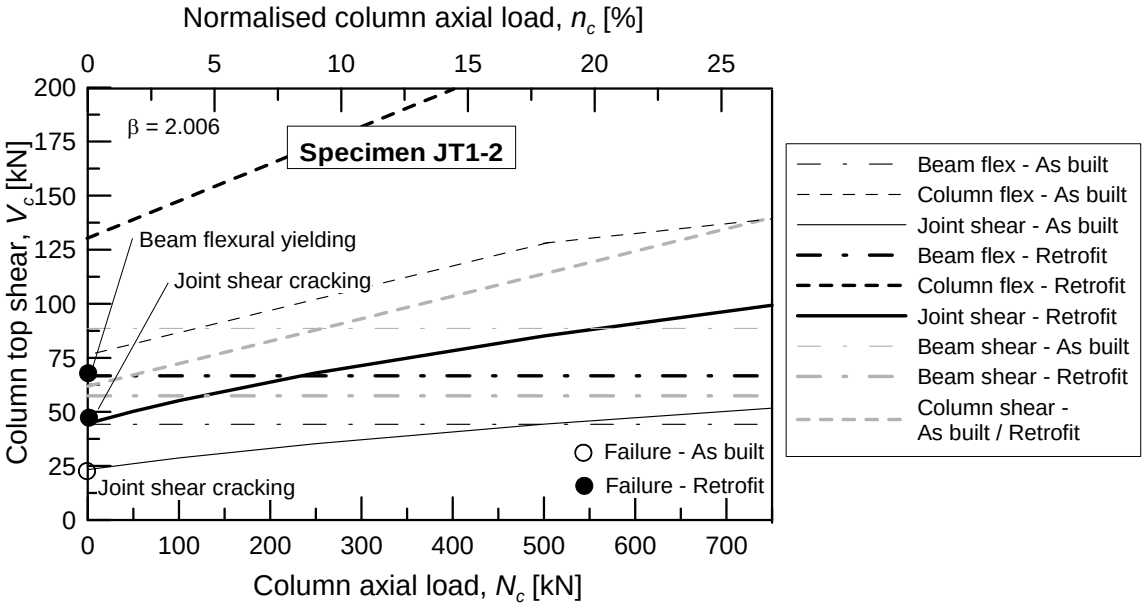

Figure F 3: Hierarchy of strength for β_m (JT1-2)

Verification of the anchorage

DESIGN ACTIONS

See Calculations for specimen 2DG1.

CALCULATION OF TENSILE AND SHEAR RESISTANCE (n = 6)

Tension			Shear		
	uncracked	**cracked**		**uncracked**	**cracked**
$N_{R,s}$ =	404.6 kN		$V_{R,s}$ =	202.4 kN	
$N_{R,c}$ =	**81.7 kN**	**57.3 kN**	$V_{R,cp}$ =	**163.4 kN**	**114.5 kN**
$N_{R,p}$ =	88.4 kN	69.9 kN	$V_{R,c}$ =	183.7 kN	132.0 kN
N_S =	92.1 kN [a)]		V_S =	138.5 kN [a)]	

[a)] Calculated at beam flexural yielding

Tensioned anchorage: Combined tension and shear

92.1 / 57.3 + 92.1*0.75 / 114.5 = 1.61 + 0.60 = 2.21 > 1.2 NO!

Compressed anchorage: Shear

138.5*0.5 / 114.5 = 0.60 < 1.0 OK!

PLASTIC HINGE IN UNFAVOURABLE LOCATION (see Figure 8-15)

$k_{N,m}$ = 35 kN/mm (see Sections 9.4.10 and 11.2.2)

$$K_{h,t\min} = 1 \Big/ \left(\frac{2 \cdot \sin 45°}{4 \cdot 35} + \frac{1}{600} \right) = \underline{\mathbf{85\ kN/mm}}$$

$$K_{h,c,m} = 1.5 \cdot K_{h,t,m} = \underline{\mathbf{127\ kN/mm}}$$

β_m = **1.704** (θ_b = 0.35; θ_c = 0.40)

Hierarchy of strength (β = 1.704)

Sequence	Event
5	$V_{c,beam\text{-}hinge}$ = 66.7 kN
6	$V_{c,beam\text{-}ultimate}$ = 78.7 kN
2	$V_{c,beam\text{-}shear}$ = 57.7 kN [a)]
7	$V_{c,column\text{-}hinge}$ = 129.4 kN (N_c = 0)
8	$V_{c,column\text{-}ultimate}$ = 152.7 kN (N_c = 0)
4	$V_{c,column\text{-}shear}$ = 61.9 kN (N_c = 0) [a)]
1	$V_{c,joint\text{-}shear\ crack}$ = 39.9 kN (N_c = 0)
3	$V_{c,joint\text{-}shear\ peak\ load}$ = 60.6 kN (N_c = 0)

[a)] Shear cracking

Verification of the anchorage

DESIGN ACTIONS

See Calculations for specimen 2DG1.

CALCULATION OF TENSILE AND SHEAR RESISTANCE (n = 4)

Tension			Shear		
	uncracked	**cracked**		**uncracked**	**cracked**
$N_{R,s}$ =	269.8 kN		$V_{R,s}$ =	134.9 kN	
$N_{R,c}$ =	**72.1 kN**	**50.5 kN**	$V_{R,cp}$ =	**144.2 kN**	**101.0 kN**
$N_{R,p}$ =	78.7 kN	54.3 kN	$V_{R,c}$ =	165.3 kN	118.8 kN
N_S =	78.6 kN [a)]		V_S =	117.3 kN [a)]	

[a)] Calculated at beam flexural yielding

Tensioned anchorage: Combined tension and shear

78.6 / 50.5 + 78.6*0.75 / 101.0 = 1.56 + 0.58 = 2.14 > 1.2 NO!

Compressed anchorage: Shear

117.3*0.5 / 101.0 = 0.58 < 1.0 OK!

Test JT1-3

Table F 13: Geometry of the specimens JT1-3

Beam		**Column**		**Joint**	
$L_b/2$ =	1875 mm	H_c =	3230 mm	w_j =	350 mm
h_b =	400 mm	h_c =	300 mm	h_j =	300mm
w_b =	300 mm	w_c =	350 mm	Anchorage	Type 1
Long. rein.	2 D20 + 1D16 [a)]	Long. Rein.	3+3 D20	Shear rein.	-
Shear rein.	D8 / 200 mm	Shear rein.	D8 / 150 mm		
c =	40 mm				

[a)] Symmetrical reinforcement top and bottom layer

Table F 14: Material properties of the specimen JT1-3

Concrete		**Rein. Steel**
f_c =	30.2 MPa	See specimen JT1-2 (Table D 4)
f_{ct} =	2.7 MPa	

Assessment of as-built joint

See Section 7 and assessment of specimen JT1-1 in Appendix D.

Choice of haunches dimensions and anchorage

See Chapter 9 for more details.

Table F 15: Design parameters of the haunches (JT1-3)

Haunch			
L_h =	820 mm	E_s =	200 GPa
$L_{h,eff}$ ~	480 mm	$L' = L_h \cos\alpha$ =	580 mm
A_d =	16x150 mm^2	$K_d = E_s A_d / L_h$ ~	600 kN/mm
α =	45°		
Anchorage			
Anchor Type	Bonded anchors	c_1 =	100 mm
n =	6	c_2 ~	50 mm
h_{ef} =	150 mm	s_1 =	100 mm
d_{nom} =	12 mm	s_2 =	150 mm
Steel 8.8, f_{yk} = 640 MPa, f_{uk} = 800 Mpa			

Assessment of retrofitted joint

$k_{N,m}$ = 35 kN/mm (see Sections 9.4.10 and 11.2.2)

See the calculations for the specimen JT1-2 for the calculation of β_m and the hierarchy of strength.

Verification of the anchorage

DESIGN ACTIONS

See calculations for the specimen 2DG1.

CALCULATION OF TENSILE AND SHEAR RESISTANCE (n = 6)

Tension			Shear		
	uncracked	**cracked**		**uncracked**	**cracked**
$N_{R,s}$ =	404.6 kN		$V_{R,s}$ =	202.4 kN	
$N_{R,c}$ =	**87.2 kN**	**61.1 kN**	$V_{R,cp}$ =	**174.5 kN**	**122.2 kN**
$N_{R,p}$ =	88.4 kN	75.6 kN	$V_{R,c}$ =	196.1 kN	140.9 kN
N_S =	92.1 kN [a)]		V_S =	138.5 kN [a)]	

[a)] Calculated at beam flexural yielding

Tensioned anchorage: Combined tension and shear

92.1 / 61.1 + 92.1*0.75 / 122.2 = 1.51 + 0.57 = 2.08 > 1.2 NO!

Compressed anchorage: Shear

138.5*0.5 / 122.2 = 0.57 < 1.0 OK!

PLASTIC HINGE IN UNFAVOURABLE LOCATION (see Figure 8-15)

See calculations for specimen JT1-2

Test JT1-4

Table F 16: Geometry of specimen JT1-4

Beam		**Column**		**Joint**	
$L_b/2$ =	1875 mm	H_c =	3230 mm	w_j =	350 mm
h_b =	400 mm	h_c =	300 mm	h_j =	300mm
w_b =	300 mm	w_c =	350 mm	Anchorage	Type 1
Long. rein.	2+2 D20 [a)]	Long. Rein.	3+3 D20	Shear rein.	-
Shear rein.	D8 / 200 mm	Shear rein.	D8 / 150 mm		
c =	40 mm				

[a)] D16 bars cut in the beam section ca. 50 mm from the end of the haunch

Table F 17: Material properties of the specimen JT1-4

Concrete		**Rein. Steel**
f_c =	33.6 MPa	See specimen JT1-2 (Table D 4)
f_{ct} =	3.1 MPa	

Assessment of as-built joint

See Section 7 and assessment of specimen JT1-1 in Appendix D.

Choice of haunches dimensions and anchorage

See Chapter 9 for more details.

Table F 18: Design parameters of the haunches (JT1-4)

Haunch			
L_h =	820 mm	E_s =	200 GPa
$L_{h,eff}$ ~	480 mm	$L' = L_h \cos\alpha$ =	580 mm
A_d =	16x150 mm^2	$K_d = E_s A_d / L_h$ ~	600 kN/mm
α =	45°		
Anchorage			
Anchor Type	Bonded anchors	c_1 =	100 mm
n =	6	c_2 ~	100 mm
h_{ef} =	150 mm	s_1 =	100 mm
d_{nom} =	12 mm	s_2 =	150 mm
Steel 8.8, f_{yk} = 640 MPa, f_{uk} = 800 Mpa			

Assessment of retrofitted joint

$k_{N,m}$ = 35 kN/mm (see Sections 9.4.10 and 11.2.2)

β_m = **2.006** (θ_b = 0.35; θ_c = 0.40)

Hierarchy of strength (β = 2.009)

Sequence	Event
1	$V_{c,beam\text{-}hinge}$ = 49.5 kN
4	$V_{c,beam\text{-}ultimate}$ = 60.9 kN
2	$V_{c,beam\text{-}shear}$ = 57.7 kN [a)]
6	$V_{c,column\text{-}hinge}$ = 126.7 kN (N_c = 0)
8	$V_{c,column\text{-}ultimate}$ = 159.2 kN (N_c = 0)
5	$V_{c,column\text{-}shear}$ = 67.0 kN (N_c = 0) [a)]
3	$V_{c,joint\text{-}shear\ crack}$ = 50.3 kN (N_c = 0)
7	$V_{c,joint\text{-}shear\ peak\ load}$ = 76.5 kN (N_c = 0)

[a)] Shear cracking

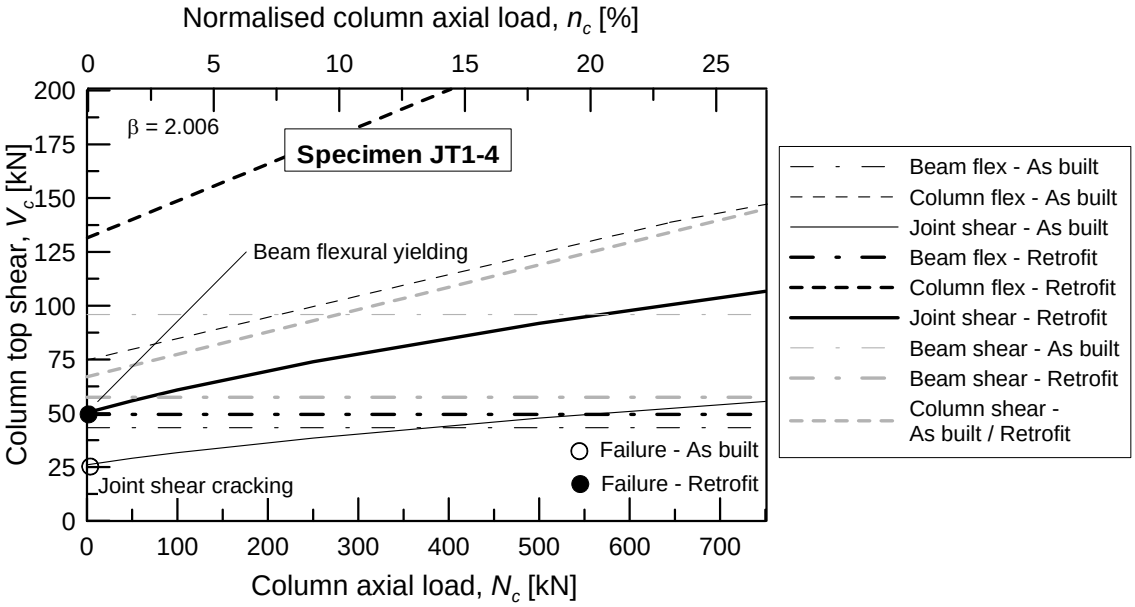

Figure F 4: Hierarchy of strength for β_m (JT4-1)

Verification of the anchorage

DESIGN ACTIONS

See calculations for the specimen 2DG1.

CALCULATION OF TENSILE AND SHEAR RESISTANCE (n = 6)

Tension			Shear		
	uncracked	**cracked**		**uncracked**	**cracked**
$N_{R,s}$ =	404.6 kN		$V_{R,s}$ =	**202.4 kN**	
$N_{R,c}$ =	108.7 kN	**76.2 kN**	$V_{R,cp}$ =	217.4 kN	**152.3 kN**
$N_{R,p}$ =	**105.3 kN**	95.2 kN	$V_{R,c}$ =	255.9 kN	183.9 kN
N_S =	68.3 kN [a)]		V_S =	102.8 kN [a)]	

[a)] Calculated at beam flexural yielding

Tensioned anchorage: Combined tension and shear

68.3 / 76.2 + 68.3*0.75 / 152.3 = 0.90 + 0.34 = 1.24 > 1.2 NO!

Compressed anchorage: Shear

102.8*0.5 / 152.3 = 0.34 < 1.0 OK!

Test JT1-5

Table F 19: Geometry of the specimen JT1-5

Beam		**Column**		**Joint**	
$L_b/2$ =	1875 mm	H_c =	3230 mm	w_j =	350 mm
h_b =	400 mm	h_c =	300 mm	h_j =	300mm
w_b =	300 mm	w_c =	350 mm	Anchorage	Type 1
Long. rein.	2 D20 + 1D16 [a)]	Long. Rein.	3+3 D20	Shear rein.	-
Shear rein.	D8 / 200 mm	Shear rein.	D8 / 150 mm		
c =	40 mm				

[a)] Symmetrical reinforcement top and bottom layer

Table F 20: Material properties of the specimen JT1-5

Concrete		**Rein. Steel**
f_c =	27.7 MPa	See specimen JT1-2 (Table D 4)
f_{ct} =	3.6 MPa	

Assessment of as-built joint

See Section 7 and assessment of specimen JT1-1 in Appendix D.

Choice of haunches dimensions and anchorage

See Chapter 9 for more details.

Table F 21: Design parameters of the haunches (JT1-5)

Haunch			
L_h =	820 mm	E_s =	200 GPa
$L_{h,eff}$ ~	480 mm	$L' = L_h \cos\alpha$ =	580 mm
A_d =	16x150 mm^2	$K_d = E_s A_d / L_h$ ~	600 kN/mm
α =	45°		
Anchorage			
Anchor type =	Concrete screws	c_1 =	100 mm
n =	6	c_2 ~	50 mm
h_{ef} =	90 mm	s_1 =	100 mm
d_{nom} =	14 mm	s_2 =	150 mm

Assessment of retrofitted joint

Based on the values indicated in the relevant ETA (European Technical Approval) the axial anchor stiffness is estimated as:

$k_{N,max}$ = 35 kN/mm (short term loading in cracked concrete)

$k_{N,min}$ = 10 kN/mm (approximately $k_{N,max}/4$)

$$K_{h,t\min} = 1 \Big/ \left(\frac{2 \cdot \sin 45°}{6 \cdot 10} + \frac{1}{600} \right) = \underline{\mathbf{40\ kN/mm}}$$

$$K_{h,t\max} = 1 \Big/ \left(\frac{2 \cdot \sin 45°}{6 \cdot 35} + \frac{1}{600} \right) = \underline{\mathbf{87\ kN/mm}}$$

$$K_{h,c,\min} = 1.5 \cdot K_{h,t,\min} = \underline{\mathbf{60\ kN/mm}}$$

$$K_{h,c,\max} = 1.5 \cdot K_{h,t,\max} = \underline{\mathbf{131\ kN/mm}}$$

β_{max} = **1.729** (verification of axial loading of the anchorage) - (θ_b = 0.35; θ_c = 0.40)

$\beta_{\min}$ = **1.076** (verification of joint shear cracking) - (θ_b = 0.35; θ_c = 0.40)

Hierarchy of strength (β = 1.076)

Sequence	Event
5	$V_{c,beam\text{-}hinge}$ = 66.7 kN
6	$V_{c,beam\text{-}ultimate}$ = 78.7 kN
3	$V_{c,beam\text{-}shear}$ = 57.7 kN [a)]
7	$V_{c,column\text{-}hinge}$ = 126.7 kN (N_c = 0)
8	$V_{c,column\text{-}ultimate}$ = 159.2 kN (N_c = 0)
4	$V_{c,column\text{-}shear}$ = 62.8 kN (N_c = 0)
1	$V_{c,joint\text{-}shear\ crack}$ = 33.3 kN (N_c = 0)
2	$V_{c,joint\text{-}shear\ peak\ load}$ = 50.7 kN (N_c = 0)

[a)] This event cannot occur, because it corresponds to the shear resistance after the formation of the plastic hinge in the beam

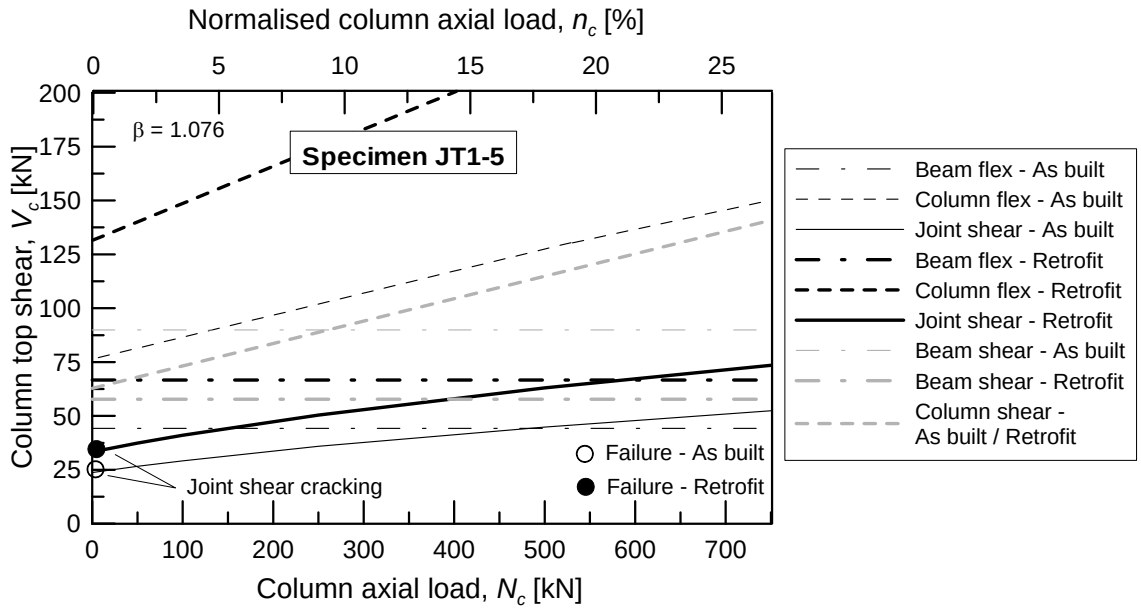

Figure F 5: Hierarchy of strength for β_{min} (JT5-1)

Verification of the anchorage

DESIGN ACTIONS

See calculations for specimen 2DG1.

CALCULATION OF TENSILE AND SHEAR RESISTANCE (n = 6)

Tension			**Shear**		
	uncracked	**cracked**		**uncracked**	**cracked**
$N_{R,s}$ =	180.0 kN		$V_{R,s}$ =	172.8 kN	
$N_{R,c}$ =	**96.2 kN**	**67.4 kN**	$V_{R,cp}$ =	**192.5 kN**	134.9 kN
			$V_{R,c}$ =	136.7 kN	**95.7 kN**
$N_{S,max}$ =	77.8 kN		$V_{S,max}$ =	117.1 kN	
$N_{S,min}$ =	48.5 kN		$V_{S,min}$ =	72.8 kN [a)]	

The verification for combined tension and shear is not necessary in this case, because $N_S/N_R > 1.0$. Furthermore, joint shear failure occurred at an earlier stage.

PLASTIC HINGE IN UNFAVOURABLE LOCATION (see Figure 8-15)

See calculations for specimen JT1-2

Test JT1-6

Table F 22: Geometry of the specimen JT1-6

Beam		**Column**		**Joint**	
$L_b/2$ =	1875 mm	H_c =	3230 mm	w_j =	350 mm
h_b =	400 mm	h_c =	300 mm	h_j =	300mm
w_b =	300 mm	w_c =	350 mm	Anchorage	Type 1
Long. rein.	2 D20 + 1D16 [a)]	Long. Rein.	3+3 D20	Shear rein.	-
Shear rein.	D8 / 200 mm	Shear rein.	D8 / 150 mm		
c =	40 mm				

[a)] Symmetrical reinforcement top and bottom layer

Table F 23: Material properties of the specimen JT1-6

Concrete		**Rein. Steel**
f_c =	29.1 MPa	See specimen JT1-2 (Table D 4)
f_{ct} =	3.3 MPa	

Assessment of as-built joint

See Section 7 and assessment of specimen JT1-1 in Appendix D.

Choice of haunches dimensions and anchorage

See Chapter 9 for more details.

Table F 24: Design parameters of the haunches (JT1-6)

Haunch			
L_h =	820 mm	E_s =	200 GPa
$L_{h,eff}$ ~	480 mm	$L' = L_h \cos\alpha$ =	580 mm
A_d =	16x150 mm^2	$K_d = E_s A_d / L_h$ ~	600 kN/mm
α =	45°		
Anchorage			
Anchor Type:	Expansion anchors	c_1 =	100 mm
n =	6	c_2 ~	50 mm
h_{ef} =	115 mm	s_1 =	100 mm
d_{nom} =	14 mm	s_2 =	150 mm

Assessment of retrofitted joint

Based on the values indicated in the relevant ETA (European Technical Approval) the axial anchor stiffness is estimated as:

$k_{N,max}$ = 56 kN/mm (short term loading in uncracked concrete)

$k_{N,min}$ = 14 kN/mm ($k_{N,max}/4$)

$$K_{h,t\min} = 1 \Big/ \left(\frac{2 \cdot \sin 45°}{6 \cdot 14} + \frac{1}{600} \right) = \underline{\mathbf{54\ kN/mm}}$$

$$K_{h,t\max} = 1 \Big/ \left(\frac{2 \cdot \sin 45°}{6 \cdot 56} + \frac{1}{600} \right) = \underline{\mathbf{170\ kN/mm}}$$

$K_{h,c,\min} = 1.5 \cdot K_{h,t,\min} = \underline{\mathbf{81\ kN/mm}}$

$K_{h,c,\max} = 1.5 \cdot K_{h,t,\max} = \underline{\mathbf{255\ kN/mm}}$

β_{max} = **2.306** (verification of axial loading of the anchorage) - (θ_b = 0.35; θ_c = 0.40)

$\beta_{\min}$ = **1.314** (verification of joint shear cracking) - (θ_b = 0.35; θ_c = 0.40)

Hierarchy of strength (β = 1.314)

Sequence	Event
5	$V_{c,beam\text{-}hinge}$ = 66.7 kN
6	$V_{c,beam\text{-}ultimate}$ = 78.7 kN
3	$V_{c,beam\text{-}shear}$ = 57.7 kN [a)]
7	$V_{c,column\text{-}hinge}$ = 126.7 kN (N_c = 0)
8	$V_{c,column\text{-}ultimate}$ = 159.2 kN (N_c = 0)
4	$V_{c,column\text{-}shear}$ = 59.3 kN (N_c = 0)
1	$V_{c,joint\text{-}shear\ crack}$ = 35.8 kN (N_c = 0)
2	$V_{c,joint\text{-}shear\ peak\ load}$ = 54.5 kN (N_c = 0)

[a)] This event cannot occur, because it corresponds to the shear resistance after the formation of the plastic hinge in the beam

See specimen JT1-5 for graphic representation of hierarchy of strength.

Verification of the anchorage

DESIGN ACTIONS

See calculations for specimen 2DG1

CALCULATION OF TENSILE AND SHEAR RESISTANCE (n = 6)

Tension			Shear		
	uncracked	**cracked**		**uncracked**	**cracked**
$N_{R,s}$ =	360.0 kN		$V_{R,s}$ =	288.0 kN	
$N_{R,c}$ =	**81.6 kN**	**57.2 kN**	$V_{R,cp}$ =	**163.2 kN**	114.4 kN
			$V_{R,c}$ =	127.6 kN	**89.3 kN**
N_S =	59.3 kN		V_S =	88.8 kN	

Verification for combined tension and shear:

Tensioned anchorage: Combined tension and shear

59.3 / 57.2 + 59.3*0.75 / 89.3 = 1.04 + 0.50 = 1.54 > 1.0 NO!

Compressed anchorage: Shear

88.8*0.5 / 89.3 = 0.50 < 1.0 OK!

PLASTIC HINGE IN UNFAVOURABLE LOCATION (see Figure 8-15)

See calculations for specimen JT1-2

CURRICULUM VITAE

Personal data

Giovacchino Genesio

Born on 7th of February, 1979
In Verona (Italy)
Married

Education

1985 – 1990	Scuola Elementare “Santa Caterina D’Alessandria”, Florence, Italy
1990 – 1993	Scuola Media “Gaetano Pieraccini”, Florence, Italy
1993 – 1998	Liceo Scientifico “Guido Castelnuovo”, Florence, Italy
1998 – 2004	Universitá degli Studi di Firenze, Florence, Italy

Working Experience

11.2004 – 06.2005	Si.In.Ter. Civil Engineer
09.2005 – 06.2011	University of Stuttgart Research Engineer, Institute of Construction Materials
Since 07.2011	IEA GmbH & Co. KG Civil Engineer

Veniet tempus quo ista quae nunc latent in lucem dies extrahat et longioris aevi diligentia. […] Itaque per successiones ista longas explicabuntur. Veniet tempus quo posteri nostri tam aperta nos nescisse mirentur.

The time will come when diligent research over very long periods will bring to light things which now lie hidden. […] A time will come when our descendants will be amazed that we did not know things that are so plain to them.

[L. A. Seneca Naturales Quaestiones, Liber VII, XXV, 4]

Verzeichnis
der bisher in der Schriftenreihe „IWB-Mitteilungen“ erschienenen Hefte:

1986/1 Institutsbericht 1983-1985 Activities

1987/1 Verdrehfähigkeit plastizierter Tragwerksbereiche im Stahlbetonbau, von Peter Langer

1987/2 Jahresbericht 1986 Activities

1987/3 Übertragbarkeit von Werkstoffkennwerten bei Glasfaser-Harz-Verbundstäben, von G. Rehm und B. Schlottke

1988/1 Zum Tragverhalten kunstharzgebundener Glasfaserstäbe im Bereich von Endverankerungen und Rissen in Beton, von Martin Faoro
(ISBN 3-9801833-0-0)

1988/2 Einfluß der Stahlkennlinie auf den möglichen Grad der Schnittkraftumlagerung bei Stahlbetontragwerken
Teil 1: Theoretische Untersuchungen, von R. Eligehausen, H. Kreller
Teil 2: Versuchsbericht, von R. Eligehausen, H. Kreller, P. Langer
(ISBN 3-9801833-1-9)

1989/1 Beiträge zur Befestigungstechnik
- Moderne Befestigungstechnik im Bauwesen - Systeme und Anwendungsbedingungen, von R. Eligehausen, W. Fuchs, M. Reuter
- Tragverhalten von Dübelbefestigungen bei Zugbeanspruchung - Loadbearing Behaviour of Anchor Fastenings in Tension, von R. Eligehausen, W. Fuchs, B. Mayer
- Tragverhalten von Dübelbefestigungen bei Querzug-, Schrägzug- und Biegebeanspruchung - Loadbearing Behaviour of Anchor Fastenings under Shear, Combinded Tension and Shear or Flexural Loading, von R. Eligehausen, W.Fuchs
- Bemessung von Befestigungen mit Stahldübeln - Zukünftiges Konzept - design of Fastenings with Steel Anchors - Future Concept, von R. Eligehausen

1989/2 Zum Weiterreißverhalten von beschichteten Geweben, von Walter Bidmon
(ISBN 3-9801833-2-7)

1989/3 Zum Tragverhalten von Übergreifungsstößen in Stahlbetonbauteilen bei Brandeinwirkung, von Roland Gerster
(ISBN 3-9801833-3-5)

1989/4 Zum nichtlinearen Trag- und Verformungsverhalten von Stahlbetonbauteilen unter Last- und Zwangeinwirkung, von Helmut Kreller
(ISBN 3-9801833-4-3)

1989/5 Untersuchungen zum Verbundverhalten gerippter Bewehrungsstäbe mit praxisüblicher Betondeckung, von Rolf Eligehausen, Helmut Kreller, Peter Langer
(ISBN 3-9801833-5-1)

1989/6 Jahresbericht 1987-1988 Activities

1990/1 SBETA Computer Program for Nonlinear Finite Element Analysis of Reinforced Concrete Structures, von V. Cervenka, R. Eligehausen, R. Pukl
(ISBN 3-9801833-6-X)

1990/2 Tragverhalten von Befestigungen unter Querlast in ungerissenem Beton, von Werner Fuchs
(ISBN 3-9801833-7-8)

1991/1 Funktionsersatzprüfungen für die Beurteilung der Eignung von kraftkontrolliert spreizenden Dübeln, von Burkhard Mayer
(ISBN 3-9801833-8-6)

1991/2 Jahresbericht 1989-1990 Activities

1992/1 Zur Korrosion von verzinktem Stahl in Kontakt mit Beton, von Klaus Menzel
(ISBN 3-9801833-9-4)

1993/1 Tragverhalten und Anwendung von Dübeln unter oftmals wiederholter Belastung, von Dieter Lotze
(ISBN 3-9803044-0-X)

1994/1 Tragverhalten von randfernen Kopfbolzenverankerungen bei Betonbruch, von Guochen Zhao
(ISBN 3-9803044-2-6)

1994/2 Zum Trag- und Verschiebungsverhalten von Kopfbolzen bei zentrischem Zug, von Johannes Furche
(ISBN 3-9803044-3-4)

1994/3 Tragverhalten von Metallspreizübeln im ungerissenen und gerissenen Beton bei der Versagensart Herausziehen, von Rolf Lehmann
(ISBN 3-9803044-1-8)

1994/4 Ein energetisches Materialmodell zur Berechnung des Tragverhaltens von zugbeanspruchtem Beton, von Gottfried Sawade
(ISBN 3-9803044-4-2)

1994/5 Zur bruchmechanischen Modellierung des Kurzzeit-Bruchverhaltens von Holz im Rißöffnungsmodus I, von Tino Schatz
(ISBN 3-9803044-5-0)

1995/1 Rotationsfähigkeit von plastischen Gelenken im Stahl- und Spannbetonbau, von Longfei Li
(ISBN 3-9803044-6-9)

1995/2 Maßstabseffekt und Duktilität von Beton- und Stahlbetonkonstruktionen, von Josko Ozbolt
(ISBN 3-9803044-7-7)

1995/3 Jahresbericht 1993-1995 Activities

1996/1 Gas Permeability as a Means to Assess The Performance Properties of Concrete, von Abebe Dinku
(ISBN 3-9803044-8-5)

1996/2 Nachbehandlungsunempfindlicher Hochleistungsbeton, von Silvia Weber
(ISBN 3-9803044-9-3)

1996/3 Zum Trag- und Verformungsverhalten von Stahlbetontragwerken unter Betriebsbelastung, von Thomas M. Sippel
(ISBN 3-9805102-0-4)

1996/4 Tragverhalten von Ankerschienen ohne Rückhängebewehrung, von Rolf Wohlfahrt
(ISBN 3-9805102-1-2)

1997/1 Jahresbericht 1996-1997 Activities

1999/1 Bemessung von zugbeanspruchten Befestigungen bei Versagensart Spalten des Betons, von Jörg Asmus
(ISBN 3-9805102-2-0)

1999/2 Jahresbericht 1998-1999 Activities

2000/1 Ökobilanzierung von Baustoffen am Beispiel des Recyclings von Konstruktionsleichtbeton, von Julian Kümmel
(ISBN 3-9805102-4-7)

2001/1 Dichtheit von Heißwasser-Langzeitspeichern aus Hochleistungsbeton, von Martin Jooß
(ISBN 3-9805102-3-9)

2001/2 Zum Trag- und Rotationsverhalten von Stahlbetontragwerken mit nicht-linearer Schnittgrößenermittlung, von Eckhart Fabritius
(ISBN 2-9805102-5-5)

2001/3 Jahresbericht 2000-2001 Activities

2001/4 Brandverhalten von Befestigungen mit großem Randabstand in Beton bei zentrischer Zugbeanspruchung, von Michael Reick
(ISBN 3-9805102-6-3)

2002/1 Zum Einfluß der Oberflächengestalt von Rippenstählen auf das Trag- und Verformungsverhalten von Stahlbetonbauteilen, von Utz Mayer
(ISBN 3-9805102-7-1)

2002/2 Zum Durchstanzen von Flachdecken im Bereich von Rand- und Eckstützen, von Henrik Vocke (ISBN 3-9805102-8-X)

2002/3 Tragverhalten und Bemessung von eingemörtelten Bewehrungsstäben, von Hannes A. Spieth (ISBN 3-9808542-1-3)

2002/4 Tragverhalten von Einzelverbunddübeln unter zentrischer Kurzzeitbelastung, von Juraj Meszaros (ISBN 3-9808542-0-5)

2002/5 met@BiM - Ein semantisches Datenmodell für Baustoff-Informationen im World Wide Web (Anwendungen für Beton mit rezyklierter Gesteinskörnung), von Marcus Schreyer (ISBN 3-9805102-9-8)

2003/1 Tragverhalten von Verbunddübeln unter zentrischer Zugbelastung im ungerissenen Beton – Gruppenbefestigungen und Befestigungen am Bauteilrand, von Bernhard Lehr (ISBN 3-9808542-2-1)

2003/2 Tragverhalten von Kunststoffdübeln im ungerissenen und gerissenen Beton, von Thilo Pregartner (ISBN 3-9808542-3-X)

2005/1 Jahresbericht 200/04 Activities

2006/1 Zum Tragverhalten von Injektionsdübeln in Mauerwerk, von Andrea Meyer (ISBN 3-9808542-5-6)

2006/2 Behavior and Testing of Fastenings to Concrete for Use in Seismic Applications, von Matthew S. Hoehler (ISBN 3-9808542-7-2)

2007/1 Ein Verbundelement für nichtlineare Finite Elemente Analysen – Anwendung au Übergreifungsstöße, von Steffen Lettow (ISBN 978-3-9808542-9-0)

2007/2 Anwendung von Ankerstäben in Rahmenecken, Rahmenendknoten und Stütze-Fundament-Verbindungen, von Markus J. Bruckner (ISBN 978-3-9811682-0-4)

2007/3 Verbundverhalten von eingemörtelten Bewehrungsstäben unter zyklischer Beanspruchung, von Isabelle N. Simons (ISBN 978-3-9811682-1-1)

2008/1 Jahresbericht 2005/07 Activities

2011/1 Jahresbericht 2008/10 Activities

2011/2 Tragverhalten und Bemessung von Injektionsdübeln unter Quer- und Schrägzugbelastung im Mauerwerk, von Georg Welz (ISBN 978-3-9811682-3-5)

2012/1 Seismic Assessment of RC Exterior Beam-Column Joints and Retrofit with Haunches Using Post-Installed Anchors, von Giovacchino Genesio (ISBN 978-3-9811682-4-2)